

# Antarctic Meteorites XXII

Papers presented to the  
Twentysecond Symposium  
on Antarctic Meteorites



June 10-12, 1997

NATIONAL INSTITUTE OF POLAR RESEARCH,  
TOKYO

国立極地研究所

**Tuesday, June 10, 1997**

0900 - 1200 Registration Auditorium (6th Floor)

0925 - 0930 Opening Address **Takeo Hirasawa**  
Director-General  
National Institute of  
Polar Research

\*Speaker

**Chairmen: Noguchi T. and Ebihara M.**

**Page**

|           |             |   |     |
|-----------|-------------|---|-----|
| <b>1</b>  | 0930 - 0945 | <b>Ichikawa O* and Kojima H.</b><br>A new member of CR clan chondrite: Petrology and mineralogy of Yamato-793261  | 61  |
| <b>2</b>  | 0945 - 1000 | <b>Noguchi T.*</b><br>Matrix and some clasts in Vigarano (CV3) chondrite  | 156 |
| <b>3</b>  | 1000 - 1015 | <b>Kimura M.* and Ikeda Y.</b><br>Anhydrous and aqueous alterations of Mokoia and Kaba CV3 chondrites   | 83  |
| <b>4</b>  | 1015 - 1030 | <b>Takeda Ha.* and Kojima H.</b><br>Refractory inclusions in the Yamato-86751 CV3 chondrite: II   | 185 |
| <b>5</b>  | 1030 - 1045 | <b>Hiyagon H.*</b><br>A preliminary study of oxygen isotopes in an Allende CAI using an ion microprobe  | 56  |
| <b>6</b>  | 1045 - 1100 | <b>Miura Y.N.* and Nagao K.</b><br>Noble gas compositions in individual chondrules of the Allende CV3 chondrite   | 118 |
| <b>7</b>  | 1100 - 1115 | <b>Nakamura T.*, Zolensky M.E., Hörz F., Takaoka N. and Nagao K.</b><br>Impact-induced loss of primordial noble gases from experimentally shocked Allende meteorite                   | 135 |
| <b>8</b>  | 1115 - 1130 | <b>Mostefaoui S., Hoppe P., Zinner E. and El Goresy A.*</b><br>IN SITU survey for interstellar graphite in unequilibrated chondrites: Evidence from C-, N-, and H-isotopic signatures | 121 |
| <b>9</b>  | 1130 - 1145 | <b>Naraoka H.* and Shimoyama A.</b><br>Carbon isotopic compositions of Antarctic carbonaceous chondrites with relevance to the alteration and existence of organic matter             | 140 |
| <b>10</b> | 1145 - 1200 | <b>Bérczi Sz.* and Lukács B.</b><br>Compositional trends in Fe and Mg contents of chondrites  | 6   |
|           | 1200 - 1300 | Lunch Time  |     |

## Special Session: Martian Meteorites

| <b>Chairmen: Ikeda Y. and Misawa K.</b> |             |  | <b>Page</b> |
|---|-------------|--|-------------|
| <b>11</b>                               | 1300 - 1315 | <b>Kaiden H.*, Mikouchi T. and Miyamoto M.</b><br>Cooling rates of olivine xenocrysts in the EET79001 shergottite  | 75          |
| <b>12</b>                               | 1315 - 1330 | <b>Kaneda K.*, McKay G. and Le L.</b><br>Comparison between synthetic and natural Nakhla pyroxenes: Minor elements composition   | 80          |
| <b>13</b>                               | 1330 - 1345 | <b>McKay G.A.*, Lofgren G.E. and Mikouchi T.</b><br>Textural relationships among carbonates, shocked feldspathic glass, and pyroxene in martian meteorite ALH84001   | 106         |
| <b>14</b>                               | 1345 - 1400 | <b>Kojima H.*, Miyamoto M. and Warren P.H.</b><br>The Yamato-793605 martian meteorite consortium   | 91          |
| <b>15</b>                               | 1400 - 1415 | <b>Ikeda Y.*</b><br>Petrology and mineralogy of the Y-793605 martian meteorite   | 64          |
| <b>16</b>                               | 1415 - 1430 | <b>Mikouchi T.* and Miyamoto M.</b><br>Major and minor element distributions in pyroxene and maskelynite from martian meteorite Y-793605 and other lherzolithic shergottites: Clues to their crystallization histories | 109         |
| <b>17</b>                               | 1430 - 1445 | <b>Ebihara M.*, Kong P. and Shinotsuka K.</b><br>Chemical composition of Y-793605, a martian lherzolite  | 22          |
| <b>18</b>                               | 1445 - 1500 | <b>Wadhwa M.*, McKay G. and Crozaz G.</b><br>Trace element distributions in Yamato 793605, a chip off the "martian lherzolite" block   | 197         |
|   | 1500 - 1530 | Tea Time   |             |
| <b>19</b>                               | 1530 - 1545 | <b>Nishiizumi K.* and Caffee M.W.</b><br>Exposure history of shergottite Yamato 793605   | 149         |
| <b>20</b>                               | 1545 - 1600 | <b>Nagao K.*, Nakamura T., Miura Y.N. and Takaoka N.</b><br>Noble gas studies of primary igneous materials of Y-793605   | 131         |
| <b>21</b>                               | 1600 - 1615 | <b>Misawa K.*, Nakamura N., Premo W.R. and Tatsumoto M.</b><br>U-Th-Pb isotopic systematics of lherzolithic shergottite Yamato 793605  | 115         |
| -- Special Lecture (I) --               |             |  |             |
| <b>22</b>                               | 1615 - 1645 | <b>Warren P.H.* and Kallemeyn G.W.</b><br>Yamato-793605 and other presumed martian meteorites: Composition and petrogenesis  | 200         |
|   | 1700 - 1900 | Reception      Lecture room (2F)   |             |

Wednesday, June 11, 1997

| <b>Chairmen: Hashimoto A. and Nagahara H.</b> |   | <b>Page</b> |
|---|---|-------------|
| <b>23</b>                                     | 0900 - 0915 <b>Nagahara H.* and Ozawa K.</b><br>Kinetically controlled stability of silicate melt at low pressures:<br>(1) Steady state   | 130         |
| <b>24</b>                                     | 0915 - 0930 <b>Ozawa K.* and Nagahara H.</b><br>Kinetically controlled stability of silicate melt at low pressures:<br>(2) Transient state  | 164         |
| <b>25</b>                                     | 0930 - 0945 <b>Hashimoto A.* and Takahashi T.</b><br>Chemical and isotopic constraints on the dynamic recycling of<br>the nebular materials   | 49          |
| <b>26</b>                                     | 0945 - 1000 <b>Sekiya M.*</b><br>Do the chondrule sizes indicate the maximum size of dust<br>aggregations in the solar nebula?  | 168         |
| <b>27</b>                                     | 1000 - 1015 <b>Tachibana S.*, Tanaka T., Tsuchiyama A., Nagahara H.<br/>and Ozawa K.</b><br>Formation of forsterite by incongruent evaporation of enstatite<br>(MgSiO <sub>3</sub> )                              | 179         |
| <b>28</b>                                     | 1015 - 1030 <b>Yamanaka A.* and Tsuchiyama A.</b><br>Evaporation coefficients of sodium from Na <sub>2</sub> O-SiO <sub>2</sub> melts by<br>thermogravimetry  | 214         |
| <b>29</b>                                     | 1030 - 1045 <b>Tsuchiyama A.* and Tachibana S.</b><br>Evaporation rates of forsterite in the primordial solar nebula  | 194         |
| <b>30</b>                                     | 1045 - 1100 <b>Kimura S.*, Kaito C., Tamura N., Saito Y. and Koike C.</b><br>Experimental studies on correlation between particle shape and<br>infrared absorption of magnesium oxide particles                   | 85          |
| <b>31</b>                                     | 1100 - 1115 <b>Bérczi Sz.*, Brezsnýánszky K., Detre Cs., Ditrói-<br/>Puskás Z., Fáy N., Holba A., Józsa S., Kubovics I.,<br/>Lukács B., Szakmány Gy. and Tóth I.</b><br>High titanium basalts in the solar system | 9           |
| <b>32</b>                                     | 1115 - 1130 <b>Lukács B.* and Bérczi Sz.</b><br>Statistical analysis of NIPR meteorite compositions, II.:<br>Comparison of sequences of differentiated rocks from an<br>asteroidal sized body and earth           | 94          |
| <b>33</b>                                     | 1130 - 1145 <b>Sato K.* and Miyamoto M.</b><br>Infrared diffuse reflectance spectra of CR chondrites:<br>Comparison with asteroids  | 165         |
| <b>34</b>                                     | 1145 - 1200 <b>Hiroi T.*</b><br>Origin of Vesta-like asteroids suggested from planetary surface<br>alteration trend of VIS-NIR reflectance spectra of HED<br>meteorites   | 52          |
|   | 1200 - 1300 Lunch Time  |             |

| <b>Chairmen: Mikouchi T. and Sugiura N.</b> |  | <b>Page</b> |
|---|--|-------------|
| <b>35</b>                                   | 1300 - 1315 <b>Arai T.*, Warren P.H., Papike J.J., Shearer C.K. and Takeda H.</b><br>Trace element chemistry of volcanic glasses in lunar meteorites Y 793274 and QUE 94281                    | 3           |
| <b>36</b>                                   | 1315 - 1330 <b>Yugami K.*, Takeda H., Kojima H. and Miyamoto M.</b><br>Modal abundances of minerals of primitive achondrites and the endmember mineral assemblage of the differentiation trend | 220         |
| <b>37</b>                                   | 1330 - 1345 <b>Chikami J.*, Takeda H., Yugami K., Mikouchi T. and Miyamoto M.</b><br>Zn behavior in chromite and daubreelite in some achondrites   | 15          |
| <b>38</b>                                   | 1345 - 1400 <b>Takeda H.*, Mikouchi T. and Miyamoto M.</b><br>Mg-rich pyroxene cores in a eucrite with type 4 chemical zonings of pyroxene   | 182         |
| <b>39</b>                                   | 1400 - 1415 <b>Kita N.T.*, Togashi S., Terashima S., Morishita Y and Yurimoto H.</b><br>Search for <sup>60</sup> Ni anomaly in MET-78008 ureilite using ion microprobe                         | 88          |
| <b>40</b>                                   | 1415 - 1430 <b>Honda M.*, Nagai H., Ebihara M. and Shinotsuka K.</b><br>Natural radioactivities in the Brenham pallasite   | 58          |
| <b>41</b>                                   | 1430 - 1445 <b>Kallemeyn G.W.*</b><br>Compositional relationships among Winona-like and other possibly related meteorites  | 78          |
| <b>42</b>                                   | 1445 - 1500 <b>Jabeen I.*, Kusakabe M., Nagao K. and Nakamura T.</b><br>Oxygen isotope studies of Tsukuba chondrite, HED meteorites and Allende chondrules                                     | 72          |
|   | 1500 - 1530 Tea Time   |             |
| <b>43</b>                                   | 1530 - 1545 <b>Fukuhara T.*, Funaki M. and Nagai H.</b><br>Measurement of natural remanent magnetization of iron meteorites  | 37          |
| <b>44</b>                                   | 1545 - 1600 <b>Wasilewski P.J.*, Dickinson T.L., Connerney J.E. and Funaki M.</b><br>Asteroid magnetic records - Possible insight from the analysis of large meteorites                        | 203         |
| <b>45</b>                                   | 1600 - 1615 <b>Funaki M.* and Danon J.</b><br>Natural remanent magnetization of Nova petropólis iron meteorite   | 43          |
| -- Special Lecture (II) --                  |  |             |
| <b>46</b>                                   | 1615 - 1715 <b>McCoy T.J.*, Dickinson T.L. and Lofgren G.E.</b><br>Experimental and petrologic studies bearing on the origin of aubrites   | 103         |

Thursday, June 12, 1997

| <b>Chairmen: Tomeoka K. and Kita N.</b> |  | <b>Page</b> |
|---|--|-------------|
| <b>47</b>                               | 0900 - 0915 <b>Fujita T.*</b><br>Origin of the barred olivine like fragment in the ordinary chondrite  | 34          |
| <b>48</b>                               | 0915 - 0930 <b>Nakamuta Y.* and Motomura Y.</b><br>Chemical composition and structural state of plagioclase in the Y-791067 chondrite  | 137         |
| <b>49</b>                               | 0930 - 0945 <b>Imae N.* and Kojima H.</b><br>On the relationship between opaque mineral assemblages and subtype in CO3 chondrites  | 66          |
| <b>50</b>                               | 0945 - 1000 <b>Matsuoka K.*, Nakamura T., Takaoka N., Nagao K. and Nakamuta Y.</b><br>Thermal metamorphism of carbonaceous chondrites with CM affinity: Evidence from mineralogy and noble gas abundance | 100         |
| <b>51</b>                               | 1000 - 1015 <b>Yamahana Y.*, Tomeoka K. and Sekine T.</b><br>Shock metamorphism of the Murchison CM2 chondrite in shock stage S4-S5: An experimental study   | 211         |
| <b>52</b>                               | 1015 - 1030 <b>Tomeoka K.* and Kojima T.</b><br>Evidence for fluidization due to water migration in a dark inclusion in the Vigarano CV3 chondrite   | 191         |
| <b>53</b>                               | 1030 - 1045 <b>Taniguchi Y.* and Hashizume K.</b><br>A search for the Q-nitrogen: Nitrogen and rare gas isotopes in Yamato-791717 (CO3)  | 188         |
| <b>54</b>                               | 1045 - 1100 <b>Sugiura N.* and Kiyota K.</b><br>Isotopic compositions of carbon and nitrogen in Mezo Madaras measured with a SIMS  | 171         |
| <b>55</b>                               | 1100 - 1115 <b>Murae T.*</b><br>Search of PAHs in carbonaceous chondrites by a fluorescence microscope   | 124         |
| <b>56</b>                               | 1115 - 1130 <b>Minamitani M., Okazaki R., Takaoka N.*, Nakamura T. and Nagao K.</b><br>Production rates of cosmogenic He, Ne, and Ar in chondrites   | 113         |
| <b>57</b>                               | 1130 - 1145 <b>Okazaki R.*, Takaoka N., Nakamura T. and Nagao K.</b><br>Noble gases in E-chondrites  | 160         |
|   | 1145 - 1245 Lunch Time & Poster Session  |             |

| <b>Chairmen: Fukuoka T. and Kimura M.</b> |  | <b>Page</b> |
|---|--|-------------|
| <b>58</b>                                 | 1245 - 1300 <b>Murakami T.*</b><br>A database for meteorites on World Wide Web   | 126         |
| <b>59</b>                                 | 1300 - 1315 <b>Yada T.*, Yano H., Nakamura T. and Takaoka N.</b><br>Petrology and mineralogy of Antarctic micrometeorites  | 208         |
| <b>60</b>                                 | 1315 - 1330 <b>Yano H.* and Noguchi T.</b><br>Sample processing and initial analysis techniques for Antarctic micrometeorites  | 217         |
| <b>61</b>                                 | 1330 - 1345 <b>Detre C.H.*, Don G., Dosztály L., Kákay-Szabó O., Solt P., Bérczi Sz., Török K., Lukács B., Tóth I. and Uzonyi I.</b><br>"Autochthonous" spherule occurrences in the Carpathian basin   | 18          |
| <b>62</b>                                 | 1345 - 1400 <b>Detre C.H.*, Don G., Dosztály L., Kákay-Szabó O., Solt P., Bérczi Sz., Török K., Lukács B., Tóth I. and Uzonyi I.</b><br>Extraterrestrial spherule layers in the Carpathian basin   | 20          |
| -- Special Lecture (III) --               |  |             |
| <b>63</b>                                 | 1400 - 1500 <b>El Goresy A.*, Chen M., Sharp T.G., Wopenka B. and Weinbruch S.</b><br>Shock-induced high-pressure phase transformations in chondritic and differentiated meteorites: Solid-state transformations, high-pressure liquidus phases, and alkali vapour fractionation | 27          |

| <b>Poster Session</b>  | <b>Page</b> |
|--|-------------|
| <b>64 Bérczi Sz., Lukács B., Földi T., Holba A., Józsa S., Marosi G., Szabó Sóni L. and Szakmány Gy.</b><br>Evolution of a small and a large rocky planetary body: Stages shown in thin sections of NASA lunar samples and NIPR Antarctic meteorites | 12          |
| <br><b>Abstract only</b>   |             |
| <b>65 Akai J. and Tari S.</b><br>Weakly ~ non-metamorphosed Antarctic CM2 carbonaceous chondrites and their mineralogical characteristics  | 1           |
| <b>66 Eugster O. and Polnau E.</b><br>Mars-Earth transfer time of lherzolite Yamato-793605   | 31          |
| <b>67 Fukuyama S. and Miura Y.</b><br>Chemical evolution of carbohydrates in origin of life  | 39          |
| <b>68 Fukuyama S., Kobayashi H. and Miura Y.</b><br>Impact metamorphosed compositions of Fe-Si-Ni-S system   | 41          |
| <b>69 Grady M.M., Verchovsky A.B., Wright I.P. and Pillinger C.T.</b><br>Carbon, nitrogen and neon in Yamato 793605 lherzolite shergottite   | 46          |
| <b>70 Itoh Y. and Fujimaki H.</b><br>Petrological study of the shock-melted Yamato-790757 LL chondrite   | 69          |
| <b>71 Marakushev A.A.</b><br>Genetic meaning of oxygen isotopic variations of chondrules in chondrites   | 97          |
| <b>72 Nayak V.K.</b><br>The Ramgarh structure - an Astrobleme (?), Rajasthan, India, an appraisal  | 143         |
| <b>73 Noguchi T. and Honjo H.</b><br>Estimation of three dimensional internal structure of some barred olivine chondrules in Allende (CV3) chondrite   | 152         |
| <b>74 Szöör G. and Rózsa P.</b><br>REE content of extremely small spherules from Borehole Nagylózs 1, NW Hungary   | 174         |
| <b>75 Wenzhu L. and Chunlai L.</b><br>Thermoluminescence in tektites and nuclear explosive and volcanic glasses  | 206         |

# **ABSTRACTS**

## Weakly- ~non-metamorphosed Antarctic CM2 carbonaceous chondrites and their mineralogical characteristics

Akai, J. and Tari, S.: Department of Geology, Faculty of Science, Niigata University  
Ikarashi 2-nocho, 8050, Niigata 950-21, Japan

**Introduction:** Many attentions were focussed on the thermal metamorphism of CM and CI chondrites and some data have been accumulated ([1-10]). It is very characteristic in contrast to non-Antarctic carbonaceous chondrites (CC). In the metamorphism, phyllosilicates changes to olivine, through some intermediate structures ([4,5,7-9]). The cause of this metamorphism has also been variously estimated ([11-14]). Some shock effect experiments have been carried out to ascertain these possibility, using shock experiment [15]. However the possibility of heating by shock events was considered to be less. Hiroi et al. [13,14] suggested possible thermal metamorphism in many of the C,G,B and F type asteroids. Hiroi et al. interpreted thermal metamorphism after extensive aqueous alteration in parent body. The different degrees of thermal metamorphism may depend partly on the different degrees of water contents and depths. More data are necessary to ascertain these scenarios or have the other. The ratio of thermally metamorphosed CC / unheated CC may become fundamental data. Using as many Antarctic CM2 type carbonaceous chondrite specimens available as possible, we are going to obtain the ratio in Antarctic meteorites. In the study we searched for the metamorphic evidences in the constituent minerals, especially phyllosilicates in CM2 CC. Summarizing previous data also, the authors will describe the thermal transformation process of phyllosilicates. We further describe constituent minerals by TEM.

### Specimens

The following 14 Antarctic carbonaceous chondrites specimens were examined. (CC which have been examined by the author are also contained here)

CI1 : Yamato (Y) -82162, CI2 : Yamato (Y) -Y-86720, Belgica (B) -7904

CM2: Yamato (Y) -74662, Y -791198, Y-793321, Y-793595, Y-82042, Y-82054, Y-82098, Y-86695, Asuka (A)-881334, A-881458 and A-881955.

### Results and discussions

Among these specimens Weakly -- slightly metamorphosed and non-metamorphosed types are as follows :

Weakly - very weakly metamorphosed : Y-793321 (300-500 C), Y-793595 (< 250 C?), A-881458 (< 250 C?), Y-82042 (slightly - non-metamorphosed?)

Unheated specimens : Y -74662, Y -791198, A-881955

The data indicates that thermally metamorphosed CC are abundantly contained in the Antarctic CM and CI CC. In very weakly metamorphosed specimens characteristic 14 Å diffraction were detected. This may be initial stage of decomposition of 7 Å serpentine

structure. Summarizing these data, decompositional sequence of serpentine minerals during thermal metamorphism were estimated. More detailed examinations may be, in some cases, necessary to detect very weak metamorphism on the other specimens which have been previously reported as unheated. Thus, continuous metamorphic degrees from very weak to intense ones are expected, assuming inner heating processes in the parent body. In Y-793595, Y-84042 and A-881458 which may have experienced very weakly metamorphism, characteristic streaks with 14 Å diffraction maxima from patchy structures were associated with main 7 Å spots.(Fig.1). This may correspond to initial stage of decomposition of 7 Å serpentine structure.

Recent investigation on Y-793595 indicated that polygonal serpentine which is rarely found in the terrestrial environments were contained (Fig.2). The other characteristics of phyllosilicates and related layer lattice minerals are almost similar to those in non-Antarctic CC: tochilinite and regularly mixed tochilinite and serpentine structures etc.

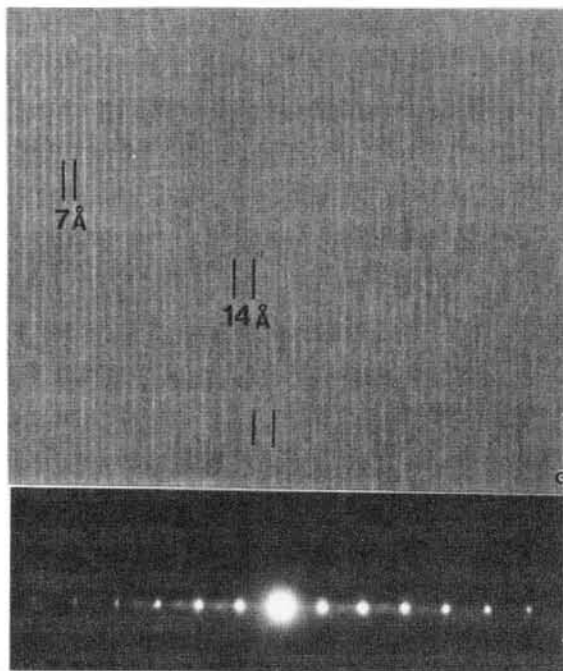


Fig.1 : TEM image of serpentine mineral with 14 Å extra diffractions.

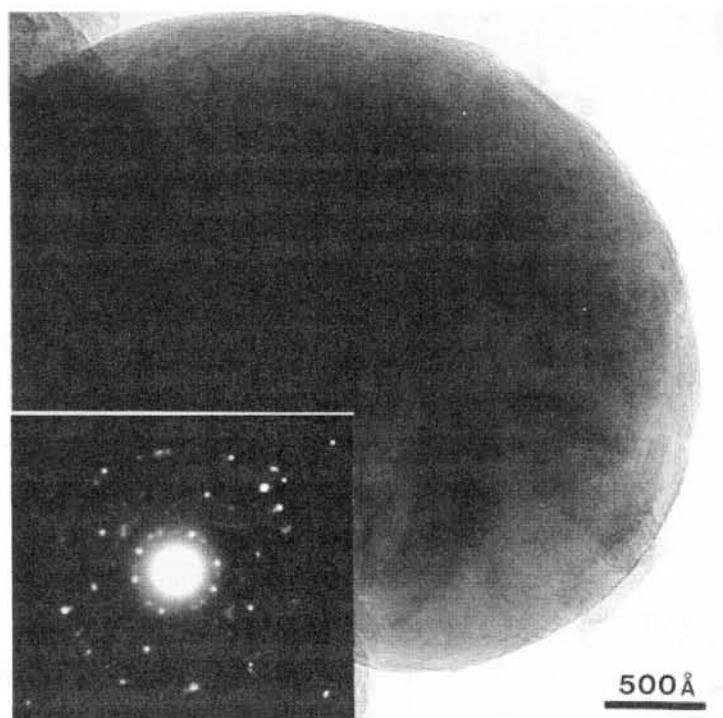


Fig.2: TEM image of polygonal serpentine which consists of 18 sectors.

References : [1] Akai,J. (1984) Paper to 9th Symp. Antarct. Meteor. 59-61. [2] Kojima, H., Ikeda, Y. and Yanai, K. (1984) Mem. Natl. Inst. Polar Res. Sp. Iss. 35, 184 - 199. [3] Akai, J. and Kanno, J. (1986) Mem. Natl. Inst. Polar Res. Sp. Iss. 41, 259-275. [4] Akai, J. (1988) Geochim. Cosmochim. Acta vol. 52, 1539-1599. [5] Akai, J. (1990) Proc. NIPR Symp. Antarct. Meteor., No.3, 55-68. [6] Akai, J. (1992) Proc. NIPR Symp. Antarct. Meteor., No.5, 120-135 [7] Tomeoka, K., Kojima, H. and Yanai, K. (1989a) Proc. NIPR Symp. Antarct. Meteor., 2, 36-54. [8] --- (1989b) Proc. NIPR Symp. Antarct. Meteorites, 2, 55-74. [9] Zolensky, M. E., Barret, R. and Prinz, M. (1989). Papers Presented to the 14th Symp. Antarct. Meteor., June 6-8, 1989., Natl. Inst. Polar Res., 24-26. [10] Ikeda, Y. (1991) Proc. NIPR Symp. Antarct. Meteor., 4, 187-225. [11] Miyamoto, M. (1991) Meteoritics, 26, 111-115. [12] Kimura, M. and Ikeda, Y. (1992) Proc. NIPR Symp. Antarct. Meteor., 5, 74-119. [13] Hiroi, (1993) Science, 261, 1016 [14] Hiroi, (1996) Lunar and Planet Sci. 28, 1 [15] Akai, J. and Sekine, T. (1994) Proc. NIPR Symp. Antarct. Meteor. 7, 101-109.

# Trace Element Chemistry of Volcanic Glasses in Lunar Meteorites Y 793274 and QUE 94281

T. ARAI<sup>1,2</sup>, P. H. WARREN<sup>2,1</sup>, J. J. PAPIKE<sup>3</sup>, C. K. SHEARER<sup>3</sup>, AND H. TAKEDA<sup>4</sup>

<sup>1</sup>Mineralogical Institute, Graduate School of Science, University of Tokyo, 7-3-1 Hongo, Tokyo 113, Japan.

<sup>2</sup>Institute of Geophysics, UCLA, Los Angeles, CA 90095-1567, U.S.A.

<sup>3</sup>Institute of Meteoritics, Department of Earth and Planetary Science, University of New Mexico, Albuquerque, NM 87131-1126, U.S.A.

<sup>4</sup>Research Institute, Chiba Institute of Technology, Tsudanuma, Narashino, Chiba 275, Japan.

**Introduction:** Lunar volcanic glasses are thought to represent primitive lunar basalt compositions since they are geochemically less evolved than crystalline mare basalts [1,2]. Thus they provide valuable insights into lunar interior. Last year we reported probable pristine volcanic glass spherules found in lunar breccia meteorites, Y793274 and QUE94281 [3]. We concluded they are probably of volcanic origin from the standpoint of major element chemistry, due to their inter- and intra-sample homogeneity, high Mg/Al ratio, and absence of exotic inclusions. These volcanic glasses are poor in TiO<sub>2</sub> (0.37 ~ 1.22 wt%), and classified as Very Low Ti (VLT). We also proposed a common source crater pairing of Y793274 and QUE94281 on the grounds that they show analogous texture, and that they include pyroxene fragments of almost identical compositions and exsolution feature, and volcanic glasses with remarkably similar compositions, especially for TiO<sub>2</sub> [3,4,5]. This study presents trace element chemistry of these volcanic glasses, aiming for further understanding of lunar interior and confirmation of their source crater pairing.

**Samples and Methods:** We studied PTSs of Y793274, 91-2 (Y79) provided by the National Institute of Polar Research, and two PTSs of QUE94281, 6 (QUE6) and 8 (QUE8), by the Antarctic Meteorite Working Group. Glasses were all analyzed with a Cameca IMS 4f ion microprobe operated by the University of New Mexico/Sandia National Laboratories consortium. A primary beam of O<sup>-</sup> is focused to a spot of 25 μm in diameter for REEs (La, Ce, Nd, Sm, Eu, Dy, Er, Yb) and trace elements (Co, Sr, Ba). Oxide interferences such as BaO on Eu (<sup>151</sup>Eu-<sup>135</sup>Ba<sup>16</sup>O and <sup>153</sup>Eu-<sup>137</sup>Ba<sup>16</sup>O) are corrected by empirical relations among <sup>151</sup>Eu/<sup>153</sup>Eu, and <sup>135</sup>Ba/<sup>137</sup>Ba and BaO/Ba observed in silicate glasses. The numbers of analyzed glasses were limited because half of them are not large enough for the analyses or include cracks. As a result, four glasses from QUE8, two glasses from QUE 6, and one from Y79 were analyzed.

**Results and Discussion:** Concentrations of major and trace elements, and sizes of analyzed glasses are shown in Table 1. Rare earth element abundances of glasses analyzed, normalized to CI chondrite values [6] are plotted in Fig. 1. The glasses both from QUE6 and 8 show REE patterns slightly LREE enriched with abundances between 7 and 22 × CI chondrite and small negative Eu anomalies ([Sm/Eu]<sub>N</sub> = 0.9 - 1.5). Although only one analysis is available for Y79, the REE pattern of this Y79 glass is almost identical to those of QUE, with abundances 10 × CI chondrite. They are similar to that of Apollo 17 VLT glass and B-1 variety of Apollo 14 (A14) green glass [7,8], in spite of the fact that A14 green B glass has larger (-) Eu anomalies ([Sm/Eu]<sub>N</sub> = 6 -14) than glasses in QUE and Y79. QUE and Y79 glasses show

negative linear correlation in the plots MgO vs. TiO<sub>2</sub> and MgO vs. CaO, analogous to those of Apollo 14 and 17 VLT glasses [3], which is consistent of similarities of REE patterns and abundances for QUE and Y79 to those of A14 and A17 VLT glasses.

Barium and Sr behave incompatibly in basaltic systems both in partial melting and crystallization processes. For glasses in QUE and Y79, Ba, Sr, Ce are negatively correlated with MgO (Fig. 2a), and have positive linear correlation with TiO<sub>2</sub> (Fig. 2b), although Ba in the most Mg-poor glass (Q8-S6) does not fall on the linear correlation with TiO<sub>2</sub>.

Low concentration of Co of glasses in QUE and Y79 tends to confirm their volcanic, not impact origin. Even though Co is highly compatible, Co is inversely correlated with MgO (Fig. 2a) and positively linked with TiO<sub>2</sub>, except Q8-S6 (Fig. 2b). Cobalt also shows positive correlation with Ba (also except Q8-S6), which is a strongly incompatible element. These correlations found in QUE and Y79 glasses have been also reported for Apollo 15 (A15) green glass [9,10]. As suggested by Shearer et al. [9], these correlations were probably not produced not by fixed-pressure magmatic processing, but plausibly by a polybaric melting as proposed by Longhi [11] and Delano [12]. The systematic Co vs. incompatible elements and Co vs. MgO variations for QUE and Y79 VLT glasses are consistent with those for other VLT glasses and support "polybaric-melting" origin of VLT glasses.

We have reported that glasses both in QUE and Y79 show two clusterings for higher-Ti (TiO<sub>2</sub> = 0.99 - 1.22 wt%) and lower-Ti (TiO<sub>2</sub> = 0.37-0.67 wt%) [3]. Yet, consistent linear correlations for Ba, Sr, Ce, Co were found encompassing both Ti groups, which indicates these two groups may have been derived by similar processes from the same or closely related magma sources.

**Summary:** (1) Although only one glass analysis is available for Y79, REE pattern and concentration, incompatible elements behavior (Ba, Sr) and compatible element (Co) behavior of Y79 glasses are almost identical to those of QUE. These observations confirm their source crater pairing. (2) Analyses of REE and incompatible elements indicate that the QUE and Y79 glasses are analogous to Apollo14 green B and Apollo17 VLT glasses. (3) The systematic variation involving Co, incompatible elements and MgO for QUE and Y79 glasses supports "polybaric-melting" origin of VLT glasses.

**Acknowledgments-** We thank M. Wiedenbeck and G. W. Fowler for technical assistance for operating ion probe.

**References:**

- [1] Delano J. W. (1986) Proc. LPSC, 16th, D201-D213.
- [2] Longhi J. (1987) JGR, 92, E349-E360.
- [3] Arai T. et al. (1996) Proc. NIPR Symposium on Antarctic Meteorites, 21, 4-7.
- [4] Arai T. et al. (1996) LPS XXVII, 33-34.
- [5] Warren P. H. & Arai T. (1997) LPS XXVIII, 1499-1500.
- [6] Anders E. and Grevesse N. (1989) GCA, 53, 197-214.
- [7] Shearer C. K. & Papike J. J. (1993) GCA, 57, 4785-4812.
- [8] Shearer C. K. et al. (1991) EPSL, 102, 131-147.
- [9] Shearer C. K. et al. (1996) GCA, 60, 509-528.
- [10] Galbreath K. C. et al. (1990) GCA, 54, 2265-2575.
- [11] Longhi J. (1992) GCA, 56, 2235-2251.
- [12] Delano J. W. (1996) LPS, XXVII, 301-302.

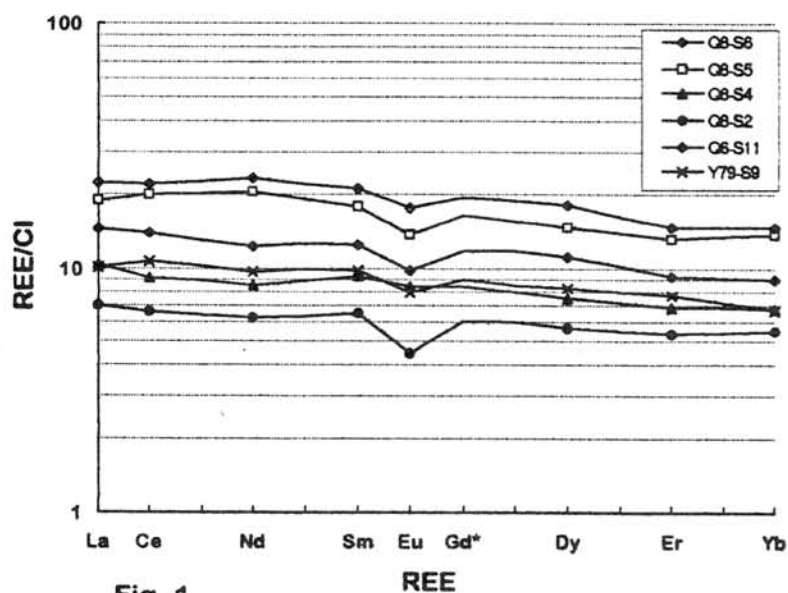


Fig. 1.

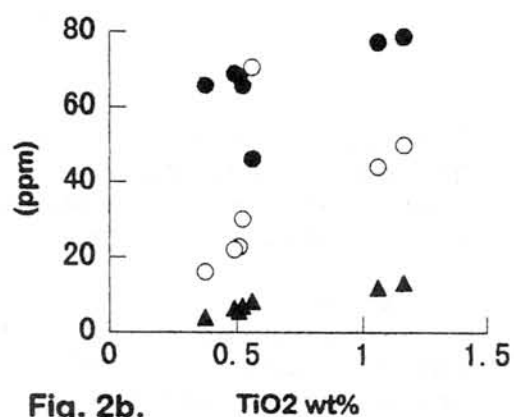


Fig. 2b.

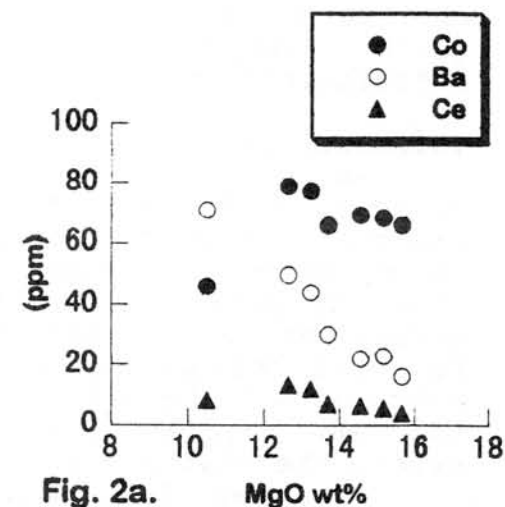


Fig. 2a.

Table 1.

|   | QUE8  |       | QUE6  |       | Y79           | A14*   | A17*      |
|---|-------|-------|-------|-------|---------------|--------|-----------|
|   | Q8-S2 | Q8-S4 | Q8-S5 | Q8-S6 | Q6-S1(Q6-S11) | Y79-S9 | Green VLT |
| Diameter or long dimension of fragment (um) | 75.0  | 70.0  | 125.0 | 47.5  | 70.0          | 100.0  | 50.0      |
|   |       |       |       |       |               |        | B-1       |
| Major Elements (wt%)                        |       |       |       |       |               |        |           |
| SiO <sub>2</sub>                            | 44.59 | 44.98 | 46.13 | 48.44 | 46.03         | 46.46  | 45.74     |
| TiO <sub>2</sub>                            | 0.37  | 0.51  | 1.06  | 0.56  | 0.53          | 1.19   | 0.49      |
| Al <sub>2</sub> O <sub>3</sub>              | 9.71  | 9.46  | 8.60  | 10.91 | 10.23         | 8.77   | 9.79      |
| FeO   | 18.77 | 18.94 | 19.20 | 16.31 | 17.43         | 19.24  | 18.39     |
| MnO   | 0.26  | 0.27  | 0.26  | 0.26  | 0.23          | 0.24   | 0.26      |
| MgO   | 15.67 | 15.17 | 13.23 | 10.50 | 13.97         | 12.89  | 14.55     |
| CaO   | 9.14  | 9.21  | 9.41  | 11.31 | 10.57         | 9.69   | 9.23      |
| Na <sub>2</sub> O                           | 0.26  | 0.22  | 0.35  | 0.34  | 0.20          | 0.43   | 0.11      |
| K <sub>2</sub> O                            | 0.03  | 0.02  | 0.04  | 0.03  | 0.04          | 0.04   | 0.08      |
| Cr <sub>2</sub> O <sub>3</sub>              | 0.49  | 0.50  | 0.56  | 0.39  | 0.40          | 0.57   | 0.49      |
| V <sub>2</sub> O <sub>5</sub>               | 0.03  | 0.02  | 0.03  | 0.04  | 0.01          | 0.04   | 0.02      |
| NiO   | 0.02  | 0.01  | 0.03  | 0.02  | 0.04          | 0.03   | 0.02      |
| Total                                       | 99.36 | 99.31 | 98.90 | 99.11 | 99.68         | 99.59  | 99.18     |
| Trace Elements (ppm)                        |       |       |       |       |               |        |           |
| Co  | 65.92 | 68.26 | 77.42 | 46.24 | 65.79         | 78.88  | 69.05     |
| Sr  | 57.22 | 58.62 | 60.43 | 71.75 | 78.92         | 65.91  | 62.48     |
| Ba  | 16.13 | 22.81 | 44.22 | 70.76 | 30.13         | 49.99  | 22.00     |
| La  | 1.65  | 2.44  | 4.43  | 3.41  | 3.35          | 5.21   | 2.35      |
| Ce  | 4.01  | 5.54  | 11.97 | 8.33  | 7.06          | 13.28  | 6.46      |
| Nd  | 2.83  | 3.88  | 9.21  | 5.54  | 4.36          | 10.54  | 4.39      |
| Sm  | 0.96  | 1.37  | 2.84  | 1.83  | 1.45          | 3.10   | 1.44      |
| Eu  | 0.25  | 0.47  | 0.77  | 0.55  | 0.63          | 0.98   | 0.44      |
| Dy  | 1.38  | 1.83  | 3.57  | 2.71  | 1.73          | 4.36   | 2.00      |
| Er  | 0.86  | 1.10  | 2.08  | 1.47  | 0.96          | 2.33   | 1.23      |
| Yb  | 0.89  | 1.11  | 2.21  | 1.47  | 1.20          | 2.37   | 1.09      |

\* Shearer & Papike (1993)

# COMPOSITIONAL TRENDS IN FE AND MG CONTENTS OF CHONDRITES

Sz. Bérczi<sup>1</sup> & B. Lukács<sup>2</sup>

<sup>1</sup> Eötvös University, Dept. of Petrology and Geochemistry & Dean's Office, H-1088 Budapest, Rákóczi út 5. Hungary

<sup>2</sup> Central Research Institute for Physics, RMKI, Bp. 114. Pf. 49. H-1525 Budapest, Hungary

## ABSTRACT

The total iron content of chondrites may serve as estimation for the initial condition for the parent body thermal evolution, therefore we wanted to see the validity of the noticeable result of Wiik (1956) on the two lines of constant total Fe content for chondrites in the light of the new Catalog of Antarctic Meteorites (Yanai, Kojima, Haramura, 1995). We carried out statistical calculations on the 443 compositional data in this catalog.

## INTRODUCTION

40 years ago H. B. Wiik deduced that among chondrites 2 groups do exist with constant total Fe content: one with cca. 27 weight % and one with 21 %. Although Wiik's result was based on no more than 30 chondrites it contained far more carbonaceous chondrites than those of Urey and Craig (1953). The carbonaceous chondrites needed normalisation to volatile free basis in order to show that constant Fe lines reflect inner compositional changes. The database of NIPR contains 443 chondrites, measured by a single person (Haramura) with the same method and apparatus, and this work made it possible to extend the statistical weight of the results. In addition

- i) Antarctic conditions are the best for survival with small chemical reaction rate after fall, and
- ii) chemical reactions cannot change much the total Fe content.

## 2. THE DATA

First we reconstruct the modern equivalent of Urey & Craig Clusters displaying the 443 points of the NIPR database (Yanai, Kojima, Haramura, 1995), as Fig. 1. It resembles the HR Diagram of stars, the field being spanned again by two basic parameters.

Wiik had only 30 reliable meteorite compositions, not enough for detailed statistical analyses; he thus chose a graphic display. On our Fig. 1 the 2 strips can be seen, but they are not too narrow and at the highest non-oxide point of L's the strips seem to touch. Interestingly enough, this point fits on the Urey-Craig trajectory, connecting the centres of gravity of the 2 Urey-Craig Clusters.

## 3. STATISTICAL ANALYSIS OF THE NIPR CHONDRITE DATA

Of course, the direct use of the NIPR data field would introduce selection effects. The NIPR collection contains some 8000 meteorites, of which more than 3500 are identified for type and cca. 3000 of them are chondrites. The investigators, very practically, selected for analysis relatively higher percentages of rarer types than of more frequent ones. So one cannot directly calculate distributions from the *measured* samples.

However, the selection was random within each van Schmus-Wood box, since composition was not known before selection. Therefore the estimate is undistorted for the distribution of any quantity  $x$  on

the full field of identified meteorites if all van Schmus-Wood boxes are inflated to the sizes before selection.

The results are: Fig. 2 is the distribution of Fe/Si on the whole field, normalised to 2987. Fig. 3 is the same but for Mg/Si.

Now let us see the moments for the whole field of 2987 chondrites. Formally we get the result,  $x = \text{Fe/Si}$ ,  $y = \text{Mg/Si}$

|       |                                       |  |
|-------|---------------------------------------|--|
| Total | $\langle x \rangle = 1.517 \pm 0.013$ | $\langle y \rangle = 0.857 \pm 0.0016$ |
|       | $\sigma_x = 0.258$                    | $\sigma_y = 0.034$                     |
|       | $n = 420$                             |  |

However the result for  $x$  has no physical meaning at all, since Fig. 2 clearly shows that  $f(x)$  has 2 well separated peaks. The best fit with the sum of two Gaussians give for  $f(x)$  that

|  |
|--|
| $N_1 \approx 1105$ , $n_1 \approx 213$                                       |
| $\langle x \rangle_1 \approx 1.215 \pm 0.0066$ , $\sigma_{1x} \approx 0.096$ |
| $N_2 \approx 2882$ , $n_2 \approx 207$                                       |
| $\langle x \rangle_2 \approx 1.694 \pm 0.0084$ , $\sigma_{2x} \approx 0.123$ |

The 2 distributions do not overlap at  $2\sigma$ , so they (not only the peaks) are well separated at more than 95% significance level.

#### 4. CONCLUSIONS

We have got back Wiik's 2 fundamental groups for Fe content, on a statistics 14 times larger than Wiik's one and with a full statistical analysis. One group is peaked around  $\text{Fe/Si} = x \approx 1.694$  ("High group"), the other around  $\text{Fe/Si} = x \approx 1.215$  ("Low group"). As further analysis (not given here) shows, the first contains almost solely C, H and E chondrites, the second L and LL ones. The old result of the pioneering work is still valid.

On the other hand, in Mg content there is a dominant central peak around  $\text{Mg/Si} = 0.857$  (which, in detailed analysis, corresponds to H, L and LL), with two, significantly existing and separate, but very small secondary peaks at 0.693 (E) and 0.937 (C).

A quite recent new chondritic type, R, seems to have its peak just in the touching of the 2 subdistributions of Fig. 2, around  $x = 1.457 \pm 0.013$ , at least if calculated from 3 available data (Palme, Weckwerth & Wolf, 1996). They practically do not contain non-oxidised Fe. In addition they seem extremely rare (only 10 of them are known); in addition 9 of the 10 are highly brecciated mixtures. (It was impossible to incorporate the R's into the analysis here, because no relative weight of R's is known to the Antarctic chondrites; the Japanese classification started well before the discovery of R's, therefore up to now no Antarctic meteorite was classified as R.) It is the best to wait until the nature of R chondrites will be clarified better.

#### ACKNOWLEDGEMENTS

Authors would like to thank Drs. K. Yanai, H. Kojima and H. Haramura for illuminating discussions. Partly supported by MKM 694/96, OMFB-MÜI TP.55/96 and OTKA T007410.

#### REFERENCES

- Bérczi Sz., Holba Agnes & Lukács B. (1996): *Antarctic Meteorites XXI*, NIPR, Tokyo, p. 17-19  
Palme H., Weckwerth G. & Wolf D. 1996: *LPSC XXVII*, p. 991-992  
Urey, H. C., and Craig, H. (1953): *GCA* 4. 36-82  
Wiik, H. B. (1956): *GCA* 9. 279-289  
Yanai, K., Kojima, H., Haramura, H. (1995): *Catalog of the Antarctic Meteorites*, NIPR, Tokyo

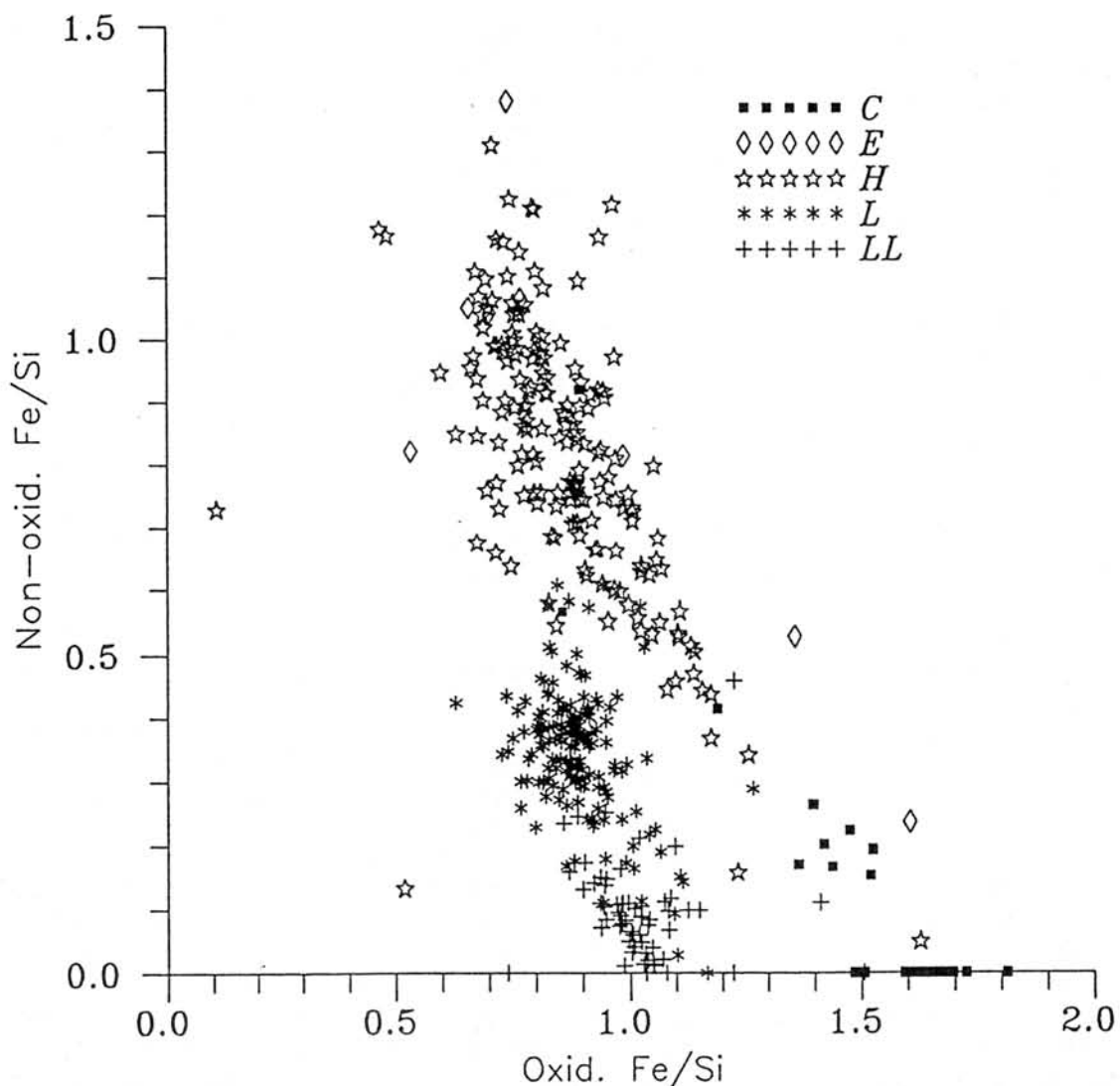


Fig. 1: The NIPR meteorites on the oxidised-non-oxidised Fe/Si plane

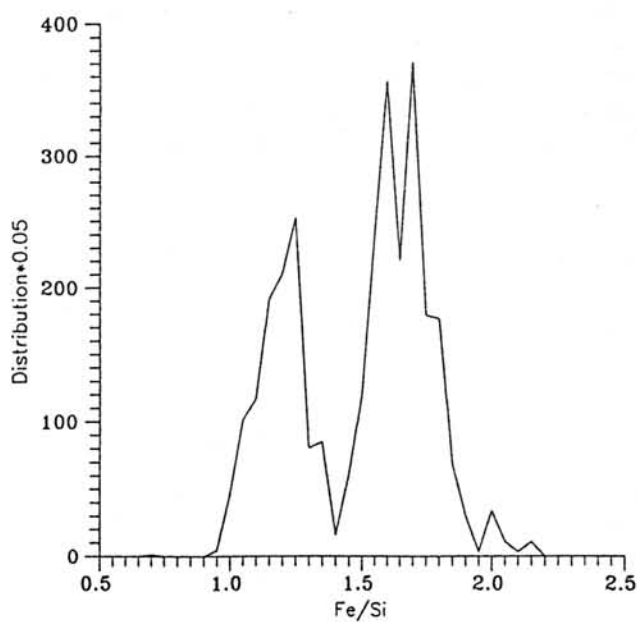


Fig. 2: The distribution of Fe/Si in NIPR chondrites

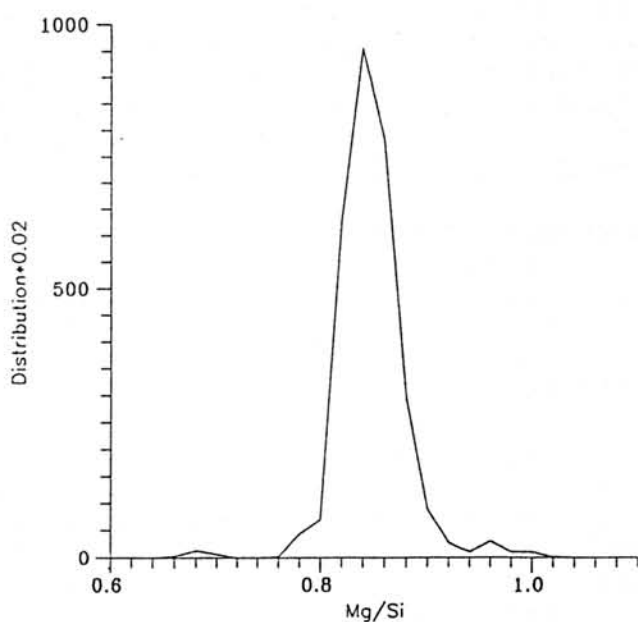


Fig. 3: The distribution of Mg/Si in NIPR chondrites

## HIGH TITANIUM BASALTS IN THE SOLAR SYSTEM

Bérczi Sz.<sup>1</sup>, Brezsnayánszky K.<sup>2</sup>, Detre Cs.<sup>2</sup>, Ditrófi-Puskás Z.<sup>1</sup>,  
Fáy Nóra<sup>3</sup>, Holba Agnes<sup>3</sup>, Józsa S.<sup>1</sup>, Kubovics I.<sup>1</sup>, Lukács B.<sup>3</sup>,  
Szakmány Gy.<sup>1</sup>, Tóth I.<sup>4</sup>

<sup>1</sup> Eötvös Univ. Petrology Dept., H-1088 Budapest Múzeum krt. 4/a

<sup>2</sup> Geological Institute of Hungary H-1143 Budapest Stefánia út 14.

<sup>3</sup> CRIP RMKI H-1525 Bp. 114. Pf. 49., Budapest, Hungary

<sup>4</sup> Konkoly Observatory, H-1525 Bp. 114. Pf. 67., Budapest, Hungary

### ABSTRACT

Reviewing the Ti/Si relations in the Solar System we concentrate on anomalous Ti enrichments. It seems that the enrichment was connected mainly with differentiations in residual liquids of upper mantle origin, especially on Earth, Luna and the unidentified angrite parent body. Here we compare data for chondrites, achondrites, lunar and terrestrial basalts on the basis of the NIPR Antarctic Meteorite Catalog, Apollo samples and Carpathian Basin geologic investigations.

### THE PROBLEM

The surprisingly high Ti content of lunar surfaces is an old problem in selenology. In some "blue" lunar basaltic layers the weight share of TiO<sub>2</sub> is above 10 % while the standard Solar System abundance is smaller by 2 orders of magnitude. Even in Archean terrestrial basalts it is not above 1 % (Condie, 1981). So either Luna has been composed of a very special assemblage, or lunar volcanism was very special.

It is rather difficult to choose until real in situ work does not become again possible. Still, the NIPR Catalog of Antarctic Meteorites (Yanai, Kojima & Harammura, 1995), henceforth the Catalog, is an excellent database to investigate this problem (appended, where necessary, with some terrestrial and lunar data), because it is the largest available cross section of the Solar System. By comparing the Solar System Ti data to lunar ones and by trying to find lunar analogons one may get some insight into the lunar Ti "anomaly". Henceforth no specific reference is given if the source is the Catalog.

### COMPOSITIONAL DATA

Chondritic data show that the primordial Ti/Si ratio is cca. 0.003. The highest chondritic ratio measured is cca. 0.0065, except for C chondrites where this value is the average. We have no explanation for this C chondrite speciality; maybe this is a condensational dependence on the primordial temperatures in the nebula.

Now let us see the effects of thermal/gravitational transformation/differentiation. In one wide group of achondrites the average does not go above 0.003; this group contains mesosiderites, lodranites, aubrites and ureilites. The opposite group is that of "volcanic" achondrites. Let us see first the diogenite -> howardite -> eucrite sequence. There a gradual (Mg -> Al,Ca) substitution is seen, which may be interpreted as nonequilibrium thermodynamic process when ascending mantle material crosses the thickening (Al,Ca)-rich crust of the parent body (Lukács & Bérczi, 1997) With substantial variations, the averages are as follows:

| Rock       | <Ti/Si> |
|------------|---------|
| Diogenites | 0.005   |
| Howardites | 0.011   |
| Eucrites   | 0.019   |

It seems as if the Ti enrichment were parallel with the (Mg -> Al,Ca) substitution. Such a phenomenon gets a simple explanation if the viscosity and/or melting point of the lava, caeteris paribus, decreases with Ti content.

But if this is true, similar trend should be seen on planetary basalts. Indeed, the Martian Ti/Si level, if calculable from the only 2 measured samples of the Catalog, is 0.017, near to eucrites and old and new terrestrial values.

Still there are a few Solar System basalts well above the eucritic Ti level. Lunar "red" (Apollo 12, 14 & 15) basalts are at Ti/Si ~ 0.1, and "blue" ones (Apollo 11 & 17) at ~0.4. The lower tail of the reds is represented in the Catalog by Yamato-793169, Yamato-793274 & Asuka-881757, but blues have not been identified so far on Antarctica. (Lunar anorthosites are at the double of chondritic level.) But lunar basalts do have analogons for Ti level in the Solar System.

## DISCUSSION

One such is the angrites. They are rather rare and the Catalog has only 2 measured samples, the archetypic Angra dos Reis and Asuka-881371. Hence the angrite level is  $Ti/Si = 0.05 \pm 0.02$ , comparable to the lunar red one. The other analogons are some C/T Carpathian Basin basalts. (That time is the prehistory of the Basin whose actual formation ended in the Miocene.) Mecsek (Harangi, 1994) and Gyergyóditró (Lengyel, 1957; Pál Molnár, 1995) basalts are at the red lunar level and Szarvaskő (Szentpétery, 1953; Lengyel, 1957) ones at the lunar blue one (for the comparison see Bérczi & Lukács, 1996). The Carpathian Basin is special, but not quite singular; much older "red" kimberlites are known from Greenland (Nixon, 1987).

The lunar bulk composition may or may not be special, but at some spots the formation processes of the Carpathian Basin produced lunar Ti level from terrestrial bulk one. So probably rather the lunar volcanic mechanism produced the high enrichment in Ti. Unfortunately just now the details of the lunar mechanism cannot be investigated, while in the Carpathian Basin the process was so complicated that one cannot tell apart the important and irrelevant details for high Ti content.

Still, we can give here the comparative Fig. 1. It is a completed form of a similar Figure in Bérczi & Lukács (1996), and for lunar data see the references therein. The samples are lunar red and blue basalts, the analogous Mecsek and Szarvaskő ones, and the measured shergottites (Zagami & ALH-77005), angrites (Angra dos Reis & Asuka-881371) and basaltic lunars (Yamato-793169, Yamato-793274 & Asuka-881757) of the Catalog.

The picture is partly interpretable. Both red samples (lunar and Mecsek) show anticorrelation between Ti and Mg, conform with the idea that somehow the more and more thicker and aluminiferous crust makes the lava enriched in Ti. Of course, it is not advisable to calculate correlation coefficients from 2 or 3 points, but at least the locations of the angrite, basaltic lunar and shergottitic points support an anticorrelation. But, in the contrary, for both blue data (lunar and Szarvaskő) the correlations are positive.

At this moment there are no lunar expeditions. Still, a comparative investigation on lunar basalts, basaltic meteorites (lunar or not) and Carpathian Basin basalts may help. We close this presentation with a statement and a question.

1) Lunar "blue" basalts are still absent among measured lunar meteorites.

2) Where is in the Solar System the angrite parent body having mimicked a substantial planet with thick and more or less aluminiferous crust?

#### ACKNOWLEDGEMENTS

Discussions with Dr. S. Harangi are acknowledged. Partly supported by: the Hungarian-Japanese S&T Cooperation "Impact and Extraterrestrial Spherules" 31/96; OTKA T/014958, MÜI-TP-15/95 & OMFB-96-97-47-1265-MÜI-TP-055/96.

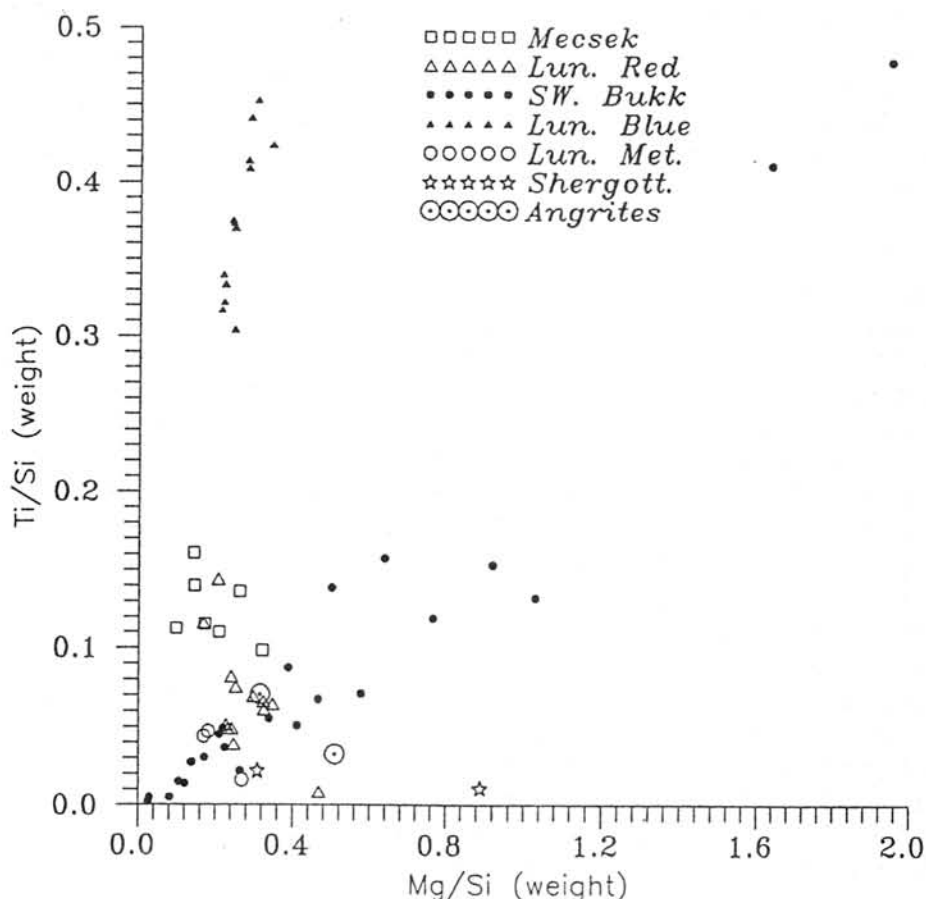


Fig. 1

#### REFERENCES

- Bérczi Sz. & Lukács B., 1996: KFKI-1996-08  
 Condie K. C., 1981: Archean Greenstone belts. Elsevier, Amsterdam  
 Harangi Sz., 1994: Lithos 33, 303  
 Lengyel E., 1957: Ann. Inst. Geol. Publ. Hung. XLVI/2  
 Lukács B. & Bérczi Sz., 1997: in this Volume  
 Nixon P. H. (ed.), 1987: Mantle Xenoliths. J. Wiley & Sons, N.Y.  
 Pál Molnár E., 1995: Petrologic and Geologic Investigations on the Gyergyóditró Syenite Complex. University Press, Szeged  
 Szentpétery Zs., 1953: Ann. Inst. Geol. Publ. Hung. XLI/1  
 Yanai K., Kojima H. & Haramura H., 1995: Catalog of the Antarctic Meteorites. NIPR, Tokyo

**EVOLUTION OF A SMALL AND A LARGE ROCKY PLANETARY BODY:  
STAGES SHOWN IN THIN SECTIONS OF NASA LUNAR SAMPLES AND  
NIPR ANTARCTIC METEORITES**

*Sz. Bérczi,<sup>1</sup> B. Lukács,<sup>2</sup> T. Földi,<sup>4</sup> Á. Holba,<sup>2</sup>*

*S. Józsa,<sup>1</sup> G. Marosi,<sup>3</sup> L. Szabó Sóki,<sup>3</sup> Gy. Szakmány,<sup>1</sup>*

<sup>1</sup> Eötvös University, Dept. Petrology, H-1088 Budapest, Múzeum krt 4/a. Hungary,

<sup>2</sup> Central Research Institute for Physics RMKI, H-1525 Budapest 114. P.O.B. 49. Hungary,

<sup>3</sup> Eötvös University, Dept. Educational Technology, H-1088 Budapest, Rákóczi út 5. Hungary

<sup>4</sup> GEMINILUX, H-1117 Budapest, Irinyi u. 36/b. Hungary

**ABSTRACT**

This contribution is a 25 minutes videofilm made on the basis of two remarkable thin section sets of NIPR Antarctic Meteorites and NASA Lunar Samples. Eötvös University, Department of Petrology and Geochemistry had the occasion for a long term of loan and parallel studies of these two sets. Our movie intends to show the multiple usefulness and benefits of such synthesis studies by selecting and arranging most of the available thin section samples according a theoretically plausible, but in some respects hypothetical evolutionary sequence of a smaller (NIPR set, chondritic and an evolved asteroidal body) and of a larger (NASA set, lunar body with using stratigraphical knowledge) celestial body. We intended to show the beauties of such petrologic microscopy work, and to give enthusiasm for students and teachers in their extraterrestrial geology and cosmopetrographical studies and lectures, too.

**INTRODUCTION**

Thermal evolution of a rocky celestial body strongly depends on the size (and so the mass) of the body. Active period with products of layers on the surface could last ca. 100 Ma on an asteroidal sized body with ca. 100-200 kms in diameter, while this interval for the Moon lasted for more than 2 Ga.

Meteorites are fragments of different asteroidal sized bodies. Mineralogical and textural characteristics of various meteorites reveal processes, which help to arrange them into types and classes. Many important processes can be fitted into a global evolutionary picture if we assume, that larger bodies suffered thermal transformation during their early lifetime, when radioactive heating warmed up them. This way main chondritic processes of early classifications to types of Prior, then Urey and Craig, further developments by Wiik, Keil and Fredriksson, and to petrologic class definition of Van Schmus and Wood serve as parallel partial processes in this global picture.

Studies of lunar stratigraphy (ie. Wilhelms, 1987) sketched important global picture of the lunar thermal evolution, although no exact geologic timescale could have been connected to this sequence of events. Nevertheless, the main periods of pre-Nectarian, Nectarian, Imbrian, Eratosthenian and Copernican stratigraphic units reflected, that earlier interval of inner activity ceased and a later interval of only impact type outer events followed in the lunar evolutionary history.

Lunar samples from the 6 Apollo missions first corresponded rock types to the principal geologic provinces on the Moon and radioactive dating of the samples projected this stratigraphic units to the idealised column of the absolute age system. Petrologic studies revealed the main great evolutionary periods in the early history of the Moon: crust formation by flotation of feldspars in the early magma ocean, and the later second period of extrusion of partial melts from the lunar mantle to the surface, so filling large impact basins forming lunar maria.

This film is a first step to show planetary evolutionary events on the smaller rocky bodies in the Solar System. Later films will show Martian and Terrestrial evolution, but on the background of a common Solar System perspective, emphasizing that any bodies could have preserved an important time-section of celestial body evolution which is not available yet on the others

**CHONDRITIC PARENT BODY AND EVOLVED ASTEROIDAL THERMAL HISTORY:  
THIN SECTIONS OF THE NIPR ANTARCTIC METEORITE SAMPLES**

The film begins with the exposition of chondritic texture (hand specimen of ALHA 761 and thin section of CO3 Yamato 791717). The first remarkable thermal transformational sequence shown is the metamorphosis throughout the van Schmus Wood petrologic classes, where we used H3 (Yamato 791428), H4 (ALHA 77233), H5 (Yamato 74079) and H6 (Yamato 74014). Throughout this sequence

we focus attention to (1) equilibration of chondrules and matrix, (2) chondrule fading and obscuring, and (3) changes in iron grain size distribution. Then questioning H the five chondrite types are shown on the Fe+FeS vs. Fe-oxides field gradually adding to Urey and Craig's H and L, the E, LL and C types. The diagram is drawn from the database of the Catalog of Antarctic Meteorites (Yanai, Kojima, Haramura, 1995). The five types are shown by color plots, where color refers to chemical composition connected to chondritic metallurgy. The five types average compositional ratio for Fe (red), FeO (green) and C (blue) content gives the color of the plots, but the next scene shows these data calculated for all available van Schmus - Wood boxes. These colors show alternation throughout the sequence of petrologic classes. The summary of this first part of the film is given by projecting the corresponding Fe compounds of these colors to the metallurgic field, where petrologic classes (numbers) show evolutionary paths. These evolutionary paths are formed from the data of the Fe compounds of the Fe+FeS vs. Fe-oxides field. We can see the main trends of first reduction, then oxidation and the transformation of this sequence to a layered structure of the chondritic parent body (Lukács & al. 1997.)

The second great period of an asteroidal sized body consists of two main events: migration of molten iron to the core and extrusion of mantle partial melts to the surface so forming there the parent rocks of basaltic achondrites. (see for example; Takeda et al. 1997, & Ykeda et al. 1996.) The iron accumulation into the core process is illustrated by a sequence of increasing Fe-Ni metal containing meteorites: mesosiderite (ALHA 77219), pallasite (Yamato 8451), and a large metallic clast containing late petrologic class chondrite sample (L6 of Yamato 790126, from the NIPR volume of Yanai et al. 1987.), and finally an iron (Yamato 791076, from the NIPR volume of Yanai et al. 1987.). The achondrites are represented by eucrites, first crystalline (hand specimen of Yamato 793169, and its thin section from NIPR volume of Yanai et al. 1987., and set thin section of Yamato 791195), and brecciated (Yamato 82009 from the NIPR volume of Yanai et al. 1987, and set thin section of Yamato 74450). The residual achondrites are represented a lodranite (thin section of Yamato 791493 of NIPR volume of Yanai et al. 1987.) and ureilites (thin section of ALHA 78262 of NIPR volume of Yanai et al. 1987, and set thin section of ALHA 77257). Summary of this second great period of evolved asteroidal body is also shown on metallurgic compositional field and asteroidal cross sections. We say good bye to Antarctic meteorites by showing some nice on site photographs of field occurrence about ALHA 77290, ALHA 77255 and Yamato 74077 of the NIPR volume of Yanai et Iguchi, 1981.

#### THERMAL EVOLUTION OF THE LUNAR BODY: THIN SECTIONS OF THE NASA LUNAR SAMPLES

Lunar stratigraphy first determined the two main geologic provinces of terra and mare on the Moon and worked out the detailed stratigraphic column of basic units. The initial target region was the Southern Imbrium Basin region, where the best exposition of the overlapping basic units was found. The basic unit of lunar stratigraphy was the Fra Mauro Formation (and two other Imbrium ejecta related formations). Late Imbrian (earlier Procellarian) layers of mare were overlapped by first Eratosthenian (without ray) crater units, then later the younger (with ray system) Copernican crater units. The initial pre-Imbrian system was later subdivided to Nectarian and pre-Nectarian (Wilhelms, 1987).

The 384 kilograms of lunar samples collected and brought to the Earth by Apollo expeditions revealed the petrologic events of lunar thermal history. Of the three main rock types found (anorthosites, basalts and breccias) two could be corresponded to the two great geologic provinces: anorthosites to terra and basalts to mare. These two main rock types represent two great differentiations periods in the lunar thermal history. The thin sections of the NASA Lunar Sample set are shown in this sequence of the two main differentiations periods (Meyer, 1987).

Two thin sections represent lunar terra. the 60025 anorthosite exhibits all important and nice characteristics of the shocked and brecciated ancient rocks which once had cumulate texture but impacts transformed it. The three main shock phenomena of (1) undulatory extinction, (2) kink banding and (3) twinning are all well represented in textural regions of 60025 anorthosite sample. The largest shock effect of diaplectic glass formation is shown on 78235 norite sample. It represents the other terra rock type, the intrusive ANT suite, and its plagioclase feldspar was mostly transformed to maskelynite. Summary of these first differentiations period shows the magma ocean in which flotation of plagioclase feldspars accumulated anorthositic crust, into which ANT suite rocks later intruded. The great basin forming impacts continue the lunar history.

Basins contain those layers which form the other great lunar geologic province rocks: basalts. They are represented with three very nice thin sections of 12002, 12005 and 70017. Both exhibits somewhat different texture corresponding to the depth of crystallisation in a ca. some 10 m thick lava flows. 12002 shows porphyritic texture with variolitic matrix, 70017 is extremely rich in sector zoned pyroxenes embedded poikilitically to large feldspars, while 12005 has the most slowly crystallized texture. 74220 orange glass sample can also be connected with this second part of lunar volcanism, but they represent pyroclastic soil, the orange soil. The 40-60 mikrometer sized orange spherules are primary liquid compositions from lunar mantle and spread around a lava-fountain in the Taurus-Littrow landing site of Apollo 17.

Finally brecciated rocks represent the final common fate of rocks from any kind of thermal history periods. 14305 breccia contains large anorthositic recrystallized fragment and a poikilitic grain, while 72275 sample has breccia-in-breccia hierarchic texture proving that repeated impacts fragmented and lithified together surface and near-surface rocks during the last 3 Ga.

## SUMMARY

It is a great challenge to have the occasion to use these two remarkable thin section sets of NIPR and NASA. We had this occasion for almost two years at the Eötvös Loránd University, Department of Petrology and Geochemistry, Budapest, Hungary. We focused our work on parallel using of the two sets.

From the video film raw material of the beautiful cosmic materials thin sections we reconstructed a (many aspects hypothetical) story of the main events in the thermal history of a small (chondritic, evolved asteroidal) and a larger (the lunar) rocky celestial body. Thanks to the richness of the two collections such events were well represented and could give a cross section of both types of rocky bodies.

Our film is the beginning in a work, where new films will expose comparisons between other types of processes, which formed the planetary bodies in our neighbourhood and which help to approach the celestial bodies, (and among them to Earth) with a Solar System perspective.

## ACKNOWLEDGEMENTS

Authors and film makers express grateful thanks for the loan of the two nice cosmic material set to their home institutes: the National Institute of Polar Research, Department of Antarctic Meteorites and the NASA Lyndon B. Johnson Space Center, Planetary Materials Laboratory, personally to Drs. Keizo Yanai and Hideyasu Kojima and Dr. James L. Gooding. We also thank the background possibilities given by Ministry of Culture and Education, Hungary, Dr. Imre Kubovics and Dr. László Dinya, undersecretaries of ministry, Dr. Gyula Tófalvi, director of Hung. Space Office, Dr. Miklós Szabó, rector, Dr. Ádám Kiss, dean, Dr. András Galács, v.dean, Dr. György Buda, institute director, Dr. Zúárd Ditrói-Puskás, head of department, Dr. László Megyesi, head of video-center at education technology. This work was helped by MKM 694/96 and OMFB 96-97-47-1265-MŰI-TP-055/96 grants.

## REFERENCES

- Y. Ikeda, M. Ebihara, M. Prinz; Petrology and chemistry of silicate inclusions in the Miles IIE iron. *Antarctic Meteorites XXI*. 54-56. NIPR, Tokyo, Japan.
- B. Lukács, Sz. Bérczi: 1997. Statistical Analysis of the NIPR (Japan) antarctic chondrites: paths of thermal evolution of parent bodies. *LPSC XXVIII*. (Abstract). p.853-854. LPI., Houston
- C. Meyer: 1987. *The Lunar Petrographic Thin Section Set*. NASA JSC Curatorial Branch Publ. No. 76. Houston, Texas, USA.
- H. Takeda, K. Yugami, D. Bogard, M. Miyamoto; 1997. Plagioclase-augite rich gabbro ... *LPSC XXVIII*. 1409-1410. Houston, Texas, USA.
- K. Yanai, M. Iguchi: 1981. *Photographic Catalog of the Selected Antarctic Meteorites*. NIPR, Tokyo.
- K. Yanai, H. Kojima: 1987. *Photographic Catalog of the Antarctic Meteorites*. NIPR, Tokyo.
- K. Yanai, H. Kojima, H. Haramura: 1995. *Catalog of Antarctic Meteorites*. NIPR, Tokyo.
- D. E. Wilhelms; 1987. *The Geologic History of the Moon*. U.S.G.S. Prof. Paper No. 1348. Washington D.C.

# Zn behavior in chromite and daubreelite in some achondrites

Jun Chikami<sup>1)</sup>, Hiroshi Takeda<sup>2)</sup>, Keiko Yugami<sup>1)</sup>, Takashi Mikouchi<sup>1)</sup> and Masamichi Miyamoto<sup>1)</sup>

<sup>1)</sup>Mineralogical Institute, Graduate School of Science, University of Tokyo, Hongo, Tokyo, 113, JAPAN, <sup>2)</sup>Chiba Institute of Technology, 2-17-1, Tsudanuma, Narashino City, Chiba 275, JAPAN

## Introduction

Zn is a volatile, chalcophile element like Cd, Se, Te and so on. We found that spinel grains in primitive achondrites and ureilites contain significant Zn content, while those in HED meteorites do not contain detectable Zn, and that troilite grains coexisting with spinels do not contain detectable Zn in primitive achondrites, ureilites or HED meteorites [1]. El Goresy suggested that the daubreelites coexisting with troilite in Odessa iron meteorites display variable chemical composition with strong fluctuations in their Zn content [2]. Daubreelite is a common component of many troilite nodules. It occurs mainly as exsolution lamellae of varying sizes parallel to (0001) of troilite [2]. The type of intergrowth between troilite and daubreelite suggests exsolution from an FeS-CrS [3] or and FeS-Cr<sub>1-x</sub>S system [4]. Zn contents as high as 8 wt% were recorded in several grains of daubreelite in the Odessa iron meteorite [2], whereas the Zn content in chromites of the Odessa iron meteorite is 1.39 wt% [5]. These studies indicate that Zn is not only present in significant amounts in sphalerites and chromites, but also in daubreelites.

In order to understand Zn behavior between daubreelite and chromite, both of which have spinel structure, we studied primitive achondrites (Y75305 and Y74025) containing both daubreelite and chromite. We also performed mineralogical studies of an H7 chondrite, a eucrite, and a SNC meteorite to understand systematically the geochemical and crystal chemical behavior of Zn content from chondrite to achondrite.

## Sample and experimental techniques

Polished thin sections (PTSs) of Y75008 (H7 chondrite), Y75305, 52-2 and Y74025, 52-4 (winonaites) and A881394 (eucrite) were supplied from National Institute of Polar Research (NIPR). A PTS of Zagami was supplied from the meteorite collection of the Planetary Materials Database of University of Tokyo.

We studied the sample using an optical microscope, a scanning electron microscope and electron probe microanalyzers (JEOL EPMA JCSA-733 at the Ocean Research Institute, University of Tokyo and JEOL EPMA JCSA 733-mkII and JEOL EPMA JCSA-8900L at the Geological Institute, University of Tokyo). 13 elements (Si, Ti, Al, Mn, Fe, Mg, Ca, Na, K, Cr, V, Ni and Zn) were measured in chromites and ilmenites, using an accelerating voltage of 15 kV and a beam current of 12 nA. 9 elements (Co, Fe, Ni, Cr, P, S, Si, Mn and Zn) were measured in troilite and daubreelite, using an accelerating voltage of 25 kV and a beam current of 20 nA. Counting times at peak wavelengths were 10S. Counts were accumulated 6 times for the eucrite and Zagami and 2 times for other meteorites. The background intensity was measured for each element at both sides of the peak wavelength.

## Results

Y75008 is an H7 chondrite [6] which consists mainly of olivine, orthopyroxene and FeNi metal, with minor augite, plagioclase, troilite, chromite and Ca-phosphate [7]. The chromite grains in Y75008 show Al<sub>2</sub>O<sub>3</sub> zoning. Al<sub>2</sub>O<sub>3</sub> increases at first and then decreases from the core to rim [7]. The ZnO content of chromites in Y75008 is 0.3-0.4 wt%. Troilites do not contain detectable ZnO.

Y75305, 52-2 is a winonaite and consists of major orthopyroxene and FeNi metal and minor olivine, augite and troilite [7, 8]. Y75305 contains daubreelite, chromite, apatite and schreibersite as accessory minerals. Focusing especially on Zn, we reanalyzed these minerals using EPMA. Daubreelites contain only small amounts of ZnO

(0.08-0.1 wt%), while chromites contain much higher amounts (1.0-1.5 wt%). Troilites do not contain detectable Zn. These data are consistent with those of Kimura et al., [8].

Y74025 is also a winonaite. Y74025, 52-2 was previously investigated by Kimura et al., [8]. We analyzed PTS, Y74025, 52-4. Y74025, 52-4 consists of major olivine, orthopyroxene, plagioclase and troilite and minor FeNi metal and augite. It contains schreibersite and daubreelite as accessory minerals. The ZnO content of daubreelites is 0.11-0.14 wt% slightly higher than in Y75305, 52-2. Troilites coexisting with daubreelite do not contain detectable ZnO. Chromites were not found in Y74025, 52-4, but Kimura et al. [8] reported 1.28 wt% ZnO in chromites in Y74025, 52-2.

A881394, 92-2 is a cumulate eucrite depleted in volatile elements [9]. It has possibly been metamorphosed [9]. It mainly consists of pyroxene and plagioclase. Its opaque minerals are mostly chromite, but rare troilite is also present. In a previous study, we found no detectable ZnO in chromites or in troilites [1]. In this study, we increased the counting time of the EPMA analysis to achieve a detection limit of 0.015 wt% for zinc. Under these conditions we measured 0.02-0.04 wt% ZnO in chromites.

Zagami is a Martian meteorite. It mainly consists of pyroxene and maskelynite. Intergrown ulvöspinel, ilmenite and pyrrhotite are also contained in the mesostasis as accessory minerals. Ulvöspinel ( $Mt_{37}Usp_{63}$ ) occurs as irregular or subhedral grains [10]. Ulvöspinel grains show chemical zoning. Ilmenite occurs in subordinate amounts as anhedral grains intergrown with ulvöspinel or less commonly as crystallographically oriented lamellae within ulvöspinel grains [10]. The ZnO contents of ulvöspinel are 0.05-0.09 wt% and those of ilmenite are 0.03 wt%. These concentrations are consistent with those obtained by INAA analysis [11]. Pyrrhotite does not contain detectable Zn.

## Discussion

Johson and Prinz reported that among CO3 carbonaceous chondrites, chromites in ALH77307 and Kainsaz (3.0 and 3.1) have ZnO under the detection limit of 0.04 wt%, whereas Ornans (3.3) and Warrenton (3.6) chromites contain 0.1-0.3 wt% ZnO [12]. Similarly, non-reequilibrated chromites in Semarkona (LL3) have Zn under the detection limit, whereas all other chromites in LL and L chondrites of higher petrographic type contain >0.1 wt% ZnO. We found also that the ZnO content of the Y75008 H7 chondrite is 0.3-0.4 wt%, whereas Y75305 and Y74025 winonaite chromites contain even higher ZnO contents (1.0-1.5 wt%). Palme et al., compared the bulk Zn content of H7 chondrites with primitive achondrites [13], and found that primitive achondrites contain higher Zn contents than H7 chondrites. The high Zn contents in chromites of primitive achondrites may result from chromites having crystallized under reducing conditions from a sulfide melt containing chalcophile Cr, Mn and Zn.

Stolper and McSween [10] compared the average concentrations of some trace and minor elements in shergottites with those in terrestrial, eucritic and lunar basalts. The Zn abundance in shergottites is almost 80% of that in terrestrial basalts, while the Zn abundance in eucrite and lunar basalts is only 1-3% of that in terrestrial basalts. The difference in the ZnO content of chromite (0.02-0.04 wt%) in eucrites and ulvöspinel (0.05-0.09 wt%) in Zagami can be explained by the difference in bulk Zn contents between eucrites and shergottites. The high concentration of Zn in the SNC meteorites may be attributed to secondary volatile enrichment during the Martian volcanism.

Y74160 is a LL7 chondrite with a bulk Zn concentration at CI levels, whereas other volatile, chalcophile elements are depleted [14]. Chromite in Y74160 contains 0.6 wt% ZnO. Calculation of bulk Zn content from the modal abundance and the ZnO concentration of chromite shows that the chromites are the reservoir of almost all the Zn in this meteorite. LEW88774 is an unusual ureilite containing spinels. These spinels also contain ZnO up to 0.6 wt%, as abundant as in LL7 chondrites. The spinels in this ureilite are also the reservoir of almost all the Zn in

LEW88774 [15]. Moreover, a similar situation is observed for the Acapulco primitive achondrite. Comparison of the bulk Zn concentration of Acapulco with that calculated from the modal abundance and ZnO concentration of chromites confirms that almost half of the bulk Zn content is contained in chromite despite the fact its modal abundance is only 1.3 %. We calculated roughly how much of the bulk in the Y74025 winonaite Zn is contained in chromite. Almost 70 % of the Zn is contained in chromite and about 15 % in daubreelite, although modal abundances of both chromite and daubreelite are very low. This fact suggests that Zn may be preferentially retained in chromite rather than in daubreelite. On the other hands, Odessa iron meteorite contains much more Zn in daubreelite than in chromite, although both minerals have the spinel structure. If we adopt an idea that chalcophile Zn prefers the spinel structure, Zn should be preferentially concentrated in thiospinel (daubreelite), contrary to our observations in primitive achondrites. One possible explanation of these unexpected behavior could be that daubreelite in primitive achondrites may have formed later during sulfidization, after chromite took considerable Zn out of the primary melt. However further study is required by taking into account the bulk Zn content of Odessa and crystallographic aspects of Zn concentration in the tetrahedral site of spinel structure. 30 % of all Zn in Zagami is contained in ulvöspinel and ilmenite, although modal abundances of ulvöspinel are only 2 vol.% and those of ilmenite only 0.5 vol.%.

### Conclusions

- (1) Chromite appear to be the major reservoir of Zn in primitive achondrites and ureilites.
- (2) In less differentiated meteorites (primitive achondrites and ureilite) the Zn content of chromites is much higher than in eucrites and Zagami.
- (3) The Zn content of ulvöspinel and ilmenite in Zagami is a little higher than that of chromite in eucrites. This can be attributed to the difference in the bulk Zn concentration between SNC meteorites and eucrites.
- (4) The Zn concentration in meteorites can be explained by the bulk Zn concentration and the structure type of Zn-containing minerals.
- (5) In primitive achondrites Zn is concentrated in chromite, while in the Odessa iron meteorite, it is concentrated much more in daubreelites rather than in chromites. This may be caused by a different order of crystallization between primitive achondrites and Odessa.

### Acknowledgment

We are indebted to NIPR and the Planetary Materials Database of University of Tokyo for samples. We thank Mr. O. Tachikawa at the Mineralogical Institute, and Mr. H. Yoshida at the Geological Institute, University of Tokyo for their technical assistance. We thank Drs. A. El Goresy and G. McKay for helpful discussion. This work was supported by JSPS Research Fellowship for Young Scientists (J. C.)

### References

- [1] Chikami J. et al., (1997) LPSC, 225-226. [2] El Goresy A. (1967) GCA, 31, 1667-1676. [3] Vogel R. and Heumann T. (1950) N. Jahrb. Min. Monatsh. 175-190. [4] Ramdohr P. (1964) Carnegie Inst. Washington Y. B. 63, 217-218. [5] Bunch T.E. et al., (1970) Contr. Mineral. and Petrol., 25, 297-340. [6] Yanai K. and Kojima H. (1995) Catalog of the Antarctic Meteorites, NIPR, Tokyo [7] Yugami K. (1997) PhD thesis, Min. Inst., Univ. of Tokyo, 113pp. [8] Kimura M. et al., (1992) Proc. NIPR Symp. Antarct. Meteorites 5, 165-190. [9] Takeda H. et al., (1996) Proc. NIPR Symp. Antarct. Meteorites 9, 170-172. [10] Stolper E. and McSween H.Y. (1979) GCA, 43, 1475-1498. [11] Laul J.C., et al., (1986) GCA, 50, 909-926. [12] Johnson C. A. and Prinz M, (1990) GCA, 55, 893-904. [13] Palme H. et al., (1981) GCA, 45, 727-752. [14] Takeda H. et al., (1984) EPSL, 71, 329-339. [15] Chikami J. et al., (1997) Meteoritics and Planetary Science, in press

## "Autochthonous" Spherule Occurrences in the Carpathian Basin

Csaba H. DETRE<sup>1</sup>; György DON<sup>1</sup>; Lajos DOSZTÁLY<sup>1</sup>; Orsolya KÁKAY-SZABÓ<sup>1</sup>; Péter SOLT<sup>1</sup>; Szaniszló BERCZI<sup>2</sup>; Kálmán TÖRÖK<sup>2</sup>; Béla LUKÁCS<sup>3</sup>; Imre TÓTH<sup>4</sup>; Imre UZONYI<sup>5</sup>

<sup>1</sup> Geological Institute of Hungary, H-1143 Budapest, Stefániaút 14, Hungary

<sup>2</sup> Department of Petrology, University Loránd Eötvös, H-1088 Budapest, Rákóczi út 5.

<sup>3</sup> Central Institute for Physics, Hung., Acad., Sci., H-1121 Budapest, Konkoly-Thege út 29-33.

<sup>4</sup> Konkoly Astrophysical Observatory, H-1121 Budapest, Budapest, Konkoly-Thege út 13-15.

<sup>5</sup> Institute of Nuclear Research, Hung., Acad., Sci., H-4001 Debrecen, Bem tér 18/c.

The Carpathian Basin is the most rich extraterrestrial occurrence territory of the world. Except of few geochronological interval, here all of the geological formations include the various types of extraterrestrial spherules.

The autochthonous position of the spherules within the rocks, is one of the greatest problem in the spherule research. Therefore, in this presentation "spherule layers" are considered as geometrically limited spherule occurrences in sure syngenetic and autochthonous situations with the bedrocks.

Autochthonous situations are considered in the case of spherules embedded in hard sediments, e.g. firestones, compact carbonatic rocks, in extremely case in granite (see Jakabska, K. 1989)

Spherule layers in chronological range :

-- Precambrian granite : Magnetic, probably meteoroid spherules from the granites of the Gemerids, from South Slovakia

-- Upper Devonian : compact and cherty limestone of the Szendrő Mts. in North-East Hungary. Glassy spherules of impact origin, probably connected to the Frasnian-Famennian (F/F) impact event. The exact stratigraphical situation of the layers is under investigation.

-- Permian-Triassic Boundary : Bükk Mts., North Hungary. Very small (diameter : 1-10 microns) magnetic spherules in compact and cherty limestones, dolomitic limestones. The thickness of the layers cca. 10-30 cm. This type of spherules can be considered as interstellar ones (see Miono, S. 1995; Detre, Cs. et al. 1997).

-- Middle Triassic : From the Anisian compact limestones of the Balaton Highland, Aszófő, very rich glassy spherule occurrences (of impact origin) are known, parallelized with Ammonoite fauna : Middle Anisian, Balatonites balatonicus Zone.

-- Upper Triassic : In the compact and/or cherty limestones of the Bakony and Buda Mts., Middle Hungary, very rich glassy, impact spherules were found. Their most important character is the extremely high, 2-4% Barium content. The data were yielded from EDAX and PIXE analyses. The distribution of the spherules in the strata is chaotic.

-- Upper Cretaceous : Barium rich glassy impact spherules also are known in the various Upper Cretaceous spherule layers of the Bakony Mts., whose thickness are no more than 10 cm. These occurrences considered as arguments of the Upper Cretaceous "impact-drum-fire" (see Detre, Cs. et al. 1997).

-- Cenozoic : A number of spherule occurrences in the Carpathian Basin should be excluded from the "spherule layers, because they are found in loose sediments.

-- Holocene : The field-reworking of the Kaba meteorite fall area has provided very rich magnetic, meteoroid spherule occurrences (see Solt, P. 1996).

References :

- Detre, Cs.H. et al. 1997 : The comparison of P/Tr and K/T boundaries on the basis of cosmic spherules found in Hungary; 28th LPSC Abstracts, pp.297-298.
- Jakabska, K. 1989 : Spherical accessories ("spherules") in the Gemic Granites, Geol. Zbor. Geol. Carp., 40,3, pp.305-322.
- Miono, S. 1996 : Astronomical Significance of Microspherules Recovered from Paleozoic and Mezozoic Chert in Japan, in : Detre, Cs. et al. (eds) "Spherules and Global Events", KFKI Report, 1996-05/C, pp.23-34., Budapest.
- Solt, P. 1996 : Exploration of Spherules in the Kaba Meteorite Fall Area, 21th NIPR Symp., Abstr., p.158.

Supported by the Hungarian-Japanese ST Co-operation " Impact and Extraterrestrial Spherules"

Hungarian Space Office

Hungarian National Scientific Fundation (OTKA) Grant T 014958

## Extraterrestrial Spherule Layers in the Carpathian Basin

Csaba H. DETRE<sup>1</sup>; György DON<sup>1</sup>; Lajos DOSZTÁLY<sup>1</sup>; Orsolya KÁKAY-SZABÓ<sup>1</sup>; Péter SOLT<sup>1</sup>; Szaniszló BÉRCZI<sup>2</sup>; Kálmán TÖRÖK<sup>2</sup>; Béla LUKÁCS<sup>3</sup>; Imre TÓTH<sup>4</sup>; Imre UZONYI<sup>5</sup>

<sup>1</sup> Geological Institute of Hungary, H-1143 Budapest, Stefániaút 14, Hungary

<sup>2</sup> Department of Petrology, University Loránd Eötvös, H-1088 Budapest, Rákóczi út 5.

<sup>3</sup> Central Institute for Physics, Hung., Acad., Sci., H-1121 Budapest, Konkoly-Thege út 29-33.

<sup>4</sup> Konkoly Astrophysical Observatory, H-1121 Budapest, Budapest, Konkoly-Thege út 13-15.

<sup>5</sup> Institute of Nuclear Research, Hung., Acad., Sci., H-4001 Debrecen, Bem tér 18/c.

The Carpathian Basin is the most rich extraterrestrial occurrence territory of the world. Except of few geochronological interval, here all of the geological formations include the various types of extraterrestrial spherules.

The autochthonic position of the spherules within the rocks, is one of the greatest problem in the spherule research. Therefore, in this presentation "spherule layers" are considered as geometrically limited spherule occurrences in sure syngenetic and autochthonic situations with the bedrocks.

Autochthonic situations are considered in the case of spherules embedded in hard sediments, e.g. firestones, compact carbonatic rocks, in extremely case in granite (see Jakabska, K. 1989)

Spherule layers in chronological range :

-- Precambrian granite : Magnetic, probably meteoroid spherules from the granites of the Gemerids, from South Slovakia

-- Upper Devonian : compact and cherty limestone of the Szendrő Mts. in North-East Hungary. Glassy spherules of impact origin, probably connected to the Frasnian-Famennian (F/F) impact event. The exact stratigraphical situation of the layers is under investigation.

-- Permian-Triassic Boundary : Bükk Mts., North Hungary. Very small (diameter : 1-10 microns) magnetic spherules in compact and cherty limestones, dolomitic limestones. The thickness of the layers cca. 10-30 cm. This type of spherules can be considered as interstellar ones (see Miono, S. 1995; Detre, Cs. et al. 1997).

-- Middle Triassic : From the Anisian compact limestones of the Balaton Highland, Aszófő, very rich glassy spherule occurrences (of impact origin) are known, parallelized with Ammonoite fauna : Middle Anisian, Balatonites balatonicus Zone.

-- Upper Triassic : In the compact and/or cherty limestones of the Bakony and Buda Mts., Middle Hungary, very rich glassy, impact spherules were found. Their most important character is the extremely high, 2-4% Barium content. The distribution of the spherules in the strata is chaotic.

-- Upper Cretaceous : Barium rich glassy impact spherules also are known in the various Upper Cretaceous spherule layers of the Bakony Mts., whose thickness are no more than 10 cm. These occurrences considered as arguments of the Upper Cretaceous "impact-drum-fire" (see Detre, Cs. et al. 1997).

-- Cenozoic : A number of spherule occurrences in the Carpathian Basin should be excluded from the "spherule layers, because they are found in loose sediments.

-- Holocene : The field-reworking of the Kaba meteorite fall area has provided very rich magnetic, meteoroid spherule occurrences (see Solt, P. 1996).

References :

- Detre, Cs.H. et al. 1997 : The comparison of P/Tr and K/T boundaries on the basis of cosmic spherules found in Hungary; 28th LPSC Abstracts, pp.297-298.
- Jakabska, K. 1989 : Spherical accessories ("spherules") in the Gemic Granites, Geol. Zbor. Geol. Carp., 40,3, pp.305-322.
- Miono, S. 1996 : Astronomical Significance of Microspherules Recovered from Paleozoic and Mesozoic Chert in Japan, in : Detre, Cs. et al. (eds) "Spherules and Global Events", KFKI Report, 1996-05/C, pp.23-34., Budapest.
- Solt, P. 1996 : Exploration of Spherules in the Kaba Meteorite Fall Area, 21th NIPR Symp., Abstr., p.158.

Supported by the Hungarian-Japanese ST Co-operation " Impact and Extraterrestrial Spherules"

Hungarian Space Office

Hungarian National Scientific Fundation (OTKA) Grant T 014958

## CHEMICAL COMPOSITION OF Y-793605, A MARTIAN LHERZOLITE

Mitsuru Ebihara, P. Kong and K. Shinotsuka Department of Chemistry, Graduate School of Science, Tokyo Metropolitan University, Hachioji, Tokyo 192-03, Japan

**Introduction** Yamato-793605 was once classified as a diogenite and was later reclassified as a shergottite [1]. This meteorite is not a typical shergottite, but is grouped with lherzolitic shergottites, being similar to ALH 77005 and LEW 88516 [2]. As Y-793605 is small (17 g), in contrast to ALH 77005 (482.5 g), a consortium study was organized under the direction of Paul Warren and Hideyasu Kojima. A piece (weighing 209 mg) of the specimen was allocated to our proposed study. In this study, we analyze the sample using instrumental neutron activation analysis (INAA) for major and trace elements, radiochemical neutron activation analysis (RNAA) for siderophile trace elements and inductively coupled plasma mass spectrometry (ICP-MS) for rare earth elements, Th and U so that the meteorite can be characterized based on the chemical composition. For comparison, ALH 77005 was also analyzed by INAA and RNAA.

### Analytical procedures

The Y-793605 sample allocated for this consortium study is an aggregate of lithic fragment with black glasses [3]. The sample in chips was easily crushed in an agate mortar. The roughly ground sample was then divided into two portions, 123 mg and 86 mg. A larger portion was used for NAA and a smaller portion was used for ICP-MS. Another lherzolitic shergottite, ALH 77005, was allocated by the Meteorite Working Group. Several chips weighing about 500 mg of the sample was carefully crushed and ground in an agate mortar. An aliquant of this powdered specimen (119 mg) was used for NAA at first and then reused for RNAA. In RNAA, a total of 9 elements (Mo, Ru, Ag, W, Re, Os, Ir, Pt, Au) were aimed to determine. Precise determination of rare earth elements (including Y), Th and U was performed by ICP-MS [4].

### Results and discussion

Figure 1 shows the relative abundances of 17 elements including most major elements for Y-793605 and ALH 77005. Literature values for ALH 77005 are also plotted for comparison. As clearly observed, Na and K are largely depleted in our Y-793605 sample compared with those in ALH 77005. In contrast to Na and K, Al, another plagiophile element, is not equally low in our sample. Alkaline elements are known to be susceptible to redistribution due to weathering on Antarctica, but its effect must not be significant. Titanium is also slightly depleted in Y-793605 compared with that in ALH 77005. Except these several elements, both Y-793605 and ALH 77005 have essentially identical abundances of the elements plotted in Fig. 1.

It may be worth pointing that Na, K and Ga (another plagiophile element; [5]) have essentially the same CI-normalized abundances in ALH 77005. Aluminum has a slightly higher abundance. As all these plagiophile elements must have behaved similarly during igneous differentiation, a slightly high abundance of Al reflects its refractory nature. The difference in volatility among remaining three plagiophiles caused no significant change. Zinc has an order of magnitude higher abundance than Se, which is contradictory to the order of volatility. Apparently, Se is depleted because of the effective uptake into the core due to its chalcophile nature. As shown in Fig. 1, Co and Ni are largely fractionated in both Y-793605 and ALH 77005. Cobalt and Ni are hardly fractionated from each other in the process of condensation. The thermal process in the ordinary chondrites also scarcely fractionates them [6]. Melting experiment of the metal-silicate system, however, showed that Co can be fractionated from Ni, with Ni more preferably entering the metal phase; the degree of fractionation of Co and Ni is highly dependent on the oxygen fugacity involved in the melting [7, 8]. CI-normalized abundance of Ni is slightly but consistently higher than those of typical refractory siderophiles such as Os and Ir. Presumably, Ni is partitioned into silicate greater than

refractory siderophiles, possibly caused by a slightly elevated oxygen fugacity.

In Figure 2, REE (including Y), Th and U abundances in Y-793605 are compared with those in ALH 77005. All data for ALH 77005 are from literatures and were obtained by RNAA. Our ICP-MS values for Y-773605 are systematically lower than the literature data for ALH 77005. The abundance patterns are very similar for both meteorites at a glance, but a faint, but systematic difference can be observed; light REE are more depleted in Y-793605 compared with those in ALH 77005, with the relative difference between two meteorites decreasing with increasing the atomic number of REE. Bulk samples of Y-793605 and ALH 77005 have no Eu anomaly in the CI-normalized REE abundance patterns. Yet, the ion probe study on ALH 77005 revealed that whitlockite has a negative Eu anomaly whereas maskelynite has a positive Eu anomaly [9]. This suggests that whitlockite and plagioclase were crystallized after the parental material for both meteorites was isolated from the parent magma and further suggests that the plagioclase separation didn't occur to the parent magma on a large scale, from which the source material (melt) for the ALH 77005 (and also Y-773605) cumulates was produced. REE and other incompatible lithophiles were largely present in the melt phase and were mechanically trapped with rather than incorporated into the cumulate phase and were distributed into constituent, non-cumulate minerals according to their partition coefficients in the later stage of crystallization of meteorites.

The most characteristic feature of the REE abundance patterns of Y-793605 (and of ALH 77005) is the presence of a hump in the middle to heavy REE span (around Dy for Y-773605); in the lighter REE span, the abundance increases, whereas the abundance decrease in the heavier REE span. Similar patterns can also be observed for other shergottites such as Zagami, EET 79001, Shergotty and QUE 94201 but the REE abundances for Y-793605 (and ALH 77005) are slightly different from those of the remaining shergottites in that the REE abundances in Y-793605 is lower and has less steep inclination in the light REE region. It may be noted that the REE abundance for LEW 88516 [10, 11] resembles those for Y-793605 and ALH 77005. Apparently, such a difference must be related to the difference in genesis of lherzolitic shergottites and the remaining (normal) shergottites.

Siderophile abundances normalized to CI values for Y-793605 and ALH 77005 are shown in Fig. 3. In general, siderophile abundances for ALH 77005 are systematically higher than those for Y-793605, but relative abundances are strongly similar for Y-793605 and ALH 77005. As its too low abundance, Re couldn't be reliably determined for Y-793605. Warren and Kallemeyn [12] discussed the Re abundances in some SNC meteorites and eucrites and came to conclude that the oxygen fugacity of the SNC parent magma has changed to be increased after the late accreting materials were mixed with the source region of SNC meteorites. Indeed, Mo and, in particular, W have relatively high abundances in Y-703605 and ALH 77005, just like as Ga, suggesting these elements are mostly present as oxide rather than metallic form in the formation of the (young) SNC parent magma.

Like other shergottites, Y-793605 as well as ALH 77005 have Ni/Co ratios lower than the CI value. According to the laboratory partitioning experiment, Ni is partitioned more greatly into solid metal and sulfide liquid than Co [7, 13]. This implies that the mantle becomes depleted in Ni compared with Co if equilibrium partitioning of Ni and Co occurred between metal-sulfide melt (which corresponds to the core of the shergottite parent body, presumably Mars) and the silicate (corresponding to mantle, from which shergottites must have derived). Nickel is grouped with compatible elements while Co is with indifferent elements in the mantle genesis of the shergottite parent body [14]. Nevertheless, Ni is more depleted than Co in the shergottite parent body mantle, suggesting that Ni was partitioned into the core much greater larger than Co. Considering that the Co and Ni abundances in lherzolitic shergottites are higher than refractory siderophiles, partition of Co and Ni into the metal-sulfide core is hindered by increasing the stability of oxide species (NiO and CoO), especially at the late stage of accretion,

when the segregation of core must have simultaneously occurred.

Tungsten and Mo are generally modeled as siderophile elements in cosmochemistry, i. e., in consideration of condensation behavior from the nebula of solar composition. Geochemically, Mo and W behave as incompatible elements, with Mo being more siderophile and chalcophile than W [15, 16]. Therefore, the partition coefficient of W into metal is decreased greatly with increasing oxygen fugacity. On the other hand, Mo is more easily sulfurized than W and a significant portion of the Mo exist as sulfide in ordinary chondrites, especially equilibrated ordinary chondrites [17]. Our observation of Mo and W in Y-793605 and ALH 77005 suggests that the segregation of W into the core is insufficient whereas Mo is significantly trapped into the metal-sulfide core.

**References** [1] Yanai K. (1995) *Lunar Planet Sci.* **XXVI**, 1533-1534. [2] Mikouchi T. and Miyamoto M. (1966) *Meteor. Planet. Sci.* **31**, A89-A90. [3] Kojima H., Miyamoto M., Yanai K. and Warren P. H. (1997) *Proc. NIPR Sympos. Antarctic Met.*, **10**, submitted. [4] Shinotsuka K. and Ebihara M. (1997) *Anal. Chim. Acta* **338**, 237-246. [5] Warren P. H. and Kallemeyn G. W. (1997) *Proc. NIPR Sympos. Antarctic Met.*, **10**, submitted. [6] Kong P. and Ebihara M. (1997) *Geochim. Cosmochim. Acta*, in press. [7] Schmitt W., Palme H. and Wänke H. (1989) *Geochim. Cosmochim. Acta* **53**, 173-185. [8] Holtheid A. and Palme H. (1996) *Geochim. Cosmochim. Acta* **60**, 1181-1193. [9] Harvey R. P., Wadhwa M, McSween H. Y., Jr. and Crozaz G. (1993) *Geochim. Cosmochim. Acta* **57**, 4769-4783. [10] Dreibus G., Jochum K. H., Palme H., Spettel B., Wlotzka F. and Wänke H. (1992) *Meteoritics* **27**, 216-217. [11] Treiman A. H., McKay G. A., Bogard D. D., Mittlefehldt D. W., Wang M.-S., Keller L., Lipschutz M. E., Lindstrom M. M. and Garrison D. (1994) *Meteoritics* **29**, 581-592. [12] Warren P. H. and Kallemeyn G. W. (1996) *Meteor. Planet. Sci.* **31**, 97-105. [13] Jones J. H. and Drake M. J. (1986) *Nature* **322**, 221-228. [14] Treiman A. H., Drake M. J., Janssens M.-J., Wolf R. and Ebihara M. (1986) *Geochim. Cosmochim. Acta* **50**, 1071-1091. [15] Newsom H. E. and Palme H. (1984) *Earth Planet. Sci. Lett.* **69**, 354-364. [16] Lodders K. and Palme H. (1991) *Earth Planet. Sci. Lett.* **103**, 311-324. [17] Kong P. and Ebihara M. (1996b) *Earth Planet. Sci. Lett.* **137**, 83-93.

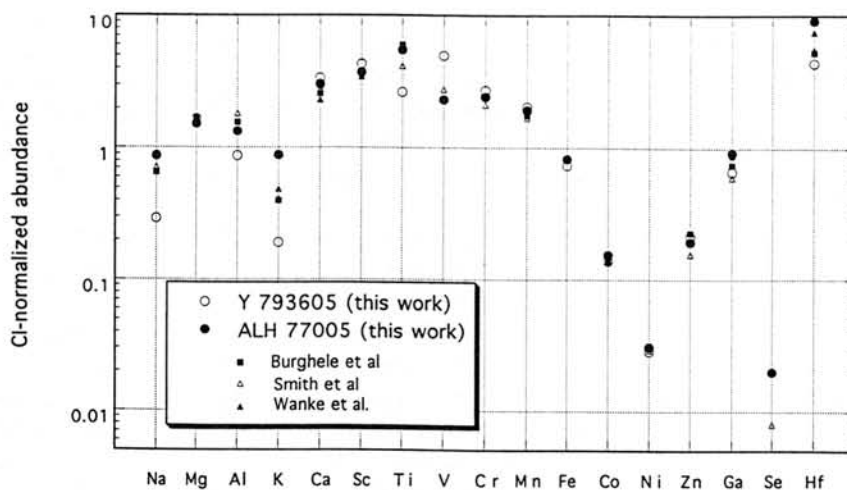


**Fig. 1** CI-normalized abundances of 17 elements including most major elements for Y-793605 and ALH 77005. Literature values for ALH 77005 are also plotted for comparison. Generally, Y-793605 and ALH 77005 have essentially identical chemical composition, suggesting a genetic link between them.

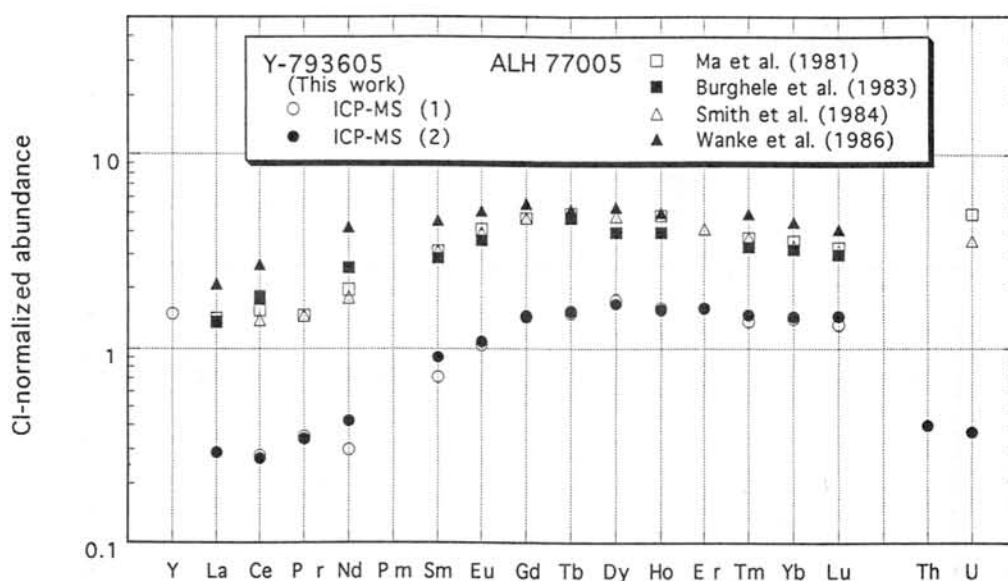


**Fig. 2** CI-normalized abundances of REE, Th and U for Y-793605 determined by ICP-MS. Literature values of REE abundances for ALH 77005 are also shown for comparison. Our ICP-MS values for Y-793605 are systematically lower than those for ALH 77005, but the abundance patterns are very similar, being characterized by a gradual increase at light REE span and a decrease at heavy REE span.

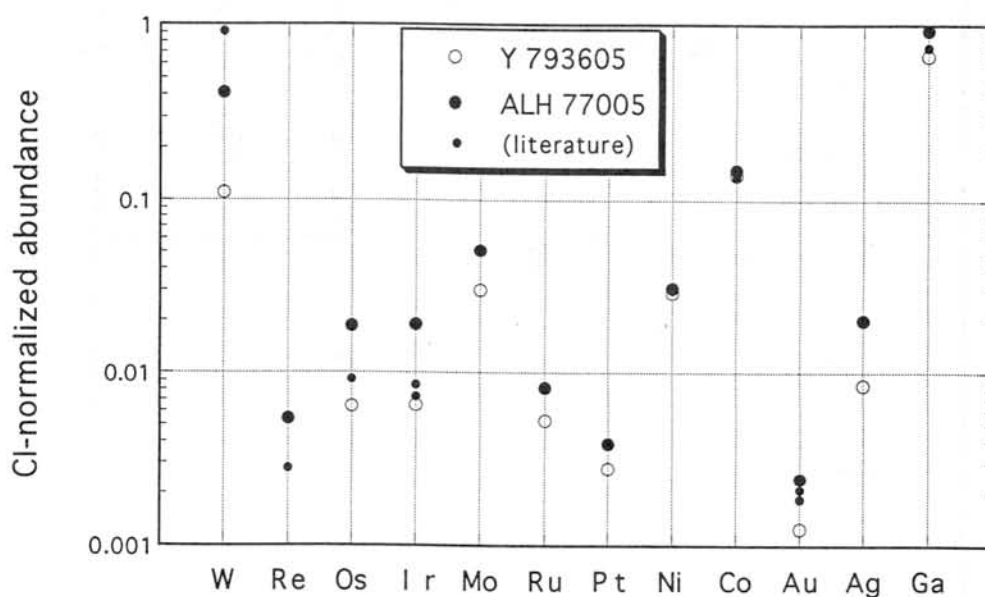
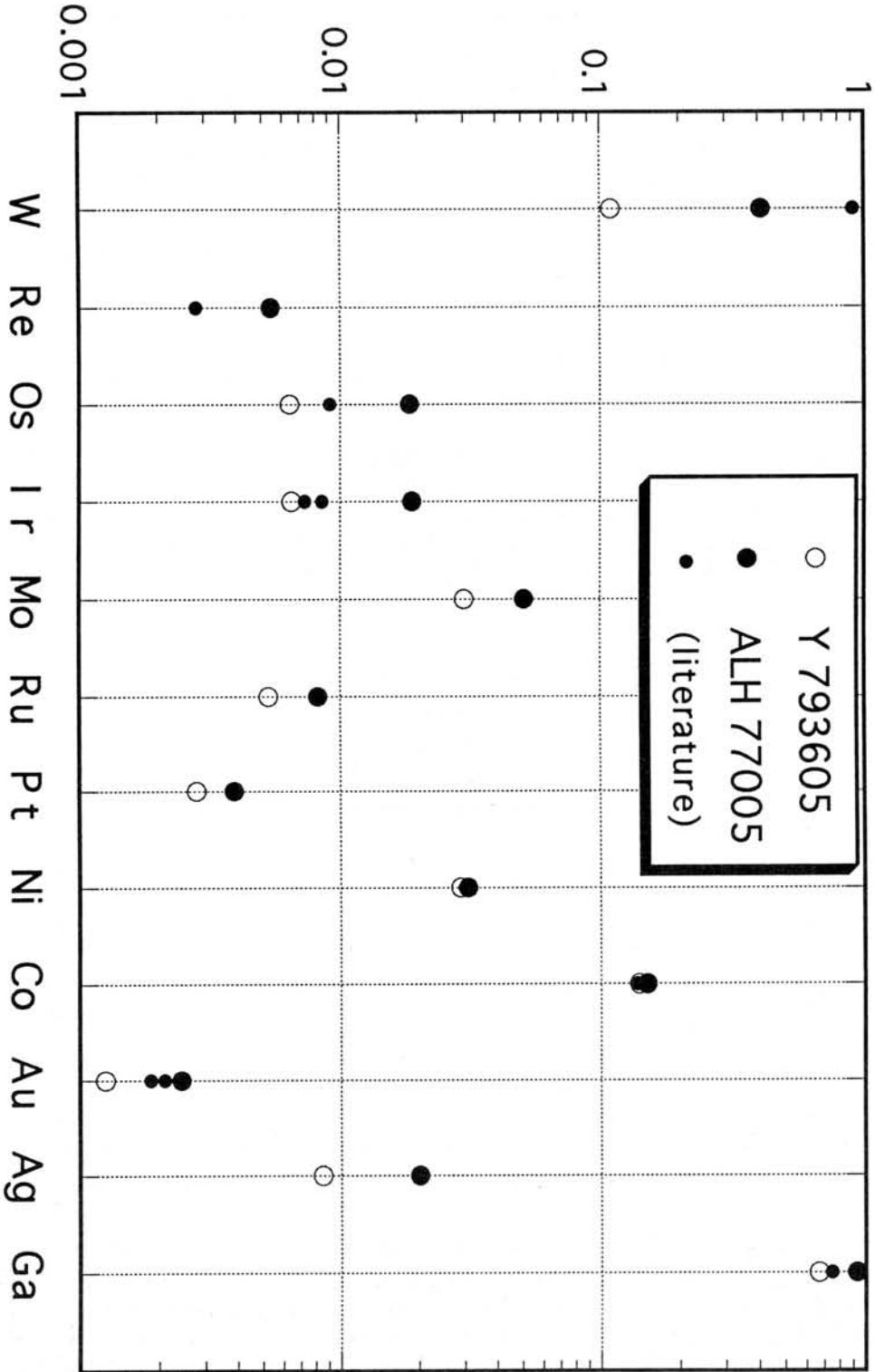


**Fig. 3** CI-normalized abundances of siderophile elements. Siderophile abundances are considerably variable compared with CI abundances; only Os/Ir ratios are exactly chondritic. Nickel is more depleted than Co, possibly due to a preferential uptake of Ni into the core. Gallium and W are highly abundant compared with other siderophile elements, suggesting that these elements hardly behaved as siderophiles when the parental material for Y-793605 and ALH 77005 formed. Again, Y-793605 bears a close resemblance to ALH 77005 in siderophile abundances.

# Cl-normalized abundance



# SHOCK-INDUCED HIGH-PRESSURE PHASE TRANSFORMATIONS IN CHONDRITIC AND DIFFERENTIATED METEORITES: SOLID-STATE TRANSFORMATIONS, HIGH-PRESSURE LIQUIDUS PHASES, AND ALKALI VAPOUR FRACTIONATION.

A. El Goresy<sup>1</sup>, M. Chen<sup>2</sup>, T G. Sharp<sup>3</sup>, B. Wopenka<sup>4</sup>, and S. Weinbruch<sup>5</sup>

- 1) Max-Planck-Institut für Kernphysik, Postfach 103980, D-69029 Heidelberg, Germany; E-Mail: GORESY@SELKET.MPI-HD.MPG.DE,
- 2) Institute of Geochemistry, Academia Sinica, Guangzhou, China
- 3) Department of Geology, Arizona State University, Tempe Arizona 85287-1404, USA
- 4) Department of Earth and Planetary Sciences, Washington University, St. Louis, MO 63130, USA
- 5) Fachbereich Materialwissenschaft; Technische Hochschule Darmstadt, Petersenstr. 23, 64295 Darmstadt Germany;

## Introduction:

Heavily shocked chondritic meteorites display a variety of deformation features including intergranular fractures, mosaicism, planar deformation features (PDFs), and sharply defined shock melt veins [1]. The melt veins contain two distinct high-pressure assemblages: a) a coarse-grained polycrystalline assemblage and b) complex fine-grained assemblages [2-4]. The adjacent matrix is usually sharply separated from the veins, heavily fractured, and contains plagioclase glass that was believed to have been formed by solid-state transformation to maskelynite, retaining its stoichiometric plagioclase composition [5-10]. Shock-induced features in SNC meteorites are, in contrast, distinct from those in chondritic meteorites. No melt veins with high-pressure minerals were found [11]. Instead, very small melt pockets consisting of dendritic olivine and pyroxene in a quenched silicate glass matrix were reported [11]. The original intercumulous plagioclase is believed to have undergone shock-induced solid-state transformation to the amorphous mineral glass maskelynite keeping the original textures and stoichiometry [11, 23-25]. The dynamically induced features in chondritic and SNC meteorites seem to follow a systematic progressive shock pattern which may allow the construction of shock classification schemes for chondritic and SNC meteorites [10]. These schemes were constructed through comparison with features produced in high-velocity dynamic experiments. However, it is important to stress the fact that shock experiments up to 133 GPa have failed so far to produce any high-pressure species found in veins in chondritic meteorites [12]. We hence argue that a comparison of experimentally shock-induced deformations in millimetre-sized objects and deformational features produced on kilometre-sized asteroids or even the much larger planets may pose considerable scaling problems. An understanding of the P-T conditions prevailed, and a qualitative estimate of the duration of the high-pressure pulse during the shock events on chondritic and SNC parent bodies requires a careful characterisation of all phases present and delineation of the textural relationships. We present results of investigations on the heavily shocked L6 chondrites M'bale, Peace River, Sixiangkou, and Tenham and the SNC meteorite Shergotty that contains the classical occurrence of maskelynite.

### Chondritic meteorites:

Detailed investigations using SEM, EMPA, Laser Raman microprobe (LRM) and HRTEM and analytical HRTEM were conducted. The mineralogical composition of the high-pressure coarse-grained assemblage vary among the studied meteorites. It reflects not only differences in the peak pressures and temperatures but also the cooling histories after decompression. In Sixiangkou and Tenham the assemblage consists of a polycrystalline aggregate of ringwoodite (up to 6  $\mu\text{m}$  in size) and low-Ca majorite (up to 10  $\mu\text{m}$  in size) identical in composition to those of olivine and orthopyroxene, respectively, in the less deformed matrices of these meteorites. In Peace River LRM indicates that the assemblage contains wadsleyite and minor ringwoodite intergrowth along with orthopyroxene. In contrast, TEM studies on M'bale indicates a complex assemblage of residual ringwoodite that is pervasively replaced by olivine.

The composition of the fine-grained assemblage also vary among the four meteorites [13]. In Sixiangkou it consists of idiomorphic majorite-pyrop<sub>SS</sub> (Mj<sub>73.8</sub>Na-Mj<sub>4.7</sub>Ca-Mj<sub>4.2</sub>Py<sub>15.8</sub>Uv<sub>1.5</sub>) + magnesiowüstite (Wü<sub>54</sub>-Per<sub>46</sub>). These findings lead to the conclusion that the shock event formed a silicate melt of Sixiangkou bulk composition and that both majorite-pyrop<sub>SS</sub> and magnesiowüstite crystallised from this melt under high pressures and temperatures. High-pressure static experiments [14] put constraints to temperature and pressure during the crystallization of the majorite-pyrop<sub>SS</sub> + magnesiowüstite in Sixiangkou to be from 2050 to 2300 °C and 20 to 24 GPa, respectively. The peak pressures previously estimated for melt veins appear to be grossly overestimated by ~ 60 GPa [1, 15]. In Tenham we find the assemblage majorite-pyrop<sub>SS</sub> (Mj<sub>75.2</sub> Na-Mj<sub>4.1</sub> Ca-Mj<sub>3</sub> Py<sub>16.2</sub> Uv<sub>1.5</sub>) + magnetite. [16]. The presence of magnetite as the second most abundant phase after garnet is surprising because it is not a mineral known from high pressure experiments. The disordered and poorly crystalline condition of magnetite suggests that either magnetite formed as an alteration product of a higher pressure phase such as magnesiowüstite or wüstite, or the magnetite itself was the high pressure phase that has been partially altered [16]. If wüstite were the primary high-pressure phase, it could have disproportionated at low pressures to metallic Fe plus magnetite, which are both present. The P-T conditions of crystallization cannot be interpreted from the magnetite + majorite<sub>SS</sub> assemblage [16]. In contrast, both Peace River and M'bale contain a Fe-rich phase with olivine stoichiometry (Fa<sub>38</sub>-Fa<sub>43</sub>) + majorite-pyrop<sub>SS</sub> (Mj<sub>90.4</sub>Na-Mj<sub>1.8</sub>CaMj<sub>1.8</sub>Py<sub>5.2</sub>Uv<sub>0.7</sub> to Mj<sub>63.7</sub>Na-Mj<sub>5.4</sub>Ca-Mj<sub>3.4</sub>Py<sub>12.9</sub>Uv<sub>1.2</sub>) in Peace River and (Mj<sub>73.9</sub>Na-Mj<sub>3.5</sub>Ca-Mj<sub>-3.4</sub>Mj<sub>5.4</sub>Ca-Mj<sub>16.8</sub>Py<sub>17.7</sub>Uv<sub>1.5</sub>) in M'bale [13]. Although the bulk compositions of these chondrites are very similar, the compositions of their garnets vary considerably. Mori [17] reported MgSiO<sub>3</sub>-rich glass (pseudomorph after MgSiO<sub>3</sub> perovskite) plus magnesiowüstite from an unknown chondrite. In addition, recently Sharp et al. [18] reported the assemblage MgSiO<sub>3</sub>-ilmenite and amorphized (Mg,Fe)SiO<sub>3</sub>-perovskite polymorphs of orthopyroxene and ringwoodite as liquidus phases in veins in the Acfer 040 L6 chondrite. This assemblage is not predicted by the liquidus phase diagram [14] for the Allende carbonaceous chondrite.

The sharp transition of veins, where localized melting took place, to a matrix, where presumably only solid-state transformations occurred, is not yet understood [1, 9]. Materials in the neighbouring matrices previously described as "maskelynite" are usually smooth with little or no intergranular fractures, while plagioclase grains with PDFs are fractured [19]. The smooth grains are always surrounded by numerous radiating cracks that have extensively shattered the neighboring silicates, chromite, and troilite [19]. The radiating cracks are indicative of volume increase due to expansion [19]. The smooth grains in Peace River and Tenham do not have the predicted

stoichiometric plagioclase compositions [19]. Grains in Peace River are highly enriched in  $K_2O$  in comparison to the fractured plagioclase (up to 3.6 wt. % vs. 0.8 wt. %  $K_2O$ ), and have a cation/anion ratio of 6/10  $[(Na\ K\ Ca\ Fe)_{0.973}\ (Al\ Si)_{5.08}\ O_{10}]$  [19]. Smooth grains previously reported in Tenham to be maskelynite [5, 9, 20] are Na- and K- rich glasses compositionally unrelated to plagioclase. Our findings indicate that they are glasses that were quenched at high-pressure from melts that are compositionally distinct from maskelynite or plagioclase. LRM investigations showed that the grains in Peace River are not amorphous glass (and thus definitely are not maskelynite, as previously reported), but rather a new mineral that has the structure of tetrahedrally coordinated silicon. We conclude, that the material in Tenham and Peace River that previously was thought to be maskelynite did not form by solid-state transformation to diaplectic glass [5, 9, 20], but rather by local melting of plagioclase, followed by Na and K metasomatism causing the enrichment of the mineral melts in the alkalis [19]. Both Na and K originated from the melt veins through shock-induced evaporation. Na was not entirely lost from the melt veins since it was in part incorporated in the majorite-pyroxene that appeared as the liquidus phase at high-pressures and -temperatures [2, 13, 21]. The presence of the pervasive radiating cracks around the smooth material in Peace River and Tenham indicates that the grains must have experienced considerable volume increase due to expansion. The expansion, evidently induced a second high-pressure event, with a magnitude (presumably few GPa) lower than the shock induced peak pressures, caused the pervasive fracturing of the meteorite matrices [19]. This second high-pressure event must have taken place after solidification of the alkali-rich melt under high-pressures [19].

#### **SNC Meteorites:**

Maskelynite was first described by Gustav Tschermak from Shergotty [22]. It has been considered to be a diaplectic glass that was formed by shock-induced solid-state transformation of plagioclase during impact events on the parent planet [11, 23-25]. The material in Shergotty was reported to have retained its stoichiometric plagioclase composition and pre-shock chemical igneous zoning [11, 23-25]. The overwhelming majority of the grains (more than 97%) are smooth with no cleavage, no contraction cracks, and no shock-induced fractures. They also display offshoots of smooth "maskelynitic" material into fractures of the adjacent pyroxene, thus attesting that a liquid was injected in the fractures after passage of the shock wave. The grains also contain schlieren of molten pyroxene. The lack of cleavage, cracks, and specifically shock-induced fractures in the grains and their long offshoots indicate that these textural features were erased in a melting event. Similar to their analogues in Peace River and Tenham, the smooth grains in Shergotty are always surrounded by numerous radiating cracks that have extensively shattered the neighboring pyroxene, titanomagnetite, and troilite. This is indicative of volume increase of the glass that was quenched from the melt under high-pressure and expanded upon pressure release [19]. The Raman spectra confirm that the grains are not crystalline: the spectra of the "maskelynite" grains cannot be distinguished from those obtained on the non-stoichiometric glass in Tenham and they are characteristic of amorphous silicate glass. Systematic EMPA profiles across smooth grains reveal distinct chemical signatures in that they do not possess the typical zoning of igneous feldspars. The curves for An- and Ab-contents are flat, do not display a systematic complementary behavior, and the compositional range is extremely narrow (An<sub>57.6</sub> Ab<sub>42.3</sub> Or<sub>0.7</sub> to An<sub>55</sub> Ab<sub>45</sub> Or<sub>0.9</sub>) indicating homogenization. In many cases the chemical composition of individual grains follows the same trend: decrease or increase in both An- and Ab- contents with constant Or-contents. Grains of a silica mineral also occur adjacent to "maskelynite". They have the typical wedge-shaped morphology of

orthorhombic  $\beta$ -tridymite and hence must have crystallized as such from the Shergotty magma. They display two sets of well-oriented coherent lamellae of two  $\text{SiO}_2$  species. The silica grains also are surrounded by pervasive radiating cracks which have heavily fractured pyroxene, "maskelynite", titanomagnetite, and troilite. This is strongly suggestive of volume increase triggered by the inversion of a high-pressure to a low-pressure polymorph of silica.

Our results indicate that the grains previously described as maskelynite in Shergotty [11, 23-25] are evidently formed by shock-induced melting and subsequent quenching to a glass under high-pressure. Our results call for a careful and detailed scrutiny of "maskelynite" in the other SNC meteorites in order to assess its nature. Our findings in Shergotty will have important implications as to the interpretation of the discordant Shergottite ages.

#### References:

- [1] Stöffler D. et al. (1991) *GCA*, **55**, 3845. [2] Chen M. et al. (1996) *Science*, **271**, 1570. [3] Mori H. and Takeda H. (1985), *Lunar Planet. Sci.* **16**, 579. [4] Sharp T. G. et al. (1996), *Lunar Planet. Sci.* **XXVI**, 1175. [5] Price G. D. et al. (1979) *Contr. Mineral. Petrol.*, **71**, 211. [6] Putnis A. & Price G. D. (1979) *Nature*, **280**, 217. [7] Price G. D. et al. (1983) *Can. Min.*, **21**, 29. [8] Price G. D. (1983). *Phys. Earth & Planet. Inter.*, **33**, 137. [9] Langenhorst F. et al. (1995) *GCA*, **59**, 9, 1835. [10] Stöffler D. et al. (1991) *GCA*, **55**, 3845. [11] Stöffler D. et al. (1986) *GCA*, **6**, **50**, 889-904. [12] Xie X., Dai C., Chen M., and El Goresy A. (1997) *Meteoritics* **32**, in press. [13] Chen M. et al. (1996) *Meteoritics*, **31**, Suppl., A27. [14] Agee, C.B. et al. (1995) *JGR* **100** B9, 17725-17740. [15] Langenhorst F. et al. (1995) *GCA*, **59**, 9, 1835. [16] Sharp T. G. et al., (1996) *Lunar Planet. Sci.* **XXVII**, 1175-1176. [17] Mori, H. (1994) *J. Mineral. Soc. Japan* **23**, 171-178. [18] Sharp T. G. et al. (1997), *Lunar Planet. Sci.* **XXVIII** [19] El Goresy A. et al. (1997), *Lunar Planet. Sci.* **XXVIII**. [20] Binns R. A. (1967) *Nature*, **213**, 1111. [21] Chen M. et al. (1996) *LPSC XXVII*, 211. [22] Tschermak G. (1872) *Sitzungsbr. Kaiserl. Akad. Wiss. Wien, Math. -Naturwiss. Kl.*, **65**, 122-146. [23] Duke M. B. (1968) *Shock Metamorphism of Natural Materials, Mono Book Corp.*, 613-662. [24] Smith J. V. and Hervig R. L. (1979) *Meteoritics*, **14**, 121-142. [25] Stolper E. M. and McSween H. Y. Jr. (1979) *GCA*, **43**, 1475-1498.

## MARS-EARTH TRANSFER TIME OF LHERZOLITE YAMATO-793605

Otto Eugster and Ernst Polnau

Physikalisches Institut, University of Bern, Sidlerstrasse 5, 3012 Bern, Switzerland

In the framework of a consortium study of martian meteorite Yamato-793605 (hereafter Y-79) organized by H. Kojima, M. Miyamoto, P. Warren, and K. Yanai (Kojima et al., 1997) we obtained a sample for the determination of the cosmic-ray exposure age and the abundances of trapped noble gases. Y-79 (recovered mass 18 g) shows strong affinities in petrography and mineral chemistry to two other martian meteorites Allan Hills 77005 (ALH77) and Lewis Cliff 88516 (LEW88) as demonstrated by Mikouchi and Miyamoto (1996a,b). These meteorites were classified as lherzolitic shergottites, that strongly differ from the basaltic shergottites Elephant Moraine 79001 (EET79), Queen Alexandra Range 94201 (QUE94), Shergotty, and Zagami in mineralogical and chemical composition. Hence these two classes of martian meteorites do not appear to originate from the same parent magma.

Before having analyzed Y-79 we have shown that the above mentioned meteorites originate from three different asteroidal or cometary impact events on Mars (Eugster et al., 1997). The time of Mars ejection is given by the sum of the cosmic-ray exposure age and the terrestrial age. The following ejection times were obtained: EET79 - 0.8 Ma ago, Shergotty, Zagami, and QUE94 - 2.8 Ma ago, and ALH77 and LEW88 - 3.8 Ma ago. In this work we shall show that Y-79 yields the same cosmic-ray exposure age (and, assuming a typically brief terrestrial age, also the same ejection time) as the latter two and, thus, belongs to the same ejection event as ALH77 and LEW88. The terrestrial age of Y-79 is presently not known; but because the terrestrial ages of the martian meteorites are typically relatively short the ejection times are not significantly higher than the cosmic-ray exposure ages.

Table 1. Results of He, Ne, and Ar measurements of Y-793605

| Sample (g) | $^4\text{He}$                    | $^{20}\text{Ne}$ | $^{40}\text{Ar}$ | $^4\text{He}$ | $^{20}\text{Ne}$ | $^{22}\text{Ne}$ | $^{36}\text{Ar}$ | $^{40}\text{Ar}$ |
|------------|----------------------------------|------------------|------------------|---------------|------------------|------------------|------------------|------------------|
|            | $10^{-8}\text{cm}^3\text{STP/g}$ |                  |                  | $^3\text{He}$ | $^{22}\text{Ne}$ | $^{21}\text{Ne}$ | $^{38}\text{Ar}$ | $^{36}\text{Ar}$ |
| 0.02079    | 35.4                             | 1.21             | 188.6            | 4.54          | 0.884            | 1.211            | 1.29             | 557              |
|            | $\pm 1.2$                        | $\pm 0.04$       | $\pm 8.0$        | $\pm 0.05$    | $\pm 0.012$      | $\pm 0.035$      | $\pm 0.10$       | $\pm 40$         |
| 0.02053    | 34.9                             | 1.19             | 197.0            | 4.72          | 0.910            | 1.241            | 1.15             | 593              |
|            | $\pm 1.1$                        | $\pm 0.04$       | $\pm 10.0$       | $\pm 0.09$    | $\pm 0.020$      | $\pm 0.080$      | $\pm 0.10$       | $\pm 55$         |
| average    | 35.2                             | 1.20             | 192.8            | 4.63          | 0.897            | 1.226            | 1.22             | 575              |
|            | $\pm 1.0$                        | $\pm 0.04$       | $\pm 5.0$        | $\pm 0.10$    | $\pm 0.015$      | $\pm 0.015$      | $\pm 0.07$       | $\pm 20$         |

The results of this work are given in Tables 1 and 2. The cosmic-ray exposure age of Y-79 (Table 3) was calculated based on the concentrations of cosmogenic  $^3\text{He}$ ,  $^{21}\text{Ne}$ , and  $^{38}\text{Ar}$ . The production rates were derived using the method of Eugster and Michel (1995) and are given in Eugster et al. (1997). The average cosmic-ray exposure age,  $T_{\text{av}} = 4.4 \pm 1.0$  Ma for Y-79 agrees within errors with those of ALH77 and LEW88.

The ejection time from Mars is given by the sum of the cosmic-ray exposure age, that is, the transfer time from Mars to Earth, and the terrestrial age, that is, the time since the meteorite fell on Earth. The terrestrial ages of the martian meteorites are in the range of a few thousand to about 300'000 years (cf. Nishiizumi and Caffee, 1996). Thus, the ejection of Y-79 from Mars occurred 4-5 Ma ago. This time agrees within errors with that observed for ALH77 and LEW88. The three Iherzolites yield an average ejection age of about  $4.0 \pm 0.5$  Ma whereas that for the shergottites QUE94201 (2.91 Ma), Shergotty (2.71 Ma) and Zagami (2.76 Ma) is  $2.79 \pm 0.12$  Ma (Eugster et al., 1997).

Table 2. Cosmogenic and trapped noble gases in Iherzolites

| Meteorite              | Cosmogenic                       |                    |                      |                      | Trapped                          |                      |
|------------------------|----------------------------------|--------------------|----------------------|----------------------|----------------------------------|----------------------|
|                        | $^3\text{He}$                    | $^{21}\text{Ne}$   | $^{38}\text{Ar}$     | $^{22}\text{Ne}$     | $^{20}\text{Ne}$                 | $^{36}\text{Ar}$     |
|                        | $10^{-8}\text{cm}^3\text{STP/g}$ |                    |                      | $^{21}\text{Ne}$     | $10^{-8}\text{cm}^3\text{STP/g}$ |                      |
| Y-793605               | 7.60<br>$\pm 0.30$               | 1.09<br>$\pm 0.10$ | 0.241<br>$\pm 0.012$ | 1.207<br>$\pm 0.020$ | 0.23<br>$\pm 0.10$               | 0.178<br>$\pm 0.020$ |
| ALH77005 <sup>1)</sup> | 6.17                             | 0.75               | 0.18                 | 1.19                 | 1.12                             | 0.187                |
| LEW88516 <sup>2)</sup> | 6.98                             | 0.90               | 0.25                 | 1.227                | 0.35                             | 0.74                 |

<sup>1)</sup> Bogard et al. (1984); <sup>2)</sup> Average for data of Ott and Löhr (1992), Becker and Pepin (1993), Bogard and Garrison (1993), Eugster and Weigel (1992), and Eugster et al. (1997).

Table 3. Cosmic-ray exposure ages of Iherzolites

| Meteorite | $T_3$            | $T_{21}$         | $T_{38}$         | $T_{av}$         |
|-----------|------------------|------------------|------------------|------------------|
|           | Ma               |                  |                  |                  |
| Y-793605  | 4.8<br>$\pm 0.5$ | 5.0<br>$\pm 0.7$ | 3.4<br>$\pm 0.4$ | 4.4<br>$\pm 1.0$ |
| ALH77005  | 3.8              | 3.2              | 2.9              | 3.3<br>$\pm 0.5$ |
| LEW88516  | 4.4              | 4.4              | 3.2              | 4.0<br>$\pm 0.8$ |

We conclude from the noble gas isotopic studies that the Mars ejection times of the basaltic shergottites and the Iherzolites do not overlap: the former ones were ejected in two events - 0.8 Ma (EET79) and  $2.8 \pm 0.1$  Ma (QUE94, Shergotty, and Zagami), whereas the latter ones (ALH77, LEW88, and Y-79) in a earlier event  $4.0 \pm 0.5$  Ma ago.

### Acknowledgments

We thank the National Institute of Polar Research, Tokyo, for the sample of martian meteorite Yamato-793605 and H. Kojima, M. Miyamoto, P. Warren, and K. Yanai for organizing the consortium study. M. Zuber assisted in the sample preparation, P. Guggisberg in mass spectrometry, and B. Balsiger in the preparation of the manuscript. This work was supported by the Swiss National Science Foundation.

## References

- Becker R.H. and Pepin R.O. (1993) Nitrogen and noble gases in a glass sample from the LEW88516 shergottite. *Meteoritics* **28**, 637-640.
- Bogard D.D., Nyquist L.E., and Johnson P. (1984) Noble gas contents of shergottites and implications for the Martian origin of SNC meteorites. *Geochim. Cosmochim. Acta* **48**, 1723-1739.
- Bogard D.D. and Garrison D.H. (1993) Noble gases in LEW88516 shergottite: Evidence for exposure age pairing with ALH77005. In *Lunar Planet. Sci.* **24**, 139-140.
- Eugster O. and Weigel A. (1992) Exposure histories of lodranites, shergottite LEW88516 and CK-chondrites. *Meteoritics* **27**, 219.
- Eugster O. and Michel Th. (1995) Common asteroid break-up events of eucrites, diogenites, and howardites and cosmic-ray production rates for noble gases in achondrites. *Geochim. Cosmochim. Acta* **59**, 177-199.
- Eugster O., Weigel A., and Polnau E. (1997) Ejection times of martian meteorites. *Geochim. Cosmochim. Acta*, in press.
- Kojima, H., Warren, P.H., and Miyamoto, M. (1997): The Yamato-793605 martian meteorite consortium. *Antarctic Meteorites XII*, Natl. Inst. Polar Res., Tokyo, this issue.
- Mikouchi T. and Miyamoto M. (1996b) Comparative mineralogy of antarctic Iherzolitic shergottites ALH77005, LEW88516, and Y793605. *Meteoritics and Planetary Science* **31**, A89-A90.
- Mikouchi T. and Miyamoto M. (1996a) A new member of Iherzolitic shergottite from Japanese Antarctic Meteorite Collection: Mineralogy and Petrology of Yamato-793605. *Antarctic Meteorites XXI*, 104-106, Natl. Inst. Polar Res., Tokyo.
- Nishiizumi K. and Caffee W. (1996) Exposure history of shergottite Queen Alexandra Range 94201. In *Lun. Planet. Sci.* XXVII, 961-962.
- Ott U. and Löhr H.P. (1992) Noble gases in the new shergottite LEW88516. *Meteoritics* **27**, 271.

# Origin of the barred olivine like fragment in the ordinary chondrite

**Takashi Fujita**

Institute for study of the Earth's Interior, Misasa, Tottori-ken 682-01, Japan

## Introduction

Barred olivine chondrule is characterized by olivine lamellae aligned to the same direction and spherical olivine shell connecting the bars. Based on the reproduction experiment (cf. [1, 2]), the melting temperature and the subsequent cooling rate of barred olivine is higher than the other chondrule texture. On the other hand, there is another type of "barred olivine" texture observed in the ordinary chondrites. They are characterized by lamellar olivine aligned to the same direction, and in its sense, they are similar to the typical barred olivine chondrule. However, the interstices of the olivine shows a holocrystalline texture of pyroxene and plagioclase, and the barred texture is not rimmed with the spherical shell but with the granular texture, both indicating a slower cooling rate than the typical barred olivine chondrule. In this study, to clarify the origin of such holocrystalline granular and barred olivine texture (hereafter called GBO temporary), mineralogy and composition of such textures among four ordinary chondrites, Moorabie(L3), Y-790448(LL3), Y-82055(L3), and Y-82058(L3) were studied.

## Description

Polished thin-section of the specimens were studied with an optical microscope, scanning electron microscope, and electron probe micro analyzer (JXA-8800). In the Moorabie and Y-790448(LL3), macro-sized clast of the GBO texture was observed, while the size of the GBO in the Y-82055(L3) and Y-82058(L3) are not so different from the normal chondrule. The respective texture is described in the following.

### 1 Moorabie (L3) (Figs.1a,b)

The GBO show a macro size (10X8X3mm) composed of olivine (around Fo86), pyroxene (En80Fs12Wo8-En53Fs7Wo40) and plagioclase (Ab8-16An82-92Or0-1). The rim of the fragment shows a granular texture of 10 to 200 micron meters (mostly, a few tens micron meters), while the core shows a barred olivine texture, in which each bars shows 20-30 micron meters in thickness. The orientation of the olivine bars are nearly the same side by side, but in the macroscopic view, the extinctions of the bars show a wavy pattern. Extinction direction of the bars are nearly parallel to the a-axis of olivine. Interstices of the olivines are filled with pyroxene and plagioclase. Besides the form and orientation of olivines, there is no definite texture for distinguish the core and rim. The fragment includes chromite, metal and ilmenite grains, and the ilmenite often include small Zr-rich grains sized about 1 micron meter. In the edge of the fragment, crystals show a broken surface, which was also observed in the other GBO texture described below.

### 2 Y-790448(LL3) (Fig.2a)

The occurrence of GBO in Y-790448 is reported previously [3], the texture is sized 2.5 X 3mm in a thin section, and composed of olivine (Fo79-75), pyroxene (En63Fs23Wo13-En53Fs20Wo27) and plagioclase (Ab12An88-Ab17An83) and accessory chromite and ilmenite. In the barred core, thickness of the bars are 20-50 micron meters. Extinction direction of the bars are nearly parallel to the a-axis of olivine, while a structure connecting the each bars was not observed. In the granular rim, composition of olivine is richer in Fe than the barred core. Chromite in the core is sized about few tens micron meters, and finer chromite grains are concentrated in the core-rim boundaries.

### 3 Y-82055(L3)(Fig.2b) and Y-82058(L3)

In the section of Y-82052, GBO with 0.8X1.2 mm is observed. In this fragment, thickness of the olivine bars in the core are about 10 micron meters. In the section of Y-82058, two GBO with 1X1.2mm and 0.7X1 mm in size were observed. Both fragment

show a barred texture and granular texture of olivine, pyroxene and plagioclase. The fragment 1 include a chromite sized 100 micron meters. In the fragment 2, olivine bar show a connection like a shell of the typical BO chondrule, while such texture is not observed in the fragment 1.

### **Discussion**

The ferroan composition, existence of the chromite grains in the GBO textures show an affinity to a type II chondrule [4]. On the other hand, the broken edge of the crystals observed in the rim of the GBO textures show a fragmentation process between the crystallization process and accumulation to the parent body. The holocrystalline texture, composed of olivine, pyroxene and plagioclase shows a similarity to lithic fragment observed in the ordinary chondrite (cf.[5,6]). Based on the similarity of mineralogy, Hutchison (1992) regarded chondrule with GBO like texture as a kind of igneous inclusion [7].

The GBO fragment of macro size and that of normal chondrule size shows a similar mineralogy and texture. In the reproduction experiment, formation of barred olivine needs the highest melting temperature (cf.[1,2]). Therefore, the barred core may be formed faster than the granular rim, whether the barred texture was crystallized insitu, or was a relict of exotic texture. However, in the most case, obvious discontinuity could not observed between the barred core and granular rim except for the difference in the crystal morphology. In the GBO in Y-790448, discontinuity between the barred texture and granular rim is evident. Concentration of chromite at the core rim boundary show the crystallization of chromite and subsequent formation of granular texture under the existence of the barred core.

The formation of the barred texture in the core remains some problem. The macro size of barred texture in the Moorabie and Y-790448 sample are larger than the normal barred olivine chondrule in the same samples. If the barred texture was crystallized in situ, it is difficult to explain the formation of barred texture without the shell connecting the each bars. On the other hand, in the normal barred olivine chondrule, sets of olivine bars with different orientation is often observed. So, it may be difficult to form a macro barred texture with only one orientation by the same process. The other possibility is remained for consideration. In the GBO texture, the barred olivine show a direction nearly parallel to a-axis. The direction is common to the cleavage of olivine. If the coarse olivine with cleavage is sited in the melt, the melting of the olivine along the cleavage and subsequent recrystallization may form a barred olivine like texture. If it was the case, the coexistence of the barred texture and granular texture is easily explained.

Besides the above problem, complex history is needed for the formation of the GBO texture. For example, for the formation of GBO texture in the Y-790448, four or five process is needed; (a) formation of barred olivine texture by remelting of the coarse olivine (if it was the case) or crystal growth, (b) deformation of the barred texture, (c) crystallization of the granular texture, and (d) deformation of GBO texture in the edge. It is difficult to distinguish whether recycling of chondrule or some planetary environment is responsible for such complex history. However, to explain the broken edges of crystals always observed in the GBO texture implies the texture is a fragment of coarser texture even in the macro sized fragment.

### **References**

- [1] Tsuchiyama, A., Nagahara, H., and Kushiro, I. (1980): Earth Planet Sci. Lett., **48**, 155-165. [2] Connolly Jr, H.C. and Hewins, R.H. (1995): Geochim. Cosmochim. Acta. **59**, 3231-3246 [3] Fujita, T. and Kitamura, M. (1994): Papers presented to the 19th Symposium on Antarctic Meteorites, 33-36. [4] McSween, H.Y. (1977) : Geochim. Cosmochim. Acta, **41**, 477-491. [5] Kennedy, A.K., Hutchison, R., Hutcheon, I.D., and Agrell, S.O. (1992): Earth Planet Sci. Lett., **113**, 191-205. [6] Bischoff, A., Geiger, T., Palme, H., Spettel, B., Schultz, L., Scherer, P., Schluter, J. and Lkhamsuren, J. (1993): Meteoritics, **28**, 570-578. [7] Hutchison, R. (1992): J. Volcanol. Geotherm. Res., **50**, 7-16.

**Fig.1 a)** Photograph of a section of the Moorabie. horizontal scale=1 cm. Large transparent region embedded in the chondritic host is the GBO fragment.**b)** Mg concentration map of a part of the GBO texture. Bright, gray, and dark parts indicates olivine(ol), pyroxene(px), and plagioclase(pl) respectively (black line in the right is a crack ).Barred texture (left) is embedded in the granular texture.

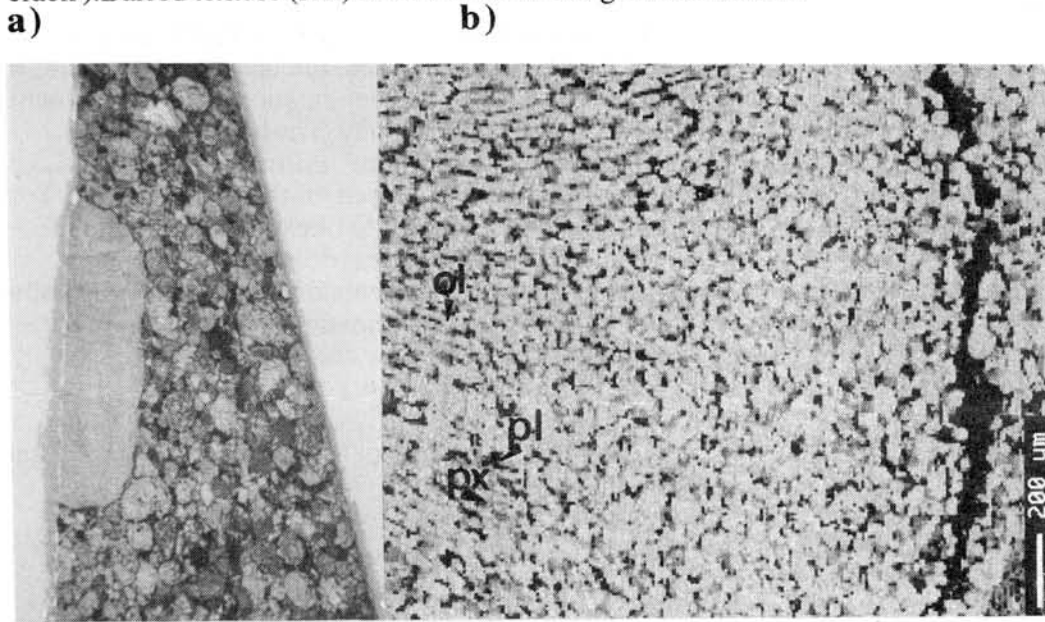
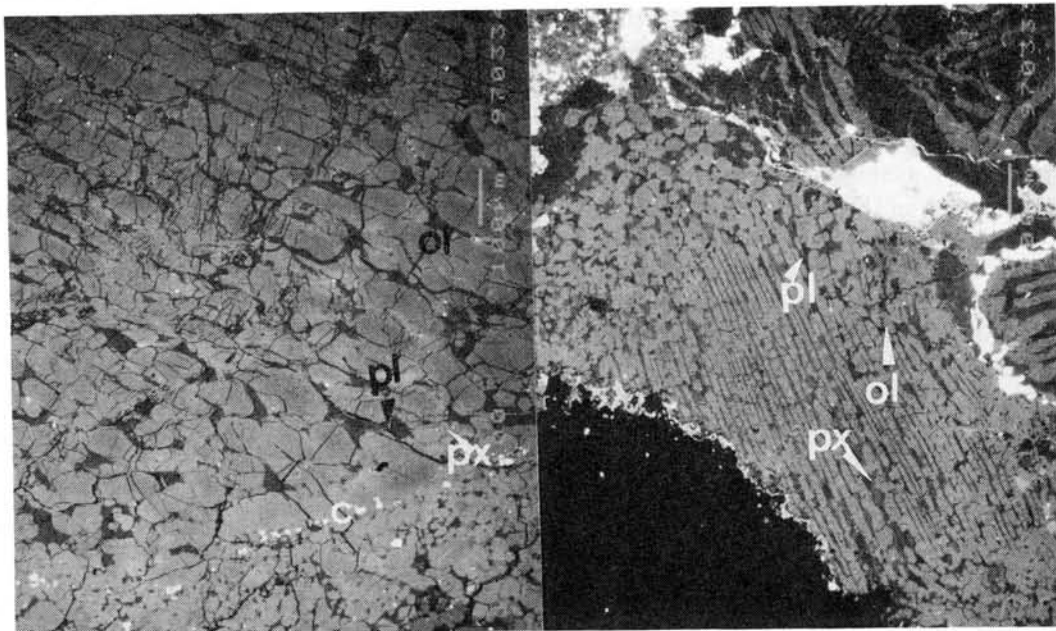


**Fig.2**

Back scattered electron image of the GBO texture in (a)Y-790448, and (b) Y-82058. Bright, gray, and dark parts indicates olivine(ol), pyroxene(px), and plagioclase(pl) respectively .horizontal scale=1mm. Chromites (C:white grains) concentrates in the core rim boundary in the Y-790448. In the Fig.2b, GBO texture can be observed in the chondrule size.

**a) Y-790448**

**b) Y-82055**



## Measurement of Natural Remanent Magnetization of Iron Meteorites

Tetsuya FUKUHARA<sup>1</sup>, Minoru FUNAKI<sup>2</sup> and Hiroyuki NAGAI<sup>1</sup>

<sup>1</sup>Department of physics, Faculty of Science, Shinshu University,

3-1-1 Asahi Matsumoto Nagano 390

<sup>2</sup>National Institute of Polar Research, 9-10 Kaga 1 Itabashi Tokyo 173

It is known that magnetic anomaly maps of limited areas on the moon have been constructed from selected intervals of Apollo 15 and 16 subsatellite magnetometer data (Hood et al, 1981). The data from which the maps were constructed were collected at altitudes of between 15km and 60 km above the surface of the moon. From these maps we know that there are some magnetic anomalies at the moon between 10 to 50 nT. On the other hand, we can explain the magnetic anomaly if there is a mass which has more than  $2\text{g/cm}^2$  of density and Natural Remanent Magnetization (NRM) of more than  $8 \times 10^{-1} \text{Am}^2/\text{kg}$  at a depth of more than 1m below the surface of the moon (Schultz & Srnka, 1980). If there are iron meteorites under the surface of the moon, it is possible that these may be the cause of the magnetic anomaly. To elucidate the magnetic anomaly we must first know the NRM value of iron meteorites. Unfortunately the NRM value of iron meteorites have never been examined statistically, so, in this paper, we have examined the NRM value of about 30 kinds of iron meteorites. We have also examined the magnetic anisotropy of "Toluca" and "Y790724" (both are iron meteorites as classified under Octahedrite) to study the cause of NRM. Samples which were measured for their NRM value were less than 100g in mass because it is impossible to measure more than 100g samples by using the spinner magnetometer. To measure the magnetic anisotropy of the iron meteorites, the samples were cut into cubes because the magnetic anisotropy depends on the shape of the sample. Cubic sub-samples were demagnetized by Alternating Field Demagnetization up to 0.1T and then each sub-sample had four different directions of Saturation Isothermal Remanent Magnetization (SIRM) applied by an electromagnet. Each coordinate axis was determined arbitrarily. The SIRM value was measured by using the spinner magnetometer. The results of measuring the NRM value of iron meteorites of less than 100g showed that the intensities of the NRM value of iron meteorites are from  $10^{-2} \text{emu/g}$  to  $10^{-4} \text{emu/g}$  and the NRM intensity may depend on Ni content (Fig. 1). The results also showed that some magnetic anisotropy was present in the samples and it is possible that the cause of these magnetic anisotropies are due to crystallomagnetic anisotropies.

**References**

**L.L.HOOD, C.T.RUSSELL & P.J.COLEMAN, JR**, 1981, *Journal of Geophysical Research*, Vol.86, 1055-1069

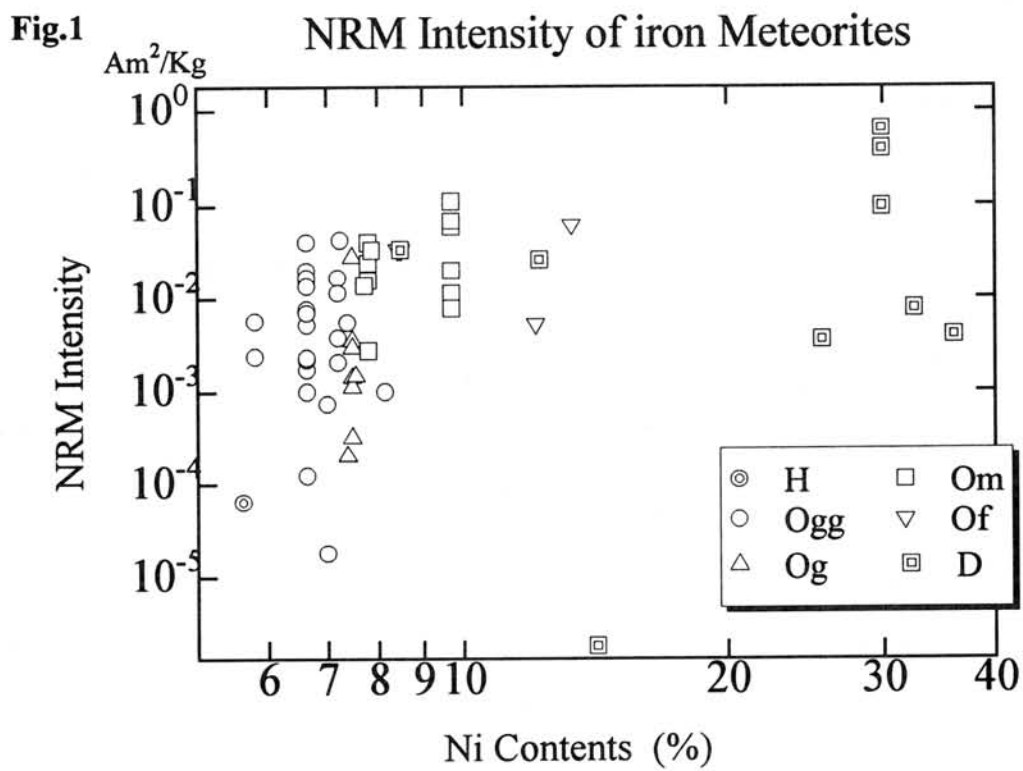
**Peter H.SCHULTZ & Leonard J.SRNKA**, *Nature*, Vol.284 6 March 1980, 22-26

**Ilmo T.KUKKONEN & Lauri J.PESONEN**, 1983, *Geol.Soc.Finland* 55, 2, 157-177

**Aviva BRECHER & Michael CUTRERA**, 1976, *J.Geomag.Geolectr*, 28, 31-45

**Aviva BRECHER & Lisa ALBRIGHT**, 1977, *J.Geomag.Geolectr*, 29, 379-400

**Takesi NAGATA**, 1979, *Proceedings of the 3rd symposium on antarctic meteorites* 238-249



# CHEMICAL EVOLUTION OF CARBOHYDRATES IN ORIGIN OF LIFE

S.Fukuyama and Y. MIURA

Department of Chemistry and Earth Sciences, Faculty of Science  
Yamaguchi University, Yoshida, Yamaguchi 753, Japan

## 1. Inorganic to organic compositions by shock wave energy

Miller (1953)[1] synthesized nitrogen-bearing amino acid from inorganic compounds by shock wave energy of spark. Similar organic compounds of nitrogen-bearing composition are formed by other shock wave energy of thunder storm, volcanic eruption, hydrothermal vent in deep sea, asteroids or cosmic ray bombardments. However, he did report only nitrogen-bearing organic materials.

Miller (1995)[2] reported all types of organic compounds after shock-wave experiments, where major organic compounds are carbohydrates (71%) and minor those of nitrogen-bearing amino-acid (29%). This suggests that major organic compound in primordial anoxic Earth or sea-water by shock wave energy is carbohydrates.

Yamanaka(1973) [3] reported energy acquirement by oxidation from low-molecule carbohydrates, though he discussed only monomers. Previous all organic compounds reported in meteorites or primordial Earth are monomer of organic compounds. There are few reports on polymers or oligomers on carbohydrate organic compounds.

Carbohydrates can be used as primordial organic compounds if there are characteristic activity to make pseudo-life organic molecules discussed in this study.

## 2. Characteristic significance of carbohydrates

Miura (1994, 1996, 1997) [4,5,6] reported that some carbohydrate of composition  $(CH_2O)_n$  show oligomers of lactide and poly-lactide, and that there are various monomers of formaldehyde, acetic acid, lactic acid, ribose and glucose, and that lactic acid  $(C_3H_6O_3)$  reveals  $SO_3$  molecules of oligomer structure  $\{(C_3H_4O_2)_z\}$  with characteristic activity as supramolecule [7] from polyoxymethylene and polyglycolic acid. The  $SO_3$  molecules can be synthesized under acid liquid condition and high temperature less than 200 degree Celsius.

This suggests that active carbohydrates can be formed widely on primitive seawaters on the Earth and Mars during shock wave energy or simple heating of interior activity.

## 3. Chemical evolution of life

Chemical evolution of life [1-6, 8-12] can be summarized in the following steps:

- (a) Conversion of inorganic  $CO_2$  and  $H_2O$  to organic compounds  $(CH_2O)_n$  by shock wave energy.
- (b) Conversion from monomers  $(CH_2O)_n$  to oligomer  $SO_3$  and polymers by heating.
- (c) Oligomer  $SO_3$  shows pseudo-life activity by fermentation process of spheroidal prokaryotes.
- (d) Conversion of inorganic  $CO_2$ ,  $H_2O$  and  $N_2$  to simple organic monomers of carbohydrate  $HCHO$  and  $HCN$ , sugars, amino acids and bases, and nucleic acids and proteins, and finally to life precursors and primitive organisms on the condition of circulation system of seawater, atmosphere and crustal solid rocks like the Earth.

Although the monomers  $(CH_2O)_n$  are important energy transporting molecules, intermediate organic oligomers with characteristic activity have not been reported previously in terrestrial rocks [8,9,10] or meteorites [11-13], nor in synthetic experiments [14].

Although sugars and RNA or DNA giant molecules are significant for life evolution, there are few detailed study of carbohydrate molecules with characteristic activity from low to high degrees of polymerization. A large amount of carbohydrate oligomers can be explained more detailed reaction in the above (a) process.

However, it takes long time to form anaerobic bacterias by chemical evolution. The difference in amounts between large carbohydrates and small nitrogen-bearing organic compounds results in long history of about 1 Ga to form life-precursors of prokaryotic cell on primordial Earth and Mars.

The following various species of primitive life are considered to be formed in primordial Earth and Mars [6,10].

- (a) Anaerobic bacteria (3.8Ga to ca.2.9Ga),
- (b) Photosynthetic bacteria (3.3Ga to 2.9Ga),
- (c) Anaerobic prokaryotes (2.9Ga to 2.4Ga),
- (d) Aerobic prokaryotes by modern photosynthesis (1.8Ga to ca.1.0Ga),
- (e) Eukaryotes (1.5Ga to 1.3Ga, 0.8Ga to 0.7Ga, and 0.5Ga to 0.0), and
- (f) Algae and metazoans (0.7Ga to 0.5Ga).

Before producing first primitive life on the Earth and Mars, it takes ca. 1 Ga due to its complex chemical evolution. During anaerobic or photosynthetic bacteria, the main organic materials are (CH<sub>2</sub>O)<sub>n</sub> composition as follows (cf. Table 1):

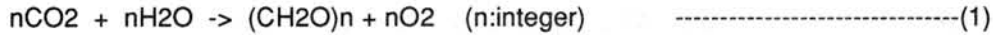


Table 1. Characteristic cyclic system of carbohydrate oligomers in primitive Earth and Mars [1,6,11].

Water and carbon dioxide → (by shock wave energy) → (CH<sub>2</sub>O)<sub>n</sub> monomers → (dehydration) → SO<sub>3</sub> oligomers → (fermentation with enzyme-like activity) → (copying) → (CH<sub>2</sub>O)<sub>3</sub> → (polylactic acid : Giant molecules) → (hydrolysis) → monomer → Water and CO<sub>2</sub> (inorganic) →

#### 4. Pseudo-life organic molecules

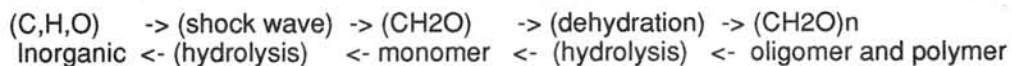
We proposed pseudo-life organic molecules in this study as follows [6].

- 1) Composition is C-H-O of carbohydrates.
- 2) Duplication system is found as polymer of molecular weight less than 200,000.
- 3) Energy system is based on early fermentation.
- 4) Characteristic activity is explained by supramolecules of enzyme-like activity.
- 5) Circulation of elements of early Earth is based on inorganic, organic (polymer) to inorganic compounds.
- 6) Evidences of monomers of carbohydrates is found in carbonaceous chondrites and IDPs.

#### 5. Recyclic process of characteristic carbohydrates

Recyclic process of carbon-bearing materials is inevitable process for life generation (Table 1)[6].

- 1) Inorganic compounds of C,H and O change to monomer of carbohydrates.
- 2) Monomers change to oligomers by heating.
- 3) Oligomers change to polymers by dehydration and heating.
- 4) Polymers change to monomer and inorganic C,H and O by hydrolysis.



#### References:

- [1] S.L.Miller (1953): Science, 117, 528-529.
- [2] S.L.Miller (1955): J.Am.Chem.Soc., 77, 2351-2358.
- [3] T.Yamanaka(1973): Space Life Sci., 4, 490-504.
- [4] Y.Miura(1994): Astro.Soc. Pacific Conf. Series, 63, 259-264.
- [5] Y.Miura(1996): Proc. 29th ISAS Lunar and Planet.Sympo. (ISAS, Japan), 29, 289-292.
- [6] Y.Miura(1997) : Conf. Early Mars (LPI), No.916, 54-56.
- [7] J.-M.Lehn (1995): Supramolecular Chemistry, 271pp. VCH, Weinheim, Germany.
- [8] M.R.Walter , R.Buick and J.Dunlop (1980): Nature, 284, 443-446.
- [9] J.W.Schopf (1993): Science, 260, 640-646.
- [10] J.W.Schopf (1977): Precambrian Research, 5, 143-173.
- [11] C.Chyba and C.Segan (1992): Nature, 355, 125-132.
- [12] D.S.McKay, E.K.Gilson, K.H.Thomas-Keperta, H.Vali, C.S.Romanek, S.J.Clemett, X.D.F. Chillier, C.R.Maechilling and R.N. Zare (1996): Science, 273, 924-930.
- [13] R.Hayatsu, S.Matsuoka, R.G.Scott, M.H.Studier and E.Anders (1977): Geochim. Cosmochim. Acta, 41, 1325-1339.
- [14] D.K.Gilding and A.M. Reed (1979): Polymer, 20, 1459-1646.

# IMPACT METAMORPHOSED COMPOSITIONS OF Fe-Si-Ni-S SYSTEM

S.Fukuyama, H.Kabayashi and Y. Miura  
*Department of Chemistry and Earth Sciences, Faculty of Science  
Yamaguchi University, Yoshida, Yamaguchi 753, Japan*

## 1. Introduction

There is few systematic report on impact indicator of composition and structure. Impact craters on the Earth are considered to be formed by iron meteorite bombardments, because effect of air layer can stop direct impacts of comets or stony meteorites on the surface of the Earth [1]. The main purpose of the study is to elucidate characteristic signature of impact composition.

## 2. Relation of compositional change by impacts

Compositional change (f) of impact metamorphosed materials can be classified by three places during every impact moment as follows [1]:

- 1) In vapor plume (as fine-grained glassy breccias and dusts):  
 $f(\text{impact}) = f(\text{projectile of iron meteorites}) + f(\text{target rock}) - f(\text{volatile elements})$
- 2) In jetting stream (as various sized grains of glassy breccias):  
 $f(\text{impact melt}) = f(\text{projectile}) + f(\text{target rock}) - f(\text{light elements})$
- 3) In walled cracked rock (as cracked target rocks of impact craters):  
 $f(\text{impact solid}) = f(\text{target rock}) + f(\text{projectile})$

Thus we have to check compositions of the surface and cutting planes of the spherules and grains to analyze whether this grains are formed at one of the above three progressive processes. The followings are one of analytical processes in impact metamorphosed (or evolved) spherules and grains [1]:

- 1) Compositional changes below and above the geological boundary.
- 2) Detailed compositional analyses of spherules and grains.
- 3) New analytical methods for spherules and grains.

## 3. Composition of Fe-Ni-Si-Mg-S system

There are a few reports on systematic compositions of impact spherules and fragments by NASA-JSC [2]. Analytical electron microscopical (AEM) data of these particles in the space of the Earth are summarized as follows:

- (a) Meteoritic origin (shown as C) of the particles are 41% (from 403 analyses) with mixed composition of Fe-Ni-Si-Mg-S system. This C grains are only found in iron meteoritic crater on the Earth, though those are difficult to find in impact craters without projectiles on the Earth.
- (b) Terrestrial contamination from natural particles (shown as TCN) from volcanic ashes are 10% (from 403 data) with mixed composition of Si-Al-Na-K-Ca-Fe system mainly from feldspar and quartz compositions, where there are a few atoms of Ni, S or Mg compared with those of the meteoritic origins. These grains are also found at jetting stream or wall cracked rocks of the meteoritic or impact craters on the Earth.
- (c) Mixed compositions which are originated from meteoritic and terrestrial sources classified as unknown particles. This is applied as significant information on vapor plume and jetting stream of impact craters on the Earth.

## 4. Meteoritic impact composition

Meteoritic compositions of Fe-Ni and Fe-Ni-S are melted from kamacite and troilite, respectively, of iron meteoritic compositions. Those of Si-Mg-Fe are originated from olivine or pyroxene of chondritic meteoritic composition. However Mg and Fe elements of the Si-Mg-Fe system are difficult to identify the sources of minerals on the terrestrial surface by impacts. Therefore, characteristic composition of impact on the terrestrial surface is obtained as Fe-Si-Ni-S system in this study. The meteoritic compositions of Fe-Si-Ni-S system are usually changed as various stages between those of vapor plume or jetting stream with impact metamorphism. In fact, minor content of Ni or S is changed after the various reactions during the impacts.

The shapes of the particles formed by impacts are spherules, fragments or particles with micrometer size. The texture of glassy states of these impact grains is changes by various cooling and crystallization rate during and after impact.

## 5. Spherules from K/T geological boundary

Spherules from Cretaceous-Tertiary (K/T) geological boundary which was formed by impacts on Middle America with distributed as global scale, show Fe-Si-Ni-S composition in Danish samples [3,

4]. This indicates that the K/T boundary is confirmed by spherule composition of Fe-Si-Ni-S system (cf. Table 1). However, as the various reactions between vapor or jetting stream, some of Fe-Si-Ni-S system should be changed to Fe-Si system by distributing the minor content of Ni or S. This example is obtained at the K/T boundary grains in Hokkaido, Japan.

## 6. Impact craters on the Earth

Impact craters of the Barringer (U.S.A.), Wolf Creek (Australia), and Ries (Germany) show mixed impact compositions of Fe-Si-Ni-S system as listed in Table 1 [1,3,4]. Those of vein in shocked quartz with iron meteorite by mixing show various contents of Fe-Si system with or without Ni or S.

Takamatsu crater [3] shows anomalous grains of Fe-Si-Ni-S system, though there is minor contamination of Cl, Ti or Al. There are various contaminations of the grains, where some grains are originated by secondary melting during formation of glassy blocks.

Akaogi crater of Anami-Oshima, Kogoshima Prefecture, Japan, shows 26% grains from meteoritic impact origin of Fe-Si-Ni-S system, and 74% grains from terrestrial igneous origin as mixed compositions. These data are obtained as cutting cross section of each magnetic spherules, though rounded spherules did not show Fe-Si-Ni-S system only from secondary reacted outer-surface.

Referenced data of Unzen volcanic ash from Mt. Unzen, Kyushu island, show Si-Fe-Ti-Al-Mg-K system from feldspar or mafic compositions after the jetting volcanic spherules formed on the tree around the volcano. This suggests that there are feldspar compositions of Al and K, and mafic composition of Mg from the volcanic spherules, and that there are few compositions of Ni or S from volcanic spherules.

Table 1. AEM analytical data of meteoritic impacts with Fe-Si-Ni-S [1,3].

| Oxides*          | Danish KT<br>SK12 | Barringer<br>crater B8 | Wolf Creek<br>crater W20 | Ries crater<br>R5-2 | Takamatsu<br>TK15 | Anami-Oshima<br>S7 |
|------------------|-------------------|------------------------|--------------------------|---------------------|-------------------|--------------------|
| SiO <sub>2</sub> | 13.5              | 44.2                   | 2.5                      | 8.7                 | 8.2               | 8.6                |
| FeO              | 80.4              | 46.5                   | 89.9                     | 82.9                | 63.2              | 90.4               |
| MgO              | 0.0               | 0.0                    | 0.0                      | 0.0                 | 0.0               | 0.0                |
| CaO              | 1.2               | 1.3                    | 0.0                      | 0.0                 | 0.0               | 0.0                |
| NiO              | 2.3               | 8.0                    | 7.7                      | 1.5                 | 5.0               | 1.0                |
| SO <sub>2</sub>  | 2.6               | 0.0                    | 0.0                      | 0.0                 | 6.5               | 0.0                |
| Total            | 100.0             | 100.0                  | 100.1                    | 93.1                | 82.9              | 100.0              |

\* The value is weight percent calculated as oxides.

## 7. Purified composition after multi-impacts

There are many reports on pure iron spherule of regolith breccias on the Moon [5,6], which are explained by secondary reaction by solar wind after impact. However, such reduction observed only Fe-spherules in glassy breccias cannot be explained by impact texture. Thus it is found in this study that Fe-pure composition of spherule can be obtained by multi-stage impacts on air-less Moon surface [3].

Thus compositional changes are proposed at impact metamorphism as listed in Table 2.

Table 2. Compositional change of spherule grains in the Moon and large impact craters [3].

|  |
|--|
| 1. First simple impact:<br>f(impact melt in spherule) = f(mixed compositions from iron meteorite Fe-Ni and target rocks Si-Al-Ca)  |
| 2. Secondary or multi-impacts:<br>f(mixed compositions from iron meteorite Fe-Ni with target rocks Si-Al-Ca systems) :<br>changes to<br>f(pure composition of Fe spherules) :<br>by impact vaporization (short reaction) and solar wind bombardment (long reaction). |

## References:

- [1] Y. Miura et al. (1995): Shock Waves Proc., 19, 399-410
- [2] CDPET (1986): Cosmic Dust Catalog (NASA-JSC, U.S.A.) 129pp.
- [3] Y. Miura et al. (1997): Shock wave, Japan, 447-450.
- [4] Y. Miura (1991): Shock Waves, 1, 35-41.
- [5] R. V. Morris (1976): Proc. Lunar. Sci. Conf. 7th, pp.315-335.
- [6] G. W. Pearce et al. (1975): Lunar Science VI, pp.634-636.

# NATURAL REMANENT MAGNETIZATION OF NOVA PETROPÓLIS IRON METEORITE

Minoru FUNAKI<sup>1</sup> and Jacques DANON<sup>2</sup>

*National Institute of Polar Research, 9-10 Kaga 1, Itabashi Tokyo 173*

*2:Centro Brasileiro de Pesquisas Físicas, Rua Dr. Xavier Sigaud, 150 22290-180 Rio de Janeiro RJ Brasil*

## 1. Introduction

An iron meteorite, Nova Petropólis, was found at Nova Petropólis, Rio Grande do Sul, Brazil, in 1967 (Grunewaldt, 1983). It has been classified into the medium octahedrite IIIA with chemical composition of 7.8%Ni, 19.9ppm.Ga, 36.5ppm.Ge, 9.4ppm.Ir (Graham et al., 1985). A part of the sample was cut by a diamond saw for magnetic studies from the original mass 305kg in weight. Extracted taenite lamellae resulting from Widmanstätten structure were examined by the Mössbauer spectroscopy at room temperature (Azevedo et al., 1987). The results indicated that lamellae consist 15%  $\alpha$ -FeNi, 62% Ni rich  $\gamma$ -FeNi, 20% paramagnetic  $\gamma$ -FeNi (<30%Ni), and 3% iron oxide.

## 2. Basic magnetic properties

A sample of Nova Petropólis was etched by HCl during 10 days. In this treatment, Ni-rich taenite lamellae (lamellae sample) resulting from the Widmanstätten structure was extracted. Magnetic hysteresis properties (Table 1) were obtained for the bulk sample and lamellae sample. Their coercive forces are rather small ( $H_C \leq 3.3$ mT) and they decrease furthermore by the heat treatment. The value  $H_{RC}$  of pre- and post-heating bulk sample is larger ( $H_{RC}=51.7$ mT) than the lamellae sample ( $H_{RC} \leq 10$ mT).

Thermomagnetic ( $I_S$ - $T$ ) curves were obtained from room temperature to 800°C. The  $I_S$ - $T$  curve of bulk sample is irreversible with  $T_c=535, 750$  and  $590^\circ\text{C}$  in the 1st run cycle, and with  $T_c=590$  and  $750^\circ\text{C}$  in the 2nd run cycle. Unstable  $T_c=535^\circ\text{C}$  which appeared in the 1st run heating curve is almost consistent with phase transition temperature of tetrataenite ( $\gamma'$  phase), but it may be due to decomposition of some unstable taenite to kamacite and/or taenite, because this iron did not include high coercive minerals as  $\gamma'$  phase. Phase transition at  $T_c=750$  and  $590^\circ\text{C}$  correspond to the phase transition of  $\alpha \rightarrow \gamma$  and  $\gamma \rightarrow \alpha$  respectively of kamacite with 7%Ni.

Table 1. Magnetic hysteresis and thermomagnetic properties.

| sample   | weight (g)              | $I_S$<br>Am <sup>2</sup> /kg | $I_R$<br>Am <sup>2</sup> /kg | $H_C$<br>mT | $H_{RC}$<br>mT | $T_c$ (°C)     |           |
|----------|-------------------------|------------------------------|------------------------------|-------------|----------------|----------------|-----------|
|          |                         |                              |                              |             |                | heating        | cooling   |
| Bulk     | 0.03062                 | 207.7                        | 0.175                        | 0.55        | 51.7           | 535, 750       | 590       |
|          | (post-heating to 850°C) | 211.5                        | 0.1                          | 0.4         | 57.7           | 750            | 590       |
| Lamellae | 0.00124                 | 140                          | 12.2                         | 3.3         | 7.2            | -320, 570, 745 | -400, 575 |
|          | (post-heating to 850°C) | 167                          | 1.3                          | 0.2         | <1.0           | -400, 750      | -400, 580 |

The  $I_s$ - $T$  curve of lamellae sample showed clearly defined the Curie point at  $T_c=560$  and  $750^\circ\text{C}$  in the heating curve and  $580^\circ\text{C}$  in the cooling curve. The magnetization related to  $T_c=560^\circ\text{C}$  decreased to small in the 2nd run cycle. This unstable  $T_c$  may be comparable with  $T_c=535^\circ\text{C}$  observed in the bulk sample.  $T_c=750$  and  $580^\circ\text{C}$  are phase transition temperature of kamacite with 7%Ni. The principal magnetic minerals of these lamellae samples are estimated to be unstable taenite and kamacite with 7%Ni.

### 3. Natural remanent magnetization

Natural remanent magnetization (NRM) of Nova Petropólis was very stable against AF demagnetization to 100mT. It was not demagnetized thermally before  $400^\circ\text{C}$ , subsequently it was decayed gradually to  $630^\circ\text{C}$ . A systematic directional change was observed during the demagnetization. The NRM direction was measured pre- and post-AF demagnetization to 30mT. They scattered widely with normal and reverse inclination. The characteristics of NRM direction were not changed drastically by AF demagnetization to 30mT.

### 4. Microscopical Observation

On the etched sample for the microscopical observations, taenite lamellae less than  $100\mu\text{m}$  in width resulting from the Widmanstätten structures invaded boundary of polygonal kamacite crystals from 1 to 4mm in diameter. They insetted cloudy taenite partially and their intervals were more than 0.8mm. Developed Neumann lines from 10 to  $100\mu\text{m}$  intervals appeared in the kamacite field, but their directions were sometimes random among the kamacite crystals.

A half of sample was partially painted by magnetic fluid (Bitter pattern) to observe the magnetic domain structures, and other half one was etched slightly. In this sample, clearly defined several sets of lines appeared by the Bitter pattern. As some lines were succeeded by the Neumann lines which appeared directly by the etching (Fig. 1), the lines observed by the Bitter pattern seem to be Neumann lines. The lines by Bitter pattern remained even if the sample was demagnetized thermally up to  $480^\circ\text{C}$ , but they disappeared when the sample was demagnetized at  $580^\circ\text{C}$ . Subsequently in the demagnetized sample, however, the lines appeared clearly by the etching.

### 5. Discussion

The principal magnetic mineral in Nova Petropólis is kamacite with 7%Ni identified by the phase transition temperature at  $750^\circ\text{C}$  and  $590^\circ\text{C}$  in the  $I_s$ - $T$  curves. This result supports the chemical composition 7.8%Ni reported by Graham et al. (1985). Tetrataenite may not exist in Nova Petropólis, estimating small  $H_c=3.3\text{mT}$  and  $H_{RC}=7.2\text{mT}$  values of the lamellae samples.

In general, the stable NRM of ordinary chondrites is carried by only tetrataenite, but there is no evidence of tetrataenite in Nova Petropólis, though the NRM is stable more than 100mT. The Bitter pattern shows where is the strong magnetic gradient; the dense magnetic field lines irradiate from the areas accumulating magnetic fluid. The lines observed by the pattern disappeared between  $480$  to  $580^\circ\text{C}$  and the NRM was demagnetized at  $580^\circ\text{C}$ . This consistency suggests that the NRM is carried by the Neumann lines for Nova Petropólis. It is difficult to explain why Neumann lines carry the stable NRM, because the lines can be seen clearly by chemical etching even if the sample was demagnetized thermally at more than  $580^\circ\text{C}$ . We have estimated that the reason is the magnetic discontinuity due to the Neumann lines produced by the strain in kamacite crystal.

The NRM directions scattered widely in spite of the stable NRM against AF

demagnetization. It is contrasted to Bocaiuva (IAB) whose directions of the stable NRM aligned along a great circle consisting with the dominant plane of developed tetrataenite lamellae (Funaki et al., 1988). Probably the reason of scattered NRM is due to the polycrystallin structure of Nova Petropolis. Consequently, the NRM direction of subsamples may reflect those of the dominant Neumann lines of the larger crystals. Since the Neumann lines have been considered to produce by shock about 10 kbar during segmentation of the parent body by collision, the NRM might have been acquired at that time.

## 6. Conclusion

Nova Petropolis consists of polycrystallin kamacite with Fe93%Ni7%, and taenite with Fe50%Ni50% and cloudy taenite resulting from Widmanstätten structures, while tetrataenite may not exist. Well-developed Neumann lines carried unusually stable NRM which survived higher than 100mT by AF demagnetization and up to 580°C by thermal demagnetization. The NRM directions of subsamples scattered widely and that may result from the directions of Neumann lines developed in the polycrystallin kamacite. These NRMs might have been acquired by shock about 10 kbar during segmentation of the parent body by collision.

## References

- Azevedo, I.S., Scorzelli, R.B. Danon, J. and Zucolotto, M.E. (1987): *Meteoritics*, 22, 320.  
Funaki, M., Taguchi, I., Danon, J., Nagata, T. and Kondo, Y. (1988): *Proc. NIPR Symp. Antarct. Meteorites*, 1, 231-246.  
Graham, A.L., Bevan, A.W.R. and Hutchison, R. (1985): *Catalogue of meteorites. British Museum (Natural History)*, 246.  
Grunewaldt, H. (1983): *Nova Petropolis: An.Acad. brasil. Cienc.*, 55, (1), 138-139.

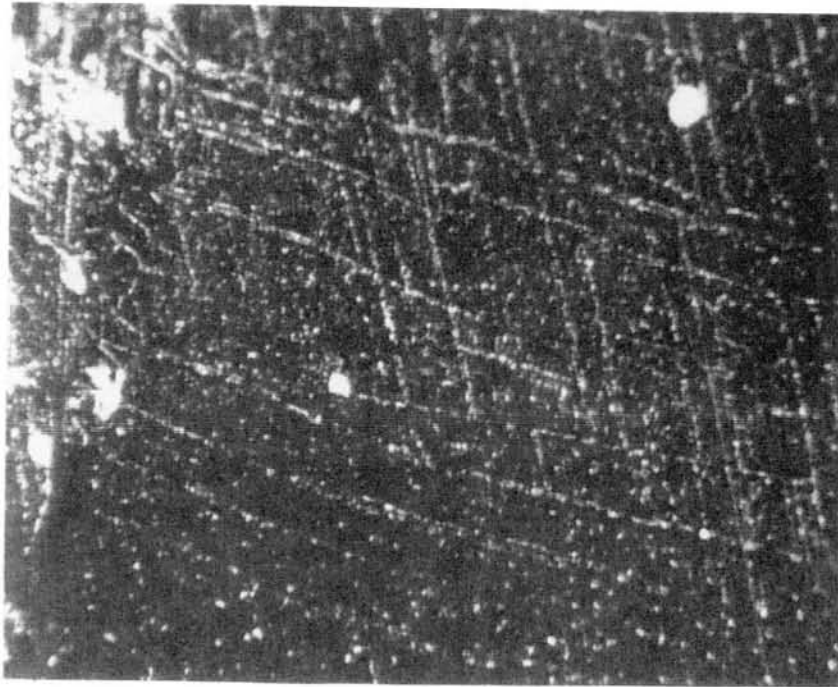


Fig. 2 Neumann lines observed by Bitter pattern on the demagnetized sample at 480°C.

## Carbon, Nitrogen and Neon in Yamato 793605 Lherzolitic Shergottite

Monica M. Grady<sup>1,2</sup>, A. B. Verchovsky<sup>2</sup>, I. P. Wright<sup>2</sup>, and C. T. Pillinger<sup>2</sup>

<sup>1</sup>Department of Mineralogy, The Natural History Museum, Cromwell Road, London SW7 5BD, UK.

<sup>2</sup>Planetary Sciences Research Institute, The Open University, Walton Hall, Milton Keynes MK7 6AA, UK.

**Introduction:** Yamato 793605 (hereinafter Y79) is a 16 g-sized shergottite, originally recognised as a possible martian meteorite by Yanai et al. [1]; measurement of its oxygen isotopic composition confirmed this classification [2, 3]. Subsequent investigation of the petrology and mineralogy of the meteorite [4, 5] placed Y79 in the sub-group of lherzolitic shergottites, along with two other Antarctic meteorites ALHA 77005 and LEW 88516. Y79 contains areas and veins of shock melt [4, 5], and thus, like the shergottites EET A79001 and Zagami, Y79 might also contain trapped martian atmospheric species. Primarily, though, meteorites like Y79 have the potential to relay information regarding processes taking place at depth within the martian lithosphere. It is against a backdrop of the light element geochemistry of martian and terrestrial mantle materials that we have placed our study of carbon, nitrogen and neon in Y79. In the terrestrial scheme, lherzolites are materials from the upper mantle, often represented at the Earth's surface as ultramafic xenoliths entrained in high-level intrusive or extrusive volcanic rocks. Within these xenoliths, carbon may be represented as elemental forms (graphite, diamond) as well as carbonates. Additionally, carbon occurs in terrestrial basalts as a coating of elemental carbon along grain boundaries, as dissolved  $\text{CO}/\text{CO}_2/\text{CO}_3^{2-}$  in silicate minerals [6], in phosphates, and also as fluid inclusions.

**Method:** The relatively low concentrations of carbon, nitrogen and noble gases in terrestrial igneous rocks necessitates the use of specialised analytical protocols; one such technique is "stepped combustion", whereby carbon, nitrogen and noble gases are removed from the sample by heating through a temperature sequence in the presence of oxygen. For gases released at an individual step, carbon is converted to carbon dioxide gas, or nitrogen to the molecular form, which can then be admitted to appropriate mass spectrometers for isotope analysis; the temperature at which the combustion occurs is diagnostic of the original form of the element (organic, elemental, etc.; ref. 7). Trapped gases (carbon dioxide, nitrogen, noble gases) are liberated when the host assemblage begins to soften or melt; carbonates and nitrates, on the other hand, decrepitate at a recognisable decomposition temperature

to give either carbon dioxide or nitrogen irrespective of whether or not oxygen is present. Application of the stepped combustion technique enables the effects of contaminant terrestrial organic compounds or adsorbed atmospheric gases to be resolved from indigenous species, and thus discounted, since materials of this nature are usually released at temperatures less than 450°C. The same techniques can also be applied to martian basalts.

A small fragment of Y79 weighing ~ 100 mg was provided by Dr Kojima and the NIPR, as part of the consortium study. The material was coarse-grained, and contained abundant black melt glass, presumably shock-produced. To prevent loss of any trapped martian gases, the material was not powdered; rather, small chips representing the bulk sample were removed from the main fragment, for analysis. A single chip was analysed for carbon (4.058 mg), and three small chips taken together for nitrogen/noble gas determination (total weight = 18.972 mg).

**Results:** Carbon: The meteorite has the lowest carbon abundance of any martian meteorite analysed so far. Once terrestrial contamination has been removed, Y79 contains only 7.3 ppm carbon with a  $\delta^{13}\text{C} \sim -19\text{‰}$ . Carbon can be divided into four separate components, identified on the basis of combustion temperature and isotopic composition: (1) carbonates (possibly calcite; 1.2 ppm with  $\delta^{13}\text{C} \sim -23\text{‰}$ ); (2) magmatic carbon (1.1 ppm;  $\delta^{13}\text{C} \sim -33\text{‰}$ ); (3) martian atmospheric species and (4) cosmogenic carbon. The isotopically-light carbonate in Y79 conforms to the observations made on other shergottites [8], that these meteorites have not been altered by surficial fluids in contact with the martian atmosphere, but rather contain carbonates produced from primary magmatic fluids.

Nitrogen: Y793605 contains 6.7 ppm nitrogen with  $\delta^{15}\text{N} \sim +20\text{‰}$ , results which are comparable with data from other shergottites. Again, as discussed for carbon, some 73% of the nitrogen is liberated below 600°C; given its isotopic composition, this component is most probably a mixture of adsorbed terrestrial atmosphere with terrestrial organic species. Above this temperature, the variation in  $\delta^{15}\text{N}$  with temperature indicates that several components are present. Above 1300°C is cosmogenic nitrogen;  $\delta^{15}\text{N}$  of +50‰ is a lower limit, implying either incomplete extraction of the component, or mixing with a more  $^{14}\text{N}$ -enriched species (presumably magmatic nitrogen). Between 950°C to 1100°C, 0.03 ppm nitrogen is released, attaining a maximum  $\delta^{15}\text{N} \sim +150\text{‰}$ . Comparison with nitrogen liberated from other shergottites implies that this component is atmospheric nitrogen trapped from the martian atmosphere, again mixed with isotopically lighter magmatic

nitrogen. So, as for carbon, nitrogen in Y79 is a mixture of cosmogenic, magmatic and atmospheric species.

**Neon:** Neon data were acquired simultaneously with nitrogen, but the small temperature increments selected for the analysis resulted in low quantities of the noble gases being released, amounts close to that of the system blank. Only  $^{21}\text{Ne}$  yielded an abundance ( $2.2 \times 10^{-8} \text{ cm}^3\text{g}^{-1}\text{STP}$ ) much higher than the blank, a concentration which, on the basis of  $^{21}\text{Ne}/^{22}\text{Ne}$  and  $^{20}\text{Ne}/^{22}\text{Ne}$  ratios can be rationalised as a mix of  $\sim 10\%$  terrestrial atmospheric neon (from the blank) with cosmogenic neon. From the production rate models of Eugster and Michel for the average chemical abundances and shielding of basaltic achondrites, and assuming the chemistry of Y79 is closer to that of a diogenite than a eucrite, then a very approximate  $^{21}\text{Ne}$  exposure age can be calculated. The resulting value of  $\sim 4$  Myr is, broadly speaking and given the assumptions made, reasonably consistent with the exposure ages of other shergottites ( $\sim 2.5 - 3.5$  Myr; ref. 10).

**Conclusions:** The carbon chemistry of Y79 is very similar to that of other lherzolithic shergottites, although Y79 has a lower overall carbon abundance and heavier isotopic composition, resulting from the influence of martian atmospheric and spallogenic components (the latter despite the short exposure age). Fewer data are available for nitrogen in shergottites, but comparison with the results that have been published show that, as for carbon, Y79 has such a low nitrogen abundance that its overall  $\delta^{15}\text{N}$  is influenced by atmospheric and spallogenic components. In terms of its carbon and nitrogen geochemistry, Y79 is a fairly typical martian igneous rock, unaltered by surficial fluids but retaining a clear magmatic signature in the form of  $^{13}\text{C}$ -depleted carbonates and high temperature carbon dissolved in silicates.

**References:** [1] Yanai, K. *Lunar Planet. Sci. Conf.*, 26, 1533-1534, 1995; [2] Mayeda T.K. et al. *Lunar Planet. Sci. Conf.*, 26, 917-918, 1995; [3] Clayton R.N and Mayeda T.K., *Geochim. Cosmochim. Acta*, 60, 1999-2017, 1996; [4] Mikouchi T. and Miyamoto M., *Proc. NIPR Symp. Antarct. Met.*, 21, 104-106, 1996; [5] Mikouchi T. and Miyamoto M., *Met. Planet. Sci.*, 31, A89-A90, 1996; [6] Mathey D.P. et al., *Geochim. Cosmochim. Acta*, 53, 2377-2386, 1989; [7] Wright I.P. and C.T. Pillinger, *USGS Bulletin* 1890, 9-34, 1989; [8] Grady M. M. et al., *J. Geophys. Res. Planets*, 102, 6750-6760, 1997; [9] Eugster O. and Michel T., *Geochim. Cosmochim. Acta*, 59, 177-199, 1995; [10] Eugster O. et al., *Lunar Planet. Sci. Conf.*, 27, 345-346, 1996.

## Chemical and isotopic constraints on the dynamic recycling of the nebular materials

Akihiko Hashimoto<sup>1</sup> and Tetuya Takahashi<sup>2</sup>, <sup>1</sup>Department of the Earth and Planetary Sciences, <sup>2</sup>Institute of the Low Temperature Sciences, Hokkaido University, Sapporo 060, JAPAN

Shu et al. [1996] attempted an astrophysical modelling of chondrite formation based on their theoretical prediction of the bipolar outflow from T-Tauri stars. We have noticed that several essential features of chondritic meteorites, including the lithophile element fractionation, redox state difference, oxygen and many other isotopic compositions, were left unanswered. In their model only the characteristics of the bipolar outflow were taken into consideration. Watanabe [1995] has studied theoretically the structure of the viscous accretion disk where outflow emerges, and found its non-linear cyclic behavior. His model calculation can provide a fair estimate of physical (e.g. temperature) conditions of the disk where the outflow emerge, if the disk's opacity is given. The latter, however, strongly depends on the state of dust materials under the conditions.

Meteoritic evidence is undoubtedly a master key to the evolution of the nebular nebula. We identify the following meteoritic properties as constraints to develop, with reasonable assumptions, our idea of "dynamic recycling" of chondritic materials that should be driven by the combined action of viscous momentum transfer and bipolar outflow. We make a temporal use of the estimate by Watanabe [1995, also per. comm.] for properties of the accretion disk and bipolar outflows, but hope to constrain them in turn with more quantitative arguments.

(1) **Two trends of lithophile element fractionations:** Carbonaceous chondrites (CM, CV, and CO types) are relatively enriched in Al, Ca, Ti, and other refractory lithophile elements relative to the solar elemental abundances, while ordinary and enstatite chondrites in general are depleted in these elements [Larimer and Anders, 1967]. The latter two chondrite classes have uniform bulk Si/Mg atomic ratios that are resolvable from each other and higher than that of carbonaceous chondrites [Larimer, 1979].

(2) **Redox states of chondrites:** Carbonaceous chondrites overall exhibit a high oxidation state. Ordinary- and enstatite-chondrites are more reduced than C-chondrites in this order [Urey and Craig, 1953].

(3) **<sup>16</sup>O enrichment in petrographic components in chondrites:** An up to 40‰ enrichment of pure <sup>16</sup>O relative to SMOW is known for CAIs [Clayton *et al.*, 1977]. FUN inclusions have additional, mass-dependent isotope fractionations [Lee *et al.*, 1980; Wasserburg *et al.*, 1977]. Chondrules in carbonaceous chondrites have lesser but distinct <sup>16</sup>O enrichments [Clayton *et al.*, 1983].

(4) **Presence of <sup>26</sup>Al at the time of formation:** The majority of normal coarse- and fine-grained CAIs have canonical <sup>26</sup>Al/<sup>27</sup>Al values of  $\sim 5 \times 10^{-5}$ , while FUN inclusions and chondrules have no live <sup>26</sup>Al at the time of formation [MacPherson *et al.*, 1995].

(5) **Cooling rates of chondrules and CAIs:** Chondrules exhibit textures believed to have formed in melting and rapid cooling, from  $\sim 100$  to a few 1000 K/hr depending on their textural types and chemical compositions [Hewins, 1988]. CAIs' estimated cooling rates are much smaller,  $\sim 1$ -10 K/hr [Stolper and Paque, 1986], both for normal and FUN CAIs.

Shu *et al.* [1996] proposed a model that CAIs formed during the embedded phase of the nebular disk, by melting and evaporation of chondritic dustballs in the bipolar outflow (x-winds), and chondrules during the revealed phase by a similar process but not much of evaporation. Kuramoto [per. comm.] argues that during the embedded phase the amount of the material which originates from such recycling should account for only a negligible fraction of the disk material, due to a predominantly abundant nebular material that falls onto the disk surface from the outer nebular envelope. Watanabe, therefore, suggests that both CAIs and chondrules must be produced during the revealed phase which we observe as a classical T-Tauri star. We envisage formation of CAIs and chondrules as follows.

By the action of angular momentum transfer of yet intensively studied mechanism, the nebular material consisting of gas and dust gradually falls inward to the sun. Larger dust grains lose their momentum by decoupling from the gas motion and fall faster than the gas and finer dust would. At typical  $R_x$  (distance from the center of the protosun)  $< 0.1$  AU, bipolar flows emanate from the disk where temperature is supposed high. Adopting the parameters (mass flux:  $1 \times 10^{-7}$  M $\odot$ /yr, turbulent Mach number: 0.01, luminosity: 2.5 L $\odot$ , and  $R_x$ : 0.08 AU), Watanabe obtain the temperature and pressure on the midplane of

the disk to be  $\sim 0.04$  atm and 1800 K, and the temperature at the disk surface (shade) to be 1000 K. At a smaller  $R_x$  these values become larger. Using vacuum evaporation rates of a chondritic material, obtained by Wang [1995], it would take 50 days at 2000 K to produce a molten CAI with a diameter of 10 mm (nearly a maximum size of actual CAIs observed in carbonaceous chondrites) from a pore-free, compact, chondritic dustball of 25 mm in diameter. Although an ambient pressure, reactions with  $H_2$ , and a diffusional efficiency of the generated vapor would affect actual evaporation rate, this estimate is within the predicted residence time, a few to 100 days, of dust grains with  $d = 10$  to 100  $\mu m$  before they are lifted up by the outflow. Thus, CAIs can be produced inside the disk before they are launched. Travelling in the temperature gradient from 2000 to 1000 K within a few to 100 days means a cooling rate of 0.5-20 K/hr, being consistent with a range of experimentally determined cooling rate for CAIs,  $\sim 1$ -10 K/hr.

The conditions are too extreme for chondrules to form, as basically most of the Mg and Si contained in the chondritic material become vapor. The vapor, however, should migrate by turbulent mixing to a cooler part near the disk surface, and recondense as ultra-fine dust particles of nano- to micrometers. Their aggregates, with frequent, large dust grains that escaped from evaporation, would be launched by the outflow. When this happens, they are exposed to an intense solar radiation. Effective melting temperatures of ultra-fine dust, which can be 0.8 times as low as those of the bulk materials, and probably "fractal melting" as suggested by Shu et al., would ease melting of the fluffy dustballs. The melting must be brief because once their surface become compact, the effective melting point is abruptly raised to that of the bulk material. This would explain frequent occurrence of sub-rounded crystals in actual chondrules, that must have escaped total melting due to large grain size. The cooling must be rapid with this mechanism, but it is yet to be investigated whether it explains the actual cooling rates of chondrules.

We agree with M. Thieme [1996] that the non-mass-dependent oxygen isotope effects, or  $^{16}O$  enrichment, in CAIs and chondrules inside carbonaceous chondrites are caused by chemical kinetics between oxygen radical ( $O^*$ ) and abundant, oxygen-bearing molecules such as CO and  $CO_2$ . The oxygen radical is most likely provided by photodissociation of  $H_2O$  [Shu et al., 1996] near the surface of the disk which are exposed to the intense sunlight. The oxygen radical rich in pure  $^{16}O$  is adsorbed onto dust surface and incorporated into the solid. We assume that dust grains become "saturated" with the  $^{16}O$ -rich radical by the time they reach within  $\sim 0.1$  AU from the sun. According to Watanabe, the activity of the protosun and concomitantly of the nebula has a non-linear cycle. It is possible that the chemical kinetics to generate 40‰ enrichment in  $^{16}O$  was complete during the high activity stage owing to a sufficient flux of high energy UV, thus chondritic dust quenched this signature, while during the low activity stage the chondritic dust inherited incomplete reaction. Alternatively,  $^{16}O$  enrichment in the solid was diluted with normal oxygen isotopes of CO during evaporation and recondensation of dust before chondrule formation.

During evaporation of chondritic dustballs to generate CAIs their oxygen isotopic composition did not change for two possible reasons: Davis et al. [1990] and Wang [1995] showed that the oxygen isotopic compositions of forsterite and a synthetic chondritic material did not change by vacuum evaporation when evaporation occurred from the solid forsterite, but they became significantly mass-fractionated when evaporation was done from the molten state. This led them suggest that normal CAIs formed by evaporation of chondritic materials that occurred mostly from the solid state, while FUN CAIs formed from the molten chondritic material. Alternatively, normal CAIs formed nearly in equilibrium state due to a confining effect by the ambient pressure, in which case mass-dependent isotope fractionations are very small [Richter and Davis, 1997]. We suggest that FUN CAIs were produced near the inner edge of the accretion disk,  $R_x < 0.08$  AU, where temperature is higher due to intense solar radiation (hence consistent with the evaporation from the molten state), and the pressure is lower (actually it is closer to vacuum between the protosun and the inner edge of the disk [Shu et al., 1996]). Normal CAIs formed behind the edge,  $R_x > 0.08$  AU, where temperature is relatively lower and pressure is high. The large mass fractionations in Mg and Si isotopes observed in FUN CAIs, and the lack, or very small magnitudes, of such fractionations in normal CAIs also support this idea.

Clayton and Jin [1995] proposed a nuclear reaction origin of excess  $^{26}Al$  from Mg by bombardment of solar energetic particles, as opposed to its synthesis in late star developments such as super novae. As a consequence of extensive evaporation of chondritic materials, there must have been abundant Mg vapor inside the disk where CAIs formed. Solar energetic particles may penetrate to certain depths of the disk, and react with Mg to form  $^{26}Al$ . Because Al is very refractory, it would immediately condense onto

existing solids, viz. CAIs. The enrichment of  $^{26}\text{Al}$  into CAIs would be efficient if CAIs stayed long at the place; the large size of CAIs prevent them from being easily carried away by the outflow until successful launches. The Group-II REE pattern of fine-grained CAIs suggests that they were recondensates from the gas that contained all of the elements except for super-refractory ones. Therefore  $^{26}\text{Al}$  must have been incorporated inside f-g-CAIs more efficiently than c-g-CAIs would, explaining the observation that f-g-CAIs are often more enriched in  $^{26}\text{Al}$  than the latter. FUN CAIs, on the other hand, did not acquire  $^{26}\text{Al}$  because the generated vapor that contained Mg was efficiently removed from their vicinity due to the nature of virtual vacuum evaporation as invoked from their oxygen, magnesium, and silicon isotope mass fractionations. The lack of excess  $^{26}\text{Al}$  in chondrules is explained in several ways. (a) The nuclear production rate of  $^{26}\text{Al}$  is very small compared to a typical residence time scale of the vapor, as the vapor accompanies outflows with no problem. (b) Alternatively, chondrules formed during low activity stages of the non-linear bipolar flow cycle, when the energy and flux of solar energetic particles were diminished.

It is believed that the solar nebula started out as a cold interstellar medium. At  $\sim 100$  K the nebula contained an overwhelming,  $\text{H}_2$ -dominant gas and dust that consists of silicate materials ("dust"), carbon-rich material ("tar"), and icy material rich in  $\text{H}_2\text{O}$  ("ice") according to Wood and Hashimoto [1993]'s criterion. The dust aggregates that had grown in size by mutual sticking became concentrated in the midplane, causing dust enrichment relative to the nebular gas. By evaporation of  $\text{H}_2\text{O}$  ice, the inner part of the accretion disk was more oxidized compared to the canonical nebular oxygen fugacity; at  $R_x \sim 0.1$  AU evaporation and recondensation of chondritic dust generated chondrules with high FeO content, CAIs, and less metal. As CAIs and chondrules were transported by the bipolar outflow, the disk became enriched in these recycled materials of high-temperature origin. The overall chemical composition of the disk at a distance from the sun became more refractory relative to the solar elemental abundances. This accounts for the origin of carbonaceous chondrites. As the disk activity went down, they in turn became a starting material to form ordinary and enstatite chondrites, because there is not much material left to fall on from the surrounding nebula. The ice had evaporated and gone via the outflow to the space and also via the funnel flow to the sun [Shu et al., 1996]. Therefore, the dust aggregates of the second generation were enriched in carbon (tar) relative to oxygen ( $\text{H}_2\text{O}$ ), creating a reducing environment. At this stage temperature was not high enough even at  $R_x < 0.1$  AU to cause nearly total evaporation of solid grains. Partial evaporation of chondritic materials is known to generate Si-rich vapor relative to Mg under both equilibrium [Grossman, 1972] and non-equilibrium [Hashimoto, 1983] conditions, and also for fractionated nebular systems [Wood and Hashimoto, 1993]. Therefore, recondensated materials inside the disk during a late, less-active phase must be enriched in Si relative to Mg. Fluffy dustballs were then lifted by the outflow and became molten by the mechanism outlined above. Because the outflow's density and speed were significantly smaller than those in the active, revealed phase of the nebula, the Mg-rich evaporation residues that must have grown in size by coagulation could not be lifted by the outflow. They must have accumulated in close orbits to the sun and finally fallen to the latter.

## References

- (1) Clayton, D.D., and Jin, L. 1995. *Astrophys. J.* **451**, L87-L91.
- (2) Clayton, R.N., Onuma, N., Grossman, L., and Mayeda, T.K. 1977. *Earth Planet. Sci. Lett.* **34**, 209-224.
- (3) Clayton, R.N., Onuma, N., Ikeda, Y., Mayeda, T.K., Hutcheon, I.D., Olsen, E.J., and Molini-Velsko, C. 1983. *Chondrules and Their Origins*, ed. E.A. King (Houston, Lunar Planet. Inst.), pp. 37-43.
- (4) Davis, A.M., Hashimoto, A., Clayton, R.N., and Mayeda, T.K. 1990. *Nature* **347**, 655-658.
- (5) Grossman, L. 1972. *Geochim. Cosmochim. Acta* **36**, 597-619.
- (6) Hashimoto, A. 1983. *Geochem. J.* **17**, 111-145.
- (7) Hewins, R.H. 1988. *Meteorites and the Early Solar System*, ed. J.F. Kerridge and M.S. Matthews (Univ. of Arizona Press), pp. 660-679.
- (8) Larimer, J.W., and Anders, E. 1967. *Geochim. Cosmochim. Acta* **31**, 1239-70.
- (9) Larimer, J.W. 1979. *Icarus* **40**, 446-454.
- (10) Lee, T., Mayeda, T.K., and Clayton, R.N. 1977. *Geophys. Res. Lett.* **7**, 493-496.
- (11) MacPherson, G.J., Davis, A.M., and Zinner, E.K. 1995. *Meteoritics* **30**, 365-386.
- (12) Richter, F.M., and Davis, A.M. 1997. *Lunar Planet. Sci.* **XXVIII**, 1161-62.
- (13) Shu, F.H., Shang, H., and Lee, T. 1996. *Science* **271**, 1545-52.
- (14) Stolper, E., and Paque, J.M. 1986. *Geochim. Cosmochim. Acta* **50**, 1785-1806.
- (15) Thiemens, M.H. 1996. *Chondrules and the Protoplanetary Disk*, ed. Hewins, R.H., Jones, R.H., and E.R.D. Scott, Cambridge Univ. Press, pp. 107-118.
- (16) Urey, H.C., and Craig, H. 1953. *Geochim. Cosmochim. Acta* **4**, 36-82.
- (17) Wang, J. 1995. Ph.D. Thesis, University of Chicago.
- (18) Wasserburg, G.J., Lee, T., and Papanastassiou, D.A. 1977. *Geophys. Res. Lett.* **4**, 299-302.
- (19) Watanabe, S. 1995. *The Fall Meeting of the Japan Society of the Planetary Science*, pp.104 [abstract].
- (20) Wood, J.A., and Hashimoto, A. 1993. *Geochim. Cosmochim. Acta* **57**, 2377-88.

**ORIGIN OF VESTA-LIKE ASTEROIDS SUGGESTED FROM PLANETARY SURFACE ALTERATION TREND OF VIS-NIR REFLECTANCE SPECTRA OF HED METEORITES.** TAKAHIRO HIROI, Department of Geological Sciences, Brown University, Providence, RI 02912, USA.

### **1. Introduction**

Asteroid 4 Vesta has been long known to have a basaltic surface composition similar to HED meteorites [1]. Vesta's surface heterogeneity was detected from its reflectance spectra at various rotational phases [2], suggesting the possibility of eucrite or howardite covered surface with large craters excavating diogenite and dunite layers [3]. The existence of such craters was supported by a recent 4-color observation of Vesta by Hubble Space Telescope [4], which also suggests existence of old basaltic crust. These two studies suggest that the impact events which created those craters did not resurface Vesta globally.

On the other hand, 20 small (5-10 km) Vesta-like asteroids (Vestoids) were found inside Vesta family and in between the Vesta-family orbit and the 3:1 Kirkwood Gap [5]. Although it seems obvious that these Vestoids in Vesta-family were created in a collisional event with Vesta, the origin of Vestoids, especially those outside Vesta family, is not clear [6]. Analyses of reflectance spectra of Vesta and Vestoids showed significant compositional differences or space weathering of Vestoids in comparison with HED meteorites [7].

In this paper, the reflectance spectra study [7] is revisited to see any space weathering trend among Vestoids suggesting their origin in comparison with fresh HED powders and two HED samples altered by a natural impact melting process and an artificial irradiation by laser beam.

### **2. Experimental**

Telescopic reflectance spectra of Vesta and 20 Vestoids were taken from [5], and laboratory reflectance spectra of HED meteorites powders ( $<25 \mu\text{m}$ ) were taken from [7]. As a simulant of a space-weathered HED meteorite, reflectance spectra of Johnstown diogenite sample ( $<75 \mu\text{m}$ ) before and after laser-irradiation were taken from [8].

In addition, a relatively dark portion of from Padvarninkai eucrite was ground into powder of  $<25 \mu\text{m}$  and its reflectance spectrum was measured. The portion of Padvarninkai eucrite has dispersed troilites and possibly oxides, finely crystallized melt grains, and other mineral fragments, suggesting its shock origin [9].

### **3. Effects of Laser-Irradiation and Shock**

Reflectance spectra (0.3-2.6  $\mu\text{m}$ ) of Johnstown diogenite (untreated and laser-irradiated) and Padvarninkai eucrite (bulk and impact melt) are shown in Fig. 1. As shown in Fig. 1a, both the laser-irradiated diogenite and the impact melt of eucrite are much darker and their absorption bands around 1 and 2  $\mu\text{m}$  seem to be much weaker than their untreated or bulk samples. Similar effects were reported for shocked enstatite and labradorite [10].

When these spectra are scaled to 1.0 at 0.56  $\mu\text{m}$  in Fig. 1b, it becomes clear that the altered samples show weaker 1 and 2  $\mu\text{m}$  bands, redder (increasing reflectance toward longer wavelength) around the 2  $\mu\text{m}$  band, and slightly altered (smoothed) visible spectral profile in the 0.3-0.75  $\mu\text{m}$  range. Although these two alteration processes are very different except for the fact that both produce glass grains, apparent spectral alteration effects shown here are not too different.

#### 4. Trend of Spectral Alteration of Vestoids

In order to find any trend of spectral alteration of Vestoids in comparison with fresh HED meteorites and the altered ones, the following spectral parameters are defined:

$$1\text{-}\mu\text{m band depth} = \ln R_M - \ln R_C$$

$$\text{Visible redness} = \ln R_M - \ln R_{55}$$

where  $R_M$  indicates the reflectance maximum around  $0.74 \mu\text{m}$ ,  $R_C$  at the  $1\text{-}\mu\text{m}$  band center, and  $R_{55}$  at  $0.55 \mu\text{m}$  as defined in [7]. A plot of the  $1\text{-}\mu\text{m}$  band depth vs. the visible redness is shown in Fig. 2.

As seen in Fig. 2, there is a trend of spectral alteration (broken lines) where the altered HEDs (M and L) and majority of Vestoids in Vesta family (filled squares) have shallower  $1\text{-}\mu\text{m}$  bands and redder visible spectral profiles than the fresh HEDs (H, E, and D). This trend is the same with the space weathering trend known for lunar samples and possibly the S asteroids. On the other hand, majority of Vestoids outside Vesta family (open squares) do not follow the above trend but have redder visible spectral profiles and similar  $1\text{-}\mu\text{m}$  depths to the fresh HEDs.

#### 5. Origin of Vestoids and HED meteorites

The result suggests a possibility that many Vestoids in Vesta family are altered HEDs which could come from Vesta and Vestoids outside Vesta family came from a different source. In that case, Vestoids outside Vesta family could be the remnants the impactor which collided with Vesta at an oblique impact angle and escaped toward the 3:1 Kirkwood Gap, producing ejecta from Vesta which became Vestoids in Vesta family and HED meteorites. And the reason why Vesta's spectrum seems fresher than many Vestoids should be due to partial resurfacing event on Vesta which excavated fresher internal materials of Vesta and must have occurred after Vestoids in Vesta family were ejected from Vesta.

However, the results here will not eliminate the possibility that Vestoids were non-HED asteroids which had a grazing impact with Vesta [6]. In this case, some of such asteroids had greater interaction with Vesta causing themselves coated with HED materials from Vesta and became members of Vesta family. Other Vestoids had lesser interaction with Vesta, thus were not covered with HED materials so extensively, and escaped toward the 3:1 Kirkwood Gap. The reason why Vesta seems to be fresher than Vestoids, in this case, is that Vestoids have different mineral composition underneath the HED coating, which have been gradually lost, making Vestoids' spectra less similar to HEDs than Vesta.

**Acknowledgments:** Antarctic meteorites were loaned from National Institute of Polar Research and Meteorite Working Group, Juvinas eucrite from the Field Museum of Natural History, and the other meteorites from the Planetary Materials Database Collection of Mineralogical Institute, University of Tokyo. The author especially thanks Drs. H. Takeda and A. Yamaguchi for Padvarninkai eucrite and Dr. J. Wasson for permission of using reflectance spectrum of Laser-irradiated Johnstown diogenite. Reflectance spectra of the above meteorite samples were measured at RELAB in Brown University. RELAB is a multiuser facility operated under NASA grant NAGW-748.

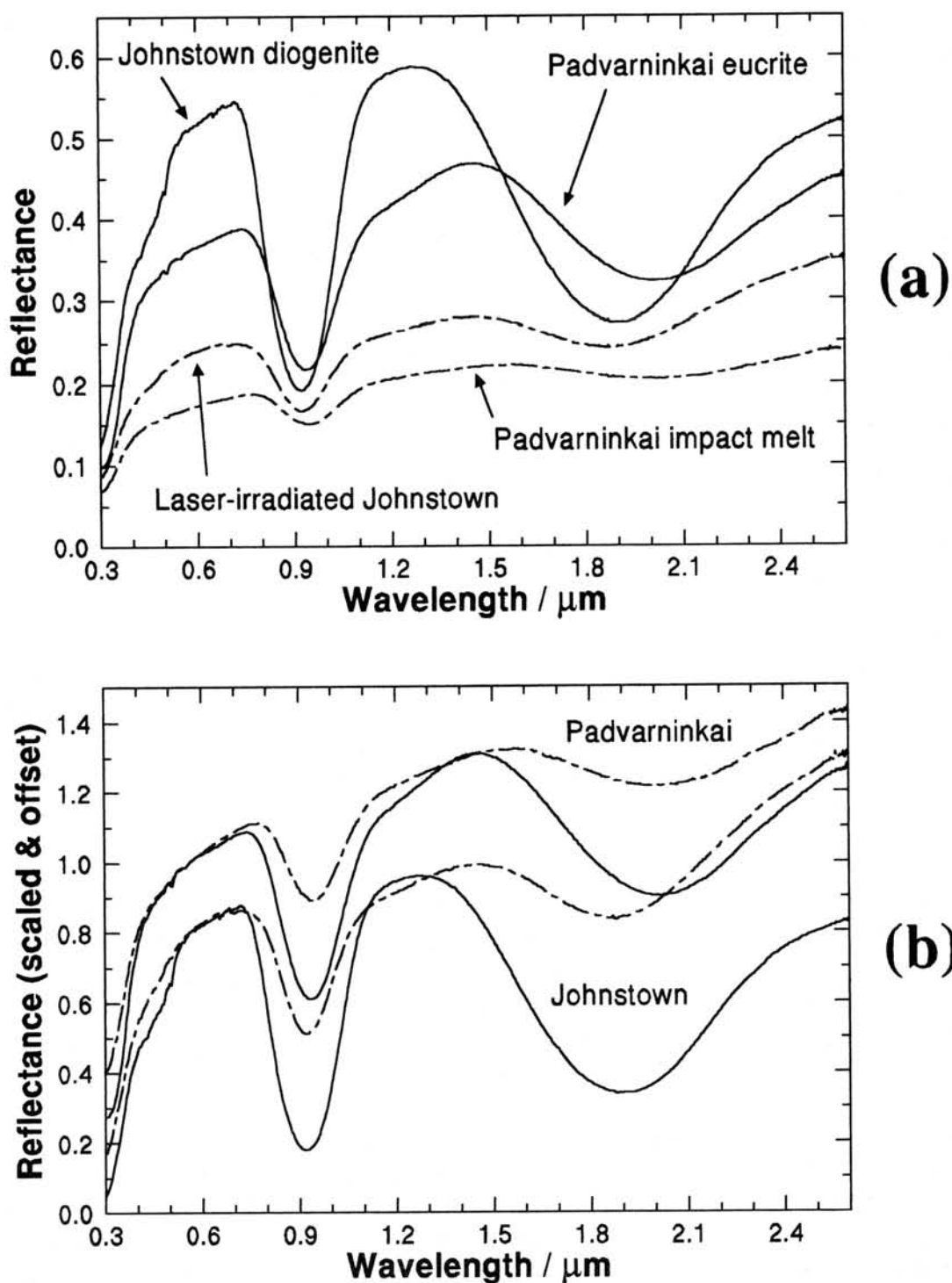


Fig. 1. Visible-NIR reflectance spectra of Johnstown diogenite samples ( $<75 \mu\text{m}$ ) before and after laser-irradiation experiment [8], and the bulk [7] and impact melt samples ( $<25 \mu\text{m}$ ) of Padvarninkai eucrite. Reflectances are plotted in actual value in (a), and scaled to 1.0 at 0.56  $\mu\text{m}$  and offset in (b).

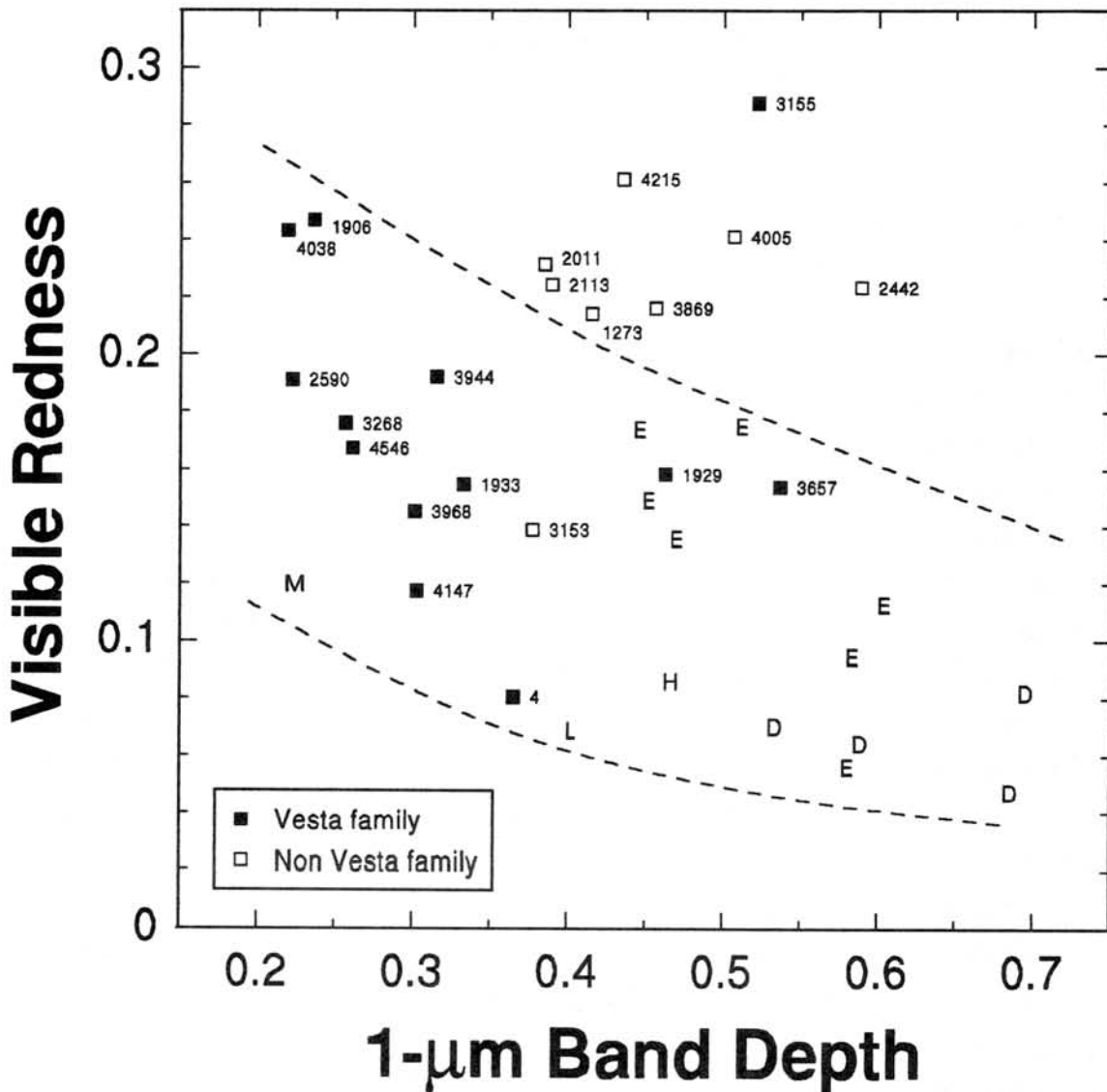


Fig. 2. A plot of the 1-μm band depth vs. the visible redness of reflectance spectra of Vesta, Vestoids, and fresh and altered HED meteorites. Filled squares indicate Vestoids in Vesta family, open squares Vestoids outside Vesta family, with asteroid number listed next to each marker. H, E, and D indicate howardite, eucrite, and diogenite, respectively. M and L indicate the impact melt sample of Padvarninkai eucrite and the laser-irradiated sample of Johnstown diogenite.

**References:** [1] McCord T. B. *et al.* (1970) *Science* **168**, 1445-1447. [2] Gaffey M. J. (1983) *Lunar Planet. Sci.* **14**, 231-232. [3] Gaffey M. J. (1997) *Icarus* (in press). [4] Binzel R. P. (1997) *Icarus* (in press). [5] Binzel R. P. and Xu S. (1993) *Science* **260**, 186-191. [6] Wasson J. T. (1995) *Meteoritics* **30**, 595. [7] Hiroi T. *et al.* (1995) *Icarus* **115**, 374-386. [8] Wasson J. T. *et al.* (1997) *Lunar Planet. Sci.* **28**, 1505-1506. [9] Yamaguchi A. (1997) Personal communications. [10] Adams J. B. *et al.* (1979) *Lunar Planet. Sci.* **10**, 1-3.

# A Preliminary Study of Oxygen Isotopes in an Allende CAI Using an Ion Microprobe

Hajime HIYAGON

Department of Earth and Planetary Physics, University of Tokyo,  
Yayoi 2-11-16, Bunkyo-ku, Tokyo 113, JAPAN

## Introduction

Calcium-Aluminum-rich Inclusions (CAIs) in chondritic meteorites have great importance in understanding early history of the solar system because (1) they apparently retain information of the high temperature events (such as evaporation/condensation processes) in the early solar system, (2) they show the oldest ages in the solar system materials, (3) they show distinct isotopic anomalies in oxygen (and also in titanium, calcium, etc.) and (4) they also show isotopic anomalies in  $^{26}\text{Mg}$  most likely due to *in situ* decay of  $^{26}\text{Al}$  [e.g., 1, 2, 3]. Since it is known that there are grain to grain variations in the oxygen isotopic compositions even in a single CAI, it would be important to analyze micro-distributions of oxygen isotopic compositions to understand the processes which formed CAIs. An ion microprobe would provide a powerful tool for this [e.g., 4-7]. The purpose of this study is to develop the technique of *in situ* spot analysis of oxygen isotopes (both for  $^{17}\text{O}/^{16}\text{O}$  and  $^{18}\text{O}/^{16}\text{O}$  ratios) in CAIs using an ion microprobe. This is an ongoing project and I will report recent technical improvements in our laboratory and some preliminary results on an Allende CAI.

## Experimental

In the last NIPR Symposium on Antarctic Meteorites, I presented a paper about *in situ* spot analysis of oxygen isotopes in an Allende chondrule, which was done using a CAMECA ims-6f ion microprobe in the University of Tokyo. In the present work, I modified some analytical conditions. In order to analyze oxygen isotopes in individual minerals (e.g., spinel) in a CAI, the size of the  $\text{Cs}^+$  primary beam (10kV) was tuned to be  $\sim 20\mu\text{m}$  in diameter. Negative secondary ions of  $^{16}\text{O}$ ,  $^{17}\text{O}$   $^{16}\text{O}^1\text{H}$  and  $^{18}\text{O}$  accelerated at -9.5kV were analyzed at a mass resolving power of  $\sim 5000$ . In order to improve counting statistics, I tried to use two detectors in the present analysis like a method used in UCLA [5,6]: a Faraday cup (for  $^{16}\text{O}$ ) and an electron-multiplier-based ion counting system (for other ions). A normal-incidence electron gun was used for charge compensation. All the samples were prepared as thin sections; their surface was polished and gold-coated ( $\sim 200\text{\AA}$  in

thickness). Burma spinel, San Carlos olivine and Miyake-jima anorthite were used as terrestrial standards.

### **Technical Problems and Preliminary Results**

The use of a stronger beam intensity ( $\sim 0.2\text{nA}$  for a  $\sim 20\mu\text{m}\phi$  beam in the present study vs  $\sim 1\text{nA}$  for a  $\sim 80\mu\text{m}\phi$  beam in the previous work) and two detectors enabled a better precision ( $<1$  permil) even within a relatively short analysis time ( $\sim 20$  minutes) at a face value. However, it turned out that the overall reproducibility was not as good as expected, especially when the analytical condition (e.g., beam shape) was modified slightly. The cause for this is not certain at present, but the observed variation in the  $^{17}\text{O}/^{16}\text{O}$  and  $^{18}\text{O}/^{16}\text{O}$  ratios seems to follow the slope 1 correlation rather than the slope 1/2 correlation (i.e., instrumental mass fractionation). This suggests that some kind of instability in the ratio of detection efficiencies of the two detectors is one possible cause for the variation of the results.

So far, one coarse-grained Type A CAI from Allende meteorite was analyzed. In spite of the problems stated above, all spinel grains so far analyzed (5 grains) show relatively tight cluster (within  $\pm 5\%$ ) in the oxygen three-isotope-diagram with  $^{16}\text{O}$ -rich compositions (both  $\delta^{17}\text{O}$  and  $\delta^{18}\text{O}$  values more than 40‰ lower than those for melilite grains), and the results for spinel and melilite are connected with a slope 1 correlation line. (Note that the analyses for the two minerals were conducted on the same day with the same condition of the ion probe, so that the difference in the oxygen isotopic compositions of these minerals is real.) However, better precision and reproducibility are required to better understand micro-distribution of oxygen isotopic compositions in CAIs.

### **References**

- [1] MacPherson et al. (1988), in *Meteorites and the Early Solar System* (eds., Kerridge and Matthews), pp746-807, Univ. Arizona Press, Tucson.
- [2] MacPherson et al. (1995), *Meteoritics* **30**, 365-386.
- [3] Clayton (1993), *Ann. Rev. Earth Planet. Sci.* **21**, 115-149.
- [4] Yurimoto et al. (1994), *Earth Planet. Sci. Lett.*, **128**, 47-53.
- [5] Choi et al. (1997) *Earth Planet. Sci. Lett.*, **146**, 337-349.
- [6] Leshin et al. (1997) *Geochim. Cosmochim. Acta* **61**, 835-845.
- [7] Saxton et al. (1996), *Meteoritics* **31**, A123.

## Natural Radioactivities in the Brenham Pallasite.

M. Honda<sup>1)</sup>, H. Nagai<sup>1)</sup>, M. Ebihara<sup>2)</sup>, and K. Shinotsuka<sup>2)</sup>

1). Department of Chemistry, College of Humanities and Sciences, Nihon Univ. Sakurajosui, Setagaya, Tokyo 156; 2). Department of Chemistry, Faculty of Science, Tokyo Metropolitan Univ., Hachioji, Tokyo 192-03

In the course of study on cosmogenic nuclides in the stone phase, non-magnetic fraction, and the metal phase, of the Brenham pallasite, we learned that the detections for the radiogenic nuclides,  $^4\text{He}$  and  $^{40}\text{Ar}$ , are difficult, because of the lowest contents (Honda et al, 1996; Nagao et al, 1996). The variations of the productions of cosmogenic nuclides, such as  $^3\text{He}$ ,  $^4\text{He}$  and Argon isotopes and the radio nuclides, in the fragments are found to be extensive by factors of more than 100, which are functions of shielding in the large meteoroid. On the other hand, radiogenic nuclides are supposed to be essentially uniformly distributed, independent of the cosmogenic products.

Some limits in the contents of K and Th + U, could be indicated from the data of excess  $^{40}\text{Ar}$  and  $^4\text{He}$  in the samples, especially recovered from the deep interior which have the lowest contents of cosmogenic nuclide (Nagao et al, 1966). In general for the estimation of K, the important was to determine cosmogenic ratios of  $^{38}\text{Ar}/^{36}\text{Ar}$ , = 1.6--1.75, in the metal (Voshage and Feldmann, 1979), as well as those in stone, as a function of shielding (Fig. 1). Quantitatively, the contents of radiogenic  $^{40}\text{Ar}$  in the metal and in the stone phase, olivine and sulfides, were estimated to be of  $<0.01$  ppmK (Fig. 2).  $^{40}\text{Ar}$  found in the samples were practically entirely from air,  $(7 - 96) \times 10^{-8}$  cc/g both from the stone and metal samples. In the metal,  $(10 - 0.03) \times 10^{-8}$  cc/g  $^{38}\text{Ar}$  have been observed. Only in AMNH881, a high  $^{40}\text{Ar}$ ,  $260 \times 10^{-8}$  cc/g in metal, was found, which has not been interpreted well. If there was no serious escape of radiogenic  $^4\text{He}$ , the contents of Th and U can be estimated at  $10^{-12}$  g/g or lower.

In this paper, we report direct determinations for potassium in the olivine phase of Brenham. The difficulty in this approach is to remove terrestrial contamination of K, which have been introduced by weathering. Decontaminated samples, 100-500mg, were prepared by washing in 1:1 HCl at room temperature. After neutron irradiation, signal of  $^{42}\text{K}$  at 1525 keV gamma,  $t_{1/2} = 12.36$  hrs, produced by  $^{41}\text{K}(n,\gamma)^{42}\text{K}$  was observed within 24 hrs.

The contamination of K was found to be concentrated in the dark

fractions, which are secondary sulfide minerals of iron and nickel, and carbon. The grains of 700 - 75 micrometers are collected by sieve and attacked with (1:1) HCl for more than 3 hrs at room temperature. The irradiated samples were dissolved with HF + nitric acid, or fused with sodium peroxide after addition of K carrier. Potassium tetra-phenyl-borate was recovered. So far, HCl is a convenient reagent to remove >99% of impurities, but some loss, 20%, of the olivine components could not be avoided. The examination for other elements was also performed (Table 1). Even though the contents of Ni and Co seem to indicate the degree of decontamination, the lower level of K could not be traced well by them. The first task is simply to select the least weathered fragments. The best to find such samples was to examine opaque minerals hand picked from original stones and measure K in the HCl solutions by atomic absorption.

Lower contents of heavy lithophile elements like K are rather common among pallasites (Megrue,1968; Miura,1995) and ureilites. The highest level has been reported at 2 ppmK, but none of them lower than 0.1 ppm. In this work, a far lower K content has been confirmed, but still it is not quite certain about the real original value. Quantitative analyses for Th and U are expected to follow those of K. The extensive segregations of lithophile elements from olivine, and sulfides, can be correlated to the formation mechanism of pallasites.

Ref. Honda M. et al (1996) Meteoritics, 31,A63, Megrue G.H.(1968) JGR 73, 2027, Miura Y.N.(1995) dissertation, Nagao K. et al (1996) 21st Symposium,p.128, Voshage H. and Feldmann H. (1979) EPSL 45,293.

Table 1. Compositions of Brenham non-magnetic-fractions:

| Brenham pallasite |               |         |                  |        |              |            |            |            |
|-------------------|---------------|---------|------------------|--------|--------------|------------|------------|------------|
| sample ID         | N 94          | Ward    | Reed 4           | Reed 3 | Reed 1       |            | Ward dark  |            |
| Element           |               |         | Fine:Coarse      | amber  | Coarse       | Fine       | (sulfides) |            |
| HClwash           | 6 N           | 6 N     | 6 N              | unwash | 2 N          | 1 N        | 1N         | unwash     |
| Na, ppm           | 70            | 80      | 79               | 113    |              | 101        | 101        | 160        |
| Al, ppm           |               | 74      |                  |        |              |            |            |            |
| <b>K, ppm</b>     | <b>0.01 #</b> | ----    | <b>0.43;0.55</b> | -----  | <b>0.5 #</b> | <b>1.1</b> | <b>15</b>  | <b>332</b> |
| Ca, ppm           | 35            | 67      |                  |        |              |            |            |            |
| Sc, ppm           | 0.95          | 0.94    | 1.12             | 0.93   | 0.87         | 0.85       | 0.4        |            |
| Cr, ppm           | 150           | 157     | 150              | 187    | 210          | 340        | 854        |            |
| Mn, ppm           | 2923          | 2856    | 2650             | 2500   | 2206         | 2135       | 503        |            |
| Fe, %             | 10.1          | 9.9     | 9.3              | 9.0    | 10.0         | 19.8       | 56         |            |
| Co, ppm           | 8±2           | 15±1    | 5±1              | 28±3   | 29±2         | 128        | 1352       |            |
| Ni, ppm           | 270±142       | 270±117 | 170±109          | 243±18 | 175±70       | 1145±50    | 14700      |            |
| As, ppm           | 0.036         | 0.076   | 0±0.03           | 0.01   | 0.016        | 0.44       | 5.5        |            |
| La, ppb           |               |         |                  |        |              |            | 2000       |            |
| Th, g/g           |               |         |                  |        |              |            |            | 5±3*E-7    |

#: JRR3, E14 n/sec.cm<sup>2</sup>

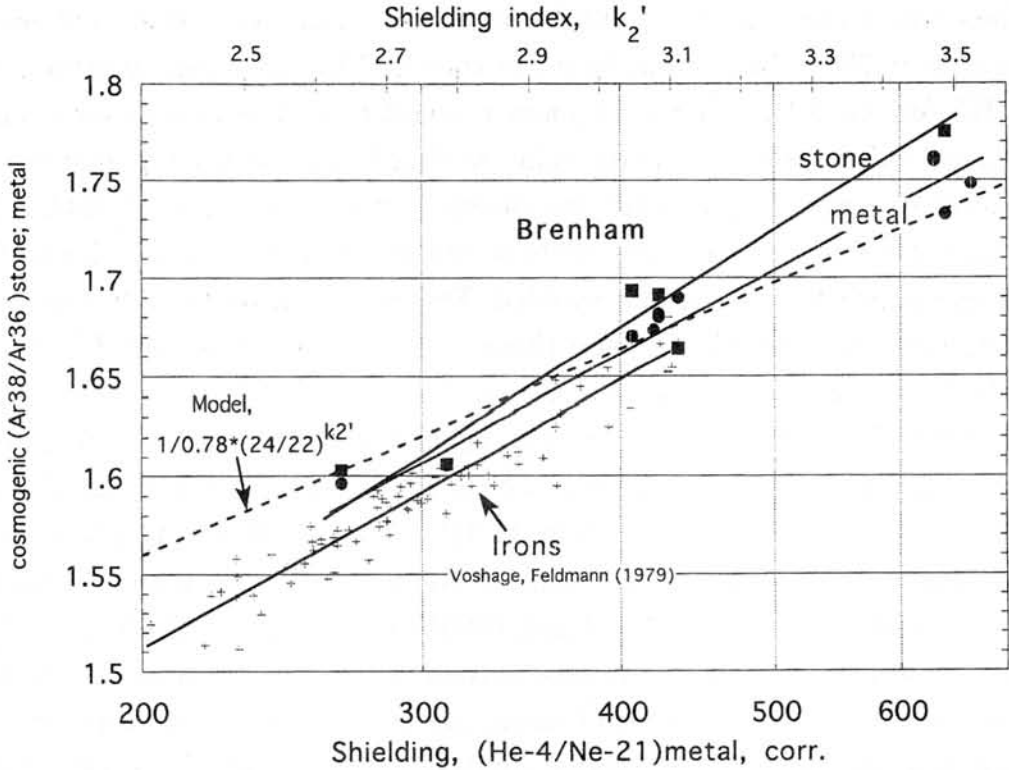


Fig. 1 Ar-38/Ar-36 vs. shielding found in metal and stone phase of Brenham.  $k_2' = 2.24 \cdot \log(\text{He4/Ne21})_m - 2.80$ . Slightly higher 38/36 were observed in stone phase, probably due to additional contributions of Ca.

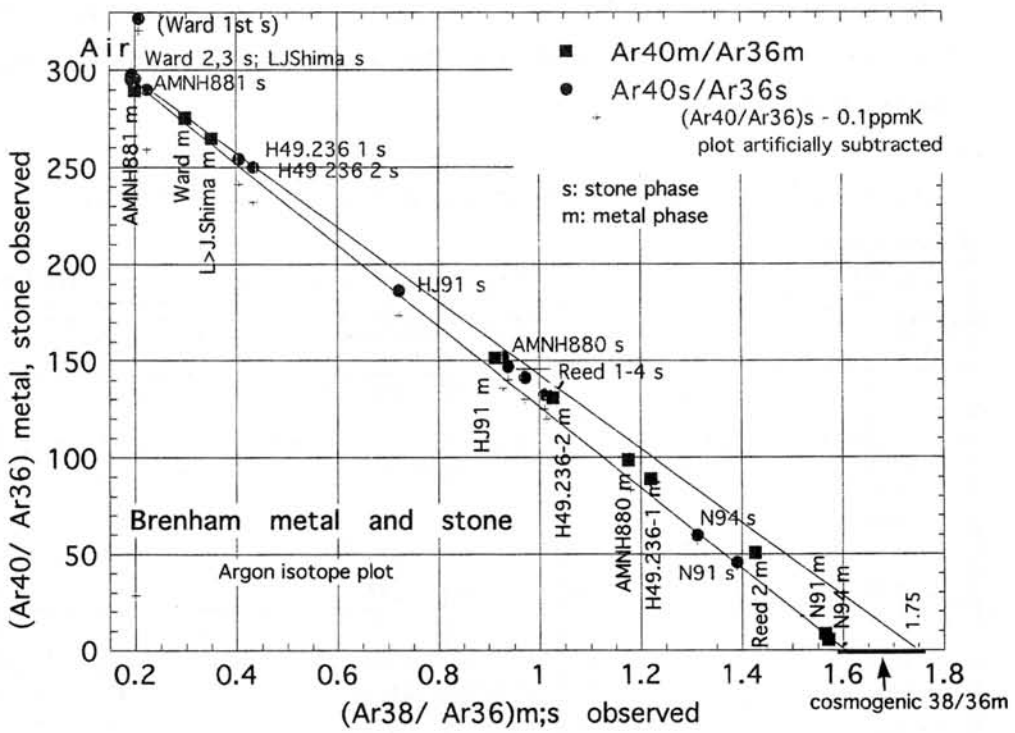


Fig.2 3 isotope plot of Argon in stone and metal of Brenham. Under the plots of stone data, lower levels by reduction of 0.1ppmK are indicated with "+". Only Argon data, "Ward 1st", indicate an exceptionally high value presumably due to contamination in the massspectrometer.

# A new member of CR clan chondrite: Petrology and mineralogy of Yamato-793261

Osamu ICHIKAWA<sup>1</sup> and Hideyasu KOJIMA<sup>1,2</sup>

<sup>1</sup>Department of Polar Science, The Graduate University for Advanced Studies,  
National Institute of Polar Research, 1-9-10 Kaga, Itabashi-ku, Tokyo 173

<sup>2</sup>National Institute of Polar Research, 1-9-10 Kaga, Itabashi-ku, Tokyo 173

**Introduction** Yamato-793261 (Y-793261) chondrite was classified as a CR2 (Yanai and Kojima, 1995). The characteristics of Y-793261 are as follows: anhydrous mafic silicates are reduced (Mg-rich), the matrix is mainly composed of phyllosilicates, and the Co/Ni ratio of the metal is nearly the same as that of CI chondrites. These characteristics are coincide with those of CR clan. But, petrographically, Y-793261 is different from known CR clan chondrites in having average chondrule diameter (320  $\mu\text{m}$ ), low abundance of Fe-Ni metal (1vol%), and high matrix abundance of 60%. This study focuses on the classification of this anomalous chondrite.

**Petrography** Y-793261,51-1 is composed of chondrules, mineral fragments, and matrix. Chondrules are divided into some large chondrules and many small chondrules. Large chondrules are 0.6 to 1.2 (average: 850  $\mu\text{m}$  in average)  $\mu\text{m}$  in diameter, and small chondrules are 90 to 450  $\mu\text{m}$  (average: 210  $\mu\text{m}$  in average). The average size of all chondrules is 320  $\mu\text{m}$ . Large chondrules seem to have dark rims under a microscope. But these can not be distinguished between dark rim and host matrix under a BSE image. Phyllosilicates in chondrules were very rare. Therefore, all chondrules in Y-793261 have hardly experienced aqueous alteration. One chondrule which includes many large metal grains in interior looks like typical CR chondrule. But other chondrules are not including large metal grains. Large opaque mineral grain were hardly observed in the matrix.

The matrix appears opaque under an optical microscope. The matrix of Y-793261 is mainly composed of phyllosilicates. The matrix abundances vary among CR chondrites (Weisberg *et al.* 1993). Y-793261 matrix has high abundance of 60%. The matrix/chondrule ratio for Y-793261 is 1.5, whereas it is 0.6 to 1.1 for most CR chondrites.

**Mineralogy** Most of olivines in magnesian chondrules are between 0 and 1 mol% Fa, and contain 0.0-0.38 wt% MnO and 0.09-0.70 wt% Cr<sub>2</sub>O<sub>3</sub>. On the other hand,

olivines in ferroan chondrules show wide compositional range (up to 70 mol% Fa), and shows compositional zoning. These olivines contain 0.10-0.62 wt% MnO and 0.17-0.85 wt% Cr<sub>2</sub>O<sub>3</sub>. In particular, one small olivine grain which is about 40 μm in diameter shows distinct chemical compositional zoning from magnesian core to ferroan rim. The FeO contents decrease from rim to core, but the MgO contents increase from rim to core (Fa<sub>2-28</sub>). In addition, the CaO and MnO contents increase from core to rim, but Cr<sub>2</sub>O<sub>3</sub> contents decrease from core to rim. These zoning profiles are similar to those of a type II chondrule in ALHA77307 (CO3) (Scott and Jones, 1990) and Semarkona (LL3) (Jones, 1990). Pyroxenes in magnesian chondrules are low-Ca pyroxene with minor high-Ca pyroxene and fassaitic pyroxene with Al<sub>2</sub>O<sub>3</sub> content of more than 5.0 wt%. Ferroan chondrules include low-Ca pyroxene and high-Ca pyroxene. All pyroxene fragments are low-Ca pyroxene. Pyroxenes in ferroan chondrules plot on a line with inclination of the solar Fe to Mn ratio. Pyroxenes in magnesian chondrules and ferroan chondrules contain Cr<sub>2</sub>O<sub>3</sub> up to 1.99 wt% and 0.92 wt%, respectively. Phyllosilicates occurs mainly in the matrix. The chemical compositions of phyllosilicates in the matrix are plotted under the serpentine solid solution line. Alkali contents in it are relatively high (up to 2.5 wt% Na<sub>2</sub>O+K<sub>2</sub>O). Metal occurs in chondrule interior, chondrule rim, and matrix. The Co/Ni ratio of the metal in Y-793261 is nearly the same as that of CI chondrites.

**Discussion** The CR clan consists of five kinds of chondrites: CR chondrites, LEW 85332, Acfer 182, ALH 85085-like chondrites, and Bencubbin-like chondritic breccias (Weisberg et al. 1995). They have dramatically different petrographic characteristics. Their mineralogical, bulk chemical, and oxygen and nitrogen isotopic similarities indicate that they are closely related. CR chondrite group is a main group in the CR clan. The meteorite which is satisfied following 7 items is classified into CR clan chondrite.

- (1) Mg-rich mafic silicates,
- (2) hydrous matrix and/or dark inclusions,
- (3) high modal abundances of Fe-Ni metal,
- (4) Fe-Ni metal having a solar Ni:Co ratio,
- (5) solar abundances of refractory and moderately volatile lithophiles, and highly depleted abundances of volatile lithophiles,
- (6) similar oxygen isotopic compositions of whole rock, and
- (7) anomalously high <sup>15</sup>N abundances.

The characteristics of Y-793261 are: anhydrous mafic silicates are reduced (Mg-rich), the matrix is mainly composed of phyllosilicates, and the Co/Ni ratio of the metal is

nearly the same as that of CI chondrites. In addition, Y-793261 contain low abundance of Fe-Ni metal (1vol%). This chondrite is considered to be member of CR clan, even, there are no the data of (5), (6), and (7) in Y-793261.

On the other hand, the each subgroup of CR clan have shown petrographic differences in:

- (1) chondrule sizes,
- (2) modal abundances of components,
- (3) degree of hydration,
- (4) relative abundance ratio of chondrule textural types, and
- (5) distribution and textural setting of Fe-Ni metal.

Petrographic features of Y-793261 are as follows: having much smaller chondrules (average chondrule diameter is 320  $\mu\text{m}$ ), low Fe-Ni metal abundance (1vol%), and high matrix abundance of 60%. These features of Y-793261 are difference from known CR clan chondrites. So Y-793261 is classified into new type of CR clan chondrite.

### **References**

- Yanai K and Kojima H., comp. (1995) Catalog of the Antarctic Meteorites.
- Weisberg M. K., Prinz M., Clayton R. N., Mayeda T. K., Grady M. M., and Pillinger C. T. (1995) Proc. NIPR Symp. Antarct. Meteorites 8, 11-32.
- WEISBERG M. K., PRINZ M., CLAYTON R. N. and MAYEDA T. K. (1993) Geochim. Cosmochim. Acta 57, 1567-1586.
- Scott E. R. D. and Jones R. H. (1990) Geochim. Cosmochim. Acta 54, 2485-2502.
- Jones R. H. (1990) Geochim. Cosmochim. Acta 54, 1785-1802.
- PRINZ M., WEISBERG M. K., CLAYTON R. N. and MAYEDA T. K. (1993) Lunar and Planetary Science XXIV. Houston, Lunar Planet. Inst., 1185-1186.
- PRINZ M., WEISBERG M. K., CLAYTON R. N., MAYEDA T. K. and EBIHARA M. (1994) Meteoritics 29, 519-520.

# PETROLOGY AND MINERALOGY OF THE Y-793605 MARTIAN METEORITE

Yukio Ikeda

Ibaraki Univ., Dept. of Earth Sciences, Japan

Y-793605 is a lherzolitic shergottite and is very similar in texture and mineralogy to the other two lherzolitic shergottites [1,2], ALHA77005 [3,4] and LEW88516 [5,6], but it is not a pair with the latter two. It has two lithologies, poikilitic and non-poikilitic, and consists mainly of olivine, pigeonite, augite, maskelynite, chromite, ilmenite, non-rhyolitic glass, and pyrrhotite. Small magmatic silicate inclusions occur in olivine and pigeonite, consisting of aluminous high-Ca and low-Ca pyroxenes, rhyolitic glass, feldspathic glass, silica-predominant glass, chromite, and/or ilmenite.

Chromite occurs in olivine, in pigeonite, and in contact with maskelynite. Chromite shows chemical zoning, and the compositional ranges of chemical zoning differ among chromites with different occurrence (Fig. 1); chromite in olivine is the richest in  $Al_2O_3$  as a whole, showing chemical zoning from Al-poor cores to Al-rich rims. Chromite in pyroxene is the richest in  $Cr_2O_3$ , and discontinuous in composition to chromite in olivine. Chromite in contact with maskelynite is the richest in  $TiO_2$ , showing remarkable zoning from Ti-poor cores to Ti-rich rims. The Ti-poor cores of chromite in contact with maskelynite are similar in composition to chromite in pyroxene. These compositional ranges and zoning patterns of chromites indicate that there is compositional discontinuity between chromites in olivine and pyroxene.

Host pyroxene of Y-793605 is mainly pigeonite, and small grains of augite occur in contact with maskelynite. Pyroxene in magmatic silicate inclusions occurring in olivine and pyroxene is similar in major element compositions to the host pyroxene, but is decidedly different in minor element contents; the inclusion pyroxene is richer in  $Al_2O_3$  and  $TiO_2$  and poorer in  $Cr_2O_3$  than the host pyroxene.

Rhyolitic glass in magmatic silicate inclusions has a wide compositional range of alkali and silica contents. The K/Na atomic ratios of the rhyolitic glass range from less than 0.1 up to about 1.0, and they differ among silicate inclusions even if they occur in one olivine grain.

Compositional discontinuity of chromites in olivine and pyroxene, difference in minor element contents between host and inclusion pyroxenes, as well as heterogeneity of rhyolitic glass in magmatic silicate inclusions, suggest that magma mixing took place between crystallization stages of olivine and pyroxene.

Y-793605 experienced secondary alteration. Olivine, opaque minerals (chromite, ilmenite, pyrrhotite), and non-rhyolitic glass have altered at their rims and along fractures in them by introduction of Si, K, and/or S, and loss of Ti, Cr, Mg, Ca, and/or Na, but maskelynite and pyroxene remain unaltered. The alteration may have taken place in Antarctica.

References. [1] Mikouchi, T. and Miyamoto, M. (1996) MAPS 31, Supl., A89-90 (Abst). [2] Mikouchi, T. and Miyamoto, M. (1996) Antarct. Meteor., Papers presented to the 20th Symp. Antarct. Meteor., NIPR, 104-106 (Abst). [3] McSween Jr., H.Y. et al. (1979) EPSL 45, 275-284. [4] Ikeda, Y. (1994) Proc. NIPR Symp. Antarct. Meteor. 7, 9-29. [5] Harvey, R.P. et al. (1993) GCA 57, 4769-4786. [6] Treiman, A.H. et al. (1994) Meteoritics 29, 581-592.

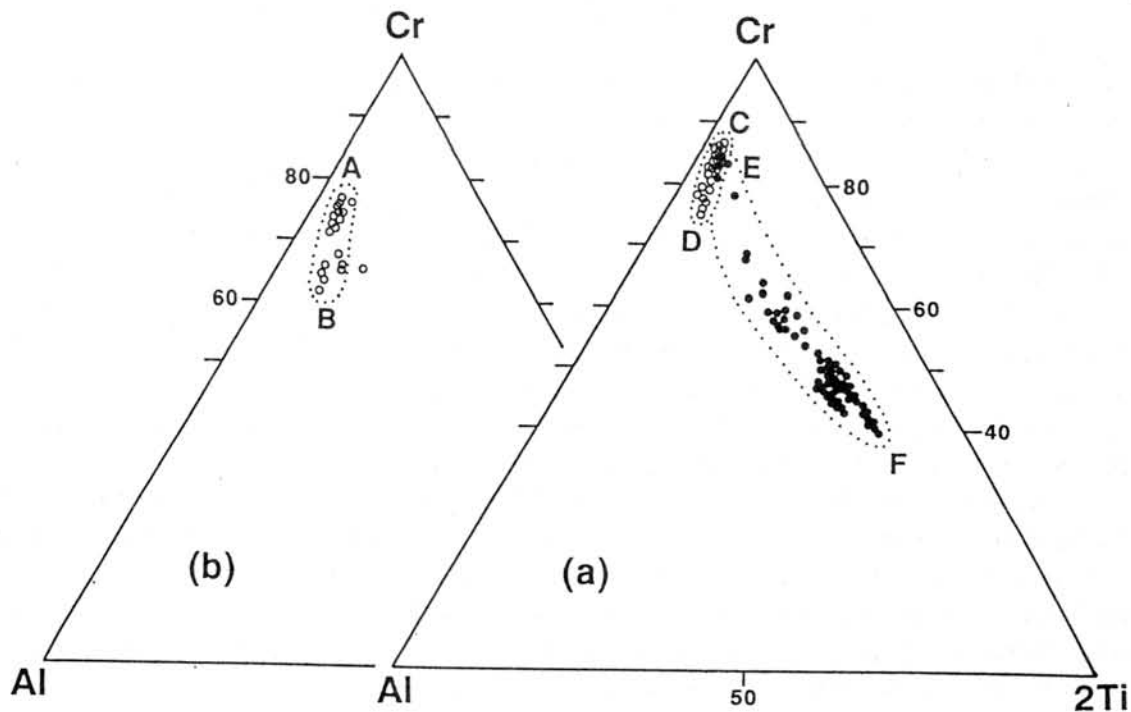


Fig. 1. Chemical compositions (atomic ratio) of chromites in Y-793605. (a) chromite in pigeonite (open circles) has compositional zonation from C to D, and that in contact with maskelynite (solid circles) from E to F. (b) chromite in olivine (open circles) has zonation from A to B.

## On the relationship between opaque mineral assemblages and subtype in CO3 chondrites

N. Imae and H. Kojima

National Institute of Polar Research, Tokyo 173, Japan

A lot of opaque mineral assemblages of metal in the core and corrosion product of sulfide and/or oxide in the rim (OACRs) have been found from unequilibrated chondrites (e. g., Imae, 1994). It has been considered that the assemblages were formed by the subsolidus reaction such as sulfidation and/or oxidation of metals and oxidation of sulfides (e. g., Rubin, 1991; Imae, 1994) though the petrogenesis is in debate. We found that OACRs are especially rich in CO3. It has been reported that CO3s have experienced thermal metamorphism, and metamorphic sequence (subtype) has been proposed (McSween, 1977; Scott and Jones, 1990). Rubin (1989) clarified that there is a relationship between chondrule size and metamorphic sequence in CO3; when metamorphism proceeds, chondrule size tends to become larger. It is highly expected that there is also similar relationships between the grains size and/or rim thickness of OACRs and metamorphic sequence. Since OAs must be more sensitive to the temperature change than silicates, the grain size and rim thickness of OACRs, and the mineral assemblages might become a better indicator of metamorphism. Then we started to study CO3s in National Institute of Polar Research (NIPR) to clarify the general relationship between OACRs and the metamorphic sequence and/or subtype, and obtained preliminary new results.

There are 27 CO3s in NIPR. We found that OACRs commonly occurs from all samples of available Japanese antarctic CO3s (17) by the observation of polished thin sections (PTSs) under the optical microscope (OM) (Table 1). We measured the grain diameter and the rim thickness under the OM from one PTS (about 0.2~1 cm<sup>2</sup>) per a chondrite. The number density of OAs are much smaller than that of chondrules. All OAs do not show the feature of OACR. Then, the number of measurable grains are from a few to about 80 per one PTS (Table 1). Rim is found as sulfide, oxide or the mixture of sulfide and oxide composing two layer. The distinction between the sulfide and the oxide was not be done when the thickness of the rim was measured. In the present study, we only distinguished whether oxide can be found or not in the sample.

The measured grain diameter is in the range of 20-140  $\mu\text{m}$ , and the measured rim thickness is in the range of 4-50  $\mu\text{m}$  for 17 CO3s. Then we found that a larger grain tends to have a thicker rim for each chondrite. We should take into account the cross sectional effect of meteorite samples in order that the distribution of the grain size and the rim thickness may be determined precisely. However, in the present study, we simply averaged the measured size and thickness for simplicity. Fig. 1 shows that a larger grain in average ( $D_{\text{mean}}$ ) has a thicker rim in average ( $d_{\text{mean}}$ ). This means that the relationship that a larger grain tends to have a thicker rim is also satisfied between different CO3s. On the other hand, we determined the number density of OACRs since it is expected that the number density is related to the size and thickness distribution. The relationship between the number density and  $d_{\text{mean}}$  shown in Fig. 2 shows that the number density of OACRs of the sample with a thicker rim is lower.

17 CO3s was subclassified based on the mean fayalite content determined by the random analyses by an electron microprobe analyzer. The source data of random analyses were used as same as Yanai and Kojima (1995). The definition of subtype based on the mean fayalite content appeared in Sears et al. (1991) was used.

Our compilation of the thickness with the subtype is shown in Fig. 3. The similar

relationship can be seen between the grains size of OACRs and the subtype. Most striking feature is that when the subtype is lower,  $D_{\text{mean}}$  and  $d_{\text{mean}}$  are lower, then oxides are found in the PTS, on the other hand, the subtype is higher,  $D_{\text{mean}}$  and  $d_{\text{mean}}$  are larger, then oxide is not found in the sample but sulfide is a dominant opaque mineral except metals. The error of the size and the thickness would be large because the number of the measurement is not abundant, nevertheless, we can conclude that there is a tendency that when the subtype is higher, size and thickness is larger. The boundary that oxide appears or disappears can be determined from Fig. 3. The relationship between the subtype and the number density of OACRs was also shown (Fig. 4). In summary, we found new CO3 features. These might reflect the systematically different thermal history for CO3s.

References:

- Imae N. (1994) *Proc. Japan Acad.* **70**, Ser. B, 133-137.  
 McSween Jr. H. Y. (1977) *Geochim. Cosmochim. Acta* **41**, 477-491.  
 Rubin A. E. (1989) *Meteoritics* **24**, 179-189.  
 Rubin A. E. (1991) *Am. Min.* **76**, 1356-1362.  
 Scott E. R. D. and Jones R. H. *Geochim. Cosmochim. Acta* **54**, 2485-2502.  
 Sears D. W. G. et al. (1991) *Proc. of the NIPR Symp. on Antarctic Meteorites* **4**, 319-343.  
 Yanai K. and Kojima H. (1995) *Catalog of the Antarctic meteorites*. NIPR, Tokyo.

Table 1. Studied 17 CO3 samples

| Name      | Abbreviation | PTS No. | Measured number of OACRs |
|-----------|--------------|---------|--------------------------|
| ALH-77003 | A            | 89-2    | 22                       |
| ALH-77307 | B            | 85-1    | 81                       |
| Y-791131  | C            | 51-1    | 6                        |
| Y-791433  | D            | 51-1    | 4                        |
| Y-791717  | E            | 62-5    | 10                       |
| Y-791745  | F            | 51-1    | 15                       |
| Y-791746  | G            | 51-1    | 7                        |
| Y-791748  | H            | 51-2    | 30                       |
| Y-794088  | I            | 51-1    | 22                       |
| Y-81002   | J            | 51-1    | 15                       |
| Y-81020   | K            | 56      | 17                       |
| Y-81067   | L            | 51-1    | 69                       |
| Y-81068   | M            | 51-1    | 20                       |
| Y-82004   | N            | 51-1    | 17                       |
| Y-82050   | O            | 101-2   | 4                        |
| Y-82094   | P            | 91-1    | 16                       |
| Y-8339    | Q            | 51-1    | 23                       |

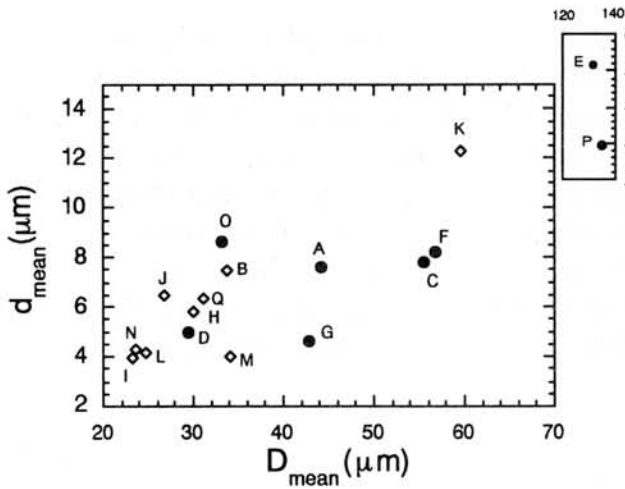


Fig. 1. The relationship between  $D_{\text{mean}}$  and  $d_{\text{mean}}$ : open symbol: oxide is contained in PTS. closed symbol: oxide is not contained in PTS (sulfide is dominant.).

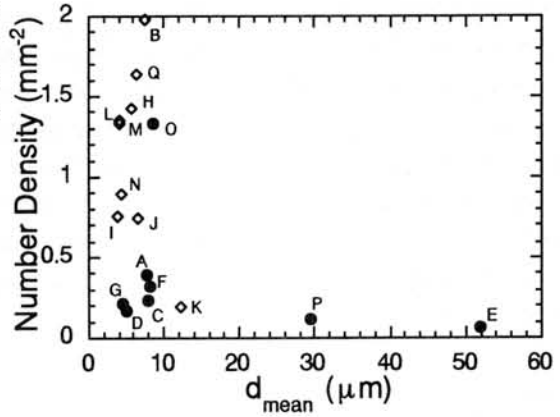


Fig. 2. Number density of OACRs of CO3s and  $d_{\text{mean}}$ : open symbol: oxide is contained in PTS. closed symbol: oxide is not contained in PTS (sulfide is dominant.).

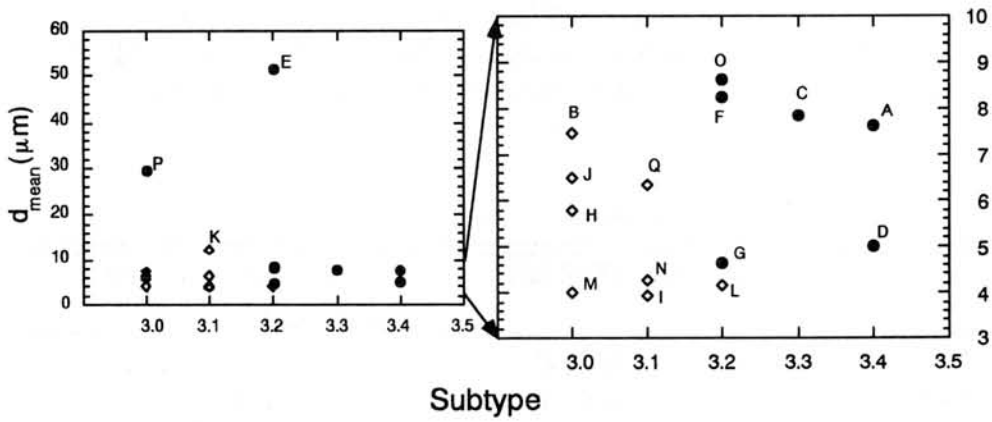


Fig. 3. The relationship between subtype and  $d_{\text{mean}}$ : open symbol: oxide is contained in PTS. closed symbol: oxide is not contained in PTS (sulfide is dominant.).

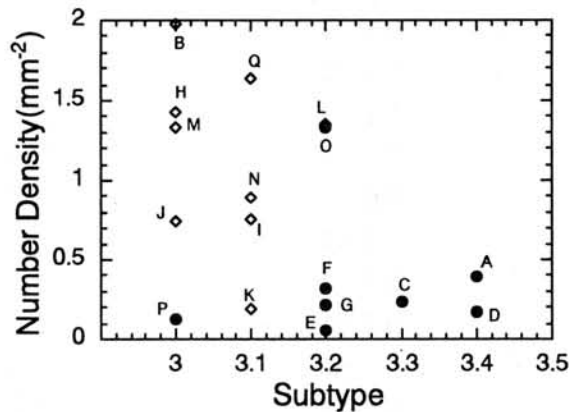


Fig. 4. The relationship between subtype and the number density. open symbol: oxide is contained in PTS. closed symbol: oxide is not contained in PTS (sulfide is dominant.).

# Petrological study of the shock-melted Yamato-790757 LL Chondrite

Yasuo Itoh and Hirokazu Fujimaki

Institute of Mineralogy, Petrology, and Economic Geology,  
Tohoku University, Sendai, Miyagi 980-77, Japan

## Introduction

Yamato-790757 is a shock-melted LL chondrite. Since it is seriously re-crystallized, the petrological type is not determined in the meteorite catalogue reported by NIPR (1987). The thermal and chronological histories of some of the shock-melted Antarctic chondrites were already investigated and reported (e.g., Okano et al., 1990; Fujimaki et al., 1992; Fujimaki et al., 1993). The brief description and preliminary report of Yamato-790757 are included in the catalogue, and it is obvious that the compositional ranges of the included minerals are rather wide, but much narrower than those in the unequilibrated chondrites. We have carried out petrological examination of the shock-melted Yamato-790757 chondrite. The analytical results of the minerals and glasses as well as sample description are reported in this paper.

## Sample Description

Yamato-790757 is a shock-melted LL chondrite. It consists of chondrules, lithic fragments, and nearly crystalline matrix with brown glasses. Only a few chondrules have sharp boundaries, but the others are severely deformed. The crystallinity of the matrix is as good as that of the equilibrated ordinary chondrites.

The size of the thin section provided by NIPR is 10 mm x 10 mm. Most of the chondrules are deformed and do not look like a chondrule. Only eight clear chondrules can be noticed in the thin section. Three of them are obviously radial pyroxene chondrules, and two barred olivine chondrules. The others seem either porphyritic or cryptocrystalline chondrules. All the other chondrule-like crystal aggregates have unclear boundaries. A few lithic fragments consisting of poikilitic olivine and pyroxene can be found. A few rounded aggregates of minerals appear to be totally deformed chondrules, but were treated as lithic fragments. The rounded shapes of the lithic fragments are similar to the shock-deformed lithic fragments (e. g., Rubin, 1985). Minerals in the fragments are mostly anhedral. Matrix is well re-crystallized and contains clear glasses. Euhedral minerals exist in the glasses. Metal and sulfide globules are spread in the matrix.

The total volume % of silicate minerals amounts to approximately 82 %, and melt glasses in matrix to 13%. Since the sample is an LL chondrite, opaque minerals is only 5%. Although brown rust stain can be recognized under the microscope, alteration is not serious. Olivine is dominant and pyroxene associates. The mineral grains are deformed; mosaicism of olivine is obvious and planar fracture as well as undulatory extinction are common for large anhedral olivine crystals. The planar fracture is also common for large anhedral pyroxene crystals, and the undulatory extinction is prevalent. Neither plagioclase feldspar nor maskelynite was found in the thin section. Although melt pockets and veins can be noticed, no opaque vein was found. The investigated sample must have been impacted very severely since its features accord with those of shock stage 6 proposed by Stöffler et al. (1991).

## Mineral Analyses

Olivine, pyroxenes, glass, metallic iron were analyzed by an EPMA. The analytical results of the cores of the large (longer than 150 $\mu$ m) anhedral olivine, and low-Ca pyroxene in the matrix, lithic fragments, and chondrules are shown in the frequency diagram on the left in Fig. 1. Since the data include the analytical results of only cores of the large crystals, the number is limited. The number of large anhedral pigeonite and subcalcic augite are very small, the obtained analytical results of the cores are also presented in the left pyroxene quadrilateral in Fig. 1. On the right column, the analytical results

of the small euhedral olivine, low-Ca pyroxene, pigeonite, and augite coexisting with the impact glass ( Fig. 1).

The number of the analytical results do not represents the modal abundance. The large anhedral crystals are mostly olivine, and low-Ca pyroxene follows. The large pigeonite and subcalcic augite are very rare. The euhedral olivine coexisting with melt glass is limited in number. In contrast, the euhedral pigeonite is abundant and low-Ca pyroxene is rather abundant in the melt glasses.

The compositional ranges of the large anhedral olivine crystals in the matrix is wide (Fa<sub>21-30</sub>). The average Fa molecule is about 26, and close to the peak of the olivine distribution in Fig. 1. In contrast, the compositional frequency distribution of the small euhedral olivine has no significant peak. The average composition of the small olivine coexisting melt glass tends to be rich in FeO compared with the anhedral olivine.

The number of the large anhedral low-Ca pyroxene in the sample is very small, and so is the available results. The Fe/(Fe+Mg) ratios are very scattered and ranges from 15 to 27. The atomic ratios of the euhedral low-Ca pyroxenes are rather concentrated around 22 of the Fe/(Fe+Mg) ratio as shown in Fig 1.

The sample contains only small amount of large anhedral pigeonite and subcalcic augite. Therefore, the number of analyses are only a few. Euhedral pigeonite and augite in the melt glasses are abundant.

The compositional trends for the large anhedral olivines and low-Ca pyroxenes were examined. The compositional differences between cores and rims were presented against the size of the minerals in Fig. 2. Since some of those minerals are irregular, two different positions of their rims were analyzed. Both were indicated by an open square and open triangle. Some are normally zoned, others are reversely zoned, and no systematic zonation was recognized. Their compositional trends do not correlate with the size. Although all the minerals are smaller than several hundred microns, significant difference can be noticed between core and rim. The difference is, however, narrower than that of olivine and pyroxene in unequilibrated chondrites.

The compositional variations of melt glasses are presented in Fig. 3. The glasses in the barred-olivine chondrules seem to have different chemical tendency. The glasses are chemically heterogeneous, and they differ much even in a single chondrule. All of them are rich in SiO<sub>2</sub>, and poor in MgO. Most of them are enriched in both Al<sub>2</sub>O<sub>3</sub> and

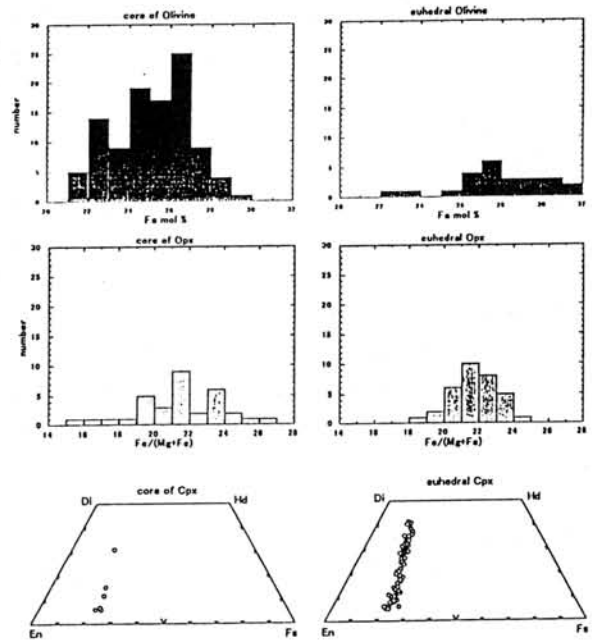


Fig. 1 Frequency diagram of olivine and low-Ca pyroxene, and quadrilateral of pigeonite and cpx.

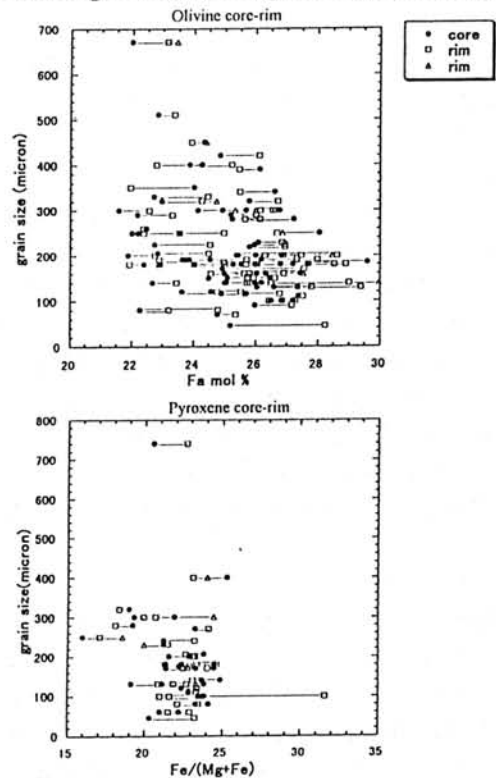


Fig. 2. Compositiona difference between core/rim

Na<sub>2</sub>O. The K<sub>2</sub>O-SiO<sub>2</sub> diagram demonstrates that the shock melt glasses are poor in K<sub>2</sub>O, but glasses in barred-olivine chondrules in Yamato-790757 contains more than 1 % K<sub>2</sub>O.

#### Implication

Chemical compositions of the cores of the large and anhedral olivine and low-Ca pyroxene are considerably variable, and their zoning trends are irregular. The impact should have heated up a part of the parent body in a very short time, but presumably tend to have homogenized mineral compositions and canceled irregular zoning within minerals. Therefore, the observed chemical features of the minerals in the sample were rather homogenized by the impact, and should have been similar to those in an unequilibrated chondrite before the impact. The large anhedral minerals could have partly kept their original features before the impact.

The impact glasses are dacitic to rhyolitic compared with the terrestrial counterparts. They are enriched in plagioclase component. The silicic nature could have derived from incongruent melting of low-Ca pyroxene. However, not so many euhedral olivine crystals are included in the glass. Instead, many euhedral orthopyroxenes, pigeonites, and subcalcic augites appear in the impact glasses. Therefore, postulated incongruent melting may not work, but melted matrix itself must have been silicic.

#### References

Fujimaki, H., Ishikawa, K. and Aoki, K., (1992), Fujimaki, H., Ishikawa, K. Kojima, H., Aoki, K. (1993), NIPR (1987), Okano, O., Nakamura, N., Nagao, K., (1990), Rubin, A. E., (1985), Stöffler, D., Keil, K. Edward, D. E.. (1991)

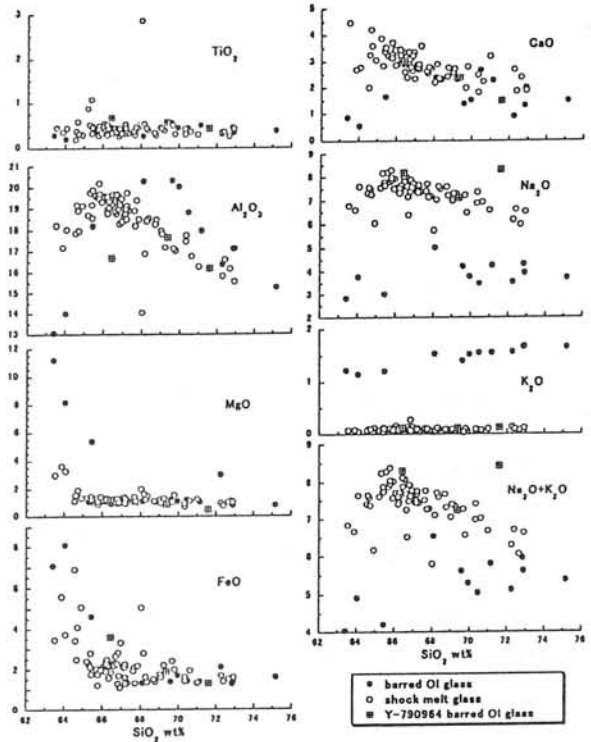


Fig. 3. Compositional variation of glass

# Oxygen isotope studies of Tsukuba chondrite, HED meteorites and Allende chondrules

I. Jabeen<sup>1</sup>, M. Kusakabe<sup>1</sup>, K. Nagao<sup>1</sup> and T. Nakamura<sup>2</sup>

1) Institute for Study of the Earth's Interior, Okayama University, Misasa, Tottori-682-01

2) Department of Earth & Planetary Sciences, Faculty of Science, Kyushu University, Fukuoka 812-81

## Introduction

Oxygen isotopes play a unique role in determining the precursor materials, formation processes and genetic relationships among different types of meteorites. The three isotope plot ( $^{17}\text{O}/^{16}\text{O}$  vs  $^{18}\text{O}/^{16}\text{O}$ ) has the property that ordinary chondrites, achondrites and carbonaceous chondrites are resolved into distinct major fields. In the present study oxygen isotope data has been determined for the Tsukuba meteorite, four eucrites, three diogenites, two pallasites and various Allende chondrules. The relationship among the stony and iron meteorites is also discussed.

## Technique

Oxygen isotope determination of different types of meteorites is carried out using laser probe technique. The sample (2-3 mg) is irradiated with  $\text{CO}_2$  laser under 300 mbar  $\text{BrF}_3$  atmosphere<sup>1,2</sup>. The liberated oxygen is cryogenically purified and introduced directly into the micro-inlet system of the stable isotope mass spectrometer (SIRA12). The calibration of system is done on the basis of VSMOW-SLAP scaling<sup>3</sup>. For this purpose international reference water samples VSMOW, SLAP, GISP & MSA6 were decomposed with  $\text{BrF}_3$  and the released oxygen was measured against the working standard ( $\text{O}_2$  gas of five 9 purity) to determine  $\delta^{17}\text{O}$  and  $\delta^{18}\text{O}$  values.

## Discussion

$\delta^{17}\text{O}$  and  $\delta^{18}\text{O}$  isotopic composition are reported for the recent fall Tsukuba meteorite<sup>4</sup>, some HED achondrites and Allende chondrules. The Tsukuba meteorite falls among the ordinary chondrites (H Type) group<sup>5</sup>. It also supports the relationship among H-chondrites and IIE irons on the basis of oxygen isotopes (Fig 1)<sup>6</sup>.

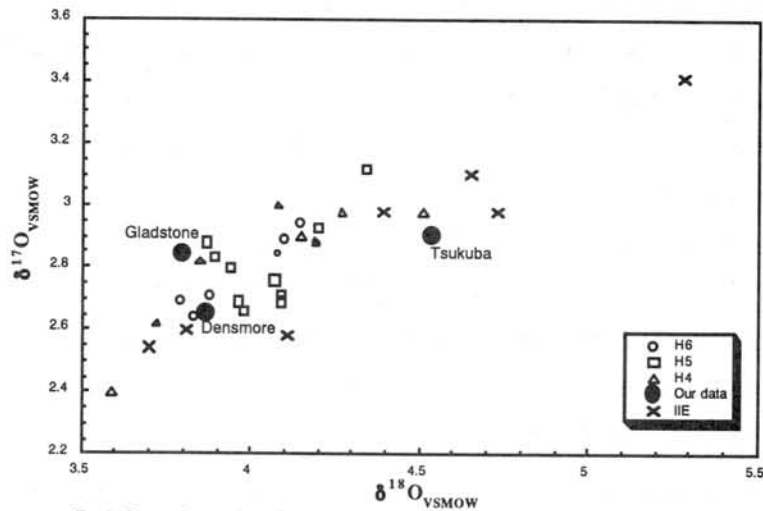


Fig. 1: Oxygen isotope data of ordinary H chondrites & IIE irons (Clayton, 1978, 1991)

Among the HED meteorites, the oxygen isotope data of eucrites, diogenites and pallasites also suggests origin from a common parent body. The analysis is done for four eucrites, Stannern, Juvinas, CamelDonga and Millbillillie. The Millbillillie eucrite consists of a fine grained part and a coarse grained one. The oxygen isotope study has shown a difference of oxygen isotopes between the two parts, the coarse one been heavier to about 0.5‰ in  $\delta^{18}\text{O}$  than the fine one. The  $^{244}\text{Pu}$ -Xe ages has also shown a difference of 60 m.y. between the two parts<sup>7</sup>. Among the three diogenites, Y-791199, 87 and Tatahouine are consistent in  $\delta^{17}\text{O}$  &  $\delta^{18}\text{O}$  values with the previous reported data<sup>8</sup>. Y-791000, 89 is falling somewhat far from the others diogenites suggesting a relationship to IIIAB irons<sup>9</sup>(Fig. 2)

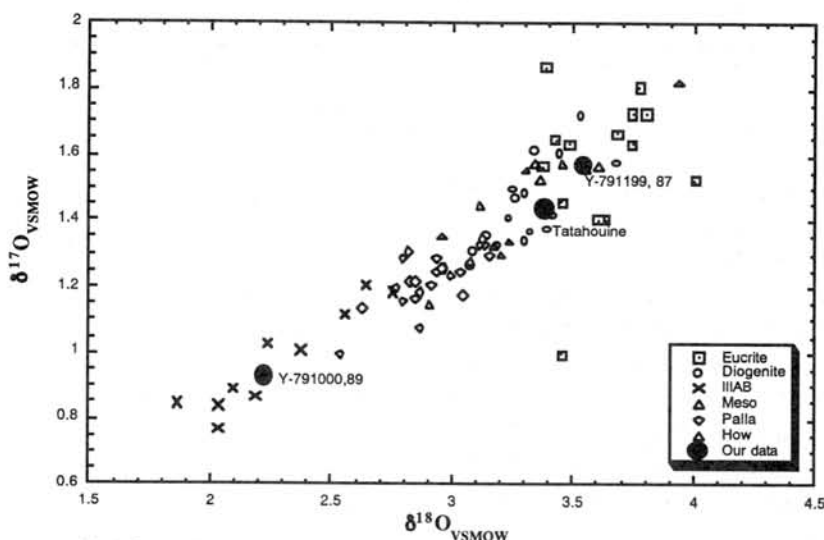


Fig.2: Oxygen isotope data of HED meteorites, Pallasites & IIIAB irons (Clayton 1996)

The oxygen isotope determination is done on about 20 Allende CV3 chondrules. This study revealed that the CV3 chondrules; mostly the porphyritic olivine PO, porphyritic olivine-pyroxene POP and the glassy ones, are showing mass dependent fractionation processes which produces a slope 1/2 on the three isotope plot of oxygen. The data by other researchers has shown the Allende chondrules to be lying with a slope 1 line on a three isotope of oxygen defined by CAI<sup>10,11</sup>. Nevertheless, there is still a reference of some PO chondrules data falling among the ESP (Eagle Station Pallasites)<sup>8</sup>. The Barred Olivine chondrules are falling near the terrestrial fractionation line farther off the other chondrules, suggesting a different source or a different formation process (Fig.3). The probe analysis of PO and POP chondrules shows that the Na<sub>2</sub>O content cannot be related with  $\delta^{17}\text{O}$  &  $\delta^{18}\text{O}$  values, leading to the suggestion that the chondrule formation didn't essentially took place in an open system.

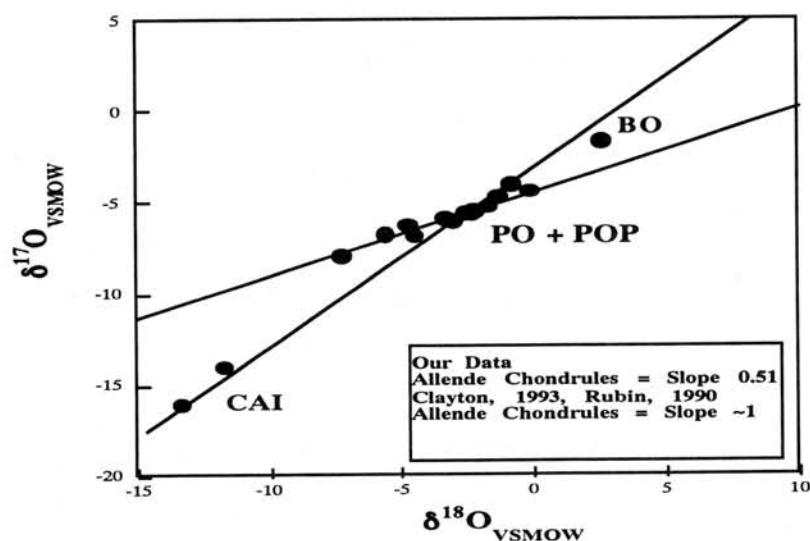


Fig.3: Oxygen isotope studies of Allende Chondrules

## References

1. Sharp, Z. D., 1990, GCA, V. 54, P. 1353-1357.
2. Rumble, D. III. and Hoering, T. C., 1994, Acc. Chem. Res., V. 27, p. 237-241
3. Jabeen I., Kusakabe, M., 1997, Chemical Geology-IGS (submitted)
4. Yoneda, S., Shima, M., Nagao, K., Okada, A., Kita, N. T., Togashi, S., Okuyama, Y. and Bunno, M., 1996, Meteoritics & Planetary Science, V. 31, p. A157-A158
5. Clayton R. N. and Mayeda, T. K., 1978, EPSL, V.40, p. 168-174.
6. Clayton R. N., Mayeda, T. K., Goswami, J. N. and Olsen, E. J., 1991, GCA, V. 55, p. 2317-2337.
7. Miura, Y. N., Nagao, K., Sugiura, N., Fujitani, T., Warren, P. H., 1996, GCA (submitted)
8. Clayton R. N. and Mayeda, T. K., 1996, GCA, V. 60, p. 1999-2017.
9. Haack, H. Scott, E. R. D., Love, S. G., Brearley, A. J. and McCoy, T. J., 1996, GCA, V. 60, P. 3103-3113.
10. Rubin. A. E., Wasson, J. T., Clayton, R. N. and Mayeda, T. K., 1990, EPSL, V. 96, p. 247-255
11. Clayton, R. N., 1993, Ann. Rev. EPS., V. 21, p. 115-49

# Cooling rates of olivine xenocrysts in the EET79001 shergottite

Hiroshi KAIDEN, Takashi MIKOUCHI, and Masamichi MIYAMOTO

*Mineralogical Institute, Graduate School of Science, University of Tokyo, Hongo, Tokyo 113, Japan.*

## INTRODUCTION

The Elephant Moraine (EET) 79001 achondrite is one of the SNC (Shergottite-Nakhilite-Chassignite) group which is inferred to have formed on Mars [e.g., 1]. It is a basaltic shergottite and contains two distinct igneous lithologies (designated A and B). Several studies on thermal histories of the shergottites have been carried out mainly on the basis of the compositions and compositional zoning of pyroxenes and/or maskelynites which are major minerals in the meteorites [2-4]. It is also important to study other phases such as olivine xenocrysts occurring in lithology A in the hope that they might record igneous history as well. The objective of the present study is to examine chemical zoning of olivine xenocrysts in the EET79001 shergottite and to constrain its thermal history.

## SAMPLES AND ANALYTICAL TECHNIQUES

Two polished thin sections of EET79001 were supplied by The Meteorite Working Group. Electron probe microanalysis was performed on a JEOL JXA-733 microprobe at the Ocean Research Institute, University of Tokyo. The chemical zoning profiles of olivine xenocrysts in lithology A of EET79001 were measured by line analyses at intervals of 3  $\mu\text{m}$ . The acceleration voltage was 15 kV and beam current was 12 nA.

## CALCULATION PROCEDURES

In order to estimate the cooling rates of olivine xenocrysts in EET79001, it was assumed that the compositional gradients of the Fa components of olivine grains are controlled by atomic diffusion and that initial profiles are uniform [5] and then the diffusion equation was numerically solved using finite difference approximation.

We have employed two kinds of diffusion coefficient independently determined by BUENING and BUSECK [6] and MISENER [7], respectively. The Fe-Mg diffusion coefficient in olivine depends on temperature, composition, and oxygen fugacity. MISENER [7], however, did not report a dependence on oxygen fugacity conditions for his experiments. Because coexisting Fe-Ti oxide (titanomagnetite and ilmenite) compositions in EET79001 suggest oxygen fugacity equilibration near that of the quartz-fayalite-magnetite (QFM) buffer [8], we have used the same expression as MIYAMOTO et al. [5].

The pyroxene compositions suggest that the temperature at which pyroxene crystallized is 1200 °C from pyroxene geothermometry [9]. Compositions of coexisting Fe-Ti oxides in lithology A of EET79001 determine the temperature of 790 °C [3]. Therefore, we calculated cooling rates for the temperature range of 1200-800 °C.

## RESULTS

The observed and calculated zoning profiles for Fe-poor ( $\text{Fa}_{23-36}$ ) and Fe-rich ( $\text{Fa}_{39-44}$ ) olivine xenocrysts, which are strongly zoned with Mg-rich cores and Fe-rich rims, in lithology A are shown in Fig. 1. Cooling rates that give the best fit between calculated profiles and observed ones are also provided in Fig. 1. If it is assumed that olivines cooled linearly, cooling rates are proportional to the diffusion coefficient and thus cooling rates derived from the

diffusion coefficient of BUENING and BUSECK [6] (0.1–0.9 °C/h) are 40–50% higher than those of MISENER [7] (0.07–0.6 °C/h).

## DISCUSSION

Lithologies A and B of EET79001 consist predominantly of clinopyroxene (pigeonite and augite) and maskelynite (shocked plagioclase glass) [10] and have many similarities in mineralogy to each other and to the other basaltic shergottites [1]. In addition, lithology A contains xenocrysts of olivine, orthopyroxene, and chromite. This xenocryst assemblage is considered to be a disaggregated plutonic rock assimilated by a basaltic shergottite magma, because olivines in the poikilitic area of the lherzolitic shergottites are chemically homogeneous and have the composition that corresponds to that of olivine xenocryst cores in lithology A of EET79001 [3, 4, 11, 12].

BREARLEY [13] concluded that the cooling rate of the Zagami shergottite is about 0.02 °C/h through the temperature interval 1100–950 °C on the basis of the width of pyroxene exsolution lamellae, whereas MCCOY et al. [2] estimated cooling rates of 0.1–0.5 °C/h based on sizes of the plagioclase (maskelynite) crystals. On the other hand, TREIMAN and SUTTON [14] inferred cooling rates of 5–20 °C/h derived from the textures and compositional zoning in Zagami's pigeonites.

MCCOY et al. [2] suggested that the Zagami shergottite experienced a two-stage magmatic history in which slow cooling occurred in a deep-seated magma chamber followed by rapid cooling in a shallow intrusion or thick lava flow. Their inferred cooling rates of 0.1–0.5 °C/h correspond to crystallization during the second stage in a near-surface environment. Our results that olivine xenocrysts in EET79001 cooled at the rate of 0.1–0.9 °C/h ([6]) and 0.07–0.6 °C/h ([7]) are broadly consistent with those estimated by MCCOY et al. [2].

## CONCLUSIONS

By investigating chemical zoning profiles, we have evaluated cooling rates of olivine xenocrysts in the EET79001 shergottite. The cooling rates we estimated are consistent with those of MCCOY et al. [2], who suggested relatively rapid cooling of the shergottites in a near-surface environment.

## ACKNOWLEDGMENTS

We thank The Meteorite Working Group for the samples.

## REFERENCES

- [1] MCSWEEN H. Y., JR. (1994) *Meteoritics* **29**, 757–779.
- [2] MCCOY T. J. et al. (1992) *Geochim. Cosmochim. Acta* **56**, 3571–3582.
- [3] MCSWEEN H. Y., JR. and JAROSEWICH E. (1983) *Geochim. Cosmochim. Acta* **47**, 1501–1513.
- [4] HARVEY R. P. et al. (1993) *Geochim. Cosmochim. Acta* **57**, 4769–4783.
- [5] MIYAMOTO M. et al. (1986) *J. Geophys. Res.* **91**, 12804–12816.
- [6] BUENING D. K. and BUSECK P. R. (1973) *J. Geophys. Res.* **78**, 6852–6862.
- [7] MISENER D. J. (1974) *Geochemical Transport and Kinetics*, Publ. 634, pp. 117–129, Carnegie Institute, Washington, DC.
- [8] STOLPER E. and MCSWEEN H. Y., JR. (1979) *Geochim. Cosmochim. Acta* **43**, 1475–1498.
- [9] LINDSLEY D. H. and ANDERSEN D. J. (1983) *Proc. Lunar Planet. Sci. Conf. 13th*, A887–A906.
- [10] STEELE I. M. and SMITH J. V. (1982) *Proc. Lunar Planet. Sci. Conf. 13th*, A375–A384.
- [11] MCSWEEN H. Y., JR. et al. (1979) *Science* **204**, 1201–1203.
- [12] MIKOUCHI T. and MIYAMOTO M. (1996) *Meteorit. Planet. Sci.* **31**, Suppl., A89–A90.
- [13] BREARLEY A. J. (1991) *Lunar Planet. Sci. XXII*, 135–136.
- [14] TREIMAN A. H. and SUTTON S. R. (1992) *Geochim. Cosmochim. Acta* **56**, 4059–4074.

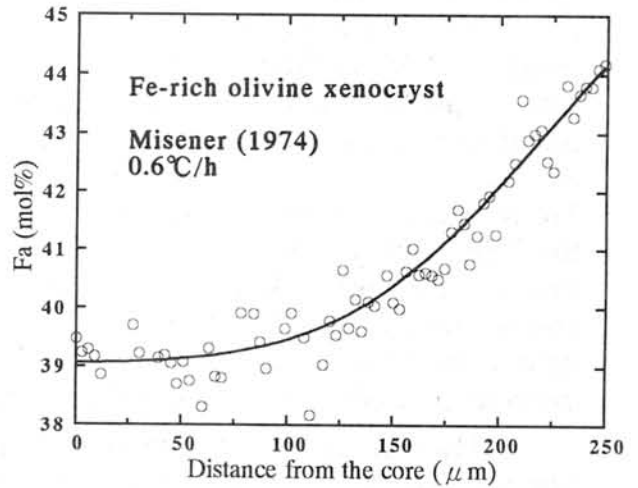
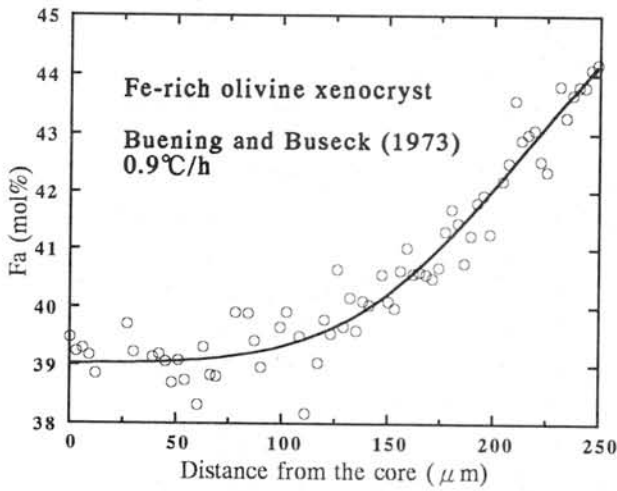
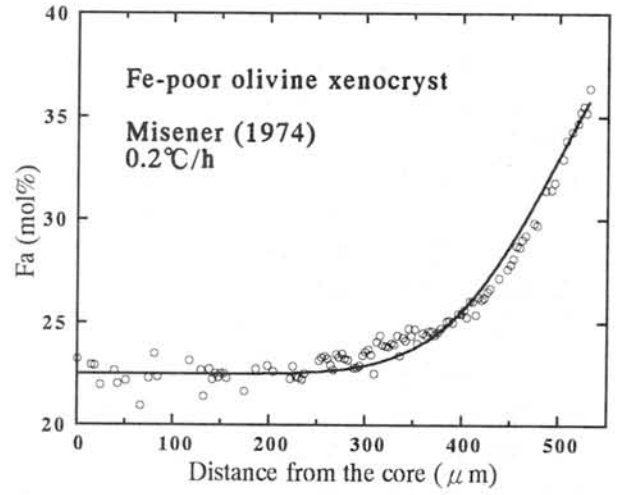
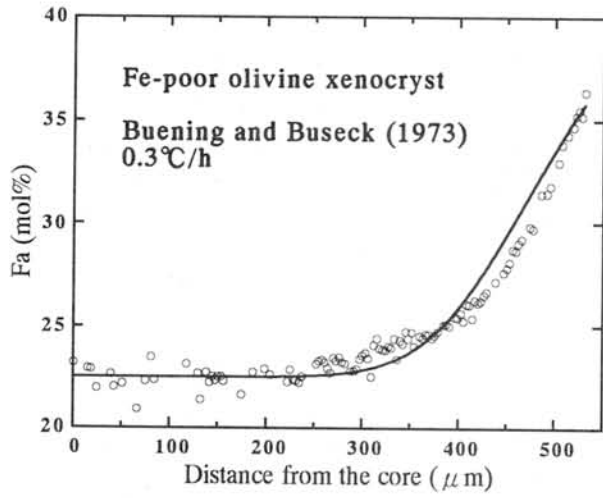


**Fig. 1** Observed (circle) and calculated (solid line) chemical zoning profiles of Fe-poor and Fe-rich olivine xenocrysts in EET79001. The calculated profiles were obtained by using the diffusion coefficients of BUENING and BUSECK [6] (left) and MISENER [7] (right) in the temperature range of 1200–800 °C.

**COMPOSITIONAL RELATIONSHIPS AMONG WINONA-LIKE AND OTHER POSSIBLY RELATED METEORITES.** G.W. Kallemeyn, Department of Chemistry, Faculty of Science, 1-1 Minami-Ohsawa, Hachioji, Tokyo 192-03, Japan.

Winona, Kakangari, Mount Morris (Wis.), Pontlyfni and chondritic xenoliths from Cumberland Falls were originally proposed as a new group of 'forsterite' chondrites by Graham et al. (1977). Prinz et al. (1980) purged Kakangari and Cumberland Falls xenoliths, added ALHA77081, Acapulco and Tierra Blanca, and called the new group winonaites. Later, Acapulco became the 'type' member of the acapulcoites, and ALHA77081 joined that group. In recent years, several Antarctic finds have been added to the list of Winona-like meteorites (Yamato 74025, Yamato 75300 and Yamato 75305).

Kallemeyn (1996) showed that Pontlyfni has characteristics at the extreme of the winonaites, and might not be a true winonaite, but only closely related. It has the lowest values for  $f_a$  (0.9) in olivine and  $f_s$  (0.5) in low-Ca pyroxene. Bulk compositional analyses of replicate samples of Pontlyfni by INAA show that its composition is distinct from the other Winona-like meteorites. Pontlyfni has close to CI abundances of refractory lithophiles. The Ca/Al atom ratio (~0.7) is indistinguishable from the range of typical chondritic ratios. Yamato 74025 appears to be related to Pontlyfni. An INAA analysis by Kimura et al. (1992) shows a very similar lithophile abundance pattern. The Pontlyfni REE have a small light-REE relative enrichment, whereas the Yamato 74025 REE have a small light-REE relative depletion. The patterns are complementary and may result from slight differences in plagioclase and orthopyroxene mineral abundances in analyzed samples. By comparison Winona, Mount Morris and Tierra Blanca have very fractionated refractory lithophile abundance patterns, the REE display a characteristic "W" pattern. Their Ca/Al atom ratios (~0.5) are lower than typical chondritic meteorite values. The overall lithophile element abundance patterns for Winona, Mount Morris (Wis.) and Tierra Blanca are similar to those of silicate inclusions from the IAB meteorite, Udei Station, previously analyzed by this author (Kallemeyn and Wasson, 1985).

The siderophile/chalcophile element abundance pattern (CI, Mg-normalized) in Pontlyfni is relatively flat, with abundances generally a little higher than CI abundances. Only the highly volatile Zn is very low ( $0.2 \times \text{CI}$ ). Yamato 74025 appears to be depleted in metal and sulfide, but the abundance pattern is very similar to that of Pontlyfni. It is probably not (completely) due to weathering. Winona, Mount Morris (Wis.) and Tierra Blanca have highly variable siderophile/chalcophile element abundance patterns ( $2.0-0.2 \times \text{CI}$ ). These meteorites are all very weathered, so the variability may be due in part to the effects weathering on the metal and sulfides.

The Winona-like meteorites as a whole encompass a relatively wide range on an oxygen 3-isotope plot, overlapping several other groups and unique meteorites (e.g., IAB, III CD, Mundrabilla, ALHA77255). Therefore, oxygen isotopic composition alone is not a sufficient parameter for classification. Pontlyfni and Yamato 74025 have  $\Delta^{17}\text{O}$  values that are outliers to the other Winona-like meteorites (Clayton and Mayeda, 1996).

It was suggested that all of the winonaites except Pontlyfni underwent some degree of partial melting (Benedix et al., 1995). The relatively

unfractionated lithophile element abundance pattern for Pontlyfni would seem to corroborate this notion, but the similarly unfractionated pattern for Yamato 74025 would seem to argue against such scenario. Whether or not Pontlyfni and Yamato 74025 originated on the same parent body as the other Winona-like meteorites is unclear. The other Winona-like meteorites may be more closely related to IAB silicate inclusions.

References:

- Benedix G.K., McCoy T.J. and Keil K. (1995) *Lunar Planet. Sci Conf.*, XXVI, 99-100.  
Clayton R.N. and Mayeda T.K. (1996) *Geochim. Cosmochim. Acta*, **60**, 1999-2017.  
Graham A.L., Easton A.J. and Hutchison R. (1977) *Min. Mag.*, **41**, 201-210.  
Kallemeyn G.W. (1996) *Meteoritics Planet. Sci.*, **31**, A68-A69.  
Kallemeyn G.W. and Wasson J.T. (1985) *Geochim. Cosmochim Acta*, **49**, 261-270.  
Kimura M., Tsuchiyama A., Fukuoka T. and Iimura Y. (1992) *Proc. Symp. Ant. Met.*, **5**, 165-190.

## Comparison between synthetic and natural Nakhla pyroxenes : Minor elements composition

K. Kaneda (Mineralogical Institute, Graduate School of Science, University of Tokyo 113, Japan), G. McKay (SN4, NASA – JSC, Houston, TX 77058), L. Le (Lockheed Martin, 2400 NASA Rd. 1, Houston, TX 77058)

**Introduction:** Nakhla, one of the SNC meteorites, is mainly composed of ~80% augite, ~5% olivine and ~15% mesostasis. The pyroxenes of Nakhla show cumulate texture and have igneous elemental zoning, especially Mg, Fe, Al and Ti. Hence, they can be the clues that give us information about the formation process of Nakhla and the composition of its parental magma. A series of crystallization experiments were performed over a range of cooling rates using a synthetic Nakhla composition. By comparing the compositions of synthetic pyroxenes from this experiment with natural pyroxenes in Nakhla, we are attempting to get additional constraints on the formation of this meteorite. From the starting material and synthetic pyroxene compositions of this and previous experiments [1][2], we can estimate the compositions of a melt from which pyroxenes having similar composition to Nakhla pyroxenes would crystallize. We plan to test this composition through additional crystallization experiments.

**Experiment:** An experimental starting material, named NJ3, was made by mixing the starting materials of our previous experiments, NJ2 and NL, half and half. NJ3 and earlier synthetic materials are plotted in a quadrilateral diagram (Fig.1). In all experiments, we set the oxygen fugacity at QFM, generally believed to approximate the  $fO_2$  of Martian magma.

125 mg pellets of NJ3 were placed on 8 mil Pt-Rh loops. Then we put them in the Deltech furnace at 1350 °C for 48 hours to homogenize the charges, then quenched to room temperature. The homogenized charges have similar composition to the NJ3 starting material, except for volatile elements, Na, K and P (Table 1). Homogenized charges were put back in the furnace a few degrees below the liquidus temperature and held at constant temperature or cooled at various cooling rates to about 200 degrees below the liquidus, then quenched to room temperature. The cooling rate of each experiment is shown in Table 2. The thin sections of quenched charges were analyzed with a Cameca Camebax Electron Microprobe at the Johnson Space Center.

**Results:** Analyzed charges contain zoned pyroxenes, Cr-Ti spinels and small amount of glass or mesostasis. In pyroxenes, from core to rim, Mg and Ca contents decrease and Fe content increases. Ti and Al contents slightly increase. The core compositions of the synthetic pyroxenes of NJ3 and pyroxenes from our earlier starting compositions are plotted in Hd-Fs-En-Di quadrilateral diagram, along with natural Nakhla pyroxenes (Fig.2). Regardless of different cooling rates, NJ3 pyroxenes fall in almost same area, at slightly higher Ca contents than Nakhla pyroxenes. Therefore, the NJ3 composition is little more Ca-rich than that of the Martian magma.

Fig.3a and 3b show MgO-Al<sub>2</sub>O<sub>3</sub> and the MgO-TiO<sub>2</sub> plots of NJ3 synthetic pyroxenes, respectively. In the MgO-Al<sub>2</sub>O<sub>3</sub> plot, the trends of synthetic pyroxenes of each experiment show a steep slope and are almost parallel to the Nakhla pyroxene trend in the MgO rich area (MgO > 11.5~12.5wt%). In the MgO poor area, the synthetic pyroxene trends have a gentler slope than those in the MgO rich area, because Mg-rich pyroxenes crystallized rapidly and the pyroxenes that crystallized after that did not contain sufficient Mg.

In the MgO-TiO<sub>2</sub> plot, Ti contents of synthetic pyroxenes have gentle slope in the Mg poor area and steep slope in the Mg rich area, similar to the MgO-Al<sub>2</sub>O<sub>3</sub> plot. The point where the gentle slope meets the steep slope is the same on the MgO-Al<sub>2</sub>O<sub>3</sub> plot. The MgO vs. TiO<sub>2</sub> slope of the Nakhla pyroxene trend, however, is different from that of the synthetic pyroxene trend in the MgO rich area, showing a significantly steeper slope.

By taking those 2 plots into consideration, we could decide that the synthetic pyroxene cores of NJ3 must contain more than 12 wt% MgO and that pyroxenes with less MgO should not be compared with Nakhla cores. Therefore, only synthetic pyroxene compositions in the Mg rich area are plotted in the Al<sub>2</sub>O<sub>3</sub>-TiO<sub>2</sub> plot (Fig.4). Al and Ti contents in earlier experimental pyroxenes, except for NJ, do not overlap the range of Nakhla pyroxene. Only the high Al-Ti range of NJ pyroxenes falls in the low Al-Ti range of Nakhla pyroxenes. The Al and Ti contents in the new experimental NJ3 pyroxenes, are in good agreement with those in the Nakhla natural pyroxene cores. Synthetic pyroxenes of each NJ3 experiment show similar slopes of the trend in the Al<sub>2</sub>O<sub>3</sub>-TiO<sub>2</sub> plot (Fig.5). The trends of NJ3 pyroxenes, however, are little different from that of

Nakhla pyroxenes, which shows a steeper slope. The early crystallized synthetic pyroxene cores, which are plotted in the low Al and Ti area of NJ3, have similar Al content to Nakhla pyroxenes in the low Al-Ti range, and thus we believe the Nakhla parental melt had a similar Al content to the NJ3 starting material. However, the Ti content in NJ3 pyroxenes is little higher (~0.05wt%) than that in Nakhla pyroxenes, and therefore the NJ3 starting material is little more rich in Ti than the Nakhla parental magma.

**Discussion:** To estimate a new starting material composition from which synthetic pyroxenes having similar composition to Nakhla pyroxene can be crystallized, we should not calculate the element contents in wt%, but atom%. Reflecting the results of the NJ3 experiments, the composition of new starting material should be more Ti-rich and less Ca-rich than NJ3. The Al and Mg contents in the NJ3 pyroxene cores are in good agreement with those of Nakhla pyroxene cores, therefore, Al, Mg, Si and  $M^{+2}$  ( $M^{+2}$ : Mg + Ca + Fe + Mn) contents (atom%) in NJ3 should be applied to the new material without changing. K and P contents in NJ3 pyroxenes are also similar to those in Nakhla pyroxene and should be applied like above. NJ3 pyroxenes are less Na rich and more Cr rich than Nakhla pyroxenes, but these elements are not so important to estimate new composition, and Na is difficult to control in our experiments because of volatility.

The low Ti pyroxenes are plotted in Fig.6. In this plot, there is a correlation between  $TiO_2$  (wt%) content in the pyroxenes and  $Ti / M^{+2}$  in the starting materials. From the low Ti content, 0.12 wt%, in Nakhla pyroxenes, the Ti content in new materials is estimated as 0.63 atom%.

Fig.7 shows Wo (mol%) vs. Wo (atom%) plot. (Wo (mol%) = Wo mol% in synthetic pyroxenes and Wo (atom%) =  $Ca / M^{+2}$  atom% in the starting materials.) Like Fig.6, the plots in Fig.7 show a correlation line and we can estimate the Ca contents in new composition by using this correlation. Wo mol% in Nakhla pyroxenes is ~39 mol% and Ca content in new material turns out to be ~32 atom% in Wo (atom%), which is 12.63 atom% of the whole material.

The Mn content in the synthetic pyroxenes is proportional to Fe, because Mn acts as Fe in a pyroxene. We set the Fe and Mn contents as 19.59 and 0.48 atom% of whole material, respectively.

In conclusion, the composition of the calculated new starting material is shown in Table 3. Crystallization experiments using this new material will soon be conducted. We expect that synthetic pyroxenes which have similar composition to Nakhla's will be crystallized from this new starting material.

**Acknowledgment:** This experiments were conducted while the first author (K. Kaneda) was an LPI summer intern at the NASA Johnson Space Center. We gratefully acknowledge Dr. V. Yang and J. Wagstaff for help with the Camebax electron microprobe, and Dr. T. McCoy, Dr. V. Lauer, and Dr. B. Hanson for the help with Deltech furnaces. This work was supported by NASA Cosmochemistry research program (RTOP 152-12-40-21 to GM).

**References:** [1] McKay et al. (1993) LPSC XXIV, 965-966 [2] McKay et al. (1994) LPSC XXV, 883-884

**Table 1**  
composition of NJ3

|       | NL1   | NJ2   | NJ3   | hc    |
|-------|-------|-------|-------|-------|
| Na2O  | 0.97  | 1.20  | 1.09  | 0.77  |
| MgO   | 5.21  | 4.00  | 4.61  | 4.52  |
| Al2O3 | 2.84  | 8.60  | 5.72  | 5.76  |
| SiO2  | 48.88 | 50.20 | 49.54 | 49.74 |
| P2O5  | 0.00  | 0.70  | 0.35  | 0.16  |
| K2O   | 0.20  | 2.80  | 1.50  | 1.00  |
| CaO   | 13.88 | 11.90 | 12.89 | 12.95 |
| TiO2  | 1.06  | 1.00  | 1.03  | 1.02  |
| Cr2O3 | 0.08  | 0.10  | 0.09  | 0.08  |
| MnO   | 0.73  | 0.40  | 0.57  | 0.56  |
| FeO   | 26.16 | 19.10 | 22.63 | 22.26 |

hc : homogenized charge

**Table 2**  
cooling rates

|     |            |
|-----|------------|
| 654 | isothermal |
| 655 | isothermal |
| 656 | isothermal |
| 657 | 2°C/h      |
| 658 | non-linear |
| 659 | 4°C/h      |
| 660 | non-linear |
| 661 | 2°C/h      |
| 662 | 1.5°C/h    |
| 664 | 1°C/h      |
| 666 | 2°C/h      |

**Table 3**  
composition of the new material

|       | atom% | wt%   |
|-------|-------|-------|
| Na2O  | 2.24  | 1.17  |
| MgO   | 6.79  | 4.62  |
| Al2O3 | 6.64  | 5.71  |
| SiO2  | 48.78 | 49.47 |
| P2O5  | 0.29  | 0.35  |
| K2O   | 1.87  | 1.49  |
| CaO   | 12.63 | 11.96 |
| TiO2  | 0.63  | 0.85  |
| Cr2O3 | 0.05  | 0.06  |
| MnO   | 0.48  | 0.58  |
| FeO   | 19.59 | 23.75 |

Fig. 1 The compositions of starting materials. (projected from olivine)

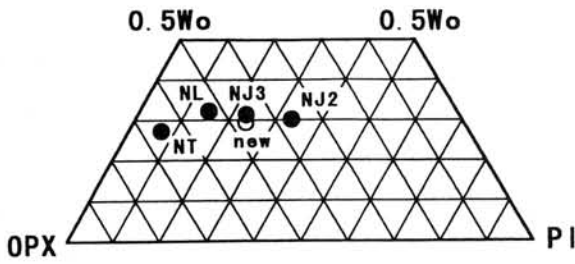


Fig. 2 Compositions of the synthetic and natural Nakhla pyroxenes.

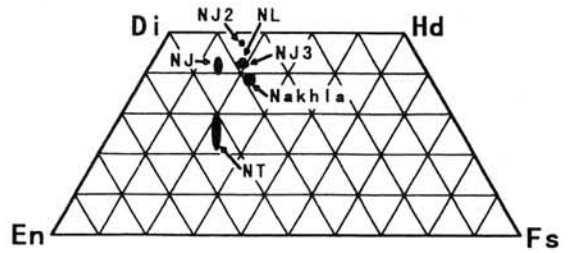


Fig. 3a MgO-Al<sub>2</sub>O<sub>3</sub> plot of the NJ3 synthetic pyroxenes.

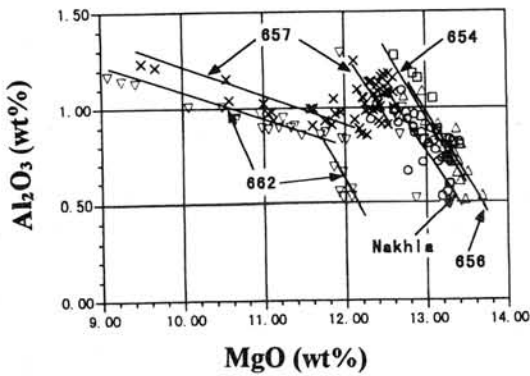


Fig. 3b MgO-TiO<sub>2</sub> plot of the NJ3 synthetic pyroxenes.

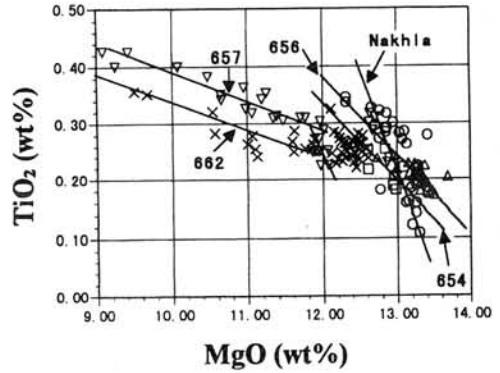


Fig. 4 Al<sub>2</sub>O<sub>3</sub>-TiO<sub>2</sub> plot of the synthetic pyroxenes.

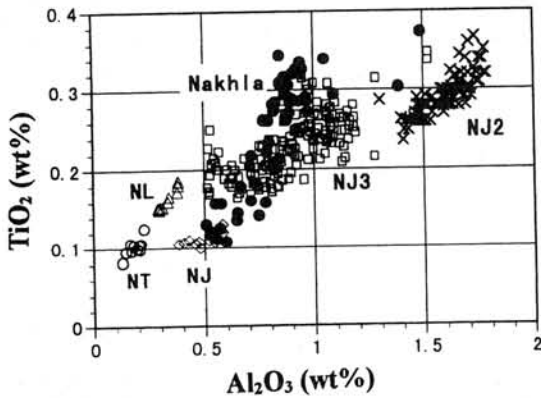


Fig. 5 Al<sub>2</sub>O<sub>3</sub>-TiO<sub>2</sub> plot of the NJ3 synthetic pyroxenes.

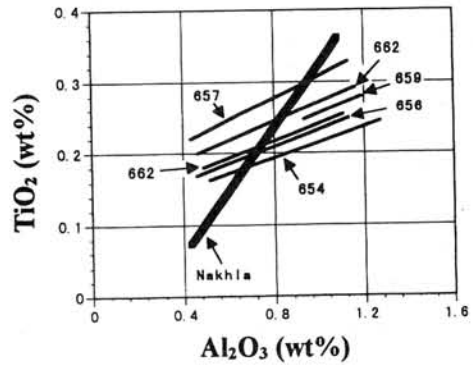


Fig. 6 Ti-M plot of the synthetic pyroxenes.

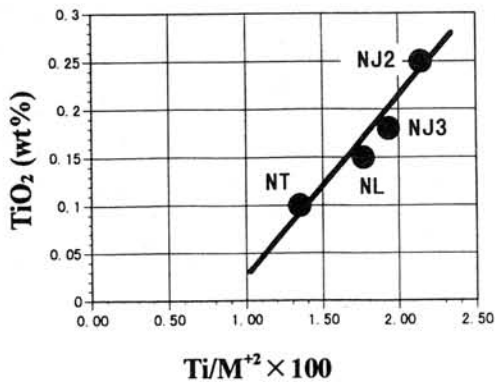
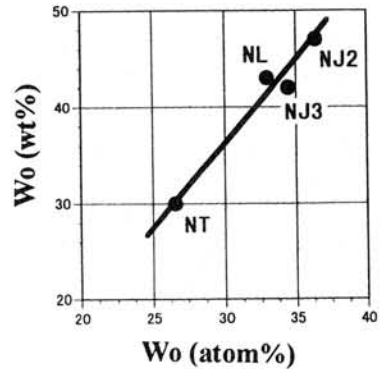


Fig. 7 Wo(mol%)-Wo(atom%) plot of the synthetic pyroxenes.



## **ANHYDROUS AND AQUEOUS ALTERATIONS OF MOKOIA AND KABA CV3 CHONDRITES.**

M. Kimura and Y. Ikeda, Institute of Astrophysics and Planetary Science, Faculty of Science, Ibaraki University, Mito 310, Japan

### **Introduction**

Almost all chondrules in Allende CV3 chondrite were secondarily subjected to anhydrous alteration, consisting of 1) alkali-Ca exchange reaction to form nepheline, sodalite and Ca-silicates such as hedenbergite and wollastonite, 2) secondary zonation of olivine, and 3) replacement of enstatite by ferroan olivine [1,2].

On the other hand, aqueous alteration to produce phyllosilicate took place in some oxidized CV3 chondrites such as Kaba and Mokoia [3,4]. Dehydration reaction was also observed in some dark inclusions in Allende [5]. Thus, various alteration reactions have been noticed for CV chondrites. In order to explore the relationships between the anhydrous and aqueous alterations of chondrules, we carried out a detailed mineralogical and petrological study of chondrules in Kaba and Mokoia, in comparison with those in the other CV chondrites.

### **Aqueous Alteration of Kaba**

Phenocrystic olivines in Kaba chondrules are Fo<sub>95-100</sub> without chemical zoning toward groundmasses. Some olivines (Fo<sub>99-96</sub>) in fragmental chondrules and isolated minerals directly contact the ferroan matrix without zonation. Low-Ca pyroxenes in chondrules do not show replacement texture by ferroan olivine. Primary groundmass phases are devitrified glass and plagioclase (An<sub>80-98</sub>). They typically occur in the central parts of chondrules. All chondrules studied here do not contain feldspathoids. Therefore, chondrules in Kaba did not experience the anhydrous alteration.

Our observation also shows that chondrules in Kaba were extensively subjected to the aqueous alteration. Phyllosilicates occur commonly in the peripheral parts of chondrules. They replaced glass and plagioclase in groundmasses, and often pyroxene. In all chondrules, olivines do not show any replacement texture by phyllosilicates. Saponite is identified in Kaba chondrules, consistent with previous works [*e.g.*, 3].

The aqueous alteration in Kaba have been considered to take place in the CV chondrite parent body at low temperatures, below 100°C [3]. Such low temperatures are consistent with no zoning of olivine in Kaba, because diffusion of Fe and Mg hardly occur below about 600°C [1].

## **Anhydrous and Aqueous Alteration of Mokoia**

Olivine phenocrysts in Mokoia chondrules are Fo<sub>81-99</sub> in the cores, whereas Fo<sub>62-98</sub> in the rims. They usually show normal zoning toward groundmasses. The ferroan rims are usually 10-20 microns in width. The atomic Mg/Mg+Fe ratios of pyroxenes are 0.97-1.00 in Kaba and Mokoia chondrules. Thus, the ferroan olivine rims were not equilibrated with coexisting pyroxenes in Mokoia. The olivine zonation was secondarily formed under subsolidus condition like that in Allende chondrules [1]. Low-Ca pyroxenes in Mokoia are abundantly replaced by ferroan olivines (Fo<sub>53-77</sub>), similar to those in Allende [1]. The secondary zonation of olivine and replacement of pyroxene are observed in all Mokoia chondrules.

Nepheline and sodalite are encountered in more than 30% of Mokoia chondrules. These feldspathoids replaced primary glass and plagioclase in groundmasses, like those in Allende. Two Mokoia chondrules contain hedenbergite (En<sub>0-2</sub>Fs<sub>49-50</sub>Wo<sub>49-50</sub>) and wollastonite in the groundmasses. Such Ca-rich phases are by-products of the alkali-Ca exchange reaction [2]. Our observations indicate that Mokoia chondrules also experienced the anhydrous alteration.

In addition, Mokoia chondrules experienced the aqueous alteration. Phyllosilicates formed around zoned olivine, low-Ca pyroxene and feldspathoids. Na-phlogopite as well as saponite commonly occur in Mokoia chondrules, as already noticed [4].

The distinct zonation of olivine in Mokoia chondrules is inconsistent with the estimated formation temperatures of phyllosilicates as mentioned before. Accordingly, we suggest that the aqueous alteration, possibly in the parent body, may have followed the anhydrous alteration which took place at about 600-800°C [2], possibly in the nebula [6].

**Acknowledgments:** We thank Dr. R. Hutchison for loaning thin sections of Kaba and Mokoia.

**References:** [1] Ikeda and Kimura (1995) Proc. NIPR Symp. Antarct. Meteorites, 8, 97-122. [2] Kimura and Ikeda (1995) Proc. NIPR Symp. Antarct. Meteorites, 8, 123-138. [3] Keller and Buseck (1990) Geochim. Cosmochim. Acta, 54, 2113-2120. [4] Tomeoka and Buseck (1990) Geochim. Cosmochim. Acta, 54, 1745-1754. [5] Kojima and Tomeoka (1996) Geochim. Cosmochim. Acta, 60, 2651-2666. [6] Ikeda and Kimura (1997) Abs. Workshop on Parent Body and Nebular Modification of Chondritic Materials.

# Experimental Studies on Correlation between Particle Shape and Infrared Absorption of Magnesium Oxide Particles

°Seiji Kimura, Chihiro Kaito, Nobuyasu Tamura,  
Yoshio Saito<sup>1</sup> and Chiyoeko Koike<sup>2</sup>

Department of Physics, Ritsumeikan University, Kusatsu, Shiga 525, Japan.

<sup>1</sup>Department of Electronics and Information Science, Kyoto Institute of Technology, Sakyo-ku, Kyoto 606, Japan.

<sup>2</sup>Department of Physics, Kyoto Pharmaceutical University, Yamashina, Kyoto 607 Japan.

**Introduction** A spectral studies to understand the nature of interplanetary dust become more important as the progress of the precision of the astronomical observations, so that the laboratory studies on optical properties of grains have received considerable attention. Although an optical constants of the particles are of importance from viewpoint of a planetary science, the optical constants are hardly obtained because the formation of planetary interested grains is difficult. A systematic studies for making clear a correlation among the shape, crystal structure and absorption spectrum of the grains have not been performed thus far. In a previous paper, it was shown experimentally that  $\alpha$ -Al<sub>2</sub>O<sub>3</sub> particles of different shape are produced and those infrared spectra are changed clearly by the difference of the shape [1]. Although the correlation between the effects on shape of grains and their spectra is a problem of very importance in spectroscopy, the definite experimental results on these problem are not found and not sufficient in agreement with theoretical considerations.

Possibly no other solid than MgO has been studied so much for the purpose of examining the correlation between particle shape and infrared spectrum [2]. The reason for this may be the ease with which a highly crystalline cubes of MgO are simply produced by burning Mg ribbon in air [3]. Although a calculation to obtain absorption spectrum is performed on the assumption that the shape of MgO particles are cubes or sphere, the effects of spectrum due to difference of particle shape is not sufficiently discussed. Because it is impossible to be produced the spherical MgO particles. In order to clarify the correlation between the shape of particles and absorption spectrum, the spherical MgO particles have been produced and the infrared spectrum of particles both cube and sphere have been measured. The shape dependence on absorption spectra are discussed with the results of absorption spectrum obtained theoretically.

Experimental method A cubic MgO particles were produced by evaporating Mg powder in a mixture gas of Ar and O<sub>2</sub> of total 13kPa. A spherical MgO particles were produced by heating the cubic MgO particles in air at 1000°C for 20 hours. For electron microscopic analysis, their particles were dispersed in ethyl-alcohol and mounted on a carbon holey film supported by a standard electron microscopic grid. The particles were also mixed into KBr powder in order to measure infrared spectrum, then KBr pellets embedded the particles were formed using a tablet punching device. The transmittance of KBr pellets was measured with a fourier transform infrared spectrometer (Horiba Co. Ltd., FT-210). The observation of the shape of particles was carried out using Hitachi H-7100R electron microscope.

Results and discussion Figure 1 shows an electron microscopic (EM) images and the corresponding infrared (IR) spectra of (a) the cubic MgO particles and (b) the spherical MgO particles. Figure 1(b) indicates that the cubic MgO particles was changed into the spherical shape. It is also seen that both particles shown in Fig.1 form the chain-like network among the grains. IR spectra show the peak shift due to difference of the shape of particles, i.e. when the shape of the particles became sphere, the wavelength of the main peak in IR spectra shifted to shorter value. According to the shape effect of surface mode introduced theoretically by Bohren and Huffman, the peak shift toward shorter wavelength and the peak position are in good agreement with the results of the theoretical expectation [2]. However, the feature of spectrum is apparently different from that of spectrum calculated. Although IR spectrum of spherical MgO grains shows a double peaks pointed by an arrow, it is expected that their peak is not seen in the spectra calculated. As shown in Fig.1(b), it can be thought that the shape of MgO particles is ellipsoid rather than sphere because of being aggregated with each other. However, the appearance of double peaks which can not be seen in the cubic shape can not explain even if the particle shape is not sphere but ellipsoid. In the theoretical consideration, the double peaks are never seen in the spherical shape. The such peak appears in the short wavelength region in both the cube and ellipsoid shapes. But in the present experiment, it was found that the double peaks appeared at long wavelength region on the spherical shape. This may be due to the size distribution of the produced grains. Experimental studies on this point are in progress.

Acknowledgement This work is supported by a Research Fellowships of the Japan Society for the Promotion of Science for Young Scientist (Kimura).

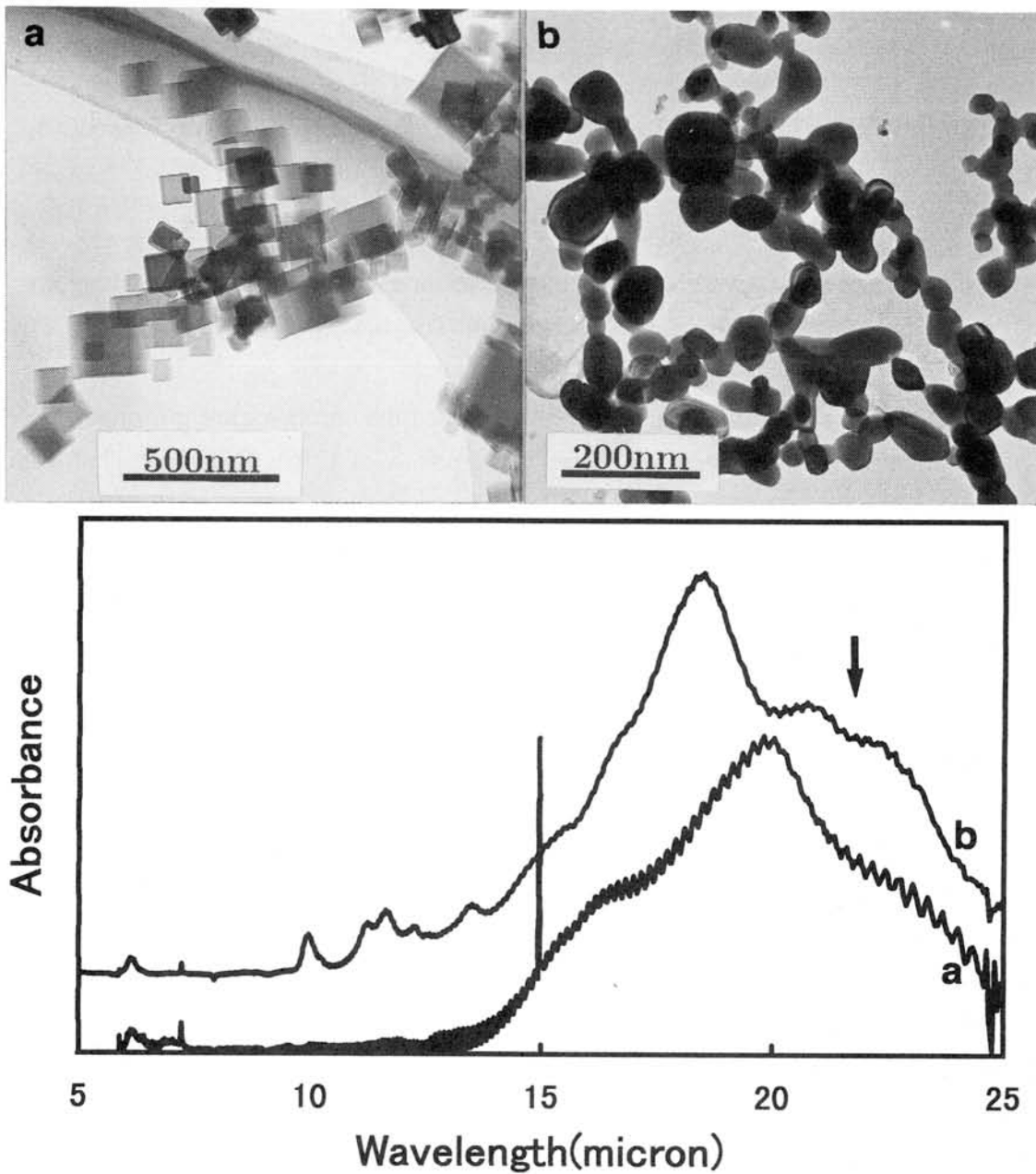


Fig.1 EM images and infrared spectra of (a) cubic MgO particles and (b) spherical MgO particles.

References (1) S. Kimura, K .Kamei, N. Tsuda, Y. Saito, C. Koike and C. Kaito: Proc. NIPR Symp. Antarct. Meteorites, 9, 240-246, 1996. (2) C. F. Bohren and D. R. Huffman, Absorption and Scattering of Light by Small Particles, Woly, 1983. (3) J. T. Luxon, D. J. Montgomery and R. Summit, Phys. Rev. 188, 1345-1356, 1969.

# SEARCH FOR $^{60}\text{Ni}$ ANOMALY IN MET-78008 UREILITE USING ION MICROPROBE

Noriko T. Kita<sup>1</sup>, Shigeko Togashi<sup>1</sup>, Shigeru Terashima<sup>1</sup>, Yuichi Morishita<sup>1</sup>,  
and Hisayoshi Yurimoto<sup>2</sup>

<sup>1</sup>Geological Survey of Japan, 1-1-3 Higashi, Tsukuba, Ibaraki 305, Japan.

<sup>2</sup>Dept. Earth and Planetary Science, Faculty of Science, Tokyo Institute of Technology,  
2-12-1 Ohkayama, Meguro-ku, Tokyo 152, Japan.

**Introduction:** The ultramafic nature of ureilites limited the chronological information because most of the ureilites do not contain any significant amounts of U-Th, REE, and alkali elements [1]. The search for the  $^{60}\text{Ni}$  isotopic anomaly from the decay of short lived nuclide  $^{60}\text{Fe}$  (half life of 1.5 Ma) is important for the study of the ureilite early history. The initial ( $^{60}\text{Fe}/^{56}\text{Fe}$ ) in the solar system was estimated to be  $(1.6 \pm 0.5) \times 10^{-6}$  from CAI [2]. Earlier work on bulk ureilite analyses by conventional method could not find any detectable anomaly [3]. Since the half life of  $^{60}\text{Fe}$  is very short, a sample with a high Fe/Ni such as silicates should be analyzed to detect a small isotopic anomaly. The Fe/Ni ratio of 3,000 is required to detect 1 permil anomaly for the material which formed 5 Ma after CAI formation.

In this study, we have developed the technique for the precise Ni isotopic analyses in olivine and low Ca-pyroxene grains using the ion probe Cameca IMS-1270. In-situ analyses using ion probe has a great advantage of obtaining high Fe/Ni phases in the ureilite by avoiding the thick reduced rim (about 100  $\mu\text{m}$ ) which contains reduced iron grains, metallic inclusions and veins. We measured Fe-Ni systematics of MET-78008 ureilite. The old U-Pb age of  $4.563 \pm 0.006$  Ga has been obtained for this meteorite [4], so that the sample is a good candidate for detecting an  $^{60}\text{Ni}$  isotopic anomaly.

**Ion Probe Analyses:** Olivine and low Ca-pyroxene grains of 0.3 - 1 mm in size from MET 78008 were mounted in epoxy, polished and Au coated (200 nm). The Cameca IMS-1270 ion probe at the Geological Survey of Japan was used in this study. The  $\text{O}^-$  primary ion beam (accelerating voltage of -13kV) was shaped to a 40  $\mu\text{m}$  diameter spot with intensity of 25-30 nA. Secondary ions (+10kV) were measured with mass resolution power of 4,500. The energy slit was open widely (75 V width) in order to collect more than 90% of the ion sputtered from the surface. The analyzed area was limited to 20  $\mu\text{m}$  square using the field aperture, which reduced the tailing of the mass spectrum. Although the present tuning of the mass spectrometer sacrifices transmission down to 25%, the effect of interference peaks of hydrides and oxides were reduced to less than  $10^{-4}$  even for samples with low Ni contents of less than 100 ppm.

For chemical analyses runs,  $^{28}\text{Si}$ ,  $^{56}\text{Fe}$ ,  $^{59}\text{Co}$ , and  $^{60}\text{Ni}$  were analyzed. The matrix effect according to the Fe content of olivine was calibrated using terrestrial standards with known Fe, Co, and Ni concentrations [5]. For low Ca pyroxene, we only used terrestrial peridotite orthopyroxene which is more Mg rich than ureilitic low Ca-pyroxene, so that there may be systematic error from matrix effect in Ni and Co concentrations.

Isotopic analyses runs consist 80 cycles of counting  $^{60}\text{Ni}$  for 5 sec,  $^{61}\text{Ni}$  for 25 sec, and  $^{62}\text{Ni}$  for 8 sec using Electron Multiplier by pulse counting mode with dead time of 14 nsec. Typical counting rate of  $^{60}\text{Ni}$  for San Carlos olivine (2,700 ppm Ni) was in the range of  $(7-14) \times 10^4$  cps. We did not measure  $^{58}\text{Ni}$  and  $^{64}\text{Ni}$ , which have isobaric interferences from Fe and Zn.

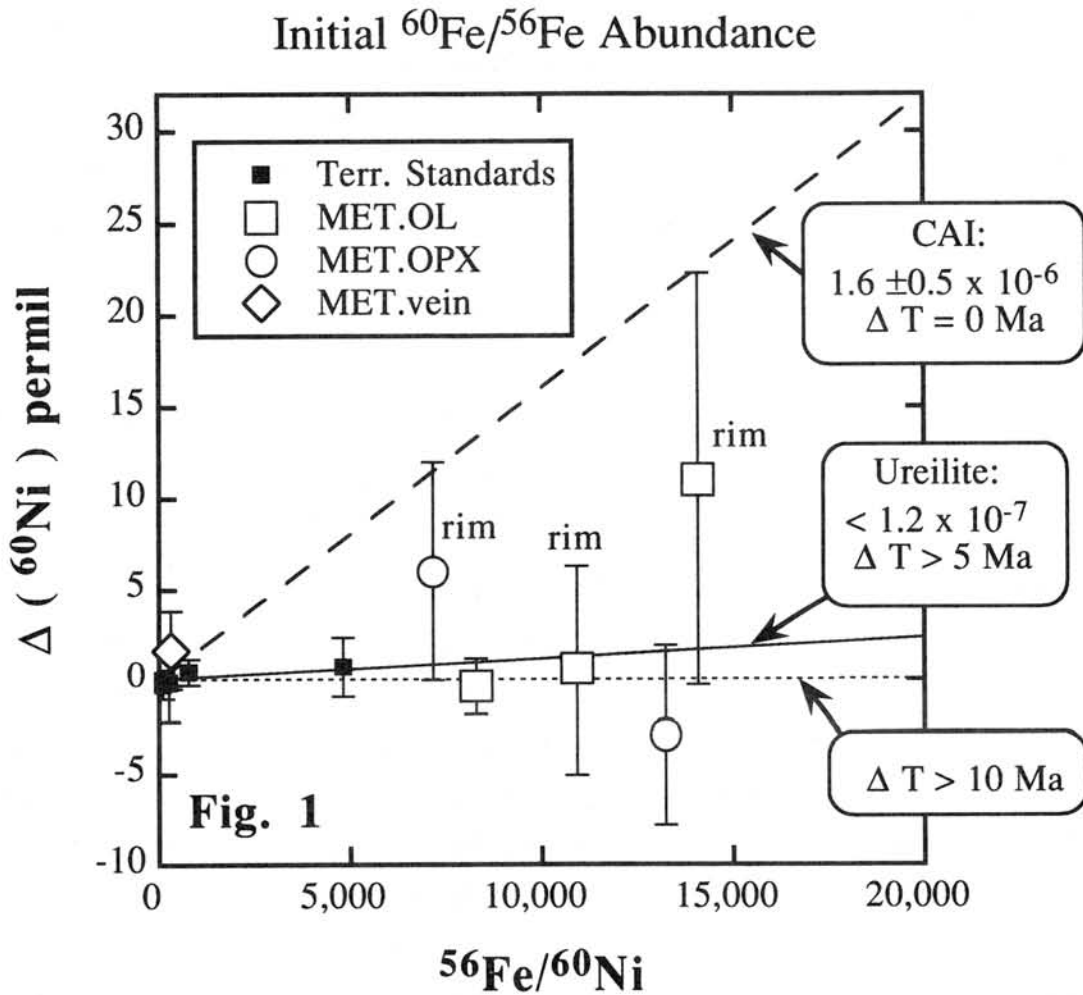
**Results and Discussion:** The fragments of ureilite olivine and pyroxene grains used in this study consist of homogeneous core and reduced rim contact with carbon-metallic vein. Thickness of reduced rim is about 100  $\mu\text{m}$ . Some of low Ca pyroxene grains contain small metallic particles. We measured (1) core olivine, (2) core pyroxene, (3) olivine near the reduced rim, (4) low Ca pyroxene near metallic particles, (5) metallic grain in carbon vein. Measured  $^{59}\text{Co}/^{56}\text{Fe}$  and  $^{60}\text{Ni}/^{56}\text{Fe}$  ratios of core olivine and pyroxenes different spots did not differ more than 3%, indicating homogeneous compositions. The Ni and Co concentrations of each phase are shown in Table 1. The calculated Fe/Ni ratio of silicate phases were between 2,000 and 4,000, which is much higher than bulk analyses of PCA 82506 ureilite of 130 [3].

For the isotopic runs, the analytical error (2 sigma mean) of single analysis was in the range of 1 permil for San Carlos olivine, and 3-4 permil for ureilitic olivine. The measured  $^{60}\text{Ni}/^{61}\text{Ni}$  ratios were corrected for the isotopic mass fractionation effect by comparing measured  $^{61}\text{Ni}/^{62}\text{Ni}$  ratios of the San Carlos olivine standard and the ureilite samples. The  $^{60}\text{Ni}$  excess after the mass fractionation correction, expressed as  $\delta(^{60}\text{Ni})$ , were plotted against  $^{56}\text{Fe}/^{60}\text{Ni}$  ratios in Fig. 1. The average of the 12 olivine analyses showed  $\delta(^{60}\text{Ni}) = -0.4 \pm 1.4$  permil, which is normal within an error. Other data showed larger errors, though all of them are normal within analytical errors. The upper limit of  $^{60}\text{Fe}/^{56}\text{Fe} < 1.2 \times 10^{-7}$  was obtained using most precise result from olivines. Using this upper limit and the initial abundance ratio of CAI [2], the formation age interval between CAIs and MET-78008 is obtained to be  $5.6 \pm 0.6$  Ma. Although the detection of  $^{60}\text{Ni}$  anomaly was unsuccessful, the present result indicates that the ureilite formed at least 5 Ma after the formation of the solar system.

**References:** [1] Torigoye-Kita et al. (1995) GCA 59, 4087-4091. [2] Birck and Lugmair (1988) EPSL 90, 131-143. [3] Shukolyukov and Lugmair (1993) EPSL 199, 159-166. [4] Torigoye-Kita et al. (1995) GCA 59, 2319-2329. [5] Kita et al. (1997) LPSC 28, 737-738.

Table 1. Fe, Co Ni concentrations in silicates of MET78008 ureilite.

| mineral   | location | Fe(%) | Co ppm | Ni ppm | Fe/Ni |
|-----------|----------|-------|--------|--------|-------|
| olivine   | core     | 16.7  | 41     | 70     | 2,399 |
| olivine   | rim      | 16.7  |        | 54     | 3,118 |
| olivine   | rim      | 11.1  | 28     | 28     | 3,997 |
| low Ca Px | core     | 9.6   | 23     | 25     | 3,781 |



## The Yamato-793605 martian meteorite consortium

Hideyasu Kojima<sup>1</sup>, Masamichi Miyamoto<sup>2</sup> and Paul H. Warren<sup>2,3</sup>

<sup>1</sup>National Institute of Polar Research, 9-10, Kaga 1-chome, Itabashi-ku, Tokyo 173, JAPAN

<sup>2</sup>Mineralogical Institute, Grad. School of Sci., University of Tokyo, Hongo, Tokyo 113, JAPAN

<sup>3</sup>Institute of Geophysics, University of California, Los Angeles, CA 90095-1567, USA

**Introduction** Yamato-793605 is a small, 16-gram meteorite that was originally assumed to be a common Antarctic diogenite. In 1994, Mittlefehldt [1] discovered that another, much larger Antarctic “diogenite” had been misclassified. That meteorite, ALH84001, is not a diogenite, because, among other differences, it is comparatively rich in ferric iron and contains preterrestrial carbonates. Mittlefehldt [1] deduced that ALH84001 is instead related to the “SNC” meteorites of presumed martian origin. Yanai [2] and Mayeda et al. [3] soon found evidence from mineralogy and oxygen isotopes, respectively, indicating that Y-793605 (at that time still known by an informal preliminary designation: “Y79-25”) is another member of the SNC/martian group.

Currently, only a total of 12 meteorites from Mars have been identified, of which half are from Antarctica [4]. Apart from ALHA77005, which belongs partly to the USA, Y-793605 is the first martian meteorite in the Japanese Antarctic collection. Its relatively small mass poses a severe constraint for efforts to utilize it as a geologic sample of the parent planet. Under such circumstances, care must be taken to balance and coordinate sample investigation efforts, to ensure that a wide variety of sample properties are measured, and yet conserve sample mass for the most essential measurements, and for future studies. The best way to achieve such a coordinated study is by organizing investigators under the proactive management of a consortium.

The NIPR recognized the need for a consortium to study Y-793605 as soon as the martian affinity of the meteorite was established [2, 3]. The authors volunteered to lead the consortium, and the NIPR approved our proposal in mid-1995. We received numerous sample requests, nearly all from researchers who had extensive previous experience in the study of meteorites from the Japanese and/or American Antarctic collections. Sample requests for investigation of the cosmic-ray exposure (CRE) history of Y-793605 were particularly encouraged, because the similarity between Y-793605 and ALHA77005 and LEW88516 was already apparent [2]. One of the most important goals of the consortium is to determine how the CRE of Y-793605 compares with that of these two similar meteorites. Most samples were sent to investigators in May, 1996.

**Macroscopic Observations on Yamato-793605** On fresh igneous surfaces, the rock appears to consist of roughly 60 vol% pyroxene, 35% olivine, 5% maskelynite and 1% black opaque phases. The pyroxene is pale olive green, and occurs mainly as coarse oikocrysts that enclose smaller (0.5-1.0 mm) and relatively euhedral medium-brown olivines. The opaque phases are scattered and very small (<<0.5 mm). This mode features a slightly higher pyroxene/olivine ratio, and lower maskelynite, compared to modes reported for the ALHA77005 and LEW88516 shergottitic peridotites [5, 6]. The significance of this disparity is unclear, however, because only a small fraction of the surface was “fresh igneous,” and the thin sections later produced for the consortium (see below) reveal considerable cm-scale heterogeneity — as has also been noted for ALHA77005 [4].

Much (probably >>50%) of the meteorite’s original surface was covered by fusion crust. On one surface, we noted fairly extensive rusting. A few tiny, elongate grains of bright white material, possibly evaporite weathering products, were noted, clustered in several small regions of the surface. However, weathering products seem quite rare in the thin sections that were later produced for the consortium. Apparently, Y-793605 is, by Antarctic meteorite standards, moderately weathered.

A large fraction (roughly 30%) of the rock consists of globby enclaves and veins of a dark grey aphanitic or glassy material that presumably, by analogy with similar lithologies in ALHA77005 and LEW88516 [7], formed by shock melting. Analogous materials in ALHA77005 and LEW88516 are commonly termed simply “glass” [4]. Actually, these globs and veins seem in general largely crystalline (albeit extremely fine-grained), and far from pure glass (see, for example, ALHA77005,83-1, shown on page 52 of Yanai and Kojima [8]). The shapes of the glassy-aphanitic shock-melt enclaves in Y-793605 are rounded (not angular), but they are typically elongated, and in places they connect with narrow veins of the same material. These veins are in some places remarkably thin (<<0.3 mm). In a few small areas, the glassy impact melt material appears to be

diffusely scattered amidst surviving crystals of the original igneous-cumulate lithology. During processing for the consortium, the large combined surface area of the 2-gram, multi-fragment sample Y-793605,10 was examined carefully for content of the glassy impact melt lithology. The observed contents (Table 1) indicate an average for Y-793605,10 of roughly 11 vol%, which is considerably below the meteorite average (roughly 30%). However, the consortium (Mittlefehldt and Nagao) also received two small samples of relatively pure glassy impact melt lithology.

**Curatorial Processing of Yamato-793605** Even before the consortium commenced, a mass of 30 mg was allocated to R. N. Clayton for an oxygen-isotopic measurement [3] that confirmed Yanai's [2] suspicion that Y-793605 is related to the 11 other meteorites of presumed martian origin. Initial processing for the consortium took place in the normal sample-processing area of the NIPR, using the usual array of stainless steel tools. Apart from polished thin sections, the main allocation for the consortium was in the form of Y-793605,10. The original mass of Y-793605,10 was 1.992 g. It consisted of many lumps, as large as 958 mg, derived exclusively (or nearly so) from the interior of the meteorite. Division of Y-793605,10 into subsamples suitable for consortium allocations was accomplished in a clean room at UCLA, where the 958-mg chip was broken into smaller pieces using an agate mortar and pestle. These allocations are summarized in Table 1. D. Mittlefehldt's composite group at NASA-JSC received the largest allocation. Other senior JSC personnel involved include: D. Bogard (noble gases and CRE), L. Nyquist (isotope geochemistry, igneous chronology), and M. Lindstrom (bulk composition). Mittlefehldt has also passed the samples studied for bulk composition to M. Lipschutz (Purdue University), for determination of additional trace elements. Similar arrangements for sharing of samples involve N. Nakamura (Kobe U.) in combination with M. Tatsumoto and W. Premo (USGS, Denver), K. Nagao (Okayama U.) in combination with N. Takaoka (Kyushu U.), and P. Warren (UCLA) in combination with T. Fukuoka (Gakushuin U.).

In addition to allocations of approximately representative materials from Y-793605,10, several allocations were made targeting specific components of the meteorite. As described above, Y-793605 contains scattered globs and veins of a dark grey glassy-aphanitic material. Roughly similar glassy enclaves in the EETA79001 and Zagami shergottites have been found to contain C, N and noble gases in proportions (including isotopic ratios) remarkably similar to the atmosphere of Mars as measured by the Viking probe [9, 10]. Thus, the NASA-JSC group led by D. Mittlefehldt received, in addition to their main allocation, a 152-mg sample of "glass"-rich material (Y-793605,71), and K. Nagao received, in addition to his main allocation, a 60-mg sample of "glass"-rich material (Y-793605,73). Mittlefehldt was also allocated a 16-mg piece from the surface of the meteorite (Y-793605,75) for a study of weathering products. K. Nishiizumi was allocated a 24-mg of near-surface material (Y-793605,77) in order to study CRE effects as a function of depth. Finally, T. Mikouchi was allocated a few grains of pyroxene and olivine for crystallography.

Not counting the earlier allocation of a polished thin section (PTS) to K. Yanai, six PTS were produced for the Y-793605 consortium, from two separate parent chips (Y-793605,50 and Y-793605,51), which had original masses of 464 and 375 mg, respectively. Both Y-793605,50 and Y-793605,51 were originally derived from the same 4.2 g subsample (many fragments) of the meteorite, Y-793605,6; Y-793605,10 was also derived partly from Y-793605,6. Except for Y-793605,51-3 (23 mm<sup>2</sup>), the PTS have similar areas of 30 (Y-793605,50-1) to 41 (Y-793605,51-2) mm<sup>2</sup>. Thus far, PTS have been loaned to Y. Ikeda (Ibaraki U.), H. Kojima (NIPR), D. Mittlefehldt and G. McKay (NASA-JSC, collaborating with G. Crozaz, Washington U.), M. Miyamoto (U. Tokyo), P. Warren (UCLA, collaborating with A. Davis, U. Chicago), and K. Yanai (Iwate U.).

**Reconnaissance Results from Consortium Thin Sections** Despite their comparatively large sizes, the consortium thin sections are diverse in mode and texture. Maskelynite is far more abundant in Y-793605,51-1 than in the other sections. As in ALHA77005 and LEW88516 [7], abundance of maskelynite is correlated with a hypidiomorphic-granular texture. Typical, maskelynite-poor portions of the rock are poikilitic, with pigeonite oikocrysts up to 8 mm across (i.e., the complete span of Y-793605,51-4) enclosing pleochroic cumulus olivines. In Y-793605,51-3, cumulus olivines are as large as 2.2×0.7 mm, but in Y-793605,50-1 none is larger than 0.9×0.9 mm. Aphanitic-glassy quenched impact melt (the grey-black material in macroscopic view) is not as abundant in any of the thin sections as it appears from macroscopic observations of the complete meteorite. The highest proportion of the glassy impact melt lithology among the thin sections is 3 vol%, in Y-793605,51-3.

The Y-793605,50 thin sections are virtually devoid of the glassy impact melt lithology. Fusion crust is absent or virtually absent in all of the consortium thin sections.

For purposes of consortium planning, we studied olivine compositions in Y-793605,50-2 and Y-793605,51-1, employing an automated JEOL JXA733 electron probe analyzer (EPMA) at the NIPR. In nonpoikilitic areas (most of Y-793605,51-1 and several large areas within Y-793605,50-2), the average olivine core Mg/(Mg+Fe) is  $66.2 \pm 0.9$  mol% (43 analyses), but in the poikilitic area of Y-793605,50-2, the average is  $69.1 \pm 0.7$  mol% (4 analyses). These results are in excellent agreement with data reported for the poikilitic and nonpoikilitic textural domains in Y-793605,51-2 by Mikouchi and Miyamoto [11]. They are also remarkably similar to results reported for the two textural domains in LEW88516 [7]. Olivine compositions in ALHA77005 are significantly more magnesian, with average Mg/(Mg+Fe)  $\approx 72$  mol% ([7]; and other sources cited by Meyer [4]).

**Conclusions** The Y-793605 consortium has arranged for this important meteorite to be studied for a wide range of properties, at leading laboratories in Japan, the USA and Europe. The present volume contains only some of the consortium's early results, from studies that could be accomplished relatively quickly. The bulk composition, including trace elements, closely resembles those of the ALHA77005 and LEW88516 martian meteorites [12]. All evidence thus far indicates a that Y-793605 is remarkably similar to both ALHA77005 and LEW88516, especially the latter.

**Acknowledgements** We thank the NIPR, and especially Prof. Keizo Yanai, for collecting this important meteorite, and then very generously allocating over 1/5 of its original mass for our consortium study. This research was supported in part by NASA grant NAGW-3808.

**References** [1] Mittlefehldt D. W. (1994) *Meteoritics* **29**, 214-221. [2] Yanai K. (1995) *Lunar Planet. Sci. XXVI*, 1533-1534. [3] Mayeda T. K. et al. (1995) *Lunar Planet. Sci. XXVI*, 917-918. [4] Meyer C. (1996) *Mars Meteorite Compendium — 1996*, NASA Johnson Space Center. [5] Treiman A. H. et al. (1994) *Meteoritics* **29**, 581-592. [6] Wadhwa M. et al. (1994) *Geoch. Cosmoch. Acta* **58**, 4213-4229. [7] Harvey R. P. et al. (1993) *Geoch. Cosmoch. Acta* **57**, 4769-4783. [8] Yanai K. et al. (1987) *Photographic Catalog of the Antarctic Meteorites*, NIPR. [9] Bogard D. D. and Johnson P. (1983) *Science* **221**, 651-654. [10] Marti K. et al. (1995) *Science* **267**, 1981-1984. [11] Mikouchi T. and Miyamoto M. (1996) *Antarctic Meteorites XXI*, 104-106. [12] Warren P. H. and Kallemeyn G. W. (1997) *Antarctic Meteorites XXII*, this volume.

Table 1. Distribution of chip samples for the Y793605 consortium (listing does not include PTS samples).

| parent sample                                       | investigator             | institution           | type of investigation   | mass (mg) | vol% impact melt lithology |
|---|--------------------------|-----------------------|-------------------------|-----------|----------------------------|
| Y-793605,10   | Ebihara, M.              | Tokyo Metropolitan U. | bulk composition        | 209       | 5-10                       |
|   | Eugster, O.              | U. Bern, Switzerland  | noble gases, CRE        | 39        | 10-20                      |
|   | Grady, M.                | Open U., U. K.        | noble gases, carbon     | 14        | nd*                        |
|   | Mittlefehldt, D., et al. | NASA-JSC, USA**       | chronology + (see text) | 102       | 10                         |
|   | Nagao, K.                | Okayama U.            | noble gases, CRE        | 572       | 15                         |
|   | Nakamura, N.             | Kobe U.               | igneous chronology      | 132       | 10                         |
|   |                          |                       |                         | 20        | nd*                        |
|   | Nishiizumi, K.           | U. California, USA    | CRE                     | 218       | 10                         |
|   |                          |                       |                         | 188       | 5-10                       |
|   | Warren/Fukuoka           | UCLA/Gakushuin U.     | bulk composition        | 63        | 5-10                       |
| 19  |                          |                       |                         | nd*       |                            |
|   |                          |                       | 285                     | 10        |                            |
|   |                          |                       | 27                      | nd*       |                            |
| Y-793605,71   | Mittlefehldt, D., et al. | NASA-JSC, USA         | noble gases, CRE +      | 152       | 70                         |
| Y-793605,75   | Mittlefehldt, D.         | NASA-JSC, USA         | weathering products     | 16        | nd*                        |
| Y-793605,73   | Nagao, K.                | Okayama U.            | noble gases, CRE        | 60        | 80                         |
| Y-793605,77   | Nishiizumi, K.           | U. California, USA    | near-surface CRE        | 24        | 80                         |
| Y-793605,90 & ,91                                   | Mikouchi, T.             | U. Tokyo              | crystallography         | 14        | 0                          |
| Total mass of chip samples allocated for consortium |                          |                       |                         | 2154      |                            |

\* nd = not determined (but probably  $\ll 10$  vol%)

\*\* also (M. Lipschutz) Purdue U., USA

# STATISTICAL ANALYSIS OF NIPR METEORITE COMPOSITIONS, II: COMPARISON OF SEQUENCES OF DIFFERENTIATED ROCKS FROM AN ASTEROIDAL SIZED BODY AND EARTH

B. Lukács & Sz. Bérczi

Central Research Institute for Physics RMKI, H-1525 Budapest 114. P.O.Box 49. Hungary  
Eötvös University, Dept. Petrology and Geochem., H-1088 Budapest, Rákóczi ut 5. Hungary

## ABSTRACT

More than 550 bulk chemical compositional measurements in the Catalog of Antarctic Meteorites (Yanai, Kojima, Haramura, NIPR, 1995) represent various layers and so different levels of differentiation from the thermally evolved meteoritic parent bodies. Our comparison of this dataset with the terrestrial data (1) emphasizes common roots and common trends in the differentiation history of different sized bodies, and (2) focuses our attention to the main gradual differences in partial melting in the mantle and in the final stage of differentiation.

## INTRODUCTION

After reconstructing the main events for Fe compounds of the thermal evolution of an asteroidal sized meteorite parent bodies we make a comparison of gradual differentiation in them and Earth. There were common main trends in evolution on both small and large bodies, i.e. accumulation of iron core by separation from the primordial mineral assemblage or differentiation in the mantle via extruding partial (basaltic) melts to the surface. But the finer details of differentiation are various, and Earth, as the largest rocky planet, is expected to be the most differentiated.

Earlier studies of evolutionary paths of chondritic parent bodies in the Fe+FeS vs. Fe-oxides compositional field (Bérczi, Holba, Lukács, 1995) have shown that thermal history of a chondritic parent body advanced toward iron accumulation and outflow of iron to form a core (Lukács & Bérczi, 1997). The existence of the basaltic achondrites proves that partial melts (probably from the mantle) form layers on asteroidal bodies.

One way to advance towards differentiation is volcanic activity when lighter partial melts from the mantle erupt to the surface. We may call theoretical considerations to sketch the main trends on chemical composition of lavas produced in such a process. These main trends were formed by two characteristics of the parent body. One is its mass, and the effect of gravity, the other is the temperature reached, which also depends on the mass of the parent body (see Bérczi & al. 1997).

As a result of gravity we may infer gravitational separation of the most distinctive two phases, that of iron and silicates. After formation of iron core further separation depends on duration of molten state in the mantle and existence of convection. In the region where no convection mixes separated layers, long term differentiation may approach an ideal barometric height formula for compounds, which represent the main constituent chemical elements Fe, Mg and Al. Because of its higher atomic weight FeO compounds should be separated first on a long term heated planetary body, and further separation in the Mg-Al silicates closes this great trend of separation of components. On the basis of such crude theoretical considerations we may account an iron cored, FeO enriched mantled, MgO enriched upper mantled and mainly Al<sub>2</sub>O<sub>3</sub> enriched crusted planetary body as the most evolved type (with our Fe, Mg, Al silicates simple system). We wanted to see if such trends may be seen from the comparison of meteoritic data and terrestrial data sets. The Catalog of Antarctic Meteorites (Yanai, Kojima, Haramura, NIPR, 1995) made it possible not only using many achondritic compositional data

but to project all these main separation events on the chondritic meteorite compositional background.

### MAIN TRENDS IN PLANETARY DIFFERENTIATION

We show 3 compositional fields where chondritic, achondritic and terrestrial compositions were compared. They all are normalized to Si (in weight) and are Fe/Mg, Al/Mg and Al/Fe plots respectively (terrestrial data were taken from the standard literature). On all compositional maps we can see two differentiation sequences. One is for achondrites, the other for Earth. The achondritic sequence has higher total Fe content than the terrestrial sequence. Both sequences span a wide range of Mg content. As we know from both theoretical considerations and from terrestrial geology the higher Mg end is the earlier in formation, and lower Mg containing basalts are the younger differentiates of the mantle. The chondritic cloud of data can be found at higher total Fe contents because metallic Fe was not separated yet by iron core forming first differentiation.

The higher Fe content of achondritic sequence shows that the separation of Fe compounds on a smaller body could have not been so effective as on a larger body (Earth). That is just expected from lower gravity. Thickening of the crust resulted in lavas gradually poorer in Mg as time advanced. Earlier high Mg containing komatiites were followed by later picrites and finally recent low-Mg lavas on the Earth. Similarly, we may infer such a sequence of events on a differentiated asteroidal body too. First diogenitic, later howarditic and finally eucritic lavas were there erupted onto the surface. Although ureilites seem to begin this sequence, we do not know yet their origin.

Next period of differentiation may result in separation of Al containing phases from the mantle compositions, because of the lower density of aluminous minerals which are the main carriers of this element. The Al/Mg map shows that projection of compositions in this respect also exhibit parallel trends both for achondrites and Earth. But achondritic basalts has lower Mg content in this field too, because some part of iron is yet always present in them, and they share the Mg, Fe compositional (mineralogical) sites together. On Earth's surface these sites are partly occupied by Ca, too.

Ca/Al plot shows that the two elements are strongly correlated, but on the most evolved Earth sometimes Al is more enriched when the outermost layers are considered. This shows that a larger body may reach more detailed, finer barometric height formula stratification of the main chemical elements - even if the carriers are minerals - than the smaller asteroidal bodies.

### ACKNOWLEDGEMENTS

This work has been supported by OMFB 96-97-47-1265-MÜI-TP-055/96 grant.

### REFERENCES

- Bérczi Sz., Holba Á., Lukács B.: 1995. Evolution of the Chondrite Parent Bodies I.: Correlation Among Ferrous Compounds. *Acta Mineralogica et Petrographica, Szeged*, XXXVI, 143-152
- Yanai K., Kojima H., Haramura H.: 1995. *Catalog of Antarctic Meteorites*. National Institute of Polar Research, Tokyo.
- Bérczi Sz. & al. 1997: Evolution of a Small and a Large Rocky Planetary Body... (this Volume)
- Lukács B. & Bérczi Sz. 1997: Statistical Analysis of NIPR (Japan) Antarctic Meteorites I. Paths of Evolution of Chondritic Parent Bodies? *LPSC 28*, 384, Houston

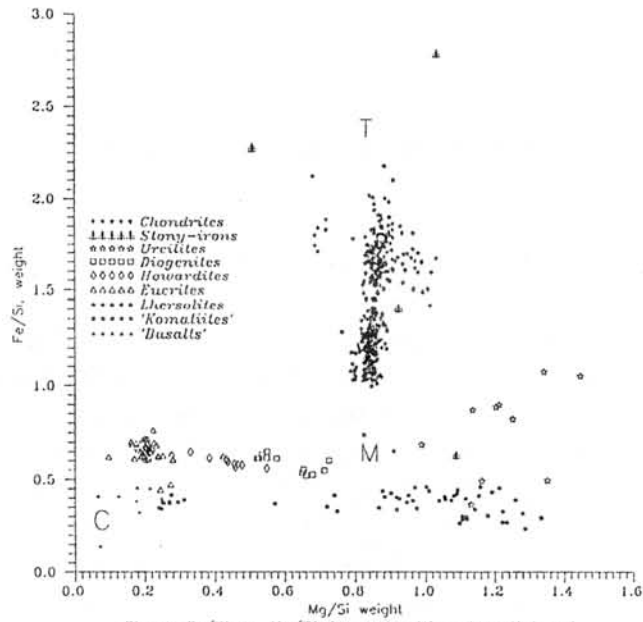


Fig. 1: Fe/Si vs. Mg/Si for meteoritic primordial and differentiated, and terrestrial differentiated rocks.

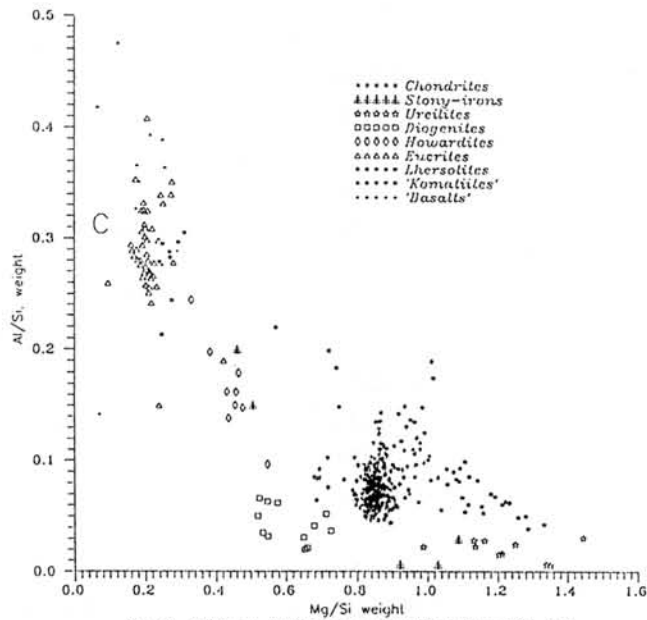


Fig. 2: Al/Si vs. Mg/Si for meteoritic primordial and differentiated, and terrestrial differentiated rocks.

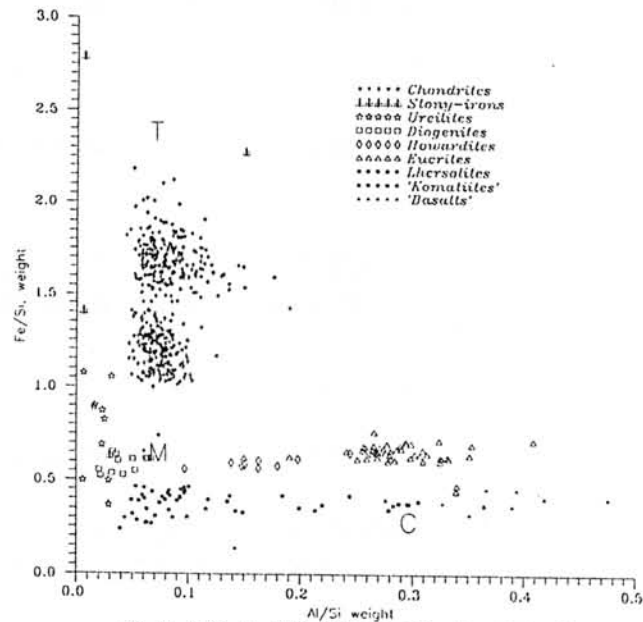


Fig. 3: Fe/Si vs. Al/Si for meteoritic primordial and differentiated, and terrestrial differentiated rocks.

# GENETIC MEANING OF OXYGEN ISOTOPIC VARIATIONS OF CHONDRULES IN CHONDRITES

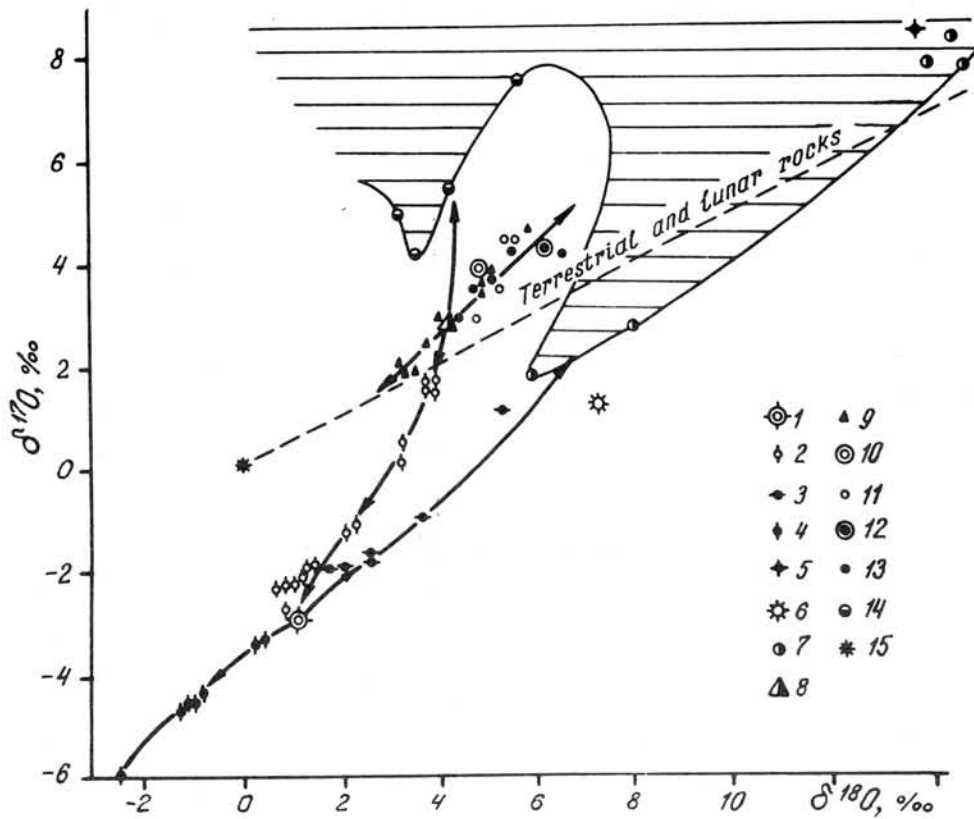
A.A.Marakushev

Institute of Experimental Mineralogy, Russian Academy of Sciences  
Chernogolovka, 142432, Moscow Region, Russia

In previous papers (Marakushev, 1994; Marakushev et al., 1995) the two-stage (I and II) evolution model of the parental planets of meteorites was substantiated: I- under a high pressure of the hydrogen envelopes of their protoplanets in progressively increasing reduced environment and II- after migration of these envelopes under increasingly oxidized conditions. The model accounts for the relic nature of the diamondiferous mineralization of chondrites, which is related exclusively to the stage I. The high hydrogen pressure at this stage is responsible for the origin of diamond as well as for the generation of oxygen isotope anomalies in chondrites as shown by arrows in Figure.

Hydrogen initiated production of water phase, anomalously accumulating heavy oxygen isotopes, as it may be represented by reaction in terms of conventional symbols of normative minerals:  $2\text{Mg}_{1.5}\text{Fe}_{0.5}\text{SiO}_4$  (initial oxygen) +  $\text{H}_2 = \text{Fe} + \text{Mg}_2\text{SiO}_4$  (anomalous light) +  $\text{MgSiO}_3$  (anomalous light) +  $\text{H}_2\text{O}$  (anomalous heavy). It may depict the transition from ordinary chondrite melts, ( $\delta^{17}\text{O} = 2.7$ ,  $\delta^{18}\text{O} = 4.1$ ‰), to carbonaceous chondrite melts, ( $\delta^{17}\text{O} = -2.6$ ,  $\delta^{18}\text{O} = 1.6$ ‰), as the result of separation of water phase, ( $\delta^{17}\text{O} = 7.5$ ,  $\delta^{18}\text{O} = 5.6$ ‰), under the high hydrogen pressure of fluid envelope of parental chondritic protoplanets. The transition is traced by oxygen isotopic variations of barred chondrules (BO) of the Allende (C3) meteorite. These barred chondrules clearly defined genetic links between ordinary and carbonaceous (C3) chondrites both the oxygen isotopic compositions and the iron number of silicates: 27(LL)-24(L)-16(H)- from 12 to zero (Allende barred chondrules). This sequence reflects the progressively increasing reduced conditions under which chondrite magmatism evolved.

The parental planets of carbonaceous chondrites are differentiated into meteoritic types C3-C2-C1 enumerated in order of increasing content of water accumulating heavy oxygen isotopes ( $\delta^{17}\text{O} = 10.2$ ,  $\delta^{18}\text{O} = 17.4$ ‰). Corresponding anomalous oxygen isotopic trend is most clearly pronounced in the porphyry chondrules and melanocratic inclusions of the Allende chondrite.



Oxygen isotopic compositions of chondrules in carbonaceous (C3, C2, C1) and ordinary (H, L, LL) chondrites (Clayton et al., 1983) in correlation with meteoritic water ocean water, lunar and terrestrial rocks (Clayton et al., 1977; Robert et al., 1992). 1-4- carbonaceous chondrite Allende C3 (1) and its chondrules: barred chondrules (2), porphyry chondrules and melanocratic inclusions (3), granular calcic chondrules and leucocratic inclusions (4); 5-6- carbonaceous C1 (5) and C2 (6) chondrites; 7- water of carbonaceous chondrites; 8-9- ordinary H-chondrites (8) and their chondrules (9); 10-11- ordinary L-chondrites (10) and their chondrules (11); 12-13- ordinary LL-chondrites (12) and their chondrules (13); 14- water of ordinary chondrites; 15- ocean water. Region of water oxygen isotopic composition in chondrites is shown by hatching. Pointed by arrows trends of oxygen isotopic variations of chondrules are the result of extraction of heavy oxygen isotopes from chondrite melts by the water phase under the high hydrogen pressure:  $2\text{FeO}(\text{initial oxygen}) + \text{H}_2 = \text{Fe} + \text{FeO}(\text{anomalous light}) + \text{H}_2\text{O}(\text{anomalous heavy})$

Oppositely directed trend of calcic granular chondrules and leucocratic inclusions is represented in Allende chondrite by minerals that are particularly poor in heavy oxygen isotopes (‰) as far as olivine ( $\delta^{17}\text{O} = -23.0$ ,  $\delta^{18}\text{O} = -28.5$ ), fassaite ( $\delta^{17}\text{O} = -16.3$ ,  $\delta^{18}\text{O} = -21.7$ ), spinel ( $\delta^{17}\text{O} = -39.3$ ,  $\delta^{18}\text{O} = -38.0$ ). The minerals of this kind reflect the most influence of hydrogen on chondritic melts producing reactions of this sort  $\text{SiO}_2 + \text{H}_2 = \text{SiO} + \text{H}_2\text{O}$ ,  $\text{Al}_2\text{O}_3 + 2\text{H}_2 = \text{Al}_2\text{O} + 2\text{H}_2\text{O}$ . They are accompanied by extremely contrast distribution of light and heavy oxygen isotopes between components of chondritic melts ( $\text{SiO}$ ,  $\text{Al}_2\text{O}$ ) and separating water ( $\delta^{17}\text{O} = 9.5$ ,  $\delta^{18}\text{O} = 21.5$  ‰). The participation of such anomalous compounds ( $\text{SiO}$ ,  $\text{Al}_2\text{O}$ ) in crystallization of melts is accompanied by separation of native metals ( $2\text{MgO} + 2\text{SiO} = \text{Mg}_2\text{SiO}_4 + \text{Si}$ ,  $\text{MgO} + 3\text{Al}_2\text{O} = \text{MgAl}_2\text{O}_4 + 4\text{Al}$ ). They are mixed with iron native phase in chondrites.

At the second stage (II) parental planets of chondrites lost fluid envelopes. Low-pressure minerals (plagioclase + pyroxene + olivine) and volcanic glass were formed at this stage. The distribution of oxygen isotopes between them follows the law of normal mass fractionation as well as between the minerals in terrestrial and lunar rocks.

**References:** Clayton, R.N., Onuma, N., Ikeda, Y., et al. Oxygen isotopic compositions of chondrules in Allende and ordinary chondrites.- *Chondrules and their origins*. 1983. Vol. 18. P. 37-43. Clayton, R.N., Onuma, N., Grossman, L., Mayeda, T.K. Distribution of the pre-Solar component in Allende and other carbonaceous chondrites.- *Earth Planet. Sci. Lett.* 1977. Vol. 34. Robert, F., Rejou-Michel, A., Javoy, M. Oxygen isotopic homogeneity of the Earth: New evidence.- *Earth Planet. Sci. Lett.* 1992. Vol. 108. P. 1-9. Marakushev, A.A. Two stage evolution of the terrestrial planets recorded in diamond-bearing chondrites.- *Papers presented to the Nineteenth symposium on Antarctic meteorites*. Tokyo, 1994. P. 200-202. Marakushev, A.A., Mitreikina, O.B., Zinovieva, N.G., Granovsky, L.B. Genesis of diamondiferous mineralization in meteorites.- *Antarctic meteorites XX (Paper presented to the twentieth symposium on Antarctic meteorites)*. Tokyo, 1995. P. 148-149.

# THERMAL METAMORPHISM OF CARBONACEOUS CHONDRITES WITH CM AFFINITY: EVIDENCE FROM MINERALOGY AND NOBLE GAS ABUNDANCE

K. Matsuoka <sup>1)</sup>, T. Nakamura <sup>1)</sup>, N. Takaoka <sup>1)</sup>, K. Nagao <sup>2)</sup>, and Y. Nakamuta <sup>1)</sup>

<sup>1)</sup> Department of Earth and Planetary Sciences, Faculty of Science, Kyushu University, Fukuoka 812-81

<sup>2)</sup> Institute for study of Earth's Interior, Okayama University, Misasa, Tottori 682-01

**Introduction** CI and CM carbonaceous chondrites are the most primitive samples of solar system materials, but are affected by secondary aqueous alteration. Recently, several unusual carbonaceous chondrites with CI-CM affinities that experienced thermal metamorphism after aqueous alteration have been found among the Antarctic meteorites. They are Belgica(B)-7904, Yamato(Y)-82162 and Y-86720, which had been studied by a research consortium [1]. They are important samples that have experienced more advanced evolution processes than usual CI-CM carbonaceous chondrites. In the subsequent studies, some other heated CM carbonaceous chondrites were recognized. Y-793321 CM chondrite has an 'intermediate phase' in matrix phyllosilicate, which was formed by a transformation from a serpentine-type phyllosilicate to a mineral with olivine structure by heating [2]. Y-86789 is also an unusual heated CM carbonaceous chondrite, which has textural, mineralogical, and compositional details very similar to those of Y-86720 [3]. It is important to know a relationship between noble-gas abundance and degree of thermal metamorphism which can be given by mineralogical studies. In this study, we report electron-microscope, X-ray, and noble-gas isotope studies on three unusual heated CM carbonaceous chondrites, Y-793321, B-7904, and Y-86789.

**Experimental Method** Polished thin sections and polished sections were prepared from meteorite chips of Y-793321, B-7904 and Y-86789. They were studied using an optical microscope and an electron-probe microanalyzer (EPMA: JEOL JCSA-733 Superprobe) equipped with wave-length dispersive X-ray spectrometers (WDS). WDS analyses were obtained at 15 kV and 10 nA with a focused beam  $\sim 3 \mu\text{m}$  in diameter.

Portions of matrices of approximately  $100 \times 100 \times 100 \mu\text{m}$  in size were extracted from the polished sections under a binocular microscope using an edged tool. The extracted matrices were mounted on thin glass fibers with  $10 \mu\text{m}$  in diameter and were exposed to Cr  $K\alpha$  X ray in a Gandolfi camera. The X-ray photographs were scanned by a photo densitometer and the output data from the densitometer were taken into a computer in order to read precise peak

positions.

Small chips of Y-793321, B-7904 and Y-86789 (32.6 mg, 43.4 mg, and 59.5 mg, respectively) have been analyzed for noble gases with a modified VG5400 mass spectrometer at the Institute for Study of the Earth's Interior, Okayama University [4]. The samples were heated stepwise at 600, 800, 1000, 1200, 1500 and 1850°C in the Ta-furnace.

**Texture and Chemical Composition** Y-793321 shows petrological feature similar to normal CM chondrites; it consists of chondrules, fine-grained chondrule rims, matrix, anhydrous silicate clasts and PCPs: No influence of a heating event is recognized in its texture, but totals of the electron microprobe analyses of the matrix show slightly higher than those of Murchison matrix, suggesting dehydration of matrix phyllosilicates during a heating event. B-7904 consists of chondrules, matrix, rims, and anhydrous silicate clasts. Unlike normal CM chondrites, PCPs are absent in B-7904 instead high abundance of small Fe-sulfide grains (<20µm in size), primarily troilite, spreads throughout the matrix. Some chondrules are altered and have very fibrous texture. Y-86789 has matrix texture similar to that of B-7904 but chondrules differ from those of B-7904: All chondrules are perfectly altered by extensive aqueous alteration and replaced by very fibrous dehydrated phyllosilicate-like materials. Chemical compositions of matrices of B-7904 and Y-86789 show very high analytical total (>90 wt%), suggesting their matrix phyllosilicates are nearly perfectly dehydrated by heating events.

**X-Ray Analyses** The X-ray powder patterns of matrices in B-7904 and Y-86789 show broad forsterite peaks and no reflection of phyllosilicate minerals, indicating that matrix phyllosilicates were dehydrated and decomposed to incompletely crystallized olivines during heating events. Furthermore, the X-ray powder pattern of Y-86789 matrix shows weak broad peaks of enstatite, which means that forsterite and an amorphous silica-rich phase began to transform to enstatite [2]. This suggests that Y-86789 was more intensively heated than B-7904, and the degree of heating decreases in the order of Y-86789 > B-7904.

**Noble-Gas Analyses** Concentrations of trapped noble gases decrease in the order of Y-793321, B-7904, and Y-86789 (Fig. 1): <sup>20</sup>Ne-A2 concentrations are 50%, 2%, and 0.5%, respectively, of those of the Murchison CM chondrite. The trapped-gas concentration reflects degree of heating which the meteorites have experienced, because trapped gases in low retentive sites appear to have been lost from the meteorites. Y-86789 is affected by heating most intensively among the three samples, and Y-793321 is least affected. Concentrations of trapped <sup>132</sup>Xe-Q show the same trend as <sup>20</sup>Ne-A2 (Fig. 1). The concentrations of <sup>132</sup>Xe-Q in

both B-7904 and Y-86789 at 600°C and 800°C are very low (Fig. 2), suggesting that the two meteorites were heated up to 800°C.

On the other hand, concentrations of radiogenic  $^{40}\text{Ar}$  in Y-793321 and B-7904 are  $3.40 \times 10^{-6}$  and  $4.13 \times 10^{-6} \text{ cm}^3\text{STP/g}$ , respectively. With K contents of Y-793321 and B-7904 [5], K-Ar ages of Y-793321 and B-7904 are calculated to be 1.4Ga and 1.8Ga, respectively. They are considerably shorter than 3.4Ga for CM chondrites that was calculated from literature data on  $^{40}\text{Ar}$  [6,7] and K [8] contents, suggesting that the K-Ar chronometers of these samples were reset by loss of  $^{40}\text{Ar}$  during heating event. Therefore, these K-Ar ages have a possibility to date the heating event.

**Degree of Heating** Our mineralogical and noble-gas data of the three meteorites indicate the order of degree of heating to be Y-86789 > B-7904 (>800°C) > Y-793321. This result is consistent with the order of heating deduced from contents of labile trace elements [9], Y-86720 (>700°C) > B-7904 (>600°C), because Y-86720 is a paired meteorite with Y-86789 [3]. But it is not consistent with the order, B-7904 (>750°C)  $\geq$  Y-86720 (700-750°C) > Y-793321 (300-350°C), determined by TEM observation [2] based on transformation of phyllosilicate to olivine.

**References** : [1] IKEDA, (1992) Proc. NIPR Symp. Meteorites, **5**, 49-73. [2] AKAI, (1992) Proc. NIPR Symp. Meteorites, **5**, 120-135. [3] MATSUOKA et al., (1996) Proc. NIPR Symp. Meteorites, **9**, 20-36. [4] MIURA et al., (1995) Geochim. Cosmochim. Acta, **59**, 2105-2113. [5] HARAMURA et al., (1983) Mem. Natl Inst. Polar Res., Spec. Issue **30**, 109-121. [6] MAZOR et al., (1970) Geochim. Cosmochim. Acta, **34**, 781-824. [7] BOGARD et al., (1971) Geochim. Cosmochim. Acta, **76**, 4076-4083. [8] KALLEMEYN et al., (1981) Geochim. Cosmochim. Acta, **45**, 1217-1230. [9] PAUL and LIPSCHUTZ, (1990) Proc. NIPR Symp. Meteorites, **3**, 80-95.

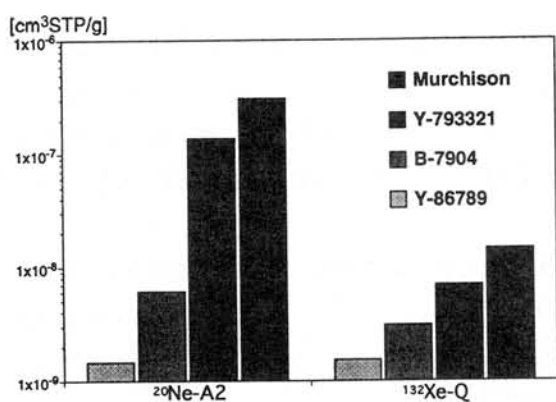


Fig. 1. Concentrations of total  $^{20}\text{Ne-A2}$  and  $^{132}\text{Xe-Q}$  releases.

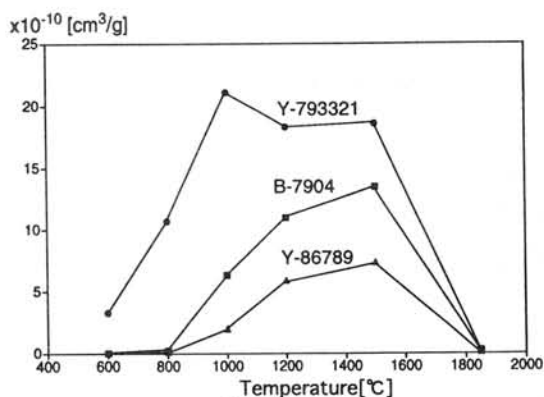


Fig. 2. Release patterns of  $^{132}\text{Xe-Q}$ .

## **EXPERIMENTAL AND PETROLOGIC STUDIES BEARING ON THE ORIGIN OF AUBRITES.**

T. J. McCoy<sup>1</sup>, T. L. Dickinson<sup>2</sup>, and G. E. Lofgren<sup>3</sup>, <sup>1</sup>Department of Mineral Sciences, MRC 119, National Museum of Natural History, Smithsonian Institution, Washington DC 20560, USA, <sup>2</sup>Physics Department, Catholic University of America, Washington DC 20064, USA, <sup>3</sup>Code SN4, NASA/Johnson Space Center, Houston, TX 77058, USA.

### **Introduction**

Igneous products are present in virtually every meteorite and their study is fundamental to understanding the formation of meteorites. Igneous processes have operated in a range of environments from the solar nebula to complete melting and differentiation of asteroids. Unfortunately, few groups of achondrites, stony-irons or irons can be confidently associated with a likely chondrite precursor. Thus, it is difficult to study the full spectrum of igneous processes from chondrule formation, asteroidal partial melting to total melting acting on a common starting material. Enstatite meteorites, however, are an important exception to this rule. As a class, enstatite meteorites exhibit highly reduced mineralogies and a common oxygen isotopic composition (Clayton *et al.*, 1984). This group includes chondrites (EL, EH); impact-melt rocks, breccias and clasts from the EL and EH chondrite parent bodies; achondrites (aubrites); stony-irons; and irons.

We have conducted a variety of experimental and petrologic studies designed to elucidate the origin of aubrites. Igneous processes have been partially duplicated by laboratory experiments and shed significant new light on the melting of ordinary and carbonaceous chondrites [1,2]. Less progress has been made in understanding the melting of enstatite chondrites, in large part because of the experimental difficulty of reproducing their highly reduced nature. We have developed techniques to replicate these highly reducing conditions.

### **The Paradigm and Remaining Problems**

A simplified model for the origin of aubrites begins with an enstatite chondrite which is heated to the point of partial melting. The partial melts, both basaltic and Fe,Ni-FeS, are removed from the source region. Continued heating completely melts this ultramafic residual material, which subsequently crystallizes to form the coarse-grained, igneous aubrites. While this model may be broadly correct in concept, several questions and objections have arisen over the details of such a model. It is these questions which our experimental and petrologic work are attempting to address. These questions include: (1) What happened to the basaltic partial melts? (2) Is aubritic oldhamite a nebular relict or an igneous crystallization product? (3) Can aubrites be derived by melting of known enstatite chondrites?

### **What happened to the basaltic partial melts?**

Differentiation of any likely chondritic precursor should produce a significant quantity of basaltic material. Despite this fact, brecciated aubrites contain a relative paucity of basaltic clasts. A number of theories have been proposed to explain their absence in aubrites, including their loss by explosive volcanism early in the history of the solar system [3]. Alternatively, a small number of sulfur-rich, silicate clasts have been identified in aubrites [4] which may sample these basaltic materials. Partial melting experiments of enstatite chondrites (discussed below) have played a key role in predicting the compositions of this missing component and future experiments may further broaden the range of materials removed during partial melting.

### **Is aubritic oldhamite a nebular relict or an igneous crystallization product?**

The highly-reducing conditions under which aubrites formed caused elements which are normally lithophile (e.g., Ca, Mg, Mn, Cr) to behave as siderophiles, forming a variety of unusual sulfides such as oldhamite (CaS), niningerite (MgS), alabandite (MnS) and daubreelite (FeCr<sub>2</sub>S<sub>4</sub>). Among these, oldhamite has garnered attention because it is the major REE carrier in aubrites (100-1000 x CI, implying REE partition coefficients between oldhamite and the bulk aubrite of the same magnitude)

[5,6], has an extraordinarily high melting temperature (~2450°C) as a pure substance, and some grains have REE abundances and patterns similar to those of unequilibrated enstatite chondrites [7,8]. These latter facts have led some authors to argue that many oldhamite grains are nebular relicts which survived igneous processing [7,9,10]. In contrast, textural evidence [6], REE patterns in some oldhamite grains [7], and oldhamite containing phases which condense at lower temperatures [6] all support an igneous origin. Despite this interest, relatively few experimental studies have been conducted to investigate the partitioning of REE. We have conducted experiments to evaluate these partition coefficients and to investigate the dependence of partitioning on oldhamite composition, temperature, oxygen fugacity, and low temperature annealing.

Our experiments [11] were run in sealed silica tubes and utilized a starting composition similar to aubrites, which included metallic Al and Mg as oxygen getters to produce the low  $fO_2$  appropriate to aubrite formation. The starting composition was doped with REE elements at the wt.% level. Charges were run at 1200-1300°C for 2 days. These experiments crystallized oldhamite at temperatures of 1200-1300°C from a silicate melt of aubrite-like composition, far below the melting temperature of pure oldhamite. The strongest control on REE partitioning is the composition of the crystallizing oldhamite. Calcium-poor oldhamite (63-79% CaS) produces a LREE-depleted, HREE-enriched pattern with a negative Eu anomaly. In contrast, Ca-rich oldhamite (88-89%CaS) produces a bowed pattern with a positive Eu anomaly. Temperature also strongly influences partitioning. Partition coefficients increase with decreasing temperature. Experiments run for 2 days at 1200°C and annealed at 800°C for 9 days exhibit larger partition coefficients for Eu and Gd. Partition coefficients measured in this work [11], and by other authors [10,12] are generally around unity.

Measured partition coefficients are clearly inconsistent with a simple igneous origin in which oldhamite is the first crystallizing phase and REE abundances are determined solely by high temperature partitioning between the oldhamite and bulk liquid. Partition coefficients near unity are consistent with the nebular model, but enstatite chondrite partial melting experiments (discussed below) suggest such an origin is unlikely. We suggest instead that oldhamite REE patterns were established by a complex process of partial melting, melt removal, fractional crystallization with oldhamite of varying compositions crystallizing from isolated melt pools, subsolidus annealing and exsolution of Mg, Mn, Cr, and Fe-rich phases, producing a wide range of REE patterns.

### **Can aubrites be derived by melting of known enstatite chondrites?**

Although aubrites clearly derived from a highly reduced precursor like enstatite chondrites, several authors have argued that aubrites were not derived by melting of known enstatite chondrites. Several arguments have been made that aubrites and enstatite chondrites formed on different parent bodies [13] and we do not disagree with this conclusion. More relevant to this discussion, several differences exist between aubrites and known enstatite chondrites (e.g., Ti abundances in troilite, presence of pigeonite in aubrites, [13]) and these features are not easily explained by igneous fractionation. Our recent petrologic [14] and experimental work [15] sheds some light on these issues.

The Bustee aubrite contains an oldhamite-pyroxene clast. Rounded oldhamite spheres 1-4 mm in diameter comprise ~30% of the clast and include large osbornites (TiN) and titanian troilite (17.2-25.2 wt.% Ti) and smaller niningerite, heideite, daubreelite, metal and forsterite. This clast is unique in containing the most Ti-rich troilite found in aubrites, as well as the Ti-rich phases osbornite and heideite. Thus, this occurrence may shed some light on the origin of the Ti enrichment in aubritic troilite relative to EC troilite. Previous workers have proposed that Ti could be enriched in aubritic troilite through immiscibility in the Fe-Ni-S system [16], preferential fractionation of Ti-rich FeS [17] or melting of osbornite [18]. However, no immiscibility exists in the Fe-Ni-S system; temperature and density difference between Ti-rich and Ti-poor troilite are too small to produce fractionation; and the occurrence of Ti-rich troilite with osbornite in Bustee suggests that melting of osbornite is not producing the Ti-rich troilite. Instead, we suggest that co-crystallization with and/or exsolution from oldhamite provides such a mechanism. Indeed, our oldhamite experiments demonstrated immiscibility in the Fe-Ca-S system [11].

Oldhamite efficiently excludes Ti, which can be preferentially incorporated into troilite, thus providing a mechanism for enriching aubritic troilite in Ti and weakening arguments against a derivation of aubrites from known enstatite chondrites.

Our latest efforts [15] have focused on a direct assessment on EC melting by conducting partial melting experiments on Indarch (EH4). In our current experiments, a graphite crucible containing ~160 mg of powdered Indarch and an alumina crucible containing Cr metal are sealed in an evacuated silica tube. Thus, the sample should stay at the Cr-Cr<sub>2</sub>O<sub>3</sub> buffer at all temperatures, which closely duplicates the intrinsic oxygen fugacity of enstatite chondrites. Samples were melted at 1000-1500°C for 4-24 hours. Textures of the charges ranged from unconsolidated powder (1000°C) with only Fe,Ni-FeS melting through total melting (1500°C). Significant separation of rounded Fe,Ni-FeS spheres occurs between 1400-1425°C. Metal in the 1100-1425°C charges contains between 5.0-8.4 wt.% Si, indicating that highly-reducing conditions were maintained during the run. The 1000-1100°C and 1450-1500°C charges lack sulfides. This almost certainly results from volatilization and, at low temperature, reaction with the Cr buffer. The 1200-1425°C charges contain two sulfides: one Fe-rich and the other Mg-rich (1200-1300°C) or Mn-rich (1400-1425°C). At all temperatures, the Mg,Mn-rich sulfide contains wt.% levels of Ca and Cr. In none of these charges were any relict sulfide grains observed. Silicate melt is absent at 1000°C. From 1100-1500°C, the melt becomes systematically depleted in SiO<sub>2</sub>, Na<sub>2</sub>O and K<sub>2</sub>O and enriched in CaS and MgO. The decreasing SiO<sub>2</sub> and increasing MgO likely reflect increased melting of enstatite. Increasing CaS reflects increases in both Ca and S in the melt, with S reaching 6.0 wt.% in our 1425°C charge. Decreasing Na<sub>2</sub>O and K<sub>2</sub>O reflects their preferential incorporation into the melt at low temperatures and increasing volatilization at high temperatures.

Several implications can be gleaned from these and previous [19,20] experiments. Significant S can be accommodated in the silicate melt at reducing conditions. As [20] pointed out, S most likely combines with Ca and Mg in the silicate melt and can crystallize oldhamite upon cooling. An important conclusion of this work is that at temperatures as low as 1200°C, relict sulfides are not observed and Ca, Mg, Mn and Cr are incorporated into either a sulfide or silicate melt. We find that oldhamite is not a stable phase at temperatures down to 1200°C where silicate melt exists and could not survive igneous processing on the aubrite parent body, in agreement with [20] and contrary to the suggestion of [7,9,10]. In addition, we observe significant exchange of elements between different phases (e.g., Si between metal and silicate melt; Ca between sulfide and silicate melt). This movement of elements might produce compositions not readily predicted on the basis of equilibrium melting relations alone and could explain the origin of some features of aubrites (e.g., the presence of oldhamite and forsterite).

### Summary and Future Work

Recent experimental and petrologic studies have elucidated the origin of aubrites by melting of enstatite chondrites. Past objections to a direct derivation from known enstatite chondrites seem weakened in light of this work. In addition, a relict nebular origin for aubritic oldhamite seems doubtful. A significant number of experiments remain to be conducted. The most important of these will examine the cooling and crystallization of partial melts and melting and crystallization of the residue. The latter experiments should serve to further our knowledge about the genesis of aubrites.

**REFERENCES:** [1] Jurewicz et al. (1993) *GCA* 57, 2123-2139. [2] Jurewicz et al. (1995) *GCA* 59, 391-408. [3] Wilson and Keil (1991) *EPSL* 104, 505-512. [4] Fogel (1994) *Meteoritics* 29, 466-467. [5] Floss et al. (1990) *GCA* 54, 3553-3558. [6] Wheelock et al. (1994) *GCA* 58, 449-458. [7] Floss and Crozaz (1993) *GCA* 57, 4039-4057. [8] Crozaz and Lundberg (1995) *GCA* 59, 3817-3831. [9] Kurat et al. (1992) *Meteoritics* 27, 246-247. [10] Lodders (1996) *MAPS* 31, 749-766. [11] Dickinson and McCoy (1997) *MAPS* 32 (in press). [12] Jones and Boynton (1983) *LPSC XIV*, 353-354. [13] Keil (1989) *Meteoritics* 24, 195-208. [14] McCoy (1996) *MAPS* 31, A86. [15] McCoy et al. (1997) *LPSC XXVIII*, 903-904. [16] Brett and Keil (1986) *EPSL* 81, 1-6. [17] Fogel et al. (1988) *LPSC XIX*, 342-343. [18] Casanova (1992) *Meteoritics* 27, 208-209. [19] Dickinson and Lofgren (1992) *LPSC XXIII*, 307-308. [20] Fogel et al. (1996) *LPSC XXVII*, 371-372.

## Textural Relationships Among Carbonates, Shocked Feldspathic Glass, and Pyroxene in Martian Meteorite ALH84001

G. A. McKay<sup>1,2</sup>, G. E. Lofgren<sup>1</sup>, and T. Mikouchi<sup>2</sup>

<sup>1</sup>SN4, NASA Johnson Space Center, Houston TX 77058, USA

<sup>2</sup>Mineralogical Institute, Graduate School of Science, University of Tokyo, Tokyo 113, Japan

**Introduction.** ALH84001, originally classified as a diogenite, was subsequently recognized by [1] as a Martian meteorite. It differs from other Martian meteorites in that it is a coarse-grained orthopyroxene cumulate containing ~1% carbonate [1,2]. It has attained enhanced importance as a result of the recent announcement of possible evidence for relict biogenic activity, especially in the carbonates [3]. The issue of biogenic activity is of great philosophical and scientific importance, and yet remains highly controversial. Understanding the origin and history of the carbonates in this sample is one key to resolving this controversy. Unfortunately, the origin of the carbonates is itself controversial, even to the point of disagreement over the temperature of formation by several hundreds of degrees [e.g., 2-5], and the age of the carbonates relative to major events that have affected this sample [e.g., 2,9].

The general petrography of ALH84001 was described by [2,3], and many workers have studied the petrography and chemical compositions of carbonates [e.g., 4-7,9]. The sample was initially formed as an igneous orthopyroxene and chromite cumulate with interstitial plagioclase. Subsequently, the sample suffered mechanical granulation along sheared zones (probably from shock), recrystallization of the granular material, and at least one shock event after the recrystallization. The plagioclase was converted to feldspathic glass, but this glass differs significantly from plagioclase stoichiometry [e.g., 1], is chemically heterogeneous (see below) and may not be a simple product of shock-induced solid-state transition to a disordered state. At some point during these events, carbonates were introduced into the sample. However, the age of the carbonates is not yet well understood [10,11], and even the timing of their formation relative to other events affecting this sample is unclear, as is the mechanism of carbonate formation. This abstract presents data that provide additional constraints on the origin and history of the carbonates.

**Samples and analytical methods.** We studied three polished thin sections of ALH84001 (.64, .82, .88) that were allocated to the consortium led by Duck Mittlefehldt. We used optical microscopes, the Cameca SX-100 electron microprobe at the Johnson Space Center (JSC) for elemental mapping and quantitative analyses, and both the Cameca SX-100 at JSC and the Hatachi S4500 FEG-SEM at the Mineralogical Institute, University of Tokyo, for BSE imaging.

**Modes of Carbonate Occurrence.** Carbonate has been reported in four textural modes: (1) rounded objects called concretions, globules, rosettes, or disks, depending on the author; (2) interstitial grains between granular pyroxene grains in recrystallized zones; (3) large veins filling cracks (we interpret these as disks viewed edge-on [6]); and (4) material filling fractures and pockets in cumulus pyroxene grains. Here we will focus on the first two modes, and describe a fifth mode.

**Globules.** Globules often occur in clusters (Fig. 1), and show striking concentric zoning, from cores of ferroan dolomite to rims with alternating bands of magnesite and ferroan magnesite [e.g., 1-4, 6]. Some compositions are metastable [e.g., 4,6]. Typically, the rounded form and distinctive rims are most often well-developed on the portions of globules facing feldspathic glass (Fig 1). This observation led Treiman [2] to propose that the carbonates formed by chemical replacement of preexisting plagioclase, prior to the event that converted the plagioclase to maskelynite. However, Kring *et al.* [9] pointed out that replacement of plagioclase would mainly occur along twin boundaries, grain boundaries, and cracks, and thus be unlikely to produce rounded shapes. Such rounded shapes are more characteristic of growth in an isotropic medium. Therefore, they proposed that the carbonates formed by chemical replacement of shock-produced feldspathic glass (maskelynite), and thus post-dated the shock event.

However, as illustrated in Fig. 1, the carbonates have been mechanically disrupted, and isolated fragments of carbonate rims are dispersed within the glass, along with fragments of pyroxene. Moreover, bands of glass appear to invade the carbonates (e.g., globule on

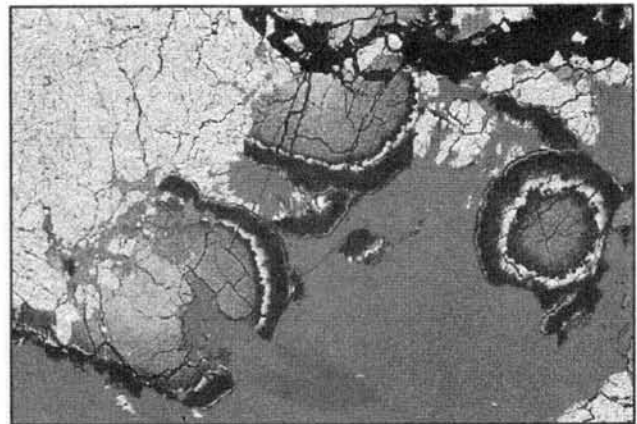


Fig. 1. BSE image of carbonate globules in ALH84001, 82. Dark gray unfractured material is feldspathic glass. Light gray is pyroxene. Radial zoning and prominent banded rims are visible in carbonate globules. Rounded shapes and well-developed rims are most often found on portions of carbonates facing glass. Note isolated fragments of carbonate rims in glass, and band of glass cutting across rim and invading globule on left. Also note that pyroxene is fragmented and dispersed in glass. Width of field is 350  $\mu\text{m}$ .

left in Fig. 1), cutting sharply across the rim. We believe these observations require that the carbonate formed prior to a major shock event that mobilized the feldspathic glass and mechanically disrupted the carbonates. The observations are thus inconsistent with formation of carbonates by replacement of maskelynite unless that maskelynite was formed by an earlier event, and *remobilized* by a *second* event.

*Interstitial grains between granular pyroxenes.* In some annealed areas, interstices between granular pyroxene grains are filled by feldspathic glass. In other areas, however, the interstices are filled by carbonates [2,6]. Kring *et al.* [9] noted this similar textural niche for feldspar and carbonate, and proposed that, along with the globules, this interstitial carbonate was also formed by chemical replacement of glass. Fig. 2 shows a portion of an annealed crushed zone with carbonate and feldspathic glass occupying interstices between granular pyroxene. The carbonate in this region exhibits chemical zoning that is very similar to that in the globules: There is a central region of Ca-enriched carbonate surrounded by a discontinuous rim of magnesite (dark) and ferroan magnesite (light), and an outer band of magnesite. It is likely that these carbonate patches are connected in the third dimension. A similar feature was reported by Treiman [2]. We proposed [6] that the similarity in zoning between globules and interstitial regions is a necessary consequence of chemical fractionation during growth from a limited supply of material, and that the metastable compositions inside the solvus between dolomite-siderite ss and magnesite-ankerite ss are the result of rapid growth.

*A new textural mode of carbonate: Filling the interstices between relict grains in feldspathic glass.* We recently discovered a new mode of occurrence, in which carbonate forms a lacy 3-dimensional network that is enclosed in feldspathic glass (Fig. 3a) [12]. A higher magnification view (Fig 3b) reveals what appear to be outlines of granular or subhedral crystals occupying the space between the carbonate grains. Note, especially, the straight and nearly parallel sides of the glass area indicated by the arrow. We believe the only reasonable interpretation of this texture is that the carbonate in this area grew in the interstices between a cluster of preexisting grains.

We are not yet certain as to the nature of the material filling the space within the carbonate network. Because of the fine grain size, and the presence of carbonate in the third dimension, it is difficult to determine whether this material is optically isotropic. However, areas in Fig 3a that are free of carbonate through the entire thickness of the thin section show no apparent birefringence. The chemical composition is generally feldspathic, but more careful analyses will be required to determine whether the material deviates from feldspar stoichiometry. On the basis of currently available data, the most likely interpretation is that these features are relict grains of feldspar that have

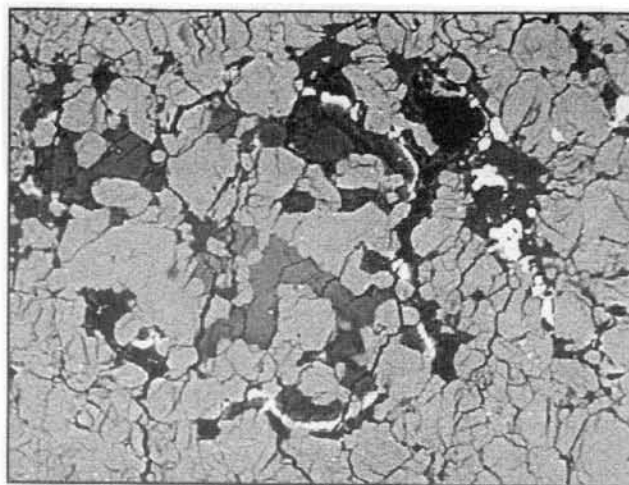


Fig. 2. BSE image of carbonate and feldspathic glass in interstices between granular pyroxenes in crushed zone. Pyroxene is medium gray, feldspathic glass is dark gray unfractured region at right with bright chromite, carbonate is fractured and zoned from medium gray (center) to dark gray with partial "rim" of ferroan magnesite (light) sandwiched between two bands of magnesite (dark). Width of field is 150  $\mu\text{m}$ .

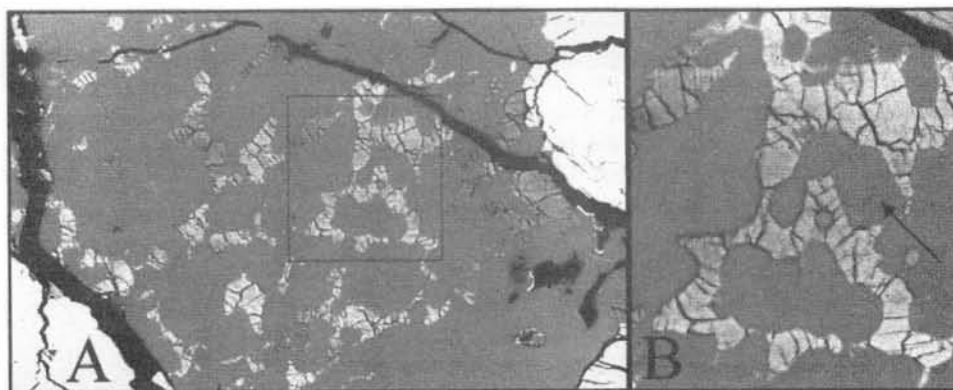


Fig. 3. BSE image of lacy carbonate filling interstices between relict grains in area of feldspathic glass. **A.** Overall view of glass region (medium gray, unfractured) containing lacy network of carbonates (light gray to dark gray, highly fractured). Dark magnesite grains at right contain bright bands of ferroan magnesite. Light phase at left and right is pyroxene. Width of field is 200  $\mu\text{m}$ . **B.** Higher magnification view of region outlined by rectangle in A. Note the euhedral or granular crystal shapes outlined by the interstitial carbonate, especially the euhedral area indicated by the arrow. Width of field is 45  $\mu\text{m}$ .

been converted to glass by shock.

It seems clear from Fig. 3 that this textural form of carbonate grew in the interstices between small granular or euhedral feldspar grains. Also, this carbonate must have simultaneously or after the feldspar. There are several possibilities for the origin of this carbonate-feldspar assemblage: (1) Both minerals could have grown simultaneously in a metamorphic recrystallization or annealing event like the one in which the granular pyroxene formed [1,2]. (2) The plagioclase could have formed first, with void space somehow being present between the grains, and the void space was subsequently filled by carbonate (unlikely, because the presence of void space between euhedral plagioclase is difficult to explain). (3) The carbonate could have replaced another interstitial mineral such as pyroxene (unlikely, because in areas like Fig. 2, where carbonate is interstitial to granular pyroxene, it clearly did not replace pyroxene). (4) Both minerals could have crystallized simultaneously during or after a shock event (shock melting of feldspar and carbonate was suggested by [7]), with the euhedral crystals being a high pressure mineral such as that reported by El Goresy *et al.* [8]. In this case, not all carbonate need necessarily have been melted by the shock event. Perhaps the globules are unmelted. If so, however, it would be necessary to explain the similarity in chemical composition between melted and unmelted carbonates. More work will be required to distinguish between these (or other) possibilities for the origin of this texture.

**Summary of petrographic observations constraining models for carbonate formation.** There are a number of key petrographic observations that any model for the origin of carbonates in ALH84001 must explain. These include: (1) Occurrence of carbonate in several textural settings, including (a) globules or disks, (b) filling of interstices between granular pyroxene grains and (apparently) granular plagioclase, (c) large veins, and (d) filling of small fractures and pockets within cumulus pyroxene. (2) Prevalence of well-developed rim sequences and round shapes on sides of globules facing feldspathic glass rather than pyroxene. (3) Similarity of chemical zoning in carbonates for all textural modes, and presence of metastable compositions between dolomite-ankerite ss and magnesite-siderite ss [e.g., 2, 4, 6]. (4) Radial and oscillatory nature of zoning in globules [e.g., 6]. (5) Crystallographically controlled boundary between magnesite and ferroan magnesite in the globule rim sequences, typically marked by striking euhedral crystal faces [e.g., Fig. 1b in 6]. (6) Presence of abundant magnetite and Fe sulfide in the ferroan magnesite band of globule rims [e.g., 3]. (7) Brittle fracture and mechanical disruption of globules, and presence of globule (especially rim) and pyroxene fragments in adjacent feldspathic glass. (8) Presence of bands of feldspathic glass cutting sharply across rim sequences in some globules. (9) Optical and chemical heterogeneity of most areas of feldspathic glass. (10) Unfractured nature of feldspathic glass, compared with highly fractured nature of other minerals, which are often radially fractured around glass [see 8].

**Discussion.** At present, we have no comprehensive explanation of carbonates that is consistent with all the observations listed above. However, we can draw a few conclusions. The presence of globule fragments in feldspathic glass requires disruption of preexisting carbonates prior to or at the same time as introduction or mobilization of the glass. As pointed out by Kring *et al.* [9] the rounded globule morphology is not consistent with formation of globules by replacement or dissolution of crystalline plagioclase, but rather suggests growth in an isotropic media. They proposed that this media was glass. However, the mechanical disruption of globules and their intrusion by feldspathic glass indicates that the globules were already present at the time the glass formed (or last moved). Thus either the carbonates formed in a medium other than glass, or the glass was remobilized after the carbonates were formed. Details of the mechanism of globule disruption and entrainment in glass are unclear.

The interstitial nature of carbonate in granular regions between both pyroxene and relict plagioclase seems inconsistent with chemical replacement of only pyroxene or plagioclase alone, to form carbonates. It is highly unlikely that carbonates were formed by replacement of one phase in some areas and the other phase in different areas. Perhaps a third interstitial phase was present and has been replaced, but we see no evidence for such a phase. The most likely explanation of interstitial carbonate is that it formed prior to or during annealing of the granular zones.

It is clear that much work remains to be done to understand the enigmatic carbonates in ALH84001.

**References:** [1] D. Mittlefehldt (1994) *Meteoritics* 29, 214-221. [2] A. Treiman (1995) *Meteoritics* 30, 294-302. [3] D. McKay *et al.* (1996) *Science* 273, 924-930. [4] R. Harvey and H. McSween (1996) *Nature* 382, 49-51. [5] J. Bradley *et al.* (1996) *GCA*, 60, 5149-5155. [6] G. McKay and G. Lofgren (1997) *LPS XXVIII*, 921-922. [7] E. Scott *et al.* (1997), *LPS XXVIII*, 1271-1272. [8] A. El Goresy *et al.* (1997) *LPS XXVIII*, 329-330. [9] D. Kring *et al.* (1997) Conference on Early Mars\*. [10] M. Wadhwa and G. Lugmair (1997) Conference on Early Mars.\* [11] D. Bogard and D. Garrison (1997) Conference on Early Mars\*. [12] G. McKay *et al.* (1997) abstract for Meteoritical Society meeting, submitted\*.

\*These abstracts can be downloaded from the LPI Web Site at <http://cass.jsc.nasa.gov/meetings/recentmeetings.html>

# Major and minor element distributions in pyroxene and maskelynite from Martian meteorite Yamato-793605 and other lherzolitic shergottites: Clues to their crystallization histories

Takashi Mikouchi and Masamichi Miyamoto

Mineralogical Institute, Graduate School of Science, University of Tokyo, 7-3-1 Hongo, Bunkyo-ku, Tokyo 113, Japan.

## Introduction.

SNC (Shergottites-Nakhlites-Chassignite) meteorites are widely believed to have originated on the planet Mars from many lines of evidence [e.g., 1], and they are of great importance to get an insight into magmatic and mantle processes within Mars. A new Antarctic Martian meteorite Yamato-793605 (Y793605) has been extensively studied by a consortium investigation organized by National Institute of Polar Research (NIPR), Tokyo [2] and all shows its close affinities to lherzolitic shergottites ALH77005 and LEW88516 in both mineralogy and chemistry [e.g., 3-10]. Lherzolitic shergottites are mainly composed of two different textures, poikilitic and non-poikilitic, in a cm scale heterogeneity [e.g., 11, 12]. In the poikilitic area, large pyroxene oikocrysts enclose rounded olivines (~1 mm) and euhedral chromites (~0.5 mm), and maskelynite is rarely observed. The non-poikilitic area is composed of subequal amounts of olivine, maskelynite and pyroxene. The sizes of olivine and maskelynite are larger than those in the poikilitic area. In both textures, pyroxenes and maskelynites are zoned in major and minor elements, providing us with useful informations on their crystallization histories. We analyzed chemical zoning of major and minor elements in pyroxene and maskelynite from three lherzolitic shergottites by electron microprobes and here discuss the petrogenetic relationship of Y793605 to ALH77005 and LEW88516 and their crystallization histories.

## Samples and Analytical Technique.

Chemical analyses were made on polished thin sections of Yamato-793605 (Y793605,51-2) and ALH77005 (ALH77005,93-1) supplied by NIPR and LEW88516 (LEW88516,24) supplied by The Meteorite Working Group (MWG), NASA Johnson Space Center. Quantitative wavelength dispersive analyses were performed on a JEOL 733 electron microprobe (Ocean Research Institute, University of Tokyo) and a JEOL JCM 733 mk II microprobe (Geological Institute, University of Tokyo). Microprobes were operated at 15 kV accelerating voltage, and beam current was 12 nA. We employed a defocused beam of ~10  $\mu\text{m}$  in diameter to minimize loss of volatile elements during maskelynite analysis. However, the actual composition will be more alkali-rich, because volatile loss is inevitable during analysis.

## Major and Minor Element Zoning in Pyroxene and Maskelynite. Y793605

Y793605,51-2 is about 9 x 6 mm in size, and is composed of pigeonite, olivine, augite, maskelynite, chromite and several other accessory minerals [e.g., 4]. The thin section is principally poikilitic in texture, but contains a small non-poikilitic (interstitial) area [e.g., 4] (Fig. 1). The pyroxene oikocryst (~8 mm) in the poikilitic area is zoned from a Ca-poor composition ( $\text{En}_{76}\text{Fs}_{21}\text{Wo}_3$ ) to a little Ca- and Fe-rich composition ( $\text{En}_{66}\text{Fs}_{23}\text{Wo}_{11}$ ). The structural state of the lowest-Ca pyroxene is unknown, but observation by an optical microscope indicates a monoclinic crystal system. Broad augite bands (~1 mm wide) are usually present rimming the oikocryst, but small patches are also observed within the oikocryst. They are zoned from  $\text{En}_{52}\text{Fs}_{16}\text{Wo}_{32}$  to  $\text{En}_{46}\text{Fs}_{14}\text{Wo}_{37}$  (Fig. 2). Pyroxenes are small (~0.5 mm) and not abundant in the non-poikilitic area. Pigeonite in the non-poikilitic area is more Ca- and Fe-rich than that in the poikilitic area (Fig. 2). The composition is scattered in both Ca and Fe contents. Typically it ranges from  $\text{En}_{65}\text{Fs}_{28}\text{Wo}_7$  to  $\text{En}_{60}\text{Fs}_{27}\text{Wo}_{13}$ . Augite is from  $\text{En}_{52}\text{Fs}_{16}\text{Wo}_{32}$  to  $\text{En}_{46}\text{Fs}_{16}\text{Wo}_{38}$ . Al and Ti in pigeonites show distinct distributions between the poikilitic and non-poikilitic areas (Fig. 3). Both Al and Ti increase in the oikocrystic pigeonite ( $\text{Al}_2\text{O}_3$ : 0.3-1.5 wt%,  $\text{TiO}_2$ : 0.05-0.35 wt%), while pigeonite in the non-poikilitic area first shows a decrease of Al and Ti ( $\text{Al}_2\text{O}_3$ : 0.8-0.5 wt%,  $\text{TiO}_2$ : 0.8-0.3 wt%), and then they increase ( $\text{Al}_2\text{O}_3$ : 0.5-1.4 wt%,  $\text{TiO}_2$ : 0.3-0.6 wt%) [4]. Maskelynites are rare in the poikilitic area, and they are unehedral up to a few hundreds of  $\mu\text{m}$  in size. In the non-poikilitic area, they are lath-shaped reaching 1 mm in length. Both maskelynites are chemically zoned and their major element compositions are almost identical. They are typically  $\text{An}_{55}\text{Ab}_{44}\text{Or}_1$  in the core and  $\text{An}_{45}\text{Ab}_{52}\text{Or}_3$  in the rim. Although maskelynites in the poikilitic area do not show systematic zoning in minor elements from core to rim due to irregular shape of the grain, they are systematically zoned in maskelynites of the non-poikilitic area. FeO and MgO in maskelynites of the non-poikilitic area show unique zoning patterns (Fig. 4). FeO in the core is about 0.5 wt%. It first drops down to 0.2 wt%, and then it again slightly increases to 0.4 wt% at the edge with some decrease and

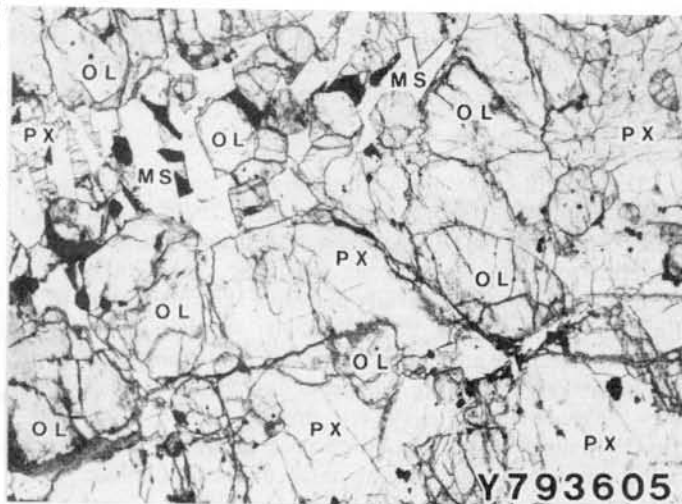


Fig. 1: Photomicrograph of Y793605. The width is ca. 3 mm. OL: olivine, PX: pyroxene, MS: maskelynite. Note that a non-poikilitic area is located around upper left.

increase. MgO is correlated with FeO. MgO in the core is 0.2 wt%. It decreases to 0.1 wt% as Fe decreases. However, it is then nearly constant towards the edge or shows a little decrease. Ti and K show increase from core to rim and do not seem to show any particular relations with Fe and Mg (Fig. 4). Ca content is nearly homogeneous in the core (CaO ~11 wt%) that corresponds to the region where Fe shows decrease.

#### ALH77005

ALH77005,93-1 (13 x 6 mm) is also mainly composed of the poikilitic areas, each reaching 6 mm in size (Fig. 5). Non-poikilitic regions are also present between the large oikocrystic pigeonites as vein-like forms (~2 mm wide). Large impact melt pockets that partially formed by skeletal olivines are observed unlike Y793605 (Fig. 5). Oikocrystic pigeonites are zoned from  $En_{77}Fs_{19}Wo_4$  to  $En_{65}Fs_{20}Wo_{15}$  (Fig. 6). Most augites in the poikilitic area are present as irregular bands of ~0.5 mm wide at the rim of the oikocryst. Small augite patches in the oikocrysts observed in Y793605 are rare. Augites are zoned from  $En_{55}Fs_{15}Wo_{30}$  to  $En_{48}Fs_{12}Wo_{40}$  (Fig. 6). Pyroxenes in the non-poikilitic areas are much smaller (~0.5 mm) than those in the poikilitic area. Pigeonite in the non-poikilitic area is clearly more Ca- and Fe-rich, and ranges from  $En_{66}Fs_{27}Wo_7$  to  $En_{61}Fs_{23}Wo_{16}$  (Fig. 6). Augite in the non-poikilitic area is from  $En_{53}Fs_{15}Wo_{32}$  to  $En_{48}Fs_{14}Wo_{38}$  (Fig. 6). Oikocrystic pigeonites show systematic increase in Al and Ti ( $Al_2O_3$ : 0.3-1.4 wt%,  $TiO_2$ : 0.05-0.3 wt%), while pigeonite in the non-poikilitic area is more Al- and Ti-rich and shows different zoning trends (Fig. 7). Both Al and Ti first decrease ( $Al_2O_3$ : 0.8-0.6 wt%,  $TiO_2$ : 0.8-0.3 wt%), and then they increase ( $Al_2O_3$ : 0.6-1.4 wt%,  $TiO_2$ : 0.3-0.7 wt%) (Fig. 7). Although maskelynites are extremely uncommon in the poikilitic area, they comprise a much larger proportion in the non-poikilitic area. Maskelynites in both areas show chemical zoning with almost identical composition in major elements. They are usually zoned from  $An_{58}Ab_{41}Or_1$  to  $An_{48}Ab_{49}Or_3$ , nearly corresponding to the reported compositions [11, 12]. Although Ikeda [13] reported crystalline plagioclase rim with reverse major element zoning, we analyzed euhedral-shaped grains without these rims. FeO and MgO in maskelynites also show unique zoning patterns like Y793605 (Fig. 8). FeO drops from 0.4 to 0.3 wt% in the core, and then it shows a little increase to 0.5 wt% toward the edge with slight decrease and increase. MgO is highly correlated with FeO. MgO decreases from 0.2 to 0.1 wt% as Fe decreases. It is then nearly constant toward the edge or shows a little increase (Fig. 8). Ti and K weakly increase from core to rim.

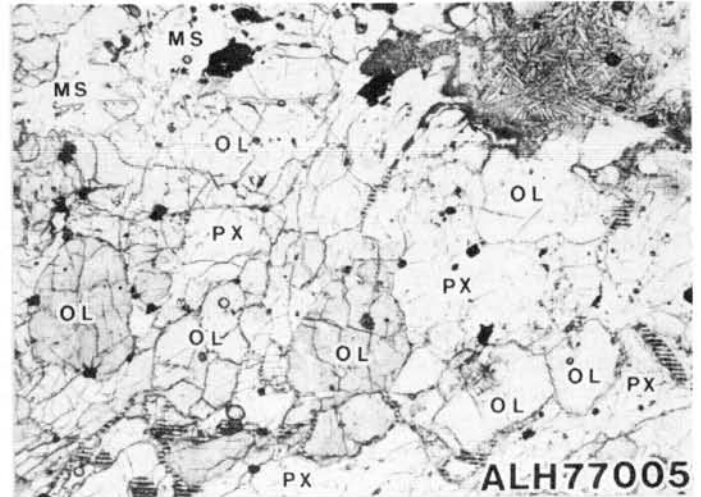


Fig. 5: Photomicrograph of ALH77005. The width is ca. 3 mm. A non-poikilitic area is observed around an upper left corner. An impact melt pocket with skeletal olivines can be seen upper right.

#### LEW88516

The poikilitic area is observed only in a small part of LEW88516,24 (10 x 7 mm) unlike Y793605 and ALH77005 (Fig. 9). Large impact melt pockets with skeletal olivines are also observed like ALH77005. Pyroxene oikocrysts are mainly pigeonite and zoned from  $En_{77}Fs_{20}Wo_3$  to  $En_{65}Fs_{21}Wo_{14}$  (Fig. 10). Augites in the poikilitic area are present at the rim of the oikocryst or small patches within the oikocryst like Y793605, and they are zoned from  $En_{55}Fs_{16}Wo_{29}$  to  $En_{48}Fs_{14}Wo_{38}$  (Fig. 10). Pyroxenes in the non-poikilitic area are pigeonite and augite. Pigeonite and augite in the non-poikilitic area range from  $En_{65}Fs_{28}Wo_7$  to  $En_{54}Fs_{28}Wo_{18}$  and from  $En_{52}Fs_{17}Wo_{31}$  to  $En_{47}Fs_{16}Wo_{37}$ , respectively (Fig. 10). Oikocrystic pigeonites (>5 x 3 mm) show systematic increase in Al and Ti like Y793605 and ALH77005 ( $Al_2O_3$ : 0.3-1.4 wt%,  $TiO_2$ : 0.05-0.4 wt%) (Fig. 11). Pigeonite in the non-poikilitic area is more Al- and Ti-rich than that in the poikilitic area (Fig. 11). Al and Ti first decrease ( $Al_2O_3$ : 0.8-0.5 wt%,  $TiO_2$ : 1.0-0.2 wt%), and then they increase ( $Al_2O_3$ : 0.5-1.4 wt%,  $TiO_2$ : 0.2-0.5 wt%) as Y793605 and ALH77005 show (Fig. 11), but more Ti-rich pigeonite is present in LEW88516. Maskelynites in both poikilitic and non-poikilitic areas are typically zoned from  $An_{58}Ab_{41}Or_1$  to  $An_{48}Ab_{49}Or_3$ . FeO and MgO in maskelynites also show unique zoning patterns like Y793605 and ALH77005 (Fig. 12). FeO drops from 0.5 to 0.3 wt% in the core, and then it a little increases to 0.5 wt% at the edge with slight decrease and increase. MgO decreases from 0.15 to 0.1 wt% as Fe decreases. It is then nearly constant towards the edge. Ti and K increase from core to rim.

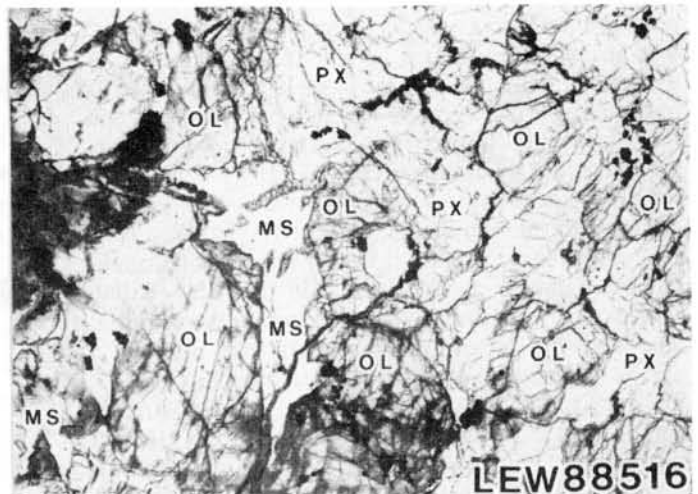


Fig. 9 Photomicrograph of LEW88516. The width is ca. 3 mm. A non-poikilitic area is observed in the left side. Black- and grey-colored regions are olivine suffering from impact.

### Constraints on the Crystallization Histories of Lherzolitic Shergottites.

It should be noted that minor element distributions in pyroxene and maskelynite from Y793605 show similar zoning patterns to those from ALH77005 and LEW88516, as suggested for major elements [e.g., 3, 4]. Thus, this study further supports an idea that Y793605 shows a close mineralogical similarities to ALH77005 and LEW88516 [e.g., 3, 4, 7, 8, 9], and also reveals additional evidence of mineralogical similarities between ALH77005 and LEW88516 [11, 12, 14]. Minor element behaviors in pigeonite and maskelynite are a key to understand the crystallization histories of lherzolitic shergottites. Both Ti and Al decreases in pigeonites of the non-poikilitic area (Figs. 3, 7, 11) suggest co-crystallization of a Ti-bearing phase, probably ilmenite [4]. Then, Al and Ti increase might indicate the end of ilmenite crystallization [4]. Decrease and increase of Fe content from core to rim in an individual grain of maskelynite in the non-poikilitic area are also important to study a crystallization sequence of the phases constituting the non-poikilitic area. Fe and Mg decrease in the maskelynite core suggest that plagioclase co-crystallized with an Fe- and Mg-bearing phase. Because an intergrowth texture of pigeonite and maskelynite is observed (e.g., Fig. 1), plagioclase and pigeonite might have co-crystallized at some stage of the non-poikilitic area formation. Fe zoning in maskelynites can give constraints on the crystallization conditions.

An explanation of the crystallization sequence of three lherzolitic shergottites might be possible employing a pseudo-liquidus diagram (Fig. 13) that is used for understanding the petrogeneses of basaltic shergottites [e.g., 15]. After crystallization of cumulus phases (e.g., olivine and chromite), oikocrystic pigeonites were formed as products of progressive fractional crystallization along arrow A-B [11]. Then, crystallization progressed to the pigeonite-augite cotectic, where pigeonite and augite co-crystallized along arrow B-C. The liquid composition reached the eutectic, where plagioclase crystallization began. It is expected that Fe in plagioclase might decrease as crystallization of three phases continues, because pyroxenes took much Fe in the melt, resulting in Fe decrease in the plagioclase core. Fe then shows increase in plagioclase, which might suggest change of geological setting (e.g., change of temperature, pressure).

We consider that this event brought about shift of phase boundaries (from solid lines to dotted lines). Although such a phase boundary shift is unknown, it is possible to consider that the composition was located in the field of plagioclase and plagioclase alone crystallized, which caused Fe increase in plagioclase (C-D). Then, the liquid composition reached the plagioclase-pigeonite cotectic (D), and pigeonite in the non-poikilitic area crystallized with a higher Fe content than oikocrystic pigeonite. This would again cause Fe decrease in plagioclase. Finally, the composition again reached eutectic (E), where augite crystallization in the non-poikilitic area began. Because at the last stage, volume of residual liquid was small, and plagioclase show enrichment in Fe at the edge. This scenario is a hypothesis, and still bears some uncertainties like phase boundary shift. To understand crystallization history of lherzolitic shergottites, further study is needed.

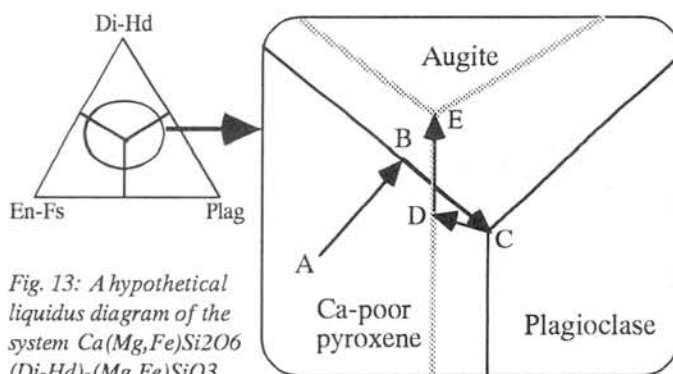


Fig. 13: A hypothetical liquidus diagram of the system  $\text{Ca}(\text{Mg,Fe})\text{Si}_2\text{O}_6$  (Di-Hd)-(Mg,Fe)SiO<sub>3</sub> (En-Fs)-plagioclase showing possible crystallization sequences of lherzolitic shergottites. Solid and dotted lines are phase boundaries. Dotted lines indicate phase boundaries after change of the geological setting. Arrows from A to E are crystallization passes.

### Conclusions.

In conclusion, minor element characteristics of Y793605 pigeonite and maskelynite show remarkable affinities to ALH77005 and LEW88516 as well as major elements. A cosmic-ray exposure age of Y793605 also accords with those of ALH77005 and LEW88516 [7, 10]. It is likely that these three meteorites shared a common petrogenesis on Mars and formed in the same igneous body as many studies propose [e.g., 4]. The same cosmic-ray exposure age of three shergottites also indicates that Y793605 was ejected from Mars by the same impact event as the other two, and reached different areas in Antarctica as different falls. Such relationship of three lherzolitic shergottites is similar to that observed in three nakhlites (Nakhla, Lafayette, and Governador Valadares). Crystallization history of lherzolitic shergottites is complex as suggested by complicated minor element zoning of maskelynite.

### Acknowledgment.

We thank NIPR and MWG for the meteorite samples and Mr. O. Tachikawa and Mr. H. Yoshida for technical assistance. Discussion with Dr. G. A. McKay of NASA Johnson Space Center was very much helpful. This work was partially supported by Society for Promotion of Space Science.

### References.

- [1] McSween H. Y. Jr. (1994) *Meteoritics* 29, 757-779. [2] Kojima H. et al. (1997) *Antarct. Meteorite Res.* 10, (submitted). [3] Mikouchi T. and Miyamoto M. (1996) *Meteoritics and Planet. Sci.* 31 (Suppl.) A89-A90. [4] Mikouchi T. and Miyamoto M. (1997) *Antarct. Meteorite Res.* 10, (submitted). [5] Misawa K. et al. (1997) *Antarct. Meteorite Res.* 10, (submitted). [6] Mittlefehldt D. W. et al. (1997) *Antarct. Meteorite Res.* 10, (submitted). [7] Nagao K. et al. (1997) *Antarct. Meteorite Res.* 10, (submitted). [8] Warren P. H. and Kallemeyn G. W. (1997) *Antarct. Meteorite Res.* 10, (submitted). [9] Ikeda Y. (1997) *Antarct. Meteorite Res.* 10, (submitted). [10] Eugster O. and Polnau E. (1997) *Antarct. Meteorite Res.* 10, (submitted). [11] Harvey R. P. et al. (1993) *Geochim. Cosmochim. Acta* 57, 4769-4783. [12] Treiman A. H. et al. (1994) *Meteoritics* 29, 581-592. [13] Ikeda Y. (1994) *Proc. NIPR Symp. on Antarctic Meteorites* 7, 9-29. [14] Wadhwa M. et al. (1994) *Geochim. Cosmochim. Acta* 58, 4213-4229. [15] Stolper E. and McSween H. Y. Jr. (1979) *Geochim. Cosmochim. Acta* 43, 1475-1498.

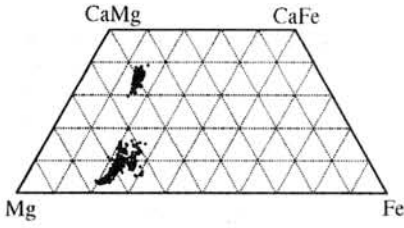


Fig. 2: Pyroxene quadrilateral of Y793605

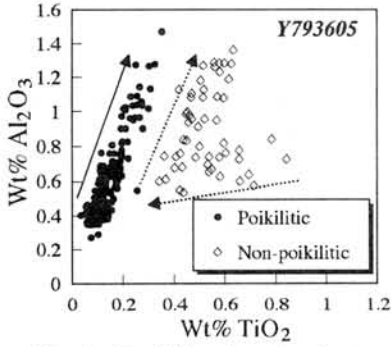


Fig. 3: Al vs Ti in pigeonites from Y793605

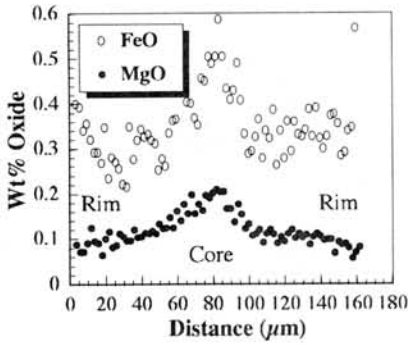


Fig. 4: Chemical zoning of maskelynite in the non-poikilitic area of Y793605

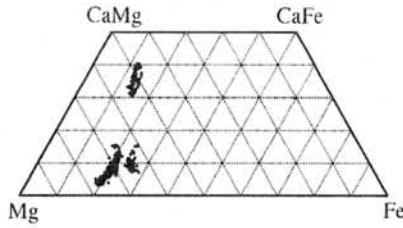
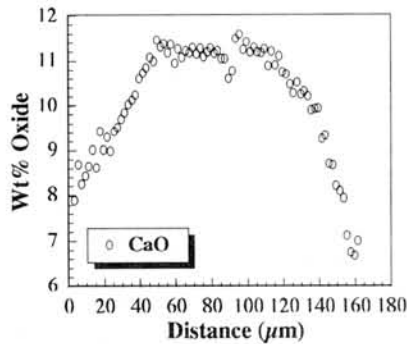
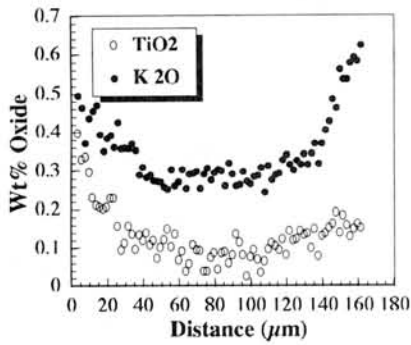


Fig. 6: Pyroxene quadrilateral of ALH77005

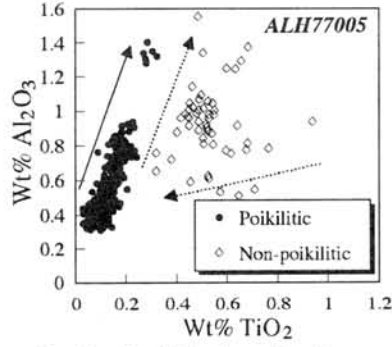


Fig. 7: Al vs Ti in pigeonites from ALH77005

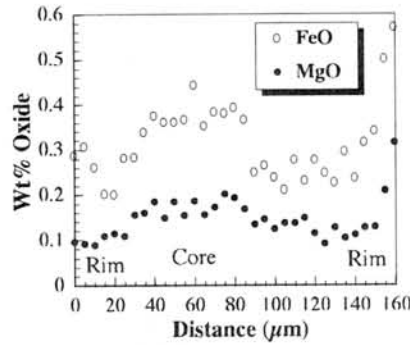


Fig. 8: Chemical zoning of maskelynite in the non-poikilitic area of ALH77005

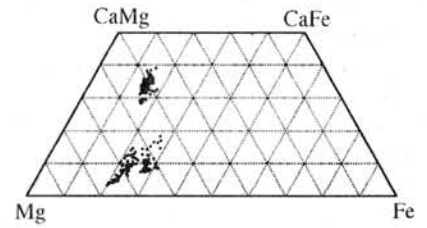
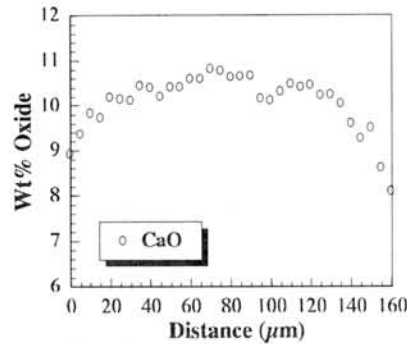
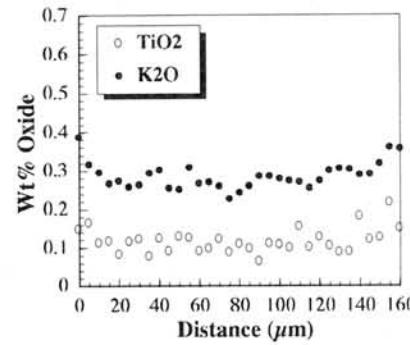


Fig. 10: Pyroxene quadrilateral of LEW88516

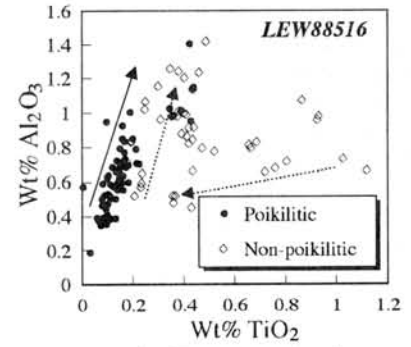


Fig. 11: Al vs Ti in pigeonites from LEW88516

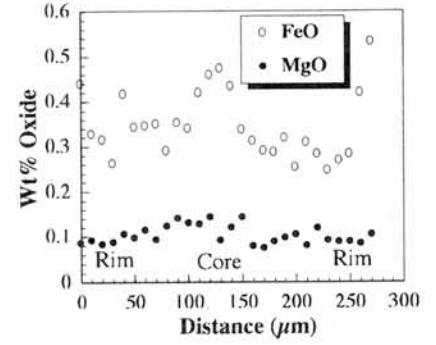
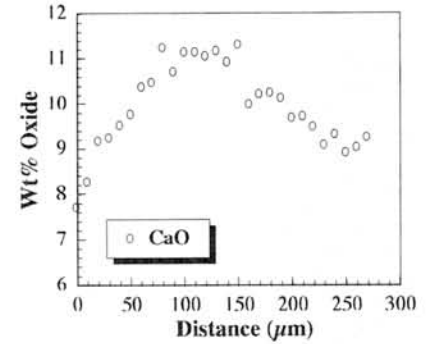
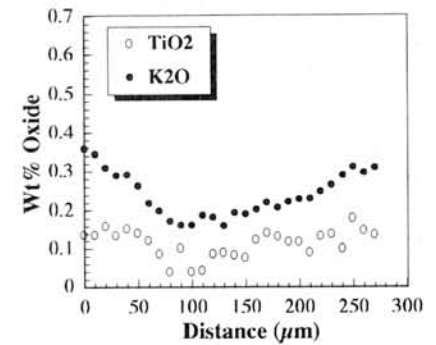


Fig. 12: Chemical zoning of maskelynite in the non-poikilitic area of LEW88516



## Production Rates of Cosmogenic He, Ne, and Ar in Chondrites

M. Minamitani<sup>1</sup>, R. Okazaki<sup>1</sup>, N. Takaoka<sup>1</sup>, T. Nakamura<sup>1</sup>, and K. Nagao<sup>2</sup>

<sup>1</sup>*Department of Earth and Planetary Sciences, Faculty of Science, Kyushu University 33, Hakozaki, Fukuoka 812-81, Japan,* <sup>2</sup>*Institute of Study for Earth's Interior, Okayama University, Misasa, Tottori 682-01, Japan*

Mineral separates of olivine, pyroxene, plagioclase, troilite and Fe-Ni metal and a bulk sample of the Alfianello L6 chondrite were analyzed for cosmogenic noble gases to determine the elemental production rates of cosmogenic He, Ne and Ar. The meteorite was powdered in a stainless steel mortar, and sieved to grain-size fractions. From these grain-size fractions, Fe-Ni metal was separated with a hand magnet and purified by selective dissolution of silicates in HF. Troilite was hand-picked from a >95 $\mu\text{m}$  fraction under a binocular. Plagioclase was separated from 26-42 and 42-67 $\mu\text{m}$  fractions using heavy liquid with a density of 2.82 g/cm<sup>3</sup>. Troilite adhering on plagioclase grains was removed by dissolution in 0.5M HCl. Olivine was hand-picked under an optical microscope in crossed polarizer from the 42-67 $\mu\text{m}$  fraction after plagioclase separation. Pyroxene in the 42-67, 67-95 and 96-133 $\mu\text{m}$  fractions was isolated by selective dissolution of olivine in 7M HCl after the separation of plagioclase.

Purity of each mineral separate was examined by analyzing qualitatively with an EPMA for elements that should not be included in the mineral. Approximately 400 to 500 grains were investigated except for the pyroxene fraction for which 50 grains were used. The purity was determined to be 92, 91, 81, 99 and 99 wt.% for olivine, pyroxene, plagioclase, troilite and metal fractions, respectively.

Duplicate measurements of noble gases were carried out at Okayama University on the mineral separates of more than 10 mg, except for the olivine separate that was only 0.8 mg available for the analysis. Concentration of cosmogenic <sup>81</sup>Kr was also determined for the cosmic-ray exposure age. Major element abundance in each mineral including Si, Mg, Fe, Al, Ca, Na, K, Cr, Mn, Ti, and S was determined by electron microprobe analyses on a thin section of a bulk meteorite sample. For the bulk elemental abundance in Alfianello meteorite, we adopt literature data (Kallemeyn et al., 1989; Michaelis et al., 1969).

With assumptions of  $P^{21}(\text{Na})=P^{21}(\text{Mg})$  and  $P^{21}(\text{Al})=1.35 \times P^{21}(\text{Si})$  (Stauffer, 1962), we have the following production rates of cosmogenic <sup>21</sup>Ne and <sup>38</sup>Ar:

$$P^{21} = 1.40[\text{Na}+\text{Mg}]+0.43([\text{Al}]+1.35[\text{Si}])+0.23[\text{S}]+0.019[\text{FeNi}], \text{ and}$$

$$P^{38} = 10[\text{K}]+1.01[\text{Ca}]+0.073[\text{FeNi}]$$

where [X] is concentration of element X as weight fraction and  $P^{21}$  and  $P^{38}$  are in units of  $10^{-8}$  cc STP/g per my. For this evaluation, we used the cosmic-ray exposure age of  $28 \pm 5$  my that was determined by the  $^{81}\text{Kr}$ -Kr method.

Compared our formula for  $P^{21}$  with that of Schultz and Freundel (1985), a good agreement is found on rates for Si, S, and FeNi. However, our rates for Mg and Al are lower by a factor of 1.2 and 1.4 than those of Schultz and Freundel (1985), respectively. The  $(^{22}\text{Ne}/^{21}\text{Ne})_c$  of bulk Alfianello is 1.11, suggestive of the typical shielding condition for chondrites, thus we can compare the production rates for Alfianello bulk (i. e.,  $0.29 \times 10^{-8}$  and  $0.038 \times 10^{-8}$   $\text{cm}^3/\text{g my}$  for  $^{21}\text{Ne}$  and  $^{38}\text{Ar}$ , respectively) with literature data. While  $P^{38}$  is lower by a factor of 1.2 than that of Eugster (1988),  $P^{21}$  agrees well with that of Nishiizumi et al. (1980). This low  $P^{38}$  is consistent with the result of Miura and Nagao (1992).

#### References

- Eugster O.(1988) GCA 52, 1649-1662.
- Miura Y. and Nagao K. (1992) Proc. NIPR. Symp. Antarct. Meteorites 5, 298-309.
- Nishiizumi K. et al. (1980) EPSL 50, 156-170.
- Schultz L. and Freundel M. (1985) in Isotopic ratios in the solar system (ed. Centre National d'Etudes Spatiales), Cepadues-Editions, Toulouse, 27-33.
- Stauffer H. (1962) JGR 67, 2023-2028.
- Kallemeyn G. W. et al. (1989) GCA 53, 2747-2767.
- Michaelis H. et al. (1969) EPSL 5, 387-394.

## U-Th-Pb ISOTOPIC SYSTEMATICS OF LHERZOLITIC SHERGOTTITE YAMATO 793605

Keiji Misawa<sup>1</sup>, Noboru Nakamura<sup>1</sup>, Wayne R. Premo<sup>2</sup> and Mitsunobu Tatsumoto<sup>2</sup>

<sup>1</sup>Department of Earth & Planetary Sciences, Faculty of Science, and Division of the Nature of the Earth, The Graduate School of Science and Technology, Kobe University, Nada, Kobe 657, Japan, <sup>2</sup>U.S. Geological Survey, MS 963, P.O. Box 25046, Denver CO 80225, U.S.A.

Nakamura et al. (1982) first proposed from U-Pb and Sm-Nd isotopic studies that Nakhla came from a relatively large, well-differentiated parent body, such as the planet, Mars. It is now widely believed that the SNC (shergottites, nakhlites, Chassigny) meteorites and one orthopyroxenite, ALH84001, possibly came from Mars. After ALH84001 was recognized as belonging to the martian group, Yanai (1995) reexamined the meteorite collection at the NIPR and found that Y-793605 has similar mineralogical and petrological characteristics to those of the shergottite meteorites. The Y-793605 meteorite is a lherzolitic shergottite, similar to ALH77005 and LEW88516 (Yanai, 1995, 1996, Mikouchi and Miyamoto, 1996a, b). Chronological studies have already been carried out on both basaltic and lherzolitic shergottites (Bogard et al., 1979, Nyquist et al., 1979, 1984, 1987, 1995, Shih et al., 1982, Wooden et al., 1982, Jagoutz and Wänke, 1986, Chen and Wasserburg, 1986, 1987, 1993, Jagoutz, 1989, Borg et al., 1997). Because isotopic systems have been disturbed most likely by intense shock, interpretation of ages obtained using these different isotope systems are very complex.

We have undertaken U-Th-Pb isotopic studies on lherzolitic shergottite, Y-793605. Yamato 793605 (408 mg) allocated from the NIPR through P.H. Warren was composed of several fragments containing ~10% fine-grained black material (shock melt). Under the binocular microscope, we recognized black-colored shock melt and numerous euhedral chromite grains. The sample was gently crushed with a stainless steel mortar and divided into three sized fractions (<63 $\mu$ m, 63-150 $\mu$ m, 150-300 $\mu$ m) using nylon cloth sieves. Olivine (OL) was handpicked from the 150-300 $\mu$ m fraction. Three separates (two pyroxene-rich phases: PX1 and PX2, and maskelynitized plagioclase: PL) were obtained from the 63-150 $\mu$ m fraction using a Frantz isodynamic separator equipped with an ethanol-filled chute. The PX1 is more magnetic and dark in color (enriched in black material) than PX2. The finest fraction (<63 $\mu$ m) was used as a whole-rock sample (WR). Four mineral separates and a whole-rock sample were leached with dilute acid in order to remove terrestrial Pb contamination.

Lead isotopic data of Y-793605 are plotted in Figs. 1a and 1b, and compared with existing data of Shergotty, Zagami, EET79001, ALH77005, and LEW88516 from Chen and Wasserburg (1986, 1987, 1993). The Pb isotopic difference among the shergottite whole-rocks suggests that they could not be derived from a single parental source reservoir. The Pb isotopic data points of five residue fractions scattered and a calculated Pb-Pb age is 3800 Ma with a large error and does not clearly indicate a later disturbance on the U-Pb system, in contrast with other shergottites. If a tie line between a 180-m.y.-old radiogenic Pb ( $^{207}\text{Pb}/^{206}\text{Pb}=0.04968$ ) and the whole-rock residue (WR,R) is drawn on a  $^{207}\text{Pb}/^{206}\text{Pb}$ - $^{204}\text{Pb}/^{206}\text{Pb}$  diagram, the PX1 and OL residues of Y-793605 and whole-rock leaches (3C,L1; 3C,L2), whole-rock (3A), whole-rock total (3C,T), whole-rock residue (3C,R), and plagioclase residue (PL,R) of Shergotty (Chen & Wasserburg, 1986) plot close to this mixing line (Fig. 1b), suggesting a young event for U-Pb fractionation.

In Fig. 2a, the U-Pb data of the leaches and residues are plotted on a modified concordia diagram (Tera and Wasserburg, 1972) after correction for initial Pb using the CDT Pb composition (Tatsumoto et al., 1973). All analyses but four (PL,L1; PX1,L1; OL,L1; and PX1,L2) plot to the left of concordia. We interpret this behavior as the result of preferential extraction of U from the fractions during leaching. If U in the leaches is combined with that from the residues and plotted using only the residue Pb values (assuming the leached Pb is predominantly secondary), the resultant data points plot to the right of concordia. A chord through the U-Pb data for PX1 leaches and residue (PX1,L1; PX1,L2; PX1,L3; PX1,R) intercepts concordia at  $4439 \pm 9$  Ma and  $212 \pm 62$  Ma. Because the PX1 separate contains abundant black glassy material, possibly impact melt, we interpret these intercept ages as suggesting a two-stage evolution whereby a 4400-m.y.-old lherzolite parent suffered a 200-m.y.-old disturbance (shock event?). The later disturbance event partially reset the U-Pb system. In Fig. 2b, the combined data points of Y-793605 are plotted along with the total data (U and Pb in the leaches are combined with those with the residues: Total) of ALH77005, Zagami,

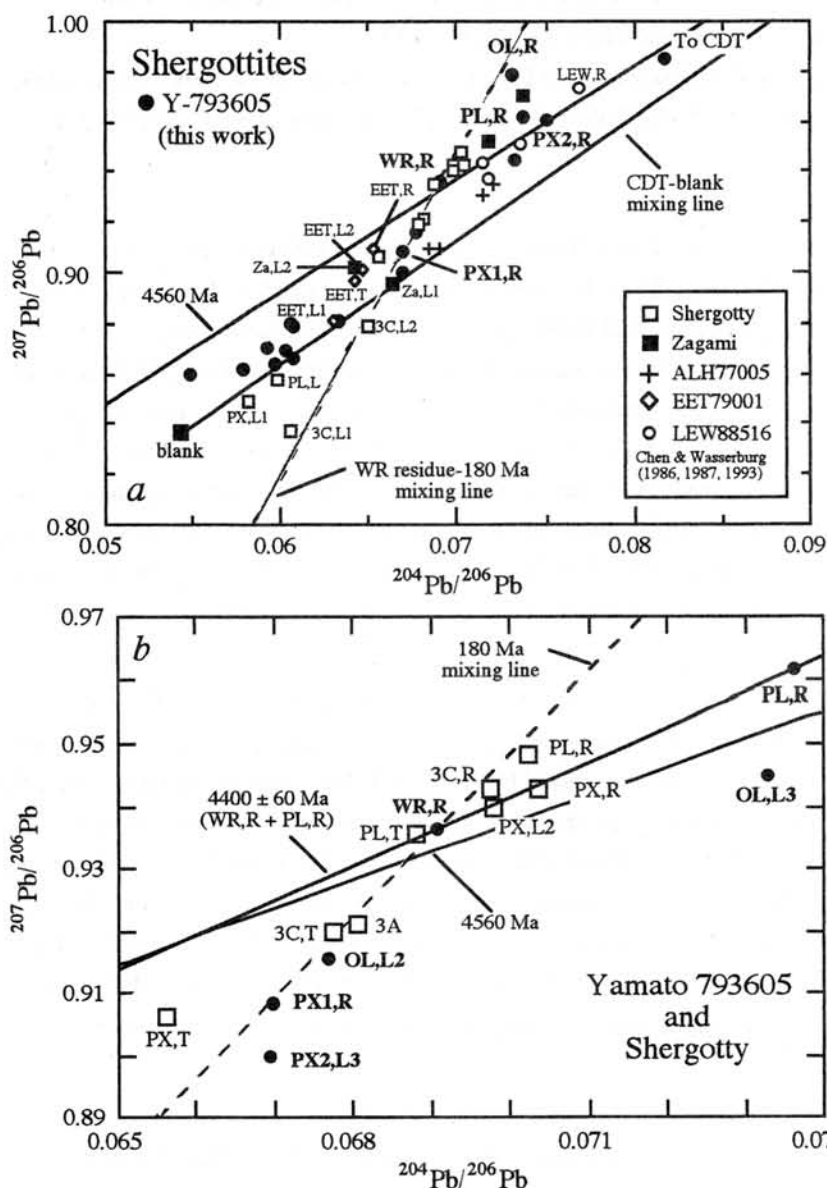


**Figure 1.**  
 (a)  $^{207}\text{Pb}/^{206}\text{Pb}$  versus  $^{204}\text{Pb}/^{206}\text{Pb}$  diagram for Y-793605 and other shergottites. Zagami, Shergotty, ALH77005, EET79001, and LEW88516 data are from Chen and Wasserburg (1986, 1987, 1993). A 4560-Ma reference line through primordial Cañon Diablo troilite (CDT) Pb (Tatsumoto et al., 1973) and a tie line between a 180-m.y.-old radiogenic Pb ( $^{207}\text{Pb}/^{206}\text{Pb} = 0.04968$ ) and WR residue is drawn. All residues of Y-793605 yield an age of  $3812 \pm 870$  Ma.

(b) Enlarged view of (a). The PX1 and OL residues of Y-793605 and 3C,L1; 3C,L2; 3C,T; 3A; 3C,R; and PL,R of Shergotty (Chen and Wasserburg, 1986) plot close to the trend of this mixing line, suggesting a young event of U-Pb fractionation.

EET79001, and LEW88516, as well as leaches and residue data of Shergotty whole-rock (Chen and Wasserburg, 1986, 1987, 1993). Similar to other shergottites, the data points of whole-rock residue (WR,R) and whole-rock "total" (WR,"T") of Y-793605 plot close to the trend of the reference chord intercepting concordia at 4560 Ma and 180 Ma.

The Pb isotopic compositions of Y-793605 indicate that a source reservoir evolved in a low m environment ( $\sim 5$ ) and confirm a low-m source of shergottites compared to volcanic rocks of the Earth.

References: Bogard, D.D. et al. (1979) *GCA* **43**, 1047-1055. Borg, L.E. et al. (1997) *LPSC XXVIII*, Chen, J.H. & Wasserburg, G.J. (1986) *GCA* **50**, 955-968. Chen, J.H. & Wasserburg, G.J. (1987) *LPSC XVII*, 113-114. Chen, J.H. & Wasserburg, G.J. (1993) *LPSC XXIV*, 275-276. Jagoutz E. (1989) *GCA* **53**, 2429-2441. Jagoutz E. & Wänke H. (1986) *GCA* **50**, 939-953. Mikouchi, T. & Miyamoto, M. (1996a) *Antarctic Meteorites XXI*, 104-106. Mikouchi, T. & Miyamoto, M. (1996b) *Meteoritics & Planet. Sci.* **31**, A89-A90. Nakamura, N. et al. (1982) *GCA* **46**, 1555-1573. Nyquist, et al. (1979) *GCA* **43**, 1057-1074. Nyquist, L.E. et al. (1984) *Meteoritics* **19**, 284. Nyquist, L.E. et al. (1987) *LPSC XVIII*, 730-731. Nyquist, L.E. et al. (1995) *LPSC XXVI*, 1065-1066. Tatsumoto, M. et al. (1973) *Science* **180**, 1279-1283. Tera, T. & Wasserburg, G.J. (1972) *EPSL* **14**, 281-304. Shih, C.-Y. et al. (1982) *GCA* **46**, 2323-2344. Wooden, J.L. et al. (1982) *LPSC XIII*, 879-880. Wooden, J.L. et al. (1979) *LPSC X*, 1379-1381. Yanai, K. (1995) *LPSC XXVI*, 1533-1534. Yanai, K. (1996) *Meteoritics & Planet. Sci.* **31**, A157.

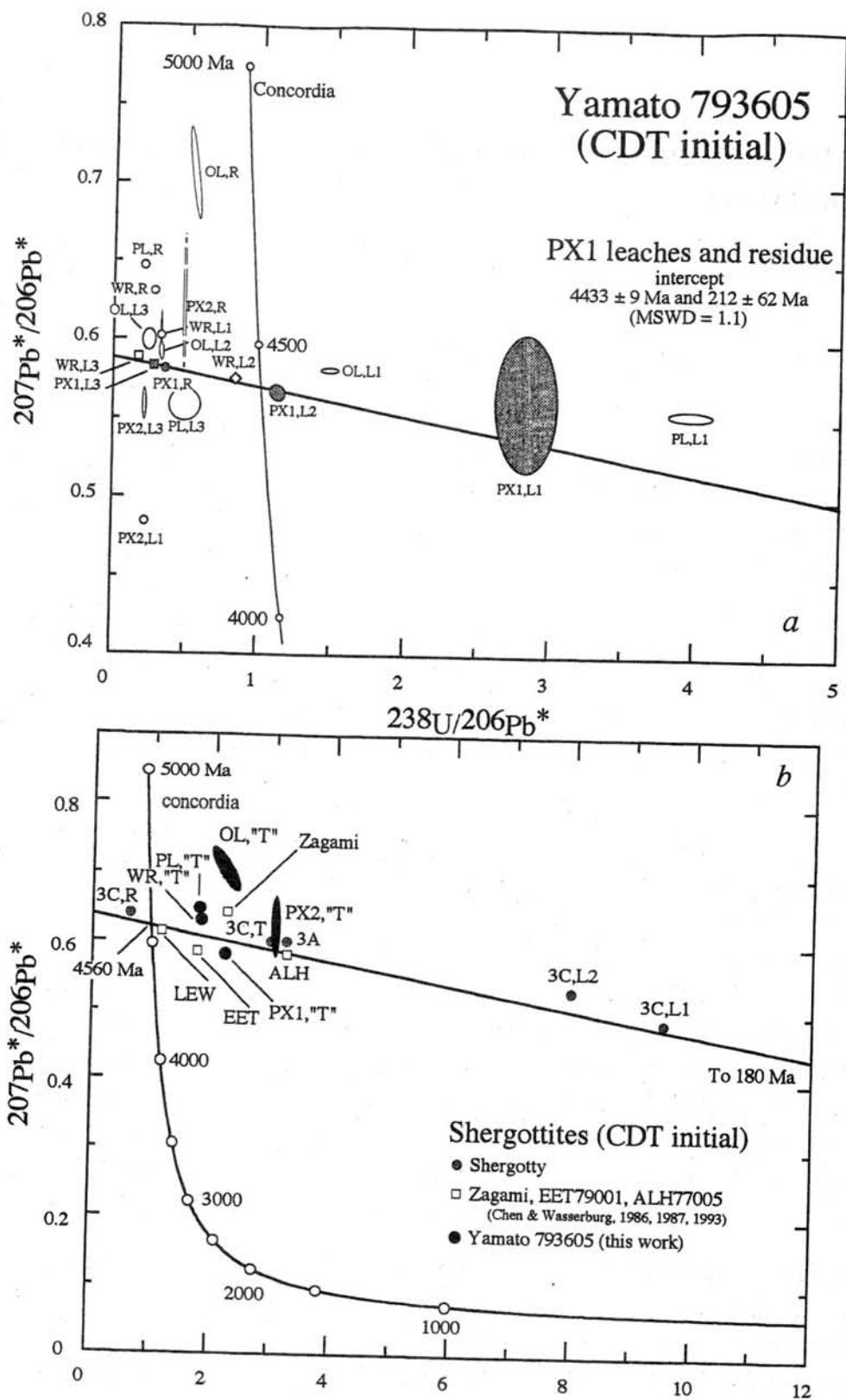


**Figure 2.**

(a) Modified concordia diagram (Tera and Wasserburg, 1972) after correction for initial Pb using Cañon Diablo troilite Pb (Tatsumoto et al., 1973). All analyses but four plot to the left of concordia, suggesting preferential extraction of U from the fractions during leaching. A chord through U-Pb data points for PX1,L1; PX1,L2; PX1,L3; and PX1,R intersect concordia at  $4439 \pm 9$  Ma and  $212 \pm 62$  Ma, suggesting a two-stage evolution of an old parent body which had experienced Pb loss due to a young disturbance event. (b) Combined data (U in the leaches are combined with that from the residues and using only the residue Pb values: "total") of four mineral fractions and a whole-rock sample of Y-793605 are plotted on a modified concordia diagram after correction for initial Pb using Cañon Diablo troilite Pb compositions along with the total data of ALH77005, Shergotty, Zagami, EET79001, and LEW88516 (Chen and Wasserburg, 1986, 1987, 1993). The chord which intercepts the concordia at 4560 Ma and 180 Ma is drawn as a reference.

# Noble gas compositions in individual chondrules of the Allende CV3 chondrite

Yayoi N. Miura<sup>1)</sup> and Keisuke Nagao<sup>2)</sup>

1) Earthquake Research Institute, University of Tokyo, Bunkyo-ku, Tokyo 113, Japan.

2) Institute for study of the Earth's Interior, Okayama University, Misasa, Tottori 682-01, Japan

**Introduction** Chondrites contain large amounts of noble gases compared with achondrites and any other differentiated materials, and it is known that noble gases are not distributed homogeneously in chondrites. Concentrations of noble gases in chondrules are several orders of magnitude lower than those in matrix, and little is known about variation of noble gas abundances and isotopic compositions for chondrules [1-4]. In order to investigate them, we have carried out noble gas analyses in each chondrule separated from the Allende as well as noble gas analyses with laser ablation technique. A part of the results including laser experiment was preliminarily reported in [5]. In this paper, we present additional result on noble gas analyses applied for individual chondrules, and characteristic features of noble gases in chondrules obtained so far are discussed.

**Samples and experiments** A fragment of the Allende CV3 chondrite, approximately 11g in weight, was roughly broken to small chips, and then, they were crushed by freeze-thaw methods. The chondrules to be measured were picked up and scraped carefully with a cutter in order to remove surrounding matrix. About half of the chondrule was used for noble gas analysis and remaining sample was (or will be) used for mineralogical observation. Noble gases were measured with a modified-VG5400 mass spectrometer at ISEI, Okayama University. Analytical procedure is essentially similar to typical one in the laboratory (e.g. [6]). Noble gases were extracted stepwisely, at 750 °C and 1800 °C. Sample weights and <sup>3</sup>He concentrations are given in Table 1.

**Results and discussion** Helium, Ne and Ar show cosmogenic signature. Significant amounts of radiogenic <sup>4</sup>He and <sup>40</sup>Ar are also contained in all chondrules. The concentrations of <sup>3</sup>He, which are likely cosmogenic origin, are almost constant except for one chondrule of #9. The range of the <sup>3</sup>He concentrations is slightly higher than the <sup>3</sup>He concentration of matrix portion of Allende from the same fragment ( $96.5 \times 10^9$  cm<sup>3</sup>/g). Although pre-irradiation of cosmic-rays is a possible reason for higher concentrations of <sup>3</sup>He in chondrules, difference of about 10 % between them may be within experimental uncertainties.

Fig. 1 shows the three isotope plot of Ne, <sup>20</sup>Ne/<sup>22</sup>Ne versus <sup>21</sup>Ne/<sup>22</sup>Ne. Neon isotopic compositions in low temperature fractions are plotted below the lines connecting between any probable trapped Ne component (the terrestrial atmospheric

Ne or possibly planetary or solar Ne) and cosmogenic Ne. The shift from the lines would be due to production of  $^{22}\text{Ne}$  from Na during cosmic-ray exposure via spallation. Low  $^{38}\text{Ar}/^{36}\text{Ar}$  is also observed in the low temperature fraction of a chondrule.

All the measured chondrules have apparently high  $^{80}\text{Kr}/^{84}\text{Kr}$ ,  $^{82}\text{Kr}/^{84}\text{Kr}$ ,  $^{128}\text{Xe}/^{132}\text{Xe}$  and  $^{129}\text{Xe}/^{132}\text{Xe}$  ratios. Because the trapped noble gas abundances are low, contribution of  $^{80}\text{Kr}$  and  $^{82}\text{Kr}$  produced via neutron captures of Br,  $^{128}\text{Xe}$  via neutron capture of  $^{127}\text{I}$  and  $^{129}\text{Xe}$  produced from now-extinct  $^{129}\text{I}$  ( $T_{1/2} = 1.7 \times 10^7$  years) are relatively effective. A plot of  $^{128}\text{Xe}/^{132}\text{Xe}$  versus  $^{129}\text{Xe}/^{132}\text{Xe}$  is shown in Fig. 2. The highest  $^{129}\text{Xe}/^{132}\text{Xe}$  ratio without blank correction obtained here is as high as 660, which was determined for the high temperature fraction of chondrule #4. All the data are plotted near a straight line, that is these chondrules have almost constant  $^{129}\text{Xe}/^{128}\text{Xe}$  ratios, indicating similar  $^{129}\text{I}$ -derived  $^{129}\text{Xe}$  retention ages among the chondrules. This must imply that time difference is less than a few million years, which agrees with reported chronological data for some chondrules (e.g. [3] for Allende and [4] for Bjurböle).

The concentrations of  $^{84}\text{Kr}$  and  $^{132}\text{Xe}$  vary more than two orders. In particularly, #9 has  $2 \times 10^{-9} \text{ cm}^3/\text{g}$  of  $^{132}\text{Xe}$ , which must have been derived from matrix and removal of matrix seems to have not been successful for this sample. The Kr and Xe in the other chondrules are much lower ( $1 \times 10^{-11} - 3 \times 10^{-10} \text{ cm}^3/\text{g}$ ). In most cases, elemental abundances of heavy noble gases fall on the terrestrial trend and does not fall on the range of chondrites.

[1] Kim J.S. and Marti K. (1994) *Meteoritics* 29, 482. [2] Swindle *et al.* (1983) *Chondrules and their origin*, LPI, pp.377, 246-261. [3] Swindle *et al.* (1983) *Geochim. Cosmochim. Acta* 47, 2157-2177 [4] Caffee *et al.* (1982) *Proc. Lunar Planet. Sci. Conf. 13<sup>th</sup>*, in *J. Geophys. Res.* 87, A303-A317 [5] Miura Y.N. and Nagao K. (1996) *Meteoritics Plant. Sci.* 31, A91. [6] Miura Y.N. *et al.* (1995) *Geochim. Cosmochim. Acta* 59, 2105-2113.

Table 1. Measured chondrules taken from the Allende CV3 chondrite.

|   | #0*     | #1 <sup>s</sup> | #3 <sup>s</sup> | #4 <sup>s</sup> |
|---|---------|-----------------|-----------------|-----------------|
| Weight (g)  | 0.00401 | 0.0272          | 0.00644         | 0.00609         |
| $^3\text{He}$ ( $10^{-9} \text{ cm}^3/\text{g}$ ) | 108     | 109             | 97.5            | 104             |

| #6 <sup>s</sup> | #7 <sup>s</sup> | #9      | #10    | #11     | #13     |
|-----------------|-----------------|---------|--------|---------|---------|
| .00596          | 0.00485         | 0.00058 | 0.0012 | 0.00206 | 0.00379 |
| 105             | 105             | 57.0    | 112    | 99.2    | 119     |

\* Mixture of small chondrules. Removal of matrix by hand was impossible. HF treatment was applied.

§ Preliminarily data for these chondrules has been presented in [5]

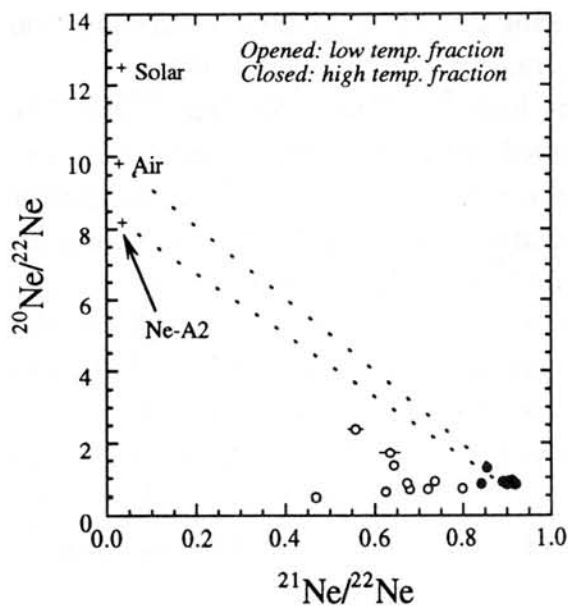


Fig. 1. Three isotope plot of Ne.  $^{20}\text{Ne}/^{22}\text{Ne}$  versus  $^{21}\text{Ne}/^{22}\text{Ne}$  for chondrules of the Allende. Neon isotopic compositions in the low temperature fractions are plotted below the lines connecting between any trapped Ne component (the terrestrial atmospheric Ne, Ne-A or solar Ne) and cosmogenic Ne.

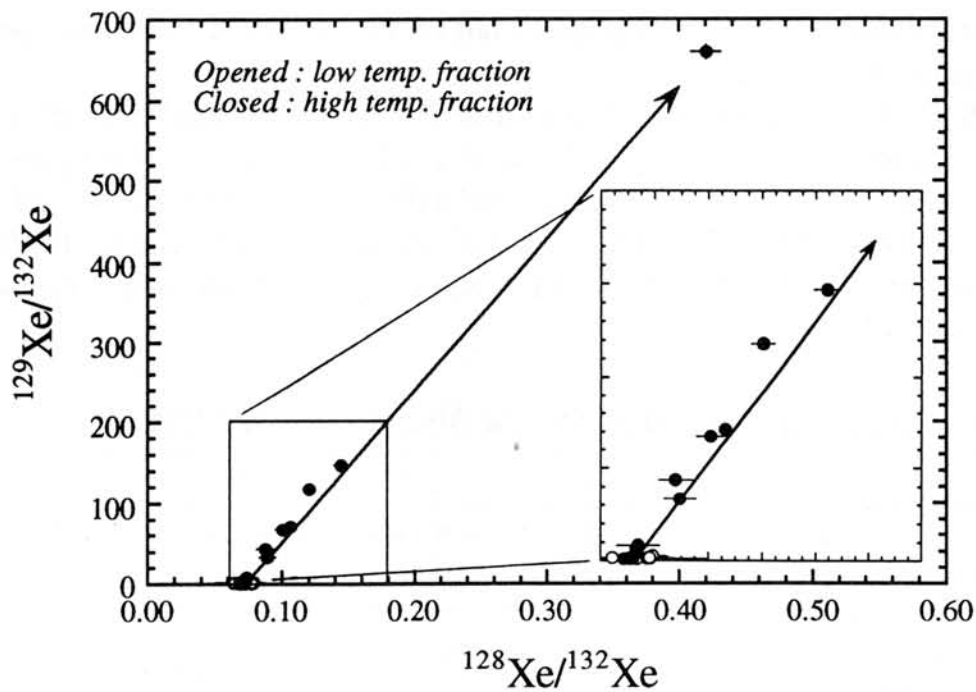


Fig. 2. Plot of  $^{128}\text{Xe}/^{132}\text{Xe}$  versus  $^{129}\text{Xe}/^{132}\text{Xe}$  for chondrules of the Allende. A line is defined by least squares fitting through the terrestrial atmospheric value for the data of high temperature fractions.

# IN SITU SURVEY FOR INTERSTELLAR GRAPHITE IN UNEQUILIBRATED CHONDRITES: EVIDENCE FROM C-, N-, AND H-ISOTOPIC SIGNATURES.

S. Mostefaoui<sup>1</sup>, P. Hoppe<sup>2</sup>, E. Zinner<sup>3</sup>, and A. El Goresy<sup>1</sup>

<sup>1</sup>Max-Planck-Institut für Kernphysik, Postfach 103980, 69029 Heidelberg, Germany  
(E-mail: smail@pluto.mpi-hd.mpg.de);

<sup>2</sup>Physikalisches Institut, Universität Bern, Sidlerstr. 5, CH-3012 Bern, Switzerland;

<sup>3</sup>McDonnell Center for the Space Sciences and Physics Department, Washington University, St. Louis, MO 63130, USA.

## Introduction:

Optical microscopic survey of unequilibrated chondrites (UCs) revealed the presence of appreciable amounts of graphite of various morphologies [1]. Graphite have been analysed for H, C, and N isotopic compositions by secondary ion mass spectrometry. Here, we report C- and N-isotopic compositions of graphite in Ucs from different chemical classes. We also report an in situ finding of graphite with abnormal <sup>15</sup>N- and D-excesses in an unusual graphite-rich chondrite, Khohar (L3).

## Petrography:

The graphite in UCs is an accessory phase. It is present as small inclusions (<20µm) in metal and troilite [1]. However, in Khohar and in Mezö-Madaras (both L3), graphite is exceptionally abundant. Here, graphite occurs in a large variety of assemblages (silicates, metal, and troilite) in chondrules, chondrule rims, and matrix. Optical microscopy revealed the existence of different graphite morphologies. The morphologies include books (single crystals), spherulitic, granular, cliftonite, and a very fine-grained (<1µm) type. In Khohar and in Mezö-Madaras, the most common morphologies are books and the fine-grained type [2]. In these chondrites, the two graphite types are present as large patches of few tens up to several hundreds of microns in diameter. The presence of mixtures of the two graphite types makes it difficult to analyze them separately with SIMs. In addition, in Khohar, a spherical object consisting of a fine-grained aggregate of Ni-poor (<2 wt%) metal and graphite is encountered in a fine-grained chondrule-free clast. Graphite was analyzed for its C-, N-, and H-isotopic compositions.

## Isotopic compositions:

*C-isotopic composition.* C-isotopic ratios of the investigated graphites of all the studied chondrites are close to normal (i.e. within the range found in terrestrial samples) and  $\delta^{13}\text{C}_{\text{PDB}}$  values are mostly negative. Fig. 1 shows  $\delta^{13}\text{C}$  in graphite from the different chondrite classes. The

diagram indicates variations in C-isotopic compositions not only among the petrologic groups, but also significant variations within a given chondrite (e.g. from -54 to -14‰ in Khohar).

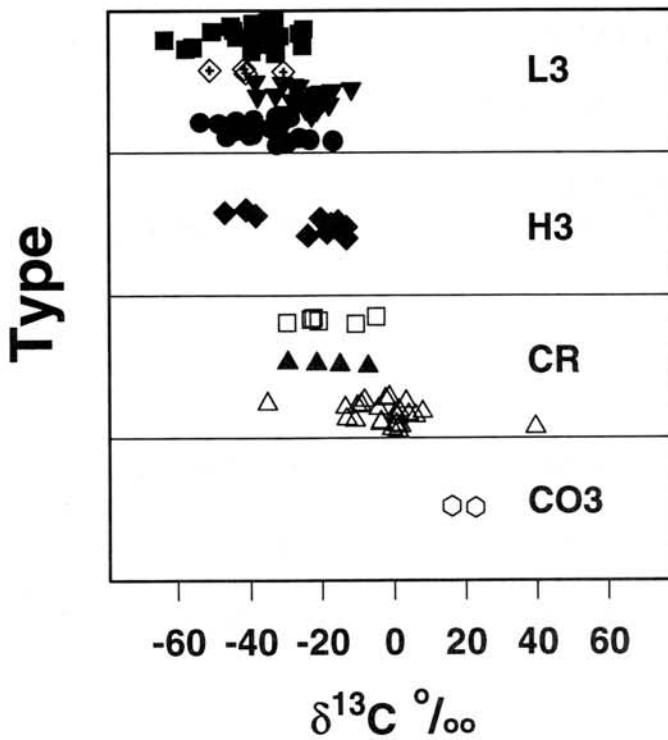


**Fig. 1:** C-isotopic composition of graphite in unequilibrated chondrites.

- Khohar; ▼ Mezo-Madaras; ■ Bishunpur;
- ◇ Inman; ◆ Grady; △ Acfer 182;
- ▲ Acfer 207; □ Acfer 214; ○ Kainsaz.

*N- and H-isotopic compositions.* N-isotopic ratios in graphites in all the studied chondrites (except Khohar) are close to normal and show  $^{15}\text{N}$  enrichments of few hundreds permil ( $\delta^{15}\text{N}$  max of +450‰, found in a graphite in Acfer 182). In Khohar, much larger variations exist and isotopically heavy N and H were encountered in the fine-grained graphite coexisting with the metal aggregate. Fig. 2 shows the results for H- and N-isotopic compositions of the fine-grained graphite in the spherical aggregate. Fig. 2A shows a plot of  $\delta\text{D}$  vs  $\text{H}^+/\text{CN}^-$ .  $\delta\text{D}$  ranges from close to normal (+65‰) up to highly anomalous values, with a maximum of +1500‰. In Fig. 2B we plotted  $^{14}\text{N}/^{15}\text{N}$  vs  $^{12}\text{C}/^{13}\text{C}$  ratios. The graphites exhibit large  $^{15}\text{N}$ -enrichments with  $^{14}\text{N}/^{15}\text{N}$  ratios as low as 117 (corresponding to  $\text{d}^{15}\text{N} = 1330\text{‰}$ ). Here, the ranges of N-isotopic compositions are comparable to those of the  $^{15}\text{N}$ -enriched graphite separates from Murchison (see Fig. 4 of [4]). Our  $^{12}\text{C}/^{13}\text{C}$  ratios in graphite have a very narrow range. In the fine-grained spherical object,  $\delta^{15}\text{N}$  is found to be inversely correlated with the N-content of the graphite. In the similar manner,  $\delta\text{D}$  is found to increase upon increase of N-content in graphite. This is evident from the negative correlation between  $\delta\text{D}$  and the  $\text{H}^+/\text{CN}^-$  ionic ratios shown in Fig. 2A. An anti-correlation can be

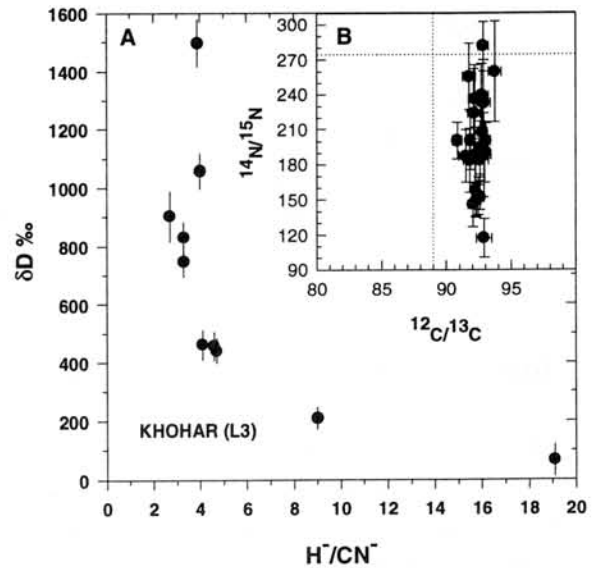


**Fig. 2:** C-, N-, and H-isotopic compositions of fine-grained graphites in a spherical metal aggregate in Khohar.

established between  $\delta^{15}\text{N}$  and  $\delta\text{D}$ , thus indicating the presence of two coexisting graphite types with two distinct D- and  $^{15}\text{N}$ -isotopic signatures.

## Discussion:

Our petrographic investigations on graphite in unequilibrated chondrites are consistent with a pre-accretion origin of the graphite. This is established through the large variations in N-, H-, and C-isotopic ratios in graphite. The distinct C-isotopic ratios in graphite from different chondrite groups (see Fig. 1) are indicative of C-isotopic heterogeneities in the solar nebula. This requires the existence of graphite as a stable phase under the solar nebular conditions. This graphite must have accreted in the solar nebula at very low temperature in order to escape oxidation [3].

The  $^{15}\text{N}$ - and D-enrichments in the fine-grained graphite in Khohar are the first *in situ* anomalies found in a chondritic meteorite. These anomalies are indicative of an interstellar origin of the graphites. The absence of large  $\delta^{15}\text{N}$  excesses in graphite of other chondrites may be explained as a result of: (1) isotopically anomalous fine-grained graphite occurs together with the isotopically normal graphite books. Due to intimate intergrowth, both are measured together. (2) terrestrial contamination during sample handling overprints the isotopic signature on the grain surfaces. In fact, after 30 minutes sputtering of graphite in Khohar to remove the outer regions,  $\delta^{15}\text{N}$  values showed considerable increase. In Mezö-Madaras, however, the similar procedure led to no significant change, attesting a possible pervasive contamination. The occurrence of D- and  $^{15}\text{N}$ -isotopic anomalies in two coexisting separate graphite types, only in the spherical metal-rich object in Khohar suggests that this object sampled only interstellar material. Here, we not only identify the possible source of graphite, but also for the first time the carrier assemblage (Ni-poor metal aggregate). We argue that these graphites originated from IMCs. The lack of C-isotopic anomalies in any graphites from the metal-rich spherical object in Khohar along with the  $^{15}\text{N}$ -isotopic anomalies underlines the strong similarities to graphite separates from Murchison [4]. Since our anomalous graphites occur in the same spherical object, this object must have sampled a specific graphite population from the IMCs. We have probably encountered a pristine assemblage consisting of Ni-poor metal with two graphite species (D-rich and  $^{15}\text{N}$ -rich) from IMCs. This is in contrast to the positive correlation between  $\delta^{15}\text{N}$  and  $\delta\text{D}$  reported from stepped combustion experiments of bulk CR chondrites [5]. The reason of such discrepancy is that the experiments of [5] were conducted on bulk graphites and hence we suspect that both graphite species (D-rich and  $^{15}\text{N}$ -rich) were measured together. Our technique demonstrates the strength of *in situ* search in identifying isotopically distinct species that are masked during stepped combustion of bulk samples.

**References:** [1] Mostefaoui S. (1996). PhD thesis. MNHN, Paris. [2] Mostefaoui S. et al. (1997) *LPS XXVIII*. [3] Mendybaev R. A. et al. (1997) *LPS XXVIII*. [4] Zinner E. et al. (1995) *Meteoritics* **30**, 209-226. [5] Ash R. D. et al. (1993) *Meteoritics* **28**, 318-319.

# SEARCH OF PAHs IN CARBONACEOUS CHONDRITES BY A FLUORESCENCE MICROSCOPE

Tatsushi MURAE

Department of Earth and Planetary Sciences, Faculty of Science, Kyushu University, Hakozaki, Fukuoka 812

Polycyclic aromatic hydrocarbons (PAHs) in Martian meteorite ALH-84001 have been used as the indirect evidence for the existence of past life on Mars by McKay et al. [1]. They detected the PAHs using a microprobe two-step laser mass spectrometer. The average PAH concentration in the interior fracture surfaces is estimated to be more than 1 part per million. All PAHs reported in the paper have a relatively small molecular weight and are extractable with organic solvents. All these compounds are fluorescent. Briggs reported the finding of three types of fluorescent organic compounds in Mokoia meteorite [2]. Two of them are water soluble, and the other is water insoluble. Claus and Nagy found 'organized elements' in grains of Orgueil and Ivuna meteorites by a microscopic examination [3]. The organized elements showed fluorescence (yellow) in ultraviolet light. Acid treatments did not seriously affect the morphology of the organized elements. Certain organic solvents affect, but not to dissolve, the organized elements. The greenish-yellow, green or pink-coloured fluorescence of the organized elements can be differentiated from bluish-white fluorescence of some of the minerals [4]. Fluorescent non-polar organic materials have been extracted from Orgueil [5] and Murchison [6].

Unextractable polycyclic aromatic macromolecules consist major parts of carbonaceous matter in carbonaceous chondrites. The molecular structures of these carbonaceous matters resemble to PAHs except the network size of their polycyclic system [7]. Graphite and fullerene gave polycyclic aromatic compounds showing similar FT-IR spectra as those of meteorite organic macromolecules on shock experiments [8]. These compounds may contain a fluorescent polycyclic aromatic part as a partial structure of the macromolecule.

We have measured fluorescence spectra on several samples of powdered carbonaceous chondrites under blue light using a Zeiss MPM 400 microscope photometer. The powdered samples are spread on an aluminum foil. The measured carbonaceous chondrites are Y-791198, Y-74662, and Murchison. These meteorites contain considerable amount of carbon (2~3%). We could find small number of fluorescent particles among non-fluorescent particles in all of these meteorite samples. Fig. 1 shows the case of Y-791198. The color of most of the fluorescent particle is yellowish green or bluish green. The fluorescence spectra of these particles showed emission maximum at 470 nm (Fig. 2). We observed similar fluorescent particles also in carbon enriched samples by acid treatments of ALH-77307 and Y-791717. In one case for Murchison, the color of fluorescence was reddish orange having the emission maximum at 630 nm.

We have also measured fluorescence spectra of some PAHs relatives (coronene, fullerene, artificial and natural graphite, and their derivatives obtained on shock experiments). The measuring methods are the same as those for the meteorite samples. Although we could observe fluorescent particles for all samples, the number of the fluorescent particles was increased after shock experiments. The emission maximum is almost the same as that of the meteorite fluorescent particles.

Most of the meteorite samples were extracted with the mixed organic solvent (benzene-methanol). Therefore, we may consider that the fluorescent particles in the meteorite samples are homologues of PAHs having much larger molecular weight. It is unclear whether these fluorescent particles are the same type of material as the organized elements found in Orgueil by Nagy et al [4].

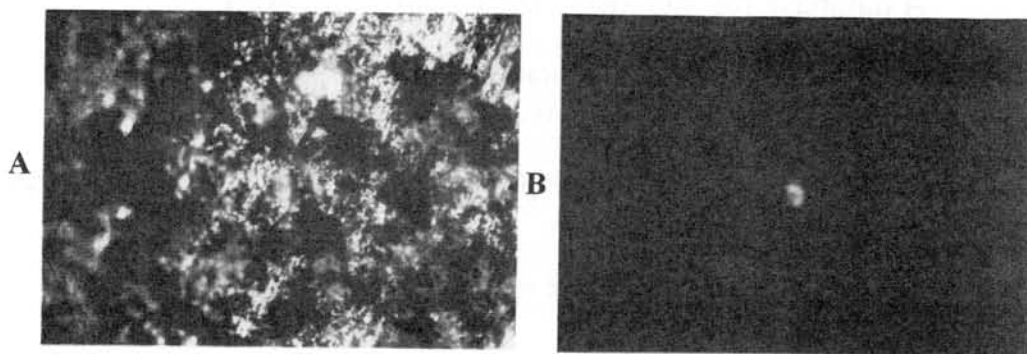


Fig. 1 Photographs of fluorescent particles in powdered Y-791198.  
**A:** under polarized white light; **B:** under blue light.

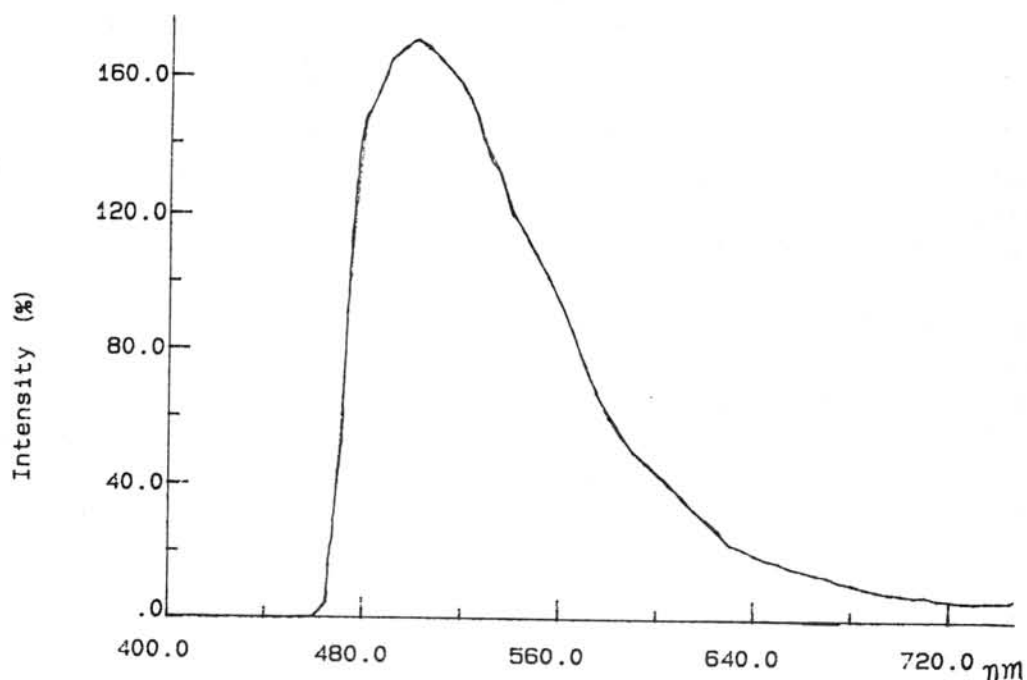


Fig. 2 A fluorescence spectrum of the same part shown in Fig. 1.

#### References:

- 1) D. S. McKay, E. K. Gibson Jr., K. L. Thomas-Keprta, H. Vali, C. S. Romanek, S. J. Clemett, X. D. F. Chiller, C. R. Maechling, and R. N. Zare, *Science*, **273**, 924-930 (1996).
- 2) M. H. Briggs, *Nature*, **191**, 1137-1140 (1961).
- 3) G. Claus and B. Nagy, *Nature*, **192**, 594-596 (1961).
- 4) B. Nagy, G. Claus, D. J. Hennessy, *Nature*, **193**, 1129-1133 (1962).
- 5) B. Alpern and Y. Benkheiri, *Earth Planet. Sci. Lett.*, **19**, 422-428 (1973).
- 6) D. W. Deamer, *Nature*, **317**, 792-794 (1985).
- 7) T. Murae, A. Masuda, T. Takahashi, *Proc. NIPR Symp. Antarct. Meteorites*, **3**, 211-219 (1990).
- 8) T. Murae, *Proc. NIPR Symp. Antarct. Meteorites*, **7**, 262-274 (1994).

## A database for meteorites on World Wide Web

Toshio Murakami

Computer Center, Gakushuin University, 1-5-1 Mejiro, Tokyo 171, Japan

METEORITE DATABASE consists of selected physical and chemical data for meteorites. The selected data set is listing below.

### CONTENTS AND SUMMARY SHEET OF "METEORITE DATABASE"

|                 |   |
|-----------------|---|
| Name            | meteorite name  |
| Group           | chemical group  |
| Type            | petrologic type                                       |
| Weathering      | degree of weathering                                  |
| %Fa             | mean composition and compositional range of olivine   |
| %Fs             | mean composition and compositional range of pyroxene  |
| Major elements  | chemical compositions of major elements               |
| FF              | Fall / Find   |
| Trace elements  | chemical compositions of trace elements               |
| Radioactive age | ages after methods of Pb-Pb, Pb-U, Pb-Th, Rb-Sm, etc. |
| Shock stage     | shock stage   |
| Oxygen isotopes | oxygen isotopes                                       |

|                              |      |
|------------------------------|------|
| Individual meteorite entries | 9239 |
| Chondrites                   |      |
| Enstatite                    | 41   |
| Ordinary                     | 2312 |
| Carbonaceous                 | 172  |
| Achondrites                  |      |
| SNC                          | 3    |
| HED                          | 181  |
| Others                       | 30   |
| Irons                        | 25   |
| Stony Irons                  | 9    |
| Others                       |      |
| Ungrouped                    | 5528 |
| Others                       | 38   |

This database system is able to be accessed from anywhere by the Internet through the World Wide Web (WWW) Browser. Some database (e.g. NASA JSC ed. Planetary Materials Curatorial Database System) have already been accessed by network. But their interface are still character based one (Fig.1). The interface of the searching system of "METEORITE DATABASE" is Graphical User Interface (GUI) (Figs.2,3). Thus searching process is very easy for a beginner.

In general, many WWW servers do not have database access mechanism built-in. They rely on the Common Gateway Interface (CGI). The CGI is a standard way of interfacing external applications with WWW servers. The search engine of this database runs as a CGI external application. WWW browsers can recognize only HTML documents. Although CGI external applications usually access information not in HTML form. They just act as a gateway between

browsers and the information. Thus this search program includes a database access mechanism and a function of generating HTML documents from result of database search. This CGI application is created by Microsoft Visual Basic because of an easy maintenance and a higher speed than other interpreter language. However, this CGI application runs only on Microsoft Windows based WWW servers (e.g. Microsoft Internet Information Server; Netscape FastTrack Server; OmniHTTPd; Fnrnd!Server).

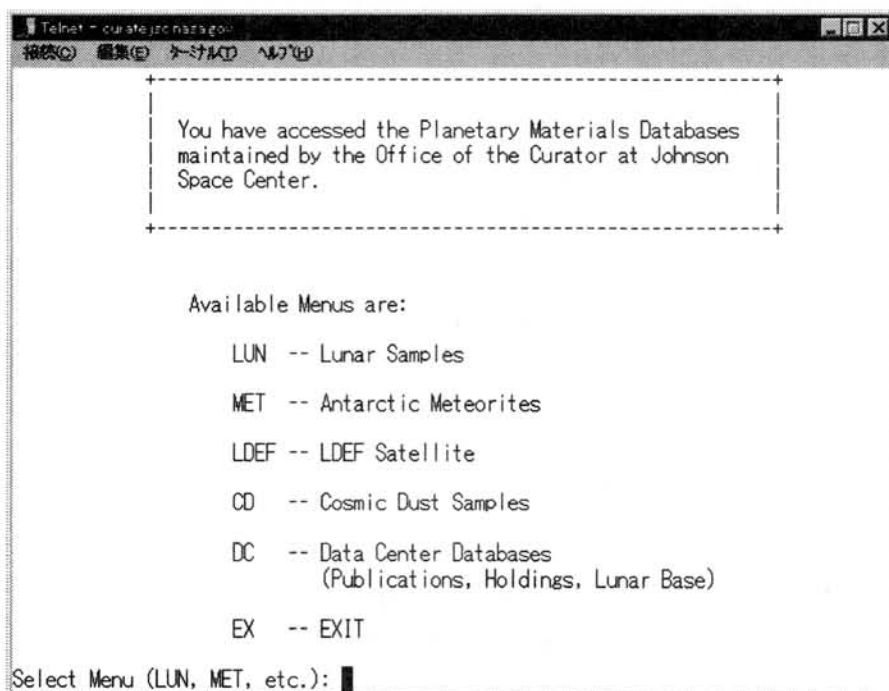


Fig.1. Example of a character based interface (NASA JSC)

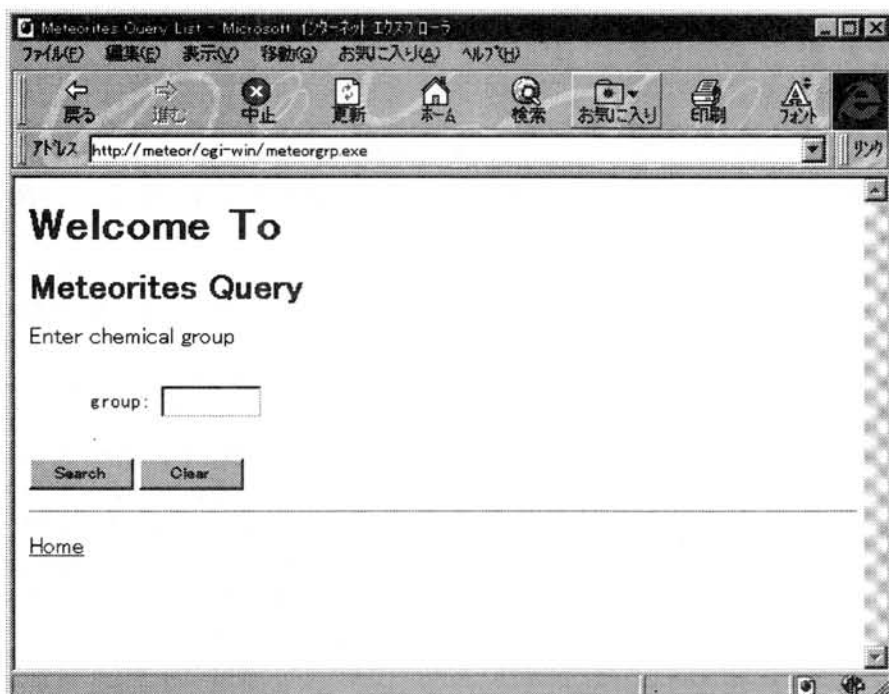


Fig.2. METEORITE DATABASE (one of search menu)

**Selected Meteorite Data**

| Name            | group | type | weathering | weight | SiO2  | TiO2 | Al2O3 | Cr2O3 | Fe2O3 | Fe       |
|-----------------|-------|------|------------|--------|-------|------|-------|-------|-------|----------|
| ALHA77299       | H     | 3    | -          | -      | 35.94 | 0.11 | 2.27  | 0.41  | -     | 13<br>15 |
| Clovis (no.1)   | H     | 3    | -          | -      | 35.4  | 0.1  | 2.06  | 0.46  | 10.29 | 9.C      |
| Grady (1937)    | H     | 3    | -          | -      | 35.9  | 0.11 | 1.95  | 0.52  | 7.93  | 7.C      |
| Sharps          | H     | 3    | -          | -      | 35.39 | 0.12 | 1.9   | 0.45  | -     | 13<br>64 |
| Study Butte     | H     | 3    | -          | -      | 34.33 | 0.13 | 2.06  | 0.5   | 14.57 | 10<br>93 |
| Suwahib (Buwah) | H     | 3    | -          | -      | 39.38 | 0.11 | 2.35  | 0.5   | -     | 9.E      |
| Willaroy        | H     | 3    | -          | -      | 33.85 | 0.13 | 2.13  | 0.48  | 22.5  | 6.7      |
| Dhaiara         | H     | 3    | -          | -      | 36.87 | 0.12 | 2.14  | 0.56  | -     | 10       |

Fig.3. Displaying search result.

### References

- [1]Bryan and Kullerud (1975) Meteoritics 10, 41-50 [2]Buchwald (1975) Handbook of iron meteorites, Univ. of California Press and Arizona State Univ. [3]Caffee et al. (1982a) Proc. LPSC 13, JGR Suppl. 87, A318-A330 [4]Caffee et al. (1982b) Proc. LPSC 13, JGR Suppl. A303-A317 [5]Caffee et al. (1988) GCA [6]Chalmers and Mason (1977) Rec. of The Australian Mus. 30, 519-531 [7]Chen and Wasserburg (1985) LPS XVI, 119-120 [8]Clarke et al. (1970) Smithsonian Contrib. Earth Sci. 5, 1-55 [9]Clarke et al. (1971) J. Geophys. Res. 76, 4135-4143 [10]Clarke et al. (1975) Smithsonian Contrib. Earth Sci. 14, 63-70 [11]Clayton et al(1976) EPSL 30, 10-18 [12]Crabb et al. (1982) GCA 46, 2511-2526 [13]Dube et al. (1977) Smithsonian Contrib. Earth Sci. 19, 71-82 [14]Esbensen and Buchwald(1979) Meteoritics 14, 573-576 [15]Ebihara(1988) [16]Fodor and Keil (1976) GCA 40, 177-189 [17]Fodor et al. (1971) Chem. Erde 30. 103-113 [18]Fodor et al. (1972) Meteoritics 7, 495-597 [19]Fodor et al. (1976) New Mexico Geol. Soc. Spec. Publ. 6, 206-218 [20]Fredriksson et al. (1969) In Meteorite Research (Ed. Millman), O. Riedl, 155-165 [21]Fredriksson et al. (1986) Meteoritics 21, 159-168 [22]Fredriksson and Kerridge (1988) Meteoritics 23, 35-44 [23]Fredriksson et al. (1975) Smithsonian Contrib. Earth Sci. 14, 41-53 [24]Gomes and Keil (1980) Brazilian stone meteorites. Univ. of New Mexico Press, pp.161 [25]Gomes et al. (1977) An. Acad. Brasil. Cienc. 49, 269-274 [26]Gomes et al. (1978) Volume Djalma Guimaraes J. de Min. Recife. 7, 67-71 [27]Gundavaram (1996) CGI programming on the World Wide Web (Tanabe tr.). O'REILLY Japan, pp475 [28]Hewins et al. (1988) 51<sup>st</sup> Ann. Meet. Met. Soc. K-3 [29]Jarosewich (1966) GCA 30, 1261-1265 [30]Jarosewich (1967) GCA 31, 1103-1106 [31]Jarosewich (1971) Meteoritics 6, 49-52 [32]Jarosewich (1984) Smithsonian Contrib. Earth Sci. 26, 111-114

[33]Jarosewich (1990) *Meteoritics* 25, 323-337 [34]Jarosewich and Dodd (1985) *Meteoritics* 20, 23-36 [35]Jarosewich and Mason (1969) *GCA* 33, 411-416 [36]Jordan et al. (1980) *Z. Naturforsch.* 35a, 145-170 [37]Keil et al. (1978) *Meteoritics* 13, 177-188 [38]King et al. (1977) *Meteoritics* 12, 13-20 [39]Levi-Donati and Jarosewich (1974) *Meteoritics* 9, 145-155 [40]Lewis and Anders (1975) [41]Manhes et al. (1975) *LPS VI*, 546-547 [42]Manhes et al. (1984) *GCA* 48, 2247-2264 [43]Mason (1973) *Meteoritics* 30, 1-7 [44]Methot et al. (1975) *Meteoritics* 10, 121-131 [45]Niemeyer and Zaikowski (1980) *EPSL* 48, 335-347 [46]Olsen and Jarosewich (1970) *Earth Planet. Sci. Lett.* 8, 261-266 [47]Olsen et al. (1978) *Meteoritics* 13, 209-225 [48]Paar et al. (1976) *Revista Brasil. De Geociencias* 6, 201-210 [49]Podsek (1970) *GCA* 34, 341-365 [50]Reynolds and Turner (1964) *JGR* 69, 3263-3281 [51]Rison and Zaikowski (1980) *Proc. LPSC* 11, 977-994 [52]Rubin et al. (1983) *Meteoritics* 18, 179-196 [53]Shukolyukov et al. (1986) *Geochem. Int.* 23(2), 130-144 [54]Tatsumoto et al. (1973) *Science* 180, 1279-1283 [55]Toselli and de Broodtkorb (1972) *Acta Geologica Lilloana* 12, 133-154 [56]Unruh et al. (1977) *EPSL* 37, 1-12 [57]Yanai and Kojima (1995) *Catalog of The Antarctic meteorites*, NIPR [58]Wolters et. al. (1996) *IIS* 2, pp587, Que. [59]Contributing editors of *Visual Basic Programmer's Journal* (1996) *The Official Visual Basic Programmer's Journal Guide to Visual Basic 4* (Three A systems, Co., Ltd. tr.), Shoeisha , pp655

**KINETICALLY CONTROLLED STABILITY OF SILICATE MELT AT LOW PRESSURES : (1) STEADY STATE.** Hiroko Nagahara and Kazuhito Ozawa: Geol. Inst., Univ. Tokyo, Hongo, Tokyo 113, Japan

Nagahara and Ozawa (1996) made evaporation experiments on silicate melt in the system MgO-SiO<sub>2</sub> (SiO<sub>2</sub> ~ 60-68 wt.), and showed that evaporation rate and kinetic barrier for evaporation are dependent on bulk composition. The rate and barrier become larger with increase in the SiO<sub>2</sub>-component in the melt. Difference in the evaporation rate and composition among the samples, which had different initial bulk composition, becomes smaller with progress of evaporation, and they reached a near steady state regarding evaporation rate, bulk composition, and texture. The near steady state is achieved soon after crystallization of forsterite begins, which was caused by bulk compositional change due to partial evaporation. The evaporation rate at the near steady state is a little larger than that of solid forsterite and is much smaller than that of melt at the beginning of evaporation. In the present study, formation of metastable melt in vacuum is studied by considering mass balance and kinetics among solid-liquid-gas, and its importance on the lifetime and thermal history of chondrule formation will be discussed.

When we consider a chondrule sphere in the solar nebula, material transfer and phase transformation among and within three phases, liquid, solid, and gas, should be treated: crystallization or dissolution between liquid and solid, elemental diffusion within liquid or solid (generally diffusion in gas can be neglected at low pressures), evaporation or condensation between liquid and gas, and that between solid and gas. The evolution of a sphere is limited by one or more of those kinetic processes. Important constraint is that evaporation (and condensation) takes place only at the surface of the sphere. The experimental residue, which is a mixture of forsterite and melt, has a surface preferentially covered with forsterite.

Achievement of the near steady state at the melt/forsterite interface at the sphere surface in the MgO-SiO<sub>2</sub> system was considered. Evaporation rate of melt is larger than that of forsterite. The flux ratio of MgO/SiO<sub>2</sub> is 2 for forsterite because it evaporates congruently in various conditions. The ratio of the melt is smaller than that of forsterite, and it varies with temperature and pressure conditions. Preferential evaporation of SiO<sub>2</sub>-rich component from the melt portion causes precipitation of forsterite, and the occupation of surface by forsterite increases. It lowers the total flux of SiO<sub>2</sub>-component and thus lowers the total evaporation from the sphere. A near steady state is thus achieved in the balance of flux ratio of MgO (or SiO<sub>2</sub>) component of melt to that of forsterite ( $J_{Mg}^{melt} / J_{Mg}^{forsterite}$ ) and the surface fraction of melt/forsterite ( $S^{melt} / (S^{forsterite} + S^{melt})$ ): the larger the  $J_{Mg}^{melt} / J_{Mg}^{forsterite}$  value, the smaller the  $S^{melt} / (S^{forsterite} + S^{melt})$  value. For the experimental conditions (1700°C, 55 wt. % of MgO mole % of melt, 61 wt. % of MgO of the bulk sphere, 0.45 of bulk melt fraction, 0.4 of  $J_{Mg}^{melt} / J_{Si}^{forsterite}$ , and 5 of  $J_{Mg}^{melt} / J_{Mg}^{forsterite}$ ), the melt fraction at the surface should be only 0.02. This is quite consistent with observation by SEM, in which the surface appears to be almost entirely covered by forsterite.

The results suggests that (1) under the control of gas-solid-melt kinetics, melt can stay even in vacuum where melt can not stay thermochemically in equilibrium with gas, (2) the lifetime of the melt-crystal mixture under the kinetic control is prolonged by more than an order of magnitude compared to homogeneous distribution of crystals and melt, and (2) barred olivine texture is the possible product of a steady state evaporation, which was formed in vacuum through a fairly long heating.

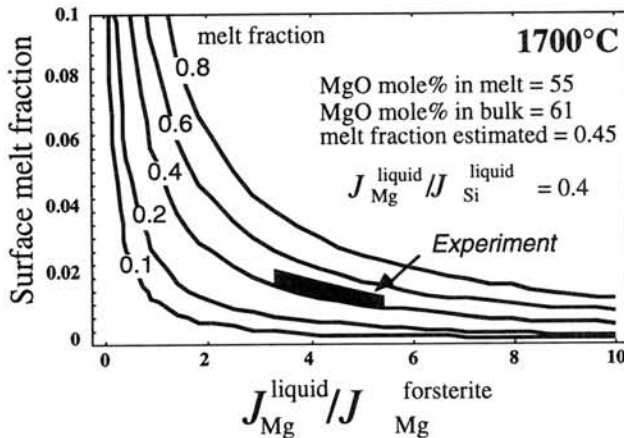


Fig. 1 Conditions for achievement of a near steady state in vacuum in the melt-solid mixtures in the MgO-SiO<sub>2</sub> system.

## Noble gas studies of primary igneous materials of Y-793605

Keisuke NAGAO<sup>1</sup>, Tomoki NAKAMURA<sup>2</sup>, Yayoi N. MIURA<sup>3</sup> and Nobuo TAKAOKA<sup>2</sup>

<sup>1</sup>*Institute for Study of the Earth's Interior, Okayama University, Misasa, Tottori-ken 682-01,* <sup>2</sup>*Earth and Planetary Sciences, Faculty of Science, Kyushu University 33, Hakozaki, Fukuoka 812-81,* <sup>3</sup>*Earthquake Research Institute, University of Tokyo, Yayoi, Bunkyo-ku, Tokyo 113*

As a part of consortium study on the Yamato 793605 martian meteorite [1], we are investigating noble gas composition and mineralogy to clarify relationships with other martian meteorites especially with the ALH77005 and LEW88516 lherzolites [2]. Cosmic-ray exposure age will give crucial information concerning the origin of Y-793605, i.e., whether this meteorite was ejected from the Mars with other known martian meteorites. Hence we will report mainly the cosmic-ray exposure history of this meteorite obtained on non-glassy part. Details have been described in [3].

Black glass materials were carefully excluded from the sample to analyze lithic materials of primary igneous rock. Mineralogical and petrologic study on the lithic material shows that this meteorite is a primary cumulate rock with close affinity to ALH77005 (and possibly to LEW88516), and is different from Shergotty. Strong shock effects, 30-50 GPa, are observed as finely fractured texture of pyroxene, maskelynite and brownish color olivine [3]. Noble gases were analyzed for two chips, 17.86 mg and 50.99 mg, by total melt and stepwise heating gas extraction, respectively, on a modified-VG5400 noble gas mass spectrometer [e.g. 4]. The meteorite samples loaded in vacuum were preheated at about 150°C overnight. Noble gas extraction temperature was 1750°C for total melt, and those for stepwise heating were 700, 1000, 1300, 1750 and 1800°C. Cosmogenic noble gases, exposure ages, and K-Ar ages are presented in Table 1, and noble gas concentrations and isotopic ratios of He, Ne and Ar are in Table 2. Kr and Xe isotopic ratios are presented in [3].

Stepwise heating of Y-793605 indicates that He is released mostly (>80% of total) at low temperatures of 700 and 1000°C with cosmogenic  $^3\text{He}/^4\text{He}$  ratio (>0.2). Radiogenic  $^4\text{He}$  concentrations could not be determined owing to low concentration and overwhelming cosmogenic He as inferred from the high  $^3\text{He}/^4\text{He}$  ratios obtained by stepwise heating as well as total melt experiments. Radiogenic  $^4\text{He}$  likely has lost recently by impact shock. Ne is dominated by cosmogenic components except for the lowest and the highest extraction temperatures for which release of small amount of trapped Ne was observed, which may be an atmospheric contamination on the sample or from a crucible. They are, however, negligible compared to the total amount of Ne.

The high ratios of cosmogenic  $^{22}\text{Ne}/^{21}\text{Ne}$  (=1.212) and  $^3\text{He}/^{21}\text{Ne}$  (7.07 and 7.49) indicate a small preatmospheric body for this meteorite, which is consistent with the small recovered mass (16 g). Production rates of cosmogenic  $^3\text{He}$ ,  $^{21}\text{Ne}$  and  $^{38}\text{Ar}$  for Y-793605 are calculated by the formulas [5] for HED meteorites and the chemical compositions for Y-793605 [6]. Since the mineral assemblage of Y-793605 lherzolite is similar to those of diogenites, we adopted the formulas for diogenites [5]. Calculated exposure ages based on the cosmogenic  $^3\text{He}$  and  $^{21}\text{Ne}$  concentrations are in good agreement among them (5.1 - 5.8 Ma). Whereas a discordant exposure age, 2.4-2.9 Ma, about half of the ages,  $T_3$  and  $T_{21}$ , is obtained from the cosmogenic  $^{38}\text{Ar}$  concentrations and the production rate  $P_{38}$  (Table 1). The short exposure age  $T_{38}$  is probably due to a low concentration of Ca in our small samples used for noble gas analyses.

Because only three martian meteorites are categorized as lherzolititic shergottites [1] until now, it is very interesting to know whether Y-793605 was ejected by a common impact event which produced the ALH77005 and LEW88516 meteorites. If we adopt the average value of  $5.4 \pm 0.3$  Ma (Table 1) based on the  $^3\text{He}$  and  $^{21}\text{Ne}$  concentrations, Y-793605 seems to have longer exposure age compared to the other lherzolites; ALH77005 ( $3.32 \pm 0.53$  Ma) and LEW88516 ( $3.98 \pm 0.58$  Ma) [7].  $^{10}\text{Be}$  exposure age,  $\geq 4.0$  Ma, is also longer than those of ALH77005 and LEW88516 [8], which is consistent with our observation. Ejection ages, i.e., exposure age plus terrestrial age, for ALH77005 and LEW88516 are proposed as  $3.52 \pm 0.60$  Ma and  $4.00 \pm 0.60$  Ma, respectively [7]. The ejection age of Y-793605 is almost the same as the exposure age owing to the short  $^{36}\text{Cl}$  terrestrial age,  $35 \pm 35$  ky (<70 ky) [8]. If the exposure and ejection ages of Y-793605 are really different from those of ALH77005 and LEW88516, Y-793605 should have originated by an additional ejection event. However, close genetic relationship among those lherzolites, i.e., they might have originated from a common magma [3], seems to indicate a common ejection event for three meteorites. If this is a case for the lherzolites, the disagreement of exposure and ejection ages among them might have produced by multistage irradiation process. In this scenario Y-793605 had been irradiated by cosmic-rays at a shallower depth in their parent body, Mars or a block ejected from Mars, before the final breakup which produced the lherzolititic meteorites. We expect to obtain information concerning the discordant ages from noble gases in remaining glassy materials of Y-793605. If the noble gases of glassy materials have martian atmospheric signature, the glasses have probably originated by an impact on Mars. On the other hand, if the glasses have short exposure age similar to those for ALH77005 and LEW88516, and no signature for martian atmosphere, the glasses have been formed by an impact in space which produced three lherzolites.

Measured  $^{40}\text{Ar}/^{36}\text{Ar}$  and  $^{129}\text{Xe}/^{132}\text{Xe}$  ratios are much lower than the high values (>2000 and

2.5, respectively) observed in martian atmosphere by the Viking lander. Upper limits for K-Ar age were calculated as  $1850 \pm 160$  and  $1420 \pm 140$  Ma for total melt and stepwise heating samples, respectively. The K-Ar ages are consistent with the young crystallization ages determined for martian meteorites except for the old one of ALH84001 orthopyroxenite. Weak signature for martian atmospheric noble gases was indicated by a small excess in  $^{129}\text{Xe}$  ( $^{129}\text{Xe}/^{132}\text{Xe} \leq 1.263 \pm 0.035$ ).

**Acknowledgments:** We wish to thank the NIPR for providing Y-793605 and Drs. H. Kojima, M. Miyamoto, K. Yanai and P.H. Warren for organizing the consortium. This work was partly supported by a Grant-in-Aid for Scientific Research No. 07454141.

**References:** [1] Kojima H. *et al.* (1997) *Proc. NIPR Symp. Antarct. Meteorites* (submitted). [2] Mikouchi T. and Miyamoto M. (1996) *Symposium on Antarctic Meteorites XXI*, 104-106. [3] Nagao K. *et al.* (1997) *Proc. NIPR Symp. Antarct. Meteorites* (submitted). [4] Miura Y.N. *et al.* (1995) *Geochim. Cosmochim. Acta* **59**, 2105-2113. [5] Eugster O. and Michel Th. (1995) *Geochim. Cosmochim. Acta* **59**, 177-199. [6] Warren P.H. and Kellemeyn G.W. (1997) *Proc. NIPR Symp. Antarct. Meteorites* submitted. [7] Eugster O. *et al.* (1997) *Geochim. Cosmochim. Acta* (in press). [8] Nishiizumi K. and Caffee M.W. (1997) *Symposium on Antarctic Meteorites XXII* (submitted).

Table 1. Cosmogenic noble gases, production rates, cosmic-ray exposure ages, and K-Ar age.

|                         | $^3\text{He}$                    | $^{21}\text{Ne}$ | $^{38}\text{Ar}$ | $^{22}\text{Ne}/^{21}\text{Ne}$ | $P_3$                               | $P_{21}$ | $P_{38}$ | $T_3$ | $T_{21}$ | $T_{38}$ | $T_{av}^{1)}$ | K-Ar           |
|-------------------------|----------------------------------|------------------|------------------|---------------------------------|-------------------------------------|----------|----------|-------|----------|----------|---------------|----------------|
|                         | $10^{-9}\text{cm}^3\text{STP/g}$ |                  |                  |                                 | $10^{-9}\text{cm}^3\text{STP/g/Ma}$ |          |          | Ma    |          |          | Ma            |                |
| Total melt<br>(17.86mg) | 89.1                             | 12.6             | 2.09             | 1.212                           | 16.1                                | 2.18     | 0.729    | 5.53  | 5.78     | 2.87     |               | $1850 \pm 160$ |
| Step heat<br>(50.99mg)  | $83.5^{2)}$                      | $11.2^{2)}$      | $1.76^{2)}$      | --                              | 16.1                                | 2.18     | 0.729    | 5.19  | 5.14     | 2.41     | $5.4 \pm 0.3$ | $1420 \pm 140$ |

1) Average of  $T_3$  and  $T_{21}$ ; 2) Total concentrations.

Table 2. Isotopic ratios of He, Ne and Ar, and noble gas concentrations in the Y-793605 martian meteorite.

|                           | <sup>3</sup> He | <sup>4</sup> He | <sup>3</sup> He/ <sup>4</sup> He | <sup>20</sup> Ne | <sup>21</sup> Ne | <sup>22</sup> Ne | <sup>20</sup> Ne/ <sup>22</sup> Ne | <sup>21</sup> Ne/ <sup>22</sup> Ne | <sup>36</sup> Ar | <sup>38</sup> Ar | <sup>40</sup> Ar | <sup>38</sup> Ar/ <sup>36</sup> Ar | <sup>40</sup> Ar/ <sup>36</sup> Ar | <sup>84</sup> Kr | <sup>132</sup> Xe |
|---------------------------|-----------------|-----------------|----------------------------------|------------------|------------------|------------------|------------------------------------|------------------------------------|------------------|------------------|------------------|------------------------------------|------------------------------------|------------------|-------------------|
| Y-793605, 73              |                 |                 |                                  |                  |                  |                  |                                    |                                    |                  |                  |                  |                                    |                                    |                  |                   |
| Total melt<br>(17.86mg)   | 89.1            | 391             | 0.2279<br>±.0026                 | 14.4             | 12.6             | 15.5             | 0.9317<br>±.0083                   | 0.8136<br>±.0062                   | 3.32             | 2.46             | 2580             | 0.7408<br>±.0069                   | 776.3<br>± 2.1                     | 82.5             | 15.8              |
| Stepwise heating(50.99mg) |                 |                 |                                  |                  |                  |                  |                                    |                                    |                  |                  |                  |                                    |                                    |                  |                   |
| 700°C                     | 37.8            | 159             | 0.2377<br>±.0013                 | 0.998            | 0.381            | 0.533            | 1.8725<br>±.0056                   | 0.7151<br>±.0031                   | 0.189            | 0.0509           | 81.5             | 0.2686<br>±.0046                   | 430.27<br>± .80                    | 32.2             | 11.6              |
| 1000°C                    | 30.5            | 140             | 0.2177<br>±.0036                 | 0.661            | 0.657            | 0.815            | 0.8115<br>±.0028                   | 0.8070<br>±.0047                   | 0.152            | 0.0786           | 136              | 0.5168<br>±.0071                   | 893.8<br>± 3.5                     | 5.42             | 1.75              |
| 1300°C                    | 13.8            | 62.2            | 0.2225<br>±.0025                 | 5.46             | 5.33             | 6.51             | 0.8391<br>±.0030                   | 0.8197<br>±.0017                   | 0.957            | 0.793            | 689              | 0.8287<br>±.0076                   | 719.82<br>± .93                    | 22.0             | 6.29              |
| 1750°C                    | 1.37            | 7.18            | 0.191<br>±.016                   | 4.89             | 4.78             | 5.88             | 0.8323<br>±.0080                   | 0.8141<br>±.0063                   | 1.25             | 1.09             | 810              | 0.8744<br>±.0080                   | 649.47<br>± .93                    | 23.9             | 4.56              |
| 1800°C                    | --              | --              | --                               | 0.045            | 0.0026           | 0.0062           | 7.26<br>±.97                       | 0.42<br>±.13                       | 0.0393           | 0.0107           | 11.8             | 0.271<br>±.022                     | 300.2<br>± 1.5                     | 0.68             | 0.16              |
| Total                     | 83.5            | 368             | 0.227                            | 12.1             | 11.2             | 13.7             | 0.883                              | 0.818                              | 2.59             | 2.02             | 1730             | 0.780                              | 668                                | 84.2             | 24.4              |

Concentrations of He, Ne and Ar are in the unit of 10<sup>-9</sup> cm<sup>3</sup>STP/g, and those of <sup>84</sup>Kr and <sup>132</sup>Xe in 10<sup>-12</sup> cm<sup>3</sup>STP/g.

## IMPACT-INDUCED LOSS OF PRIMORDIAL NOBLE GASES FROM EXPERIMENTALLY SHOCKED ALLENDE METEORITE

Tomoki Nakamura<sup>1</sup>, Michael E. Zolensky<sup>2</sup>, Fred Hörz<sup>3</sup>, Nobuo Takaoka<sup>1</sup> and  
Keisuke Nagao<sup>4</sup>

<sup>1</sup>Department of Earth and Planetary Sciences, Faculty of Science, Kyushu University 33, Hakozaki, Fukuoka 812-81, Japan, <sup>2</sup>SN2, NASA JSC, Houston TX 77058, USA, <sup>3</sup>SN4, NASA JSC, Houston TX 77058, USA, <sup>4</sup>Institute of Study for Earth's Interior, Okayama University, Misasa, Tottori 682-01, Japan

Shock effects with pressures up to 90 GPa are recorded in the primitive chondritic meteorites [e. g., 1]. Shock-wave propagation and shock heating were responsible for changes of primitive characteristics of the chondritic meteorites. Noble gases are the most volatile elements and are subject to be lost by impacts from the chondritic material. H<sub>2</sub>O, CO<sub>2</sub> and radiogenic Ar showed impact-induced loss from chondrites [2, 3] and volatile-bearing minerals [e. g., 4]. In the early stage of the solar system formation, primordial noble gases were dominant noble gases in the planetary bodies. Major components of the primordial noble gases are Q-gas and HL-gas: the former dominates primordial Ar, Kr, and Xe and locates in ill-identified carbonaceous matter called phase Q, and the latter comprises most of primordial He and Ne [5] and locates in HL diamonds of interstellar origin [e. g., 7]. The Q and the HL gases are found to be distributed in any type of primitive chondritic meteorite [8]. However, shock effects on the abundance of the primordial noble gases were not well known, except for Nakamura et al. (1996) [9] that reported essentially no loss of the primordial noble gases from Allende meteorite by a 23 GPa impact.

Shock-recovery experiments were carried out on the Allende CV3 chondrite with peak pressures of 30, 47, and 70 GPa using a single stage propellant gun at NASA JSC. To avoid adsorption and implantation of atmospheric noble gases, we have done special arrangements in the experiments: (1) A through hole with 1 mm diameter was made in a stainless sample holder, (2) Allende sample was evacuated down to  $1 \sim 4 \times 10^{-2}$  torr through the hole in the holder, (3) the sample was preheated at 180 °C for 4 hours in the gun chamber, (4) ambient air was replaced by N<sub>2</sub> gas during cool down the sample, and (5) the sample was impacted after it was cooled down to room temperature.

The carrier phases of the primordial noble gases are distributed in the matrix, thus shock effects of the matrix material could provide us clues to understand what happened during shock-loading. Cross sections of the recovered products were investigated with high magnification images on the scanning electron microscope. Fine-grained Fe-rich olivine, low-Ca pyroxene, Fe-Ni metal and sulfide in the matrix of the 30 GPa product appear to be strongly compacted but not to be melted. In the 47 GPa product the metal-sulfide minerals were melted to form many small veins in the matrix. The glassy materials rich in Ca, Si, and Fe that were located originally interstices between fine silicate grains in the matrix appear to have been melted to form irregular- to ellipsoidal-shaped melt pockets. In some portions silicate minerals in the matrix were also melted where metal and sulfide grains became rounded. The 70 GPa product shows a drastic textural change: matrix is totally melted and numerous small gas bubbles with diameters from 1 to 30 μm were produced throughout the matrix.

Major element composition of the melt is similar to that of bulk matrix except for Na depletion. The melt containing high densities of the small bubbles intruded into cracks in a metallic sample holder.

Noble-gas concentrations and isotope ratios in the three shock-loaded products and an unshocked Allende sample were determined using a noble gas mass spectrometer [e. g., 10] by a stepped heating technique with eight temperature steps, 350, 450, 600, 800, 1000, 1250, 1550, 1850 °C. Primordial  $^{20}\text{Ne}$  and  $^{132}\text{Xe}$  were separated into Q- and HL-gases, i. e.,  $(^{20}\text{Ne})_{\text{Q}}$  vs.  $(^{20}\text{Ne})_{\text{HL}}$ , and  $(^{132}\text{Xe})_{\text{Q}}$  vs.  $(^{132}\text{Xe})_{\text{HL}}$ , using Xe-Q, Xe-HL isotopic ratios [6, 11] and a  $(^{20}\text{Ne}/^{132}\text{Xe})_{\text{Q}}$  elemental ratio [11]. Concentration of heavy primordial noble gases such as  $^{36}\text{Ar}$ ,  $^{84}\text{Kr}$ , and  $^{132}\text{Xe}$  decreases in the order of the unshocked Allende, 30, 47, and 70 GPa samples:  $(^{132}\text{Xe})_{\text{Q}}$  concentrations are 9.4, 6.9, 5.9, and  $2.4 \times 10^{-10}$  cc STP / g, respectively. This indicates that phase Q lost up to 75% noble gases due to experimental shock-loading with pressures up to 70 GPa. Release patterns of  $(^{132}\text{Xe})_{\text{Q}}$  of the unshocked Allende, 30, 47, and 70 GPa samples are basically similar, although concentrations of all temperature steps are reduced. This seems to suggest that phase Q which suffered heavier shock effects has lost all noble gases including those in highly retentive sites, whereas the rest of phase Q that suffered lesser degrees of shock effects has retained most noble gases. Unlike the phase Q, HL diamonds did not lose noble gases by shock loading. Amounts of HL-gas such as  $(^{20}\text{Ne})_{\text{HL}}$  and  $(^{132}\text{Xe})_{\text{HL}}$  were relatively constant in the unshocked and the shocked samples:  $(^{20}\text{Ne})_{\text{HL}}$  concentrations are 2.2, 2.9, 2.5,  $2.1 \times 10^{-10}$  cc STP / g for the unshocked, 30, 47, and 70 GPa samples. Release patterns of  $(^{20}\text{Ne})_{\text{HL}}$  from the four samples are basically similar. Large amounts of HL-gas were extracted in 800 - 1000 °C fractions in the stepwise heating experiments. These facts suggest that the HL diamonds did not lose not only noble gases but gas-retentivity, even after 70GPa impact. It is uncertain why the HL-gas was not lost by a strong shock compression, but it is likely that the HL-gas was rigidly trapped in the crystal structure of diamonds. The preferential loss of the Q-gas from the shock-loaded samples caused elemental fractionation of the noble gases remained in the samples that tend to have higher elemental ratios of light noble gases to heavy ones, e. g., Ne/Xe, although Ar/Xe and Kr/Xe ratios did not change considerably. As for isotope compositions, shock-loading appears not to cause significant isotope fractionation except for enrichment of light and heavy Xe isotopes due to high HL/Q ratio in the shock-loaded samples.

*Acknowledgments:* The authors appreciate the technical support of Messrs. G. Haynes and W. Davidson in the shock experiments and V. Yang in electron-microprobe analyses.

References: [1] Stöfler D. et al., (1991) GCA 55, 3845 [2] Tyburczy J. A. et al., (1986) EPSL 80, 201. [3] Bogard D. et al., (1987) GCA 51, 2035. [4] Lange M. A. et al., (1985) GCA 49, 1715. [5] Huss G. R. and Lewis R. S., (1994) Meteoritics 28, 563. [6] Lewis R. S. et al., (1975) Science 190, 1251. [7] Lewis R. S. et al., (1989) Nature 339, 117. [8] Huss G. R. and Lewis R. S., (1995) GCA 58, 115. [9] Nakamura T. et al., (1996) Proc. of the 3rd NIRIM International Symp. on Advanced Materials, 33. [10] Nagao K. (1994) Proc. NIPR Symp. Antarct. Meteorite 7, 197 [11] Wieler R. et al., (1991) GCA 55, 1709.

# CHEMICAL COMPOSITION AND STRUCTURAL STATE OF PLAGIOCLASE IN THE Y-791067 CHONDRITE

Y. Nakamuta and Y. Motomura

Dept. Earth and Planetary Sciences, Faculty of Science, Kyushu University, Fukuoka 812, Japan

## Petrographic texture

The Y-791067 chondrite has bulk, olivine, and pyroxene chemical compositions corresponding to the LL-group chondrite (Yanai et al., 1987, 1995). Under a optical microscope, it shows a breccia texture and coarse-grained olivine and pyroxene clasts disperse in a fine- to medium-grained matrix. Chondritic textures are absent. Plagioclase of 50 to 100  $\mu$ m in size occurred interstitially in a matrix. The interstitial occurrence of plagioclase suggests its formation after the brecciation of the meteorite. The meteorite has been tentatively classified as petrologic type 7 chondrite by Yanai et al. (1987) because of homogeneous chemical compositions of pyroxene and olivine and the absence of chondritic textures, suggesting high recrystallization of the meteorite. Its fine- to medium-grained matrix, however, suggests lower petrologic type of the meteorite than that suggested by Yanai et al. (1987).

## Chemical composition of plagioclase

Chemical composition of plagioclase in the Y-791067 chondrite was analyzed by electron probe microanalyzer with a wave-length disperse mode, 15kv accelerating voltage, and 0.01 nA beam current. The chemical compositions of plagioclase are shown as solid circles along with those for the Dhurmsala(LL6) chondrite (open circles) on the ternary diagram with Or, Ab, and An components of plagioclase at each apex (Fig. 1). Plagioclase in Y-791067 has an uniform An content of 9.6 ( $\pm 0.6$ ) mole % and variable Or contents in the range between 3.7 and 6.2 mole % and is relatively poorer in the An component than that in the Dhurmsala chondrite.

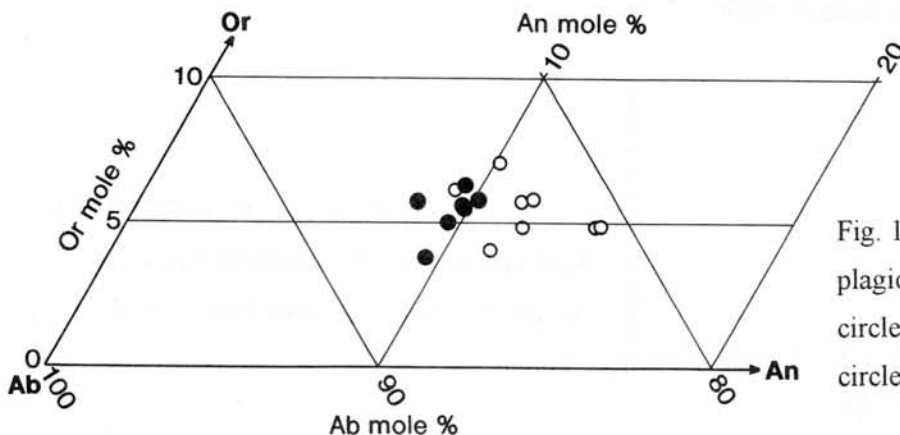


Fig. 1. Chemical composition plagioclase from Y-791067 (solid circles) and Dhurmsala (open circles) chondrites.

### Structural state of plagioclase

The x-ray powder patterns of individual plagioclase grains of about  $50\ \mu\text{m}$  in size of which chemical compositions have been analyzed were obtained by a Gandolfi camera. The distance between 1-31 and 131 reflections in the x-ray powder pattern was determined precisely with an error less than 0.01 degree ( $2\theta$ ) by applying a profile-fitting technique. The measured distance between the 1-31 and 131 reflections was corrected for the influence of Or content by using the correction diagram presented by Kroll and Ribbe (1981). The corrected distance is directly related to the structural state of plagioclase, the degree of Al/Si order in the four symmetrically non-equivalent tetrahedral sites in the framework structure, and is correlated to the equilibration temperature of plagioclase (Smith, 1972).

Plagioclases from Y-791067 are platted as solid circles together with those from the Dhurmsala LL6 chondrite (open circles) on the diagram by Smith(1972) which shows the relation between the 131 structural indicator and temperature of synthesis of plagioclase. The plagioclases from Y791067 show the temperatures in the range between 650 and 710 °C which are lower than those of the range between 680 and 800 °C for the Dhurmsala LL6 chondrite. The ranges of the temperature obtained by plagioclase from both chondrites reveal that the structural state of plagioclase is not in equilibrium, maybe due to the sluggishness of order disorder reactions of plagioclase in a dry environment which is plausibly suggested for chondrite parent bodies (Dodd,

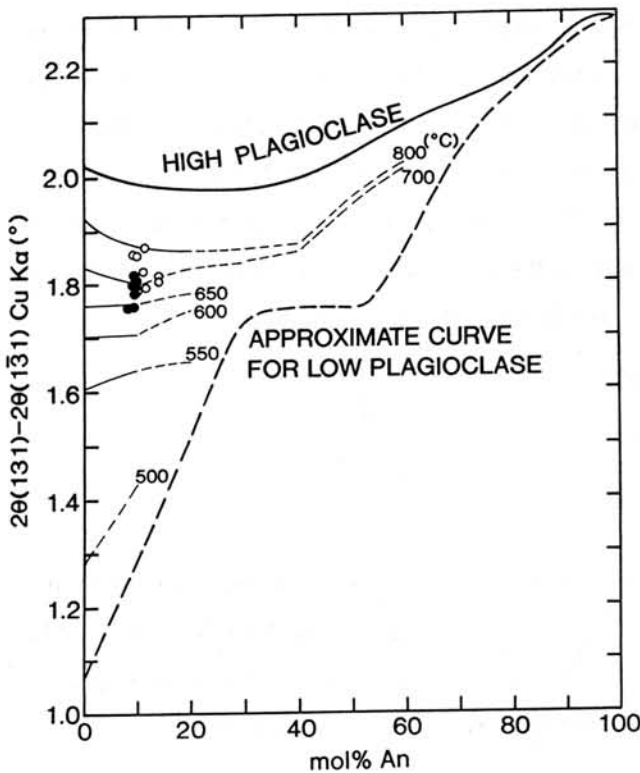


Fig. 2. Plots of pladioclase from Y-791067 ( Solid circles) and Dhurmsala (open circles) chondrits on the diagram by Smith (1972).

1981). Therefore, the temperatures estimated from Fig. 2 may correspond to the temperatures at which plagioclases crystallized from pre-existing glass during progressive alteration processes in a parent body. Then, the maximum temperature indicated by plagioclase of each chondrite corresponds to the peak temperature reached during metamorphic processes in a parent body.

The maximum temperature estimated from plagioclase for Y-791067 is 710°C and is lower than the maximum temperature of 810°C for the Dhurmsala LL6 chondrite. On the basis of the results, Y-791067 has been metamorphosed in the environment of lower temperature than the Dhurmsala LL6 chondrite and may be assigned to the petrologic type intermediate between 5 and 6. The interstitial occurrence of the plagioclase in the Y-791067 chondrite suggests that the peak metamorphic temperature has been attained after the brecciation of the meteorite.

### References

- Dodd, R. T. (1981): *Meteorites*, Cambridge University Press, London.
- Kroll, H. and Ribbe, P. H. (1980): *Amer. Mineral.*, **65**, 449-457.
- Smith, J. V. (1972): *Jour. Geology*, **80**, 505-525.
- Yanai, K. and Kojima, H. (1987): *Photographic catalog of the Antarctic meteorites*, NIPR, Tokyo.
- Yanai, K. and Kojima, H. (1995): *Catalog of the Antarctic meteorites*, NIPR, Tokyo.

## Carbon isotopic compositions of Antarctic carbonaceous chondrites with relevance to the alteration and existence of organic matter.

Hiroshi Naraoka<sup>1</sup> and Akira Shimoyama<sup>2</sup>

<sup>1</sup> Dept. of Chemistry, Tokyo Metropolitan University, Hachioji, Tokyo 192-03

<sup>2</sup> Dept. of Chemistry, University of Tsukuba, Tsukuba, Ibaraki 305

**Introduction** Bulk carbon isotopic compositions of carbonaceous chondrites may have potentials to clarify classification of the chondrites, and physical and chemical processing of the meteorite parent body. So far, the isotopic studies have been mainly reported using non-Antarctic meteorites [1]. Antarctic meteorites are not "recent-falls", but have been preserved in ice shield mostly up to several hundred thousand years. Antarctic carbonaceous chondrites may provide new opportunities to clarify the isotopic characteristics because non-Antarctic carbonaceous chondrites are rare and limited for their analyses. In this paper, the isotope ratios are reported compared to those in non-Antarctic ones, and referred from the existence of solvent-extractable and -insoluble organic matter (kerogen-like matter), since most carbon in carbonaceous chondrites is known to be present as organic carbon. The isotopic characteristics are also discussed with relevance to alteration and metamorphism on parent bodies.

The samples used in this study were Antarctic 27 carbonaceous chondrites (34 specimens) collected mainly by JARE in 1974, 1977, 1979 and 1988 field seasons [2]. Seven CM chondrites of these, carbon isotopic compositions were also determined for the residues of hot H<sub>2</sub>O, HCl/HF and heating treatment.

**Results** The  $\delta^{13}\text{C}$  values are plotted against carbon contents as large symbols in Fig. 1. Carbon contents range from 0.02 to 2.49 wt% with an average value of 1.31 wt% for all specimens. Although the concentration was determined for several CM chondrites with different sub-numbers, it is less variable with a maximum difference of 0.25 wt% in B-7904. Carbon isotopic compositions vary widely from -16.6 to +0.9‰, but within a single chondrite the largest difference was 2.5‰ found in A-881334. Most differences, however, are less than 1‰. In Fig. 1 most CM and CO Antarctic chondrites lie on a trend as shown within broken lines, where the  $\delta^{13}\text{C}$  values become larger with increasing carbon contents ("a major sequence"). In addition, an unique group is characterized by isotopically light ( $\sim -15\text{‰}$ ) carbon with relatively high carbon content ( $\sim 2.5\text{ wt\%}$ ) (indicated by oval in Fig. 1).

Hot H<sub>2</sub>O extraction decreases the  $\delta^{13}\text{C}$  values of residues by up to 6‰ compared to those of bulk samples. The isotopic differences ( $\Delta_{\text{H}_2\text{Oresidue-bulk}}$ ) are small (-2.0 to -0.4‰)

for 4 chondrites (Y-793321, B-7904, A-881280 and A-881334), while those of the others (Y-791198 and A-881458) are relatively large (-4.9 to -6.0‰).

Contrary to large isotopic variations in bulk carbon, kerogen-like matter has relatively constant  $\delta^{13}\text{C}$  values. Most kerogen-like matter has  $\delta^{13}\text{C}$  values of -15 to -13‰. Two specimens (Y-793321 and A-881458) have  $\delta^{13}\text{C}$  values of -9 to -7‰. Isotopic differences between bulk meteorites and their kerogen-like matter ( $\Delta_{\text{kerogen-bulk}}$ ) are small (-1.7 to +0.1‰) for 2 chondrites (B-7904, A-881280), intermediate (-6.2 to -2.1‰; Y-793321 and A-881334), and relatively large (-15.3 to -8.3‰) for 3 chondrites (Y-74662, Y-791198 and A-881458). The last group also has a relatively large  $\Delta_{\text{H}_2\text{Oresidue-bulk}}$  value (up to -6‰).

The heating experiment on two Asuka CM chondrites reduced their carbon contents, and made their isotopic compositions lighter (shown as arrows in Fig. 1). The  $\delta^{13}\text{C}$  values of heating residues (-15.9‰ for A-881334 and -18.9‰ for A-881458) are similar or slightly lower than that of low group of the kerogen-like matter. Mass balance calculation indicates that the released component from A-881458 is richer in  $^{13}\text{C}$  (+2.2‰) than that from A-881334 (-4.4‰).

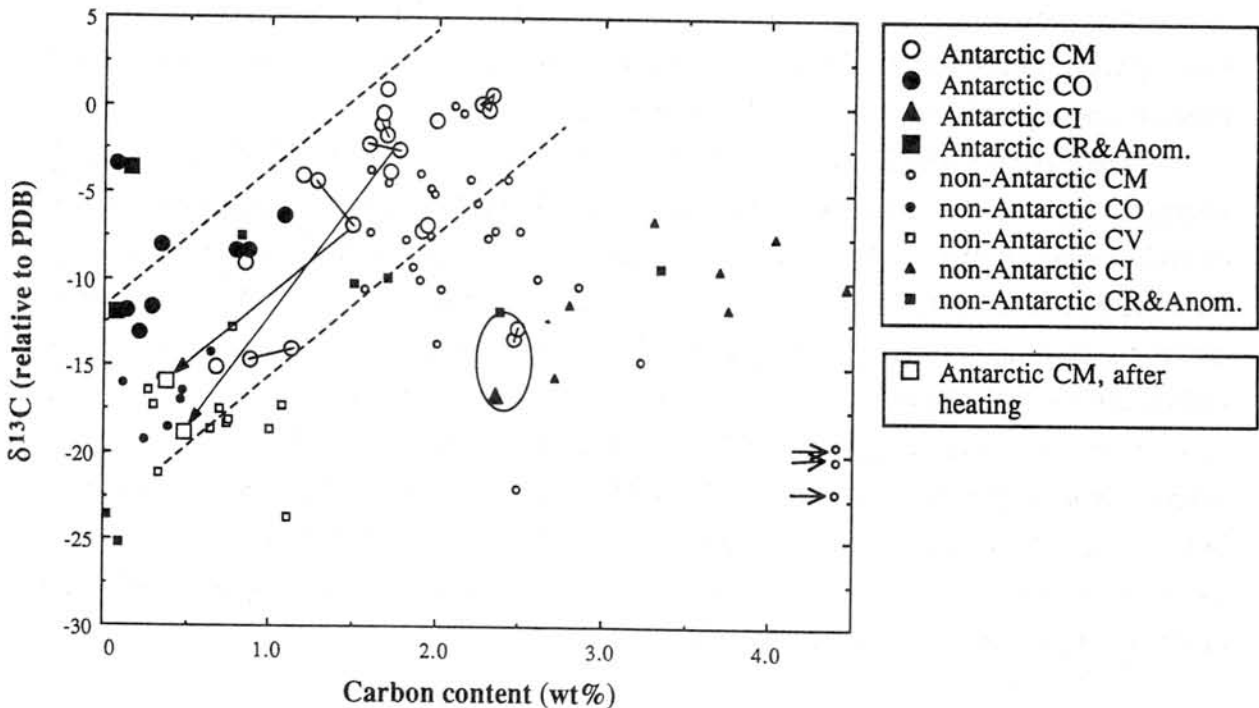


Fig. 1. Relationship between bulk carbon isotopic compositions and carbon contents of Antarctic carbonaceous chondrites with those of non-Antarctic carbonaceous chondrites. Large symbols stand for the Antarctic (this study), and small symbols for the non-Antarctic (data from Kerridge [1]). Plots of multiple analyses in a single Antarctic chondrite are tied by a line. Most Antarctic CM and CO chondrites lie on a trend ("a major sequence") as shown within broken lines, where the  $\delta^{13}\text{C}$  values become larger with increasing carbon contents. An unique group (probably altered) is indicated by the oval. By heating experiment changes in carbon content and  $\delta^{13}\text{C}$  value are projected as arrows.

**Discussion** Antarctic chondrites are generally isotopically heavier than non-Antarctic ones at the same level of carbon content (Fig. 1). The mean  $\delta^{13}\text{C}$  values of -5.8 ‰ is apparently heavier than that of non-Antarctic (-11.5 ‰: using data by Kerridge [1]). The difference may be explained by contamination of terrestrial organic carbon on non-Antarctic chondrites and/or different populations of parent bodies.

Most CM chondrites are plotted in right-over region on "a major sequence", while CO chondrites in left-under region. The feature is distinct mineralogically, but apparently continuous isotopically. The sequence may be explained by a two-end member mixing model. Isotopically heavy components (labile for physical and chemical treatments) are mixed with isotopically light components (relatively inert). It is known that the main carbon-bearing component in carbonaceous chondrites is isotopically light (~-15‰) and solvent-insoluble kerogen-like matter, which occurs in all groups of carbonaceous chondrites [3, 4]. While it is revealed that major isotopically heavy components are carbonates and solvent-extractable organic matter such as amino acid and carboxylic acid [5, 6]. They are heterogeneously distributed among the various types of carbonaceous chondrites, and may be easily removable or destructive by aqueous alteration or thermal metamorphism. The characteristics of carbon-bearing components will predict the mixing trend between low isotope ratios at low carbon contents and higher isotope ratios at higher carbon contents.

The mixing model is also supported by the experiments of  $\text{H}_2\text{O}$ ,  $\text{HCl}/\text{HF}$  and heating treatment.  $\text{H}_2\text{O}$  treatment makes the residue isotopically lighter up to 6‰ compared to those of bulk carbon. Amino acids and carboxylic acids were identified in the water extract [7]. Also  $\text{HCl}/\text{HF}$  treatment, which remove carbonate and organic matter trapped in the matrix, makes the residue isotopically lighter up to 15‰. Furthermore, heating experiment reduces carbon content, and makes the  $\delta^{13}\text{C}$  values smaller by up to 19‰. Kerogen-like matter itself may become isotopically lighter by releasing of hydrocarbons during heating considering from the much lighter residue (-18.9‰; A-881458). The two samples after heating are plotted in Fig. 1 near the severely altered specimens such as B-7904 and Y-86720. Hence, if aqueous alteration or metamorphism occurred on the parent bodies, the isotopic signature of such processes may have an identical pathway along the sequence.

## References

- [1] J. F. Kerridge (1985) *Geochim. Cosmochim. Acta*, **49**, 1707-1714. [2] K. Yanai and H. Kojima (1995) *Catalog of the Antarctic meteorites: collected from December 1969 to December 1994*, National Institute of Polar Research, Tokyo. [3] J. R. Cronin et al. (1988) In *Meteorites and the Early Solar System*, 819-857, Univ. Arizona Press, Tucson. [4] J. F. Kerridge et al. (1987) *Geochim. Cosmochim. Acta*, **51**, 2527-2540. [5] S. Epstein et al. (1987) *Nature*, **326**, 477-479. [6] G. Yuen et al. (1984) *Nature*, **307**, 252-254. [7] H. Naraoka et al. (1991) *Papers Presented to the 16th Symposium on Antarctic Meteorites*, 146-147.

# THE RAMGARH STRUCTURE - AN ASTROBLEME (?), RAJASTHAN, INDIA, AN APPRAISAL

V.K. NAYAK

Department of Applied Geology, Indian School of Mines, Dhanbad, India

## ABSTRACT

The origin of the spectacular circular structure at Ramgarh (25°20'N : 76°37'30"E), India, has been a controversial subject for nearly three decades. An appraisal of various views and suggestions with emphasis on meteorite impact and tectonism is presented. The depth to diameter ratio, raised rim, quaquaversal dips, inverted topography support its impact origin. Besides, shatter cone, shock-like lamellae and anomalous birefringence in quartz have been reported but their true nature needs to be confirmed.

A multi-disciplinary effort is suggested to establish the origin of this circular structure on a definitive basis. The problem of origin of the structure still remains inconclusive and at present it seems reasonable to consider it as 'Ramgarh Astrobleme'.

## INTRODUCTION

As an outgrowth of scientific interest and awareness of planetary surfaces generated by exploration of space, there has been a rapid acceleration in the study of terrestrial impact structures. It is now increasingly realised that impact cratering was a fundamental ubiquitous process in geology and it will unravel the mysteries of the solar system. Currently 150 terrestrial impact craters are known throughout the world and in India, Lonar is an authentic meteorite impact crater (Grieve et al. 1995).

An isolated annular shape structure at Ramgarh (25°20'N : 76°37'30"E), Kota District, Rajasthan, India, has in recent years aroused great interest to comprehend its formation. Obviously, the origin of this enigmatic feature has been a debated subject for about three decades and various views and suggestions have been proposed from time to time. These are meteorite impact, kimberlite and carbonatite intrusions, subsidence and tectonism etc.

## LOCATION

Ramgarh is located 350 km SSW of New Delhi and 110 km East of Kota City. The nearest railway station is 25 km south of Ramgarh at Baran. The feature is named after the village Ramgarh which is situated in the south-west foot hill which is breached at this point.

The remnants of temples and a fort along the crest reflect that it was a historical place of veneration and civilization. The feature is seen in the Survey of India Toposheet No. 54-C/11 and also shown cartographically and air-photographically as a hill feature (Fig. 1) in the School Atlas (1961). From the Earth Resources Technology Satellite (ERTS) imagery, Dietz and McHone (1974) suggested that Ramgarh is an impact structure which is either an eroded young crater or more likely the central uplift of an ancient astrobleme. The structure is also described in the Astronaut's Guide as an impact crater with ring of hills and a small central peak from the Landsat Image (Fig. 2) (Grieve et al., 1988). It is interesting to note that the Ramgarh structure is not fully circular but in fact is rectangular and analogous to the well-known Meteor Crater, Arizona, U.S.A. (Milton in Crawford, 1972).

## GEOLOGY AND DIMENSIONS

The Ramgarh structure abruptly stands out in monotonous sandstone of the Bhandar Group of the Vindhyan Supergroup. Ramasamy (1987, 1988) worked out lithostratigraphy and structure of the area in and around Ramgarh and showed conformable and continuous sequence of the Bhandar Group consisting of sandstone, shale and limestone within the structure and the Rewa Group consisting of Jhiri shales and Upper Rewa sandstone exposed in the central part of the basin (Figs. 3 & 4). Other observations recorded by several workers are: steep slopes on the inner sides and gentle slopes on outer sides. Good sedimentary structures are preserved and faulting and folding of strata have been recorded. Overturned rocks are seen at the crest which is covered with bouldery rocks. The sandstone is fractured and shattered at several places in the area. Also, it may be mentioned that Deccan Basalts are exposed 50 km south of the Ramgarh structure and both the basalts and Ramgarh overlie the Vindhyan Supergroup of rocks. There is a raised rim with quaquaversal dips, inversion of topography and uplifting of rocks in the centre of the structure. The outer diameter is 4 km while the inner diameter is 2 km and covers an area of 16 sq. km. The depth to diameter ratio is only 0.05. The average radius is about 3 km, height of rim from the surrounding plain is 200 m while the highest point is 240 m.

## ORIGIN OF THE STRUCTURE

A survey of the literature reveals that the origin of the Ramgarh Structure has been a controversial subject and various explanations have been proposed from time to time. These relate to meteorite impact, tectonism, carbonatite and kimberlite intrusive body, combined action of tectonic and volcanic activity, subsidence and cryptovolcanism etc. Obviously, these suggestions were mainly based on geological, geomorphological, lithostratigraphical and structural characteristics of the area and interpreted subjectively and at times speculatively. A brief review of these follows:

Mallet (1869) was the first geologist to make a general reconnaissance survey of the area but did not make any reference to the Ramgarh feature. More than a century passed until Crawford (1972) found a shatter cone in the colluvium of the central part of structure and brought to attention that Ramgarh could be some kind of impact structure. Later, Crawford (1978) while dealing with the Narmada-Son lineament remarked that the Ramgarh structure may be due to carbonatite intrusive body but not related to any lineament. Balasundaram and Dube (1973) observed shear fracturing, granulation and anomalous birefringence in quartz grains of quartzitic sandstone and thus concurred with Crawford's concept of impact origin. Ahmad et al. (1974a) discovered highly magnetic pieces and spherules from the area and considering their Ni-Fe nature favoured the impact origin of the structure. Subsequently, more analyses of the iron material already collected by Ahmad et al., and later by Bhandari and his team of the Physical Research Laboratory, Ahmedabad, showed that Ni-Fe ratio is much smaller and therefore non-meteoritic in nature. On the whole, however, Ahmad et al. (1974b) considered the origin of the structure by meteorite impact and referred it to 'astrobleme', a suggestion made earlier <sup>due to</sup> by Nayak (1984). Rakshit (1974) also postulated Ramgarh to be an extra-terrestrial gaseous body like a comet. Similar views were expressed in support of impact hypothesis by Khan (1980).

Auden (1970) personally communicated to the Director General, Geological Survey of India, with a suggestion that the Ramgarh structure could be correlated with the diamondiferous kimberlite pipe at Majhgawan in Panna District, Madhya Pradesh. Sharma (1973) geomorphologically interpreted the Ramgarh structure as a dome and topographically a circular basin formed by combined action of tectonic and volcanic activity. However, he also observed quaquaversal dips inverted topography and these characters support the impact origin. Gupta and Prasad (1976) considered Ramgarh to be a domal structure formed as a consequence of erosion of underlying limestones and shales. Ramasamy (1984)

suggested Ramgarh dome to be a tectonic feature related to regional tectonism and further provided a kinematic model to understand the evolution of domal structure. A geophysical survey of the area did not indicate any magnetic anomaly inside the Ramgarh structure (Sharma and Singh, 1970; Ahmad et al. 1974b), and thus ruled out the possibility of its formation by igneous activity. Drilling by the Geological Survey of India (Vimal Kumar and Reddy, 1984) in the central depression upto a depth of 452 m did not reveal any magmatic or igneous rock but instead encountered a great thickness of Upper Vindhyan sandstone.

### **CONCLUSIONS AND SUGGESTIONS**

Ramgarh structure is indeed a spectacular circular feature in the plain regional surrounding of the Vindhyan Supergroup. From the logical interpretation of the factual observations, it is conjectured that the origin of the Ramgarh structure can be grouped mainly into meteorite impact phenomenon and tectonism or perhaps impact induced tectonism resulted in the formation of the structure. Other explanations like carbonatite intrusion, kimberlite pipe, diapirism, igneous activity, subsidence and cryptovolcanism can be ruled out.

Considering its overall characteristics such as raised rim, depth to diameter ratio, quaquaversal dips, inverted topography, possible shock metamorphic features, it is suggested that the Ramgarh structure at present should be considered as a 'Ramgarh Astrobleme', until more definitive evidences are found and confirmed.

A few years ago in 1989-90, the author and the scientists of the Lunar Planetary Institute (LPI), Houston, U.S.A., formulated a cooperative project for an integrated 'Field, Petrological and Geochemical' study of the Ramgarh structure, however, unfortunately it could not be executed owing to various constrains.

It is strongly felt that the Ramgarh structure deserves a well-planned multi-disciplinary effort to resolve its origin on definitive basis. In addition, the determination of its age will be useful to understand its relationship with the nearby Deccan volcanic episode. Finally, it is believed that the Ramgarh structure - an Astrobleme would make an important contribution to the Earth's cratering history.

### **ACKNOWLEDGEMENTS**

The author thanks the Director, Indian School of Mines, for providing the necessary facilities for this work. He is also indebted to Dr. N. Bhandari, Physical Research Laboratory, Ahmedabad; Dr. SM Ramasamy, Bharathidasan University, Trichy and Dr. A.M.Rakshit, Geological Survey of India, for their published and unpublished material which was useful in the preparation of this contribution.

## REFERENCES

- Ahmad, N., Bhardwaj, B.D. Sajid, H.A. and Hasnain, I. (1974). Curr. Sci., India, 43 (18), 598.
- Ahmad, N., Ahmad, R., Bhandari, N., Gopalan, K. and Patel, P.P. (1974). Unpublished Report, Physical Research Laboratory, Ahmadabad, 1-14.
- Auden, J.B. (1970). Personal communication with the Director General, Geological Survey of India, Calcutta.
- Balasundaram, M.S. and Dube, A. (1973). Nature, 242, 40.
- Crawford, A.R. (1972). Nature, 237, 96.
- Crawford, A.R. (1978). Jour. Geol. Soc. India., 19 (4), 144-153.
- Dietz, R.S. and McHone. J. (1974). Meteoritics, 2, 329-333.
- Grieve, R.A.F., Wood, C.A., Garvin, J.B., McLaughlin, G. and McHone, G.Jr. (1988). Lunar Planetary Institute Report 88-03, 1-89.
- Grieve, R.A.F., Rupert, J., Smith, J. and Therriault, A. (1985). GSA Today, Geol. Soc. Amer., 5 (10), 194-196.
- Gupta, S.N. and Prasad, B. (1976). In Symposium on 'Vindhyan of Central India', 125th Geological Survey of India Anniversary Celebrations, 11.
- Khan, A.J. (1980). Geoviews, 7 (14), 173-179.
- Mallet, F.R. (1869). Mem. Geol. Surv. India, 7, 129.
- Nayak, V.K. (1984). Proc. 71st Indian Sci. Congr., Ranchi, 22-23.
- Rakshit, A.M. (1974). Unpublished Prog. Report, Geol. Surv. India.
- Ramasamy, S.M. (1984). Unpublished Ph.D. Thesis, Andhra University, India
- Ramasamy, S.M. (1987). Rec. Geol Surv. India, 113 (7), 13-22.
- Ramasamy, S.M. (1988). Rec. Geol. Surv. India, 114 (7 & 8), 15-24.
- School Atlas, 7 - Map Publication Office, Survey of India, Dehra Dun, 1961.
- Sharma, H.S. (1973). Nature, 242, 39-40.
- Sharma, J.K. and Singh, S.R. (1970). Unpublished Prog. Report, Geol. Surv. India, Calcutta.
- Vimal Kumar and Reddy, B.V.R. (1984). Unpublished Prog. Report, Geol. Surv. India, Calcutta.

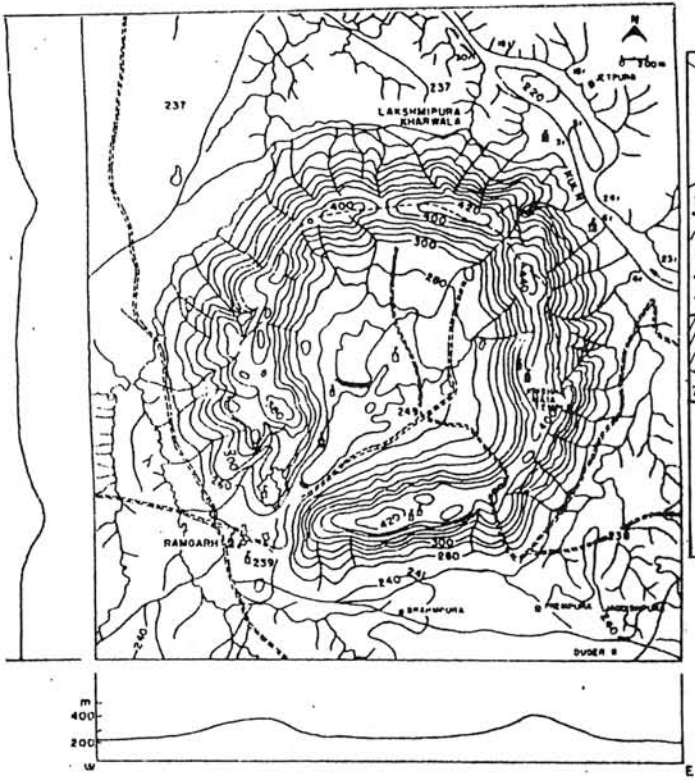


Fig. 1 - A contour plan and cross sections of Ramgarh, India

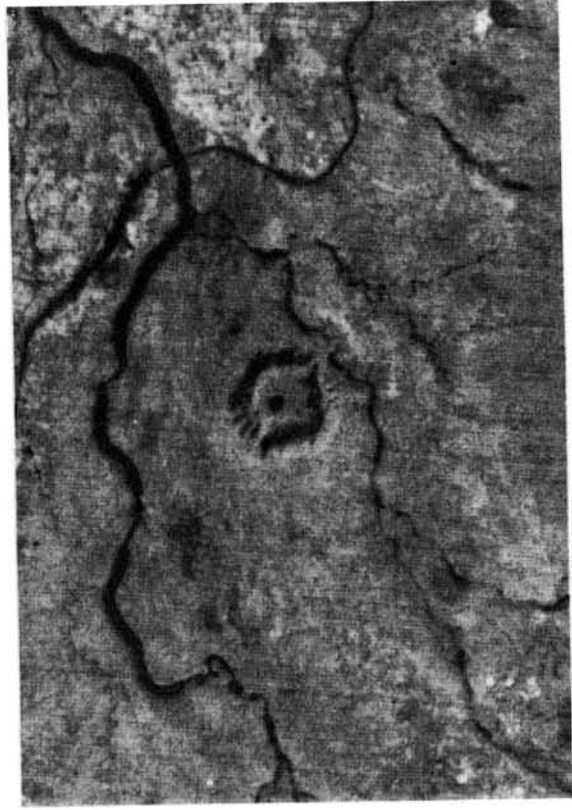


Fig. 2 - Landstat image showing a ring of hills and central peak of Ramgarh (After Grieve et al., 1988)

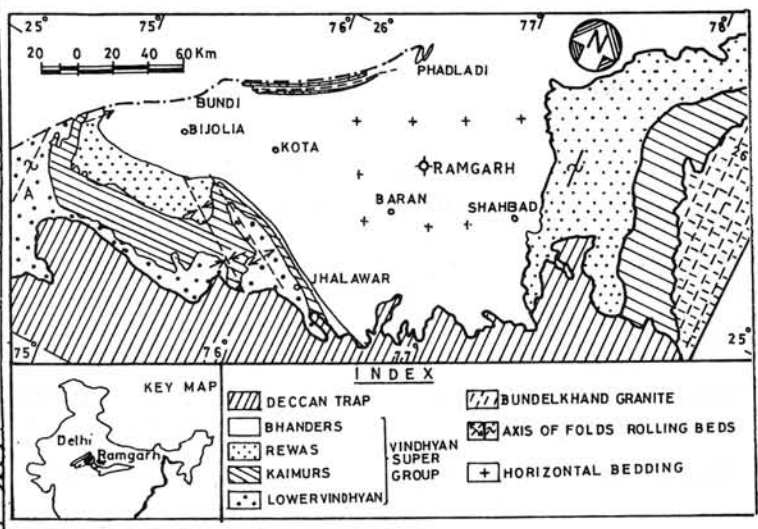


Fig. 3 - Location of Ramgarh in a geological set-up of western part of the Vindhyan Basin (After Ramasamy, 1987).

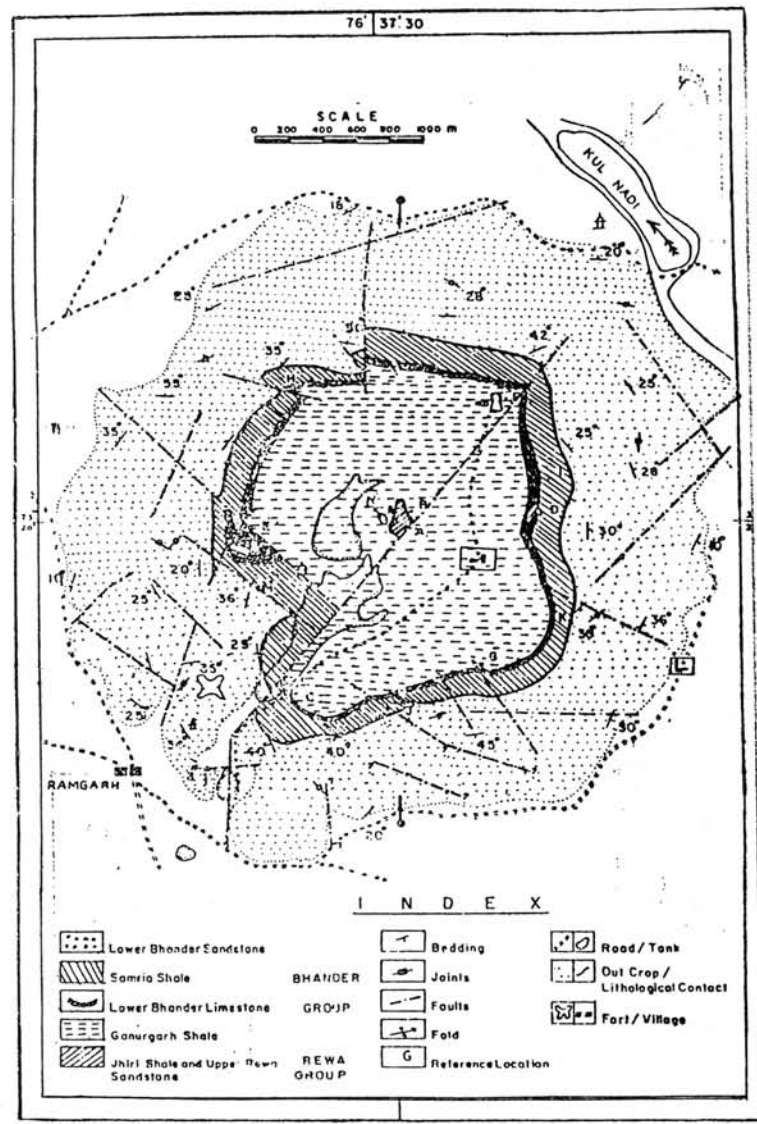


Fig. 4 - A geological map of the Ramgarh dome structure (After Ramasamy, 1988)

## EXPOSURE HISTORY OF SHERGOTTITE YAMATO 793605

K. Nishiizumi, Space Sciences Laboratory, University of California, Berkeley, CA 94720-7450,  
M. W. Caffee, Institute of Geophysics and Planetary Physics, Lawrence Livermore National  
Laboratory, Livermore, CA 94551

Cosmogenic nuclide studies of SNC meteorites have contributed significantly to our understanding of these objects. Based on cosmic-ray-produced nuclides, exposure histories, ejection conditions from the hypothesized Martian parent body, and genetic relationships between SNC meteorites are determined. In addition to those nuclides produced by galactic cosmic rays (GCR) are those produced by solar cosmic rays (SCR). Radionuclides produced by SCR reside in the uppermost few centimeters of material and their presence in meteorites indicates the degree to which a meteorite has ablated. Previous work has shown ablation to be less than 1 - 2 cm in at least three shergottites, ALH 77005, Shergotty, EETA79001, and possibly LEW 88516 [1, 2, 3]. This observation suggests that the atmospheric entry velocity and/or entry angle of these shergottites is much lower than the velocity and/or entry angle of ordinary chondrites.

We report here the results of cosmogenic radionuclide measurements in the Antarctic shergottite Yamato 793605 (Y-793605). This meteorite, the subject of a consortium investigation, has a recovered mass of 17 g. Based on the petrographical and mineralogical studies, Y-793605 is similar to and is thus associated with the lherzolitic shergottites, ALH 77005 and LEW 88516 [4]. Accordingly, the radionuclide results from Y-793605 and their interpretation will be compared with these shergottites.

By itself, the small recovered size implies a small preatmospheric size, which in turn suggests the presence of SCR effects. To investigate SCR effects in Y-793605 we measured radionuclides in both interior and exterior samples. The interior sample consisted of two small chips. Since the exact sample location of each chip was not documented we measured cosmogenic nuclides in the largest of the two (64.29 mg). The exterior chip (21.97 mg), denoted Y-793605,77 has a fusion crust on one side. The maximum thickness between the surface of fusion crust and interior is 2.5 mm. The exact distance between the exterior and interior chips is unknown but is less than 20 mm. We measured  $^{10}\text{Be}$  (half-life = 1.5 My),  $^{26}\text{Al}$  (0.705 My), and  $^{36}\text{Cl}$  (0.301 My) concentrations in both interior and exterior chips using accelerator mass spectrometry (AMS). The chemical composition of the major target elements was measured by atomic absorption spectroscopy in an aliquot solution. These results are shown in Table 1. Table 2 shows  $^{10}\text{Be}$ ,  $^{26}\text{Al}$ , and  $^{36}\text{Cl}$  results in two sub-samples of Y-793605 along with radionuclide measurements from other shergottites. The quoted errors represent a  $\pm 1\sigma$  uncertainty in the AMS measurement.

The  $^{10}\text{Be}$ ,  $^{26}\text{Al}$ , and  $^{36}\text{Cl}$  concentrations in the interior and exterior samples of Y-793605 are nearly identical, with the interior sample possessing a slightly higher concentration. There is clearly no evidence of increasing  $^{26}\text{Al}$  concentration from the interior toward the surface of the meteorite. ALH 77005 and Shergotty by contrast, had high  $^{26}\text{Al}$  activities in samples taken at the surface [1, 2], clearly indicative of SCR production of  $^{26}\text{Al}$ . In Y-793605 the somewhat higher concentration of cosmogenic nuclides in interior sample matches the pattern of GCR production. As the secondary particle flux increases with depth the radionuclide concentrations correspondingly increase. This pattern indicates that all cosmogenic nuclides in this particular sample were produced by GCRs. A reasonable interpretation is that there are no SCR effects at these sample

depths. This conclusion implies that at least 3 cm of material was ablated from the surface of this meteorite during its atmospheric entry. Therefore its preatmospheric radius was at least 4 cm. By way of comparison the ablation depth of ALH 77005 was less than 1 cm and its preatmospheric radius was 5-6 cm, based on both cosmic ray track densities and  $^{26}\text{Al}$  concentration [2].

The  $^3\text{He}$  and  $^{21}\text{Ne}$  exposure age of Y-793605 is reported to be  $5.4 \pm 0.3$  My [5]. A space exposure of this duration would result in saturated activities for both  $^{26}\text{Al}$  and  $^{36}\text{Cl}$  while  $^{10}\text{Be}$  should be near saturation.

Ca and Fe are the major target elements for production of  $^{36}\text{Cl}$ . The  $^{36}\text{Cl}$  concentrations were normalized to the measured concentrations of the relevant target elements and are shown in the last column of Table 2. For a  $4\pi$  bombardment in transit to Earth the  $^{36}\text{Cl}$  saturation activity is  $22 \pm 3$  dpm/kg (8Ca+Fe). The difference between the expected saturated  $^{36}\text{Cl}$  activity and the measured normalized  $^{36}\text{Cl}$  concentrations in Y-793605 require a terrestrial age of  $35 \pm 35$  ky (<70 ky). The terrestrial age of Y-793605 does not differ from that of LEW 88516, 21 ky [6], but is significantly shorter than that of ALH 77005,  $210 \pm 80$  ky [7, 8].

Al and Si are the major target elements for production of  $^{26}\text{Al}$ . By assuming the  $^{26}\text{Al}$  production rate from Al is 2.5 times higher than that from Si, the  $^{26}\text{Al}$  concentrations in Y-793605 can be normalized to the  $^{26}\text{Al}$  activity in L-chondrites (1.27 % Al and 18.7 % Si). This  $^{26}\text{Al}$  activity in Y-793605 (assuming 20 % Si) is 45 dpm/(kg L-chondrite) requires either exposure to GCR as an object having a small preatmospheric radius or that it was exposed to cosmic rays near the surface of larger meteoroid. The measured  $^{22}\text{Ne}/^{21}\text{Ne}$  ratio of 1.23 is also consistent with exposure under low shielding conditions [5].

The  $^{10}\text{Be}$  concentration in Y-793605 is similar to those of LEW 88516 and ALH 77005 (at the time of the fall, 19.5 dpm/kg). However, this  $^{10}\text{Be}$  concentration differs significantly from the  $^{10}\text{Be}$  concentration of other basaltic shergottites such as Shergotty, Zagami (unpublished results), and QUE 94201 (at the time of the fall). The  $^{10}\text{Be}$  production rate of Y-793605 is estimated to be 18 - 21 atom/min·kg based on the  $^{26}\text{Al}$  concentration [9]. Thus the  $^{10}\text{Be}$  exposure age of Y-793605 is 4.0 My or longer, an exposure age consistent with the noble gas exposure age of  $5.4 \pm 0.3$  My [5]. The exposure age of Y-793605 is longer than those of ALH 77005 (2.6-3.6 My) [7, 10] and LEW 88516 (3.0-4.1 My) [11, 12].

Taken together, the exposure ages of all the shergottites seemingly require at least four ejection events (0.6, 2.4, 3-4, and ~5.4 My) from their parent body. Three basaltic shergottites have exposure ages of 2.4-2.8 My. Even among those shergottites having similar cosmic ray exposure ages the different terrestrial ages indicate that each shergottite was ejected as an individual object from the parent body. In general, based on the  $^{10}\text{Be}$  concentrations, shergottites were ejected from more than a few meters depth within the parent body and therefore record no cosmic ray exposure in a  $2\pi$  geometry. However, for Y-793605 it is not possible to completely eliminate the possibility of a short pre-irradiation in the surface of the parent body. To resolve the particular conditions under which this exposure occurred  $^{53}\text{Mn}$  (half-life = 3.7 My) measurements are needed.

*Acknowledgments:* We wish to thank the NIPR for providing Y-793605. This work was supported by NASA grant NAGW-3514 and NSF grant OPP 9316272.

Table 1. Chemical composition of Yamato 793605

|             |          | Wt<br>mg | Mg<br>% | Al<br>% | K<br>ppm | Ca<br>% | Mn<br>ppm | Fe<br>% |
|-------------|----------|----------|---------|---------|----------|---------|-----------|---------|
| Y-793605    | interior | 64.3     | 15.1    | 1.92    | 340      | 2.49    | 3750      | 15.5    |
| Y-793605,77 | exterior | 22.0     | 13.7    | 1.87    | 1030     | 2.50    | 3570      | 13.9    |

Table 2. Cosmogenic radionuclide concentration in shergottites

| Sample                    | Depth from<br>surface<br>(mm) | <sup>10</sup> Be<br>(dpm/kg<br>meteorite)          | <sup>26</sup> Al<br>(dpm/kg<br>meteorite) | <sup>36</sup> Cl<br>(dpm/kg<br>meteorite) | <sup>36</sup> Cl<br>(dpm/kg<br>8Ca+Fe) |
|---------------------------|-------------------------------|--|---|---|--|
| Y-793605                  | interior                      | 17.78 ± 0.47                                       | 51.5 ± 2.0                                | 7.90 ± 0.20                               | 21.6 ± 0.6                             |
| Y-793605,77               | exterior                      | 17.09 ± 0.28                                       | 50.3 ± 1.6                                | 7.70 ± 0.12                               | 20.7 ± 0.3                             |
| ALH 77005 <sup>a</sup>    | ~ 25                          | 16.07 ± 0.58                                       | 47.9 ± 2.4                                | 4.82 ± 0.19                               | 13.3 ± 0.5                             |
| ALH 77005 <sup>a</sup>    | 1 - 10                        | 14.02 ± 0.15                                       | 73.0 ± 5.8                                | 6.07 ± 0.65                               | 18.0 ± 2.0                             |
| LEW 88516,13 <sup>b</sup> |                               | 16.70 ± 0.27                                       | 68.5 ± 1.7                                | 8.35 ± 0.12                               | 21.4 ± 0.3                             |
| QUE 94201,27 <sup>c</sup> | 0 - 5                         | 11.83 ± 0.11                                       | 58.8 ± 2.1                                | 8.23 ± 0.19                               | 11.1 ± 0.2                             |
| QUE 94201,13 <sup>c</sup> | 4 - 8                         | 12.10 ± 0.22                                       | 55.7 ± 1.7                                | 9.14 ± 0.18                               | 11.9 ± 0.2                             |
| Shergotty,2 <sup>d</sup>  |                               | 13.39 ± 0.54                                       | 100.7 ± 10.1                              | 14.6 ± 0.9                                | 21.9 ± 1.4                             |
| Shergotty,26 <sup>d</sup> | 2 - 6                         | 13.56 ± 0.54                                       | 87.7 ± 8.8                                | 13.2 ± 0.8                                | 19.5 ± 1.2                             |
| Zagami                    |                               | 19.1 ± 2.0 <sup>e</sup><br>14.6 ± 0.2 <sup>f</sup> | -   | -   | -                                      |
| EETA79001,95 <sup>d</sup> | 26 - 31                       | 4.73 ± 0.19  | 29.7 ± 3.0                                | 8.1 ± 0.6                                 | 20.7 ± 1.5 <sup>g</sup>                |

a.[2, 8] and unpublished results; b.[13]; and unpublished result; c.[14]; d.[1]; e.[15]; f.unpublished result; g.corrected with 0.6 My exposure age.

## References:

- [1] Nishiizumi K. *et al.* (1986) *Geochim. Cosmochim. Acta* 50, 1017-1021.  
[2] Nishiizumi K. *et al.* (1986) *Meteoritics* 21, 472-473.  
[3] Garrison D.H. *et al.* (1995) *Meteoritics* 30, 738-747.  
[4] Mikouchi T. and Miyamoto M. (1996) *Symposium on Antarctic Meteorite XXI*, 104-106.  
[5] Nagao K. *et al.* (1997) *Proc. NIPR Symp. Antarct. Meteorites* submitted.  
[6] Jull A.J.T. *et al.* (1994) *Lunar Planet. Sci. XXV*, 647-648.  
[7] Schultz L. and Freundel M. (1984) *Meteoritics* 19, 310.  
[8] Nishiizumi K. *et al.* (1994) *Meteoritics* 29, 511.  
[9] Michel R. *et al.* (1995) *Planet. Space Sci.* 43, 557-572.  
[10] Bogard D.D. *et al.* (1984) *Geochim. Cosmochim. Acta* 48, 1723-1139.  
[11] Bogard D.D. and Garrison D.H. (1993) *Lunar Planet. Sci. XXIV*, 139-140.  
[12] Eugster O. *et al.* (1996) *Lunar Planet. Sci. XXVII*, 345-346.  
[13] Nishiizumi K. *et al.* (1992) *Meteoritics* 27, 270.  
[14] Nishiizumi K. and Caffee M.W. (1996) *Lunar Planet. Sci. XXVII*, 961-962.  
[15] Pal D.K. *et al.* (1986) *Geochim. Cosmochim. Acta* 50, 2405-2409.

## **Estimation of three dimensional internal structure of some barred olivine chondrules in Allende (CV3) chondrite**

Takaaki Noguchi and Hirokazu Honjyo

Department of Materials and Biological Sciences, Ibaraki University,

Bunkyo 2-1-1, Mito 310, Japan

**Introduction** Petrologic studies of chondrules have been based on thin sections, in other words, two dimensional information. However, three dimensional internal structure of chondrules, spatial distribution and three dimensional compositional zoning patterns of minerals in chondrules will give a new constraint on the formation conditions of chondrules. It is known that chondrules in CV3 chondrites were reacted with surrounding nebular gas during chondrule forming event(s) (e. g. Ikeda and Kimura, 1995). Therefore, the authors used chondrules from Allende CV3 chondrite in order to investigate spatial distribution of secondary minerals in chondrules as well as that mentioned above.

**Experimental method** Chondrules were separated from chips of Allende by crushing lightly on an agate mill and by the freeze-thaw method. Because one of the purposes of this study is to investigate three dimensional internal structure of barred olivine (BO) chondrules, 4 BO chondrules were selected. Other chondrules selected are a porphyritic olivine chondrule, a porphyritic olivine pyroxene chondrule, and an olivine-, spinel-, plagioclase-bearing chondrule. These chondrules were set in molds with a flat bottom for TEM samples, and then embedded in epoxy resin. After removing solidified epoxy rods including chondrules from the molds, the ends of the solidified epoxy rods opposite to where chondrules exist were cut by a low-speed diamond saw to make flat planes parallel to the surfaces where chondrules are embedded. The samples were then fixed on slide glasses. The surfaces of the samples were ground and polished in a constant manner. After polishing, the thickness of the samples (and slide glasses) were measured five times by a micrometer. Parallelism of each cross section was fairly good, because variation of thickness of the sample was 2-4  $\mu\text{m}$ . The average spacing of each cross section was  $46 \mu\text{m} \pm 11 (1\sigma)$ . Backscattered electron images (BEIs) were taken by SEM for each cross section. The BEI photomicrographs were scanned by a flat bed scanner and processed by Adobe Photoshop™ 3.0 and NIH image 1.59 and 1.61 on Macintosh PowerMac 9500, in order to get sequential and projection stacks. In this paper, we will deal with only BO chondrules.

**Result** Sequential stacks of BO chondrules reveal that parallel planner olivine crystals (their cross section are regarded as “bars” of olivine) had nucleated from a few areas on olivine “shells” (Fig. 1). It can be seen in Fig. 1 that two groups of planner olivine crystals stopped crystallizing where two groups met. Mesostasis of the BO chondrule is altered to secondary minerals such as ferroan olivine, nepheline, and sometimes sodalite. Mesostasis indicated by arrows in this figure has quite a different texture from the other “normal” altered mesostasis. Chemical composition of these mesostases were measured by an electron microprobe. The relation between  $\text{Na}_2\text{O}$  and  $\text{K}_2\text{O}$  wt % in the unique and normal altered mesostases shows that

some analyses of the unique altered mesostasis are plotted among normal altered mesostasis and phlogopite in CAIs and chondrules (Hashimoto and Grossman, 1987; Kimura and Ikeda, 1996). This diagram suggests that the unique altered mesostasis contains a small amount of phlogopite. "Phlogopite"-bearing altered mesostasis occurs very locally within the BO chondrule. The area of the unusual altered mesostasis in contact with the surface of the chondrule is very small. Where the "phlogopite"-bearing mesostasis exists, it is more porous than the surrounding normal altered mesostasis. Effect of direction of cutting on textural variation of single BO chondrule was investigated by using projection stacks of NIH image. Figure 2 shows an example of textural variation when a BO chondrule is cut in different planes. This figure indicates that cross sections of a BO chondrule always contain olivine "bars" except for the case when the chondrule is cut parallel to the surfaces of planar olivine crystals in it.

**Discussion** (1) *Effect of cutting on texture of BOs.* As can be inferred from Fig. 2, it is natural that almost always BO chondrules display olivine "bars" on their cross sections, because the possibility of cutting a BO chondrule parallel to the surfaces of platy olivine crystals is very low. Figure 3 shows a BEI photomicrograph of a chondrule in Saratov L4 chondrite. Olivine crystals indicated by arrows extinct at the same time like olivine in BO chondrules. The morphology of olivine crystals in this figure is similar to that of Fig. 2b. The chondrule in Fig. 3 may be the rare case shown in Fig. 2b. (2) *"Phlogopite"-bearing altered mesostasis.* As noted above, the ratio of the surface area in contact with outside of the BO and the volume of the "phlogopite"-bearing altered mesostasis is very low. The very low ratio suggests that phlogopite was formed by a nebular gas - solid (chondrule) reaction. If the reaction had occurred in the meteorite parent body, it would have been very difficult to explain very localized occurrence and very low surface area/volume ratio of the mesostasis. However, it is not clear why phlogopite was formed in the area shown in Fig. 1. It may be a key to solve the problem that where phlogopite exists, it is more porous than the surrounding altered mesostasis. Tsuchiyama et al. (1997) and Kondo et al. (1997) reported holes in a porphyritic chondrule from Allende. These holes are probably connected to the surface of the chondrule due to thin cracks. If the phlogopite-bearing area in Fig. 1 was a hole before phlogopite was formed, it is thought that the surface of the hole directly came into contact with nebular gas. Phlogopite-bearing altered mesostasis was perhaps formed by the reaction with the nebular gas and the surface of the hole (normally altered mesostasis).

**Acknowledgment** The authors thank K. Amano for premission in using a Macintosh PowerMac 9500 and a high-resolution flat bed scanner.

**References** Hashimoto, A. and Grossman, L. (1987) *Geochim. Cosmochim. Acta*, 51, 1685-1704. Ikeda, Y. and Kimura, M. (1995) *Proc. NIPR Symp. on Antarct. Meteorites*, 8, 97-122. Kimura, M. and Ikeda, Y. (1996) *Papers presented to the 21st NIPR Symp. Antarct. Meteorites*, 68-39. Kondo, M., Tsuchiyama, A., Hirai, H., and Koishikawa, A. (1997) *Abstracts of 1997 Japan Earth and Planetary Science Joint Meeting*, 594 (in Japanese). Tsuchiyama, A., Kondo, M., Hirai, H., and Koishikawa, A. (1997) *Papers presented to the 28th LPSC. CD-ROM*.

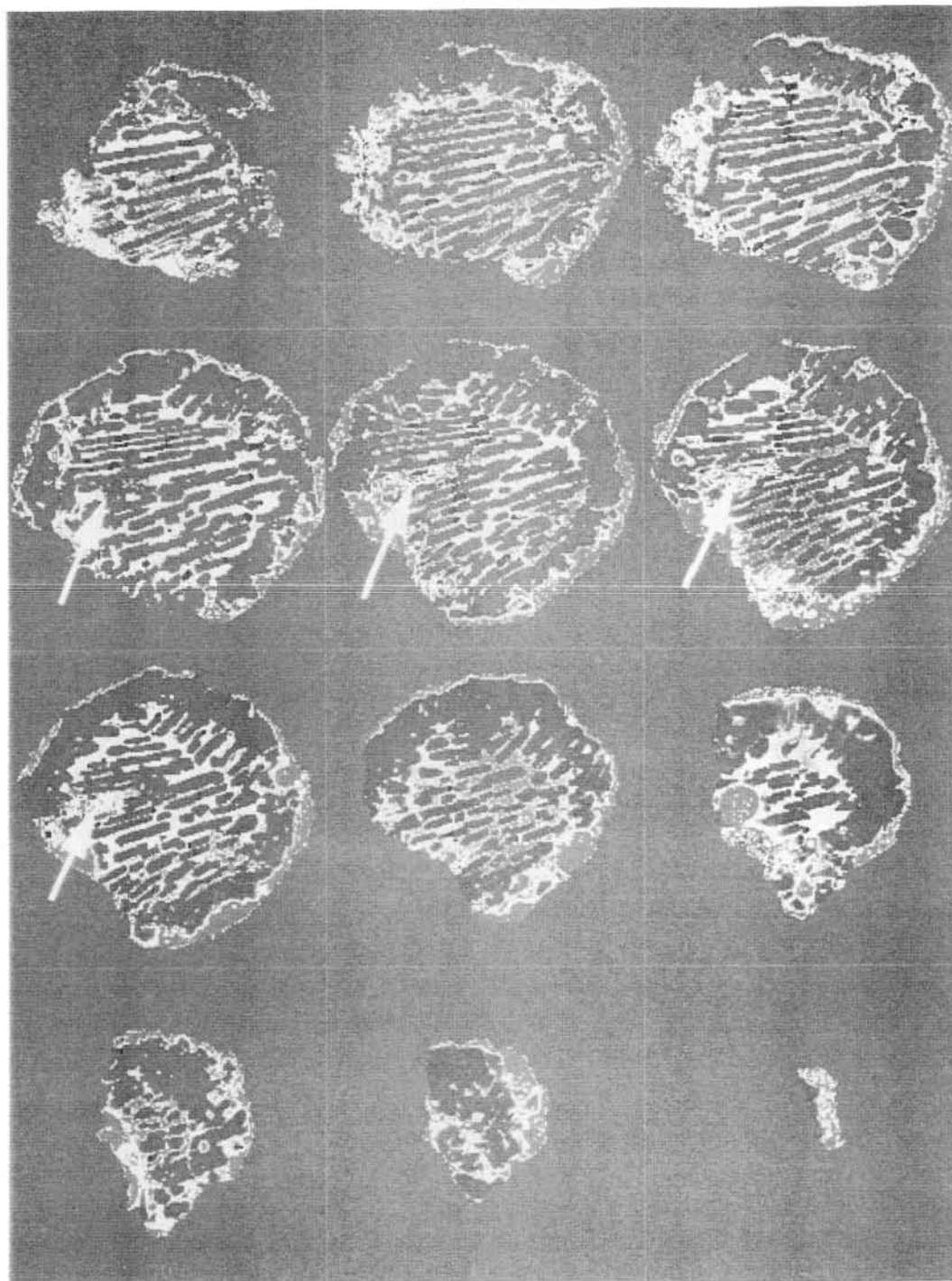


Figure 1 A sequential stack of a BO chondrule. "Phlogopite"-bearing altered mesostasis is indicated by arrows. Olivine grains occur as gray "bars" and shells. Maximum length of this chondrule is about 0.8 mm.

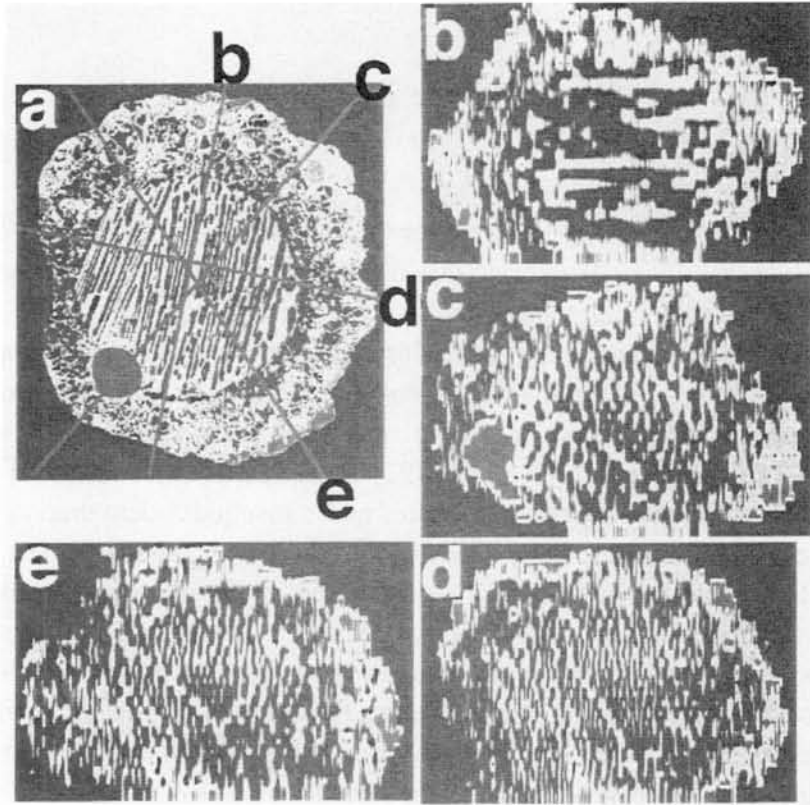


Figure 2 A projection stack of a BO chondrule. Effects of direction of cutting on the texture of single BO is displayed. Olivine grains occur as gray “bars” and shells. Maximum length of this chondrule is about 1.7 mm.

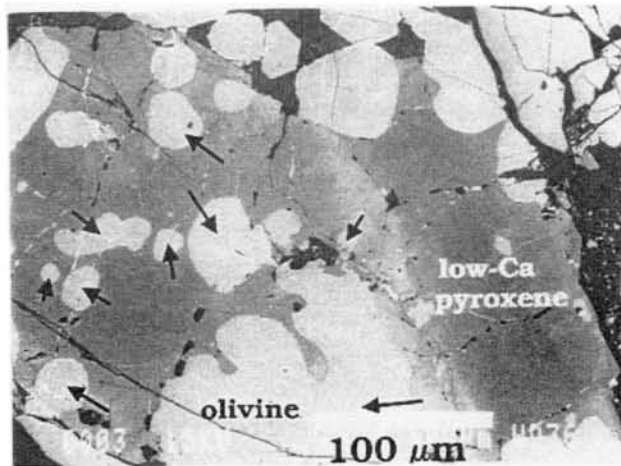


Figure 3 BEI photomicrograph of a chondrule in Saratov L4 chondrite. Olivine grains indicated by arrows extinct at the same time under an optical microscope.

## Matrix and some clasts in Vigarano (CV3) chondrite

Takaaki Noguchi

Department of Materials and Biological Sciences, Ibaraki University,

Bunkyo 2-1-1, Mito 310, Japan

**Introduction** There is growing evidence for the aqueous alteration of CV3 chondrites (e. g. Tomeoka and Buseck, 1990). However, ubiquitous evidence for the aqueous alteration has been restricted to the case of the “oxidized” sub-group of McSween (1977). Recently, an unusual dark inclusion in Vigarano which belongs to the “reduced” sub-group of McSween (1977) was investigated by Kojima and Tomeoka (1996). They suggested that the inclusion had been formed by the aqueous alteration and the subsequent dehydration by thermal metamorphism. Tanimura and Tomeoka (1997) investigated mesostases of chondrules in Vigarano and suggested that aqueous alteration and subsequent dehydration processes had occurred on the meteorite parent body. However, Kimura and Ikeda (1996) suggested that phlogopite in chondrules in Vigarano had been formed in the later stage of the reaction with nebular gas. As shown above, it is not clear whether phyllosilicates in Vigarano chondrules are the products of aqueous alteration on the parent body. And it is also not clear whether the dehydration process is a ubiquitous process during the evolution of the meteorite parent body. During a detailed SEM observation, the author found distinct evidence for aqueous alteration predating the final agglomeration of Vigarano meteorite.

**Petrography and chemical compositions** Matrix of the Vigarano meteorite contains two types of clasts which probably contain phyllosilicates. One is characterized by abundant magnetite. As shown in Fig. 1a, they occur as irregular- to subrounded-shaped clasts. Their size ranges less than 20  $\mu\text{m}$  across to about 500  $\mu\text{m}$  across. The boundaries of the clasts of this type and the host matrix are sharp in most cases (e. g. Fig. 1a). They are usually darker than the host matrix in backscattered electron images (BEIs). Grain sizes of constituent minerals of the matrix of the clasts are finer than those of the host matrix. Most of magnetite occurs as aggregates of fine-grained (less than 2-3  $\mu\text{m}$  across) crystals. In some clasts of this type, aggregates of framboidal magnetite were found (Fig. 1b). The other type of clasts are characterized by laths of magnetite. The clasts of this type are rarer than the former type. Figure 1c shows a clast of this type. The boundaries between the clasts and the host matrix are sharp as shown in Fig. 1c. The dimensions of magnetite laths are 30-50  $\mu\text{m}$  in width and 200-400  $\mu\text{m}$  in length (Fig. 1d). Thin troilite rims (less than 5  $\mu\text{m}$  thick) are often found on magnetite. Framboidal aggregates of fine-grained magnetite are rarely observed in the clasts. The clasts are also darker than the host matrix in BEIs. Grain sizes of matrix minerals of the clasts are also finer than those of the host matrix.

Chemical compositions of the host matrix, clast A (the clast shown in Figs. 1a and 1b), and clast B (the clast shown in Figs. 1c and 1d) were analyzed by electron microprobe (Fig. 2). Matrix, clast A, and clast B occupy different areas in Figs. 2a and 2b although there are overlaps among the plotted areas. These diagrams suggest that the host matrix is composed mainly of ferroan olivine and Ca-rich pyroxene, and that the matrix of clast A is

composed mainly of ferroan olivine and serpentine (or olivine and minor saponite), and that the matrix of clast B is composed mainly of saponite and minor olivine (or saponite and serpentine). Average total wt % and standard deviations of the host matrix, the matrix of clast A, and that of clast B are  $94.3 \pm 5.2$ ,  $88.8 \pm 6.4$ , and  $79.8 \pm 6.0$ , respectively. Figure 2c displays the relation between  $\text{Na}_2\text{O}$  and  $\text{K}_2\text{O}$  concentrations in the host matrix, the matrix of clast A, and that of clast B. There is a positive correlation between  $\text{Na}_2\text{O}$  and  $\text{K}_2\text{O}$  wt % of the matrices of clasts A and B. Analyses of the host matrix scatter in the diagram. However, some are plotted among the matrices of clasts A and B.

**Discussion** As noted above, phyllosilicates were rarely found in the matrix (Graham and Lee, 1992) and chondrules (Kimura and Ikeda, 1996; Tanimura and Tomeoka, 1997), and it is not clear that these phyllosilicates were formed on the meteorite parent body. Fine-grained magnetite bearing clasts in this study often include framboidal aggregates of magnetite. Framboidal magnetite has been found from CI chondrites (e. g. Kerridge et al., 1979), matrix of CM chondrites (Heyman et al., 1985), and dark inclusions in CR chondrites (e. g. Weisberg et al., 1993). Because it is regarded that these magnetite framboids were formed by aqueous alteration on meteorite parent bodies, these clasts were also probably formed by aqueous alteration on the meteorite parent body. Coarse magnetite laths observed in magnetite lath bearing clasts have not been reported yet from any types of carbonaceous chondrites. In Fig. 1c and 1d, some magnetite laths seem to have nucleated on the kamacite spherules on the surface of a chondrule and to have grown in the matrix of clast A. If the magnetite laths had been formed before accretion of the constituents of the clast, the observed texture would not have been preserved during accretion. Therefore, these magnetite laths were probably formed after accretion and during aqueous alteration on the meteorite parent body. In an unusual dark inclusion in Vigarano, there is no hydrated mineral (Kojima and Tomeoka, 1996). As opposed to the case of the dark inclusion, average total wt % of microprobe analyses of the host matrix, the matrix of clast A, and that of clast B suggest that fine-grained magnetite bearing clasts and magnetite lath bearing clasts contain phyllosilicates, and that the latter clasts contain more phyllosilicates than the former. These clasts may be one of the precursor materials of the dehydrated dark inclusions in Vigarano. If true, dehydration subsequent to aqueous alteration may not be an inevitable process in the evolution of the meteorite parent body. As noted above, there is no unique estimation of constituent minerals of the matrices of these two types of clasts. Graham and Lee (1992) found during TEM observation that there were rare saponite grains (about 5 nm across). But they found no direct evidence for the formation of saponite by "in-situ" alteration of matrix olivine. Main phyllosilicates in these clasts may be saponite, if these rare saponite grains in the host matrix were derived from the fine-grained fragments of these clasts.

**References** Graham, A. L. and Lee, M. (1992) Proc. 23rd LPSC, 435. Kerridge, J. F., MacKay, A. L., and Boynton, W. V. (1979) Science, 205, 395-397. Kojima, T. and Tomeoka, K. (1996) Papers presented to the 21st Symp. on Antarct. meteorites. 74-75. McSween, H. Y. (1977) Geochim. Cosmochim. Acta, 41, 1777-1790. Tanimura, I. and Tomeoka, K. (1997) Abstracts of 1997 Japan Earth and Planetary Science Joint Meeting, 572 (in Japanese). Tomeoka, K. and Buseck, P. R. (1990) Geochim. Cosmochim. Acta, 54, 1745-1754. Weisberg, M. K., Prinz, M., Clayton, R. N., Mayeda, T. K. (1993) Geochim.

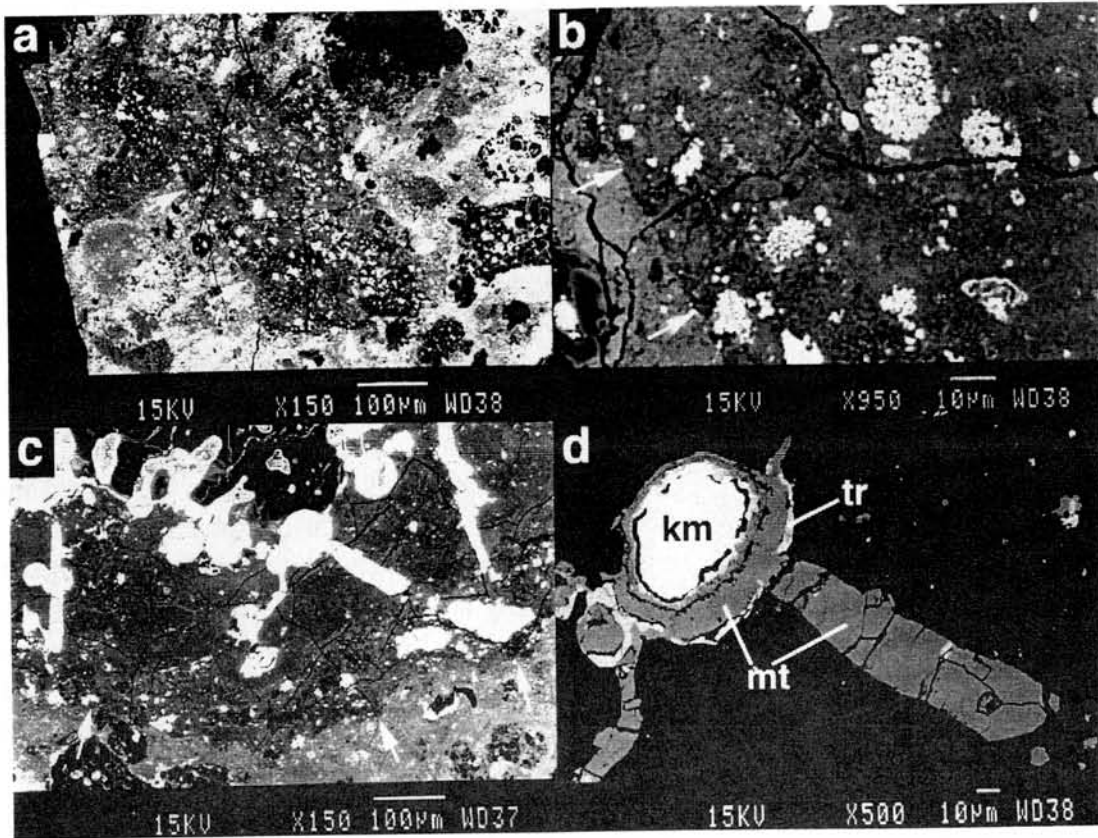
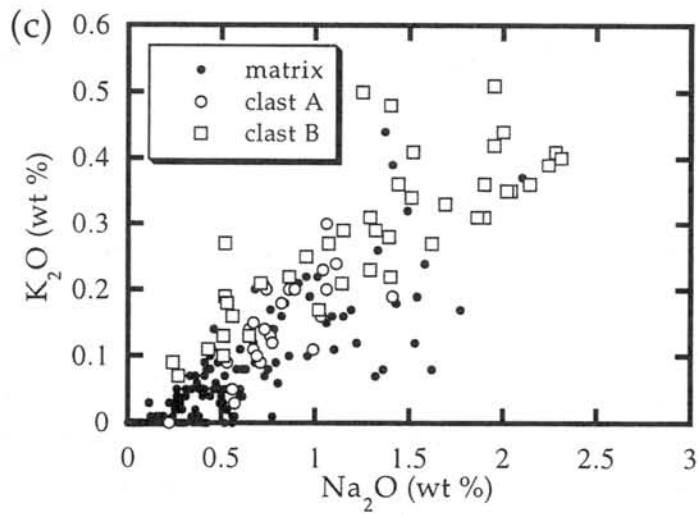
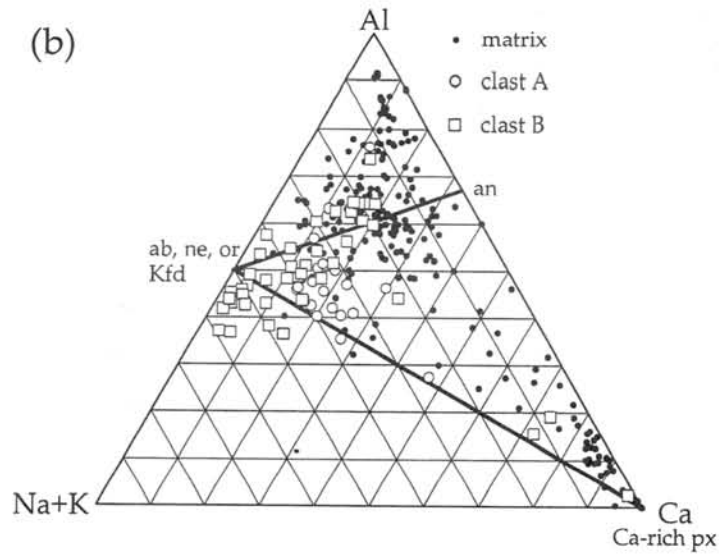
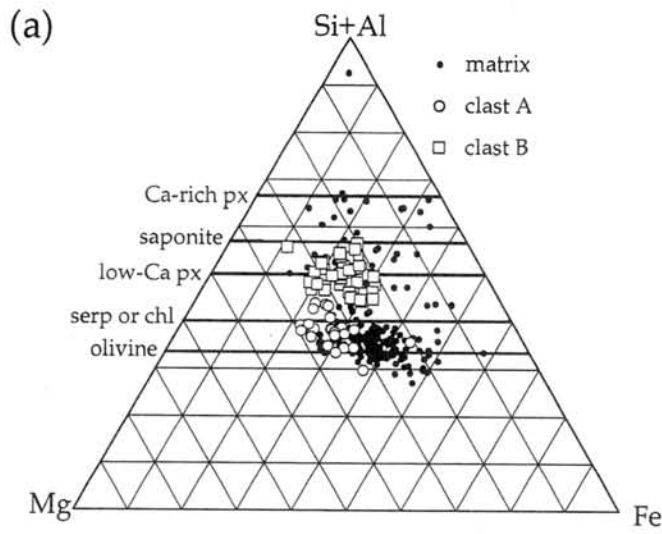


Figure 1 BEI photomicrographs of typical occurrences of clasts which probably contain phyllosilicates. a: A clast which contains abundant fine-grained magnetite. b: An enlarged image of the clast shown in 1a. Some framboidal aggregates of magnetite can be observed. The clast in Figs. 1a and 1b is called "clast A" in the text. c: A clast which contains magnetite laths. d: An enlarged image of magnetite lath in the clast shown in 1c. The clast in Figs. 1c and 1d is called "clast B" in the text. The boundaries between the host matrix and the clasts are indicated by white arrows. Abbreviations. km: kamacite; mt: magnetite; tr: troilite.

Figure 2 (opposite page) a: A ternary plot of the atomic ratios among Si+Al, Mg, and Fe of the host matrix, the matrix of clast A (shown in Figs. 1a and 1b), and that of clast B (shown in Figs. 1c and 1d). b: A ternary plot of the atomic ratios among Al, Na+K, and Ca of the host matrix, the matrix of clast A, and that of clast B. c: Na<sub>2</sub>O vs K<sub>2</sub>O concentrations among the host matrix, the matrix of clast A, and that of clast B. Abbreviations. serp: serpentine; chl: chlorite; low-Ca px: low-Ca pyroxene; Ca-rich px: Ca-rich pyroxene; ab: albite; ne: nepheline; Kfd: potassium feldspar; an: anorthite.



# Noble gases in E-chondrites

R. Okazaki, N. Takaoka, T. Nakamura, Dept. Earth & Planet. Sci., Kyushu Univ.,  
Fukuoka 812-81, and K. Nagao, Inst. Study Earth's Interior, Okayama Univ.,  
Misasa, Tottori, 682-01

**Introduction** Enstatite chondrites are enigmatic in several respects. While it is well known that host phases of trapped noble gases are carbonaceous materials for both ordinary and carbonaceous chondrites [e.g., Lewis et al., 1975; Wieler et al., 1991], those for E-chondrites are not known yet, although enstatite crystal is a possible candidate [Crabb and Anders, 1982]. Two types of trapped gases in E-chondrites have been reported: the usual planetary component and a less fractionated, sub-solar component [Crabb and Anders, 1982]. Concentrations of trapped gases decrease with increasing petrologic type of chondrites except for E-chondrites [Marti, 1967; Zähringer, 1966]. These noble gas signatures as well as highly reduced states of E-chondrites reflect conditions of the formation and evolution of their parent bodies [e.g., Keil, 1989].

Recently, Takaoka et al. (1996) have reported that great amounts of trapped gases are released by crushing Happy Canyon (EL6/7). And they suggested micro-bubbles in enstatite crystals for possible sites trapping noble gases. However, Happy Canyon has suffered impact melting. Since there are no data of crushing experiments for E-chondrites that have not suffered impact melting, it is highly important to know whether they contain micro-bubbles or not. In the present report, we analyze E-chondrites of various petrologic types including type-7 impact-melted for noble gases released by stepwise heating. This provides a reconnaissance for the next step of experiments.

**Samples and experimental methods** Measured samples are three E6-chondrites (Y-86004, Y-82189, Y-793225), E3H  $\alpha$  (Y-74370) [Zhang and Sears, 1996], E4 (Y-8414) and one EL7 (Iafegh-009) [Otto, 1992; MacCoy et al., 1995]. Approximately 50 mg was chipped from each bulk chondrite and was heated stepwise at 600, 800, 1000, 1200, 1400, 1600 and 1800°C for 15 minutes. Released gases were measured with a modified VG5400 mass spectrometers of Okayama University [Miura et al., 1993].

**Results and discussion** No primordial trapped He and Ne were detected. Radiogenic  $^4\text{He}$  and cosmogenic He and Ne are dominant, whereas Ar, Kr and Xe are mixtures of trapped, radiogenic and cosmogenic gases. We address here mainly on cosmogenic and trapped gases, and therefore cosmic-ray exposure ages as well as isotopic ratios of trapped Xe and elemental

ratios of trapped gases.

(A)Cosmogenic gases and cosmic-ray exposure ages

Isotopic ratios of cosmogenic Ne are normal except for Y-793225 and -82189. For these two stones, the  $^{21}\text{Ne}/^{22}\text{Ne}$  ratios is as low as  $\sim 0.7$ . The  $^{21}\text{Ne}/^{22}\text{Ne}$  ratio clusters round 0.7 for all temperature fractions of Y-82189, while it moves from 0.7 for low-temperature fractions of Y-793225 to 0.86 for high-temperature fractions (Fig. 1). The  $^{21}\text{Ne}/^{22}\text{Ne}$  ratio in a Na-rich phase such as plagioclase is 0.7 [Smith and Huneke, 1975; Wacker and Marti, 1983]. Probably the Y-82189 sample was extremely enriched in plagioclase. Preferential releases of cosmogenic Ne at low temperatures are compatible with this idea.

Table 1 shows the cosmic-ray exposure ages of E-chondrites measured in this work. The production rates were calculated as EH-chondrites, except for Ilafegh-009 EL7, with the production rate equations of Eugster (1988).

(B) Isotopic and elemental components of heavy noble gases

Ilafegh-009 (EL7) and Y-793225 (E6) have low ratio of  $^{134}\text{Xe}/^{132}\text{Xe}$  and  $^{136}\text{Xe}/^{132}\text{Xe}$  close to the solar Xe. Ilafegh-009 at 1000, 1200 and 1400°C fractions have approximately solar Xe ratios, and move to the air Xe ratio along with the heating temperatures (Fig. 2a). Although Y-793225 also have low Xe ratios,  $^{136}\text{Xe}/^{132}\text{Xe}$  are slightly higher than ILAFEGH-009 at all temperatures, and rarely correlated with the heating temperatures (Fig. 2b). The other samples have rather high ratios which are close to the air Xe ( $^{136}\text{Xe}/^{132}\text{Xe}=0.32\sim 0.33$ ).

Fig. 3 shows elemental ratios for heavy trapped gases released from Ilafegh-009 and Y-793225, respectively. Ilafegh-009 has the low elemental ratios ( $^{36}\text{Ar}/^{132}\text{Xe}=48.7$ ,  $^{84}\text{Kr}/^{132}\text{Xe}=0.57$  at 1200°C) relative to the average ratios ( $^{36}\text{Ar}/^{132}\text{Xe}=111.6$ ,  $^{84}\text{Kr}/^{132}\text{Xe}=1.56$ ) through all temperatures (Fig. 3a), and they are correlated with the low  $^{136}\text{Xe}/^{132}\text{Xe}$  ratios. While Y-793225 has the high ratios which are up to the planetary range (Fig. 3b) and no correlation with the  $^{136}\text{Xe}/^{132}\text{Xe}$  ratios. According to Takaoka (1994), the formation of micro-bubble should cause the fractionation of elemental and isotopic noble gas components. For this reason, there is some possibility of the presence of micro-bubbles in Ilafegh-009.

**References** Crabb J. and Anders E. (1982) *Geochim. Cosmochim. Acta*, 40. Eugster O. (1988) *Geochim. Cosmochim. Acta* 52, 1649-1662. Keil K. (1989) *Meteoritics*, 24, 195-208. Lewis R. S. (1975) *Geochim. Cosmochim. Acta* 39, 417-432. MacCoy T. J. (1995) *Geochim. Cosmochim. Acta* 59, 161-175. Marti K. (1967) *Earth Planet. Sci. Lett.*, 2, 193-196. Miura Y., Nagao K. and Fujinami T. (1993) *Geochim. Cosmochim. Acta.*, 57, 1857-1866. Otto J. (1992) *Chem. Erde* 52, 33-40. Smith S. P. and Huneke J. C. (1975) *Earth Planet. Sci. Lett.*, 27, 191-199. Takaoka N.

(1994) Noble Gas Geochemistry and Cosmochemistry, ed. by J. Matsuda, pp.23 -29. Takaoka N., Nakamura T. and Nagao K. (1996) *27th Lunar Planet. Sci. Conf.* Wacker J. F. and Murti K. (1983) *Earth Planet. Sci. Lett.*, 62 Zahng Y. and Sears D. W. G. (1996) *Meteoritics & Planet. Sci.*, 31, 647-655. Zähringer J. (1966) *Meteoritika* 27, 25-40.

Table 1: Concentrations of cosmogenic isotopes and cosmic-ray exposure ages.  $P_n$  and  $T_n$  mean production rates and exposure ages of cosmogenic nuclides  ${}^nM$ , respectively.

| Sample Name | $[{}^3\text{He}]_c$<br>( $\times 10^{-8}$ cc STP/g) | $[{}^{21}\text{Ar}]_c$ | $[{}^{38}\text{Ar}]_c$ | $({}^{21}\text{Ne}/{}^{22}\text{Ne})_c$ | $P_3$ | $P_{21}$ | $P_{38}$ | Exposure Ages (Ma)                  |       |          |
|-------------|---|------------------------|------------------------|---|-------|----------|----------|-------------------------------------|-------|----------|
|             |   |                        |                        |   |       |          |          | ( $\times 10^{-8}$ cc STP/g per Ma) | $T_3$ | $T_{21}$ |
| Y-8414      | 4.21  | 0.76                   | 0.05                   | 0.882                                   | 1.55  | 0.234    | 0.0447   | 2.71                                | 3.26  | 1.09     |
| Ilafegh     | 1.19  | 0.67                   | 0.04                   | 0.897                                   | 1.61  | 0.312    | 0.0418   | 0.74                                | 2.16  | 1.02     |
| Y-74370     | 0.40  | 0.08                   | 0.01                   | 0.832                                   | 1.53  | 0.183    | 0.0400   | 0.26                                | 0.41  | 0.24     |
| Y-86004     | 0.75  | 0.23                   | 0.03                   | 0.908                                   | 1.57  | 0.270    | 0.0469   | 0.48                                | 0.85  | 0.70     |
| *Y-82189    | 0.12  | 0.07                   | 0.01                   |   |       | 0.150    |          |                                     | 0.49  |          |
| Y-793225    | 10.41   | 1.51                   | 0.21                   | 0.928                                   | 1.58  | 0.303    | 0.0486   | 6.59                                | 4.98  | 4.31     |

\* The production rate of Y-82189 is calculated with assumption that the main target of  ${}^{21}\text{Ne}$  is Na in plagioclase and the production rate of  ${}^{21}\text{Ne}$  from Na is 0.25 times relative to that from Mg.

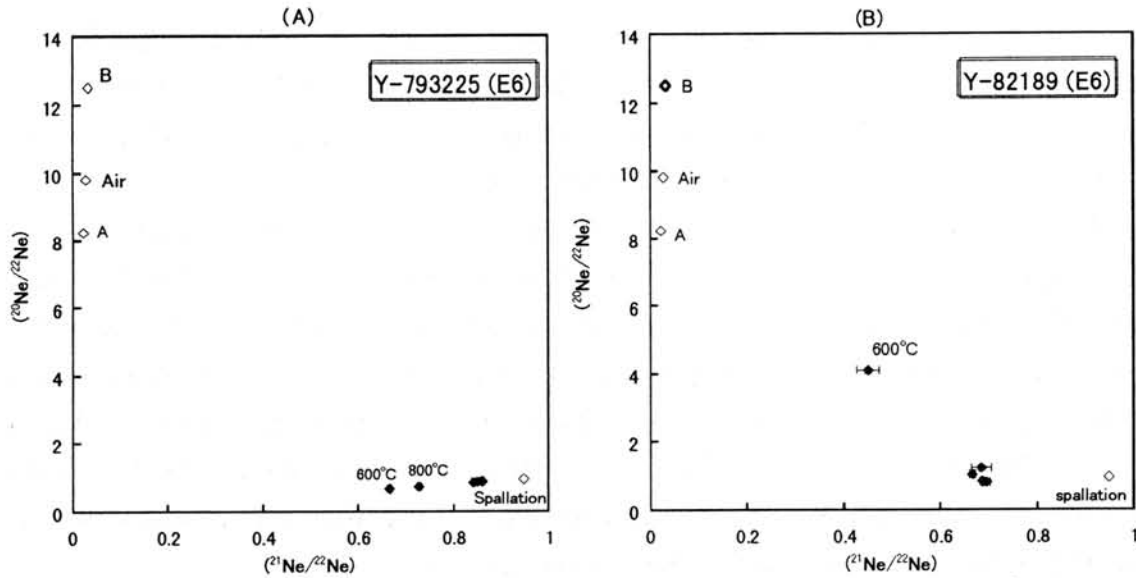


Fig. 1: Neon isotopic compositions of Y-793225 and -82189. The  ${}^{21}\text{Ne}/{}^{22}\text{Ne}$  ratios ( $\sim 0.7$ ) of two meteorites are declined by enhancement of  ${}^{22}\text{Ne}$  in the sodium-rich phases.

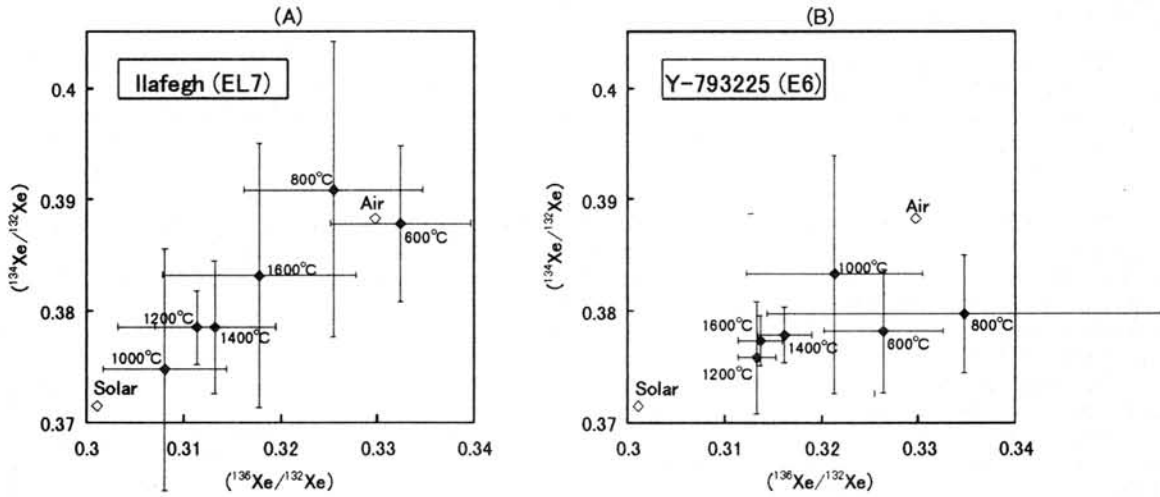


Fig. 2: Heavy Xenon isotopes of Ilafegh-009 and Y-793225. The  $^{136}\text{Xe}/^{132}\text{Xe}$  ratios of Ilafegh has wide range from the solar to the air compositions, while those of Y-793225 are somewhat confined.

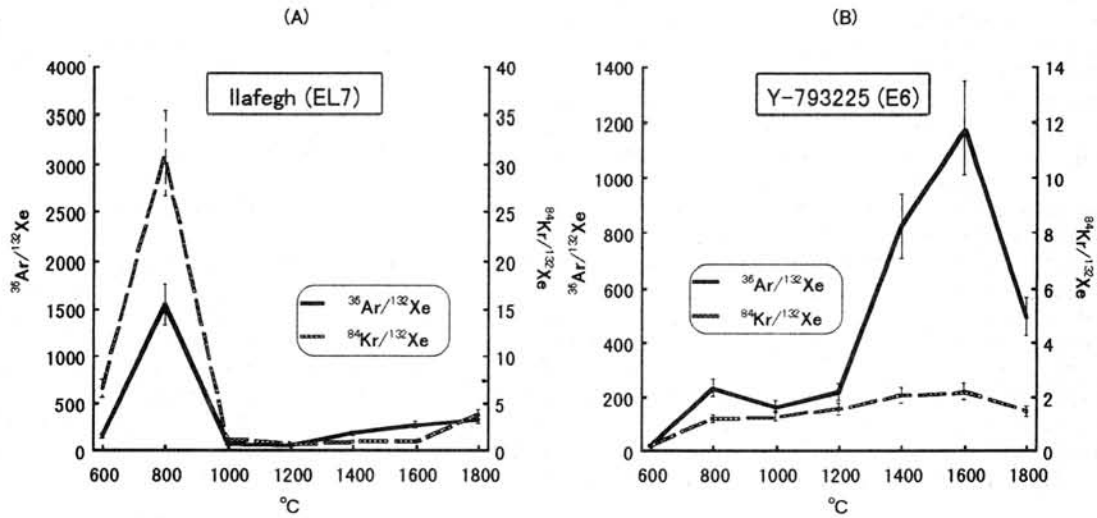


Fig. 3: Elemental ratios of heavy trapped gases released from Ilafegh-009 and Y-793225. The both meteorites has low elemental ratios relative to each average ratio, respectively. The low elemental ratios of Ilafegh are correlated with the low  $^{136}\text{Xe}/^{132}\text{Xe}$  ratios, while Y-793225 has rare such correlation.

**KINETICALLY CONTROLLED STABILITY OF SILICATE MELT AT LOW PRESSURES : (2) TRANSIENT STATE.** Kazuhito Ozawa and Hiroko Nagahara: Geol. Inst., Univ. Tokyo, Hongo, Tokyo 113, Japan

Although formation of silicate melt is thermochemically inhibited in the average solar nebula, chondrules and at least some CAIs were formed through an incipient melting stage. In order to explain the formation of silicate melt in the solar nebula, enrichment of dust has been considered. Nagahara and Ozawa (1996), however, experimentally showed that silicate melt-crystal mixture in the MgO-SiO<sub>2</sub> system, which has porphyritic or barred olivine texture, lives for a long duration at high temperatures in vacuum (for more than 1 day at 1700°C). The metastable retention of silicate melt in vacuum is explained by crystal-melt-gas kinetics including evaporation (and condensation), crystallization (and dissolution), and elemental diffusion in melt. In our companion paper (Nagahara & Ozawa, this volume), we have developed an equation to describe a steady state in a crystal-melt mixture in vacuum. The change of radius, melt fraction, degree of crystallization, melt fraction on the surface, and bulk composition in a transient state were examined in this paper.

Because evaporation takes place from the surface of a sphere, the melt near surface precipitates crystals. If elemental diffusion in the sphere is rapid enough, nucleation and growth of crystals proceed homogeneously. Thus, melt fraction of the surface is kept to be the same as that inside (Case A). On the other hand, diffusion is slow, the surface is more preferentially covered by crystals due to heterogeneous nucleation and growth. In an extreme situation, the surface melt fraction can be very small, which is quite different from melt fraction of the bulk sphere (Case B). The idea is shown in Fig. 1. Actual processes should be in between these two cases. (There can be another extreme case that melt is preferentially present on the surface (Case C). It may be a situation when Ca and Al-rich melt is present on the surface of less refractory silicate minerals.)

Figure 2 shows the change of radius, total melt fraction, degree of crystallization, and surface melt fraction with time. In Case A (curve for parameter value 1.0), the size of the sphere becomes small most quickly as far as melt is present, the melt fraction decreases most quickly, the degree of crystallization increases more quickly, and the surface melt fraction decreases less dramatically. By contrast, in Case B (curve for 0.02) the size of the sphere decreases slowly but steadily to reach total evaporation most quickly, crystallization is not significant, and the surface melt fraction decreases dramatically to reach steady value. Figure 2 shows that a nearly total melt with surface 90% covered by crystals can survive evaporation process for significantly longer duration (by 5 times of total melt without surface crystals).

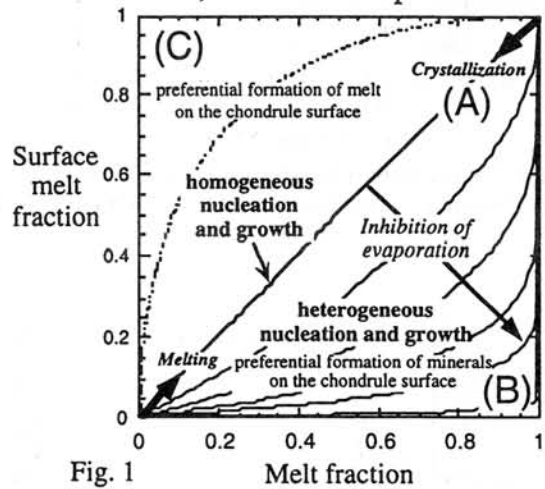


Fig. 1

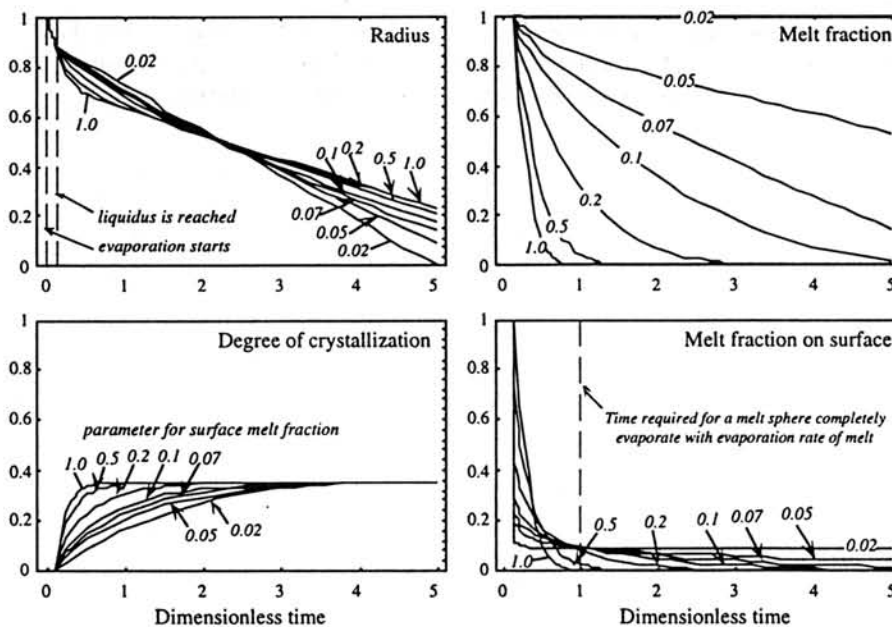


Fig. 2: Modeled change of radius, melt fraction, degree of crystallization, and surface melt fraction as a function of time normalized to the time required for complete evaporation of a melt sphere without surface crystals. The MgO-SiO<sub>2</sub> system is assumed, and thus the melt composition is fixed on liquidus after the liquidus is attained.

# Infrared Diffuse Reflectance Spectra of CR Chondrites: Comparison with Asteroids

Kimiyasu SATO, and Masamichi MIYAMOTO

*Mineralogical Institute, Graduate School of Science, University of Tokyo, Hongo, Tokyo 113, Japan*

## Introduction

Absorption bands near 3  $\mu\text{m}$  in diffuse reflectance spectra are due to the presence of hydrates and/or hydroxyl ions and the intensity of the 3  $\mu\text{m}$  band is related to the amount of hydrous minerals in a silicate sample [e.g., 1]. Molecular water in minerals shows broad absorption bands near 3400  $\text{cm}^{-1}$  (2.94  $\mu\text{m}$ ) and hydroxyls typically show sharp absorption bands near 3650  $\text{cm}^{-1}$  (2.74  $\mu\text{m}$ ) [e.g., 2, 3]. Therefore, the absorption bands near 3  $\mu\text{m}$  are the spectral signatures of hydrated silicates included in meteorites and surface materials of solar system objects.

We have previously compared the reflectance spectra near 3  $\mu\text{m}$  of asteroid 1 Ceres and 2 Pallas (commonly classified into G and B type, respectively) with those of variable carbonaceous chondrites, including thermally metamorphosed ones. We have shown that Renazzo (CR2 chondrite) is the excellent spectral match to Pallas [4]. In this paper, we measured infrared diffuse reflectance spectra of 8 CR chondrites from Antarctica and examined the spectral profiles of the absorption bands near 3  $\mu\text{m}$ . The spectral features of the 3  $\mu\text{m}$  absorption bands are compared with those of asteroids which are members of the C, G, B and F taxonomic classes.

## Samples and Experimental Techniques

CR chondrites studied in this paper are summarized in Table 1. Samples of these CR chondrites weighing approximately 50 mg were ground in a corundum mortar and passed through a 100  $\mu\text{m}$  sieve to obtain powder samples for spectral measurements. Each powder sample was dried in a desiccator for at least 48 hours in order to remove any adsorbed water from the grain surface. A specimen weighing approximately 20 mg was taken from each powder sample and used for the spectral measurements. Diffuse reflectance spectra were measured in dry-air surroundings by the use of a Fourier transform infrared spectrometer (JASCO, FT/IR-300E) equipped with a diffuse reflectance attachment at Mineralogical Institute, University of Tokyo. Spectra were taken over the range from 7900  $\text{cm}^{-1}$  (1.27  $\mu\text{m}$ ) to 400  $\text{cm}^{-1}$  (25  $\mu\text{m}$ ) at a resolution of 4  $\text{cm}^{-1}$ . An aluminum-coated mirror was used as standard. The ratio of meteorite reflectance to standard spectrum displays only mineralogical features. Diffuse reflectance spectrum of Renazzo was measured under the similar conditions and was taken over the range from 3950  $\text{cm}^{-1}$  (2.53  $\mu\text{m}$ ) to 400  $\text{cm}^{-1}$  (25  $\mu\text{m}$ ) at a resolution of 4  $\text{cm}^{-1}$ . Details of measurements are described in [4].

## Reflectance Spectra of CR Chondrites

Infrared diffuse reflectance spectra of 9 CR chondrites are shown in Fig. 1. They exhibit various intensities of the absorption bands near 3  $\mu\text{m}$ , caused by hydrous minerals. Antarctic CR chondrites show more intensive hydration bands than that of Renazzo. The shape of their 3  $\mu\text{m}$  bands is more round than that of Renazzo which assumes a triangular shape. As was mentioned above, the 3  $\mu\text{m}$  hydrated silicate bands are composed of a sharp 3650  $\text{cm}^{-1}$  feature dominantly due to hydroxyl ions and a much broader 3400  $\text{cm}^{-1}$  absorption dominantly due to interlayer molecular water. The 3  $\mu\text{m}$  absorption feature in the reflectance spectrum of Renazzo is due to the presence of hydroxyl ions in the intergrown phyllosilicates contained in matrix [5, 6, 7]. Goethite, reported as a major corrosion product of Fe-Ni alloys in Antarctic meteorites by [8], shows broad absorption bands near 3  $\mu\text{m}$ . The position of reflectance minima is about 3150  $\text{cm}^{-1}$  (3.17  $\mu\text{m}$ ). For severely weathered Antarctic meteorites, the absorption bands near 3150  $\text{cm}^{-1}$  becomes noticeable because of the presence of corrosion products [1]. The rounded shape of the 3  $\mu\text{m}$  bands of Antarctic CR chondrites are probably due to some corrosion products. Among 8 Antarctic CR chondrites, 4 meteorites which belong to EET series are paired with each other [9, 10]. Spectral profiles of EET 87747, EET 92042, and EET 92052 are almost the same and this result is consistent with the consideration that they are paired with each other. Spectral profile of EET 87770 is similar to those of other 3 EET meteorites but shows weaker absorption bands. This probably indicates that EET 87770 is terrestrially less weathered than other meteorites of EET series. Values of the integrated intensity of the 3  $\mu\text{m}$  absorption bands will be given in our next full length paper.

## Reflectance Spectra of Asteroids

The C, G, B, and F asteroids have been considered to be related to carbonaceous chondrites, on the basis of their albedos and reflectance spectra in the visible-NIR wavelength region. Telescopic reflectance spectra of low-albedo asteroids near 3  $\mu\text{m}$  were reported by [11] and we utilized their spectral data. 8 asteroids selected based on higher quality of their spectral data are summarized in Table 2 and their reflectance spectra were

compared with those of CR chondrites. Telescopic reflectance spectra of these asteroids are shown in Fig. 2. The taxonomic classifications of asteroids are based on [12].

**Comparison between CR Chondrites and Asteroids**

We have compared reflectance spectra of newly studied CR chondrites with those of 8 selected asteroids. Shown in Fig. 3 are spectral matches. As was reported by [4], spectral shapes of asteroid 2 Pallas and Renazzo are in an excellent match in the wavelength region near 3  $\mu\text{m}$ . Although its quality of telescopic spectral data is lower than that of Pallas, the overall spectral profile of 511 Davida also exhibits similarity to the Renazzo spectrum. In this study, no asteroid has been founded that has an Antarctic CR meteorite counterpart. CR chondrites from Antarctica show 3  $\mu\text{m}$  hydration bands which have been deepened and rounded probably by terrestrial weathering. Therefore, it is difficult to compare reflectance spectra of weathered meteorites with those of asteroids directly.

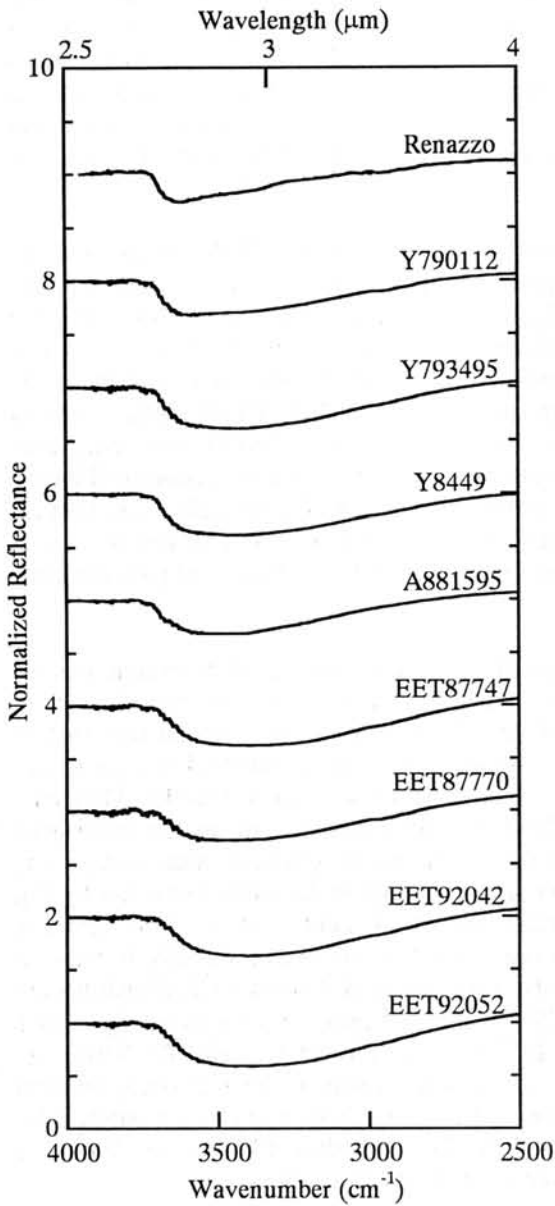


Fig. 1. Infrared diffuse reflectance spectra of CR chondrites. All spectra are scaled to 1 at 2.53  $\mu\text{m}$  and offset for clarity.

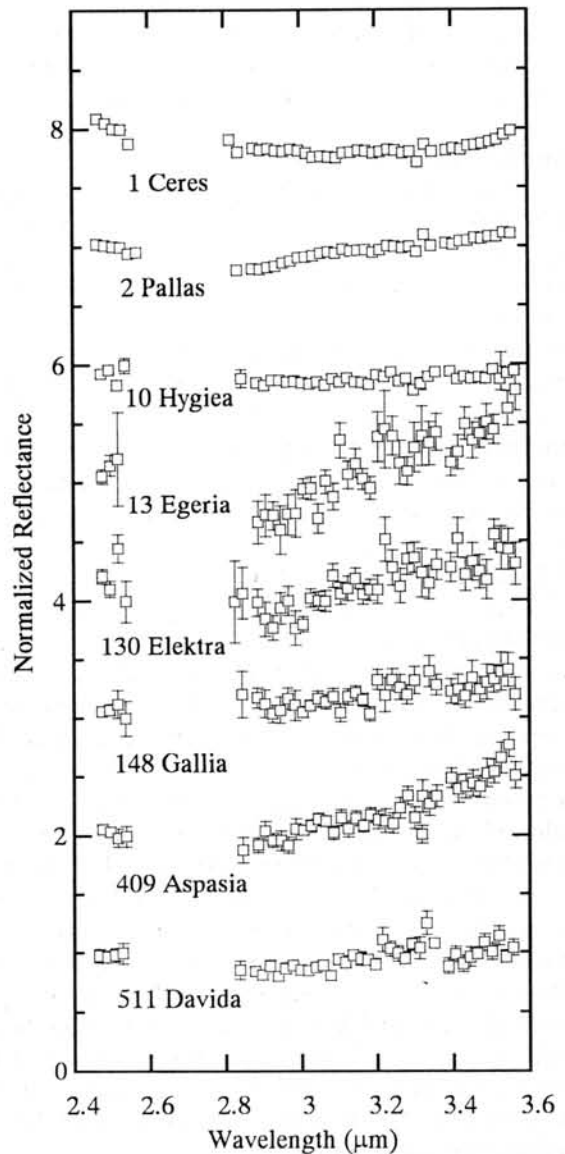


Fig. 2. Telescopic reflectance spectra of selected 8 asteroids. All spectra are scaled to 1 at 2.53  $\mu\text{m}$  and offset for clarity.

## Acknowledgment

We thank National Institute of Polar Research and Meteorite Working Group for providing Antarctic meteorite samples. Asteroidal reflectance spectra were taken from the Planetary Data System (PDS) Small Bodies Node (SBN), located in the Astronomy Department of University of Maryland.

## References

- [1] Miyamoto M. (1991) *Geochim. Cosmochim. Acta* **55**, 89-98. [2] Ryskin Ya. I. (1974) In *The Infrared Spectra of Minerals* (ed. V. C. Farmer), pp. 137-181. [3] Salisbury J. W., Walter L. S. and D'Aria D. (1988) *Mid-infrared (2.5 to 13.5  $\mu\text{m}$ ) Spectra of Igneous Rocks*. [4] Sato K., Miyamoto M. and Zolensky M. E. (1997) *Meteorit. Planet. Sci.*, in press. [5] Nelen J., Kurat G. and Fredriksson K. (1975) *Meteoritics* **10**, 464-465. [6] Zolensky M. E., Barret R. and Browning L. (1993) *Geochim. Cosmochim. Acta* **57**, 3123-3148. [7] Weisberg M. K., Printz M., Clayton R. N., Mayeda T. K., Grady M. M. and Pillinger C. T. (1995) *Proc. NIPR Symp. Antarct. Meteorites* **8**, 11-32. [8] Buchwald V. F. and Clarke R. S., JR. (1989) *Ame. Mineral.* **74**, 656-667. [9] Grossman J. N. (1994) *Meteoritics* **29**, 100-143. [10] Grossman J. N. and Score R. (1996) *Meteorit. Planet. Sci.* **31**, A161-A174. [11] Jones T. D., Lebofsky L. A., Lewis J. S. and Marley M. S. (1990) *Icarus* **88**, 172-192. [12] Tholen D. J. and Barucci M. A. (1989) In *Asteroids II*, pp. 298-315.

Table 1: CR chondrites studied in this paper

| Meteorites | Remarks             |
|------------|---------------------|
| Renazzo    | Fell 1824           |
| Y-790112   | Antarctic meteorite |
| Y-793495   | Antarctic meteorite |
| Y-8449     | Antarctic meteorite |
| A 881595   | Antarctic meteorite |
| EET 87747  | Antarctic meteorite |
| EET 87770  | Antarctic meteorite |
| EET 92042  | Antarctic meteorite |
| EET 92052  | Antarctic meteorite |

Table 2: Asteroids compared with CR chondrites

| Asteroids   | Class | Date of observation |
|-------------|-------|---------------------|
| 1 Ceres     | G     | 04/25/1987          |
| 2 Pallas    | B     | 04/24/1987          |
| 10 Hygiea   | C     | 02/01/1988          |
| 13 Egeria   | G     | 10/03/1987          |
| 130 Elektra | G     | 02/02/1988          |
| 148 Gallia  | GU    | 02/01/1988          |
| 409 Aspasia | CX    | 02/03/1988          |
| 511 Davida  | C     | 04/21/1987          |

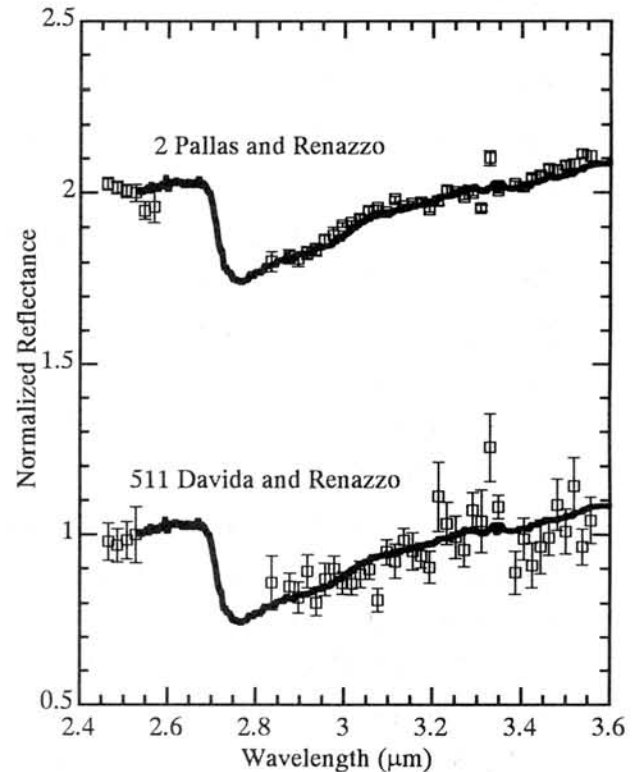


Fig. 3. Asteroid-meteorite counterparts that have similar reflectance profiles. Open squares: Telescopic reflectance spectra of asteroids. Solid curves: Diffuse reflectance spectrum of Renazzo. All spectra are scaled to 1 at 2.53  $\mu\text{m}$  and offset for clarity.

## DO THE CHONDRULE SIZES INDICATE THE MAXIMUM SIZE OF DUST AGGREGATIONS IN THE SOLAR NEBULA?

Minoru SEKIYA

*Department of Earth and Planetary Sciences, Faculty of Science, Kyushu University 33, Hakozaki, Fukuoka, 812-81 Japan*

The chondrule sizes are often considered to indicate the maximum size of the dust aggregations in the solar nebula (Eisenhour *et al.* 1994). If this is the case, planetesimals should have been formed not by mutual sticking of dust aggregations due to non-gravitational forces but by gravitational instabilities in the solar nebula.

The critical density of gravitational stability of the dust layer in the solar nebula is given by

$$\rho_c = 0.606 M_\odot / r^3 = 3.6 \times 10^{-7} (r / \text{AU})^{-3} \text{ [g cm}^{-3}\text{]}, \quad (1)$$

where  $M_\odot$  is the solar mass and  $r$  is the heliocentric distance (Sekiya 1983). On the other hand, if dust aggregations are uniformly distributed in the solar nebula, the dust density is written

$$\rho_d = 6 \times 10^{-12} f_d \exp[-(z/H)^2] (r / \text{AU})^{-11/4} \text{ [g cm}^{-3}\text{]}, \quad (2)$$

where  $f_d = 1$  and 4.2 for the regions where water vaporizes and condenses, respectively, and  $z$  is the distance from the midplane, and  $H$  is the scale height

$$H = 7.1 \times 10^{11} (r / \text{AU})^{5/4} \text{ [cm]}. \quad (3)$$

Here the Hayashi model is used (Hayashi 1981, Hayashi *et al.* 1985).

Therefore dust aggregations with sizes  $\sim 1$  mm should settle towards the midplane and make a very thin dust layer with a half-thickness  $z_d \leq 1 \times 10^7 f_d (r / \text{AU})^{3/2}$  [cm] in order that the dust density  $\rho_d$  exceed the critical density  $\rho_c$  and that the dust layer become gravitationally unstable to form planetesimals.

The rotational velocity  $v$  of the solar nebular gas is determined by the valance of the solar gravity, the centrifugal force and the gas pressure gradient:

$$v = v_K \{1 - [\rho_g \eta / (\rho_g + \rho_d)]\}, \quad (4)$$

where  $v_K$  is the circular Keplerian velocity

$$v_K = 3.0 \times 10^6 (r / \text{AU})^{-1/2} \text{ [cm s}^{-1}\text{]}, \quad (5)$$

and  $\rho_g$  is the gas density

$$\rho_g = 1.4 \times 10^{-9} f_g \exp[-(z/H)^2] (r/\text{AU})^{-1/4} \text{ [g cm}^{-3}\text{]}, \quad (6)$$

where  $f_g$  is the gas depletion factor compared with the Hayashi model, and  $\eta$  is a non-dimensional factor

$$\eta = -(\partial P_g / \partial \ln r) / (2v_K^2 \rho_g) = 1.81 \times 10^{-3} (r/\text{AU})^{1/2}, \quad (7)$$

where  $P_g$  is the gas pressure. In deriving Eq. (4), I assumed that the relative velocity of dust and gas is small enough, since I assume that sizes of dust aggregations are on the order of 1 mm. Eq. (4) shows that  $\partial v / \partial z \neq 0$  if  $\rho_g / \rho_d \neq \text{constant}$  for  $z$ . Therefore, as the dust aggregations settle towards the midplane, the shear motions arise in the nebula.

The shear instability grows if the Richardson number

$$J = -(\partial \rho_d / \partial z) g (\rho_g + \rho_d)^{-1} (\partial v / \partial z)^{-2}, \quad (8)$$

is less than the critical value  $J_c = 0.25$  (Chandrasekhar, 1961), where  $g$  is the  $z$ -component of the gravitational acceleration. As the dust aggregations settle towards the midplane, the Richardson number decreases. If the Richardson number  $J$  becomes lower than the critical value  $J_c$ , then the flow becomes turbulent, and dust aggregations would be stirred up and stop to settle further. Therefore it is supposed that the dust distribution becomes quasi-equilibrium where  $J = J_c$ . I solved this equation and obtained the dust density distribution (Fig. 1). This solution correspond to solutions of Cuzzi et al. (1993) in the limiting case of small enough dust aggregations. As seen from the figure, the quasi-equilibrium dust density  $\rho_d$  on the midplane is much smaller than the critical density  $\rho_c$ . Therefore the dust layer cannot be gravitationally unstable. On the other hand, if the gas density is 0.029 times the Hayashi model, the dust density on the midplane becomes equal to the critical value (Fig. 2).

The above calculations show that two alternative stories are considered:

- (1) Dust particles stick together by non-gravitational forces to form  $\sim 1$  km bodies. In this case, chondrule sizes do not indicate the maximum size of dust aggregations in the solar nebula. The chondrule sizes may be determined by fragmentation processes during violent chondrule formation events.
- (2) There were little aggregations larger than the chondrule sizes in the solar nebula, and the dissipation of the nebular gas led the formation of the planetesimals due to the gravitational instabilities.

Further theoretical and experimental investigations are needed to clarify which is the true story.

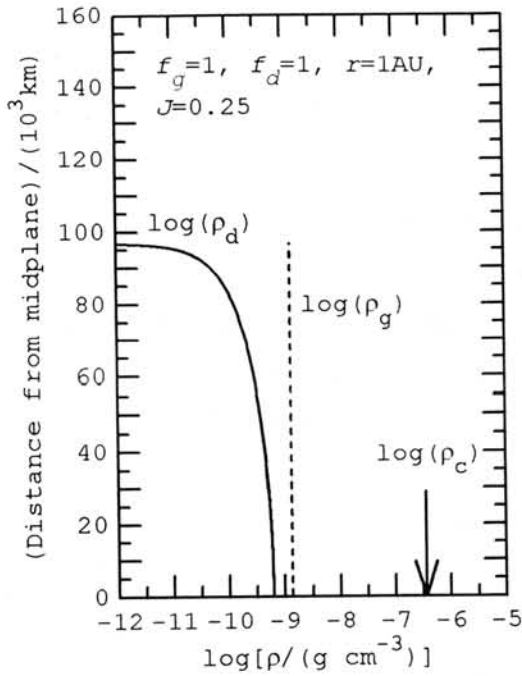


Fig. 1. The quasi-equilibrium density distributions of dust (solid line) and gas (dotted line) in the case of the Hayashi model. The critical density is shown by the arrow.

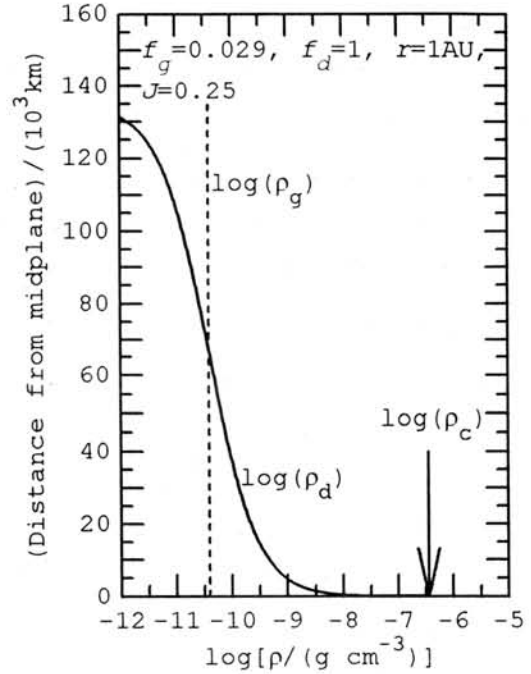


Fig. 2. Density distributions in the case where the nebular gas is depleted by  $f_g = 0.029$  compared with the Hayashi model. The dust density on the midplane is equal to the critical density.

## References

- Chandrasekhar, S. (1961) *Hydrodynamic and hydromagnetic stability*. Oxford University Press, Oxford.
- Cuzzi, J. N., Dobrovolskis, A. R. and Champney, J. M. (1993) Particle-gas dynamics in the midplane of a protoplanetary nebula. *Icarus* **106**, 102-134.
- Eisenhour, D. D., Daulton, T. L. and Buseck, P. R. (1994) Electromagnetic heating in the early solar nebula and the formation of chondrules. *Science* **265**, 1067-1070.
- Hayashi, C. (1981) Structure of the solar nebula, growth and decay of magnetic fields, and the effects of magnetic and turbulent viscosities on the nebula. *Progr. Theor. Phys. Suppl.* **70**, 35-53.
- Hayashi, C., Nakazawa, K. and Nakagawa, Y. (1985) Formation of the solar system. In *Protostars and Planets II*. (D. C. Black and M. S. Matthews, Eds.), pp. 1100-1153. Univ. Arizona Press, Tucson.
- Sekiya, M. (1983) Gravitational instabilities in a dust-gas layer and formation of planetesimals in the solar nebula. *Progr. Theor. Phys.* **69**, 1116-1130.

## Isotopic compositions of carbon and nitrogen in Mezo Madaras measured with a SIMS

Naoji Sugiura and Kaoru Kiyota

Department of Earth and Planetary Physics, Univ. of Tokyo, Tokyo, Japan

### Introduction

Mezo Madaras is known to contain isotopically anomalous nitrogen [1]. To find out the carrier of this nitrogen a polished section was examined with a SEM-EDX. Graphite-like grains were found. Some of them was examined with a SIMS and found to contain isotopically anomalous nitrogen.

### Previous study

Stepped combustion of Mezo-Madaras revealed that there are two kinds of isotopically anomalous nitrogen in this chondrite. One is isotopically heavy and fairly abundant, while the other is isotopically light and seems to be low in abundance [1].

### SEM-EDX study

Areas with low density were identified with a back-scattered electron image and then the carbon content was examined with the EDX. Because gold coating was used for the SEM observation, carbon concentration cannot be determined quantitatively. But absence of the other elements suggests that the entire grain consists of carbon and therefore it is assumed to be graphite, although the crystallographic structure has not been known.

There are three types of occurrence of the graphite.

1) Graphite-metal association: Graphite consists about 50 % of the area and the rest is made of Fe-Ni alloy. The size of the mixture is as large as 50 micrometers and the size of each graphite and metal grain is of the order of several micrometers. This is the most prevalent occurrence of graphite and predominates in terms of carbon abundance.

2) Metal-silicate association with minor graphite: Only one occurrence was observed. A clast of more than 100 micrometer consists of metal and silicate which are interwound intimately. Judging from the appearance this clast may have been molten and quenched. Graphite with irregular shape occurs on the periphery of this clast. The size of the graphite is typically 10 to 20 micrometer.

3) Metal-sulfide-silicate association with minor graphite: Only one occurrence was observed. This may be a typical fine grained rim of a chondrule, though the material inside is not spherical in shape and the thickness of this association is as much as 100 micrometers. It consists

of nearly equal abundances of sulfide, silicate and metal. Graphite occurs on the outer part of this association. The size of the graphite is typically 1 micrometer.

#### SIMS study

Some of the graphite grains were examined with a SIMS (Cameca-6F). To remove contamination, the sample was pre-combusted at 300 C for 30 minutes before the SIMS observation.

Carbon and nitrogen isotopic compositions were measured using Cs primary ions. Secondary ions were extracted with 9.5 KV. Charge up of the sample is compensated using an electron gun. Reproducibility (1 sigma) of the isotopic compositions is a couple of permil within a session of measurements if the electron gun is not in use. The reproducibility with the electron gun is not yet studied in detail, but it is expected to be better than several permil. The carbon isotopic compositions of 4 graphite (Fig.1) is considered to be the same within the error the measurements.

Since carbon is the major element, carbon isotope composition is not affected by contamination. On the other hand, nitrogen is a minor element in graphite and could be affected by contamination. Therefore, nitrogen isotopic measurements were repeated at the same spot. It was found that generally the nitrogen isotopic composition gets heavier by repeated measurements. This is interpreted as due to removal of contamination that exists near the surface. Fig.1 shows that the  $\delta^{15}\text{N}$  value is as high as 272 permil. This is slightly higher than the value (229 permil) obtained by the combustion study. Among the three types of occurrence of graphite, the metal-graphite association showed the highest  $\delta^{15}\text{N}$  value. This is interpreted to be due to the highest volume fraction of graphite in the area of analysis (about 30 micrometers in diameter) which makes the result least affected by contamination. The graphite associated with the metal-silicate clast showed lowest  $\delta^{15}\text{N}$  value which did not increase significantly by repeated measurements. It may be that the nitrogen within this graphite was isotopically homogenized with isotopically normal nitrogen in the solar system when the clast was heated to a high temperature.

#### Conclusions

Graphite was found to be a carrier of the isotopically heavy nitrogen in Mezo Madaras. Graphite with different appearance may have different nitrogen isotopic composition. Such observations are consistent with the recent report on nitrogen isotopic compositions of graphite in other chondrites [2]. It is yet to be determined if such graphite and the associated phases are presolar in origin or not.

References

- [1] N.Sugiura, K.Kiyota and K. Hashizume, Nitrogen isotopic groups of primitive ordinary chondrites, submitted to Meteoritics.  
 [2] S.Mostefaoui, E.Zinner, P.Hoppe and El Goresy, In situ survey of graphite in unequilibrated chondrites: Morphologies, C, N, and H isotopes, Lunar Planet. Sci. XXVIII, 1997.

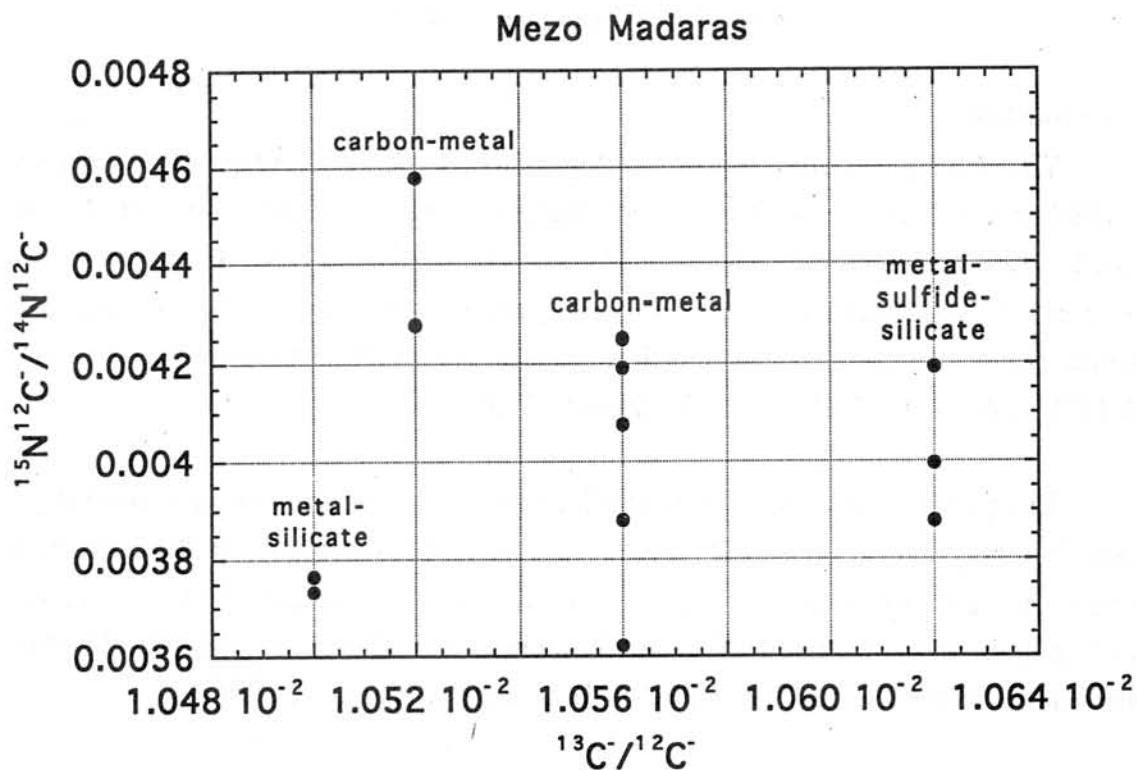


Fig.1 Carbon and nitrogen isotopic composition of four graphite in Mezo Madaras measured with a SIMS. The carbon isotopic composition was measured once for each graphite, while the nitrogen isotopic composition was measured repeatedly on the same spot. In every case, the nitrogen isotopic composition gets heavier by the repeated measurements.

# REE CONTENT OF EXTREMELY SMALL SPHERULES FROM BOREHOLE NAGYLÓZS 1, NW HUNGARY

Gyula Szöőr - Péter Rózsa

Department of Mineralogy and Geology, University of Kossuth Lajos, Debrecen,  
P. O. Box 4, Hungary, H-4010

## Introduction

The drilling ordered by the Geological Institute of Hungary was executed in 1990 in the framework of the Little Hungarian Plain mapping project. It was aimed at acquiring better knowledge of the geological structure as well as of the sedimentary sequences of the Little Hungarian Plain basin. The drilling was located in NW Hungary, SE of Sopron. Its geographic coordinates are: 47° 34' 13"N; 16° 48' 04"E. Depth of the bottom: 1335.2 m.

The penetrated geological formations and their microspherule assemblages were formerly discussed (Boldizsár et al., 1993; Rózsa et al., 1995). However, extremely small spherules with 1-3  $\mu\text{m}$  in size from lower part of this borehole have not been introduced. Similar objects were found in Middle Triassic formations of the Mecsek Mountains, S Hungary (Szöőr et al., 1996).

## Method

About 150 - 200 g of material were taken from inner part of the core samples. They were decomposed in water. The sediments dried were examined under stereoscopic microscope at 100 x in order to isolate glassy particles.

An AMRAY 1830I scanning electron microscope (SEM) was used. The photos were taken by using secondary- and backscattered electron (SE and BSE) detectors. For X-ray analysis an EDX system (SiLi detector with a 10  $\mu\text{m}$  thick Be window) was used, usually 20 kV acceleration potential, the energy resolution is 150 eV. The specimens were coated by gold or, for X-ray analysis, by carbon.

## Results and discussion

Several angular fragments and microspherules, which differ from each other, were found by SEM-EDAX analyses. These findings came from various Upper Miocene sediments (marly siltstone, claymarly siltstone, sandy silt, sandstone) intersected between 1000 and 1304 m.

These 1-3  $\mu\text{m}$  size "extremely small microspherules" have smooth surface, no structure. These spherules can not be mistaken for spores, pollens or other

biogenic objects, and they have very interesting chemical composition accumulating several rare earth elements (lantanides).

To demonstrate the above mentioned facts, a benthic foraminifer and an extremely small spherule are shown in Photo 1. Data of the chemical analysis are listed in Table 1.

**Table 1.** Composition of the pelite in a foraminifer test and its various spherules and angular fragments from borehole Nagylózs-1 (1033.0 m).

| Element  | [%]        | 61    | 61/1   | 61/2   | 61/3   | 61/4  | 61/5  | 61/6  | 61/7  |
|----------|------------|-------|--------|--------|--------|-------|-------|-------|-------|
| Na       | K $\alpha$ |       | 0.194  |        |        |       |       |       |       |
| Mg       | K $\alpha$ | 2.52  | 8.889  | 0.251  |        |       | 1.92  | 2.06  |       |
| Al       | K $\alpha$ | 16.33 | 11.15  | 6.971  | 2.758  | 7.4   | 9.96  | 6.82  | 6.75  |
| Si       | K $\alpha$ | 41.18 | 26.806 | 3.165  | 0.868  | 8.25  | 20.22 | 11.71 | 13.04 |
| S        | K $\alpha$ |       | 0.167  |        |        |       |       |       |       |
| Cl       | K $\alpha$ |       | 0.749  | 2.46   | 0.729  |       | 0.42  |       |       |
| K        | K $\alpha$ | 4.22  | 2.473  | 2.997  | 1.135  |       | 1.3   | 0.76  | 0.41  |
| Ca       | K $\alpha$ | 31.88 | 5.864  | 13.868 | 6.784  | 9.69  | 2.99  | 3.01  | 8.1   |
| Ti       | K $\alpha$ | 0.71  |        |        |        |       | 61.5  |       |       |
| Cr       | K $\alpha$ |       |        |        |        |       |       | 13.77 |       |
| Mn       | K $\alpha$ |       |        |        |        |       |       | 0.66  |       |
| Fe       | K $\alpha$ | 3.16  | 18.131 | 25.195 | 44.779 | 29.74 | 1.7   | 54.73 | 0.25  |
| Ni       | K $\alpha$ |       |        |        |        |       |       | 6.47  |       |
| Cu       | K $\alpha$ |       | 0.896  | 0.649  |        |       |       |       |       |
| Zn       | K $\alpha$ |       | 1.95   | 4.596  |        |       |       |       |       |
| La       | L $\alpha$ |       | 6.12   | 6.888  | 8.32   | 12.6  |       |       |       |
| Ce       | L $\alpha$ |       | 13.8   | 17.992 | 20.309 | 26.34 |       |       |       |
| Pr       | L $\alpha$ |       | 1.099  | 3.54   | 3.382  | 1.87  |       |       |       |
| Nd       | L $\alpha$ |       | 1.712  | 8.155  | 7.363  | 4.12  |       |       |       |
| Sm       | L $\alpha$ |       |        | 1.317  | 1.707  |       |       |       |       |
| Gd       | L $\alpha$ |       |        | 1.956  | 1.867  |       |       |       |       |
| Au       | M $\alpha$ |       |        |        |        |       |       |       | 71.46 |
| $\Sigma$ |            | 100.0 | 100.0  | 100.0  | 100.0  | 100.0 | 100.0 | 100.0 | 100.0 |

Legend:

- 61 = foraminifer test  
 61/1, 61/2, 61/3 = spherules (size is 0.8-3.3  $\mu\text{m}$ )  
 61/4, 61/5, 61/7 = angular fragments (size is 1-10  $\mu\text{m}$ )

The origin of the extremely small spherules of interesting composition built in the Badenian, Sarmatian and Lower Pannonian foraminifer tests is very problematic.

The figure of Haskin et al. (1970) compares rare earth element (REE) abundances for some lunar sample Apollo 11 materials, a composition of a North American shale, and that of a submarine andesite. The REE spectra show a uniform degree of enrichment in the lunar rocks, except for europium that shows characteristic negative anomaly. This depletion is linked with a unique geochemical feature: under highly reducing conditions europium exists as  $\text{Eu}^{2+}$  and it preferentially enters the plagioclase structure (Mason and Melson 1970. p. 144).

The paper of Wasson (1991. p. 100) demonstrated the REE patterns in "layered tektites" from Southeast Asia and in "splash-form tektites" from Australia. The tektite spectra are similar to those in post-Archean continental sediments as Wyoming shales and Luochuan loesses. The REE compositions of the samples exhibit large Eu anomalies and large and systematic depletion in  $\text{La} > \text{Lu}$ ; concentrations in the sediments are somewhat lower than those in the tektites.

The trend of REE-s from Zhamanshin impact structure, Kazakhstan is similar to the Australasian splash tektites (Taylor and McLennan 1979. p. 1562).

Sholkovitz et al. (1993) have investigated the REE composition of aerosols from Bermuda and Woods Hole. The REE spectra show large-scale fractionation between the continents, ocean and atmosphere. The precipitated samples (p. 595) of the seawater also exhibit large negative Eu anomalies and drastic depletions in the heavy REE.

The very high REE concentration of the extremely small spherules of the borehole Nagylózs-1 (see Table 1), that are smaller in orders of magnitude than the other objects, is "unique" in itself.

It is also characteristic that, in an accordance with the cosmochemical rules of the solar abundance of elements (Anders and Grevesse 1989), the concentrations of uneven atomic numbered lanthanides are less than those of even atomic numbered ones. Members following Eu and Gd could not be detected. Therefore, a negative anomaly and large depletion of La prevail in this case, too. It has to be noted that REE rich angular inclusions (61/4), and components of high Ti content (61/5) and those of Fe, Ni, Co contents (61/6) building in the tests are also found. An embedded gold grain is also noteworthy.

On the basis of our present knowledge, the genesis of these objects can not be established, we assume that this problem should be approached from a

biogeochemical point of view, and their study should be continued by comparative analysis of the extremely small spherules.

### **Acknowledgement**

A grant obtained from the OTKA Bureau, Hungary (No. T-019516) supported the investigations. This help is gratefully acknowledged.

### **References**

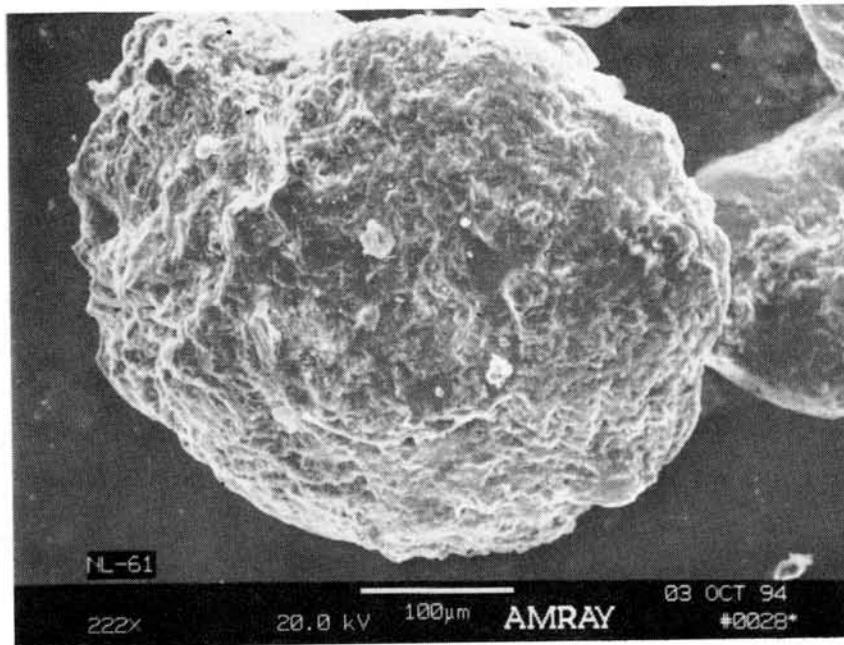
- Anders E. and Grevesse N. 1989. Abundances of the elements. – Meteorite and solar. *Geochim. Cosmochim. Acta*, 53. 197-214.
- Boldizsár I., Don Gy., Erhardt Gy., Hobot J., Ivancsics J., Kaiser M., Marsi I., Scharek P., Szeiler R., Szurkos G., Tullner T., Zsámbok I. 1993., The Geological Map Series of the Little Hungarian Plain, SOPRON - KŐSZEG. Manuscript. – Geological Institute of Hungary. Ed. by Dr. P. Scharek.
- Haskin L.A., Allen R.O., Helmke P.A., Paster T.P., Anderson M.R., Korotev R.L. and Zweifel K.A. 1970., Rare earth and other trace elements in Apollo 11 lunar samples. – *Geochim. Cosmochim. Acta, Suppl.* 1. 1213-1231.
- Mason B. and Melson W.G. 1970., *The Lunar Rocks*. – Wiley and Sons, Inc. ISBN 0 471 57530 5.
- Rózsa, P., M. Braun, Gy. Szöör. 1995. Geochemical and petrogenetic evaluation of the glassy microspherules from Upper Pannonian layers of borehole Nagylózs 1, NW Hungary. – *Antarctic Meteorites XX*. 211-219.
- Sholkovitz E.R., Church T.M. and Arimoto R. 1993., Rare Earth Element Composition of Precipitation, Precipitation Particles, and Aerosols. – *Journal of Geophysical Research*, 98, D11. 20,587-20,599.
- Szöör, Gy., E. Rálich-Felgenhauer, I. Beszeda, P. Rózsa and M. Braun. 1996., Origin of the "extremely small spherules" from the Middle Triassic of Mecsek Mts., Hungary. – *Annales Univ. Sci. Budapest. R. Eötvös. Sec. Geoph. Met.* XII. 79-86.
- Taylor S.R. and McLennan S.M. 1979., Chemical relationships irghizites, zhamanshinites, Australasian tektites and Henbury impact glasses. – *Geochim. Cosmochim. Acta*, 43. 1551-1565.
- Wasson J.T. 1991., Layered tektites: a multiple impact origin for the Australasian tektites. – *Earth and Planetary Science Letters*, 102. 95-109.
- Williams H., Turner F.J. and Gilbert Ch.M. 1982., *Petrography*. Copyright W.H. Freeman and Company.

**Photo 1.**

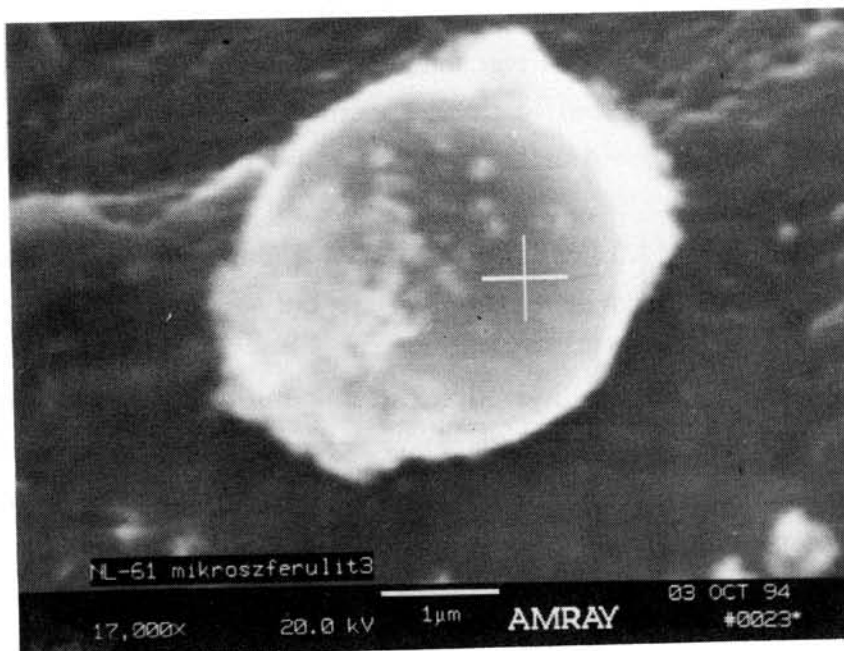
Extremely small spherule built in a foraminifer test.

- A. Benthic foraminifer in borehole Nagylózs 1, 1033.0 m (sample: NL-61).
- B. Extremely small spherule; secondary electron detector (SE) was used.

**A**



**B**



## *Formation of forsterite by incongruent evaporation of enstatite (MgSiO<sub>3</sub>)*

Shogo TACHIBANA<sup>1)</sup>, Tadashi TANAKA<sup>1)</sup>, Akira TSUCHIYAMA<sup>1)</sup>,  
Hiroko NAGAHARA<sup>2)</sup> and Kazuhito OZAWA<sup>2)</sup>

<sup>1)</sup>*Department of Earth and Space Science, Osaka University, Toyonaka 560, JAPAN.*

<sup>2)</sup>*Geological Institute, University of Tokyo, Hongo 113, JAPAN.*

### Introduction.

The elemental fractionation, which occurred in the primitive solar nebula, would be caused by condensation of gas and/or evaporation of dust particles. Thermochemical calculations have been used as a benefit method to discuss the elemental fractionation (*e.g.*, [1]). These calculations, however, assume equilibrium of the system, and have not taken the effects of gas-solid (or liquid) reaction kinetics into consideration. Some theoretical studies discussed the kinetic effects of condensation of gas in the primitive solar nebula (*e.g.*, [2,3]), and give us important information about gas-solid (or liquid) reaction. However, reaction kinetics and kinetic parameters are obtained only by experiments.

Some experimental studies have been done to obtain the evaporation rates of minerals under the primitive solar nebula conditions (*e.g.*, Fe; [4], FeS; [5], Mg<sub>2</sub>SiO<sub>4</sub>; [6]). As regards enstatite (MgSiO<sub>3</sub>), Sata *et al.* [7] and Kushiro and Mysen [8] carried out evaporation experiments, and found that enstatite evaporates incongruently under vacuum conditions. Sata *et al.* [7] found that enstatite evaporates linearly with (time)<sup>1/2</sup> under vacuum conditions, and concluded that the rate-determining process is diffusion process of cations through a residual layer although they did not find the residual layer. Kushiro and Mysen [8] found that Si-rich gas evaporates selectively from enstatite, and forsterite (Mg<sub>2</sub>SiO<sub>4</sub>) is formed as an evaporation residue. However, they did not find a residual layer of forsterite on the surface of enstatite, and did not give evaporation rates of enstatite. Hence, the purpose of the present study is to elucidate the evaporation kinetics of enstatite in more detail and obtain the evaporation rates which can be used for the discussion on the chemical fractionation in the primitive solar nebula.

### Experiments.

We used single crystals of orthoenstatite as a starting material (*c.f.*, powders were used in the previous experiments [7,8]). We synthesized a few mm-sized single crystals by

the flux method using "lithiumvanadomolybdate" ( $\text{Li}_2\text{O}_3\text{-MoO}_3\text{-V}_2\text{O}_5$ ) [9]. The crystals were stoichiometric, transparent, and elongated parallel to the c-axis. They contain  $\text{Al}_2\text{O}_3 = 0.02\text{-}1.0$ ,  $\text{MoO}_3 < 0.08$ , and  $\text{V}_2\text{O}_5 < 0.3$  wt% as impurities.

Evaporation experiments on enstatite were carried out under vacuum conditions at  $1500^\circ\text{C}$  in a tungsten-mesh furnace [10]. The total pressure of the vacuum chamber during the experiments were about  $10^{-6}\text{-}10^{-7}$ Torr. Heating duration ranged from 22hrs to 90hrs.

### Results and Discussion.

In the present experiments, we found that a single crystal of enstatite evaporates incongruently to form forsterite crystals on the surface as an evaporation residue under vacuum conditions. This incongruent evaporation behavior of enstatite is consistent with that of the previous studies. Figure 1 shows an SEI image of the surface of a run product ( $1500^\circ\text{C}$ , 22hrs). The almost whole surface is rough and covered with forsterite ( $\text{Mg}_2\text{SiO}_4$ ) crystals. The width of the forsterite layer is about  $20\mu\text{m}$ . These crystals are polycrystalline, and the length of a single crystal ranges from a few tens to a few hundred  $\mu\text{m}$ . The cross section, which was cut perpendicular to c-axis, of the same run product is shown in Fig.2. Forsterite (bright part) covers the surface of enstatite (dark part). Evaporation rates of enstatite will be discussed in the symposium.

### References.

- [1] Larimer, J.W. and Anders, E. (1967) *Geochim. Cosmochim. Acta*, **31**, 1239-1270.
- [2] Fegley, B., Jr. and Prinn, R.G. (1989) *The Formation and Evolution of Planetary Systems*, 171-211.
- [3] Yamamoto, T. and Hasegawa, H. (1977) *Prog. Theoretical Physics*, **58**, 816-828.
- [4] Tsuchiyama, A. and Fujimoto, K. (1995) *Proc. NIPR Symp. Antarc. Meteorites*, **8**, 205-213.
- [5] Tachibana, S. and Tsuchiyama, A. (1997) *in prep.*
- [6] Nagahara, H. and Ozawa, K. (1996) *Geochim. Cosmochim. Acta*, **60**, 1445-1459.
- [7] Sata, T. et al. (1978) *Rev. Int. Hautes Temp. Réfract., Fr.*, **15**, 237-248.
- [8] Kushiro, I. and Mysen, B.O. (1991) *Progress in metamorphic and magmatic petrology*, 411-433.
- [9] Ozima, M. (1982) *J. Jpn. Assoc. Mineral. Petrol. Econ. Geol.*, **3**, 97-103.
- [10] Nagahara, H. and Ozawa, K. (1997) Japan Earth and Planetary Science Joint Meeting.

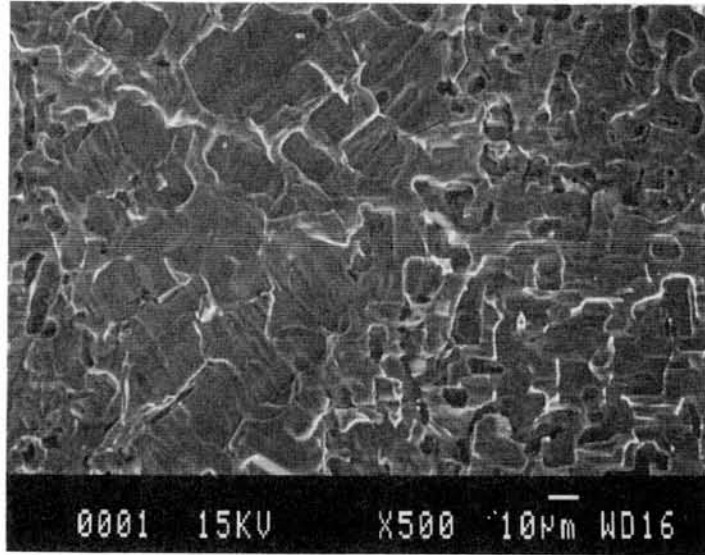


Fig.1 An SEI image of the (010) enstatite surface of a run product (1500°C, 22hrs).

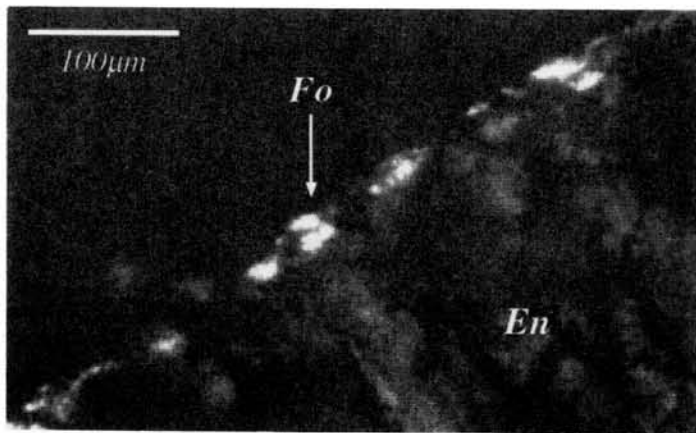


Fig.2 An optical micrograph of the cross section of a run product (1500°C, 22hrs), cut perpendicular to the c-axis (crossed nicols). The width of the polycrystalline forsterite layer is about 20 µm. Polysynthetic twinning due to proto-clino inversion is seen in the host enstatite.

## MG-RICH PYROXENE CORES IN A EUCRITE WITH TYPE 4 CHEMICAL ZONINGS OF PYROXENE.

Hiroshi Takeda<sup>1,2</sup>, Takashi Mikouchi<sup>2</sup> and Masamichi Miyamoto<sup>2</sup>.

<sup>1</sup>Research Institute, Chiba Inst. of Technology, 2-17-1 Tsudanuma, Narashino City, Chiba 275, Japan.

<sup>2</sup>Mineral. Inst., Graduate School of Sci., Univ. of Tokyo, Hongo, Tokyo 113, Japan.

### Introduction

Eucrites in the HED achondrites have been known as basalts among the oldest extruded on the surface of a Vesta-like protoplanet. Such old lava units have been proposed to explain surface features of Vesta observed by the Hubble Space Telescope [1]. However, the most abundant eucrites are brecciated and metamorphosed basalts with monomict breccia texture and homogenized Fe-rich composition of pyroxene [2]. They are called ordinary eucrite, which is a convenient name like ordinary chondrites. Takeda and Graham in 1991 [3] used degree of Mg/Fe homogenization of pigeonite (Type 1 to 6) as a measure of equilibration. Ordinary eucrites contain type 5 to 6 pyroxenes. Real quickly cooled basalts as were found in the lunar mare regions are rather rare. Pasamonte was the first eucrite, which preserves the chemical zoning of primary crystallization in a lava (Type 2). More pristine lava-like eucrites with subophitic textures and type-1 pyroxene were found in clasts of polymict breccias of Antarctic eucrites [4-6]. This paper deals with Y790447 with the type-4 pyroxene.

Arguments on the partial melting model *versus* the crystal fractionation model for the formation of the HED parent body are depend on what kind of heat sources one assumes for the melting of the chondritic materials. Stolper [7] performed melting experiments of eucrites using a metamorphosed monomict breccia. Subsequent model of the partial melting assumed heat sources by the decay of short-lived radio nucleoids. Ikeda and Takeda [8] postulated that the crystal fractionation may lead to the eucritic compositions, which solidify as a scum layers covered the surface of a thin magma ocean. Accretional and impact heating as a heat source for melting an entire surface of the HED body or for promoting global thermal metamorphism have been subjects of debate for a body smaller than the moon [9]. Impact melt veins have been observed in some eucrites such as Padvarninkai [10], but no evidence of nearly total melting has been found in the HED collections. In this paper, mineralogical evidence of a nearly totally melted eucrite is given for the basis of discussion of the heat source for the HED parent body.

### Samples and Experimental Techniques

Photographs and physical descriptions of Y790447 are given in the Catalog of Antarctic Meteorites [11]. Polished thin sections (PTS), Y790447,51-2 and Y790266 supplied by the National Institute of Polar Research (NIPR) were used for preliminary characterizations. The PTSs were studied by an optical microscope, and the chemical compositions of the minerals in Y790447 were obtained by electron probe microanalyzer (EPMA) JEOL 733 at Ocean Research Inst. (ORI) of Univ. of Tokyo. The data were compared with those of Y790266. Elemental distribution maps (Mg, Ca, Si, Al, Fe, Cr, Ti and Na) were obtained via the Chemical Map Analysis (CMA) technique of the JEOL 8900 Super Probe at the Geological Inst. of Univ. of Tokyo. and the Mg-rich cores of Y790447 were surveyed with the CMA for Mg, Si, Fe, and Ca (T. Mikouchi).

### Results

Y790447 has been reported to be a eucrite with a few pyroxenes as Mg-rich as diogenite [11]. The major pyroxenes show chemical zoning of type 4. Elemental distribution maps for Mg, Ca, Si, and Fe showed that the Mg-rich pyroxenes were detected as a very small cores in only small numbers of grains and were mantled by brownish Fe-,Ca-rich pigeonite rims similar to ordinary eucrites. The texture and compositions of Y790447 are similar to those of the Y790266 eucrite with type 4 pyroxene [12]. The Mg-rich core of the Y790266 is in the center of a large pigeonite and rimmed by Ca-Fe-rich pyroxene (Type 4) and has been interpreted as a remnant core of chemically zoned pigeonite.

The most Mg-rich portions of pyroxenes in Y790447 (up to  $\text{Ca}_4\text{Mg}_{67}\text{Fe}_{29}$ ) are found as small cores both in pyroxenes with the basaltic textures (Fig. 1a) and in pyroxene fragments set in a matrix of mixtures of breccia matrix and melt (Fig. 1b). The latter pyroxene fragment shows exsolution-like texture. The chemical zoning from the Mg-rich center to Fe-rich rims with nearly constant low-Ca contents are preserved for only a few grain but the chemical trends towards the calcic composition are similar for all zoned Fe-rich pyroxene (Fig. 2). However, an entire texture is still that of basalt (Fig. 1a) and is similar to that of Y790266. The chemical zonings of major pyroxenes ( $\text{Ca}_6\text{Mg}_{35}\text{Fe}_{58}$  to  $\text{Ca}_{37}\text{Mg}_{31}\text{Fe}_{32}$ , Fig. 2) are the same as those found in Y790266 [12]. The existence of a pyroxene grain with lamella texture in a breccia-like matrix texture favors an origin of an unmelted fragment of Mg-rich pyroxenes in type 1-2 monomict eucrites, polymict eucrites or howardites.

The type-4 zoning of the Y790266 pyroxene is from low-Ca to high-Ca compositions along the tie line of the finely exsolved Fe-rich pigeonites of the ordinary eucrites, leaving a large original Mg-rich core as a small Mg-rich remnant spot, which was not homogenized by diffusion of Mg/Fe ions. The Mg-rich core of Y790447 is similar to that of Y790266, but the texture of some fragments looks like a remnant of unmelted fragments of Mg-rich pyroxenes in a breccia, by the textural configuration given above. The diffusion of Fe-Mg also took place between the remnant fragments and the over grown Fe-,Ca-rich pyroxenes.

## Discussion

Combined chronological and mineralogical studies of monomict eucrites revealed that these eucrites (ordinary eucrites) experienced extensive metamorphic events in the early history of the crustal evolution [9,13]. However, such events were overprinted by other features such as impacts [13]. Thus, it has been difficult to decipher the heat sources from the metamorphic records of brecciated eucrites. Yamaguchi et al. [9] proposed that extrusion of lavas is heat sources, because an impact on a small body like Vesta produces only cold breccias. We report mineralogical examination of a eucrite with the evidence of melting in connection with our works on the crustal evolution of eucrites [9,14].

The type 4 pyroxene was primarily ascribed to the remnant of chemical zoning of an originally zoned pyroxene as in the type 1 pyroxene, and was interpreted as a state in the middle of Mg-Fe homogenization. By this assumption, the Mg-rich portion is a remnant of a large Mg-rich core, which was not equilibrated because of its large size. The zoning trend of the rims is towards the Ca-rich pyroxene along the tie line of the exsolved pigeonite. The presence of a Mg-rich core with an exsolution-like texture set in a matrix of mixtures of breccia matrix and melts of Y790447 (Fig. 1b) favors the origin as an unmelted portion of the Mg-rich pyroxenes in eucrites or howardites.

The chemical zoning trends of the pyroxene rims are the same as that of the type 4 pyroxenes. This trend can be explained by the over-growth of calcic pyroxene crystallized from a calcic melt, which is a product without Mg-rich unmelted fragments. We admit a possibility that the present zoning profile is also a product of partial equilibration. If the over growth is from a eucritic partial melt, it will produce the zoning trend the same as the type 1 pyroxene. The absence of such trend suggests that the melt is not an addition of a fresh melt from the next extrusion. The calcic melt can be an impact melt of the fine grained breccia matrix.

The presence of impact melts in eucrites or howardites has been known for some samples, but they are mostly in a form of vein. A good example of such shock melt vein has been reported for Padvarninkai [10]. The presence of maskelynite in Padvarninkai supports the impact origin of the melting. The absence of large scale impact melts in eucrites can be explained by an interpretation that the larger volume of melts prevent rapid cooling and the formation of glasses and facilitates crystallization as in extruded lavas. Mixtures of melts and rapid growth after the mixing have been found in the acicular plagioclase areas in Juvinas [15].

The origin of the HED meteorites should take into account the heat sources for magma ocean and global metamorphism. If we accept the above interpretation of the large scale melting by an impact on the Vest-sized body, we can propose that the heat source for the formation of a thin magma ocean is accretional one. This assumption is good for the case of the model of Ikeda and Takeda [8], in which eucrites were thin scum layers covering the surface of the thin magma ocean, like those covering the surface of the terrestrial lava lakes. Impact into such scum gives favorable heat source for the metamorphism of the monomict breccias, and driving force for stirring of magma to mix cumulates with trapped liquid.

Although we accept that the current size of the Vesta may be too small for the accretional heating to produce a magma ocean, we can still think of the following possibility. The existence of a number of Vesta fragments around the orbit of Vesta implies that the size of Vesta might have been larger to cause accretional heating. Runaway accretion will also help heating the thin surface of Vesta close to the final stage of accretion. Our discovery of a eucrite nearly totally melted described in this paper suggests that an impact can melt considerable portion of the HED body. The presence of magma ocean will help heating the surface materials from beneath for metamorphism. Hyper velocity impacts into the magma ocean, will also help for driving off Na to make calcic plagioclase as was found in A881394 [16] from the chondritic source materials.

In conclusions, (1) the presence of two types of the Mg-rich compositions in different textured areas in Y790447 implies that the Mg-rich cores are the unmelted fragments of the Mg-rich pyroxene fragments. (2) The presence of considerably melted eucrites assure that impacts into the original HED body will raise the surface temperature up to the melting points.

**Acknowledgments:** We acknowledge the NIPR for supplying us with the samples. This work was supported by a grant of the ORI and by a Grant-in-Aid for Scientific Research from the Japanese Ministry of Education, Science and Culture. We are indebted to Dr. T. Ishii and Mr. H. Yoshida for their help in microanalysis at the ORI and Geological Inst., Univ. of Tokyo, and to Drs. A. Yamaguchi, L. E. Nyquist, D. D. Bogard, D. Mittlefehldt and Profs. P. Warren, K. Keil and G. J. Taylor for discussion.

**References:**

- [1] BINZEL R. P., GAFFEY M. J., YHOMAS P. C., ZELNER B. H., STORRS A. W. and WELLS E. (1996) *Icarus*, in press.
- [2] DELANEY J. S., PRINZ M., and TAKEDA H. (1984) *Proc. Lunar Planet. Sci. Conf. 15th, J. Geophys. Res.* **89**, C251-C288.
- [3] TAKEDA H. and GRAHAM A. L. (1991). *Meteoritics* **26**, 129-134.
- [4] TAKEDA H., WOODEN J. L., MORI H., DELANEY J. S., PRINZ M., and NYQUIST L. E. (1983) *Proc. Lunar Planet. Sci. Conf. 14th, J. Geophys. Res.* **88**, B245-B256.
- [5] NYQUIST L. E., TAKEDA H., BANSAL B. M., SHIH C.-Y., WIESMANN H., and WOODEN J. L. (1986) *J. Geophys. Res.* **91**, B8,8137-8150.
- [6] TAKEDA H., MORI H. and BOGARD D.D. (1994a) *Earth Planet. Sci. Lett.* **122**, 183-194.
- [7] STOLPER E. M. (1977) *Geochim. Cosmochim. Acta* **41**, 587-611.
- [8] IKEDA Y. and TAKEDA H. (1985) *Proc. Lunar Planet. Sci. Conf. 15th, J. Geophys. Res.* **90**, C649-C663.
- [9] YAMAGUCHI A., TAYLOR G. J., and KEIL K. (1996) *Icarus* **124**, 97-112.
- [10] NYQUIST L.E., BOGARD D.D., WIESMANN H., SHIH C.-Y., TAKEDA H. and YAMAGUCHI A. (1996) *Meteoritics* **31**, A101-A102.
- [11] YANAI K. and KOJIMA H. (1995) *Catalog of the Antarctic Meteorites*. 230 pp. NIPR, Tokyo.
- [12] TAKEDA H. and YANAI K. (1982) *Mem. Natl. Inst. Polar Res., Spec. Issue* **25**, 97-123.
- [13] BOGARD D. D. (1995) *Meteoritics* **30**, 244-268. [14] NYQUIST, L., BOGARD, D., TAKEDA, H., BANSAL, B., WIESMANN, H. AND SHIH, C.-Y. (1997) *Geochim. Cosmochim. Acta*, in press.
- [15] TAKEDA H., YAMAGUCHI A., KANEOKA I. and NAGAO K. (1997) *Meteoritics and Planet. Sci.*
- [16] TAKEDA H., ISHII T., ARAI T. and MIYAMOTO M. (1997) *Proc. NIPR Symp. Antarct. Meteorites* **10**, in press.

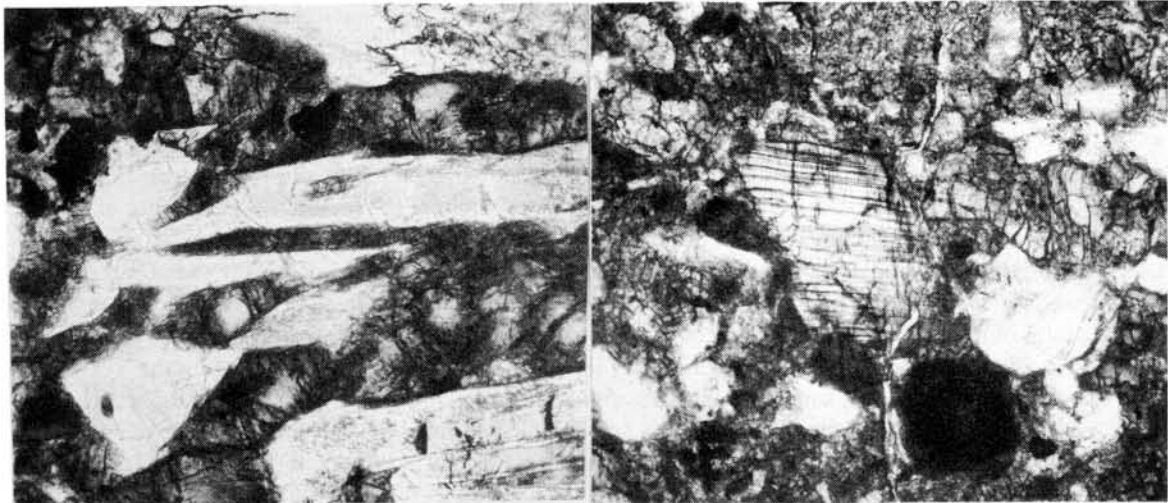


Fig. 1 (a) Basaltic textured area of Y790447. Width is 3 mm. (b) Enlarged view of the Mg-rich core of a pyroxene in Y790447. Width is 1 mm. Parallel light.

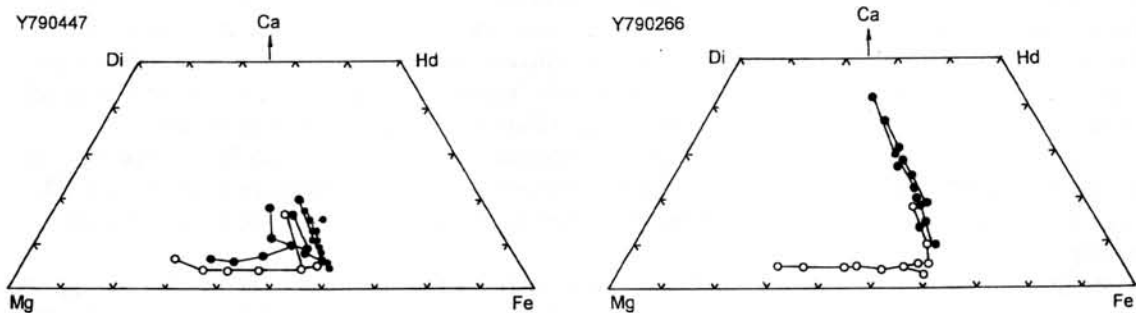


Fig. 2. Pyroxene zoning trends (dotted lines) Y790447 plotted in the pyroxene quadrilaterals. The trends are compared with that of Y790266. Different symbols indicate one traverse.

# Refractory inclusions in the Yamato-86751 CV3 chondrite: II

Hajime Takeda<sup>1</sup> and Hideyasu Kojima<sup>2</sup>, <sup>1</sup>Department of Polar Science, The Graduate University for Advanced Studies, <sup>2</sup>National Institute of Polar Research, 9-10, Kaga 1-chome, Itabashi-ku, Tokyo 173, Japan.

## **Introduction**

Refractory inclusions in chondrites consist mainly of minerals which are predicted to be formed from equilibrium condensation at high temperature by thermodynamic calculation such as spinel, perovskite, and melilite. Because of such mineral assemblages, they have been considered to have many information of the high temperature processes in the early solar nebula.

The Antarctic meteorites show relatively old terrestrial ages compared with non-Antarctic meteorites. This fact indicates possibility that the Antarctic meteorites have been ejected from their parent bodies at different period from non-Antarctic meteorites and different population from non-Antarctic meteorite; difference of region in the solar nebula, parent body or location (or depth) on their parent body. These differences may be reflected in texture, mineralogy, and bulk compositions of refractory inclusions in them. Many studies have performed on the refractory inclusions in non-Antarctic CV3 (especially for Allende meteorite), while few studies have been done on those of Antarctic chondrites.

We have reported three refractory inclusions (98-1/I-1, 99/I-1, and 93-1/I-1) in Yamato-86751 (Y-86751) Antarctic CV3 chondrite [1]. In this study, we have found additional three refractory inclusions (54-4/I-1, I-2, and I-3;) from another thin section which is numbered "54-4" of the Y-86751. We will report petrography of them, in addition to new observations about previously reported three refractory inclusions.

## **Sample Descriptions**

**98-1/I-1;** 98-1/I-1 is 3.9 mm × 3.1 mm in size. It consists mostly of coarse-grained melilites (several hundred μm in size) with minor coarse-grained pyroxenes and euhedral tiny spinel grains (20~30 μm in size). Melilite crystals are located in the margin of the inclusion. Some melilite crystals are oriented nearly perpendicular to the margin of the inclusion. Most of the pyroxenes occur in the center of this inclusion. The modal abundance of melilite and pyroxene are about 79 % and 14%. Spinel crystals are scattered in both melilites and pyroxenes. The modal abundance of spinel is about 5 %. Accessorily, perovskite, metal, and sulfide grains and metal veins are observed as accessory phases. These grains are less than 20 μm in size. Anorthite, nepheline, and sodalite occur as secondary alteration products which replace melilite and they occupy about 2 modal % of the inclusion.

**99/I-1;** 99/I-1 is 2.1 mm × 1.8 mm in size. It consists of core and multi-layered rim. The core

consists of hibonite, spinel and melilite, and contains many voids and cracks. Hibonite and/or spinel is enclosed by melilite. The voids are up to 10  $\mu\text{m}$  in size and show oval or amoeboidal shape. The hibonite crystals show blue color under an optical microscope. Blue hibonites were reported in the "Blue Angel" [2] and refractory inclusions in Murchison CM2 chondrite [3]. The rim is distinguished into five layers (innermost layer 1 to outermost layer 5) by mineral assemblages. Each layers have the thickness of about 20  $\mu\text{m}$ . Spinel in this inclusion contains less than 0.9 wt% of FeO, and olivine contains less than 1.4 wt% of FeO. Any secondary alteration products such as anorthite and nepheline have not been observed in this inclusion.

**93-1/I-1;** 93-1/I-1 is 4.3 mm  $\times$  3 mm in size. It consists mostly of spinel, melilite, and pyroxene with minor perovskite, metal, and sulfide grains. This inclusion can be divided into three portions by their textures; nodular portion, fine-grained portion, and FTA-like portion. The nodular portion is cluster of some nodules. The FTA-like portion shows a texture that is observed in the margin of "fluffy" type A inclusions (FTA's) in the Allende meteorite mentioned by [4], but is different in the point that it contains Al- and Ti-rich pyroxene. The rim which occurs on the FTA-like portion also resemble to that of the FTA's in the Allende. Spinel shows compositional zoning in Fe perpendicular to some cracks and contains up to 14.4 wt% of FeO. Anorthite and alkali-rich phase (probably nepheline and sodalite) have been observed in the fine-grained portion and FTA-like portion.

**54-4/I-1;** 54-4/I-1 is 150  $\times$  270  $\mu\text{m}$  in size. It consists mainly of spinel, pyroxene, melilite, and enclosed by a rim. Spinel shows high Fe content (20.4 ~ 24.3 wt% of FeO) and no compositional zoning. Pyroxene and melilite occur among spinel grains. The rim consists of pyroxene and is about 5  $\mu\text{m}$  in thickness. Pyroxene which occurs in interior of the inclusion contains 19.7 ~ 26.6 wt% of  $\text{Al}_2\text{O}_3$  and 4.9 ~ 10.1 wt% of  $\text{TiO}_2$  while that occurs in the rim contains less than 12.2 wt% of  $\text{Al}_2\text{O}_3$  and 4.3 wt% of  $\text{TiO}_2$ . Melilite contains 82 ~ 90 mol% of gehlenite component. A phase which appears as bright portion under a back scattered electron image occurs in some places inside of the rim. These area is 10 ~ 20  $\mu\text{m}$  in size. Analyzed data of them seem to be mixture of olivine and spinel. Alkali-rich phase (probably nepheline) occurs in the interior of the inclusion.

**54-4/I-2;** 54-4/I-2 is 300  $\times$  200  $\mu\text{m}$  in size. It consists mostly of spinel and pyroxene, and enclosed by a rim. It seems to be aggregates of individually rimmed objects. Interior of the inclusion shows porous texture. Spinel crystals appear as euhedral grains and less than 5  $\mu\text{m}$  in size. Pyroxene fills up among the spinel grains. The rim is about 5  $\mu\text{m}$  in thickness and consists of pyroxene. Spinel in this inclusion contains 22.1 ~ 26.5 wt% of FeO. Pyroxene occurs in interior of the inclusion contains 19.5 ~ 23.8 wt% of  $\text{Al}_2\text{O}_3$  and 7.2 ~ 13.8 wt% of  $\text{TiO}_2$  while that in the rim contains 9.1 wt% of  $\text{Al}_2\text{O}_3$  and 1.1 wt% of  $\text{TiO}_2$ . Alkali-rich phase (probably nepheline) is observed in some voids in the interior of the inclusion.

**54-4/I-3;** 54-4/I-3 is about 300  $\times$  200  $\mu\text{m}$  in size and shows irregular shape. It consists mostly of

spinel and pyroxene. This inclusion is also enclosed by a rim. The rim is less than 5 $\mu$ m in thickness and consist of pyroxene. Spinel contains less than 4.4 wt% of FeO. Pyroxene occurs in interior of the inclusion contains 12.4 ~ 20.7 wt% of Al<sub>2</sub>O<sub>3</sub> and 3.6 ~ 9.5 wt% of TiO<sub>2</sub>. Pyroxene in the rim contains less than 10.0 wt% of Al<sub>2</sub>O<sub>3</sub> and 0.8 wt% of TiO<sub>2</sub>. Any alkali-rich phase have not been observed in this inclusion.

### **Discussion**

Various type of refractory inclusions have observed in the Y-86751 chondrite. There are some differences from refractory inclusions in the Allende. Firstly, the Y-86751 contains less amount of large inclusion compared with the Allende which commonly contains refractory inclusions over 1 cm in size. Secondly, typical "fluffy" type A inclusions, which have been commonly observed in the Allende, have not been observed in Y-86751. On the other hand, inclusions which contain Al-, and Ti-rich pyroxene is abundant. Thirdly, refractory inclusions in the Y-86751 contain less amount of secondary alteration products compared with similar type inclusions in the Allende. In addition, grossular, which is usually observed as secondary alteration products in the Allende inclusions [5], have not been observed in any refractory inclusions in the Y-86751.

### **References**

[1] Takeda Ha. and Kojima H. (1996) *Ant. Met.* 21, 173-175. [2] Armstrong J. T. et al. (1982) *GCA.* 46, 575-595. [3] MacPherson G. J. et al. (1983) *GCA* 47, 823-839. [4] MacPherson G. J. and Grossman L. (1984) *GCA.*48, 29-46. [5] MacPherson G. J. et al. (1988) In "*Meteorites and The Early Solar System*", Univ. of Arizona Press 746-807.

# A Search for the Q-Nitrogen: Nitrogen and rare gas isotopes in Yamato-791717 (CO3).

TANIGUCHI Yoshinobu and HASHIZUME Ko

Department of Earth and Space Science, Graduate School of Science,  
Osaka University, Toyonaka 560, JAPAN

## *Introduction*

A major fraction of heavy rare gases (Ar, Kr and Xe) in primitive carbonaceous chondrites is sited in the phase-Q [1-3], whose host phase is poorly characterized. The phase-Q is insoluble by non-oxidizing acids but is lost by oxidation. Rare gases in the phase-Q have been studied well. The phase-Q commonly exists among both primitive carbonaceous chondrites and ordinary chondrites [4-6]. Nitrogen in the phase-Q may reflect a common nitrogen component existed in the primitive solar nebula. Murty (1996) reported that nitrogen in the phase-Q (in Dhajala) possess a  $\delta^{15}\text{N}$  value of  $-15\text{‰}$  [7]. Since concentrations of rare gas in the phase-Q in carbonaceous chondrites are higher than in ordinary chondrites [4-6], we planned to determine isotopic composition of Q-nitrogen involving systematic chemical treatments and step wise combustion technique.

## *Sample and Experiments*

An Antarctic meteorite Yamato-791717 (CO3) was used in this study. This meteorite was not affected by shock but experienced mild metamorphism. Yamato-791717 is classified as a "normal" CO chondrite. "Normal" CO chondrites contain only small amounts of micro diamonds and negligible amounts of silicon carbide.

An acid residue of Yamato-791717 was prepared by the Chicago procedure [1, 4, 8]. We crushed about 8 g of this meteorite to 0.1 mm size. The crushed sample was treated with 1M HCl + 10M HF and 6M HCl alternately. At the end of this cycle, the residue was washed with 3M HCl and 0.1M HCl successively.

Nitrogen, rare gases (Ne, Ar, Kr and Xe) and carbon in Yamato-791717 were extracted using step wise combustion technique. Gases were analyzed by a static quadrupole mass spectrometer (BALZERS QMG421). This mass spectrometer installed in Osaka university is tuned for precise nitrogen and rare gases isotopic measurement. The reproducibility of the  $\delta^{15}\text{N}$  value is about 1‰ when we measure  $\sim 1$  ng of standard air  $\text{N}_2$ . The amount of combusted carbon in the form of  $\text{CO}_2$  was also measured by a calibrated pirani gauge.

## *Results and Discussion*

The step wise combustion results of nitrogen and  $^{36}\text{Ar}$  in the bulk meteorite are shown in Fig1. The maximum nitrogen release peak appear at  $750^\circ\text{C}$ . The  $\delta^{15}\text{N}$  value observed here is  $-137 \pm 3\text{‰}$ . The  $^{36}\text{Ar}$  major release peak appears at the same temperature.

The major release of  $^{84}\text{Kr}$  and  $^{132}\text{Xe}$  appear at slightly higher temperature, at  $850^\circ\text{C}$  and  $900^\circ\text{C}$ , respectively. This tendency that heavier rare gases are released at higher temperature by stepped combustion was also observed in the case of Allende matrix [9].

Subsequently, an acid (HF/HCl) residue of Yamato-791717 was prepared. The acid residue weighs 0.39 wt% of the original bulk meteorite. It contains about 63% (nitrogen), 16% ( $^{36}\text{Ar}$ ), 36% ( $^{84}\text{Kr}$ ) and 36% ( $^{132}\text{Xe}$ ) of the bulk meteorite. The major nitrogen release peak appears at  $750^\circ\text{C}$  (Fig 2). The  $\delta^{15}\text{N}$  value observed here is  $-57.7 \pm 1.9\%$ . The minimum  $\delta^{15}\text{N}$  value (about  $-200\%$ ) appears at  $500\sim 550^\circ\text{C}$  however the nitrogen release is very small. The low  $\delta^{15}\text{N}$  values in these fractions can be explained by contribution of the light nitrogen originating from micro diamonds, whose  $\delta^{15}\text{N}$  value is estimated to be  $-359.5 \pm 0.8\%$  [10]. From the rare gas data, total amounts of released  $^{36}\text{Ar}$  is about  $2 \times 10^{-5}$  ccSTP/g. This  $^{36}\text{Ar}$  quantity is roughly equal to the  $^{36}\text{Ar}$  quantity in acid residues of other "normal" CO<sub>3</sub> carbonaceous chondrites [5]. Therefore we consider that the majority of the  $^{36}\text{Ar}$  in our acid residue is the Q-component argon. Heavy rare gases of acid residue have several release peaks. This result suggests that the phase-Q may actually consist of multiple phases, which are combusted at different temperatures. Unlike the release pattern observed in the bulk meteorite, there is a good peak-to-peak correlation among the release patterns of  $^{36}\text{Ar}$ ,  $^{84}\text{Kr}$  and  $^{132}\text{Xe}$ . The Q-phase (in the bulk meteorite) may be protected by other phases which are soluble by acid.

We do not have the answer yet which component observed in the acid residue is the Q-nitrogen. We plan to proceed to further chemical treatments (oxidation and gravity separation) using the acid residue. The results will be reported at the meeting.

#### Reference

- [1] Lewis R.S., Srinivasan B. and Anders E. (1975) *Science*. 190, 1251-1262.
- [2] Lewis R.S., Gross J. and Anders E. (1977) *J. Geophys. Res.* 82, 779-792.
- [3] Reynolds J.H., Frick U., Neil J.M. and Phinney D.L. (1978) *Geochim. Cosmochim. Acta* 42 1775-1797
- [4] Alaerts L., Lewis R.S. and Anders E. (1979) *Geochim. Cosmochim. Acta* 43 1399-1415
- [5] Alaerts L., Lewis R.S. and Anders E. (1979) *Geochim. Cosmochim. Acta* 43 1421-1432
- [6] Matsuda J., Lewis R.S., Takahashi H. and Anders E. (1980) *Geochim. Cosmochim. Acta* 44 1861
- [7] Murty S.V.S. (1996) *Earth and Planetary Science Letters* 141 307-313
- [8] Amari S., Lewis R.S. and Anders E. (1994) *Geochim. Cosmochim. Acta* 58 459-470
- [9] Frick U. and Pepin R.O. (1981) *Earth and Planetary Science Letters* 56 45-63
- [10] Russell S.S., Arden J. W. and Pillinger C.T. (1996) *Meteoritics & Planetary Science* 31 343-355

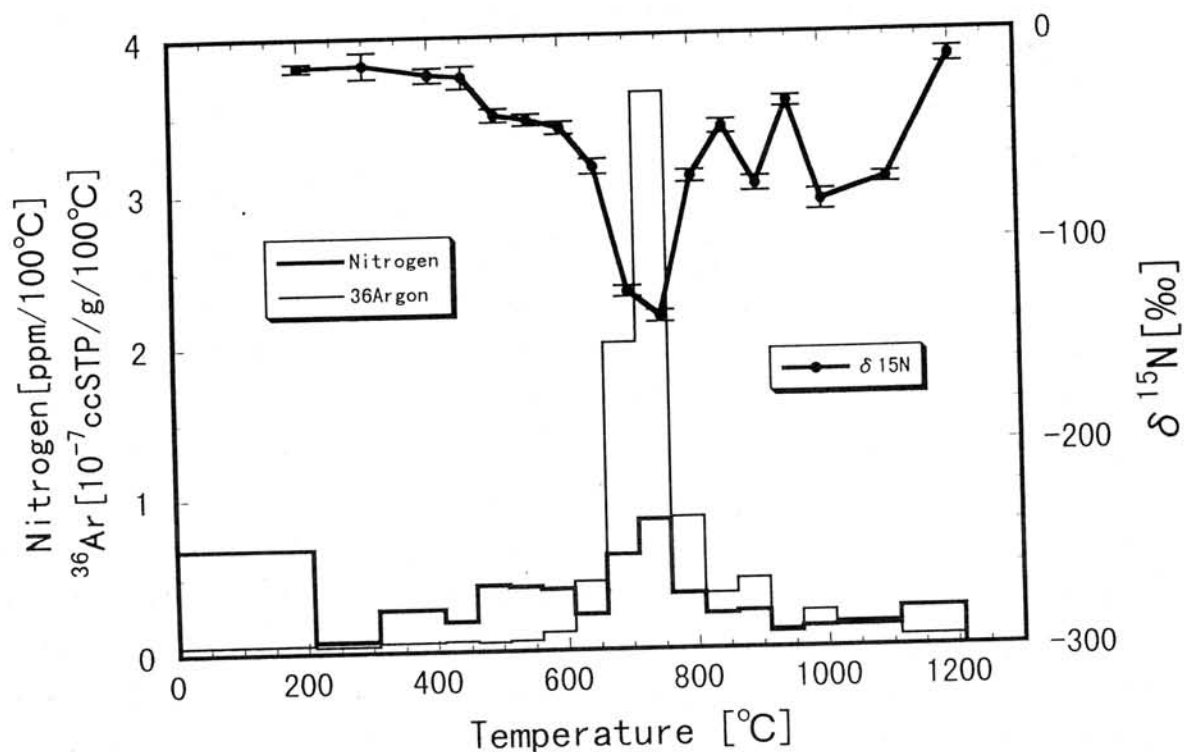


Fig.1 Step wise combustion results of the Yamato-791717 bulk meteorite  
Filled circles connected with lines, bold line and thin line denote  
nitrogen isotopic ratio, nitrogen concentration and argon concentration, respectively.

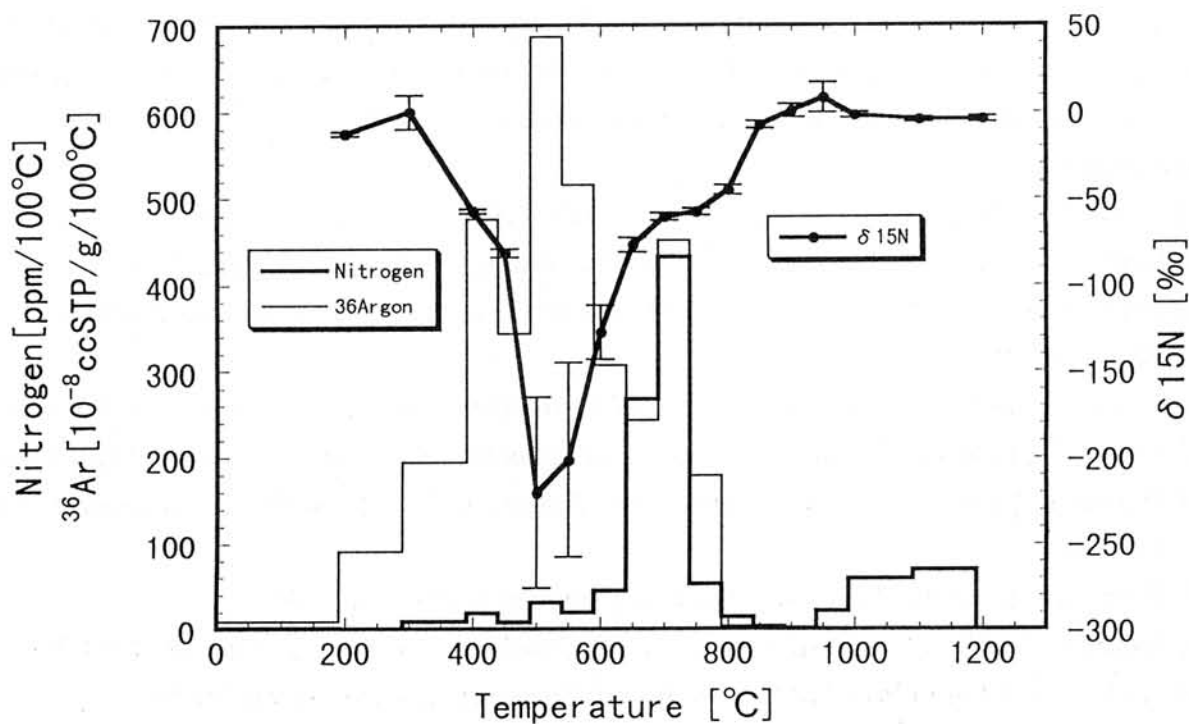


Fig.2 Step wise combustion results of the acid residue of Yamato-791717  
Filled circles connected with lines, bold line and thin line denote  
nitrogen isotopic ratio, nitrogen concentration and argon concentration, respectively.

## EVIDENCE FOR FLUIDIZATION DUE TO WATER MIGRATION IN A DARK INCLUSION IN THE VIGARANO CV3 CHONDRITE

K. Tomeoka and T. Kojima

Department of Earth and Planetary Science, Faculty of Science, Kobe University,  
Nada, Kobe 657, Japan

It has recently been suggested that dark inclusions (DIs) in CV3 chondrites were affected by extensive aqueous alteration and subsequent dehydration on the meteorite parent body [1-4]. There is also growing evidence that the bulk of the CV3 chondrites were involved in various degrees of aqueous alteration [5-9]. Some DIs contain chondrules, CAIs and/or their pseudomorphs, which are products of dehydration of aqueously altered chondrules and CAIs. The size distribution and the abundances of the chondrules, CAIs and their pseudomorphs suggest that the DIs were formerly lithic clasts of chondritic material, most likely to be the host CV3 chondrites [3]. This implies that there was a local region (or regions) in the CV parent body that was once involved in extensive aqueous activity.

In contrast to most DIs, an unusual DI (AMNH 2226-7) has been reported from Vigarano [10], which consists almost exclusively of fine grains ( $<5\ \mu\text{m}$  in diameter) mainly of Fe-rich olivine ( $\text{Fo}_{49-57}$ ) and are devoid of chondrules, CAIs, and their pseudomorphs. This DI has an especially unusual texture, i. e. a network of almost *en echelon* arcuate bands, some crosscutting one another. Such a texture has never been reported from any other meteorite. At the last year's NIPR Symposium, we described the mineralogical and petrographic details of AMNH 2226-7, but could not propose a confident model to explain the formation process of this DI [11]. At this Symposium, we present our discovery of a terrestrial analogue of the arcuate band texture and discuss formation process of this DI.

Arcuate bands appear bright and distinctive in backscattered electron images (Fig. 1). Two or more bands occur roughly parallel, forming a set of successive parallel bands. The bands typically range in apparent thickness from 0.05 to 0.3 mm and in length from 1.0 to 3.5 mm. The boundary between a band and the matrix is sharp on the convex side of each arc, while it is commonly gradational on the concave side. The gradation is due to a decrease in the abundance of Fe-rich olivine grains away from the contact. The bands are composed mainly of fine grains of Fe-rich olivine, which are relatively smaller, more densely packed, and slightly more enriched in Fe than those in the interband areas ( $\text{Fo}_{49-54}$  vs.  $\text{Fo}_{51-57}$ ).

AMNH 2226-7 has been studied by several investigators [11,12], but its origin has remained unknown. In our extensive survey we found the arcuate bands to be closely similar to the "dish structure" which is commonly observed in terrestrial siltstone and sandstone sediments, especially turbidite sequences [13] (Fig. 2). Dish structure is defined by the presence of thin, dark-colored, subhorizontal, flat to concave-upward laminations which range in thickness from sharp lines  $<0.2$  mm to diffuse zones up to 2 mm, and in width from  $<1$  to  $>50$  cm [13]. Dish structure is always found in association with finer-grained clay or organics, and the dark lines are enriched in these materials. The grain size of sands just above the dark clay-rich lines slightly increases, and the amount of clay tends to decrease upward, exhibiting a distinct gradation.

These textural characteristics closely resemble the arcuate bands in AMNH 2226-7, suggesting that a similar mechanism was involved in the formation of these materials. Dish structure has been studied by many investigators [13-17], and most of them agree that it is a secondary structure formed during the consolidation of unconsolidated deposits and its fundamental mechanism is governed by fluidization of granular aggregates. Fluidization in this case is regarded to be the process that occurs when a fluid flowing vertically through a

granular aggregate exerts drag forces on the grains to lift or suspend them against the force of gravity [18]. Various modification structures are known to form during the fluidization, which include the direct rearrangement of sediment grains and the deformation of hydroplastic, liquefied or fluidized sediments in response to external stresses [18].

If the proposal that there was extensive aqueous activity in some CV chondrites [1-4] is correct, the CV parent body can be regarded as having been initially accreted as a mixture of stone (and/or dust) and ice, as modelled for the CI and CM parent bodies [19]. In such primitive bodies, most of stony materials would initially have been composed of unconsolidated, loosely packed aggregates of grains. In the process of parent body growth, as heating developed, a large redistribution of water in the interior of the parent body would have occurred. With sufficient heating, water residing in the spaces between the grains would have become gravitationally unstable and undergone convection [19], and in such an environment, it is expected that the grains would have been fluidized and various sedimentary processes would have taken place in response to permeable water flow. The present study reveals the first evidence suggesting that such processes did indeed occur within the carbonaceous chondrite parent body.

*Acknowledgements-* We thank Dr. M. Prinz for providing the AMNH 2226-7 sample and Drs. R. Hutchison and T. Tsuji for helpful discussion. This work was supported by Grant-in-Aid of Japan Ministry of Education, Science and Culture.

## REFERENCES

1. T. Kojima, K. Tomeoka, K., H. Takeda, *Meteoritics* 28, 649 (1993).
2. A.N. Krot, E.R.D. Scott, M.E. Zolensky, *Meteoritics* 30, 748 (1995).
3. T. Kojima and K. Tomeoka, *Geochim. Cosmochim. Acta* 60, 2651 (1996).
4. A.N. Krot, E.R.D. Scott, M.E. Zolensky, *Meteoritics & Planet. Sci.* 32, 31 (1997).
5. K. Tomeoka and P.R. Buseck, *Geochim. Cosmochim. Acta* 54, 1745 (1990).
6. L.P. Keller and P.R. Buseck, *Geochim. Cosmochim. Acta* 54, 2113 (1990).
7. L.P. Keller et al., *Geochim. Cosmochim. Acta* 58, 5589 (1994).
8. M.R. Lee, A.L. Graham, R. Hutchison, *Meteoritics & Planet. Sci.* 31, 477 (1996).
9. A.J. Brearley, *Lunar Planet. Sci. XXVIII (Abstr.)* (1997).
10. C.A. Johnson et al., *Geochim. Cosmochim. Acta* 54, 819 (1990).
11. T. Kojima and K. Tomeoka, *Antarctic Meteorites XXI (Abstr.)* 74 (1996).
12. M.E. Zolensky et al., *Lunar Planet. Sci. XXVII, 1507 (Abstr.)* (1996).
13. D.R. Lowe and R.D. LoPiccolo, *J. Sed. Petrol.* 44, 484 (1974).
14. P.H. Sauffer, *J. Sed. Petrol.* 37, 487 (1967).
15. K.D. Corbett, *Sedimentology* 19, 99 (1972).
16. J.R.L. Allen, in *Sedimentary Structures, Vol. II*, 367 (Elsevier, 1982).
17. T. Tsuji and Y. Miyata, *J. Geol. Soc. Japan* 93, 791 (1987).
18. D.R. Lowe, *Sedimentology* 22, 157 (1975).
19. R.E. Grimm and H.Y. McSween, *Icarus* 82, 244 (1988).

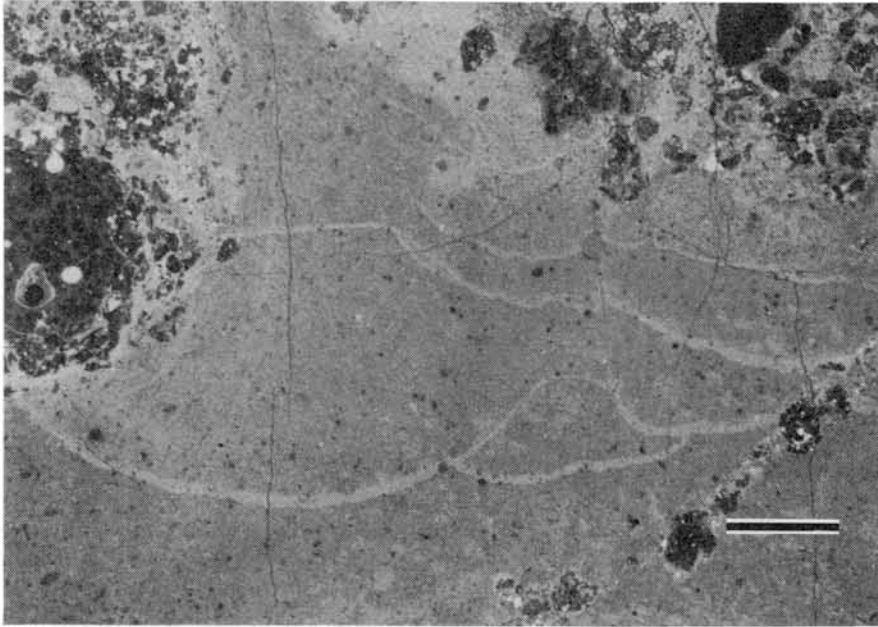


Fig. 1 A back-scattered electron image of Dark inclusion AMNH 2226-7 including arcuate bands (bright bands). Scale bar = 0.5 mm



Fig. 2 A photograph of a vertical section of a terrestrial sandstone with dish structure from the Tertiary Nichinan Group (see ref. 17). Scale bar = 30 mm

# EVAPORATION RATES OF FORSTERITE IN THE PRIMORDIAL SOLAR NEBULA

TSUCHIYAMA Akira, and TACHIBANA Shogo

Department of Earth and Space Science, Osaka University, Toyonaka 560, JAPAN

## Introduction

Evaporation is one of the most important process for chemical and isotopic fractionation in the primordial solar nebula as well as condensation. In this consequence, experimental studies on evaporation of forsterite, one of the most important Mg-silicates, have been done in vacuum [1, 2] and H<sub>2</sub>-rich conditions [3, 4]. It has been known from these experiments that forsterite evaporates congruently, and the measured evaporation rates are less than those estimated from vapor pressures in equilibrium with forsterite. Nagahara and Ozawa [3] discussed evaporation behavior of forsterite dust and accompanied isotopic mass fractionation in the primordial solar nebula by using their experimental data in H<sub>2</sub> gas. However, the evaporation rates were obtained in the experiments, where only H<sub>2</sub> were present, while O-bearing molecules (e.g., H<sub>2</sub>O), which affects forsterite evaporation, must be present in the primordial solar nebula. Accordingly, evaporation rates of forsterite in the primordial solar nebula should be generally different from those in the experiments. In the present study, evaporation rates of forsterite in the primordial solar nebula were estimated based on the previous experimental results by taking O-bearing molecules in the nebula into consideration.

## Models

Evaporation rates of forsterite (Mg<sub>2</sub>SiO<sub>4</sub>) can be obtained by Hertz-Knudsen equation. The evaporation flux of each elements,  $j_E$ , are generally expressed as follows:

$$j_E = \alpha \sum_i \frac{\nu_{E_i} (p_{E_i}^e - p_{E_i})}{\sqrt{2\pi m_{E_i} kT}} \quad (E=\text{Mg, Si, and O}), \quad (1)$$

where  $\alpha$  is the evaporation coefficient,  $\nu_{E_i}$ , the stoichiometric coefficient (the number of the element E in  $i$ -th gas species),  $p_{E_i}^e$ , the vapor pressure of  $i$ -th species in equilibrium with forsterite at temperature  $T$ ,  $p_{E_i}$ , the partial pressure in an ambient gas,  $m_{E_i}$ , the mass of  $i$ -th species, and  $k$ , the Boltzmann constant.  $\alpha$  is usually less than unity ( $0 < \alpha \leq 1$ ), and the evaporation occurs ideally at the maximum rate without any kinetic constraints.  $p_{E_i}^e$ 's are related to the free energy of formation, and can be calculated from thermodynamic data [5]. Because forsterite evaporates congruently,

$$j_{\text{Mg}}/j_{\text{Si}} = 2, \text{ and } j_{\text{O}}/j_{\text{Si}} = 4. \quad (2)$$

By solving Eqs.(1) and (2), we can obtain  $j_E$ , and thus the evaporation flux of forsterite,  $j_{\text{Fo}}$  ( $= j_{\text{Si}}$ ), as a function of  $p_{E_i}$  and partial pressures of other species in an ambient gas which are not included in Eq.(1).

**(1) Experimental conditions.** Under the experimental conditions in vacuum and in H<sub>2</sub> gas at low pressures ( $\leq 10^{-3}$  bar), thermodynamic calculations show that Mg, SiO, H<sub>2</sub>O, O<sub>2</sub>, O, OH, H<sub>2</sub> and H are major gas species in equilibrium with forsterite. The total pressure,  $P_{\text{total}}$ , is

$$P_{\text{total}} = P_{\text{H}_2} + P_{\text{H}} \quad (3)$$

as long as residual gas species by evacuation can be ignored. Because the experiments were done under evacuated conditions, partial pressures of other species can be regarded as zero. It should be noted that Nagahara and Ozawa [3] calculated  $j_{\text{Fo}}$  by ignoring  $p_{\text{H}_2}$  and  $p_{\text{H}}$  in the region where  $P_{\text{total}}$  is less than the equilibrium pressure of forsterite,  $p_{\text{Fo}}^e$  ( $\approx p_{\text{Mg}}^e + p_{\text{SiO}}^e + p_{\text{O}_2}^e + p_{\text{O}}^e$ ). However, this is incorrect because ambient gas of H<sub>2</sub> and H is present even under such

conditions.

(2) **Solar nebula conditions.** O, He and C are also taken into consideration as major elements in the nebula. S may be another important element as SiS molecules, but was not included here because  $p_{SiS}^e$  becomes important only at low temperatures ( $\leq 1000\text{K}$ ). The abundances of He and C are expressed as follows:

$$[X]/[H] = \sum v_{X_i} p_{X_i} / \sum v_{H_i} p_{H_i} \quad (X=\text{He and C}), \quad (4)$$

where  $p_{X_i}$  and  $p_{H_i}$  are partial pressures of gas species including X and H, respectively. For O abundance,

$$([O] - 2[Si] - [Mg])/[H] = \sum v_{O_i} p_{O_i} / \sum v_{H_i} p_{H_i}, \quad (5)$$

where it is assumed that Si and Mg are present as solid compounds of  $\text{SiO}_2$  and  $\text{MgO}$ . Thermodynamic calculations show that  $\text{H}_2$ , H, He, CO and  $\text{H}_2\text{O}$  are the major gas species at  $T = 1000 - 2000\text{K}$  and  $p_{\text{total}} = 10^{-10} - 1\text{bar}$  for the solar abundance of the elements, and Mg, SiO,  $\text{H}_2\text{O}$ ,  $\text{O}_2$  and O are the major species in equilibrium with forsterite. Thus, the total pressure is

$$p_{\text{total}} = p_{\text{H}_2} + p_{\text{H}} + p_{\text{He}} + p_{\text{CO}} + p_{\text{H}_2\text{O}} \quad (6)$$

in the beginning of the evaporation ( $p_{\text{Mg}} = p_{\text{SiO}} = 0$ ). If the evaporation took place in a closed system,  $p_{\text{Mg}}$  and  $p_{\text{SiO}}$  should be taken into consideration as the evaporation proceeds.

## Results and discussion

(1) **Experimental conditions.** The solution can be obtained analytically although the expression is very complicated. Fig.1a shows the ideal  $j_{\text{Fo}}$  calculated with  $\alpha = 1$  together with experimental data [1-4]. At constant temperatures, (i)  $j_{\text{Fo}}$  is almost constant irrespective of  $p_{\text{total}}$  at  $p_{\text{total}} < p_{\text{Fo}}^e$  (forsterite evaporates mainly as Mg, SiO,  $\text{O}_2$  and O, and  $\text{H}_2$  does not affect  $j_{\text{Fo}}$  in this H-poor region), and (ii)  $j_{\text{Fo}} \propto j_{\text{total}}^{1/2}$  at  $p_{\text{total}} > p_{\text{Fo}}^e$  (forsterite evaporates mainly as Mg, SiO and  $\text{H}_2\text{O}$ , or  $\text{H}_2$  affects  $j_{\text{Fo}}$  as a reducing agent). Because  $p_{\text{Fo}}^e$  decreases with decreasing  $T$ , the area of constant  $j_{\text{Fo}}$  diminishes with decreasing  $T$ . We will obtain  $\alpha$  by comparing the ideal rates with the experimental data. Strictly speaking, the evaporation coefficients for each gas species,  $\alpha_{E_i}$ , should be taken into consideration as in [6] for FeS. However, the data are not enough for forsterite, and thus the overall evaporation coefficient of  $\alpha = 0.1$  irrespective of  $T$  and  $p_{\text{total}}$  is adopted here. The errors are within the factor of about three (Fig.1b), and this value of  $\alpha$  was used for  $j_{\text{Fo}}$  in the nebula.

(2) **Solar nebula conditions.** The solution can be obtained only numerically. The calculated  $j_{\text{Fo}}$  with  $\alpha = 0.1$  is shown in Fig.2a. Three modes are recognized as shown in Fig.2a; (i) constant  $j_{\text{Fo}}$  at  $p_{\text{total}} < p_{\text{Fo}}^e$ , (ii)  $j_{\text{Fo}} \propto j_{\text{total}}^{1/2}$  at  $p_{\text{Fo}}^e < p_{\text{total}} < p_{\text{total}}^*$ , and (iii) constant  $j_{\text{Fo}}$  at  $p_{\text{total}} > p_{\text{total}}^*$ . The regions (i) and (ii) are similar to those in the experimental conditions (Fig.1), but in the mode (iii)  $\text{H}_2$  does not act as a reducing agent because  $p_{\text{H}_2\text{O}}^e/p_{\text{H}_2} \approx p_{\text{H}_2\text{O}}/p_{\text{H}_2} = \text{const.}$  (forsterite evaporates mainly as Mg, SiO and  $\text{H}_2\text{O}$  in this region too).  $p_{\text{total}}^*$  is the total pressure which divides the modes (ii) and (iii), and decreases with decreasing  $T$ . Thus, the region (iii) appears at lower temperatures. The calculated  $j_{\text{Fo}}$  is also plotted in the  $p_{\text{total}} - T$  conditions together with those estimated in the nebula at the active stage [6] in Fig.2b. It is expected from the diagram that forsterite evaporates with the modes (ii) and (iii) in the inner and outer regions of the nebula (the boundary is 0.2-1.0 AU depending on models), and the mode (i) does not appear. Life time of forsterite dust, kinetic effects on the evaporation behavior in the dynamic nebula, and isotopic mass fractionation will be discussed from the present results.

**References:** [1] Hashimoto (1990) *Nature*, **347**, 53. [2] Wang *et al* (1993) *L.P.S.*, **XXIV**, 1479. [3] Nagahara and Ozawa (1996) *G.C.A.*, **60**, 1445. [4] Takahashi (1995) Master Thesis of Osaka Univ. [5] Chase *et al.* (1985) JANAF Thermochemical Tables, 3rd Ed., pp.1856. [6] Tachibana and Tsuchiyama, *in prep.*

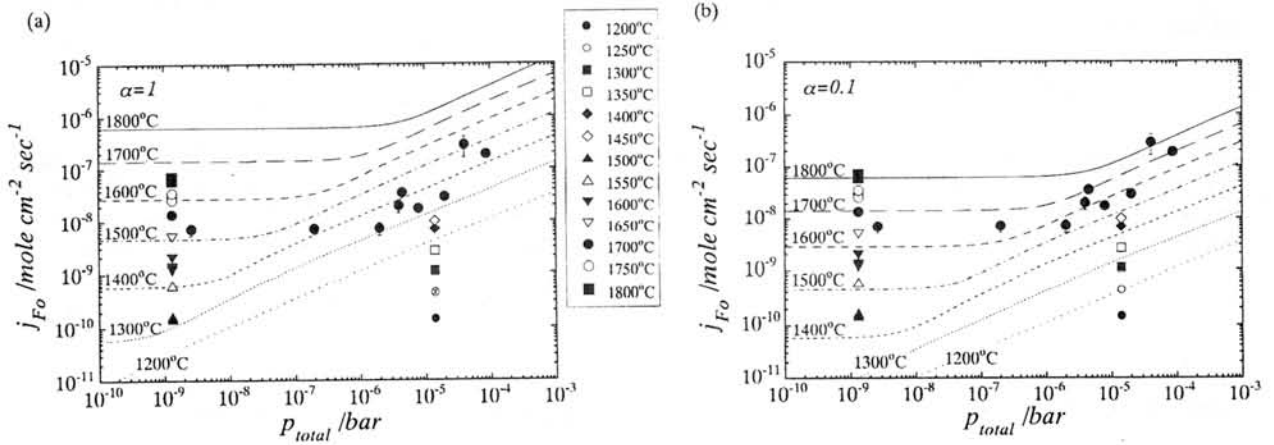


Figure 1. Calculated evaporation rate of forsterite,  $j_{Fo}$ , under experimental conditions together with experimental data [1-4]. (a) Ideal  $j_{Fo}$  calculated with  $\alpha = 1$ . (b)  $j_{Fo}$  calculated with  $\alpha = 0.1$ .

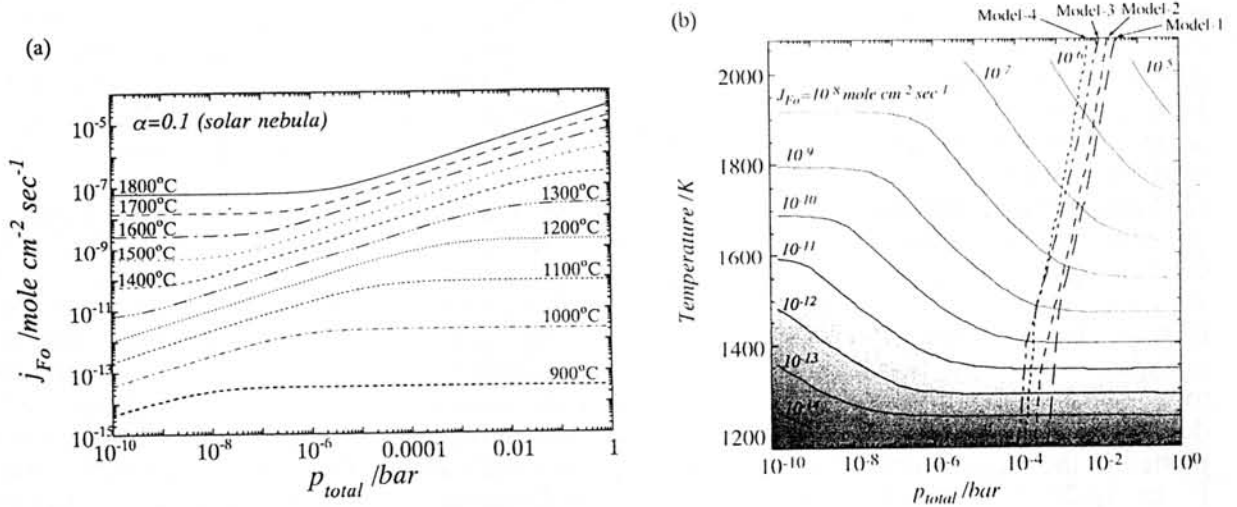


Figure 2. Calculated evaporation rate of forsterite,  $j_{Fo}$ , with  $\alpha = 0.1$  under nebula conditions. (a)  $j_{Fo}$  plotted against  $P_{total}^*$  at each  $T$ . (b)  $j_{Fo}$  plotted in the  $P_{total} - T$  conditions together with those estimated in the nebula at the active stage (1176, 678, 420 and 1573 K at 1 AU, and 1661, 1356, 840 and 1910 K at 0.5 AU in the models 1, 2, 3 and 4, respectively) [6].

**TRACE ELEMENT DISTRIBUTIONS IN YAMATO 793605, A CHIP OFF THE "MARTIAN LHERZOLITE" BLOCK.** <sup>1</sup>Meenakshi Wadhwa, <sup>2</sup>Gordon McKay, and <sup>3</sup>Ghislaine Crozaz. <sup>1</sup>Department of Geology, The Field Museum, Roosevelt Rd. at Lake Shore Dr., Chicago, IL 60302, USA; <sup>2</sup>Mineralogical Institute, Graduate School of Science, University of Tokyo, 7-3-1 Hongo, Bunkyo-ku, Tokyo 113, Japan, and Mail Code SN4, NASA Johnson Space Center, Houston, TX 77058, USA; <sup>3</sup>McDonnell Center for the Space Sciences and Department of Earth and Planetary Sciences, Washington University, St. Louis, MO 63130, USA.

**Introduction.** The SNC meteorites are believed to have originated on the planet Mars ([1] and references therein) and, until there is a sample return from this planet, they represent the only samples of the martian crust accessible for laboratory studies. As such, they can provide valuable insights regarding the geological evolution of this planet. Since there are only a few meteorites of putative martian origin (currently a total of 12), recognition of new SNC meteorites is, therefore, of great interest to meteoriticists and planetary scientists. Y793605 was only recently identified as belonging to the SNC group [2] and a consortium was organized by the NIPR to systematically study this meteorite [3]. Preliminary petrographic and geochemical studies Y793605 (hereon referred to as Y79) indicate that it most closely resembles the lherzolitic shergottites, ALH77005 and LEW88516 [4,5,6,7]. We made ion microprobe analyses of trace and minor element microdistributions in minerals of Y79; the results of this study are reported here.

**Sample Description and Analytical Methods.** We were allocated a thin section of Y79 by the NIPR consortium (Y793605, 51-4). This section is composed predominantly (>90%) of a *poikilitic* region consisting of sub-mm sized olivine grains enclosed within a large pyroxene oikocryst (~6 mm across, composed of a zoned pigeonite grain surrounded by a rim of augite), but there is also a small *non-poikilitic* region that is composed of smaller grains of pyroxene (mostly pigeonite), olivine, maskelynite and opaque minerals. The thin section was characterized by X-ray elemental mapping of major and minor elements, followed by quantitative analyses of various minerals with the Cameca SX-100 electron microprobe at the Johnson Space Center. Subsequently, trace and minor element analyses were made on several spots (selected on the basis of the electron microprobe analyses) with the Washington University modified Cameca IMS-3f secondary ion mass spectrometer.

It should be noted that we were unable to locate any Ca-phosphate minerals in our section, despite extensive mapping with the electron microprobe. However, this does not mean that there is no Ca-phosphate in this rock. In fact, Mittlefehldt et al. [7] reported the occurrence of "partly decomposed" Ca-phosphates, probably originally of igneous origin, in their sample of Y79.

**Results.** In the poikilitic region, we made ion microprobe analyses on 1 olivine, 12 pigeonite, and 2 augite spots. We also measured the REE abundances of a glassy region within a melt inclusion present in a poikilitically enclosed olivine grain. In the non-poikilitic region, we analysed individual grains of maskelynite (1), olivine (1), and pigeonite (6).

Fig. 1 presents representative REE abundances in minerals of Y79 (filled symbols). For comparison, REE concentrations in minerals of the lherzolitic shergottite ALH77005 [8] (hereafter referred to as ALH) are also shown (open symbols). Note that HREE in maskelynite and LREE in olivine are not shown since these REEs are present in these minerals below the detection limit of the ion microprobe. It can be seen that REE abundances in maskelynite and olivine of Y79 and ALH (Fig. 1a) are the same within  $2\sigma$  errors (errors plotted in Fig. 1 are  $1\sigma$  from counting statistics only). Also shown in Fig. 1a are the REE concentrations in a glassy area of the melt inclusion referred to above. The melt inclusion is predominantly glassy, although other minerals such as pyroxene (20-30 vol. %) are also present. Note that the REE patterns of the glass in this inclusion, the Y79 whole rock [6], and the ALH whole rock [9], (shown as the solid line in Fig. 1a) are all similar, although absolute abundances in the whole rocks are somewhat lower.

As in ALH, pyroxenes in Y79 have characteristic LREE-depleted patterns with small Eu anomalies (fig. 1b). However, there is an indication that the REE patterns of the low-Ca

pyroxenes of ALH (C1-normalized Tm/La ~40-60) are somewhat steeper than those of Y79 (C1-normalized Tm/La <40). In addition, five of the twelve low-Ca poikilitic pyroxenes analysed in Y79 have positive Ce anomalies ( $Ce/Ce^* \sim 1.5-4$ , where  $Ce^*$  is the interpolated Ce value between chondrite-normalized abundances of La and Pr). No Ce anomalies were found in the low-Ca non-poikilitic and the high-Ca poikilitic pyroxenes, probably because we analysed fewer of these two types of pyroxenes. Pyroxenes of other Antarctic shergottites commonly display Ce anomalies (negative and positive), which are believed to be the result of REE mobilization during weathering processes in the Antarctic.

Fig. 2 shows Y and Zr abundances vs. Ti concentrations (Figs. 2a and 2b, respectively) in low-Ca pyroxenes (poikilitic and non-poikilitic) of Y79 as well as ALH. It is evident that trace and minor element abundances in pyroxenes of Y79 and ALH are similar.

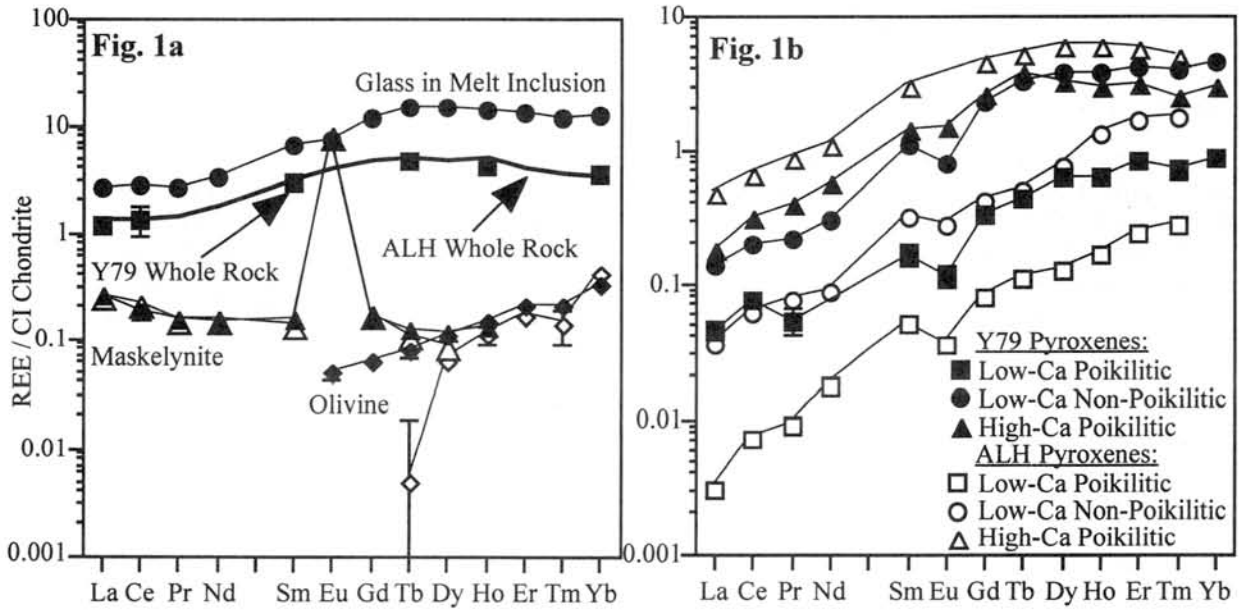
**Discussion.** The similarity of trace and minor element concentrations in minerals of Y79 and ALH (which itself is essentially indistinguishable from LEW88516; [8]) confirms the close association of Y79 with the other two lherzolitic shergottites and clearly indicates that the crystallization histories of these three rocks had much in common as suggested by other petrographic and geochemical studies [4,5,6,7]. Given that the exposure ages of all three lherzolites are similar (~3.7 Ma; [10]), it is likely that these samples were ejected by the same impact event on Mars. However, since each of the three lherzolites was collected from a different ice field in Antarctica, it is unlikely that they are paired. This situation is analogous to that of the three nakhlites (Nakhla, Lafayette, and Governador Valadares). Although these fell in different regions of the world, they exhibit striking petrographic and geochemical similarities and also have the same exposure age of ~11 Ma [11,12,13]. Based on these data, it has been suggested that all nakhlites could have originated from within the same lithologic unit on Mars [11,12]. Similarly, it is possible that the three lherzolitic shergottites were derived from the same horizon of a lherzolitic rock unit on Mars (as also suggested by [6]).

Regarding the REE composition of the Y79 parent melt, it appears that it was LREE-depleted like the parent melt compositions of the other two lherzolitic shergottites [8]. This can also be inferred from the REE pattern of the glassy region of the melt inclusion in the poikilitically enclosed olivine of Y79, which is LREE-depleted and parallel to the REE pattern of the Y79 whole rock [6] (see Fig. 1a). This is to be expected if Y79 consists of a cumulate portion (that contains a small fraction of the overall REE budget of this rock) and a trapped melt component (that has the composition of the parent melt) that essentially crystallized as a closed system. The REE composition of the glass in the melt inclusion, thus, approximately reflects the composition of the parent melt of Y79.

Like those of other SNCs, the parent magmas of lherzolitic shergottites were derived by partial melting of an already partly depleted mantle.

REFERENCES: [1] McSween H.Y., Jr. (1994) *Meteoritics* 29, 757. [2] Yanai K. (1995) *LPSC XXVI*, 1533. [3] Kojima H. and Warren P.H. (1997) *Proc. NIPR Sympos. Antarctic Met.* (Tokyo), submitted. [4] Mikouchi T. and Miyamoto M. (1996) *Meteorit. Planet. Sci.* 31, A89. [5] Mikouchi T. and Miyamoto M. (1997) *Proc. NIPR Sympos. Antarctic Met.* (Tokyo), submitted. [6] Warren P.H. and Kallemeyn G.W. (1997) *Proc. NIPR Sympos. Antarctic Met.* (Tokyo), submitted. [7] Mittlefehldt D. et al. (1997) *Proc. NIPR Sympos. Antarctic Met.* (Tokyo), submitted. [8] Harvey R.P. et al. (1993) *Geochim. Cosmochim. Acta* 57, 4769. [9] Smith M.R. et al. (1984) *Proc. 14th Lunar Planet. Sci. Conf., Part 2, J. Geophys. Res.* 89, B612. [10] Eugster O. and Polnau E. (1997) *Proc. NIPR Sympos. Antarctic Met.* (Tokyo), submitted. [11] Harvey R.P. and McSween H.Y., Jr. (1992) *Geochim. Cosmochim. Acta* 56, 1655. [12] Wadhwa M. and Crozaz G. (1995) *Geochim. Cosmochim. Acta* 59, 3629. [13] Bogard D.D. et al. (1984) *Geochim. Cosmochim. Acta* 48, 1723.

### REE in Minerals of Y793605 and ALH77005



### Low-Ca Pyroxenes of Y793605 and ALH77005

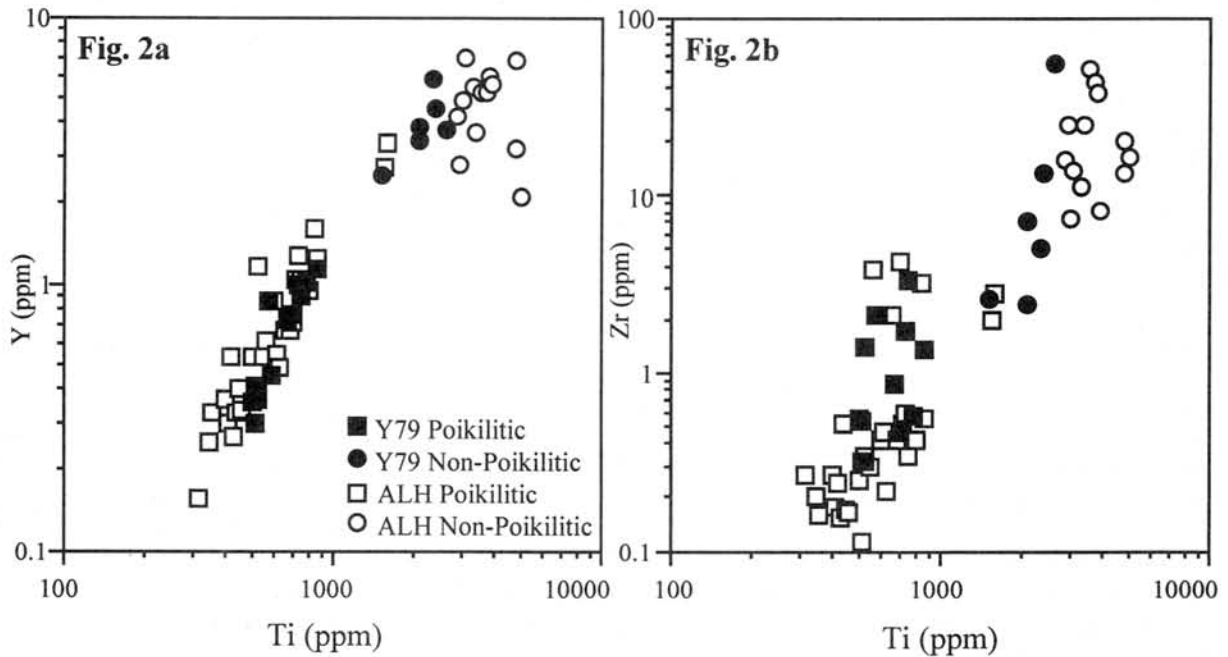


**Fig. 1:** REE in minerals of the martian lherzolites Y793605 and ALH77005. Filled symbols denote minerals of Y793605, while open symbols denote minerals of ALH77005 [8]. Filled squares in Fig. 1a are the whole rock data for Y793605 [6], while the solid line represents the whole rock data for ALH77005 [9].

**Fig. 2:** Y (Fig. 2a) and Zr (Fig. 2b) vs. Ti abundances in low-Ca pyroxenes of Y793605 (Y79; filled symbols) and ALH77005 (ALH; open symbols) [8]. Symbols in Fig. 2b are the same as in Fig. 2a.

## Yamato-793605 and other presumed martian meteorites: Composition and petrogenesis

Paul H. Warren<sup>1,2</sup> and Gregory W. Kallemeyn<sup>1,3</sup>

<sup>1</sup>Inst. Geophysics, UCLA, Los Angeles, CA 90095, USA, <sup>2</sup>Mineralogical Inst., Univ. Tokyo, Hongo, Tokyo 113, JAPAN, <sup>3</sup>Dept. Chemistry, Tokyo Metropolitan U., Hachioji, Tokyo 192, JAPAN

Abundant evidence indicates that a petrologically diverse group of meteorites, presently numbering 12 and sometimes called the SNC meteorites, are transported pieces of the igneous crust of Mars [1]. One of the most recently discovered meteorites of this type is the 16 gram Yamato-793605 peridotite [2,3]. As members of the consortium organized to study Y793605 by the NIPR [4], we are investigating the concentrations of a variety of trace elements as well as major elements in the meteorite's bulk composition. The consortium allocated for this study a 208 mg aliquot from a powder that originally weighed 308 mg. After INAA, we further subdivided the 208 mg powder into a 191 mg aliquot for future radiochemical neutron activation analysis (RNAA) plus a 17 mg aliquot for microprobe fused bead analysis, used to determine primarily Si and Mg. Samples of martian meteorites ALH77005, ALH84001, EET79001, and QUE94201 were processed in a roughly similar manner. We discuss the implications of these new data, particularly with regard to suggestions [5,6] of a close connection between shergottitic peridotites and EET79001.

Our results (Table 1) confirm previous indications [2,3] that Y793605 is a peridotite remarkably similar to ALH77005 and LEW88516. Although the ALH77005-LEW88516-Y793605 trio are commonly described as lherzolites, petrographic studies have discovered abundant clinopyroxene but no definite orthopyroxene (except where formed by slight subsolidus exsolution) in any of these rocks [1,3]. According to standard igneous nomenclature, a lherzolite must have  $\text{opx}/(\text{ol}+\text{opx}+\text{cpx}) >5\%$ . Peridotite with  $\text{opx}/(\text{ol}+\text{opx}+\text{cpx}) <5\%$  is properly termed wehrlite. The usage of "lherzolite" to describe these samples should be discouraged in favor of wehrlite, or the generic term peridotite. The Y793605 composition shows indications of a relatively low trapped liquid content. Plagiophile elements Na and Al, plagiophile/incompatible element K, and highly incompatible element La, all are depleted by small factors in Y793605 compared to the SP average.

**Origin of Y793605** All three martian peridotites have cosmic-ray exposure (CRE) ages of  $\sim 3.7$  My [9], and this age is generally assumed to record the complete duration of the journey from Mars to Earth. However, ALH77005 and LEW88516 apparently did not fall at the same time [1]. The terrestrial age of Y793605 is unknown, but its great distance from the ALH and LEW areas ( $\sim 3000$  km) would ordinarily lead to a presumption against pairing. Assuming three separate peridotite fall events, these admittedly poor statistics suggest that the 3.7 Myr event was responsible for a major fraction (1/4) of all martian meteoroids currently in near-Earth space.

The degree of compositional similarity among the three peridotites suggests derivation not only from a single layered intrusion, but from the same small region in the intrusion. Peridotitic portions of terrestrial layered intrusions typically feature heterogeneity at all scales down to cm. As a rule, aside from small-scale mineralogical/textural layering, layered intrusions are most heterogeneous near their last-crystallized regions (close to their tops, where exposed), and most homogeneous in their middle-deep interiors. Unless the three peridotites were originally only a few cm or meters apart, they probably all formed in a deep interior portion of the parent intrusion. Also suggesting derivation of these rocks from the lower portion of the parent intrusion are the consistent absence of cumulus plagioclase, and the compositions of melt inclusions in olivines [7], indicating that the parent magmas were primitive in the sense of being too poor in  $\text{Al}_2\text{O}_3$  to be plagioclase-saturated.

Models of launch off a large body, and observations from lunar meteorites, suggest that near-surface regions are strongly favored as the immediate pre-launch source locations of martian meteoroids [10]. The martian meteorites consistently lack CRE evidence for launch from depths  $\ll 5$  m, but on Mars, materials at shallow depths may be too weathered to survive the violent launch process. On balance, therefore, the pre-launch depths were probably of order 10 m. Assuming an igneous crystallization age of roughly 170 Ma (data sources: see [1]), there has been little opportunity for endogenous martian geologic activity to expose an originally deep region of the intrusion. Thus, if the original depth of formation was  $\gg 10$  m, then these materials were probably excavated to their pre-launch location(s) by a prior impact. Impacts are presumably not vastly more common, in terms of craters of a given size per year, on Mars than on Earth [11]. Thus, impact

excavation has been a very rare process on Mars over the last 170 Ma.

If a prior impact excavation is invoked, the ejecta from this impact should have been a jumbled mass of materials from many different regions of the parent intrusion. It is remarkable, then, that these three cumulate peridotites, constituting the entire 3.7 Ma CRE cluster, are so nearly identical. Related but more evolved cumulates of the same intrusion should have been launched from the 3.7 Ma crater. As an alternative to the prior impact excavation hypothesis, it might be assumed that the parent intrusion was so small that even at their original depth, these rocks were shallow enough to be launched off Mars. However, considering that they probably originated relatively deep in the cumulate pile, this model implies the entire intrusion was never more than a few tens of meters thick. In that case, production of cumulates such as these would inevitably have engendered gross compositional heterogeneity, especially layering, at a scale of the order 1/10 of the intrusion thickness, i.e., at a scale of meters. Again, the detailed scenario seems improbable for launch of three nearly identical rocks as separate meteoroids.

Wetherill [12] and Gladman [13] have argued that martian meteorites are in general unlikely to reach Earth via secondary collisions after leaving Mars. However, Gladman's [13] precise modeling of the dynamical evolution of meteoroids launched off Mars shows that roughly 20% of them quickly (time scale of order 0.2 Myr) migrate into the inner portion of the asteroid belt, where they should have significant probability for collisions with other asteroids (in this analysis of Gladman's results, I define the asteroid belt not simply on the customary basis of semimajor axis; the region of high asteroid density extends to significantly smaller heliocentric distances — we assume 2.0 AU — because most asteroid orbits are moderately eccentric). Assuming the primary meteoroid was too small to engender  $2\pi$  CRE in most of the meteoroid's volume, and that the combined duration of the trip to the asteroid belt and the subsequent journey of the collisional fragment to Earth took  $\sim 3.7$  Myr, then the CRE records would not show any significant difference vs. meteorites of more direct Mars-Earth derivation. Martian meteorites derived from secondary collisions might be expected to be generally smaller than other martian meteorites. Compared to the average martian meteorite mass of 4 kg, LEW88516 (13 g) and Y793605 (17 g) are tiny, and ALH77005 (482 g) is small. Considering the extreme compositional-petrologic similarity among these three stones, for them the secondary fragmentation model seems slightly more plausible than alternative scenarios not invoking secondary fragmentation. One advantage of assuming that a major portion of the total martian meteoroid population represents secondary fragmentation products, is that it helps to account for the enigmatically high ratio of martian to lunar meteorites [10].

**Origin of EET79001-A** The EET79001 "A" lithology consists of a fine-grained basaltic groundmass, with many small peridotitic xenoliths (lithology "X" [11]) similar to the ALH77005-LEW88516-Y793605 (SP) rock type. Lithology "A" is in igneous contact with a basaltic EET79001 "B" lithology, and its bulk composition roughly corresponds to a mixture of B with SP. McSween and coworkers [14,5] interpret A as a product of magma mixing, or else assimilation of peridotitic matter by B type magma. Mittlefehldt et al. [6] have argued instead that A formed as an impact melt, dominated by B basalt but rich in clasts of "X" peridotite, and contaminated with meteoritic Au.

We consider the EET79001-A lithology more likely an endogenously produced mixed magma than an impact melt. Our results indicate that Au is only slightly enriched in A compared to B. The Au contamination interpretation requires an assumption that the compositions of the pure igneous components are known. But Au contents of martian meteorites in general are highly diverse. Also, the lithophile element composition of A can only be roughly approximated by models mixing B plus any known variety of SP. Using literature averages for SP and EET79001-B [1] as components, the mixing ratio that satisfies mafic elements such as Mg, Sc, Co and Ni is consistently about 55:45 (B:SP), whereas the plagiophile elements Na, Al, and Ga consistently imply about 36:64; and the lightest REE, La, implies roughly 14:86. Vanadium is actually higher in the supposedly intermediate "A" than in either "B" or the most V-rich of the known peridotites (Fig. 1).

The A/B contact is gradational [14], unlike typical contacts between large clasts and groundmass in impact melt breccias, where cold clasts efficiently chill the surrounding melt [15]. The presence of only two grossly dissimilar rock types (B and "X") as discernible components in A seems an unlikely outcome from the chaotic process of impact mixing. Moreover, it seems improbable that one of only 12 martian meteorites happens to be an impact melt of relatively young age. Analogy to Earth (i.e., mainly Chicxulub) suggests that the volume of post-200 Ma impact melt

on Mars is  $\sim 4 \times 10^5 \text{ km}^3$ , or 0.06% of the volume of the martian crust. Conceivably, however, impact melting enhances the statistical likelihood for derivation of martian meteoroids from a given area, by replacing weak (brecciated and weathered) surficial rocks with strong, freshly crystallized rocks.

Thermal energy balance is potentially a severe constraint on any assimilation model [5]. However, the calculations of [5] treat the assimilation process as requiring complete equilibration of a peridotitic component into the combined magma. Much of the peridotitic component appears to have remained solid (many NASA photos, e.g. S86-37533). Mechanical admixture of solids requires less enthalpy than ideal, total assimilation. Also, admixed solids might have been concentrated, by settling or squeezing, into the marginal (next to B) magma that became EET79001 "A."

**References:** [1] Meyer C. (1996) *Mars Meteorite Compendium — 1996*, NASA Johnson Space Center. [2] Yanai K. (1995) *Lunar Planet. Sci. XXVI*, 1533-1534. [3] Mikouchi T. & Miyamoto M. (1996) *Meteor. Plan. Sci.* **31**, A89-A90. [4] Kojima H. et al. (1997) submitted to this volume. [5] Wadhwa M. et al. (1994) *GCA* **58**, 4213-4229. [6] Mittlefehldt D. W. et al. (1997) *LPS XXVIII*, 961-962. [7] Harvey R. P. et al. (1993) *GCA* **57**, 4769-4783. [8] Treiman A. H. et al. (1994) *Meteoritics* **29**, 581-592. [9] Eugster O. & Polnau E. (1997) *Proc. NIPR Sympos. Ant. Met.* **10**, submitted. [10] Warren P. H. (1994) *Icarus* **111**, 338-363. [11] Treiman A. H. (1995) *JGR-Planets* **100**, 5329-5340. [12] Wetherill G. W. (1984) *Meteoritics* **19**, 1-12. [13] Gladman B. J. (1997) *Icarus*, submitted. [14] McSween H. Y. & Jarosewich E. (1983) *GCA* **47**, 1501-1513. [15] Simonds C. H. et al. (1976) *Proc. LS Conf.* **7**, 2509-2528. [16] Warren P. H. et al. (1996) *Ant. Met.* **XXI**, 195-197.

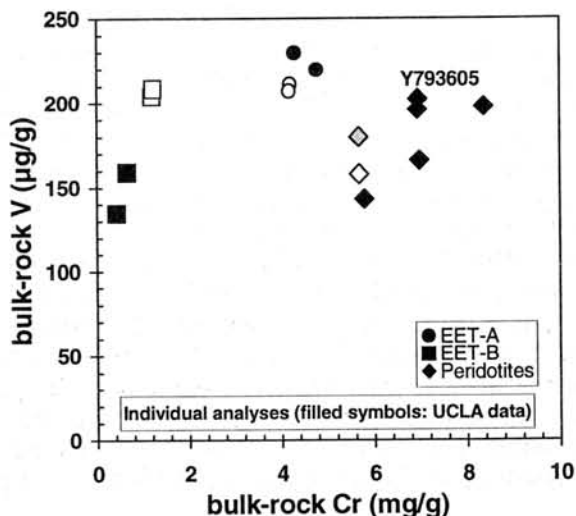
Table 1. Bulk compositions of presumed martian meteorites determined by INAA, MFBA and RNAA.

|                        | mass | Na   | Mg   | Al   | Si   | K     | Ca   | Sc   | Ti   | V    | Cr   | Mn   | Fe   | Co   | Ni   | Zn   | Ga   | La    | Sm    | Eu    | Tb    | Lu    | Hf    | Ta     | Ir   | Au    | Th    |
|------------------------|------|------|------|------|------|-------|------|------|------|------|------|------|------|------|------|------|------|-------|-------|-------|-------|-------|-------|--------|------|-------|-------|
|                        | mg   | mg/g | mg/g | mg/g | mg/g | mg/g  | mg/g | μg/g  | μg/g  | μg/g  | μg/g  | μg/g  | μg/g  | ng/g   | ng/g | pg/g  | pg/g  |
| normal uncertainty*    |      | 3%   | 4%   | 4%   | 3%   | 7%    | 3%   | 3%   | 5%   | 5%   | 4%   | 3%   | 4%   | 3%   | 5%   | 6%   | 6%   | 4%    | 4%    | 4%    | 6%    | 5%    | 6%    | 10%    | 5%   | 6%    | 7%    |
| ALH77005,128           | 615  | 3.29 | 175  | 16   | 193  | 0.22  | 21   | 19.0 | <5   | 166  | 7.0  | 3.40 | 159  | 78   | 310  | 59   | 6.9  | 0.40  | 0.48  | 0.25  | 0.17  | 0.085 | 0.57  | 0.04   | 4.1  | 260   | <0.1  |
| notable uncertainties* |      |      | 6%   |      | 6%   | 8%    |      |      |      |      |      |      |      |      |      |      |      |       |       |       |       |       |       | 30%    |      |       |       |
| ALH84001:56a           | 337  | 1.05 | 149  | 6.4  | 247  | 0.127 | 13.0 | 11.8 | 1.19 | 205  | 7.3  | 3.64 | 134  | 45   | 5.8  | 90   | 2.74 | 0.246 | 0.160 | 0.049 | 0.043 | 0.042 | 0.117 | <0.042 | 0.08 | 9.4   | <0.05 |
| ALH84001:56b           | 332  | 1.12 | 149  | 6.4  | 247  | 0.122 | 12.9 | 13.1 | 1.19 | 205  | 8.0  | 3.63 | 135  | 50   | <20  | 92   | 2.3  | 0.28  | 0.163 | 0.045 | 0.042 | 0.050 | 0.111 | <0.06  | <2.2 | <640  | 0.11  |
| notable uncertainties* |      |      |      |      |      | 12%   |      |      |      |      |      |      |      |      |      |      | 10%  |       |       |       | 21%   | 18%   |       |        |      |       | 24%   |
| EET79001,397a ("A")    | 312  | 6.6  | 72   | 38   | 241  | 0.33  | 61   | 37.2 | 5.7  | 230  | 4.29 | 3.66 | 130  | 43   | 128  | 85   | 14.2 | 0.48  | 0.78  | 0.40  | 0.32  | 0.17  | 0.97  | <0.08  | <2.3 | <2000 | <0.10 |
| notable uncertainties* |      |      |      |      |      | 12%   |      |      |      |      |      |      |      |      |      |      |      |       |       |       |       |       |       |        |      |       |       |
| EET79001,397b ("A")    | 321  | 5.9  | 88   | 31   | 236  | 0.32  | 53   | 38.0 | 4.2  | 220  | 4.76 | 3.81 | 144  | 55   | 179  | 65   | 12.8 | 0.41  | 0.76  | 0.37  | 0.32  | 0.16  | 0.08  | 0.03   | <5   | 960   | <0.07 |
| notable uncertainties* |      |      |      |      |      | 14%   |      |      |      |      |      |      |      |      | 9%   |      |      |       |       |       |       |       |       |        |      |       | 35%   |
| EET79001,399a ("B")    | 319  | 13.2 | 33   | 62   | 232  | 0.66  | 78   | 43.2 | 9.2  | 159  | 0.65 | 3.20 | 137  | 27.7 | 23   | 105  | 26.8 | 1.18  | 2.01  | 0.96  | 0.76  | 0.40  | 2.26  | 0.09   | <1.3 | <1000 | 0.14  |
| notable uncertainties* |      |      |      |      |      | 9%    |      |      |      |      |      |      |      |      | 31%  |      |      |       |       |       |       |       |       |        |      |       | 22%   |
| EET79001,399b ("B")    | 324  | 15.1 | 31   | 71   | 233  | 0.65  | 77   | 42.1 | 7.5  | 135  | 0.42 | 3.16 | 132  | 28.4 | 19   | 92   | 29.9 | 1.03  | 1.95  | 0.95  | 0.79  | 0.38  | 2.31  | 0.068  | <2.4 | <200  | 0.15  |
| notable uncertainties* |      |      |      |      |      | 10%   |      |      |      |      |      |      |      |      | 32%  |      |      |       |       |       |       |       |       |        |      |       | 11%   |
| QUE94201,19            | 305  | 10.3 | 38   | 52   | 224  | 0.32  | 82   | 49.0 | 11.9 | 124  | 1.01 | 3.65 | 149  | 24.4 | <40  | 108  | 25.9 | 0.44  | 2.55  | 1.09  | 0.93  | 0.54  | 3.4   | <0.08  | <2.4 | <500  | <0.09 |
| notable uncertainties* |      |      |      |      |      | 16%   |      |      |      |      |      |      |      |      |      |      |      |       |       |       |       |       |       |        |      |       |       |
| Y793605,10             | 310  | 2.63 | 158  | 12.3 | 212  | 0.204 | 29   | 25.0 | 2.1  | 202  | 6.9  | 3.70 | 153  | 72   | 280  | 49   | 6.8  | 0.29  | 0.45  | 0.206 | 0.168 | 0.080 | 0.51  | <0.04  | 3    | <800  | <0.06 |
| notable uncertainties* |      |      |      |      |      | 9%    |      |      |      |      |      |      |      |      |      |      |      |       |       |       |       |       |       |        | 35%  |       |       |
| Liter. avg. ALH77005   |      | 3.38 | 170  | 15.5 | 199  | 0.23  | 23.5 | 21.3 | 2.57 | 162  | 6.9  | 3.50 | 156  | 72   | 333  | 60   | 6.8  | 0.35  | 0.46  | 0.295 | 0.168 | 0.078 | 0.58  | 0.032  | 4.3  | 280   | 0.056 |
| Liter. avg. LEW88516   |      | 3.53 | 150  | 13.1 | 219  | 0.23  | 31.1 | 25.8 | 2.02 | 179  | 6.0  | 3.72 | 153  | 63   | 256  | 58   | 7.6  | 0.33  | 0.43  | 0.222 | 0.173 | 0.084 | 0.52  | 0.032  | 2.4  | 440   | 0.060 |
| Avg. 3 SP              |      | 3.18 | 159  | 13.6 | 210  | 0.22  | 27.8 | 24.0 | 2.25 | 181  | 6.6  | 3.64 | 154  | 69   | 289  | 56   | 7.1  | 0.32  | 0.45  | 0.241 | 0.170 | 0.081 | 0.54  | 0.032  | 3.2  | 360   | 0.058 |
| Lit. avg. EET79001-A   |      | 6.4  | 93   | 31.2 | 233  | 0.34  | 52   | 36.7 | 4.2  | 217  | 4.3  | 3.73 | 143  | 48   | 150  | 72   | 13.2 | 0.40  | 0.74  | 0.36  | 0.28  | 0.165 | 0.95  | 0.027  | <2.0 | ?     | 0.080 |
| Lit. avg. EET79001-B   |      | 12.8 | 40   | 58.4 | 231  | 0.64  | 77   | 47.3 | 7.4  | 177  | 1.0  | 3.31 | 136  | 30   | 28   | 94   | 24.5 | 0.87  | 1.61  | 0.76  | 0.61  | 0.31  | 1.94  | 0.079  | <2.0 | ?     | 0.135 |

Table notes: Averages shown for shergottitic peridotites ALH77005 and LEW88516 are based on a comprehensive compilation of literature data, mainly from sources cited in Meyer [1]; data for ALH77005,128 shown above were included for the ALH77005 average. Data for QUE94201,19 supercede the preliminary data set published by Warren et al. [16].

\* Uncertainties in INAA counting statistics are shown where they are large compared to normal 70% confidence levels (i.e., "normal" for moderate-high concentrations).

Fig. 1. Cr vs. V, from individual analyses of EET79001 and shergottitic peridotites. Variations are probably due to real heterogeneities, not inter-lab bias.



# Asteroid Magnetic Records - Possible Insight from the Analysis of Large Meteorites

P. J. Wasilewski  
NASA Goddard Space Flight Center

T. L. Dickinson  
Physics Department, Catholic University of America

J. E. Connerney  
NASA Goddard Space Flight Center

and M. Funaki  
National Institute of Polar Research, Japan

## Abstract

The first quantitative measurements of an asteroid's composition and structure will be made at the Eros encounter by NEAR (Near Earth Asteroid Rendezvous) spacecraft. On board is a three axis fluxgate magnetometer that will map the magnetic field of EROS. The magnetometer record, together with other data collected by NEAR, will provide important information about the connection between asteroids and meteorites.

The most recent compilation of NRM data (Pesonen et al., 1993) identified a range of several orders of magnitude in NRM intensity for any group of meteorites. At least part of this variability is probably due to magnetic contamination. Shock impact will also produce variability in the NRM data. Pesonen et al. (1993) did not shock classify the meteorites they studied. NRM data must be analyzed based on the mineralogic makeup. In addition, some meteorites have extremely noisy small scale magnetic variations and larger scale inhomogeneities in the magnetic distribution. In order to understand meteorite magnetization, detailed studies of small samples and the analysis of bulk properties of large meteorites are required.

Large sample studies will reveal the orientation of the bulk magnetization with respect to sample geometry and internal structure, while minimizing the problem of magnetic contamination. Small sample data for carbonaceous chondrites suggests coherent magnetization throughout. Large sample data is needed to verify this. Ordinary chondrites show scattered, and sometimes random, records with evidence of pockets of coherent magnetization. The ordinary chondrite meteorites are potential candidate S type asteroidal material and, therefore, large sample ordinary chondrite analyses are important. Magnetic records from large meteorites will provide the most reliable bulk meteorite magnetization records.

We have obtained several large meteorites from the Smithsonian Institute (U.S. National Museum) for a non-destructive evaluation of their magnetic properties. We are grateful to Dr. Glen MacPherson for his assistance in obtaining the meteorites. Magnetization data for Canyon Diablo (454 Kg), Allende (17.2 Kg) and ALH76009 (23.7 Kg) are presented in Table 1.

The experimental configuration for the large meteorite sample measurement technique is illustrated in Figure 1. The lower part of the Figure illustrates the orbit technique, in which the fluxgate array is positioned at different heights to record data for spherical harmonic analysis of the meteorite's magnetic field. Classic spherical harmonic analysis will illustrate the magnitude and orientation of the dipole and non-dipole components in the magnetization records of these large meteorites.

Figure 2 illustrates the NRM total magnetization and the orbit record after a 3mT alternating field demagnetization for the central orbit plane of the Canyon Diablo meteorite.

The magnetization intensity for the large meteorites is less than for small samples of the same meteorites as reported in the literature (Table 1) (e.g. Nagata et.al., 1981; and Wasilewski, 1981). The bulk magnetization of large meteorites includes cancellation due to random and inhomogeneous distributions of magnetization that would not be apparent in small samples. In ALH76009, the inhomogeneous distribution of magnetization is obvious. The true picture of the magnetization of meteorites and the connection between meteorite magnetism and the magnetization of asteroids will be a likely consequence of large meteorite magnetic analysis.

**TABLE 1**

**MAGNETIZATION DATA FOR LARGE METEORITES, COMPARATIVE SMALL SAMPLES AND LABORATORY INTRODUCED TRM IN FeNi ALLOYS OF KAMACITE COMPOSITIONS.**

|   | <b>CANYON DIABLO</b>  | <b>ALLENDE</b>   | <b>ALH76009</b>  |
|---|---|--|--|
| DIPOLE MOMENT                                   | 782.9x10 <sup>-3</sup> Am <sup>2</sup>  | 1.8x10 <sup>-3</sup> Am <sup>2</sup>                           | 6.2x10 <sup>-3</sup> Am <sup>2</sup>   |
| DIPOLE MOMENT AFTER DEMAG.                      | 515x10 <sup>-3</sup> Am <sup>2</sup>  | —  | 0.2x10 <sup>-3</sup> Am <sup>2</sup>   |
| WEIGHT  | 454 Kg  | 17.2 Kg  | 23.7 Kg  |
| DENSITY   | 7500 Kgm <sup>-3</sup>  | 2750 Kgm <sup>-3</sup>   | 2890 Kgm <sup>-3</sup>   |
| MAGNETIZATION INTENSITY                         | 12.94Am <sup>-1</sup>   | 0.288Am <sup>-1</sup>  | 0.756Am <sup>-1</sup>  |
| MAGNETIZATION PER UNIT MASS (DEMAG.)            | 17.25x10 <sup>-4</sup> Am <sup>2</sup> Kg <sup>-2</sup><br>(11.38x10 <sup>-4</sup> Am <sup>2</sup> Kg <sup>-2</sup> ) | 1.1x10 <sup>-4</sup> Am <sup>2</sup> Kg <sup>-2</sup><br>—     | 2.63x10 <sup>-4</sup> Am <sup>2</sup> Kg <sup>-2</sup><br>(0.084x10 <sup>-4</sup> Am <sup>2</sup> Kg <sup>-2</sup> ) |
| <b>SMALL BULK SAMPLES</b>                       |   | <b>(WASILEWSKI 1981)</b>                                       | <b>(NAGATA et.al. 1981)</b>  |
| MAGNETIZATION/gm                                | —   | 2.37–2.64x10 <sup>-4</sup><br>Am <sup>2</sup> Kg <sup>-1</sup> | 22.1x10 <sup>-4</sup><br>Am <sup>2</sup> Kg <sup>-1</sup>  |
| REM = NRM/SIRM<br>(SIRM = saturation remanence) | —   | 0.0042 – 0.0054  | 0.0065   |

For FeNi spheres (0–9% Nickel) acquiring a TRM in the geomagnetic field  
 TRM = 7.6 – 25.2 x 10<sup>-4</sup> Am<sup>2</sup>K<sup>-1</sup> (linear with Ni content). These spheres  
 have REM values between 0.02 and 0.03.

**FIGURE 1:**

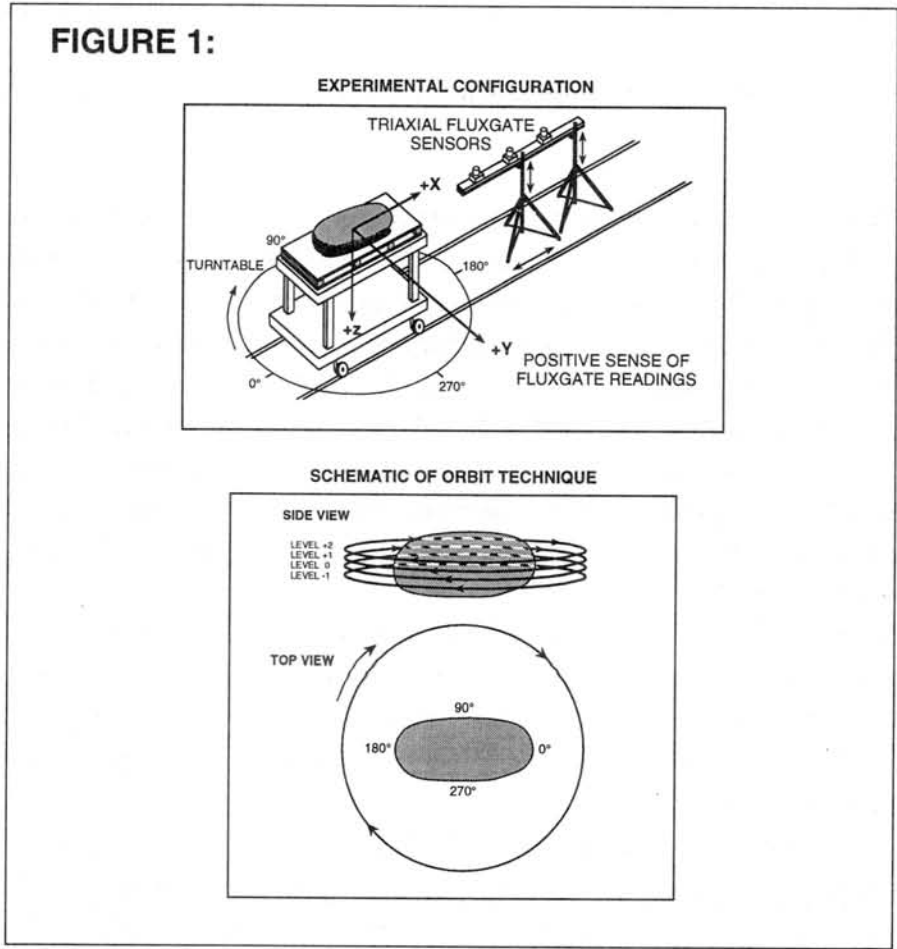
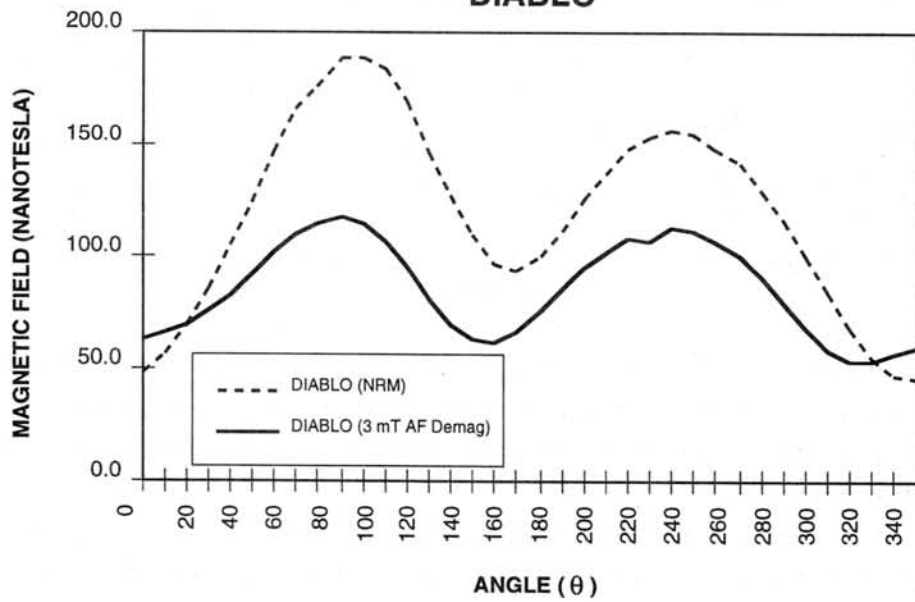


**FIGURE 2:**

CANYON DIABLO TOTAL MAGNETIZATION RECORD FOR ONE ORBIT PLANE

**DIABLO**



# THERMOLUMINESCENCE IN TEKTITES AND NUCLEAR EXPLOSIVE AND VOLCANIC GLASSES,

L Wenzhu and Li Chunlai, Institute of Geochemistry, Chinese Academy of Sciences, Guiyang 550002

The TL have been applied in studying radiation and thermal histories, terrestrial age, orbit effect and rock type of meteorites, and successfully applied to determine age of the archaeology and other earth sciences(1). The tektites are materials of specific amorphous state which scatter all over the world. Their appearance is similar to obsidian and possess air-dynamic shape of volcanic glasses. As for origin of the tektites is an endless debate from last century to now. However, major investigators, including authors, believe that the tektites are melting materials resulted from impact of asteroid or comet on the Earth(2,3). Other glasses are also scattered all over region-volcanic glasses. Their formation thermal environment apparently differ from tektites. So, this paper attempted to apply TL method for discovering thermal radiation histories of tektites, nuclear explosive and volcanic glasses.

The samples select tektites (Wen Chang, Bo Bai and layer), nuclear explosive and volcanic glasses. Experimental condition: using fine-grained suspension method; solvent is acetone; radiating body is  $^{90}\text{Sr}$   $\beta$ -particles, irradiate twenty minute; using  $\text{N}_2$  protect heating strip, the rate of heating was  $20^\circ\text{C/s}$ . Typical natural TL and artificial TL glow curves above glasses samples are shown Fig.1,2 respectively.

Table 1 Glow-peak Structure of Glasses. The Peak Temperatures are shown in  $^\circ\text{C}$

| Peak | Wen Chang |     | layer |     | Bo Bai |     | Bo Bai glass |     | N.C.glass |     | Volcanic gl. |     |
|------|-----------|-----|-------|-----|--------|-----|--------------|-----|-----------|-----|--------------|-----|
|      | NTL       | ATL | NTL   | ATL | NTL    | ATL | NTL          | ATL | NTL       | ATL | NTL          | ATL |
| 1    |           | 193 |       | 210 |        | 200 |              | 210 |           |     |              |     |
| 2    |           |     |       |     |        |     |              |     |           | 225 |              |     |
| 3    |           |     |       |     |        | 240 |              |     |           |     |              |     |
| 4    |           |     |       |     |        | 308 |              |     |           |     |              |     |
| 5    | 320       |     |       |     |        |     |              |     |           |     |              |     |
| 6    |           |     |       |     |        |     |              |     | 330       |     |              |     |
| 7    |           |     |       |     | 334    |     | 340          | 344 |           | 350 | 350          |     |
| 8    |           |     | 360   | 370 |        |     |              |     |           |     |              |     |
| 9    |           | 410 |       |     |        | 410 | 410          |     | 410       |     |              |     |
| 10   | 440       |     | 440   |     | 430    |     |              | 445 |           | 430 | 430          |     |
| 11   |           |     |       |     |        |     | 460          |     |           |     |              |     |
|      |           |     |       |     |        | 480 |              |     |           |     |              |     |

These natural TL glow curves of glass roughly divide into three classes: 1, sawtoothed type(Wen Chang, layer tektite and nuclear explosive glass);2,unsymmetry single peak type(Bo Bai tektite and glass) and 3,smooth wide peak type(volcanic glass). The artificial radiation TL glow curves very difference from NTL curves.

They also can divide into three classes: 1,Bo Bai tektite and glass, the glow curves consist of one low temperature peak (LTP)( $\sim 200^\circ\text{C}$ ) and one high temperature peak (HTP)( $\sim 410^\circ\text{C}$ ),HTP amplitude high than LTP; 2, layer tektite and nuclear explosive glass also consist of two temperature peak. However, LTP and HTP amplitude do not difference, but position of HTP is

lower ( $\sim 360^{\circ}\text{C}$ ); 3, Wen Chang tektite, their ATL pattern similar to typical symmetric ordinary chondrites.

We using equivalent dose(ED) to study and compare thermal stories of above variety glasses. If their age(T) were calculated in using TL data

$$T = \text{NTL} / \text{TL unit}$$

measure X nature dose rate

$$= \text{ED} / \text{dose rate}$$

Because of formational time of nuclear explosive glass is very accuracy, however, if data is normalized in using nuclear explosive glassy age, formation age of tektites and volcanic glass will be paradox age. So, our conclusion are that the TL of tektites lies in using this method for determining their age do not very accuracy. However, using distinguish glassy type (tektite or volcanic glass) is very successful.

**REFERENCE**

[1], Chen Y-H., D.W.G. Sears and Wang D-D, ANTARCTIC RESEARCH (CHINESE EDITION) 6, 13-31 1994  
 [2], L W-Z and Oyang Z-Y, SCIENCIA GEOLOGICAL SINICA 2, 148-157 1991,  
 [3], B.P.Glass, Tectonophysics, 171, 393-404 1990

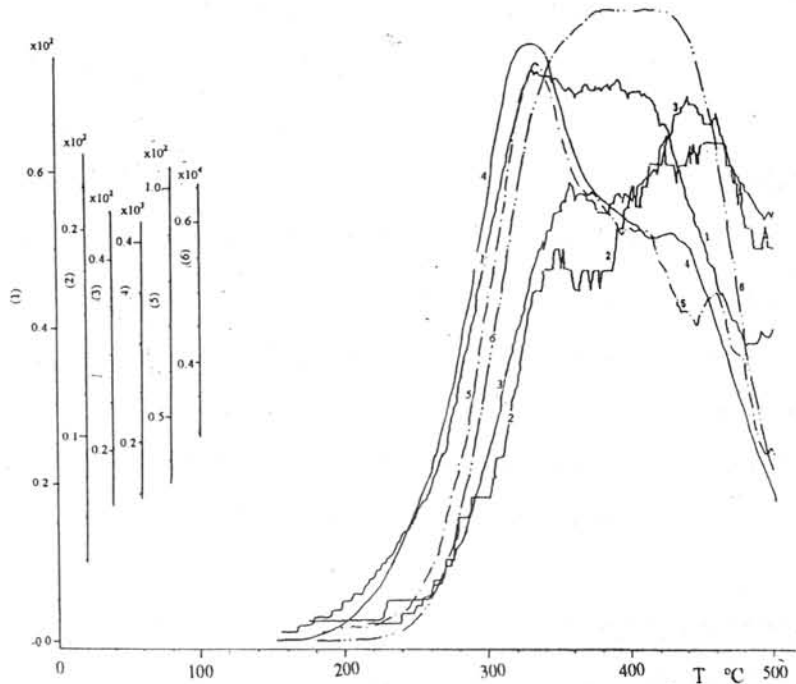


Fig.1 Natural TL glow curves of tektites, nuclear explosive glass and volcanic glass

nuclear explosive glass (1), Wen Chang tektite (2), layer tektite (3), Bo Bai tektite (4) Bo Bai glass(5), and volcanic glass

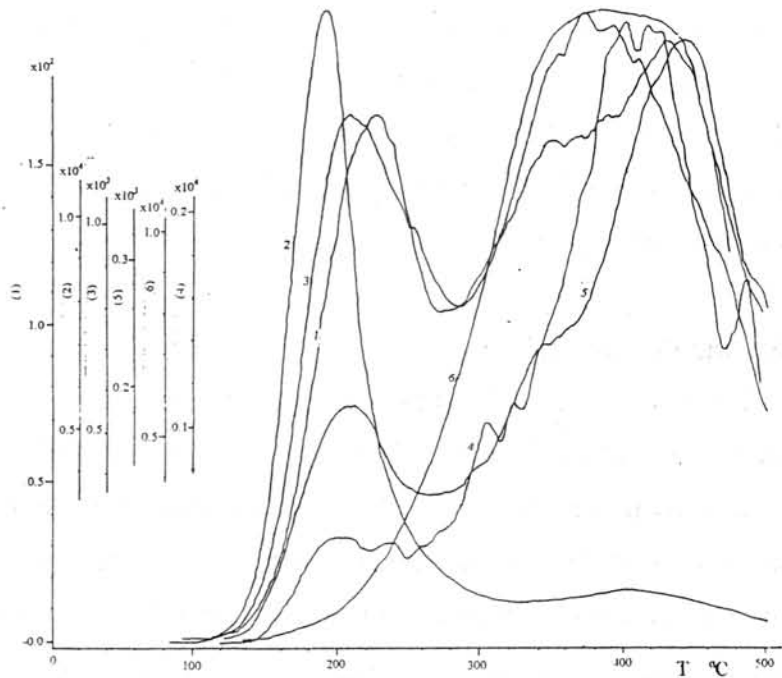


Fig.2 Artificial TL glow curves of tektites, nuclear explosive glass and volcanic glass

nuclear explosive glass (1), Wen Chang tektite (2), layer tektite (3), Bo Bai tektite (4) Bo Bai glass(5), and volcanic glass

# Petrology and Mineralogy of Antarctic Micrometeorites

T. Yada<sup>1</sup>), H. Yano<sup>2</sup>), T. Nakamura<sup>1</sup>), and N. Takaoka<sup>1</sup>)

<sup>1</sup>)Dept. Earth & Planet. Sci., Fac. Sci., Kyushu Univ., Fukuoka 812-81

<sup>2</sup>)Div. Planet. Sci., Institute of Space and Astronautical Science, Kanagawa 229

## **Introduction**

Extraterrestrial materials are thought to have accreted to the Earth at  $(40\pm 10)\times 10^6$  kg per year with a peak of mass distribution at  $1.5\times 10^{-5}$  g (Love and Brownlee, 1993); they are relatively condensed in deep sea sediment, polar ice, and stratosphere. We investigated about 20 samples of such cosmic dust particles extracted from the Antarctic ice, so called Antarctic micrometeorites, to make clear the characteristics of the micrometeorites, to elucidate their origin, and to understand the evolution of primordial materials in the early solar system.

## **Samples and methods**

Micrometeorites analyzed in this study were collected by the French expedition team at blue-ice field of Cap-Prudhomme, Antarctica in January 1991 (Maurette et al., 1992). By courtesy of Prof. Maurette, a 50-100  $\mu\text{m}$  fraction of particles were allocated to us. The fraction contains not only micrometeorites but also terrestrial material, such as single crystals of quartz, feldspar, and mica, paint chips, and so on. Black or brown, irregular shaped particles were hand-picked under a stereoscope. Then each particle was divided into two pieces. One is preserved and the other was analyzed their surface by SEM-EDS (JEOL JSM-5800). After the characterization of surfaces, they were polished and analyzed by EPMA (JEOL JCSA733) for chemical composition of inside material.

## **Results and discussions**

EDS analyses showed that the surfaces of the unmelted micrometeorites are Fe-rich and no of them have chondritic features in chemical composition on their exterior surfaces.

Based on interior texture of the micrometeorites, they are divided into three types namely: scoriaceous, phyllosilicate, and coarse-grained crystalline types, as proposed by Kurat et al. (1994). The scoriaceous micrometeorites consist mainly of Fe-rich olivine ( $\text{Fa}_{35}\text{-Fa}_{55}$ ) with many cavities due to pulse heat melt and volatile degassing with subsequent resolidification. They often contain relict refractory minerals like forsterite. The phyllosilicate micrometeorites are mainly

composed of dehydrated phyllosilicate and Fe-oxide. The dehydrated phyllosilicate has a stoichiometry similar to that of cronstedtite (Table 1). Especially, a composition of point No. 22 is almost as same as that of Murchison matrix. Inside one type micrometeorite in this category, we found a corundum grain, highly refractory minerals as observed in CAIs in C chondrites, of 10  $\mu\text{m}$  in size (Fig. 1). The coarse-grained crystalline micrometeorites consist mainly of olivine and pyroxene. One micrometeorite of this category is enstatite ( $\text{En}_{98}\text{Wo}_1$ ) with kamacite and Fe-oxide with small amounts of P, S, Si, Cr and Ni. All micrometeorites we observed have thin Fe-oxide rims on their exteriors. This implies that they were strongly heated in very short time, most likely due to their atmospheric entry. Cronstedtites are common in CM chondrites matrices, and also enstatites with kamacite and tochilinites are often found in chondrules of CM chondrites. Therefore, these micrometeorites are quite similar to CM chondrites in mineralogy although they are not fragments of CM chondrites scattered upon falling to the ice, but discrete particles when entering Earth's atmosphere, because the micrometeorites show some signs of short and intense heating, that is, thin Fe-oxide rims, olivine with many cavities, and dehydrated phyllosilicates.

The phyllosilicate micrometeorites are also analyzed for bulk composition by defocused beam with 10-20  $\mu\text{m}$  in diameter. Fig.2 shows major element abundances normalized to CI chondrite (Orgueil), matrix of CM chondrite (Murchison), and that of CR chondrite (Renazzo). The bulk compositions of the micrometeorites are similar to CM and CR rather than CI. It is consistent with the mineralogical analyses that they contain cronstedtite-like materials. Such micrometeorites are enriched in Ti and depleted in Mg, Ca, Na, Ni, and S relative to CM matrix. As potassium was not detected, adsorption of lithophile elements from terrestrial material in polar ice, as reported by Koeberl et al. (1992), should not occur in these samples.

From the mineralogy and chemical composition, the origin of the micrometeorites is considered to have a close relation to parent bodies of CM chondrites.

### **Acknowledgements**

We thank Prof. Maurette very much for giving us samples of Antarctic micrometeorites.

### **References**

Koeberl et al. (1992), Lunar Planet Sci. Conf. XXIII, 709-710, Kurat et al. (1994), Geochim. Cosmochim. Acta., 58, 3879-3904, Love and Brownlee (1993), Science, 262, 550-553, Maurette et al. (1992), Lunar Planet Sci. Conf. XXIII, 859-860

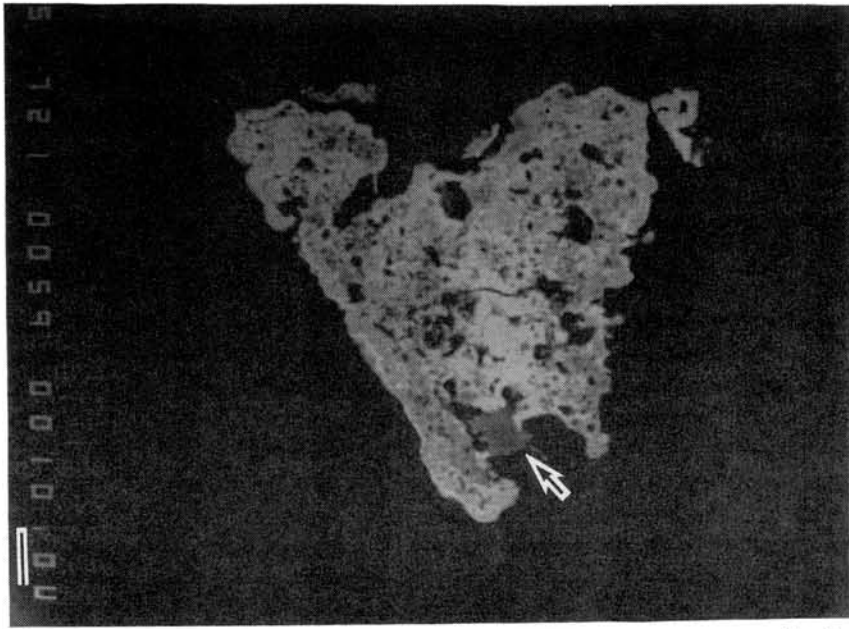
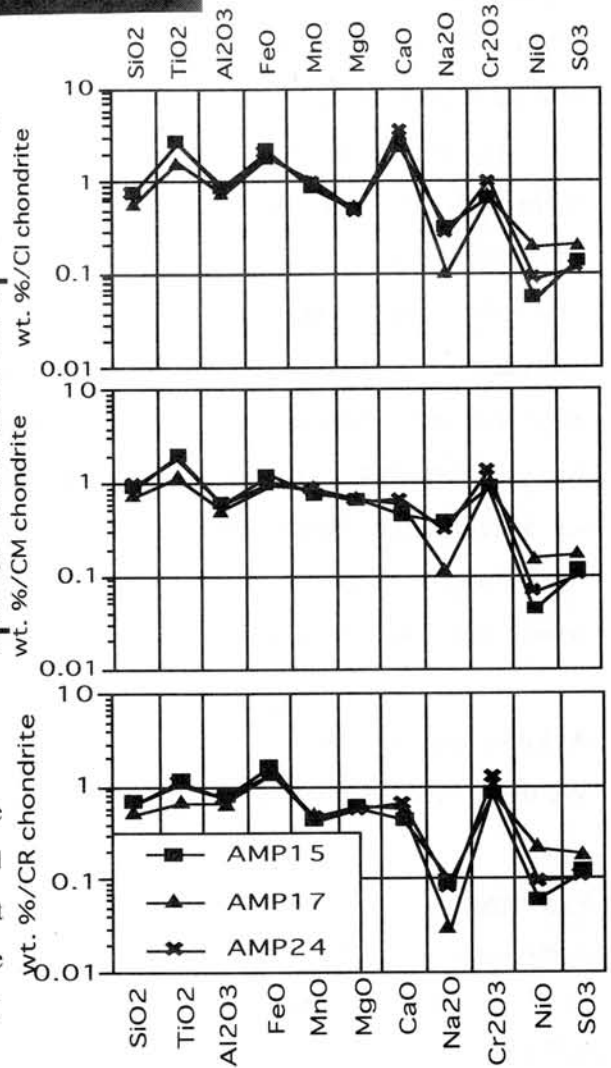


Fig. 1. A back-scattered electron image of a phyllosilicate micrometeorite, AMP17. A scale bar stands for 10  $\mu\text{m}$ . It consists mainly of Fe-rich phyllosilicates. A point of an arrow is a corundum of 10  $\mu\text{m}$  in size.

Table 1. Chemical compositions of phyllosilicates in micrometeorites

| Sample No.                     | AMP15 |       | AMP17 |       | AMP24 |       | Murchison matrix |
|--------------------------------|-------|-------|-------|-------|-------|-------|------------------|
| Point No.                      | 1     | 2     | 5     | 14    | 21    | 22    |                  |
| SiO <sub>2</sub> (wt.%)        | 26.73 | 26.62 | 29.04 | 20.29 | 32.90 | 26.34 | 23.90            |
| TiO <sub>2</sub>               | 0.08  | 0.05  | 0.08  | 0.15  | 0.18  | 0.10  | 0.06             |
| Al <sub>2</sub> O <sub>3</sub> | 1.79  | 1.76  | 3.13  | 1.12  | 1.75  | 2.33  | 2.07             |
| FeO                            | 43.75 | 55.37 | 45.27 | 52.95 | 36.26 | 34.12 | 28.20            |
| MnO                            | 0.15  | 0.16  | 0.23  | 0.07  | 0.25  | 0.06  | 0.19             |
| MgO                            | 15.37 | 10.06 | 15.98 | 9.64  | 18.00 | 10.28 | 13.80            |
| CaO                            | 0.48  | 0.47  | 0.32  | 0.57  | 0.55  | 0.76  | 1.05             |
| Na <sub>2</sub> O              | 0.06  | 0.04  | 0.03  | 0.00  | 0.06  | 0.26  | 0.12             |
| K <sub>2</sub> O               | 0.00  | 0.00  | 0.00  | 0.00  | 0.00  | 0.00  | 0.05             |
| Cr <sub>2</sub> O <sub>3</sub> | 0.57  | 0.23  | 0.32  | 0.40  | 0.61  | 0.56  | 0.41             |
| NiO                            | 0.38  | 0.03  | 0.02  | 0.54  | 0.05  | 0.22  | 1.55             |
| SO <sub>3</sub>                | 1.08  | 0.84  | 0.32  | 6.82  | 0.66  | 1.16  | 2.70             |
| P <sub>2</sub> O <sub>5</sub>  | 0.12  | 0.18  | 0.00  | 0.30  | 0.33  | 0.45  | 0.25             |
| Total                          | 90.57 | 95.81 | 94.74 | 92.83 | 91.56 | 76.62 | 74.05            |

Fig.2. Major element abundances of phyllosilicate micrometeorites normalized to those of CI chondrite, Orgueil (upper), matrix of CM chondrite, Murchison (middle), and that of CR chondrite, Renazzo (lower). These micrometeorites are similar to matrices of CM and CR chondrites rather than CI chondrites.



# SHOCK METAMORPHISM OF THE MURCHISON CM2 CHONDRITE IN SHOCK STAGE S4-S5: AN EXPERIMENTAL STUDY

Y. Yamahana<sup>1</sup>, K. Tomeoka<sup>1</sup> and T. Sekine<sup>2</sup>

<sup>1</sup> Department of Earth and Planetary Science, Faculty of Science, Kobe University, Nada, Kobe 657.

<sup>2</sup> National Institute for Research in Inorganic Materials, 1-1 Namiki, Tsukuba, Ibaraki 305.

## INTRODUCTION

Highly shocked carbonaceous chondrites are rare [1], and the shock effects on these meteorites are relatively unknown. However, if the hypothesis that the carbonaceous chondrites were once part of early planetesimals and these planetesimals accumulated through mutual collisions to form larger protoplanets [e.g. 2] is correct, they should not have escaped extensive shock processes. In this regard, Scott et al. [1] hypothesized that the high porosity of type 2-3 chondrites caused high post-shock temperature and melting at relatively low pressures, and the high volatile contents could disperse easily the shocked and melted material on release from high pressure, thus highly shocked type 2-3 chondrites normally escaped from parent bodies and formed particles that are too small to survive as meteorites. In order to gain our knowledge about the shock history of carbonaceous chondrites, we believe experimental research is a necessary step.

At the last year's NIPR Symposium, we reported the results of shock-recovery experiments of the Murchison CM2 chondrite in the shock pressure range from 7 to 21 GPa [3], which corresponds to shock stage S2 to S3 in the classification of Stöffler et al. [4]. The study showed that chondrules were flattened in the plane of shock front by shock pressures 10-20 GPa, and shock melts rich in Si, Mg, Fe, Ca and S were produced at 21 GPa. The chondrule flattening was also observed in the shock experiments of Allende [5], but the degree of flattening was found to be considerably different between Murchison and Allende [3]. We here present the results of our continuing shock-recovery experiments of Murchison in the pressure range 25-40 GPa, which corresponds to shock stage S4-S5. It has been reported that almost all of the existing CM2 chondrites are shock stage S1 (<5 GPa) [2], thus no CM2 chondrite has ever experienced such high shock pressures.

## MATERIALS AND METHODS

The shock-recovery experiments were performed by using a single stage 30-mm bore propellant gun at the National Institute for Research in Inorganic Materials. Details of the experimental procedures are described in Sekine et al. [6] and Tomeoka et al. [3].

In the present study, we initially undertook to shock Murchison samples at 25, 28, 30, and 35 GPa at room temperature. The resultant peak pressures calculated by the measured velocities turned out to be 26, 28, 30 and 38 GPa. Polished sections were made from each recovered sample by cutting along the shock compaction axis and studied by using an optical microscope, a scanning electron microscope (JEOL JSM-5800) equipped with an energy-dispersive X-ray spectrometer.

## RESULTS

**Impact at 26 GPa :** Chondrules are apparently more flattened than those in the 21-GPa sample [3]. The mean aspect ratio of 50 chondrules is 1.57 (That in the 21-GPa sample is 1.48). But, despite the increase in the degree of chondrule flattening, preferred orientation is not so pronounced; the chondrules appear to be rather more randomly oriented than those in the 21-GPa sample. Flat, thick (20-50  $\mu\text{m}$ ) cracks occur oblique to the compaction axis near the edge of the disk sample, similar to the 21-GPa sample, but no melt is observed. Most olivine and pyroxene phenocrysts in chondrules are finely fractured. Near the top and the bottom portions of the disk sample, numerous thin cracks are produced in the matrix at an interval of  $\sim 10 \mu\text{m}$  in a direction roughly perpendicular to the compaction axis, showing a finely divided banding structure.

**Impact at 28 GPa :** Chondrules are flattened nearly as much as those in the 26-GPa sample.

The mean aspect ratio of 44 chondrules is 1.56. Preferred orientation is again not so pronounced. Compared to the 26-GPa sample, more abundant thick (10-50  $\mu\text{m}$ ) cracks occur not only near the edge but also in the central portions of the sample; aggregates of extremely fine grains (<5  $\mu\text{m}$  in diameter), which are compositionally similar to the matrix, are produced in the cracks. The finely divided banding structure occurs in larger areas. Most olivine and pyroxene phenocrysts in chondrules are finely fractured, but there are still some unfractured grains. Minor melting occurs near the edge of the disk sample. The melts contain tiny spherules of Fe-Ni metal and Fe sulfide and abundant bubble-like voids, similar to that produced in the 21-GPa sample [3].

**Impact at 30 GPa :** Chondrules are flattened, but the degree of flattening is nearly as much as those in the 26- and 28-GPa samples. The mean aspect ratio of 41 chondrules is 1.58. Preferred orientation is again not so pronounced. However, the sample shows a very characteristic texture distinct from the previous samples. The finely divided banding structure occurs throughout the matrix (Fig. 1). Besides these bands, relatively thick (10-50  $\mu\text{m}$ ) cracks run throughout the sample; they run as if they go around each chondrule, forming a mesh-like network. The sample is found to be very fragile and easily disaggregates while polishing. All olivine and pyroxene phenocrysts in chondrules are finely fractured; they appear more like aggregates of very fine particles. Larger amounts of melts were produced near the edge of the disk sample.

**Impact at 38 GPa :** The sample container was cracked, and much of the sample was lost. Large portions of the remaining sample melted, and the general texture became chaotic; chondrules are finely fractured, destroyed and mixed into the matrix, thus hardly recognizable. The melts are similar in composition to the matrix, but are very heterogeneous, and tend to be more enrich in S and Ca. They contain grains of olivine and pyroxene, globules of Fe-Ni metal and sulfide, and bubble-like voids.

## DISCUSSION

The present experiments show that chondrule flattening and foliation occur in the Murchison CM2 chondrite by shock pressures to ~30 GPa. The degree of chondrule flattening is found to increase roughly in proportion to the intensity of shock pressure in the pressure range to ~25 GPa (Fig. 2). This indicates that the degree of chondrule flattening can be used as a quantitative measure of shock pressure in the pressure range to ~25 GPa. But, it does not increase in the same manner at pressures higher than 25 GPa. In the range 25-30 GPa, the orientation of flattened chondrules appears to become more irregular, thus exhibiting less pronounced foliation.

One of important changes that occurred between 25 and 30 GPa is the finely divided banding structure of the matrix. It starts to form at ~25 GPa and extends throughout the sample at ~30 GPa. The banded portions of the sample (*i.e.* matrix) are easily disaggregated to fine grains, probably because of the dense network of fine fractures and thick cracks. Most of the coarse-grained olivines and pyroxenes in chondrules are also finely fractured at 25-30 GPa. These features indicate that almost all the components in Murchison become pulverized at ~30 GPa, although the sample barely maintains its original configuration in which chondrules are uniformly embedded in a matrix.

Another important change observed in the pressure range between 20 and 30 GPa is the production of shock melts. The matrix melts locally as veins and pockets, and the amount of melts increases progressively with increasing shock pressure. At 38 GPa, the matrix melts randomly throughout the sample. These results are consistent with the experimental study of Akai and Sekine [7], who reported that phyllosilicates in Murchison decomposes to an amorphous state at pressures >32 GPa. The melts were apparently derived from the matrix, but they are generally more enriched in S and Ca. These particular elements probably have a tendency to be mobilized and incorporated in the melts by shock melting.

The present experiments reveal that the changes involving melting, evaporation and pulverization start to take place in Murchison at shock pressure 20-25 GPa, which is about the onset of shock stage S4, and these changes drastically advance with increasing pressure in the range 25-30 GPa, which is the onset of shock stage S5. The sample becomes chaotic

with major melting and destruction at 38 GPa. These results support the hypothesis of Scott et al. [1] that type 2 chondrites shocked above 20-30 GPa escaped from the parent asteroids, due to explosive expansion of shocked materials on pressure release, and formed particles that are too small to survive as meteorites.

**REFERENCES**

[1] Scott E.R.D., Keil K. and Stöffler D. (1992) *Geochim. Cosmochim. Acta* **56**, 4281-4293.  
 [2] Hayashi C., Nakazawa K. and Nakagawa Y. (1985) *Protostars and Pplanets II*, pp.1100-1154, Univ. Arizona Press.  
 [3] Tomeoka K., Yamahana, Y., Mizumoto, F. and Sekine T. (1996) *Papers presented to 19th Symp. Antact. Meteorites*, 185-188 (Abstr.).  
 [4] Stöffler D., Keil K. and Scott E.R.D. (1991) *Geochim. Cosmochim. Acta* **55**, 3845-3967.  
 [5] Nakamura T., Tomeoka K., Sekine T. and Takeda H. (1995) *Meteoritics* **30**, 344-347.  
 [6] Sekine T., Akaishi M., Setaka N. and Kondo K. (1987) *J. Mat. Sci.* **23**, 3615-3619.  
 [7] Akai J. and Sekine T. (1994) *Proc. NIPR Symp. Antarct. Meteorites* **7**, 101-109.

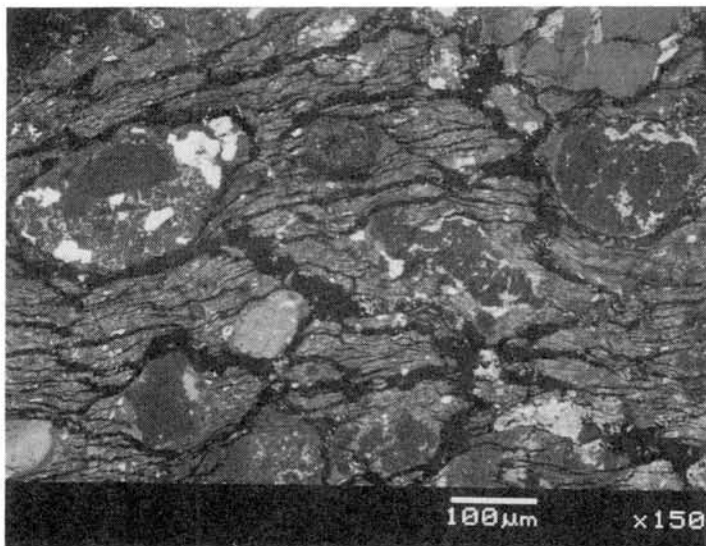


Fig. 1 A back-scattered electron image of the Murchison sample shocked at 30 GPa.

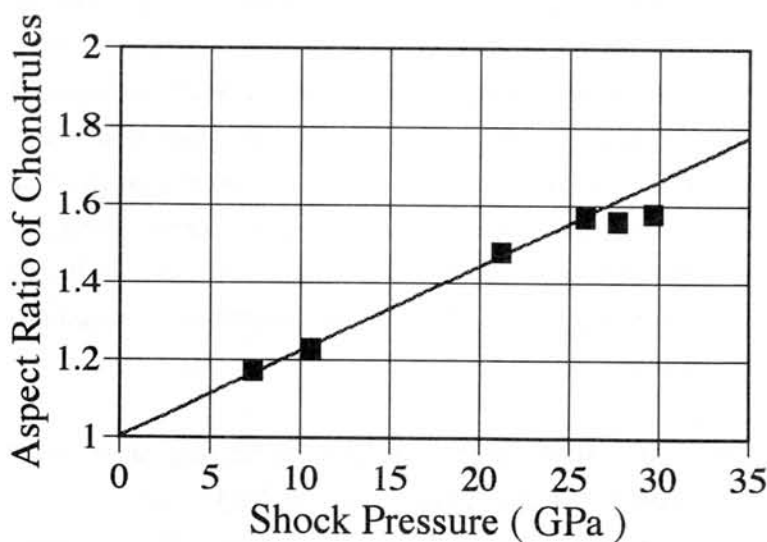


Fig.2 Relationship between mean aspect ratios of chondrules and shock pressures.

# Evaporation coefficients of sodium from $\text{Na}_2\text{O-SiO}_2$ melts by thermogravimetry

Atsuko YAMANAKA and Akira TSUCHIYAMA

Department of Earth and Space Science, Faculty of Science, Osaka University, Toyonaka  
560, Japan

**Introduction :** Chondrules were formed as isolated droplets of molten or partially molten materials. It has been known that alkalis volatilize easily from silicate melts at high temperatures. However, contents of sodium in chondrules are not so depleted compared with CI-chondrites or the cosmic abundance. This has been used as one of the important restrictions for discussing conditions of chondrule formation (for example [1], [2]). Experiments were conducted on the volatilization of sodium from silicate melts with chondrule compositions under conditions at 1 atm (for example [3]) and low pressures [4]. However, evaporation rates of sodium has not been known systematically under different conditions with different compositions. We have been trying to construct a new technique to measure evaporation rates of sodium from silicate melts using a thermogravimetry. We report here our recent experimental results on the evaporative behavior under several  $p(\text{O}_2)$  conditions at low pressures.

**Experiments :** The evaporation experiments were performed on the high temperature mass balance (SETARAM TG-92: identification limit is 1  $\mu\text{g}$  and upper limit of the temperature is 1750°C) with a vacuum system with controlled gas species. Melts in a simple system with known thermodynamical data were used in the experiments.  $\text{Na}_2\text{O-SiO}_2$  glass ( $\text{Na}_2\text{O}=24.99$  wt%,  $\text{SiO}_2=75.01$  wt%, liquidus temperature=800°C) were prepared as starting materials for experiments. The sample of about 15 mg was held on the Pt wire loop, and heated at constant temperature ranging from 1300°C to 1500°C in constant  $p(\text{O}_2)$  ranging from  $10^{-8}$  atm to  $10^{-13}$  atm controlled by  $\text{H}_2/\text{CO}_2$  mixing gases under low vacuum conditions of about  $10^{-3}$  atm. Volatility of  $\text{Na}_2\text{O}$  is much higher than that of  $\text{SiO}_2$ , and it was confirmed from comparison between mass loss and chemical analysis of the recovered sample that the measured mass loss is by volatilization of  $\text{Na}_2\text{O}$ . It was also confirmed from electron probe micro-analysis (JEOL-733) that distribution of sodium in recovered samples were homogeneous.

**Results and discussion :** Changes of vaporization mass during heating at constant temperature in constant  $p(\text{O}_2)$  are shown in Fig.1. Evaporation of  $\text{Na}_2\text{O}$  occurred non-linearly with time. Homogeneous distribution of sodium in the recovered sample eliminates

the possibility that Na<sub>2</sub>O evaporation is controlled by diffusion of sodium in the melts. Thus, the voratilization rate of sodium,  $J$ , should be controlled by surface process, and can be expressed by Heltz-Knudsen equation:

$$J = \frac{\alpha(p_{Na}^e - p_{Na})}{\sqrt{2\pi m_{Na} kT}}, \quad (1)$$

where  $\alpha$  is the vaporization coefficient ( $0 < \alpha \leq 1$ ),  $m_{Na}$  is the mass of Na gas molecules,  $k$  is the Boltzmann constant, and  $T$  is the temperature.  $p_{Na}^e$  and  $p_{Na}$  are the equilibrium and partial pressure of sodium.

To discuss our experimental results, we made two assumptions to the change in equilibrium vapor pressure by changing chemical composition of the melt, and change in vapor pressure in a gas due to evaporation of sodium.

$$p_{Na}^e = p_{Na,0}^e - f_1 g, \quad (2)$$

$$p_{Na} = p_{Na,0} + f_2 g, \quad (3)$$

where  $g$  is the measured evaporation mass, and  $f_1$  and  $f_2$  are positive constants, suffix 0 denotes initial value [5]. From eqs. (1)(2) and (3) we can obtain :

$$g = -\zeta [\exp(-\eta t) - 1],$$

$$\zeta = \frac{p_{Na,0}^e - p_{Na,0}}{f_1 + f_2}, \quad \eta = A \alpha \sqrt{\frac{m_{Na}}{2\pi k T m_{NaO_{0.5}}}} (f_1 + f_2), \quad (4)$$

where  $\alpha$  is assumed to be constant, and  $A$  is the surface area of the melt, which is assumed to be constant. We confirmed  $p_{Na,0} \sim 0$  by blank experiments. The experimental data fitted well with Eq.(4), and  $\zeta$  and  $\eta$  values were obtained by the least square method. By multiplying  $\zeta$  and  $\eta$ , we obtained  $\alpha p^e$  (Fig. 2).

Activity coefficients of our samples can be calculated from [6].  $p_{Na}^e$  was obtained from the activity coefficient and the equilibrium constant [7] of the evaporation reaction;  $Na_2O(l) = 2Na(g) + 1/2O_2(g)$  as a function of  $p(O_2)$ , and thus  $\alpha$  was obtained.  $\alpha$  is less than unity and shows temperature and  $p(O_2)$  dependence (Fig. 3).

**References :** [1] Grossmann J.N. (1988) In *Meteorites and the Early Solar System* ed. J.F. Kerridge and M.S. Matthews, pp 680-696. [2] Hewins R.H. (1991) *GCA*, 55, 935-942. [3] Tsuchiyama A. et al. (1981) *GCA*, 45, 1357-1367. [4] Yu Y. and Hewins R.H. (1997) *LPS XXVIII*, [5] Yamanaka A. et al. (1996) *Antarctic Meteorites XXI*, 210-212. [6] Rego D.N. et al. (1985) *Metal. Trans.* , 16B, 313-323. [7] Chase et al. (1985) *JANAF Thermochemical Tables 3rd Ed.*, p1577.

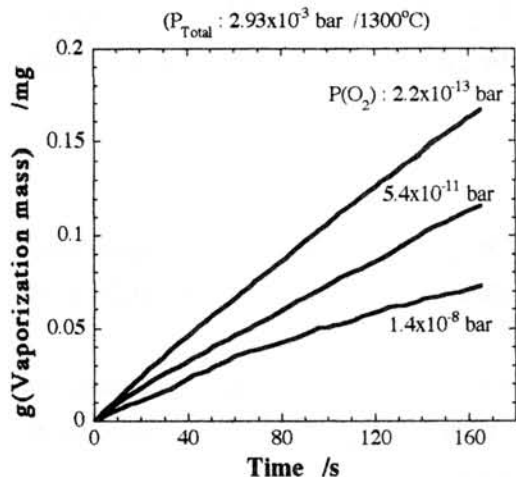


**Fig.1.** Vaporization mass plotted against the experimental time at  $1300^{\circ}\text{C}$  in the low vacuum of  $2.9 \times 10^{-3} \text{ bar}$ .

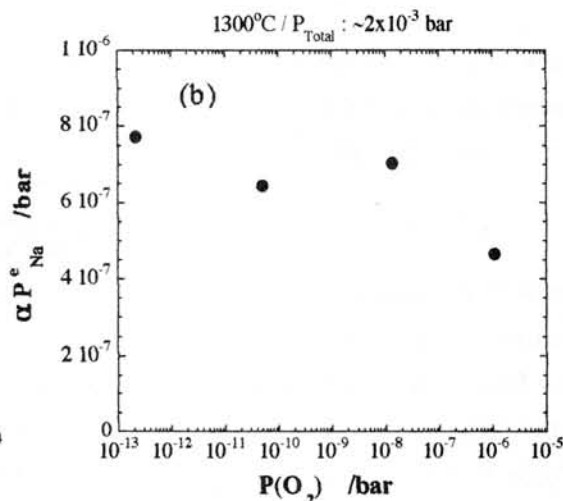
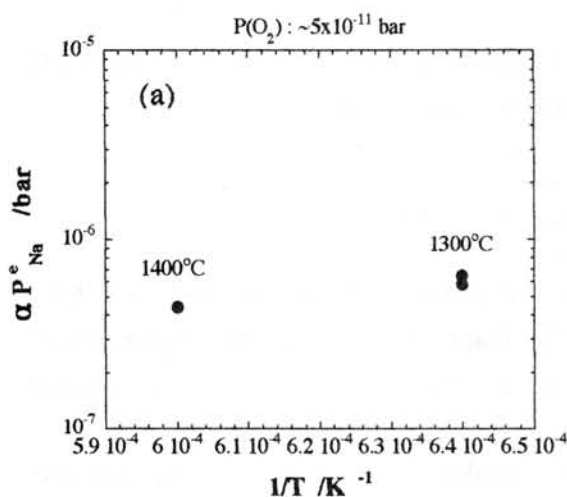


**Fig.2.**  $\alpha P_{\text{Na}}^e$  plotted against the temperature (a) and  $p(\text{O}_2)$  (b).

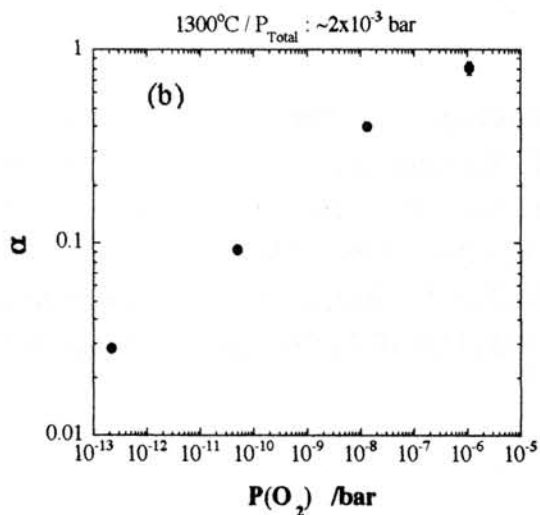
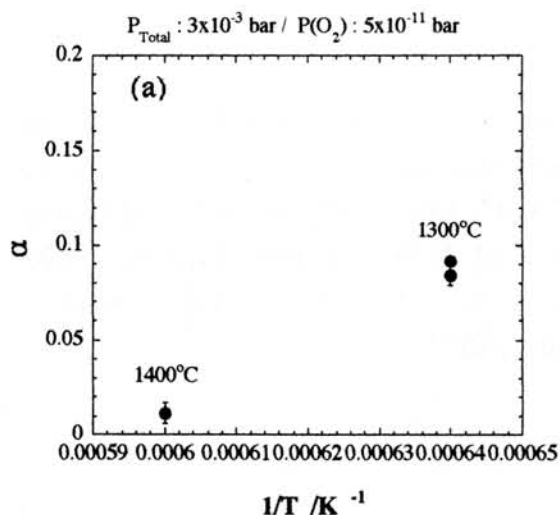


**Fig.3.**  $\alpha$  plotted against the temperature (a) and  $p(\text{O}_2)$  (b).

# SAMPLE PROCESSING AND INITIAL ANALYSIS TECHNIQUES FOR ANTARCTIC MICROMETEORITES

Hajime Yano<sup>1</sup> and Takaaki Noguchi<sup>2</sup>

1. Planetary Science Division, Institute of Space and Astronautical Science,  
3-1-1 Yoshinodai, Sagami-hara, Kanagawa, 229 Japan
2. Department of Materials and Biological Sciences, Ibaraki University,  
2-1-1 Bunkyo, Mito, Ibaraki, 310 Japan

## Introduction

Since the last decade, large (i.e. ~50-500  $\mu\text{m}$ ) and abundant (e.g. ~100 per ton of ice) micrometeorites recovered from Antarctic ice (AMM) have been appreciated as a new tool to complement other extraterrestrial materials for understanding of the microparticulate environment of the Solar System (e.g. [1][2]). Since 1994, one of the authors (HY) has been trained initial selection and processing of melted and unmelted AMM with M. Maurette's group in the CSNSM, Orsay, France, mainly for comparative studies with micrometeoroid impacts in space [3][4]. In parallel to such an effort, the Japanese Antarctic Research Expedition (JARE) team is currently preparing for their first collection of AMMs near the Showa Station and Yamato Mountains in the 1997-1999 term [5]. Thus it is our intention to establish a curation system for AMMs which is consistent with previous work outside Japan. While some detailed studies of samples from the same collection with EPMA and INAA are presented elsewhere [6][7], this paper focuses on standardising selection criteria of AMMs from mixture with terrestrial and artificial particles and sample processing for initial characterisation of the microparticles using low vacuum SEM/EDS (LV-SEM/EDS) and TEM, including ultra-microtoming technique.

## Sample Collection in Antarctica

The samples analysed in this study were collected at a blue ice field near Cap-Prudhomme, Antarctica in January 1991 by Maurette's team. The detailed procedure is presented elsewhere [1]. One bottle of "unprocessed" samples of 50-100  $\mu\text{m}$ -sized particles sieved from 1t of ice melt water, out of 100t ice in total, was allocated to us. As can be seen from past reports, one of the key issues to perform timely and systematic curation of abundant AMMs (e.g. in order of  $10^3$ - $10^4$  samples per campaign) is how quickly and precisely one can distinguish AMMs from terrestrial and artificial microparticles. The first step of this challenge is a reduction of terrestrial and artificial inclusions in sieved samples. It requires a careful choice of collection sites in terms of contamination level (i.e. remoteness from exposed lands and human bases) and thorough design and operation of "micrometeorite factory", or a ice melting and sieving instrument, on selection sites. After that, simple but reliable selection criteria of AMMs with only optical properties, morphology and X-ray EDS spectra must be established (e.g. [8] for stratospheric IDPs and [9] for impact craters on Low Earth Orbit spacecraft).

## Initial Processing

First of all the sample bottle was washed with distilled water and deposited all the grains collected on to a paper filter under an optical stereo-microscope. A new, fine paint brush being wet with the distilled water, was used as a "manipulator" to hold and move the microparticles. In the past, the following contaminants were identified and separated from AMMs:

- (1) Terrestrial morainic debris such as silicate grains from surrounding mountains,
- (2) Fragments of penguin feathers (!),
- (3) Ash ejected from the chimney of a steam generator engine used in this study,
- (4) Fragments released from plastic tubes,
- (5) Rust from corrosion of steam generator pipes and the pumps made of ordinary steel.

The first point was obvious for our sample such as crystal quartz, feldspar, mica, ilmenite suggesting continental and volcanic origin. In particular platelet grains were so abundant in this size range comparing to larger size regimes (e.g. 100~400  $\mu\text{m}$ ). Also another contaminant

frequently found was reddish coloured rust grains as reported in the last point. The 1991 collection suffered from contamination with rust particles, because tubing of three steam generators used to heat up ice melt water were made of ordinary steel. To discriminate them, we carefully turned over even black coloured grains with a wet brush and removed them if showing any detectable speck of red coloured surfaces. However this operation still leaves some ambiguity for selection because most of partially melted (scoria) AMMs have magnetite rims on exteriors and they can be oxidised during atmospheric entry and interaction with ice water. Similarly terrestrial iron particles also rust showing a red colour first (iron hydroxide), but become dark (magnetite type) after "cooking". Thus in the 50-100  $\mu\text{m}$  range, non-platelet, irregular-shaped (e.g. porous), black particles with sub- $\mu\text{m}$  to  $\mu\text{m}$  size magnetite rims are selected. Such morphological and optical features may not be unique to extraterrestrial particles unless completely melted by atmospheric entry (i.e. "cosmic spherules"; Fig. 1).

In 1994 this problem was considerably reduced for the French collection, because these tubings were replaced by stainless steel of a type used in nuclear reactors. The same careful planning is strongly recommended for the instrumentation of the forthcoming JARE collection. Nevertheless we mounted such black or glassy (olivine-like green-to-yellow colour), irregular-shaped AMM "candidates" on a multiple (6 x 6 matrix) sample holder made of brass for the low vacuum (LV)-SEM/EDS studies.

### LV-SEM/EDS Analysis

After calibration with a cobalt standard, a total of 44 AMM "candidates" with 5 cosmic spherules were investigated their SEM imagery and EDS spectrum on the LV-SEM/EDS (JEOL JSM-5310LV) attached an Oxford X-ray detector and ISIS-Link spectrum analysis software. The advantage of using LV-SEM/EDS from ordinary EDS or EPMA is that samples do not require any conductive coating nor embedding in epoxy; thus they will not be restricted to any types of further analyses even after initial qualitative determination of bulk elements for curation/cataloguing. The acceleration voltage at 15 kV in exposed times in 60-100 seconds gave sufficient count rates to characterise main peaks. In micro-morphology (typically x500~x5000 magnification in this size range), we could further identify terrestrial particles with multi-layer structure or melted droplets or clusters of large crystals. The rest appeared porous in irregular shape and were usually covered with magnetite rims in sub- $\mu\text{m}$  size.

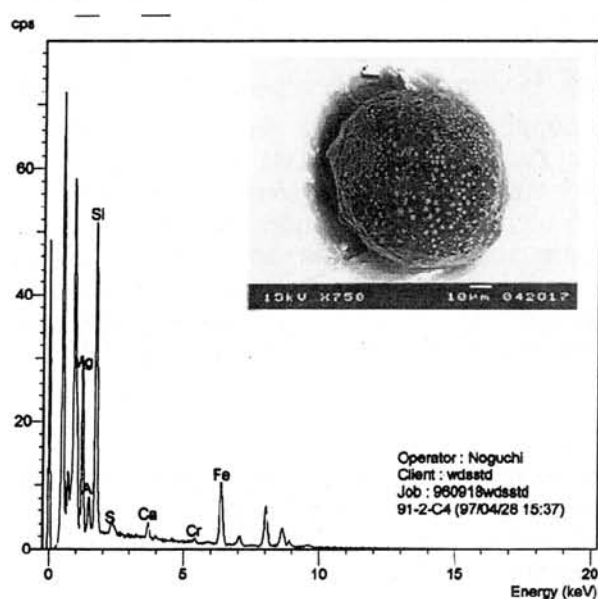


Figure 1. BEI photograph and EDS spectra for the sample 91-2-C4, a cosmic spherule with major peaks of Si > Mg > Fe > Al > Ca = S >> Cr in the order of height.  $d = \sim 88 \times 80 \mu\text{m}$ .

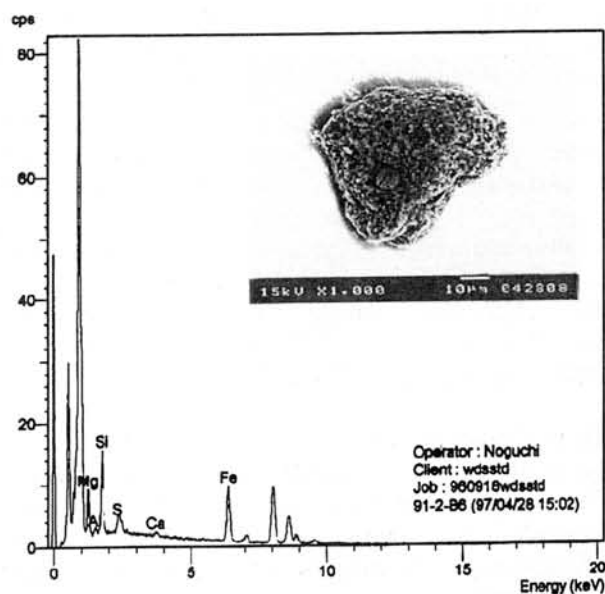


Figure 2. BEI photograph and EDS spectra for the sample 91-2-B6, a unmelted AMM candidate with major peaks of Si > Mg = Fe > S >> Al = Ca in the order of height.  $d = \sim 63 \times 50 \mu\text{m}$ .

Such porous particles typically indicated Si as the strongest peak followed by Mg being as large as or larger than Fe, suggesting anhydrous silicates (i.e. olivine and pyroxene; Fig. 2). By comparing with cosmic spherules as indicators of extraterrestrial signatures, relatively strong peaks of Al, S and Ca were apparent though Cr and Ni were only present when they were melted and enriched considerably. Other particles exhibited strong FeS (troilite) features while the others lacked Mg but enriched Al and light elements like K and Cl, suggesting another terrestrial origin.

### Ultra-Microtoming and TEM Analysis

By combining the micro-morphology and qualitative EDS results, it appeared obvious to identify unmelted or least-melted AMM candidates with chondritic features so that several of those were ultra-microtomed and proceeded to TEM analysis of their mineralogy.

Ultra-microtoming (UM) that can slice samples in an accuracy of < 100 nm with a diamond blade is a technique commonly used for thin-sectioning of biological samples and clay minerals for microanalysis. It has been adopted for mineralogical analysis of stratospheric IDPs for some years at NASA/JSC.

After embedded in epoxy resin and sliced by the UM, three AMM candidates with likely extraterrestrial EDS features were observed with TEM. As a result all the three candidates were found to include magnetite crystals in the interiors as well as exteriors, suggesting iron rust. This implies that morphological and SEM characterisations only cannot be reliable determinators of AMMs from the mixture of terrestrial and artificial grains.

### Discussion and Further Works

So what is the smoking gun of extraterrestrial origin for unmelted microparticles in Antarctic ice? The mineralogy, including detection of fission track by solar wind impacts, is surely a strong tool for it but it requires micro-manipulation for sample preparation. Detection of isotopic anomaly of heavy elements such as Ir by INAA technique is another choice while estimating cosmic-ray exposure duration with AMS and others requires much larger bulk mass than a 50-100  $\mu\text{m}$  porous particle. Thus we are currently cross checking the potential AMMs between TEM and INAA analyses. Also we are studying one sample of scoria AMMs from the 1992 collection [3] with the TEM to understand what level of clarity of mineralogy is available in the "real" AMMs. Unless we succeed to link their results with the initial survey of morphology and EDS spectrum, it seems non-trivial to establish a practical and reliable routine of cataloguing AMMs when the JARE brings tens of thousands of grains from Antarctic ice.

We should also investigate the same size range of French samples from other collection sites in 1994 with an improved "micrometeorite facility" and see if contamination level and difficulty of AMM detection reduce. The 1994 collection was the best one ever made so far, in particular because the blue ice fields were shielded from man made contamination by the heaviest snow falls ever recorded since the building of the French station of Dumont d'Urville, 44 years ago.

### Acknowledgements

We greatly appreciate M. Maurette for providing the samples that we presented here. Also M. Nakamura and his colleagues at the Tokyo Institute of Technology have kindly allowed us to use their LV-SEM/EDS. HY is supported by the Scientific Research Grant-in-Aid of the Ministry of Education, Science, Culture and Sports of Japan as a part of his research fellowship from the Japanese Society of Promotion of Science. TN is supported by the Grant-in-Aid for Scientific Research, from the Ministry of Education, Science, Sports, and Culture, Japan (No. 08640600).

### References

- [1] Maurette, M. *et al.*: *Nature*, **351**, 44-46, (1991); [2] Maurette, M. *et al.*: In *Analysis of Interplanetary Dust*, (edit.) Zolensky, M.E. *et al.*, AIP Press, 277-289, (1994); [3] Yano, H.: *Ph.D. Thesis*, University of Kent at Canterbury, Kent, U.K., (1995); [4] Yano, H., C. Engrand and M. Maurette: *Antarctic Meteorites*, **21**, 213-215, (1996); [5] Kojima, H.: *Abst. 1997 Jpn Earth & Planet. Sci. Joint Meet.*, **H21-09**, 552, (1997); [6] Yada, T. *et al.*: this volume, (1997); [7] Fukuoka, T. *et al.*: this volume, (1997); [8] CDPET: *Cosmic Dust Catalog*, NASA/JSC, Houston, Texas, U.S.A., **1-14**, (1981-1994); [9] Zolensky, M.E. *et al.*: *Proc. Second LDEF Post-Retrieval Symp.*, NASA CP-3194, 277-302, (1993).

# Modal abundances of minerals of primitive achondrites and the endmember mineral assemblage of the differentiation trend.

Keiko Yugami<sup>1)\*</sup>, Hiroshi Takeda<sup>2)</sup>, Hideyasu Kojima<sup>3)</sup> and Masamichi Miyamoto<sup>1)</sup>

1) Mineralogical Institute, Graduate School of Science, University of Tokyo, Hongo, Tokyo 113, Japan

2) Research Institute, Chiba Institute of Technology, Tsudanuma, Narashino, Chiba 275, Japan

3) National Institute of Polar Research, Kaga, Itabashi-ku, Tokyo 173, Japan

\* Present address: X-ray Laboratory, Rigaku Corporation, Matsubara-cho, Akishima-shi Tokyo 196, Japan.

## Introduction

Winonaites and IAB iron meteorites (WI) and acapulcoites and lodranites (AL) are both sub-groups of primitive achondrites, although their oxygen isotope compositions indicate that they are from the different parent body [1]. In this paper, in order to decipher a common differentiation processes for the two sub-groups, modal abundances of minerals of twenty meteorite samples of all sub-groups of primitive achondrites have been studied by chemical mapping analysis (CMA) techniques of electron probe microanalysis (EPMA). The mineral distribution maps of twenty PTSs were made from them to obtain the mode of variations of the distributions of minerals and quantitative modal abundances of minerals. Some areas rich in plagioclase and augite in the polished thin sections (PTS) were found in the Caddo County IAB iron meteorites[2]. The trends of variations of chemical compositions of minerals also showed that the end member of the variation is similar to the material found in the Caddo County. Then, the mechanism of local heterogeneous segregation of partial melts has been propose based on the information obtained by all available specimens in this study.

## Samples and Techniques

The polished thin sections (PTSs) of twelve meteorites in the AL group, Acapulco, ALH77081,4, ALH78230,51-2, ALH81187,16, ALH81261,14, EET84302,28, Y74357,62-1, Y75274,81-2, Y791491,61-2, Y8002,51-2, Y8307,51-2 and MAC88177,17, and five winonaite, Tierra Blanca, Winona, Y74025,52-4, Y75305,52-2, and Y8005,51-3, and three PTSs of Caddo County IAB iron meteorite, Caddo County, B1A, B2A, B3A and two PTSs of Y791058 (WI group), Y791058,51-2 and ,91-2 were studied. Y791058,51-2 is like an iron meteorite with silicate inclusions and Y791058,91-2 looks like an acapulcoite. The Y75008 H7 chondrite was also studied as a hypothetical standard source material for primitive achondrites for comparison. These samples were supplied from National Institute of Polar Research, Meteorite Working Group of the U.S. and Planetary Materials Database Collections of University of Tokyo. These PTSs were investigated by EPMA JEOL733 at Ocean Research Institute and Geological Institute and JEOL JXA-8900L at Geological Institute, University of Tokyo. Two dimensional CMA techniques of EPMA for nine elements (Si, Mg, Ca, Fe, Al, Cr, P, S, Ni) have been applied to twenty-one PTSs and mineral distribution maps of eighteen primitive achondrites and Y75008 chondrite were made from CMA data processed by using the public domain NIH Image program (Distribution maps of eleven minerals of each PTSs were made and combined [3]). Modal abundances of minerals of these samples were obtained from the mineral distribution maps.

## Results

Modal abundances of minerals of twenty PTSs obtained by CMA are summarized in Table 1. The volume percentage of opaque minerals varies from 5.2 % (MAC88177) to 82 % (Y791058 metal-rich PTS). Because the FeNi modal abundances are so variable, the mineral assemblages of silicates and phosphates portions of primitive achondrites are plotted in the orthopyroxene (Opx) - olivine (Ol) - (plagioclase (Plag) + augite (Aug) + phosphate) pseudo-ternary diagram (Fig. 1). The previous investigations (*e.g.* [4]) used (Opx + Aug) component as a parameter to indicate differentiation trend, but we combined Aug with Plag + phosphate to represent the differentiation trend better, because the (Plag + Aug)-rich material as was found in Caddo County can be taken as an extreme end of the differentiation trend. Ratios of volume

percentage of Ol - Opx - (Plag + Aug + phosphate) of the primitive achondrites show that their variation is in line with the local heterogeneity model, and that the plagioclase-augite-rich region of Caddo County B3A (Plag + Aug + phosphate = 96.8 %) can be taken as an endmember of the variation. The orthopyroxene-chromite-rich region of EET84302,19 (Opx = 95.1 %) and Y74357 (Ol = 83.2 %) are other types of segregated materials for the silicate portions. General trends of deviation of winonaites from the chondritic assemblages are away from the Ol corner, but Tierra Blanca is closer to the Ol corner than other winonaites. The modal abundances of minerals of some selected parts of the PTSs of Caddo County, B1A (coarser-grained region (CR) and finer-grained region (FR)), B2A (region 1 (R1) and R2), B3A (R1, R2 and R3), Gibson (R1, R2, R3 and R4), EET84302,19 (chromite-rich region (C) and metal-rich region (M) [5], Tierra Blanca (R1 and R2) and Y8005 (R1, R2, R3 and R4) are added in Fig. 1. There are considerable heterogeneities in each PTSs of Caddo County, EET84302,19 and Tierra Blanca. Caddo County, B1A FR is plotted at the region of acapulcoites. Now, the new diagram (Fig. 1), clearly show the differentiation trend of the AL group, except for EET84302. All other lodranites are plotted towards lower base line between Opx + Ol. EET84302 is just a coarse-grained version of acapulcoites. Many acapulcoites are plotted above the H7 position. Most of the primitive achondrites are distributed at near sites of the bisector of the (Aug + Plag + phosphate) corner. This trend suggests that the enrichment of low-melting-temperature components may facilitate a recrystallization process. The similarities in modal abundance variations, chemical zoning patterns of silicate minerals and opaque grain shapes in different sub-groups suggest that it is possible to envision common formation processes of all primitive achondrites. The  $fe\#s$  ( $fe\# = 100 \times Fe / (Mg + Fe)$  atomic ratio) of the mafic silicates of the WI group ( $fe\# =$  about 2 - 7) overlap with those of the Mg-rich members ( $fe\# =$  about 3 - 6) of the AL group. The presence of coarse-grained acapulcoites (some of former lodranites) does not support the old classification scheme of acapulcoite/lodranite. Fe/Mg reverse zoning at the rims of olivine can be attributed to reduction during cooling on the basis of the diffusion simulation of the cations. Primitive achondrites with larger  $fe\#s$  (than 10) of silicates that include Ca-phosphate, do not include schreibersite, and those with smaller  $fe\#s$  (than 10) that include schreibersite, do not include Ca-phosphate. Those with much smaller  $fe\#s$  include daubreelite. Such trends can be explained by oxidation-reduction condition.

Texture variations range from fine-grained recrystallized chondrite-like materials including all kind of minerals known in chondrites, to coarse-grained materials with elongated, curved or joined opaque mineral grains, often with large aggregates of FeNi metal ( $5.5 \times 2$  mm in size). Mineralogical heterogeneity of coarser-grained samples is characterized by concentration or depletion of plagioclase-augite-rich materials and iron meteorite-like materials.

## Discussions

There are some noticeable differences between the AL and WI groups. The mafic silicate-rich lodranite-like area is conspicuously missing in the WI group, and the iron-meteorite-like materials are missing in the AL group. However, these differences may be the sampling problems of the large parent body, and metal-rich trends observed in EET84302 suggest extension of the trend will lead to the Caddo County-like materials.

By combining these two groups, the entire picture of the parent body can be reconstructed. From an ideal picture reconstructed from some of the AL/WI group, a formation and evolution mechanism of these meteorite groups has been proposed as a mechanism of most basic differentiation processes of planetesimals from primitive source materials. This mechanism involves segregation and migration of partial melts such as Ca-, Al-rich silicate melt and Fe-Ni-S eutectic melt from chondritic materials.

In conclusion, the origin of primitive achondrites can be explained by local heterogeneity of materials in the parent bodies with the variation trend from recrystallized chondrite to segregation of iron meteorite plus plagioclase-augite assemblage leaving lodranite-like mafic silicates behind. Such processes are the most basic form of differentiation of primitive source materials. This model expects that concentration of partial melts, Ca-Al-rich melt and Fe-Ni-S melt may lead to plagioclase-augite-rich rocks, which have been found in this study of a IAB

iron meteorite. The above facts cannot be explained by an equilibrium partial melting model proposed by previous investigators.

We thank Dr. D. Bogard for his associate for making PTSs of Caddo County, and Mr. H. Yoshida for his technical supports. A part of the study was performed while one of the authors (H. Takeda) was at Div. of Geol. and Planet. Sci., Caltech. He is indebted to Prof. G. J. Wasserburg and Dr. W. Hsu for their discussion and supports.

**References:** [1] Clayton R. N. and Mayeda T. K. (1996) *Geochim. Cosmochim. Acta* **60**, 1999-2017. [2] Takeda H. *et al.* (1997) *LPS XXVIII*, 1409-1410. [3] Yugami K. (1996) *Ph.D. dissertation*, Univ. of Tokyo. [4] Prinz *et al.* (1983) *LPS XIV*, 616-617. [5] Takeda H. *et al.* (1994) *Meteoritics* **29**, 830-842.

Table 1. Modal abundances of minerals obtained from mineral distribution maps (volume %).

|                  | Olivine | Opx <sup>1)</sup> | Aug <sup>2)</sup> | Plagioclase | Ca-Phosphate | Chromite | Troilite | FeNi <sup>3)</sup> | Schreibersite | Daubreelite |
|------------------|---------|-------------------|-------------------|-------------|--------------|----------|----------|--------------------|---------------|-------------|
| Acapulco         | 25.2    | 41.1              | 2.5               | 14.8        | 1.21         | 0.82     | 8.7      | 5.7                | 0.01          | -           |
| ALH77081         | 27.9    | 38.7              | 7.3               | 14.2        | 0.42         | 0.94     | 3.9      | 6.6                | -             | -           |
| ALH78230         | 28.4    | 37.7              | 5.3               | 13.6        | 0.52         | 0.85     | 6.9      | 6.7                | -             | -           |
| Y8307            | 25.9    | 32.4              | 6.7               | 13.5        | 0.90         | 0.19     | 5.5      | 15.0               | -             | -           |
| EET84302,28      | 17.7    | 38.6              | 0.5               | 15.2        | 0.04         | -        | 0.2      | 27.2               | 0.62          | -           |
| Gibson           | 27.3    | 41.9              | 6.3               | 3.3         | 0.00         | 0.09     | 0.3      | 20.8               | 0.07          | -           |
| MAC88177         | 48.7    | 44.1              | 1.9               | -           | 0.03         | -        | 4.1      | 1.1                | -             | -           |
| Y74357           | 71.9    | 9.7               | 4.7               | -           | 0.09         | 0.06     | 0.3      | 13.1               | 0.27          | -           |
| Y75274           | 20.3    | 50.5              | 0.4               | 2.3         | -            | -        | -        | 25.3               | 1.23          | -           |
| Y791491          | 57.4    | 32.0              | 0.2               | 0.2         | 0.16         | 0.55     | 5.4      | 4.1                | 0.06          | -           |
| Y8002            | 31.7    | 43.7              | 1.7               | 10.0        | 0.01         | 0.04     | 0.3      | 12.2               | 0.25          | -           |
| Tierra Blanca    | 27.6    | 32.7              | 0.2               | 10.2        | 0.09         | 0.02     | 3.8      | 25.5               | 0.03          | -           |
| Y74025           | 16.0    | 41.4              | 6.1               | 14.9        | -            | -        | 14.0     | 7.0                | 0.15          | 0.51        |
| Y75305           | 5.8     | 36.5              | 0.4               | 8.6         | 0.01         | 0.12     | 9.2      | 39.0               | 0.02          | 0.29        |
| Y8005            | 11.8    | 28.4              | 6.2               | 13.5        | -            | 0.04     | 7.2      | 31.7               | 0.81          | 0.28        |
| Y791058,91-2     | 24.8    | 40.9              | 2.1               | 17.6        | 0.28         | 0.01     | 4.1      | 10.2               | 0.09          | -           |
| Caddo Co. B1A    | 26.0    | 39.9              | 5.3               | 20.4        | 0.21         | 0.03     | 4.3      | 3.7                | 0.09          | -           |
| Caddo Co. B2A    | 9.7     | 11.9              | 18.8              | 34.3        | 0.85         | 0.01     | 8.1      | 16.0               | 0.34          | -           |
| Caddo Co. B3A    | 9.6     | 11.8              | 24.8              | 35.8        | 0.00         | -        | 1.2      | 16.4               | 0.49          | -           |
| Caddo Co. B3A R3 | 0.2     | 1.3               | 25.4              | 21.4        | 0.00         | -        | 0.4      | 49.7               | 1.52          | -           |
| Y75008           | 18.4    | 36.3              | 2.7               | 4.7         | 0.37         | 1.46     | 7.2      | 29.0               | -             | -           |

1) orthopyroxene. 2) augite. 3) FeNi metal, including Fe-hydroxide, etc. -: not detected.

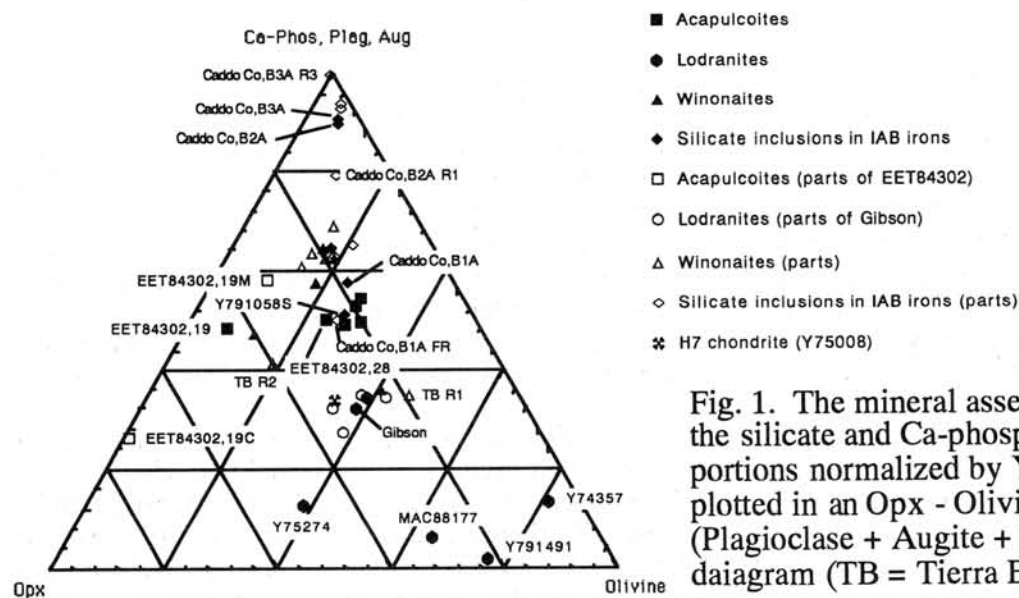


Fig. 1. The mineral assemblages of the silicate and Ca-phosphate portions normalized by Y75008 (H7) plotted in an Opx - Olivine - (Plagioclase + Augite + Phosphate) daiagram (TB = Tierra Blanca).

## AUTHOR INDEX

- |                    |                         |                 |                                     |
|--------------------|-------------------------|-----------------|-------------------------------------|
| Akai J.            | 1                       | Kong P.         | 22                                  |
| Arai T.            | 3                       | Kubovics I.     | 9                                   |
| Breznysnyánszky K. | 9                       | Kusakabe M.     | 72                                  |
| Bérczi Sz.         | 6, 9, 12, 18,<br>20, 94 | Kákay-Szabó O.  | 18, 20                              |
| Caffee M.W.        | 149                     | Le L.           | 80                                  |
| Chen M.            | 27                      | Lofgren G.E.    | 103, 106                            |
| Chikami J.         | 15                      | Lukács B.       | 6, 9, 12, 18,<br>20, 94             |
| Chunlai L.         | 206                     | Marakushev A.A. | 97                                  |
| Connerney J.E.     | 203                     | Marosi G.       | 12                                  |
| Crozaz G.          | 197                     | Matsuoka K.     | 100                                 |
| Danon J.           | 43                      | McCoy T.J.      | 103                                 |
| Detre C.H.         | 9, 18, 20               | McKay G.        | 80, 106, 197                        |
| Dickinson T.L.     | 103, 203                | Mikouchi T.     | 15, 75, 106, 109,<br>182            |
| Ditrói-Puskás Z.   | 9                       | Minamitani M.   | 113                                 |
| Don G.             | 18, 20                  | Misawa K.       | 115                                 |
| Dosztály L.        | 18, 20                  | Miura Y.        | 39, 41                              |
| Ebihara M.         | 22, 58                  | Miura Y.N.      | 118, 131                            |
| El Goresy A.       | 27, 121                 | Miyamoto M.     | 15, 75, 91, 109,<br>165, 182, 220   |
| Eugster O.         | 31                      | Morishita Y.    | 88                                  |
| Fujimaki H.        | 69                      | Mostefaoui S.   | 121                                 |
| Fujita T.          | 34                      | Motomura Y.     | 137                                 |
| Fukuhara T.        | 37                      | Murae T.        | 124                                 |
| Fukuyama S.        | 39, 41                  | Murakami T.     | 126                                 |
| Funaki M.          | 37, 43, 203             | Nagahara H.     | 130, 164, 179                       |
| Fáy N.             | 9                       | Nagai H.        | 37, 58                              |
| Földi T.           | 12                      | Nagao K.        | 72, 100, 113, 118,<br>131, 135, 160 |
| Grady M.M.         | 46                      | Nakamura N.     | 115                                 |
| Hashimoto A.       | 49                      | Nakamura T.     | 72, 100, 113, 131,<br>135, 160, 208 |
| Hashizume K.       | 188                     | Nakamuta Y.     | 100, 137                            |
| Hiroi T.           | 52                      | Naraoka H.      | 140                                 |
| Hiyagon H.         | 56                      | Nayak V.K.      | 143                                 |
| Holba A.           | 9, 12                   | Nishiizumi K.   | 149                                 |
| Honda M.           | 58                      | Noguchi T.      | 152, 156, 217                       |
| Honjo H.           | 152                     | Okazaki R.      | 113, 160                            |
| Hoppe P.           | 121                     | Ozawa K.        | 130, 164, 179                       |
| Hörz F.            | 135                     | Papike J.J.     | 3                                   |
| Ichikawa O.        | 61                      | Pillinger C.T.  | 46                                  |
| Ikeda Y.           | 64, 83                  | Polnau E.       | 31                                  |
| Imae N.            | 66                      | Premo W.R.      | 115                                 |
| Itoh Y.            | 69                      | Rózsa P.        | 174                                 |
| Jabeen I.          | 72                      | Saito Y.        | 85                                  |
| Józsa S.           | 9, 12                   | Sato K.         | 165                                 |
| Kaiden H.          | 75                      | Sekine T.       | 211                                 |
| Kaito C.           | 85                      | Sekiya M.       | 168                                 |
| Kallemeyn G.W.     | 78, 200                 | Sharp T.G.      | 27                                  |
| Kaneda K.          | 80                      | Shearer C.K.    | 3                                   |
| Kimura M.          | 83                      | Shimoyama A.    | 140                                 |
| Kimura S.          | 85                      | Shinotsuka K.   | 22, 58                              |
| Kita N.T.          | 88                      | Solt P.         | 18, 20                              |
| Kiyota K.          | 171                     | Sugiura N.      | 171                                 |
| Kobayashi H.       | 41                      | Szabó Sóki L.   | 12                                  |
| Koike C.           | 85                      |                 |                                     |
| Kojima H.          | 61, 66, 91, 185,<br>220 |                 |                                     |
| Kojima T.          | 191                     |                 |                                     |

|                 |                                 |
|-----------------|---------------------------------|
| Szakmány Gy.    | 9, 12                           |
| Szöör G.        | 174                             |
| Tachibana S.    | 179, 194                        |
| Takahashi T.    | 49                              |
| Takaoka N.      | 100, 113, 131, 135,<br>160, 208 |
| Takeda H.       | 3, 15, 182, 220                 |
| Takeda Ha.      | 185                             |
| Tamura N.       | 85                              |
| Tanaka T.       | 179                             |
| Taniguchi Y.    | 188                             |
| Tari S.         | 1                               |
| Tatsumoto M.    | 115                             |
| Terashima S.    | 88                              |
| Togashi S.      | 88                              |
| Tomeoka K.      | 191, 211                        |
| Tsuchiyama A.   | 179, 194, 214                   |
| Tóth I.         | 9, 18, 20                       |
| Török K.        | 18, 20                          |
| Uzonyi I.       | 18, 20                          |
| Verchovsky A.B. | 46                              |
| Wadhwa M.       | 197                             |
| Warren P.H.     | 3, 91, 200                      |
| Wasilewski P.J. | 203                             |
| Weinbruch S.    | 27                              |
| Wenzhu L.       | 206                             |
| Wopenka B.      | 27                              |
| Wright I.P.     | 46                              |
| Yada T.         | 208                             |
| Yamahana Y.     | 211                             |
| Yamanaka A.     | 214                             |
| Yano H.         | 208, 217                        |
| Yugami K.       | 15, 220                         |
| Yurimoto H.     | 88                              |
| Zinner E.       | 121                             |
| Zolensky M.E.   | 135                             |

